

AD-A197 314

UNITED STATES DEPARTMENT OF THE INTERIOR

GEOLOGICAL SURVEY

Pacific Enewetak Atoll Crater Exploration (PEACE) Program
Enewetak Atoll, Republic of the Marshall Islands

Part 4: Analysis of borehole gravity surveys and other geologic
and bathymetric studies in vicinity of OAK and KOA craters

edited by

Thomas W. Henry¹ and Bruce R. Wardlaw²

U.S. Geological Survey

Open File Report 87-665

Prepared in cooperation with the Defense Nuclear Agency

and funded

This document has been approved
for public release and sale; its
distribution is unlimited.

This report is preliminary and has not been reviewed for conformity with
U.S. Geological Survey editorial standards and stratigraphic nomenclature

¹Branch of Paleontology and Stratigraphy, Denver, CO 80225-0046

²Branch of Paleontology and Stratigraphy, Reston, VA 22092

TABLE OF CONTENTS

Page No.

CHAPTER 1: INTRODUCTION TO PART 4 OPEN-FILE REPORT	1- 1
GENERAL REMARKS	1- 1
PEACE PROGRAM REPORTS	1- 3
DATA ACQUISITION AND BASES	1- 3
SYNOPSIS OF CHAPTERS	1- 7
Borehole Gravity	1- 7
Paleontologic Evidence for Mixing	1- 8
Electron Paramagnetic Resonance Studies	1- 8
Bathymetric Studies of OAK Crater	1- 9
Constraints on Densification and Piping for OAK	1-10
Additional Studies of Geologic Crater Models	1-11
ACKNOWLEDGEMENTS	1-11
REFERENCES CITED	1-12
 CHAPTER 2: BOREHOLE GRAVIMETRY, OAK CRATER	2- 1
INTRODUCTION	2- 1
BOREHOLE GRAVITY ANALYSIS	2- 4
LATERAL DENSITY CHANGES	2- 6
CORRECTION FOR LATERAL DENSITY CHANGES	2- 6
CORRECTED BOREHOLE DENSITY AND POROSITY	2-14
NATURAL DENSITY AND POROSITY VARIATIONS	2-22
CHANGES RELATED TO CRATERING	2-28
SUMMARY	2-33
ACKNOWLEDGEMENTS	2-36
REFERENCES CITED	2-36
APPENDIX 2-1; Gravity Survey, Borehole E-1, Medren Island	2-54
APPENDIX 2-2; Determination of Interval Grain Density	2-56

(continued on next page)



Accession For	
NTIS GRA&I	<input checked="" type="checkbox"/>
DTIC TAB	<input type="checkbox"/>
Unannounced	<input type="checkbox"/>
Justification	
By <i>per Statement on Title Page</i>	
Distribution/	
Availability Codes	
Dist	Avail and/or Special
<i>A-1</i>	

TABLE OF CONTENTS (continued)

	Page No.
CHAPTER 3: PALEONTOLOGIC EVIDENCE FOR SEDIMENTARY MIXING	3- 1
INTRODUCTION	3- 1
MATERIALS AND METHODS	3- 1
STANDARD MICROFAUNAL SEQUENCE	3- 2
RESULTS	3- 7
Central Crater Boreholes	3- 8
Homogenized Zone	3- 8
Upwardly Mixed Zone	3- 8
Maximum Piping Zone	3- 8
Basal Mixed Zone	3-11
Statistical Analysis	3-11
Injection Dikes	3-11
Transition Boreholes	3-11
OCT-5	3-11
OFT-8	3-13
OKT-18	3-13
SUMMARY AND CONCLUSIONS	3-14
REFERENCES CITED	3-15
APPENDIX 3-1; Occurrence of Species, OAR-2/2A	3-21
APPENDIX 3-2; Occurrence of Species, OOR-17	3-23
APPENDIX 3-3; Occurrence of Species, OBZ-4	3-25
APPENDIX 3-4; Occurrence of Species, OPZ-18	3-27
APPENDIX 3-5; Occurrence of Species, OCT-5	3-28
APPENDIX 3-6; Occurrence of Species, OFT-8	3-29
APPENDIX 3-7; Occurrence of Species, OKT-13	3-30
 CHAPTER 4: ELECTRON PARAMAGNETIC RESONANCE STUDIES, OAK CRATER	4- 1
INTRODUCTION	4- 1
ELECTRON PARAMAGNETIC RESONANCE ANALYSIS	4- 1
Sample Preparation and Spectrometer Settings	4- 1
SHOCK-PRESSURE CALIBRATION OF EPR SPECTRA	4- 3
Shock-Wave Calibration Experiments	4- 3
Description of Shocked Spectra	4- 4
Pressure Calibration by Differencing Spectra	4- 7
OAK DATA	4-11
Borehole Sample Selection	4-11
Results of Borehole-Sample Analysis	4-12
Results from Debris Samples	4-14
DISCUSSION	4-19
ACKNOWLEDGEMENTS	4-20
REFERENCES CITED	4-20

(continued on next page)

TABLE OF CONTENTS (continued)

	Page No.
CHAPTER 5: BATHYMETRIC STUDIES OF OAK CRATER	5- 1
INTRODUCTION	5- 1
Objectives and General Procedures	5- 1
Terminology	5- 1
DATA BASE	5- 3
Holmes & Narver Preshot Bathymetric Map	5- 3
Holmes & Narver Postshot Bathymetric Map	5- 4
USGS 1984 Bathymetric Map	5- 4
DATA PROCESSING	5- 6
Digitized Base Contour Maps	5- 6
Derived Isopach Maps	5- 6
Map Products	5- 7
ANALYSIS	5-10
Map Derived Quantities	5-10
Water Depths	5-10
Cross Sections	5-12
Areas and Volumes	5-12
MAP CHARACTERISTICS	5-14
Holmes & Narver Preshot Contour Map	5-14
Holmes & Narver Postshot Contour Map	5-15
USGS 1984 Contour Map	5-15
H&N Postshot - H&N Preshot Isopach Map (Δ -Relief)	5-16
USGS 1984 - H&N Preshot Isopach Map (Δ -Relief)	5-17
USGS 1984 - H&N Postshot Isopach Map (Δ -Relief)	5-18
CONCLUSIONS	5-18
ACKNOWLEDGEMENTS	5-19
REFERENCES CITED	5-20
 CHAPTER 6: CONSTRAINTS ON DENSIFICATION AND PIPING, OAK CRATER	 6- 1
BACKGROUND AND SUMMARY	6- 1
BASIC FACTS AND PARAMETERS	6- 2
SHORTENING OF "CORAL" COLUMNS BY DENSIFICATION	6- 7
DENSITY PROFILES, TREATMENT, AND DOWNWARD DISPLACEMENTS	6- 8
CONTRIBUTION OF SIMPLE SUBSIDENCE TO THE OAK CRATER	6-10
CONFIDENCE ASSESSMENT	6-18
LONG-TERM SETTLING	6-23
PIPING	6-26
OTHER CONSTRAINTS; HORIZONTAL PIPING	6-29
DENSIFICATION: SUMMARY AND CRITIQUE	6-32
CONCLUSIONS	6-34
ACKNOWLEDGEMENTS	6-36
REFERENCES CITED	6-37
APPENDIX 6-1 -- PEACE Program Density Profiles	6-39
APPENDIX 6-2 -- Densities as Continuous Depth Function	6-74
Mass as Continuous Depth Function	6-75
Thickness Change as Continuous Depth Function	6-76
References Cited	6-78

(continued on next page)

TABLE OF CONTENTS (continued)

	Page No.
CHAPTER 7: INTEGRATION OF MATERIAL-PROPERTY UNITS, GRAVIMETRY, AND ADDITIONAL STUDIES OF OAK AND KOA CRATERS	7- 1
INTRODUCTION	7- 1
PRE-EVENT GEOLOGY OF OAK AND KOA CRATERS	7- 1
POST-EVENT GEOLOGY OF OAK AND KOA CRATERS	7- 7
Crater Zones	7- 7
Geologic Crater Zones	7- 7
Paleontologic Crater Zones	7-10
Seismic Crater Zones	7-15
CRATER FEATURES	7-16
Crater Material in the Lagoon	7-16
Breach Deposit in the Lagoon	7-16
Piping	7-24
Paleontologic Mixing	7-24
OAK Crater	7-29
KOA Crater	7-29
Estimates of Volume of Piped Material	7-30
Paleontologic Model of Crater Fill	7-31
Injection	7-31
Gamma Activity	7-31
Distribution of Radionuclides	7-34
Distribution of Shocked Calcite	7-37
Depression and Uplift of Structural Surfaces	7-37
COMPARISON OF OAK AND KOA CRATERS	7-37
GEOLOGIC CRATER MODEL FOR OAK AND KOA	7-42
Thinning Analysis	7-43
Stratigraphic Density Profile	7-43
General Densification and Flow Patterns	7-58
OAK Crater	7-58
KOA Crater	7-59
Relative Timing of Depositional Events	7-59
VOLUME PROBLEMS	7-61
Evidence for Piping and Lateral Flow	7-62
Surface	7-62
Crater-Fill	7-62
Subsurface	7-62
Loss of Material from Crater	7-63
SUMMARY	7-63
REFERENCES CITED	7-64

FIGURE INDEX

Figure No.	Description	Page No.
CHAPTER 1: INTRODUCTION		
1- 1	Location Map of Enewetak	1- 2
1- 2	Location map of KOA crater	1- 5
1- 3	Location map of OAK crater	1- 6
CHAPTER 2: BOREHOLE GRAVIMETRY, OAK CRATER		
2- 1	Map of Enewetak showing OAK and KOA craters and Medren Island borehole E-1 site.	2- 2
2- 2	Map of OAK crater area and gravity survey boreholes	2- 3
2- 3	Distribution of repeated gravity measurements	2- 5
2- 4	Density model of natural atoll facies changes	2- 7
2- 5	Cross section, southwest transect	2- 9
2- 6	Cross section, southeast transect	2-11
2- 7	Density model, southwest transect	2-13
2- 8	Well logs, densities, and porosity, OOR-17	2-15
2- 9	Well logs, densities, and porosity, OPZ-18	2-16
2-10	Well logs, densities, and porosity, OQT-19	2-17
2-11	Well logs, densities, and porosity, ORT-20	2-18
2-12	Well logs, densities, and porosity, OSR-21	2-19
2-13	Densities and porosity, OTG-23	2-20
2-14	Variability of BHG and gamma-gamma density	2-21
2-15	Porosity cross plots	2-23
2-16	Interval densities and porosities, southwest transect ...	2-25
2-17	Cross plot of interval grain density vs BHG porosity	2-27
2-18	Density and porosity model, southwest transect	2-29
2-19	Interval densities and porosities, southwest transect ...	2-31
2-20	Density profile, borehole E-1 (Medren Island)	2-55
CHAPTER 3: PALEONTOLOGIC EVIDENCE FOR SEDIMENTARY MIXING		
3- 1	Plot of ostracode species versus depth, OAR-2/2A	3- 5
3- 2	Plot of ostracode species versus depth, OOR-17	3- 6
3- 3	Plot of ostracode species versus depth, OBZ-4	3- 9
3- 4	Plot of ostracode species versus depth, OPZ-18	3-10
3- 5	Plot of piped specimens versus depth	3-12

(continued on next page)

FIGURE INDEX (continued)

Figure No.	Description	Page No.
 CHAPTER 4: ELECTRON PARAMAGNETIC RESONANCE STUDIES		
4- 1	EPR spectrum of powdered single crystal calcite	4- 2
4- 2	Comparison of laboratory-shocked limestone spectra	4- 5
4- 3	Comparison of "coral" spectra shocked in laboratory	4- 6
4- 4	Differencing technique, overlay of standard vs	4- 8
	unshocked limestone spectra.	
4- 5	Plot of summed differences, low- and high-field	4- 9
	components vs shock pressure.	
4- 6	Map of OAK crater showing boreholes sampled	4-13
4- 7	Sample analysis showing calculated shock pressures	4-15
	vs sample depth for OAK boreholes.	
4- 8	Depth and thickness of regions of highly shocked	4-16
	carbonates from boreholes.	
4- 9	Map of OAK crater showing debris-sample sites	4-17
4-10	Shock pressure versus range from GZ and versus	4-18
	estimated pre-event depth below sea level.	
 CHAPTER 5: BATHYMETRIC STUDIES OF OAK CRATER		
5- 1	Map of area included in Holmes & Narver and	5- 2
	USGS surveys.	
5- 2	Fathometer lines in 1984 USGS study	5- 5
5- 3	Isopach computational grid	5- 8
5- 4	Cross sections through OAK ground zero	5-13
 CHAPTER 6: CONSTRAINTS ON DENSIFICATION AND PIPING		
6- 1	Cross sections at OAK	6- 3
6- 2	Density profiles from gravimetry	6-11
6- 3	Density profiles from gamma-gamma logging	6-12
6- 4	Change in rock thickness from BHG densities, simple	6-13
	subsidence, OPZ-18 vs OSR-21, OPZ-18 vs OOR-17.	
6- 5	Change in rock thickness from BHG densities, simple	6-14
	subsidence, OTG-23 vs OSR-21, OTG-23 vs OOR-17.	
6- 6	Change in rock thickness from BHG densities, simple	6-15
	subsidence, OQT-19 vs OSR-21, OQT-19 vs OOR-17.	
6- 7	Change in rock thickness from BHG densities, simple	6-16
	subsidence, ORT-20 vs OSR-21, ORT-20 vs OOR-17.	
6- 8	Change in rock thickness form BHG densities, simple	6-19
	subsidence, OSR-21 vs OOR-17.	
6- 9	Change in rock thickness from BHG densities, simple	6-20
	subsidence, OOR-17 vs OSR-21.	
6-10	High, low, and best estimates of fraction contributed ...	6-35
	by densification to seafloor drop, OQT-19 and ORT-20.	

(continued on next page)

FIGURE INDEX (continued)

Figure No.	Description	Page No.
6-11	BHG Profile, OOR-17	6- 40
6-12	BHG Profile, OSR-21	6- 41
6-13	BHG Profile, ORT-20	6- 42
6-14	BHG Profile, OQT-19	6- 43
6-15	BHG Profile, OTG-23	6- 44
6-16	BHG Profile, OPZ-18	6- 45
6-17	Y-Y Profile, OOR-17	6- 46
6-18	Y-Y Profile, OSR-21	6- 47
6-19	Y-Y Profile, ORT-20	6- 48
6-20	Y-Y Profile, OQT-19	6- 49
6-21	Y-Y Profile, OBZ-04	6- 50
6-22	Y-Y Profile, OCT-05	6- 51
6-23	Y-Y Profile, OAR-2A	6- 52
6-24	Y-Y Profile, OIT-11	6- 53
6-25	Y-Y Profile, OKT-13	6- 54
6-26	Y-Y Profile, OPZ-18	6- 55
6-27	Thickness changes, Y-Y densities, ORT-20 & OOR-17	6-102
6-28	Thickness changes, Y-Y densities, ORT-20 & OSR-21	6-103
6-29	Thickness changes, Y-Y densities, ORT-20 & OAR-2A	6-104
6-30	Thickness changes, Y-Y densities, OQT-19 & OOR-17	6-105
6-31	Thickness changes, Y-Y densities, OQT-19 & OSR-21	6-106
6-32	Thickness changes, Y-Y densities, OQT-19 & OAR-2A	6-107
6-33	Thickness changes, Y-Y densities, OBZ-04 & OOR-17	6-108
6-34	Thickness changes, Y-Y densities, OBZ-04 & OSR-21	6-109
6-35	Thickness changes, Y-Y densities, OBZ-04 & OAR-2A	6-110
6-36	Thickness changes, Y-Y densities, OCT-05 & OOR-17	6-111
6-37	Thickness changes, Y-Y densities, OCT-05 & OSR-21	6-112
6-38	Thickness changes, Y-Y densities, OCT-05 & OAR-2A	6-113
6-39	Thickness changes, Y-Y densities, OIT-11 & OOR-17	6-114
6-40	Thickness changes, Y-Y densities, OIT-11 & OSR-21	6-115
6-41	Thickness changes, Y-Y densities, OIT-11 & OAR-2A	6-116
6-42	Thickness changes, Y-Y densities, OKT-13 & OOR-17	6-117
6-43	Thickness changes, Y-Y densities, OKT-13 & OSR-21	6-118
6-44	Thickness changes, Y-Y densities, OKT-13 & OAR-2A	6-119
6-45	Thickness changes, Y-Y densities, OPZ-18 & OOR-17	6-120
6-46	Thickness changes, Y-Y densities, OPZ-18 & OSR-21	6-121
6-47	Thickness changes, Y-Y densities, OPZ-18 & OAR-2A	6-122
6-48	Thickness changes, Y-Y densities, OOR-17 & OSR-21	6-123
6-49	Thickness changes, Y-Y densities, OSR-21 & OOR-17	6-124
6-50	Thickness changes, Y-Y densities, OOR-17 & OAR-2A	6-125
6-51	Thickness changes, Y-Y densities, OAR-2A & OOR-17	6-126
6-52	Thickness changes, Y-Y densities, OSR-21 & OAR-2A	6-127
6-53	Thickness changes, Y-Y densities, OAR-2A & OSR-21	6-128

(continued on next page)

FIGURE INDEX (continued)

Figure No.	Description	Page No.
CHAPTER 7: INTEGRATION OF MATERIAL-PROPERTY UNITS, GRAVIMETRY, AND ADDITIONAL STUDIES OF GEOLOGIC MODELS, OAK AND KOA CRATERS		
7- 1	Distribution of shallow cemented zones on Enjebi Island, EXPOE cores.	7- 2
7- 2	Relationship of discontinuities, major discontinuities, biostratigraphic zones, material-property units, and sedimentary packages in reference boreholes.	7- 3
7- 3	Cementation and sediment types, relationships to material-property units, reference boreholes.	7- 5
7- 4	Probable pre-shot surfaces for tops of Pleistocene and Pliocene in OAK and KOA areas.	7- 6
7- 5	Comparison of pre-shot ground surface and subsurface geology, OAK and KOA areas.	7- 8
7- 6	Geologic crater model	7-11
7- 7	Fence diagram of KOA crater showing relationship of crater zones and geologic horizons.	7-17
7- 8	Fence diagram of OAK boreholes OOR-17 to OPZ-18, relationship of crater and geologic horizons.	7-18
7- 9	Fence diagram of OAK boreholes OBZ-4 to OAR-2/2A, relationship of crater and geologic horizons.	7-19
7-10	Fence diagram, OAK boreholes, reef tract to OLT-14 relationship of crater and geologic horizons.	7-20
7-11	Geologic interpretation of multichannel seismic lines 101 and 103, OAK crater area.	7-21
7-12	Geologic interpretation of multichannel seismic lines 303 and 306, KOA crater area.	7-22
7-13	Isopach map showing distribution of muddy sediments, Enewetok lagoon.	7-23
7-14	Distribution of sand volcanoes on enhanced sea-floor image of OAK crater.	7-25
7-15	Comparison of number of specimens from MP-4 and -5 to percent ostracodes from crater zones in OBZ-4 and OPZ-18.	7-26
7-16	Paleontologic mixing in mixed zone of OAK crater	7-27
7-17	Paleontologic mixing in mixed zone of KOA crater	7-28
7-18	Paleontologic model of crater-fill and paleontologic mixed zones.	7-32
7-19	Borehole lithology, geologic and paleontologic crater zones, and gamma-ray logs, OAK crater.	7-33
7-20	Borehole lithology, geologic and paleontologic crater zones, and gamma-ray logs, KOA crater.	7-35
7-21	Distribution of shocked calcite and Cesium-137 and relationship to crater zones, OAK crater.	7-36
7-22	Maximum depression/uplift of Pleistocene and Pliocene surfaces, OAK crater.	7-38
7-23	Maximum depression of Pleistocene and Pliocene surfaces, KOA crater.	7-39

(continued on next page)

FIGURE INDEX (continued)

Figure No.	Description	Page No.
------------	-------------	----------

CHAPTER 7: (Continued from preceeding page).

7-24	Present-day (post-shot) location of Pleistocene and Pliocene surfaces, KOA and OAK craters.	7-40
7-25	Idealized model of geologic crater for symmetric crater and asymmetric crater on significant slope.	7-44
7-26	Horizon locations, fence diagram, OOR-17 to OPZ-18	7-47
7-27	Horizon locations, fence diagram, OBZ-4 to OAR-2/2A	7-48
7-28	Horizon locations, fence diagram, OUT-24 to OLT-14	7-49
7-29	Horizon locations, fence diagram, XBK-1 to KET-7	7-50
7-30	Graphic thinning analysis, OAK crater	7-53
7-31	Graphic thinning analysis, KOA crater	7-54
7-32	Stratigraphic density profile, borehole gravimetry	7-56
7-33	Idealized succession of major depositional events to form geologic crater.	7-57

PLATE INDEX

(All plates in map pocket)

Plate No.	Description
-----------	-------------

CHAPTER 5: BATHYMETRIC STUDIES OF OAK CRATER

- | | |
|------|--|
| 5- 1 | Digitized Holmes and Narver (1958a) Preshot Topographic and Hydrographic Map. |
| 5- 2 | Digitized Holmes and Narver (1958b) Postshot Topographic and Hydrographic Map. |
| 5- 3 | Digitized U.S. Geological Survey (1984) Postshot Bathymetric Map. |
| 5- 4 | Negative Δ -Relief Map, H&N Preshot and H&N Postshot Map Pair. |
| 5- 5 | Positive Δ -Relief Map, H&N Preshot and H&N Postshot Map Pair. |
| 5- 6 | Negative Δ -Relief Map, H&N Preshot and USGS Postshot Map Pair. |
| 5- 7 | Positive Δ -Relief Map, H&N Preshot and USGS Postshot Map Pair. |
| 5- 8 | Negative Δ -Relief Map, H&N Postshot and USGS Postshot Map Pair. |
| 5- 9 | Positive Δ -Relief Map, H&N Postshot and USGS Postshot Map Pair. |

TABLE INDEX

Table No.	Description	Page No.
 CHAPTER 1: INTRODUCTION TO PART 4 OPEN-FILE REPORT		
1- 1	Matrix of data bases and analyses	1- 4
 CHAPTER 2: BOREHOLE GRAVIMETRY, OAK CRATER		
2- 1	Corrections for lateral density changes	2-39
2- 2	Density and porosity values, OOR-17	2-41
2- 3	Density and porosity values, OPZ-18	2-43
2- 4	Density and porosity values, OQT-19	2-45
2- 5	Density and porosity values, ORT-20	2-47
2- 6	Density and porosity values, OSR-21	2-49
2- 7	Density and porosity values, OTG-23	2-51
2- 8	Density of atoll material surrounding OAK	2-52
 CHAPTER 3: PALEONTOLOGIC EVIDENCE FOR SEDIMENTARY MIXING		
3- 1	Borehole depth of examined samples	3- 3
3- 2	Foraminifer occurrences, OBZ-4	3-16
3- 3	Foraminifer occurrences, OCT-5	3-17
3- 4	Foraminifer occurrences, OFT-8	3-18
3- 5	Foraminifer occurrences, OKT-13	3-19
3- 6	Foraminifer occurrences, OPZ-18	3-20
 CHAPTER 4: ELECTRON PARAMAGNETIC RESONANCE STUDIES		
4- 1	Pressure and integrated difference data for high- resolution spectra, laboratory samples.	4-10
4- 2	Results for OAR-2A samples	4-22
4- 3	Results for OBZ-4 samples	4-23
4- 4	Results for OCT-5 samples	4-24
4- 5	Results for OET-7 samples	4-25
4- 6	Results for OFT-8 samples	4-26
4- 7	Results for OPZ-18 samples	4-27
4- 8	Results for OAK debris samples	4-28
 CHAPTER 5: BATHYMETRIC STUDIES OF OAK CRATER		
5- 1	Summary of digitized bathymetric map products	5- 9
5- 2	Water depths and vertical differences	5-11
5- 3	Summary of areas and volumes from derivative map from H&N preshot vs H&N postshot maps.	5-21
5- 4	Summary of areas and volumes from derivative map from H&N preshot and USGS postshot maps.	5-22
5- 5	Summary of areas and volumes from derivative map from H&N postshot and USGS postshot maps.	5-23
5- 6	Grand summary of areas and volumes of negative, zero, and positive Δ -relief, OAK crater.	5-24

(continued on next page)

TABLE INDEX (continued)

Table No.	Description	Page No.
CHAPTER 6: CONSTRAINTS ON DENSIFICATION AND PIPING, OAK CRATER		
6- 1	Column-height changes down OAK boreholes	6- 5
6- 2	Uniformity of horizons in OAK area	6- 6
6- 3	Column-height changes due to densification	6-17
6- 4	Probability estimates	6-22
6- 5	Column-height changes due to densification 48 to 67 days after burst and probability estimates.	6-25
6- 6	Piping hypothesis analysis	6-30
6- 7	Endpoints of segments of piecewise linear fits to density profiles from BHG.	6-56
6- 8	Endpoints of segments of piecewise linear fits to density profiles from γ - γ logging.	6-57-73
6- 9	Mass of solid in vertical columns of unit cross- section, from BHG survey data.	6-79-81
6-10	Mass of solid in vertical columns of unit cross- section, from γ - γ survey data.	6-82-101
 CHAPTER 7: INTEGRATION OF MATERIAL-PROPERTY UNITS, GRAVIMETRY, AND ADDITIONAL STUDIES OF OAK AND KOA CRATERS		
7- 1	Relationship of geologic and paleontologic zones in crater and debris blanket.	7-12
7- 2	Depth to tops of crater zones, OAK and KOA	7-13
7- 3	Paleontologic crater zones, transition sand, KOA and OAK craters.	7-14
7-4	Correlation of geologic crater zones and multi- channel seismic zones.	7-15
7- 5	Depths to material-property unit boundaries, pre- and post-shot, OAK crater.	7-45-46
7- 6	Thinning analysis of material-property units, OAK	7-51
7- 7	Depths to material-property units, pre- and post- shot, KOA crater.	7-52
7- 8	Thinning analysis of material-property units, KOA	7-52
7- 9	Stratigraphic bulk-density analysis, OAK crater	7-55

**PACIFIC ENEWETAK ATOLL CRATER EXPLORATION (PEACE) PROGRAM
ENEWETAK ATOLL, REPUBLIC OF THE MARSHALL ISLANDS**

**Part 4: Analysis of borehole gravity survey and other
geologic and bathymetric studies in vicinity of
OAK and KOA craters**

CHAPTER 1:

INTRODUCTION TO PART 4 OPEN-FILE REPORT

By

Thomas W. Henry^{1/2} and Bruce R. Wardlaw^{1/3}

GENERAL REMARKS

The Pacific Enewetak Atoll Crater Exploration (PEACE) Program was established and funded by the Defense Nuclear Agency (DNA) to resolve a number of questions for the Department of Defense (DOD) about the geologic and material-properties parameters of two craters (KOA and OAK), formed by near-surface bursts of high-yield thermonuclear devices on the northern margin of Enewetak Atoll, (fig. 1-1), Marshall Islands, in 1958. The multidisciplinary studies conducted by the USGS in collaboration with the DNA, the Department of Energy (DOE), and other organizations during 1984 through 1987 were part of a much larger research initiative by the DNA to better understand the dynamic properties of strategic-scale nuclear bursts and the relevance of the Pacific Proving Grounds (PPG) craters to issues of strategic basing and targeting of nuclear weapons.

The reader is referred to the reports cited in the succeeding section for a detailed explanation of the events leading up to the PEACE Program and the collaborative roles of the USGS, other Federal agencies, and scientists and engineers from universities and private research laboratories.

¹ Branch of Paleontology and Stratigraphy, U.S. Geological Survey.

² Denver, CO 80225-0046.

³ Reston, VA 22092.

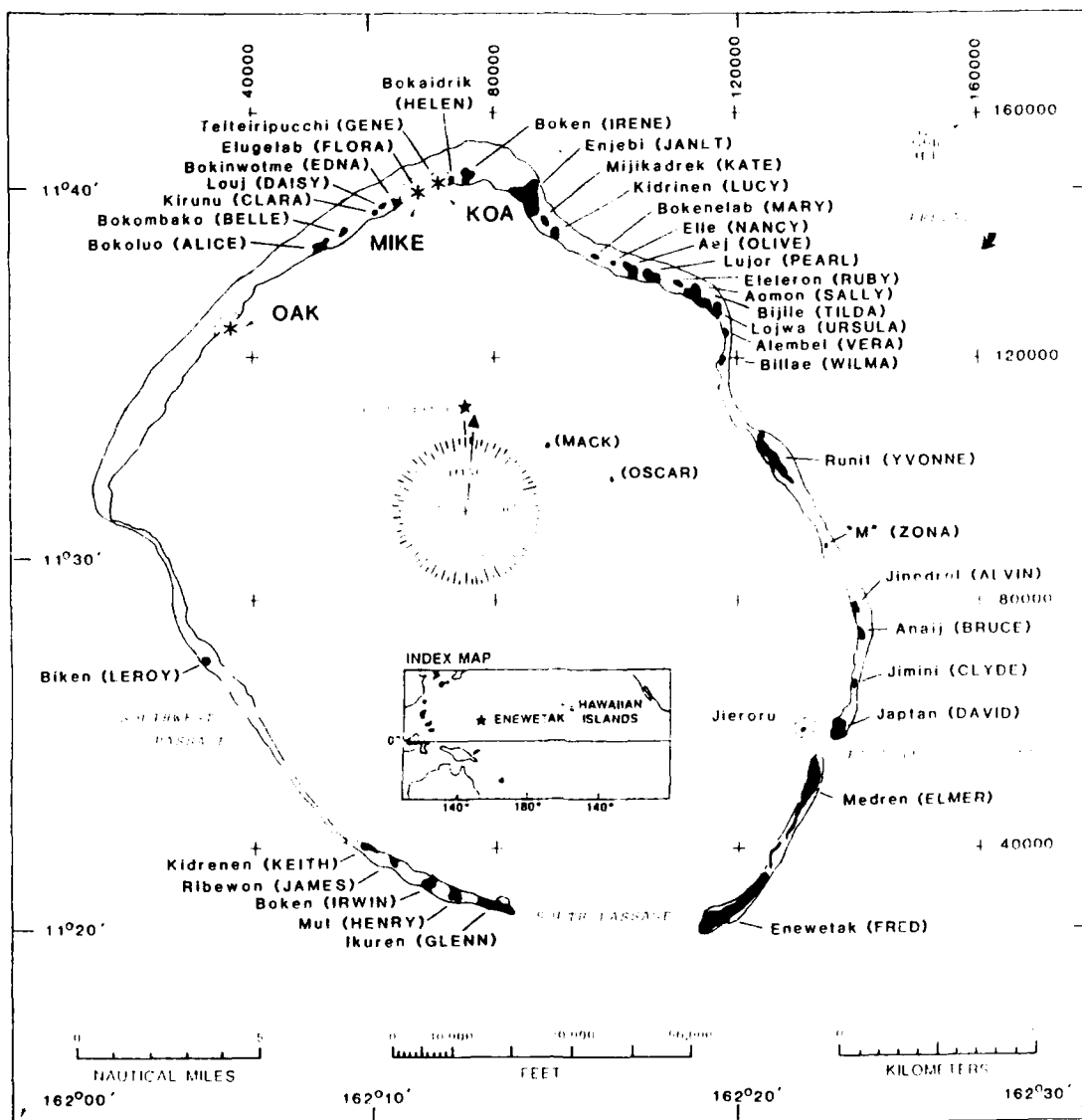


FIGURE 1-1. -- Map of Enewetak Atoll, Republic of the Marshall Islands (RMI), showing native names of principal islands and other features (military site name in parenthesis), and location of OAK, KOA, and MIKE craters. Inset map shows location of Enewetak within Pacific Ocean. Map from Henry, Wardlaw, and others (1986, p. 12, fig. 3).

PEACE PROGRAM REPORTS

This volume is the fifth and final volume of a series of four U.S. Geological Survey (USGS) Open-File Reports (Henry, Wardlaw, and others, 1986; Cronin, Brouwers, and others, 1986; and Henry and Wardlaw, 1986a) and one USGS Bulletin (Folger, 1986a) documenting geologic and geophysical data, analyses, and interpretations for the PEACE Program. Syntheses for the geologic and material-properties models for the craters are found in Wardlaw and Henry (1986, Ch. 14) and Wardlaw (1987, Ch. 7, this Report). The material-properties studies themselves, which provide quantitative parameters for computational modeling, for the most part were not conducted by USGS personnel and are published elsewhere for the DNA (e.g., Blouin and Timian, 1986a, 1986b; Borschel, Klauber, and Earley, 1986; McClelland Engineers, 1986; Mueller, 1987; Patti and Schatz, 1987 [1988], in preparation, Schatz, Patti, and Melzer, 1987 [1988], in preparation, and Simons and others, 1984).

DATA ACQUISITION AND BASES

The PEACE Program was truly a multidisciplinary endeavor. Field work for the program on Enewetak Atoll was done in two parts, the Marine Phase (mid- to late summer, 1984) and the Drilling Phase (late winter through mid-summer, 1985). The primary and derivative PEACE Program data bases and framework groups consist of the elements shown in Table 1-1. For general discussion of the fieldwork and data-acquisition procedures for the Marine Phase, the reader is referred to Folger (1986b), and, for the Drilling Phase, to Henry, Wardlaw, and others (1986, p. 29-97). For more detailed information about the field and laboratory procedures employed for a specific data set, refer to the individual Chapters or volumes (see tbl. 1-1). Many of the derivative data sets and framework groups from the Drilling Phase utilized samples from the 32 deep and intermediate boreholes drilled from the M/V Knut Constructor in the Enewetak lagoon. These boreholes (figs. 1-2 and 1-3) provide a data base upon which the subsurface geologic framework is grounded and upon which interpretations made from the geophysical and material-properties studies must be validated.

A wide array of pre-PEACE Program data from the PPG was re-examined, including (but not limited to) the following:

- (1). Published accounts in USGS Professional Paper 260 series (see Emery, Tracey, and Ladd, 1954) from the initial geologic, geophysical, and oceanographic investigations in the Marshall Islands associated with the early phases of nuclear testing.
- (2). Published reports and raw data from the geologic and geophysical studies of the PACE, EXPOE, and EASI Projects, sponsored by the DNA and conducted on Enewetak by the Air Force Weapons Laboratory (AFWL) (Couch, Fetzer, and others, 1975; Henny, Mercer, and Zbur, 1974; Ristvet, Tremba and others, 1978; Tremba, Jones, and Henny, 1981; Tremba, Couch, and Ristvet, 1982; and Tremba, 1987). For example, some of the multichannel-seismic lines from EASI were reprocessed by Grow, Lee, and others (1986), and selected PACE/EXPOE boreholes were redescribed and analyzed stratigraphically and isotopically before the Drilling Phase actually got underway (Henry, Wardlaw, and others, 1986;

TABLE 1-1. -- Matrix of data bases and analyses from PEACE Program. In heading, CH = Chapter; under heading PHASE, Marine or Drilling connotes which phase the samples were obtained originally. The pilot gravity survey in the old borehole on Medren (ELMER) Island was conducted in April 1984, hence the asterisk (*) in the appropriate column. The geologic and material-properties models for the craters are presented in Wardlaw and Henry (1986, Ch. 14) and in Wardlaw (1987, Ch. 8, this Report). U.S. Geological Survey Open-File Report 87-665 is the current volume.

DATA GROUP	PHASE	PUBLICATION	CH.	REFERENCE CITATION
Bathymetric Maps	Marine	Bull. 1678 OF-87- 665	A 5	Folger, Hampton, and others (1986); Peterson and Henry (1987*).
Side-Scan Sonar Imagery	Marine	Bull. 1678	B	Folger, Robb, and others (1986).
Single-Channel Seismic Reflection	Marine	Bull. 1678	C	Robb, Foster, and others (1986).
Multichannel Seismic Reflection	Marine	Bull. 1678	D	Grow, Lee, and others (1986).
Seismic Refraction	Marine	Bull. 1678	E	Ackermann, Grow, and Williams (1986).
Submersible Observations	Marine Both	Bull. 1678 OF-86- 555	F 11	Halley, Slater, and others (1986); Slater, Roddy, and others (1986).
Debris/Ejecta	Marine Marine Drilling	Bull. 1678 OF-86- 555 OF-87- 665*	G 3 4	Halley, Major, and others (1986); Ludwig, Halley, and others (1986); Polanskey and Ahrens (1987*).
Scuba Observations	Marine	Bull. 1678	H	Shinn, Kindinger, and others (1986).
Bottom Samples	Marine Mainly	OF-86- 555	10	Wardlaw, Henry, and Martin (1986).
Boreholes	Drilling	OF-86- 555	-	Henry, Wardlaw, and others (1986).
Lithostratigraphic Framework	Drilling	OF-86- 555	2	Wardlaw and Henry (1986a).
Biostratigraphic Framework & Mixing Studies	Drilling	OF-86- 555 OF-86- 555 OF-87- 665*	- 11 3	Cronin, Brouwers, and others (1986); Brouwers, Cronin, and Gibson (1986); Cronin and Gibson (1987*).
Geophysical Logs	Drilling	OF-86- 555 OF-87- 665*	7 6	Melzer (1986). Trullio (1987*).
Seismic Reference Survey	Drilling	OF-86- 555	9	Tremba and Ristvet (1986b).
Borehole Gravimetry	Drilling	OF-86- 555 OF-87- 665* OF-87- 665*	8 2 6	Beyer, Ristvet, and Oberste-Lehn (1986); Beyer (1987*); Trullio (1987*).
St-Isotope Framework	Marine Drilling	Bull. 1678 OF-86- 555	G 3	Halley, Ludwig, and others (1986); Ludwig, Halley, and Simmons (1986).
X-Ray Mineralogy	Drilling	OF-86- 555	4	Tremba and Ristvet (1986).
Organic Geochemistry	Drilling	OF-86- 555	5	Ristvet and Tremba (1986).
Insoluble Residues	Drilling	OF-86- 555	6	Ristvet and Tremba (1986).
Radiation Chemistry	Drilling	OF-86- 555	12	Ristvet and Tremba (1986).
Electron-Spin Resonance	Drilling Mainly	OF-87- 665*	4	Polanskey and Ahrens (1987*).
Crater-Area Bottom Samples	Drilling	OF-86- 555 OF-86-555 ----	4 10 -	Tremba and Ristvet (1986). Wardlaw, Henry, and Martin (1986). Patti and Schatz (1987) [1988?].
Crater Synthesis	Marine Both Both	Bull. 1678 OF-86- 555 OF-87- 665*	A 14 7	Folger (1986b); Wardlaw and Henry (1986b); Wardlaw (1987*).

* OF-87-665 is the current report.

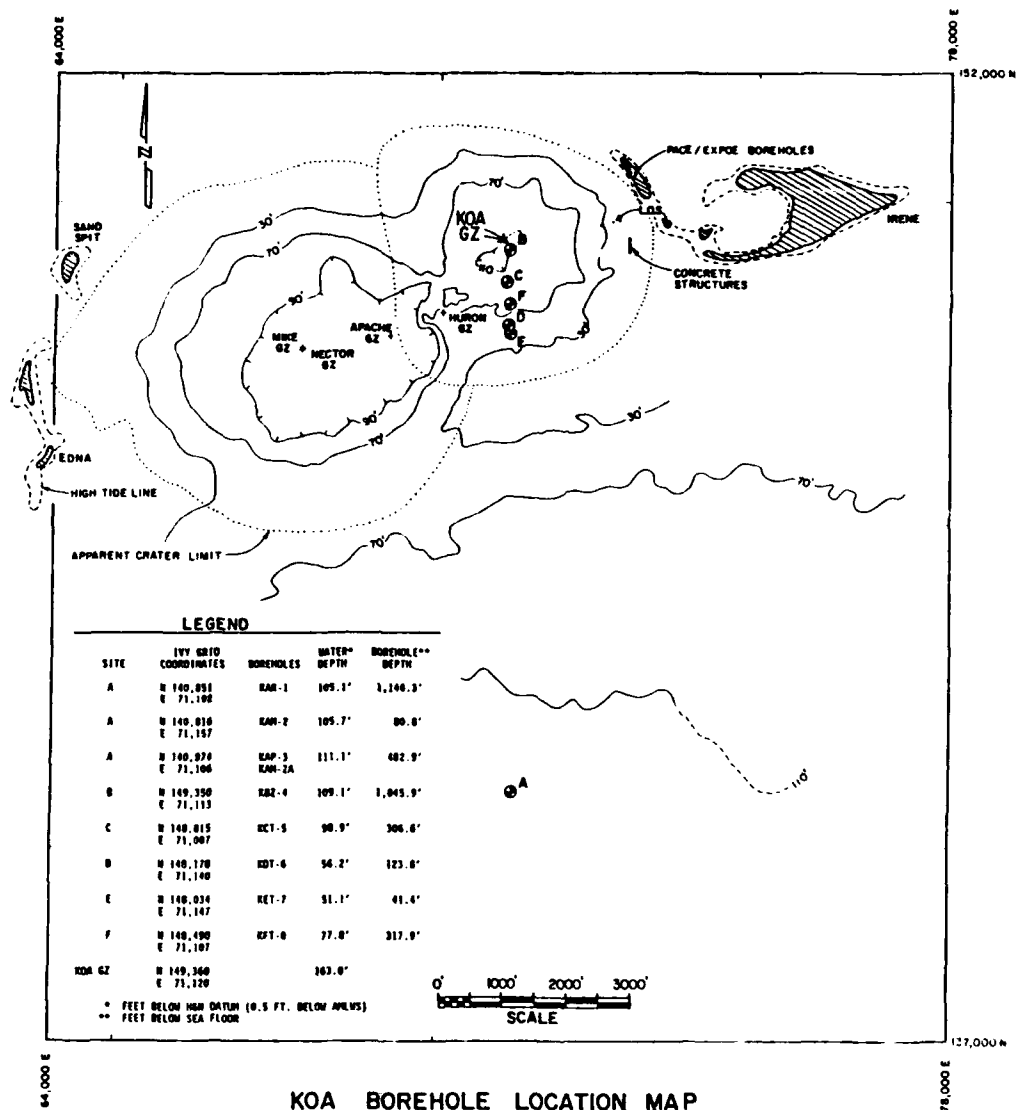


FIGURE 1-2. -- Map of KOA crater area showing borehole sites (depicted by letters) and general bathymetric contours (contour interval in feet). Map modified from Henry and Wardlaw (1986b, fig. 1-2).

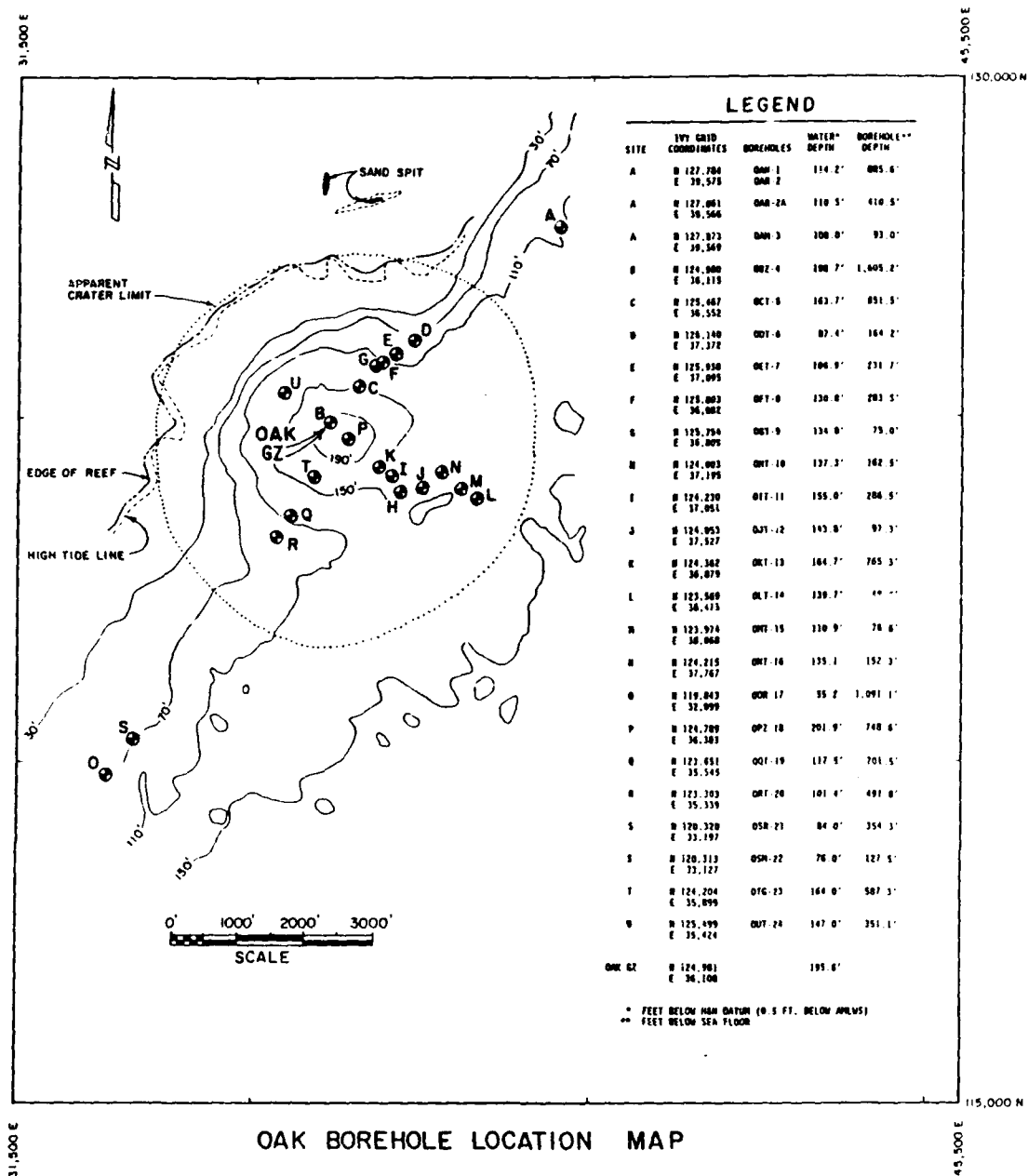


FIGURE 1-3. -- Map of OAK crater area showing borehole sites (depicted by letters) and general bathymetric contours (contour interval 10 feet). Map modified from Henry and Wardlaw (1986b, fig. 1-3).

Cronin, Brouwers, and others, 1986; Halley, Major, Ludwig, and others, 1986).

- (3). A broad spectrum of unpublished archival material from the PPG made freely available to us by the DNA and the DOE. These data include pre- and post-shot survey maps of the OAK and KOA crater areas, both black-and-white and color, stereographic aerial photographs, other kinds of aerial photographs, and pictures made (both pre- and post-testing) from ground-level of various crater features and man-made structures. The pre- and post-shot Holmes and Narver maps of OAK crater were digitized and form an essential part of the volumetric studies for the PEACE Program (Peterson and Henny, 1987, Chapter 5 of the current Report).
- (4). Other published reports, too numerous to cite here.

SYNOPSIS OF CHAPTERS OF CURRENT VOLUME

This Open-File Report consists of seven Chapters. The interrelationship of each Chapter to the overall data base is depicted in Table 1-1. Salient points of each Chapter are summarized below.

Borehole Gravity (Ch. 2; Beyer)

The borehole gravity measurements from the southwest transect of OAK crater and in the Medren (ELMER) Island borehole provide a critical set of data for bulk density and porosity of both the undisturbed stratigraphic sequence and the sediments and rock that were affected by the OAK event.

Significant densification, porosity diminution, and mass removal are indicated for discrete intervals within the boreholes in the central-crater region of OAK. Zones in which these phenomena are indicated correspond closely to the geologic crater zones and provide strong corroborative evidence for their integrity.

One of the primary goals of the gravimetry was to determine whether densification of the shallow substrate in the crater-flank region (or "wings") could account for the measured lowering of the sea floor. This is particularly critical because the bulk of the volume of the apparent crater lies within its flank region. Gravity analysis conducted in the upper parts of transition-zone boreholes (OQT-19 and ORT-20, see fig. 1-3) demonstrates conclusively that the materials (sediment, rock, and rock debris) are only slightly denser than comparable intervals of materials in reference boreholes OOR-17 and OSR-21. In fact, only perhaps about 15 percent of the documented lowering of the sea floor in the crater wings region can be explained by densification alone. Thus, for the wings region, processes other than densification clearly are also involved.

Paleontologic Evidence for Mixing (Ch. 3; Cronin, Gibson)

Paleontologic analysis of the upper 1,200 ft of strata on Enewetak established the division of the upper part of the carbonate cap into twelve discrete biostratigraphic zones (named zones AA, the youngest, through LL, the oldest -- see also Cronin, Brouwers, and others, 1986, and Brouwers, Cronin, and Gibson, 1986). For the current study, additional samples from stratigraphically undisturbed boreholes from the OAK crater area (i.e., from the reference boreholes) were examined to refine the local zonation and to more closely resolve key biostratigraphic boundaries. Several of these boundaries, combined with physical stratigraphic datums, form surfaces or marker horizons that are Lagrangian (see Chapter 6), permitting employment of a powerful tool in the analysis of crater evolution.

The microfossil studies of OAK reference-borehole plus crater samples provides significant new information about the timing and methods of emplacement¹ of materials from various biostratigraphic zones within the materials that partially infill the crater itself. This includes for the first time identification of sediments that were either at or within a few centimeters of the pre-event lagoon floor. These new data have furnished quantitative estimates of material from each zone (or group of zones) admixed in the crater fill. These estimates include volumes and percentages of materials originating from the deeper stratigraphic zones not involved in the excavation of the initial crater itself and from shallower geologic units as well. The editors emphasize that materials from stratigraphically shallower zones pose a real problem of differentiation. For example, how does one separate material that may have been emplaced from, say, zone CC from material within CC that has not moved? *Therefore, estimated volumes or percentages of material that may have been piped or otherwise moved from these shallow zones may be underestimated, perhaps grossly.*

Electron Paramagnetic Resonance Studies (Ch. 4; Polanskey, Ahrens)

EPR spectrometry was applied to measure the peak-shock stress to which calcitic materials were subjected during the OAK event. Most of the samples analyzed can be characterized as either unshocked or very heavily shocked, with few samples showing intermediate states. Samples of the "transition sand" from OPZ-18 show the greatest concentration of very highly shocked material, interpreted as originating in the proximity of ground zero and plastered onto the walls of the excavational crater. Because of subsequent collapse of the excavational crater walls and dilution by mixing with less-shocked or unshocked materials, this lining, as a discrete stratigraphic unit, is identifiable only in the OPZ-18 borehole. Surprisingly, none of the 26 samples from the ground-zero borehole OBZ-4 showed significant shock damage. However, a zone containing less concentrated, very highly shocked material can be recognized in the three transition-zone boreholes studied (OCT-5, OET-7, and OFT-8), and its base occurs at progressively shallower depths away from ground zero.

¹ The term emplacement is used as a generic term to describe the deposition of material transported from one point to another without reference to the mechanism involved.

Bathymetric Studies of OAK Crater (Ch. 5; Peterson, Henny)

Three pertinent base maps were digitized and processed with a computer to facilitate analysis of the changes in the sea-floor bottom topography (bathymetry) and corresponding volumes in the area affected by the detonation of the OAK device (June 29, 1958) and by subsequent, longer term geologic processes. These maps are: (1) the pre-shot Holmes and Narver (H&N) survey, completed three days prior to the burst; (2) the post-shot H&N map, surveyed 47 to 67 days after the burst; and (3) the USGS map, made during the Marine Phase of the PEACE Program, 26 years after the burst.

The USGS map, in the format presented by Folger, Hampson, and others (1986), was not amenable for comparison with the two H&N maps (even undigitized) primarily because the USGS depth contours are given in meters rather than feet. The irregular area common to all three base maps is shown in Figure 5-1.

OAK is a strongly asymmetric crater; part of the asymmetry is a geologic function of the reef being on one side of surface ground zero and the atoll lagoon on the other. Many independent lines of evidence demonstrate that the excavational crater was appreciably smaller and more nearly circular than the current (or apparent) crater. Using the standardized digitized data for the common area of the base maps, three pairs² of vertical-difference contour maps were prepared. These maps show that: (1) the pre-shot topographic (geologic) features significantly influenced not only the evolution and final size/shape of the crater but also the initial distribution and subsequent reworking of debris from the OAK event; (2) the area of greatest downward displacement of the sea floor between the two post-shot base maps is that of the inner crater; and (3) the entire map area was lowered (and not uniformly) an average of 23 ft by 67 days after the burst and by another 12 ft during the next 26 years. As the surface of the lagoon and crater floor in this area was lowered, areas of positive-difference in relief (i.e., those areas that were higher post-shot than pre-shot) also decreased from about 27 percent by 67 days to about 14 percent 26 years later.

Two notes of caution must be clearly understood in using these maps for quantitative estimates for cratering calculations. The first is that there is no Lagrangian marker for the pre-event lagoon floor. The second is that the debris volumes estimated from these maps are understated simply because the apparent crater of OAK extends beyond the areas mapped, including the USGS map, which encompasses the largest area.

¹ Following the glossary presented in Henry and Wardlaw (1986a), the apparent crater is defined as the locus of the zero-difference contour line surrounding a crater -- viz, the locus of points where the effects of an explosion can no longer be detected when the pre-event contours are compared with the post-event contours (fide, B.L. Ristvet.)

² A negative- and a positive-relief-difference (called Δ -relief) isopachous map was constructed for each combination of two base maps.

Constraints on Densification and Piping for OAK (Ch. 6; Trulio)

As mentioned previously, it is established from a wide array of data that the excavational crater of OAK had an appreciably smaller radius than that of the apparent crater. Because crater volume is a radius-squared function, it is evident that most of the volume of OAK is contained within its flank or "wing" area. What is (are) the significant mechanism(s) responsible for forming the wings of the large apparent craters in the PPG? Trulio presents a number of different models dealing with the PEACE Program data bases and makes a number of inferences about these mechanisms based on these models.

Using the data base from the gravimetry (Chapter 2), Trulio applies mathematical analyses to the data, from a purely physical viewpoint, and verifies Beyer's conclusion that densification (or, in Trulio's terminology, "simple subsidence") accounts for just a small part of the formation of the wings of OAK crater. As a best estimate, only about 8 percent of the sea-floor drop on the wings can be attributed to density increases caused by the burst.

Another explanation for part of the observed sea-floor lowering phenomenon is piping, or movement (driven by gravity and density differences) of a sediment/water slurry through conduits (cracks, fissures, etc.) to generally shallower depths or to the surface through vents to form "sand volcanoes". That piping occurred associated with the OAK and KOA bursts, particularly in the central crater region, is supported by independent lines of evidence (see Chapter 7 for discussion). However, at issue are: (1) the role of piping relative to other mechanisms to account for the drop in the sea floor; and (2) the amount of material transported by this mechanism. Mean values for the density of material piped up to the sea floor from beneath OAK can be derived from the combination of sea-floor base maps and gravimetry profiles. If correct, this model poses limitations on the amount of material transported out of the crater by piping. The best estimate based on this model is that the piped and residual materials differed by only about 0.2 g/cc, a density difference that can drive piping, in Trulio's words, "but weakly". Trulio cautions that the sequence of events leading to the transport of piped material out of the crater is subject to interference at many points.¹

It is suggested that plastic flow also should be considered as a plausible mechanism to account for most of the phenomenon of sea-floor lowering. Trulio points out, however, that little is known about the displacement field around a flow crater.

¹ See caveat in italics on page 1-8. The editors also emphasize that the observed "subsidence" or sea-floor lowering on the wings of the Enewetak craters studied is not reasonably attributable to one mechanism operating alone. The lowering was caused in part by densification, in part by piping (certainly upwardly and probably laterally as well), probably in part to plastic flow, and possibly to other mechanisms that may not have even been thought of yet.

Additional Studies of Geologic Crater Models (Ch. 7, Wardlaw)

The final Chapter provides an integration of the new information from the various studies presented in the current Open-File Report with the previously developed analyses of PEACE Program data. Of particular interest to the material-properties community is the formulation of a set of material-properties units for the normal stratigraphic (geologic) sequence and a discussion of the relationship of these units to the sedimentary packages presented in Wardlaw and Henry (1986a, 1986b).

Using available evidence, the pre-event geology beneath the OAK and KOA crater areas is reconstructed, including paleotopographic contour maps of several of the more significant subsurface datums. Wardlaw points out that topographic differences of the pre-event Holocene ground surfaces (i.e., the pre-1958 lagoon, reef, and island surface) between the KOA and OAK area produced differences in the surface configurations of the two craters. Differences in cementation and structural competency of key stratigraphic intervals beneath the surface ground zeros of KOA and OAK and the effects of these differences on the development of the two craters are summarized.

A study of the thinning of the stratigraphic units influenced by OAK and KOA is presented. A more comprehensive interpretation of the models for these two craters given in Wardlaw and Henry (1986b) is developed based primarily on the inferred pre-shot elevation of certain datums and thicknesses of stratigraphic intervals in contrast to their post-shot attributes. The case is made that movement of material laterally ("lateral flow") may account for much of the "subsidence" and formation of the wings.

An idealized succession of cratering and depositional events is presented.

ACKNOWLEDGEMENTS

We, the editors, extend a special note of appreciation to the following people, without whom this program would have not been possible. Lt. Col. Robert F. Couch, Jr. (U.S. Air Force and DNA Program Manager for the PEACE Program) and Byron L. Ristvet and Edward L. Tremba (both of S-Cubed Division of Maxwell Laboratories), and Robert W. Henny (Air Force Weapons Laboratory) were full scientific collaborators with us during the PEACE Program. All four of these geologists logged extensive on-site experience in the PPG prior to the current program and were principal investigators in all of various phases of the earlier AFWL investigations on Enewetak. And, in a real sense, they represent a vital component of the record of cratering studies on Enewetak. Their expertise and geotechnical knowledge were invaluable to the current program, and we owe them a profound debt of gratitude. Couch, Ristvet, and Tremba served (alternatively) as Chief Scientists aboard the Knut Constructor during the Drilling Phase of the program, and all three were on-site during parts of the earlier Marine Phase.

We would like to thank also the authors of the Chapters of the current Open-File Report for their timely response to our needs in editing, compiling,

and finalizing this volume and for their input for synthesizing the diverse data bases.

We are indebted also to John F. Schatz and L. Stephen Melzer of SAIC for constructive exchange of scientific and technical information for this volume. Melzer was on-site with us as Chief Scientist during part of the Drilling Phase field work, and it was his observations along with that of the geologists and paleontologists studying the OAK ground-zero borehole aboard the drill ship that demonstrated the reality of piping of materials from zones from far below the excavational crater into the sediment forming part of the crater fill.

The plates for Chapter 2 were laid out by James MacCornack, S-Cubed, Albuquerque, and printed by the Defense Nuclear Agency Printing Plant, Kirtland AFB, New Mexico. We thank Leonard MacDonald, head printer, for his assistance.

REFERENCES CITED

- Ackermann, H.D., Grow, J.A., and Williams, J.M., 1986, Chapter E: Seismic-refraction survey of OAK crater; 18 p., 19 figs., 1 tbl.; in Folger, D.W., editor, Sea-floor observations and subbottom seismic characteristics of OAK and KOA craters, Enewetak Atoll, Marshall Islands: U.S. Geological Survey Bulletin 1678.
- Beyer, L.A., Ristvet, B.L., and Oberste-Lehn, D., 1986, Chapter 8: preliminary density and porosity data and field techniques of borehole gravity surveys, OAK crater; 28 p., 4 figs., 10 tbls., 2 appendices; in Henry, T.W., and Wardlaw, B.R., editors, Pacific Enewetak Atoll Crater Exploration (PEACE) Program, Enewetak Atoll, Republic of the Marshall Islands; Part 3: Stratigraphic analysis and other geologic and geophysical studies in vicinity of KOA and OAK craters: U.S. Geological Survey Open-File Report 86-555.
- Blouin, S.E., and Timian, D.A., 1986a, Core description and ultrasonic logs from Enewetak Atoll: Defense Nuclear Agency, Washington, DC., Technical Report TR-86-198, 98 p., [released 3 February 1986, unclassified document].
- Blouin, S.E., and Timian, D.A., 1986b, Material properties testing in support of PEACE Program, Enewetak Atoll: Defense Nuclear Agency, Washington, DC., Technical Report TR-86-197, 458 p., [released 4 June 1986, unclassified document].
- Borshel, T.F., Klauber, W.P., and Earley, K.H., 1986, Lithological, physical, and mechanical characterization of geologic samples from Enewetak Atoll: TerraTek Research, Inc., Report TR-87-25, prepared for the Defense Nuclear Agency.

- Brouwers, E.M., Cronin, T.M., and Gibson, T.G., 1986, Chapter 11: Additional paleontologic studies, OAK and KOA craters; 18 p., 5 figs., 5 tbls., 1 pl.; in Henry, T.W., and Wardlaw, B.R., editors, Pacific Enewetak Atoll Crater Exploration (PEACE) Program, Enewetak Atoll, Republic of the Marshall Islands; Part 3: Stratigraphic analysis and other geologic and geophysical studies in vicinity of KOA and OAK craters: U.S. Geological Survey Open-File Report 86-555.
- Couch, R.F., Jr., Fetzer, J.A., Goter, E.R., Ristvet, B.L., Tremba, E.L., Walter, D.R., and Wendland, V.P., 1975, Drilling operations of Enewetak Atoll during Project EXPOE: Air Force Weapons Laboratory Technical Report AFWL-TR-75-216, Kirtland Air Force Base, New Mexico, 270 p., 17 figs., 4 tbls. [unclassified document].
- Cronin, T.M., Brouwers, E.M., Bybell, L.M., Edwards, E.E., Gibson, T.G., Margerum, R., and Poore, R.Z., 1986, Pacific Enewetak Atoll Crater Exploration (PEACE) Program, Enewetak Atoll, Republic of the Marshall Islands; Part 2: Paleontology and biostratigraphy, application to OAK and KOA Craters: U.S. Geological Survey Open-File Report 86-159, 39 p., 20 figs., 12 tbls., 3 appendices.
- Emery, K.O., Tracey, J.I., Jr., and Ladd, H.S., 1954, Geology of Bikini and nearby atolls: U.S. Geological Survey Professional Paper 260-A, 265 p., 73 pls., 84 figs., 11 charts, 27 tbls.
- Folger, D.W., editor, 1986a, Sea-floor observations and subbottom seismic characteristics of OAK and KOA craters, Enewetak Atoll, Marshall Islands: U.S. Geological Survey Bulletin 1678, 301 p., 112 figs., glossary, 2 appendices. [Chapters A - H, plus Introduction.]
- Folger, D.W., 1986b, Introduction to the volume; 7 p., 2 figs., 2 tbls.; in Folger, D.W., editor, Sea-floor observations and subbottom seismic characteristics of OAK and KOA craters, Enewetak Atoll, Marshall Islands: U.S. Geological Survey Bulletin 1678.
- Folger, D.W., Hampson, J.C., Robb, J.M., Woellner, R.A., Foster, D.S., and Tavares, L.A., 1986, Chapter A: Bathymetry of OAK and KOA craters; 35 p., 12 figs., 2 appendices; in Folger, D.W., editor, Sea-floor observations and subbottom seismic characteristics of OAK and KOA craters, Enewetak Atoll, Marshall Islands: U.S. Geological Survey Bulletin 1678.
- Folger, D.W., Robb, J.M., Hampson, J.C., Davis, P.A., Bridges, P.M., and Roddy, D.J., 1986, Chapter B: Sidescan-sonar survey of OAK and KOA craters; 18 p., 6 figs.; in Folger, D.W., editor, Sea-floor observations and subbottom seismic characteristics of OAK and KOA craters, Enewetak Atoll, Marshall Islands: U.S. Geological Survey Bulletin 1678.
- Grow, J.A., Lee, M.W., Miller, J.J., Agena, W.F., Hampson, J.C., Foster, D.S., and Woellner, R.A., 1986, Chapter D: Multichannel seismic-reflection survey of KOA and OAK craters; 46 p., 39 figs.; in Folger, D.W., editor, Sea-floor observations and subbottom seismic characteristics of OAK and KOA craters, Enewetak Atoll, Marshall Islands: U.S. Geological Survey Bulletin 1678.

- Halley, R.B., Major, R.P., Ludwig, K.R., Peterman, Z.L., and Matthews, R.K., 1986, Chapter G: Preliminary analyses of OAK debris samples; 11 p., 6 figs., 4 tpls.; in Folger, D.W., editor, Sea-floor observations and subbottom seismic characteristics of OAK and KOA craters, Enewetak Atoll, Marshall Islands: U.S. Geological Survey Bulletin 1678.
- Halley, R.B., Slater, R.A., Shinn, E.A., Folger, D.W., Hudson, J.H., Kindinger, J.L., and Roddy, D.J., 1986, Chapter F: Observations of OAK and KOA craters from the submersible; 32 p., 13 figs., 1 appendix; in Folger, D.W., editor, Sea-floor observations and subbottom seismic characteristics of OAK and KOA craters, Enewetak Atoll, Marshall Islands: U.S. Geological Survey Bulletin 1678.
- Henny, R.W., Mercer, J.W., and Zbur, R.T., 1974, Near-surface geologic Investigations at Eniwetok Atoll: Air Force Weapons Laboratory Technical Report AFWL-TR-74-257, Kirtland Air Force Base, New Mexico, 367 p. [unclassified document].
- Henry, T.W., and Wardlaw, B.R., editors, 1986a, Pacific Enewetak Atoll Crater Exploration (PEACE) Program, Enewetak Atoll, Republic of the Marshall Islands; Part 3: Stratigraphic analysis and other geologic and geophysical studies in vicinity of KOA and OAK craters: U.S. Geological Survey Open-File Report 86-555, 486 p., 92 figs., 90 tpls, 34 pls. [14 Chapters.]
- Henry, T.W., and Wardlaw, B.R., 1986b, Chapter 1: Introduction: 13 p., 3 figs., 1 tbl., in Henry, T.W., and Wardlaw, B.R., editors, Pacific Enewetak Atoll Crater Exploration (PEACE) Program, Enewetak Atoll, Republic of the Marshall Islands; Part 3: Stratigraphic analysis and other geologic and geophysical studies in vicinity of KOA and OAK craters: U.S. Geological Survey Open-File Report 86-555.
- Henry, T.W., Wardlaw, B.R., Skipp, B.A., Major, R.P., and Tracey, J.I., Jr., 1986, Pacific Enewetak Atoll Crater Exploration (PEACE) Program, Enewetak Atoll, Republic of the Marshall Islands; Part 1: Drilling operations and descriptions of boreholes in vicinity of KOA and OAK craters: U.S. Geological Survey Open-File Report 86-419, 497 p., 32 figs., 29 pls., 13 tpls., 3 appendices.
- Ludwig, K.R., Halley, R.B., Simmons, K.R., and Peterman, Z.E., 1986, Chapter 3: Sr-isotope stratigraphy of disturbed and undisturbed carbonates; 23 p., 8 figs., 6 tpls.; in Henry, T.W., and Wardlaw, B.R., editors, Pacific Enewetak Atoll Crater Exploration (PEACE) Program, Enewetak Atoll, Republic of the Marshall Islands; Part 3: Stratigraphic analysis and other geologic and geophysical studies in vicinity of KOA and OAK craters: U.S. Geological Survey Open-File Report 86-555.
- McClelland Engineers, Inc., 1986, Relative liquefaction for potential study for carbonate versus noncarbonate materials: Report No. 0186-1069, to Holmes and Narver, Inc., Honolulu, Hawaii; dated December 19, 1986; 37 p., 13 pls. [Signed by Ronald J. Ebehar, Project Supervisor, and Alan G. Young, Vice President, Marine Geosciences.]

- Melzer, L.S., 1986, Chapter 7: Downhole geophysical logs; 32 p., 16 figs., 7 tbls.; in Henry, T.W., and Wardlaw, B.R., editors, Pacific Enewetak Atoll Crater Exploration (PEACE) Program, Enewetak Atoll, Republic of the Marshall Islands; Part 3: Stratigraphic analysis and other geologic and geophysical studies in vicinity of KOA and OAK craters: U.S. Geological Survey Open-File Report 86-555.
- Mueller, C.M., 1987, Mechanical response of undisturbed cores and remolded coral sand from Enewetak Atoll: Department of the Army, Corps of Engineers, Waterways Experiment Station, Technical Report SL-87-14, Vicksburg, Mississippi, 361 p., 274 pls., 56 figs., 5 tbls. [unclassified document].
- Patti, N., and Schatz, J.F., 1987 [1988?], in preparation, Material properties tests, material compaction on shot-similar stress/strain paths, and grain size distribution on Enewetak Atoll coral specimens: Science Applications International Corporation, Report SAIC-87/1158, prepared for the Defense Nuclear Agency.
- Ristvet, B.L., and Tremba, E.L., 1986a, Chapter 5: Total organic content of lagoon benthic sediments and of subsurface samples from the PEACE drilling program; 9 p., 2 figs., 2 tbls.; in Henry, T.W., and Wardlaw, B.R., editors, Pacific Enewetak Atoll Crater Exploration (PEACE) Program, Enewetak Atoll, Republic of the Marshall Islands; Part 3: Stratigraphic analysis and other geologic and geophysical studies in vicinity of KOA and OAK craters: U.S. Geological Survey Open-File Report 86-555.
- Ristvet, B.L., and Tremba, E.L., 1986b, Chapter 6: Insoluble residue analysis of carbonate sediments from the subsurface of Enewetak Atoll; 5 p., 1 tbl., ; in Henry, T.W., and Wardlaw, B.R., editors, Pacific Enewetak Atoll Crater Exploration (PEACE) Program, Enewetak Atoll, Republic of the Marshall Islands; Part 3: Stratigraphic analysis and other geologic and geophysical studies in vicinity of KOA and OAK craters: U.S. Geological Survey Open-File Report 86-555.
- Ristvet, B.L., and Tremba, E.L., 1986c, Chapter 12: Radiation chemistry of the subsurface of OAK and KOA craters; 15 p., 5 figs., 5 tbls; in Henry, T.W., and Wardlaw, B.R., editors, Pacific Enewetak Atoll Crater Exploration (PEACE) Program, Enewetak Atoll, Republic of the Marshall Islands; Part 3: Stratigraphic analysis and other geologic and geophysical studies in vicinity of KOA and OAK craters: U.S. Geological Survey Open-File Report 86-555.
- Ristvet, B.L., Tremba, E.L., Couch, R.F., Jr., Fetzer, J.A., Goter, E.R., Walter, D.R., and Wendland, V.P., 1978, Geologic and geophysical investigations of the Enewetak nuclear craters; Final reports: Air Force Weapons Laboratory Technical Report AFWL-TR-77-242, Kirtland Air Force Base, New Mexico, 298 p. [unclassified document].
- Robb, J.M., Foster, D.S., Folger, D.W., Hampson, J.C., and Woellner, R.A., 1986, Chapter C: Single-channel seismic survey of OAK and KOA craters: 51 p., 24 figs.; in Folger, D.W., editor, Sea-floor observations and subbottom seismic characteristics of OAK and KOA craters, Enewetak Atoll, Marshall Islands: U.S. Geological Survey Bulletin 1678.

- Schatz, J.F., Patti, N., and Melzer, L.S., 1987 [1988?], in preparation, Material properties at OAK/KOA -- Summary Report: Science Applications International Corporation, Report SAIC-87/1159, prepared for the Defense Nuclear Agency.
- Simons, D., and others, 1984, Recommendations for laboratory material properties testing of core materials from the Pacific Proving Grounds: Research and Development Associates, Los Angeles, California; unnumbered report submitted to Defense Nuclear Agency.
- Shinn, E.A., Kindinger, J.L., Halley, R.B., and Hudson, J.H., 1986, Chapter H: Scuba observations of OAK and KOA craters, 39 p., 38 figs., 1 tbl.; in Folger, D.W., editor, Sea-floor observations and subbottom seismic characteristics of OAK and KOA craters, Enewetak Atoll, Marshall Islands: U.S. Geological Survey Bulletin 1678.
- Slater, R.A., Roddy, D.J., Folger, D.W., Halley, R.B., and Shinn, E.A., 1986, Chapter 13: Additional submersible studies; detailed observations of the seafloor of OAK, KOA, and MIKE craters; 153 p., 2 tbls., 4 pls.; in Henry, T.W., and Wardlaw, B.R., editors, Pacific Enewetak Atoll Crater Exploration (PEACE) Program, Enewetak Atoll, Republic of the Marshall Islands; Part 3: Stratigraphic analysis and other geologic and geophysical studies in vicinity of KOA and OAK craters: U.S. Geological Survey Open-File Report 86-555.
- Tremba, E.L., 1987 [1984], Enewetak Atoll Seismic Investigation (EASI): Phase III; Final Report: Air Force Weapons Laboratory Technical Report 84-105, Air Force Systems Command, Kirtland Air Force Base, New Mexico, 87117-6008, 122 p., 36 figs., 11 tbls. [unclassified document].
- Tremba, E.L., Couch, R.F., Jr., and Ristvet, B.L., 1982, Enewetak Atoll Seismic Investigation (EASI) Project; Phases I and II: Air Force Weapons Laboratory Technical Report AFWL-TR-82-20, Kirtland Air Force Base, New Mexico, 124 p., 38 figs., 3 tbls., 3 appendices [unclassified document].
- Tremba, E.L., Jones, G.L., and Henny, R.W., 1981, Pacific atoll cratering experiments (Project PACE 2); Results and analysis of cratering and related effects: Air Force Weapons Laboratory Technical Report AFWL-TR-81-167, Air Force Systems Command, Kirtland Air Force Base, New Mexico, 334 p., 32 figs., 8 tbls., 8 appendices [unclassified document].
- Tremba, E.L., and Ristvet, B.L., 1986a, Chapter 4: X-ray diffraction mineralogy; 49 p., 11 figs., 35 tbls., in Henry, T.W., and Wardlaw, B.R., editors, Pacific Enewetak Atoll Crater Exploration (PEACE) Program, Enewetak Atoll, Republic of the Marshall Islands; Part 3: Stratigraphic analysis and other geologic and geophysical studies in vicinity of KOA and OAK craters: U.S. Geological Survey Open-File Report 86-555.
- Tremba, E.L., and Ristvet, B.L., 1986b, Chapter 9: Seismic reference surveys; 16 p., 1 fig., 12 tbls.; in Henry, T.W., and Wardlaw, B.R., editors, Pacific Enewetak Atoll Crater Exploration (PEACE) Program, Enewetak Atoll, Republic of the Marshall Islands; Part 3: Stratigraphic analysis and other geologic and geophysical studies in vicinity of KOA and OAK craters: U.S. Geological Survey Open-File Report 86-555.

Wardlaw, B.R., and Henry, T.W., 1986a, Chapter 2: Physical stratigraphic framework; 36 p., 10 figs., 2 tpls.; in Henry, T.W., and Wardlaw, B.R., editors, Pacific Enewetak Atoll Crater Exploration (PEACE) Program, Enewetak Atoll, Republic of the Marshall Islands; Part 3: Stratigraphic analysis and other geologic and geophysical studies in vicinity of KOA and OAK craters: U.S. Geological Survey Open-File Report 86-555.

Wardlaw, B.R., and Henry, T.W., 1986b, Chapter 14: Geologic interpretation of OAK and KOA craters; 39 p., 21 figs., 2 tpls.; in Henry, T.W., and Wardlaw, B.R., editors, Pacific Enewetak Atoll Crater Exploration (PEACE) Program, Enewetak Atoll, Republic of the Marshall Islands; Part 3: Stratigraphic analysis and other geologic and geophysical studies in vicinity of KOA and OAK craters: U.S. Geological Survey Open-File Report 86-555.

Wardlaw, B.R., Henry, T.W., and Martin, W.E., 1986, Chapter 10: Benthic samples from Enewetak Atoll; 50 p., 6 figs., 12 tpls., 29 pls.; in Henry, T.W., and Wardlaw, B.R., editors, Pacific Enewetak Atoll Crater Exploration (PEACE) Program, Enewetak Atoll, Republic of the Marshall Islands; Part 3: Stratigraphic analysis and other geologic and geophysical studies in vicinity of KOA and OAK craters: U.S. Geological Survey Open-File Report 86-555.

CHAPTER 2:

ANALYSIS OF BOREHOLE GRAVITY SURVEYS AT OAK CRATER

by

L. A. Beyerl

INTRODUCTION

Borehole gravity (BHG) surveys were made in selected PEACE Program boreholes at OAK crater on Enewetak Atoll because they provide the only means to directly and accurately measure in situ bulk density of large volumes of rock and sediment that surround the boreholes and to provide data to calculate the total porosity of these materials². The differences between the density and porosity of undisturbed atoll materials and the sediment and rock involved in the excavational and apparent craters are crucial to understanding various cratering phenomena. In addition, accurate and representative density and porosity measurements of undisturbed atoll materials are important for nuclear-event calculations. The nature of BHG measurements, rationale for siting BHG boreholes, field techniques, and preliminary (apparent) BHG density data and calculated porosity values are given in Beyer, Ristvet, and Oberste-Lehn (1986).

This report presents the models used to correct the apparent (BHG) density and porosity data for large-scale lateral density changes across the reef margin (due to natural facies changes) and for smaller-scale lateral density changes due to cratering phenomena. Corrected BHG density data and calculated porosity values are described in terms of their modification due to cratering processes.

Ancillary topics include: (1) general results of the BHG survey in the E-1 borehole on Medren (ELMER) Island (Appendix 2-1), (2) brief comparison of estimates of density and porosity from BHG, gamma-gamma, and neutron logs, and (3) relationship between grain density and BHG porosity in undisturbed atoll materials. A short description of how average interval grain density was determined from the x-ray mineralogy and organic analyses studies of core samples is found in Appendix 2-2.

The locations of OAK crater and E-1 and F-1 deep boreholes referred to later in this chapter are shown in Figure 2-1. Locations of boreholes drilled at OAK crater during the PEACE Program are given in Figure 2-2, along with a table that summarizes pertinent information about the boreholes in which BHG surveys were made. Locations of two cross sections presented later in the chapter also are shown in Figure 2-2.

¹Branch of Sedimentary Processes, U.S. Geological Survey, Menlo Park, CA.

²Bulk density and total porosity are abbreviated as density and porosity in this Chapter. Porosity is calculated from a combination of in situ density and grain-density data derived from x-ray mineralogic analyses.

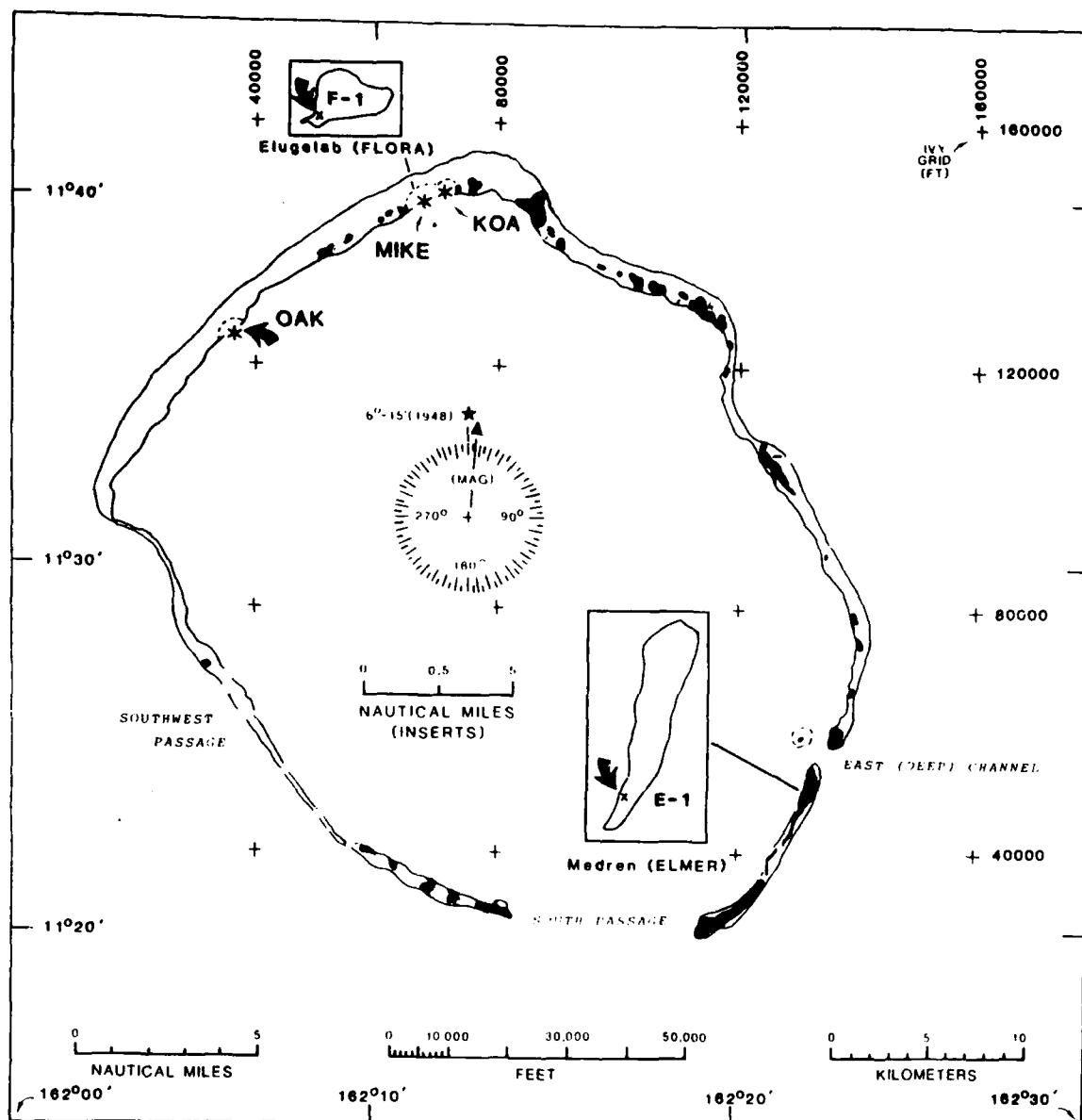


FIGURE 2-1. - Map of Enewetak Atoll showing locations of OAK, KOA, and MIKE craters and Medren (ELMER) Island. Deep boreholes E-1 and F-1 drilled in 1951 and 1952 by the USGS and AEC (Ladd and others, 1953; Ladd and Schlanger, 1960) and referred to in this paper are shown by "X"'s on the inset maps.

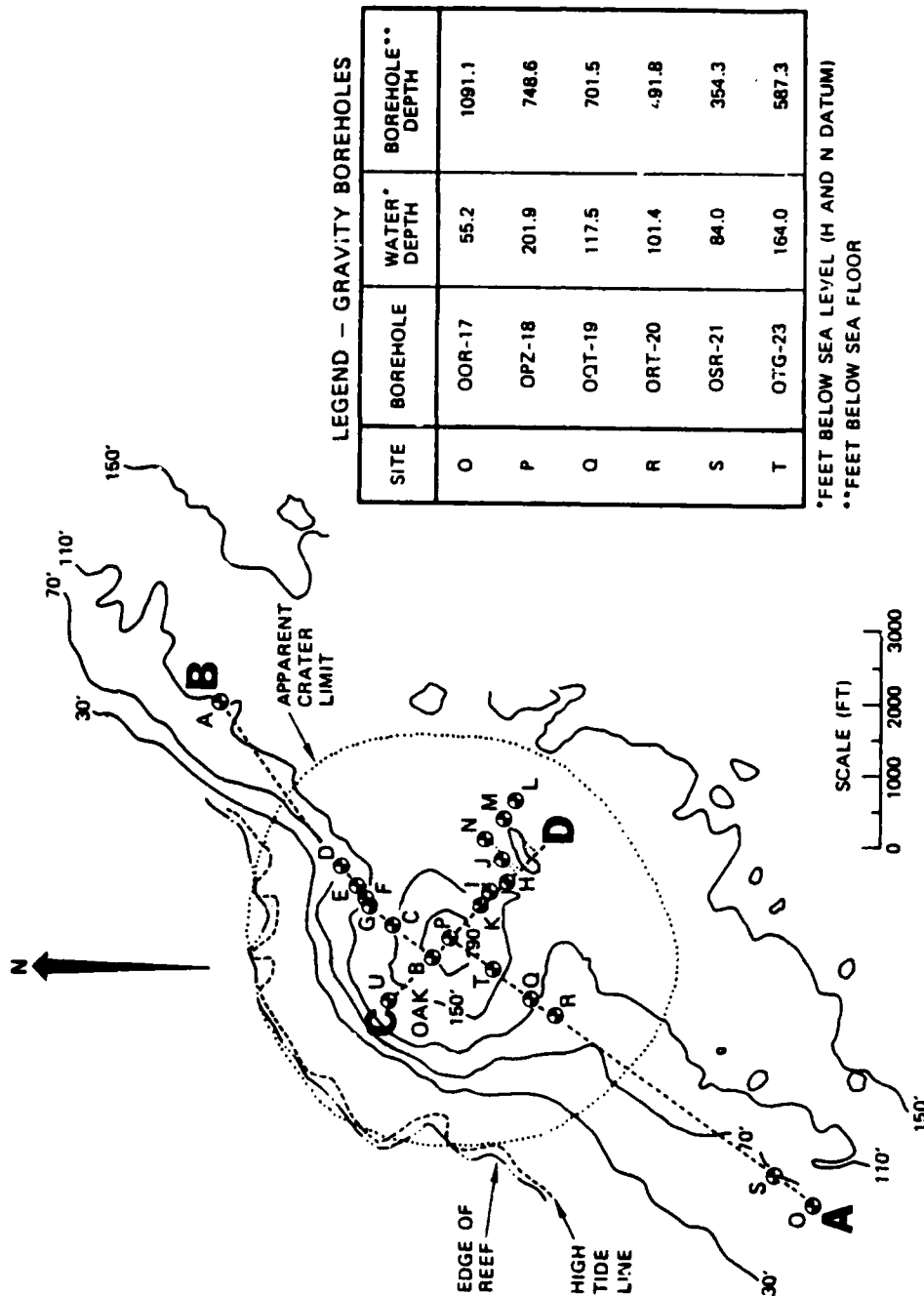


FIGURE 2-2. - Map of OAK crater and vicinity showing locations of PEACE Program boreholes and cross sections AB and CD. Inset shows designation, water depth and total subsea-floor depth of boreholes in which gravity surveys were made.

The efficacy of BHG surveys to determine subtle density differences at OAK crater depends in great part on the precision of the field measurements. This is determined by making repeated W_g/W_z measurements over the same depth interval. Of 98 intervals surveyed in six boreholes, 8 percent were repeated four or more times, 81 percent were repeated three times, 10 percent were repeated two times, and 1 percent were not repeated due to operational constraints. These repeated W_g/W_z measurements indicate that the precision of the surveys is quite high and fully adequate for the purposes of the OAK study (fig. 2-3). Standard deviations of repeated measurements are given in column 3 of Tables 2-2 through 2-7 (located at the end of the current Chapter), are illustrated graphically on BHG density and porosity profiles in subsequent figures, and are explained in Appendix 8-2 of Beyer, Ristvet, and Oberste-Lehn (1986).

BOREHOLE GRAVITY ANALYSIS

The analysis of BHG measurements at OAK crater follows the only logical path available in the absence of independent data such as a detailed surface gravity anomaly map and reliable density data from gamma-gamma and/or core measurements. BHG measurements are corrected for recognizable lateral density variations so that the corrected BHG densities are reasonably accurate measures of the atoll materials within a few tens to a few hundreds of feet of each surveyed borehole. Then, comparisons of density (and porosity) can be made between different boreholes in and near OAK crater.

Corrections can be made rationally for submarine topography (Beyer, Ristvet, and Oberste-Lehn, 1986), for large-scale lateral density charges across the reef margin that are caused by natural facies changes, and for smaller-scale lateral density changes related to cratering processes. A summary of the range of corrections calculated and applied to the BHG surveys is given in Table 2-1. Individual corrections are presented in Tables 2-2 through 2-7, located at the end of the Chapter.

Corrections cannot be made for even smaller-scale lateral density changes on the order of tens to about a hundred feet distant from each borehole, because data needed to model these very small density changes were beyond the scope of the PEACE Program. We will note where these very small-scale effects may be present. Neglect of them does not impair the objectives of the BHG phase of the PEACE Program.

Please note that these corrections are computed as vertical gravity gradients which, when multiplied by $0.25 k$, where k is the Newtonian gravitational constant, become density corrections in g/cm^3 . Lateral density variations that cause a downward positive vertical gravity gradient result in a positive density correction, whereas a downward negative gradient causes a negative density correction (see Appendix 8-2 of Beyer, Ristvet, and Oberste-Lehn, 1986).

All tables are located at the end of the Chapter.

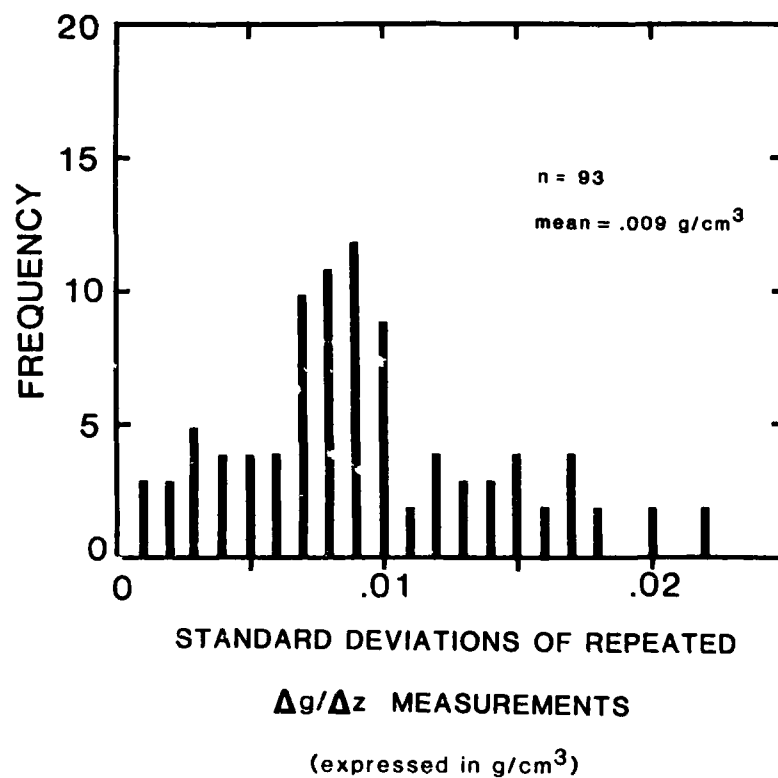


FIGURE 2-3. - Distribution of 93 sets of repeated $\Delta g/\Delta z$ measurements during borehole gravity surveys in OAK boreholes, expressed in g/cm^3 . Mean is .009 g/cm^3 and is a measure of the high quality of the borehole gravity surveys (Beyer, 1968; Black and Herring, 1983).

LARGE-SCALE LATERAL DENSITY CHANGES ACROSS REEF MARGIN

A substantial body of work by many investigators at modern Pacific atolls has shown that forereef and reef core facies generally are more highly cemented (and therefore denser) than lagoon facies, and that atoll reefs generally prograde seaward (e.g., Buigues, 1985). These relationships are believed to be present along the northwest margin of Enewetak Atoll according to B. L. Ristvet, who provided the author with a sketch of the probable distribution of facies and densities across the reef margin at OAK crater. Other PEACE Program studies (Folger, 1986a) and earlier work at Enewetak, especially deep boreholes E-1 and F-1 and the XEN series of boreholes on Engebí Island (Ladd and others, 1953; Ladd and Schlanger, 1960; Couch and others, 1975), led to this assessment of atoll margin structure. Densities provided by Ristvet were modified slightly using the BHG densities from the E-1 borehole on Medren Island (see Appendix 2-1).

Deeper density contrasts (e.g., between the volcanic core and overlying carbonate rocks of the atoll) and possible incomplete isostatic compensation of the atoll also can affect the vertical gravity gradients (and BHG densities). Corrections for these possible effects are almost certainly negligibly small and, if determined, would cause only a very small, constant dc-type shift of all density data. The absence of even a rudimentary surface gravity anomaly map and more detailed deep borehole data prevent any attempt to examine these effects.

The two-dimensional density model prepared for the atoll margin at OAK crater is shown in Figure 2-4. Vertical gravity gradient corrections were calculated for the two-dimensional model with a well-established algorithm (Talwani and others, 1959) that has been modified for borehole gravity applications. These corrections are given in column 5 of Tables 2-2 to 2-7 and probably are unnecessary but their magnitudes needed to be evaluated.

CORRECTION FOR LATERAL DENSITY CHANGES DUE TO CRATERING PROCESSES

Lateral density variations due to cratering processes also can affect the BHG densities and, therefore, were evaluated. The model used to correct for these crater-related lateral density changes was developed along the southwest transect from OPZ-18 to OOR-17 by using BHG densities (corrected for submarine topography and large-scale density changes across the atoll margin) and a correlation cross section prepared by D. Oberste-Lehn and modified by B. R. Wardlaw (fig. 2-5; correlation cross section CD, fig. 2-6, also was prepared by Oberste-Lehn and Wardlaw). The density model is shown in Figure 2-7 and was assumed to have circular symmetry about OPZ-18. Trial gravity calculations taking into account the departure of OAK crater from circular symmetry about OPZ-18 (based only on correlation cross sections) showed that the assumption of circular symmetry is valid. The size of the corrections due to crater-related lateral density changes is so small that the question of true three-dimensionality versus circular symmetry about OPZ-18 is academic. The question of the actual crater density structure along cross section CD remains. A very careful sea floor gravity survey or more BHG drillholes and surveys would shed light on this question.

Generalized 2-D Density Model through OAK Crater

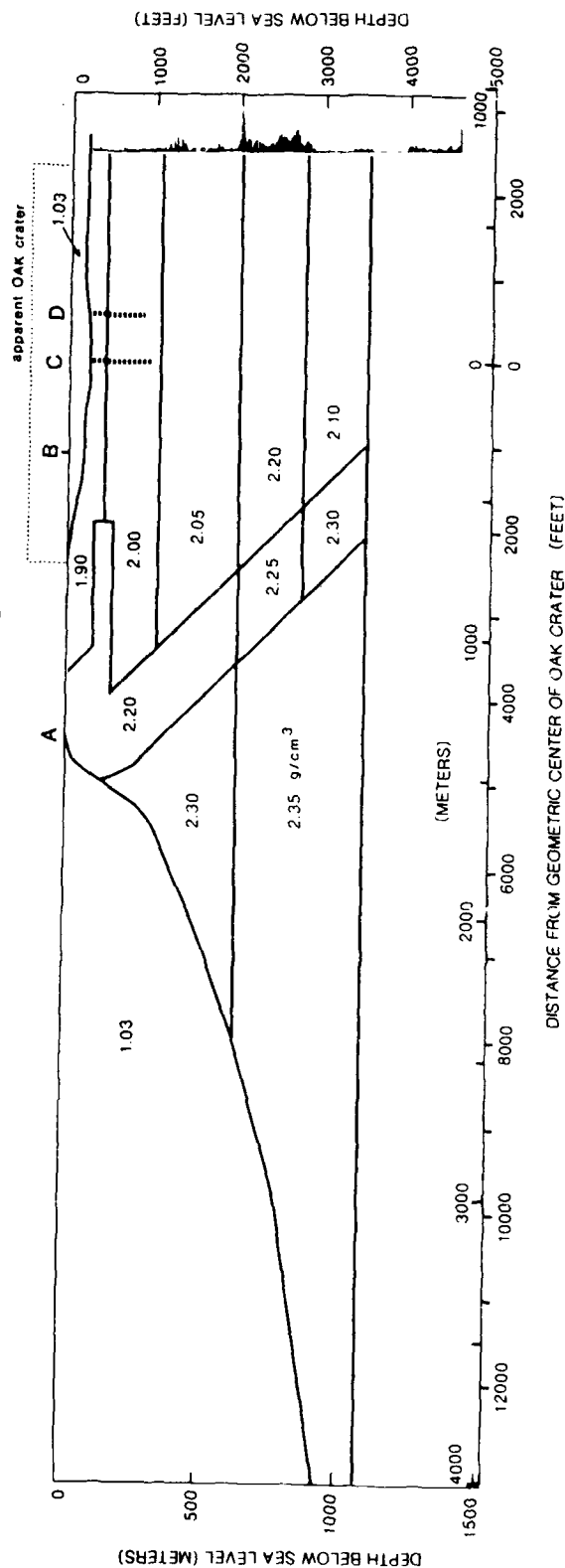


FIGURE 2-4. - Two-dimensional density model (assumed to extend as shown to great distances in directions perpendicular to page) of natural atoll facies changes in section orthogonal to reef. Labels include model element densities in g/cm³, outer reef edge ("A"), inner reef edge prior to OAK event ("B"), position of boreholes OPZ-18, OTG-23, OQT-19, and ORF-20 ("C") and position of boreholes OSR-21 and OOR-17 ("D"). Drilling time profile (near right of depth scale) is for borehole F-1 (see fig. 2-1 for location). Remember that submarine topography correction replaced seawater (1.03 g/cm³) with 1.90 g/cm³ (Beyer, Ristvet, and Oberste-Lehn, 1986). No vertical exaggeration.

BLANK PAGE

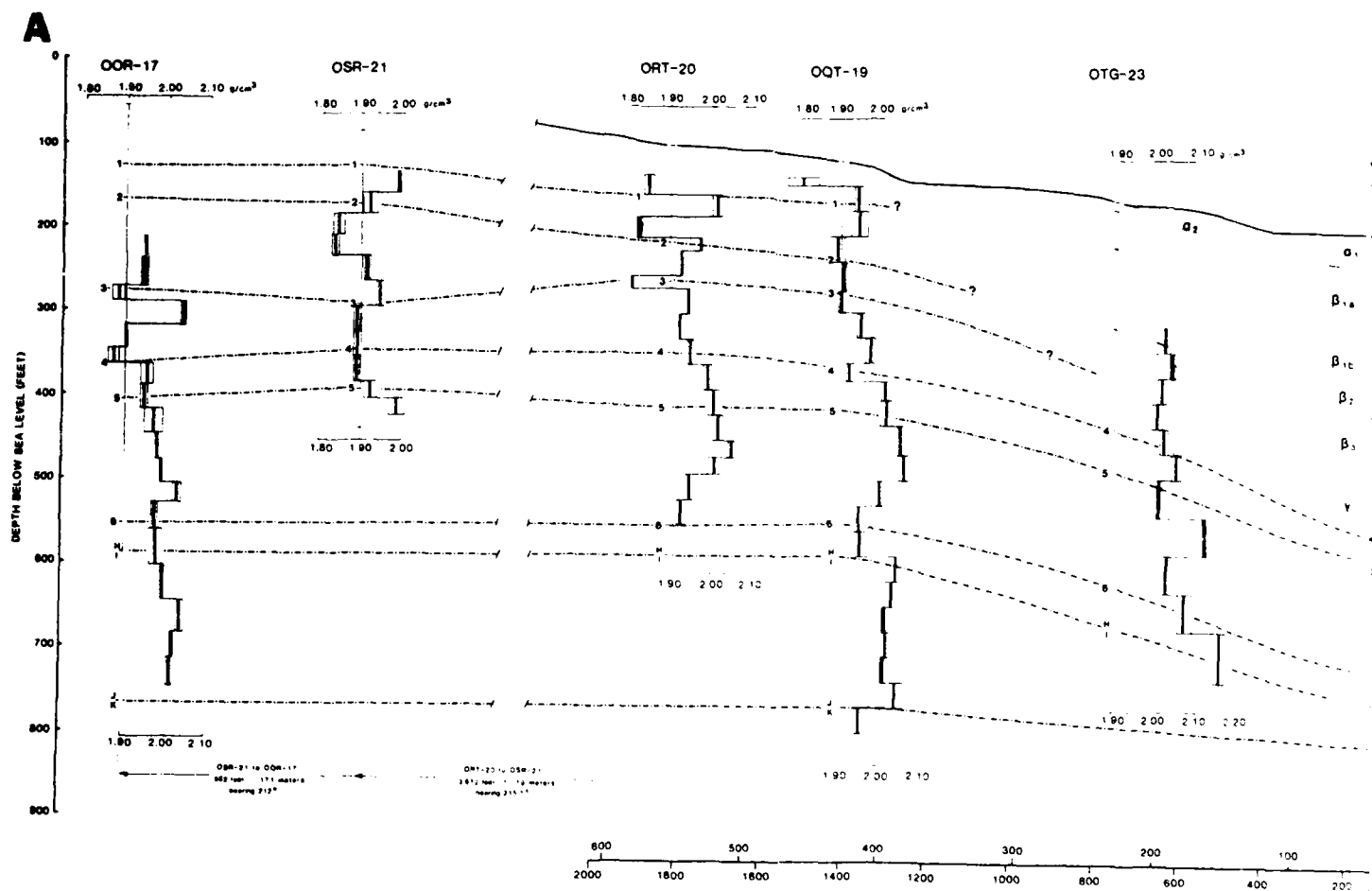
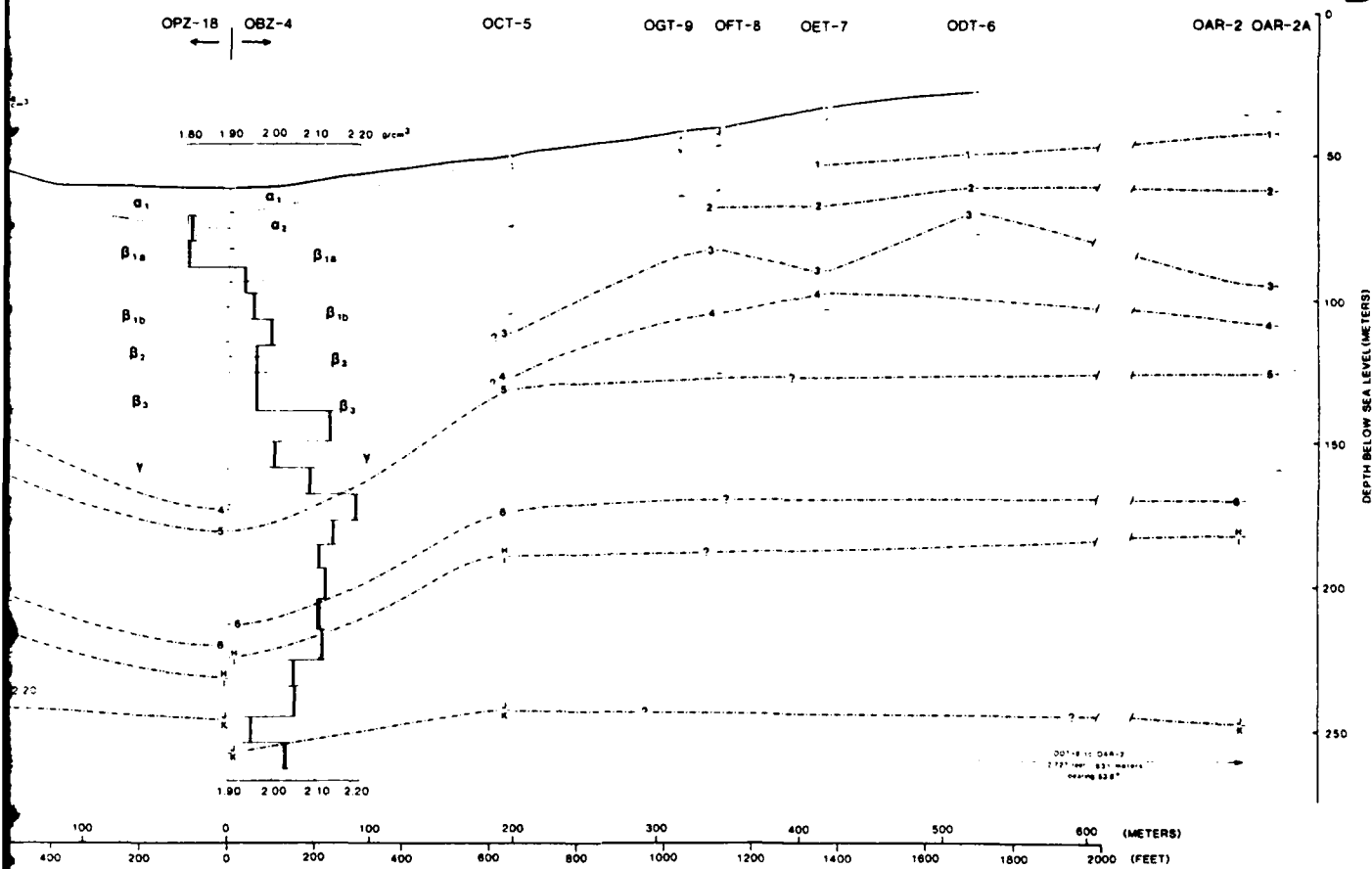


FIGURE 2-5. - Cross section AB extends from south-southwest to north-northeast through markers in OBZ-4 extending to the right and markers in OPZ-18 extending to the left zone boundaries H/I and J/K, and crater geologic zones α_1 through γ (see Wardlaw by D. Oberste-Lehn and modified by B. R. Wardlaw. BHG density profiles are superimposed scale labels "1.90" correspond to the positions of the surveyed boreholes in the c

B



ast through OAK crater (fig. 2-2). Section is broken at center with geologic to the left. Correlation lines tie disconformities 1 through 6, biostratigraphic Wardlaw and Henry, 1986a,b). This section and that of Figure 2-6 were prepared are superimposed on the section for the six surveyed boreholes. The density is in the cross section. Vertical exaggeration from OAR-20 to ODT-6 is 2X.

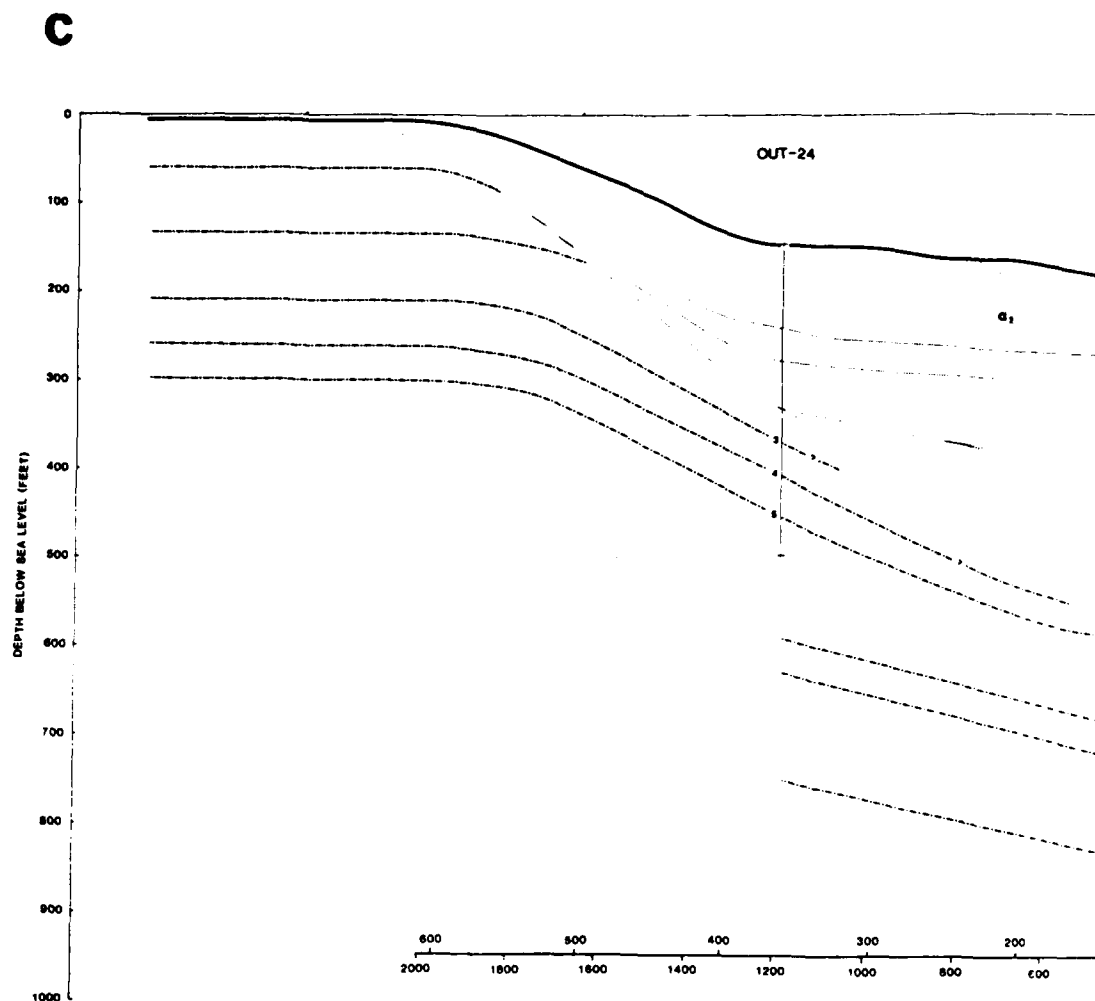
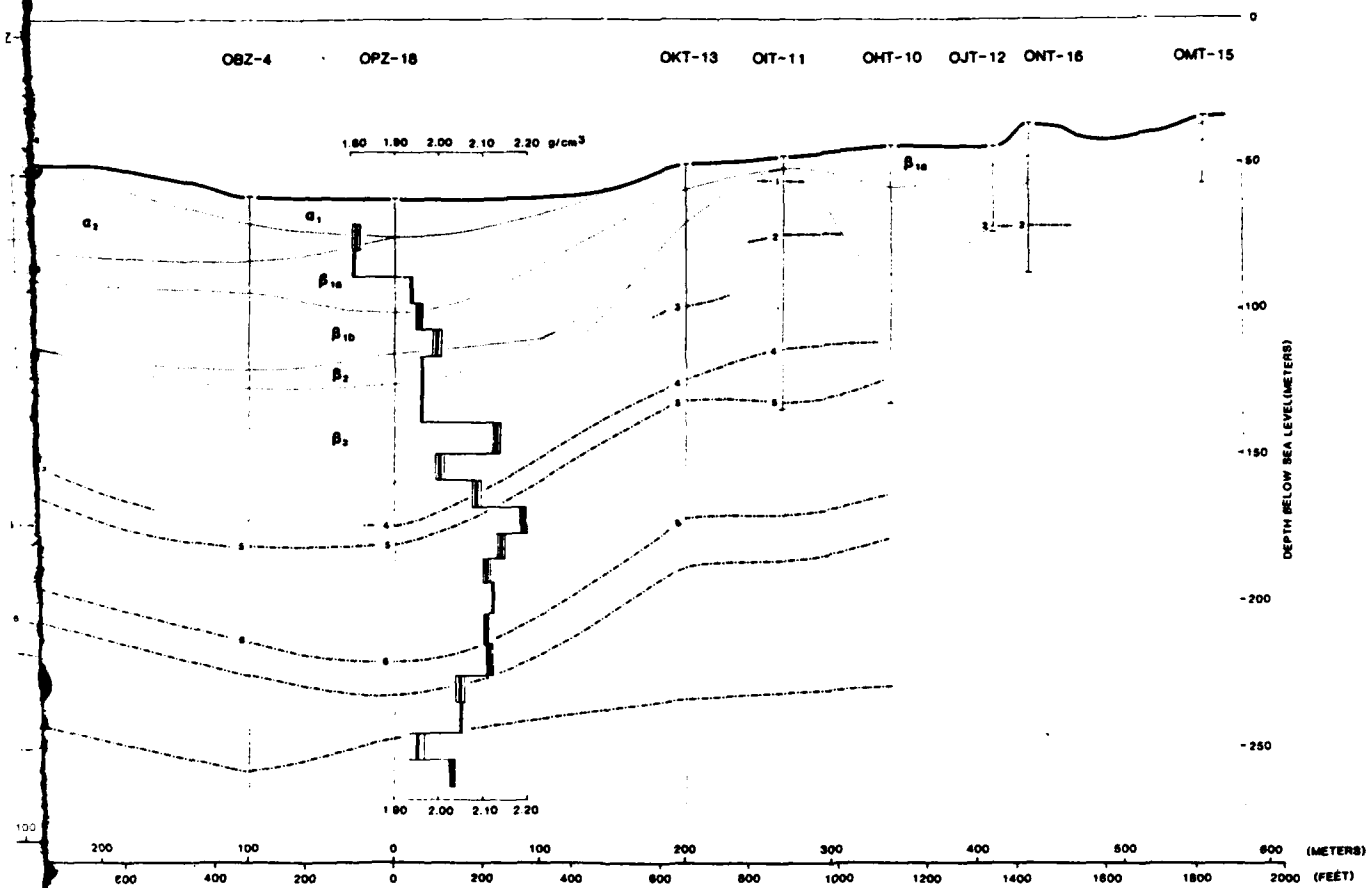


FIGURE 2-6. - Cross section CD extends from west-northwest to east-south. Figure 2-5. Only the BHG density profile of OP2-18 lies in this section in Figure 2-2. Vertical exaggeration is 2X.

D



East-southeast through OAK crater (fig. 2-2). Data are identical to those described for this section. Boreholes OJT-12, ONT-16, and OMT-15 are projected into section as shown

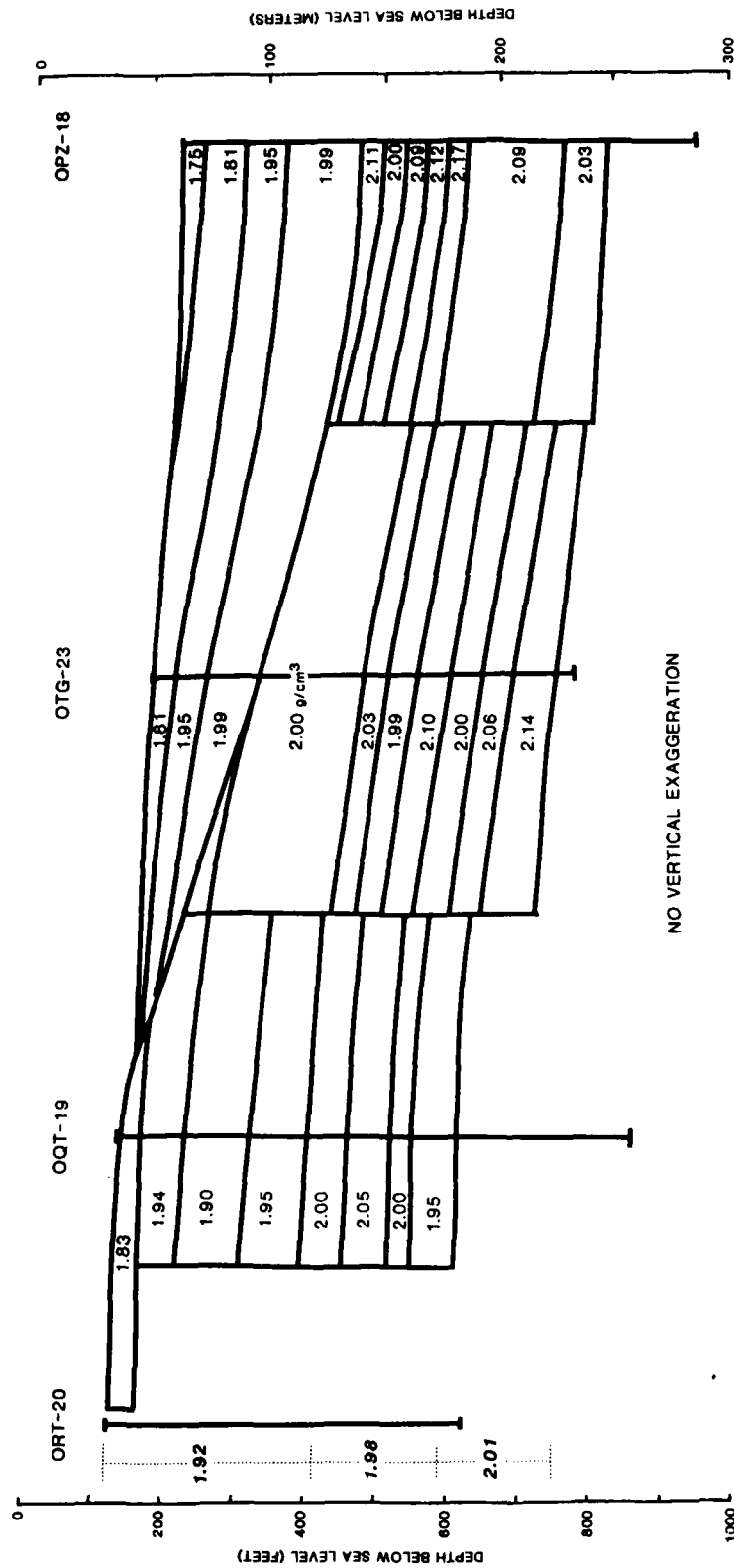


FIGURE 2-7. - Cross section along south-southwestern transect for lateral density variations caused by cratering processes. Density model is assumed to have circular symmetry about borehole OPZ-18. Densities of surrounding atoll materials as determined from BHG densities from reference boreholes OOR-17 and OSR-21 are shown next to left depth scale.

In order to perform density calculations using the model shown in Figure 2-7, the assigned densities must be recast as density contrasts relative to the surrounding medium. The density of the surrounding atoll material was determined from the BHG density profiles of reference boreholes OOR-17 and OSR-21 which were assumed to be unaltered by crater-related processes. The density model for the surrounding medium is summarized in Table 2-8, and values are shown along the left side of Figure 2-7. These reference density values were subtracted from laterally juxtaposed crater density model elements to arrive at a density contrast model.

Corrections to the BHG densities in OPZ-18, OTG-23, OQT-19, and ORT-20 were calculated from the density contrast model using a well-established algorithm for three-dimensional density elements (Plouff, 1976) modified for borehole gravity application. These corrections proved to be very small (column 6, tables 2-2 through 2-7), which could be predicted from the gentle dips of the density element boundaries as shown in Figure 2-7.

CORRECTED BOREHOLE GRAVITY DENSITY AND POROSITY AND COMPARISON WITH GAMMA-GAMMA AND NEUTRON DATA

Tabular and graphical summaries of BHG density and porosity with error estimates, grain densities with error estimates and interval-averaged density and porosity from gamma-gamma and neutron logs are presented in Tables 2-2 through 2-7 and Figures 2-8 through 2-13. Open-hole well log curves also are shown in Figures 2-8 through 2-12. Interval-averaged neutron porosity is not graphically displayed in Figures 2-8 through 2-12 because of a systematic error that has made all values too large. Interval grain density profiles are derived from individual grain density values, examination of open-hole well logs, and descriptions of cores and samples, sedimentary packages, and boreholes (Henry and Wardlaw, 1986; Wardlaw and Henry, 1986a; Holloway and Young, 1986). Errors in interval grain density are only estimates that may be increased or decreased with further information about the mineralogy of individual intervals, particularly intervals with both aragonite and calcite.

A number of questions about the reliability of the gamma-gamma density and neutron porosity logs run in OAK boreholes were raised during the analysis of the borehole data. Corrected BHG density and porosity provide a reliable standard against which gamma-gamma and neutron logs can be evaluated. In OAK boreholes, the differences between BHG density and interval-averaged gamma-gamma density decrease with increasing depth below the sea floor (fig. 2-14). This result agrees with the well-documented body of literature from the petroleum industry, which indicates that shallow-penetration radiation well logs, such as the gamma-gamma and neutron logs run in OAK boreholes, perform poorly in loosely consolidated, highly permeable sediments where formation damage caused by rotary drilling is almost always substantial.

Relatively good correspondence between BHG and gamma-gamma data is obtained for intervals deeper than 600 ft below sea level in OOR-17 and OQT-19, and deeper than 500 ft below sea level in ORT-20 where drill-induced borehole and formation damage is less because sediments are somewhat more consolidated than at shallower depths (figs. 2-8, 2-10, and 2-11). More specifically, Figure 2-14 suggests that gamma-gamma density departs

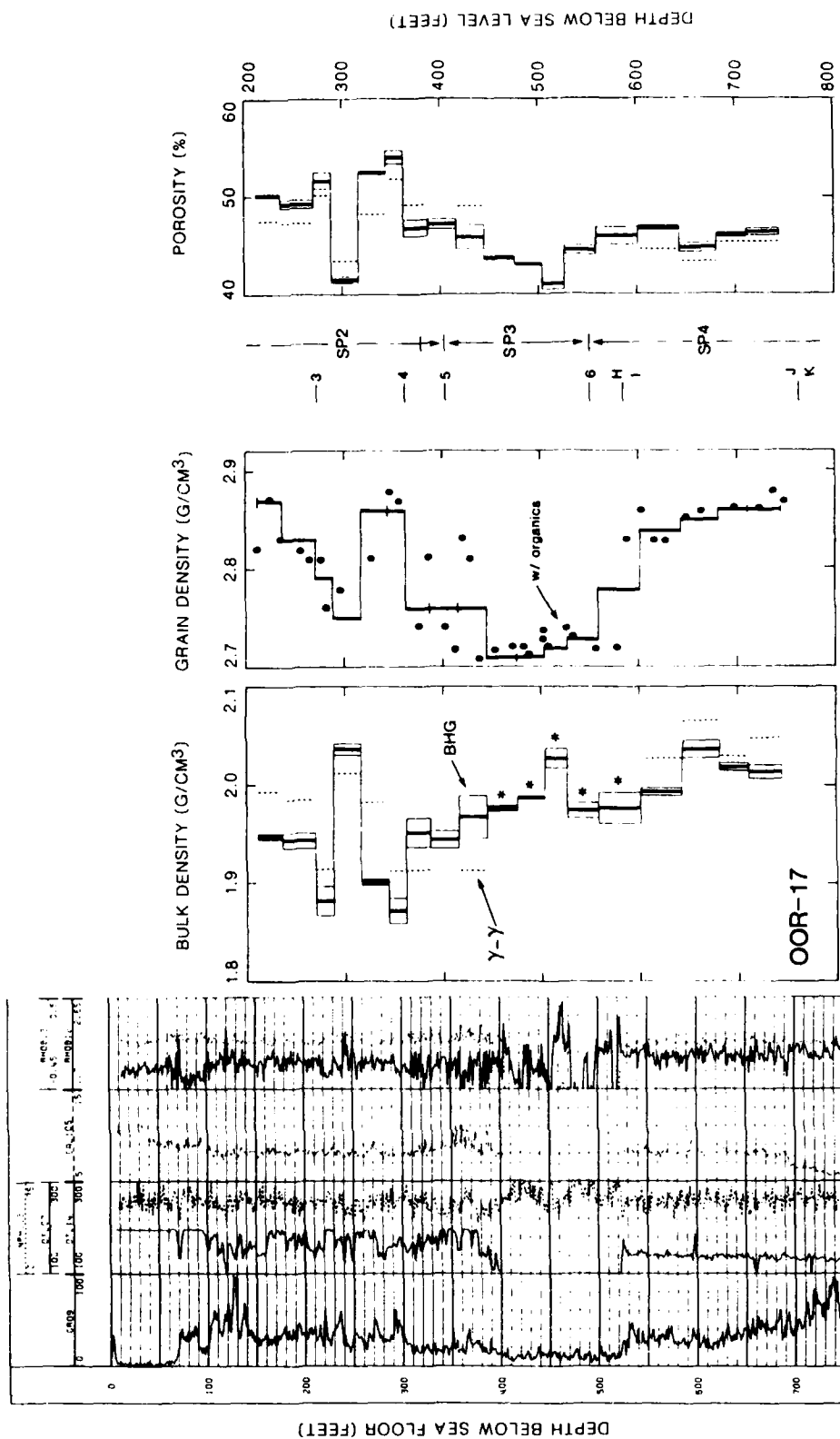


FIGURE 2-8. - Open-hole well logs, BHG and gamma-gamma density, core and interval grain density, disconformities and facies boundaries, sedimentary packages, and BHG and gamma-gamma porosity for borehole OOR-17 (left to right). Well logs from left to right are gamma-ray, multi-channel sonic, neutron porosity, caliper, gamma-gamma density, and gamma-gamma density correction. Asterisks indicate intervals where gamma-gamma log not available due to drillpipe. Interval averages of gamma-gamma density and porosity are plotted where values are outside error regions of BHG density and porosity.

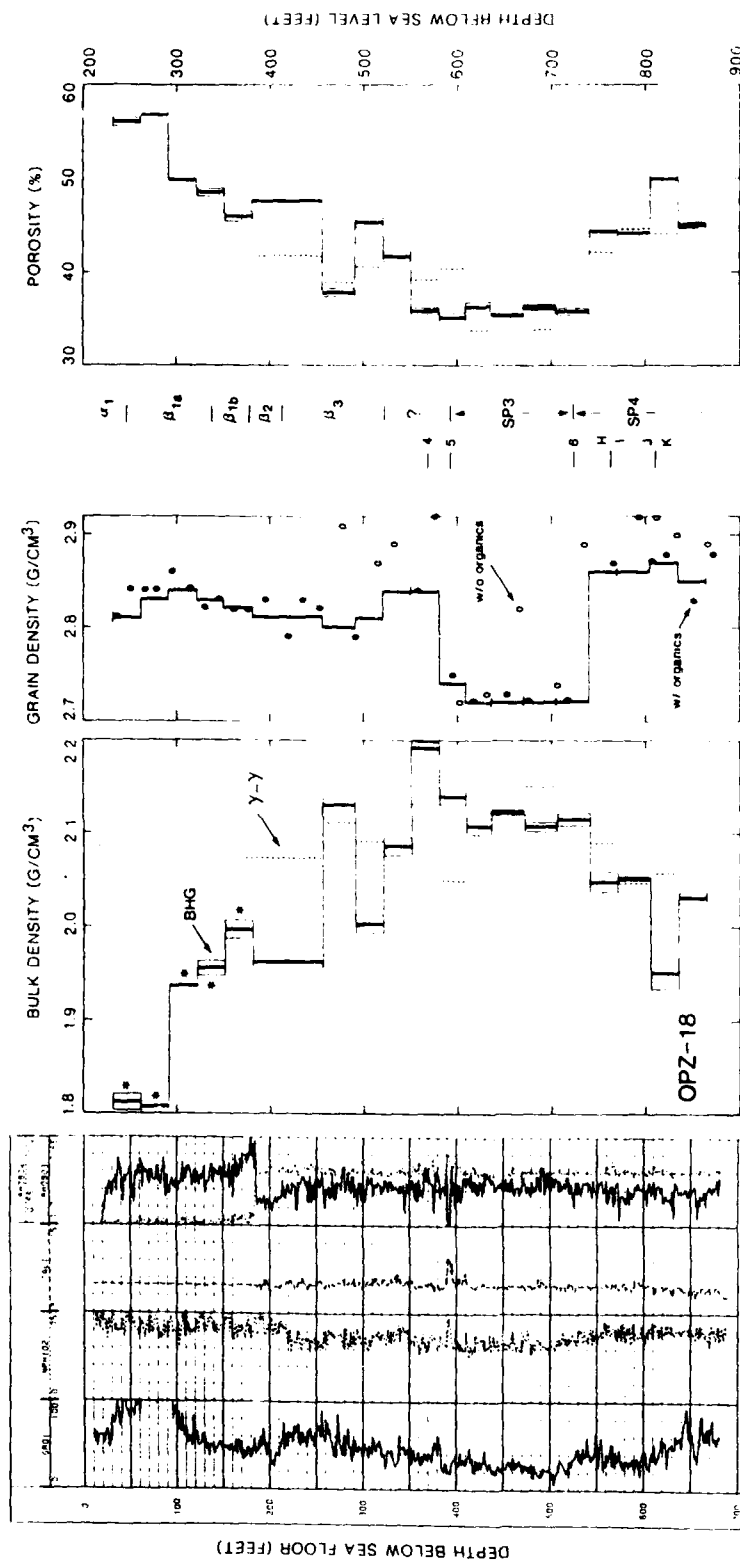


FIGURE 2-9. - Open-hole well logs, BHG and gamma-gamma density, core and interval grain density, disconformities and facies boundaries, sedimentary packages, and BHG and gamma-gamma porosity for borehole OPZ-18 (left to right). Well logs from left to right are gamma-ray, neutron porosity, caliper, gamma-gamma density, and gamma-gamma density correction. Asterisks indicate intervals where gamma-gamma log not available due to casing. Interval averages of gamma-gamma density and porosity are plotted where values are outside error regions of BHG density and porosity.

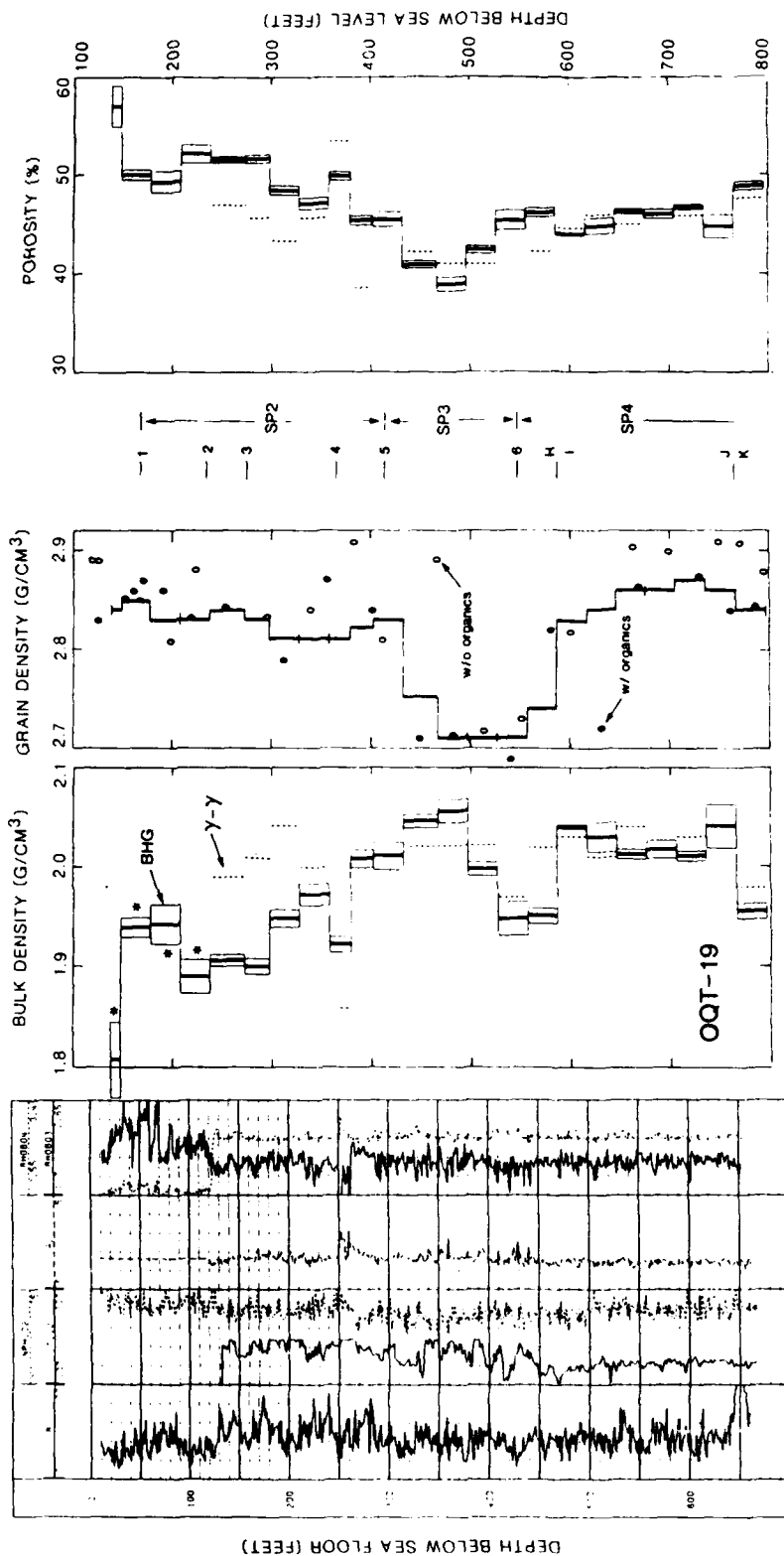


FIGURE 2-10. - Open-hole well logs, BHG and gamma-gamma density, core and interval grain density, disconformities and facies boundaries, sedimentary packages, and BHG and gamma-gamma porosity for borehole OQT-19 (left to right). Well logs from left to right are gamma ray, multi-channel sonic, neutron porosity, caliper, gamma-gamma density, and gamma-gamma density correction. Asterisks indicate intervals where gamma-gamma log not available due to casing. Interval averages of gamma-gamma density and porosity are plotted where values are outside error regions of BHG density and porosity.

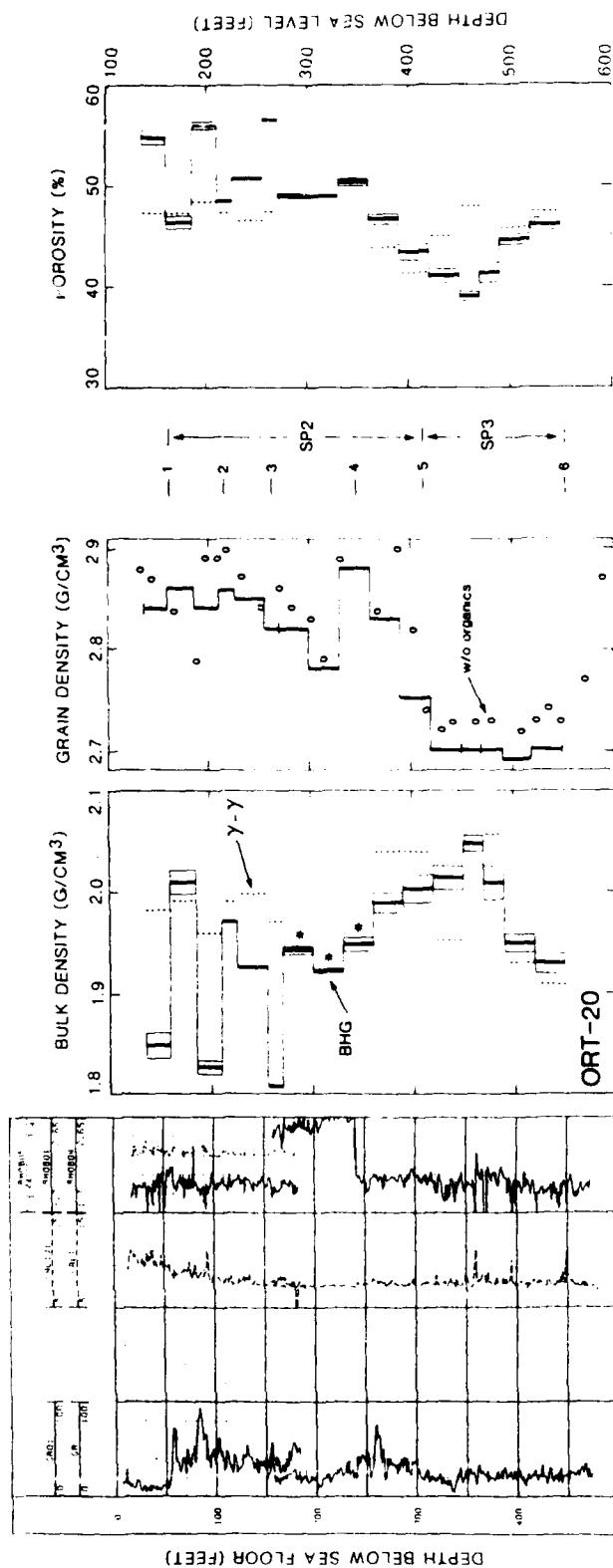


FIGURE 2-11. - Open-hole well logs, BHG and gamma-gamma density, core and interval grain density, discontinuities and facies boundaries, sedimentary packages, and BHG and gamma-gamma porosity for borehole ORT-20 (left to right). Well logs from left to right are gamma ray, caliper, gamma-gamma density, and gamma-gamma density correction (partial). Asterisks indicate intervals where gamma-gamma log not available due to casing. Interval averages of gamma-gamma density and porosity are plotted where values are outside error regions of BHG density and porosity.

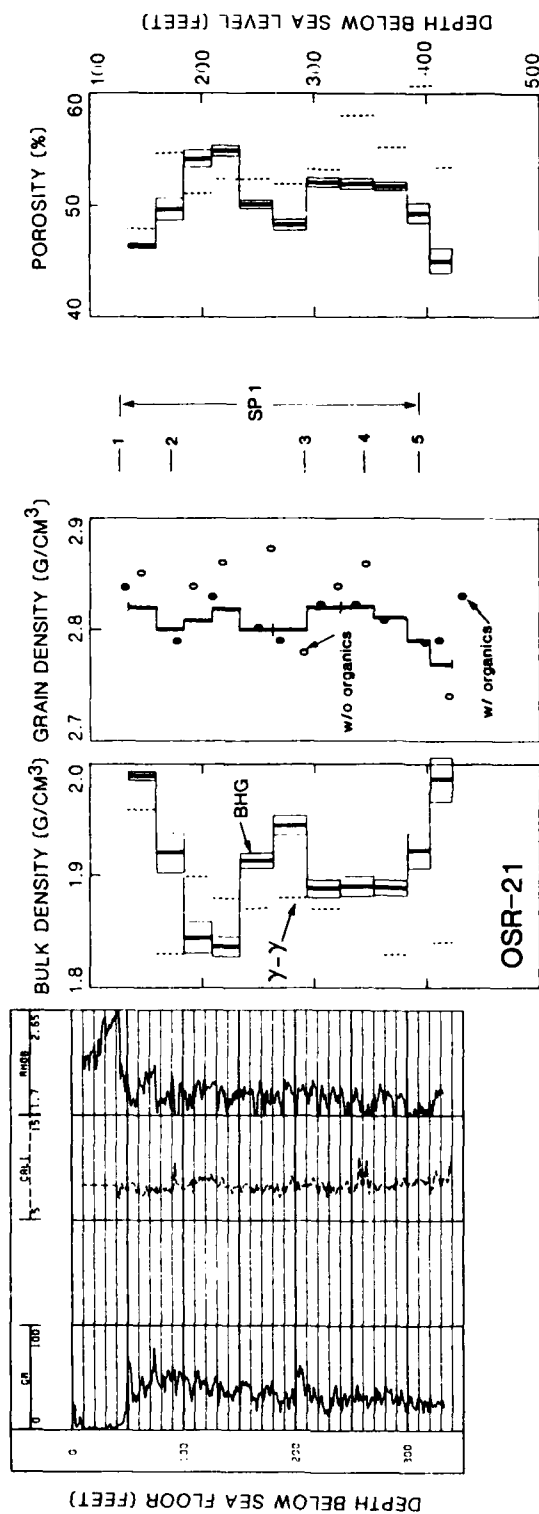


FIGURE 2-12. - Open-hole well logs, BHG and gamma-gamma density, core and interval grain density, discontinuities and facies boundaries, sedimentary packages, and BHG and gamma-gamma porosity for borehole OSR-21 (left to right). Well logs from left to right are gamma ray, caliper, and gamma-gamma density. Interval averages of gamma-gamma density are plotted where values are outside error regions of BHG density and porosity.

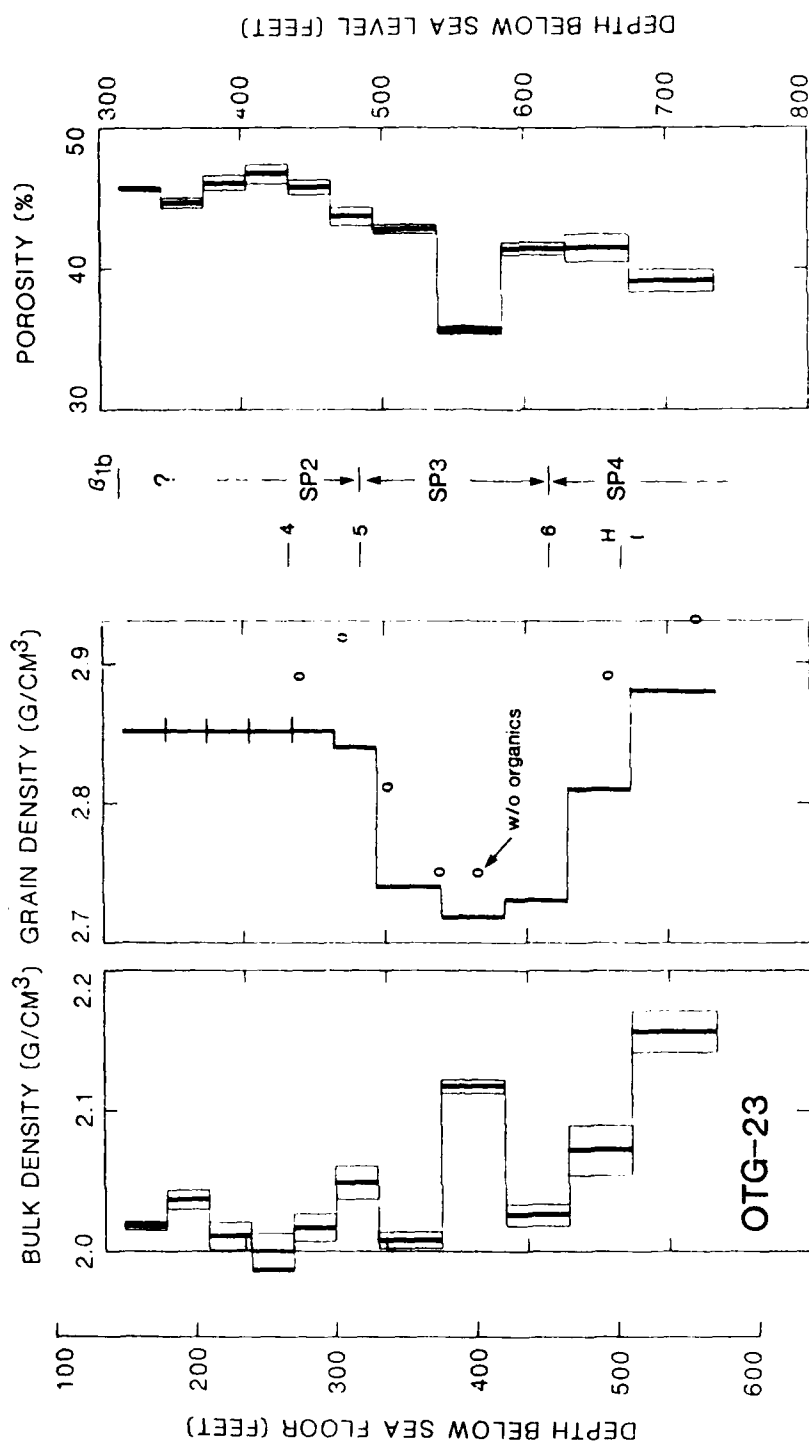


FIGURE 2-13. - BHG density, core and interval grain density, discontinuities and facies boundaries, sedimentary packages, and BHG porosity for borehole OTG-23 (left to right). No open-hole well logs were run.

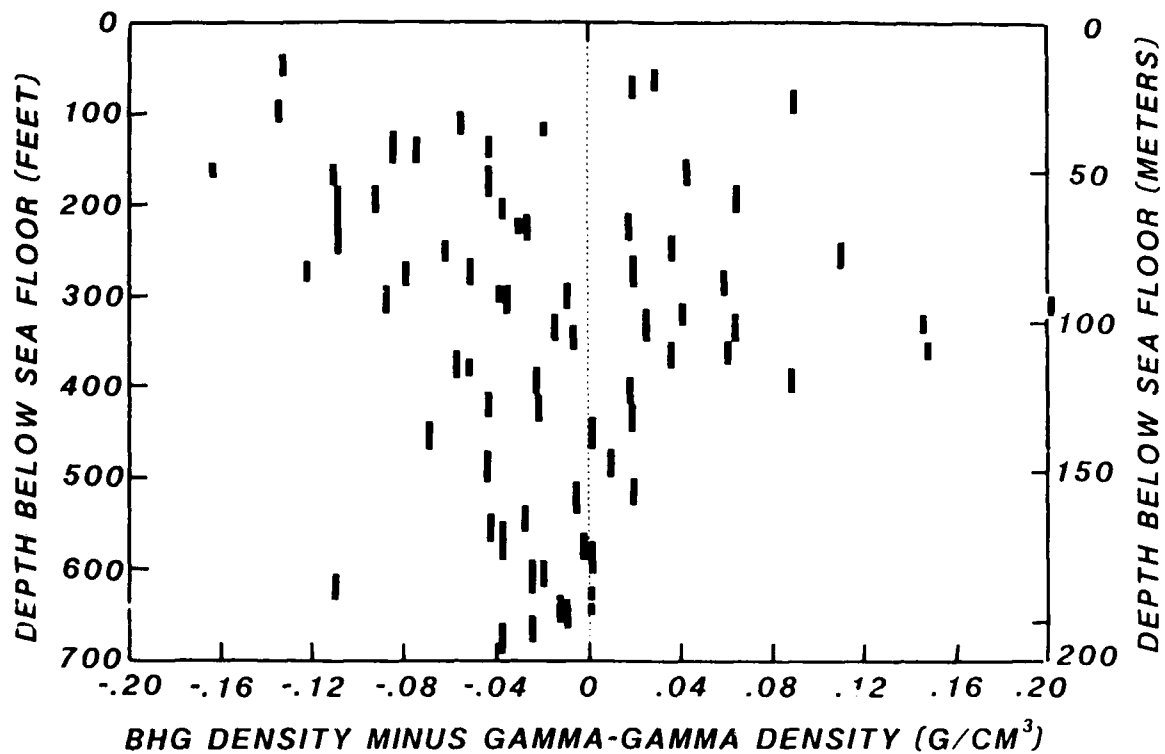


FIGURE 2-14. - Differences between BHG density and interval averages of gamma-gamma density versus depth below sea floor (bsf). Seventy differences are from boreholes OOR-17, OPZ-18, OQT-19, ORT-20 and OSR-21.

unsystematically from BHG density by as much as ± 10 percent at depths shallower than about 400 ft below the sea floor. At depths greater than about 500 ft below sea level, gamma-gamma density appears to vary from BHG density by about 2 percent or less.

Cross plots between BHG porosity and neutron porosity, gamma-gamma porosity and neutron porosity, and gamma-gamma porosity versus BHG porosity confirm that the neutron data are not adequate (fig. 2-15). These cross plots, along with Figure 2-14, emphasize the need for caution in the use of the gamma-gamma logs for quantitative density or porosity evaluation. Furthermore, bulk density and total porosity data derived from core measurements should be viewed skeptically if they differ significantly and systematically from corresponding BHG density and porosity.

NATURAL DENSITY AND POROSITY VARIATIONS OF ATOLL MATERIALS

Natural variations of density and porosity of atoll materials represent the background "noise" through which density and porosity changes caused by cratering phenomena must be determined. At the volume scale of core samples of several cubic feet, a broad range of values of densities and porosities from virtual sea-water-filled voids to dense crystalline carbonate is expected. At the volume scale of BHG studies (hundreds of thousands of cubic feet--an appropriate scale for studies of large craters), one expects the range of values of natural densities and porosities to narrow considerably because of the averaging effect. This is confirmed by the BHG surveys at OAK crater where the range of densities in reference boreholes OOR-17 and OSR-21 is not great.

At shallow depths in OOR-17, OSR-21, ORT-20 and OQT-19, density fluctuations are substantial but can be averaged to give nearly identical values (fig. 2-16). Based on the similarity of averaged BHG densities for OOR-17, OSR-21, ORT-20, and parts of OQT-19, the "noise" problem connected with natural density and porosity variations is believed to be small. However, close correspondence between individual BHG intervals from borehole to borehole can not be expected because of natural variations of density in porosity.

A general systematic relationship exists between BHG porosity and interval grain density based on data from reference boreholes OOR-17 and OSR-21 (fig. 2-17). Back reef sediments dominated by aragonite have higher porosities than sediments dominated by calcite. Effects on porosity caused by mechanical compaction and grain-size distribution and uncertainty about values of interval grain density may account for some or all of the scatter of points in Figure 2-17. Nevertheless, the rate of change of porosity with respect to aragonite content, as estimated by the dashed line, is almost identical to that found by Schmoker and Hester (1986) in a study of the late Pleistocene Miami Limestone. However, porosity values of the Miami Limestone are lower than Enewetak back-reef sediments by about 15 percent for equivalent aragonite content, emphasizing the different geologic settings of these two locations.

If bulk density is held constant, the mineral volume increase accompanying simple transformation of aragonite to calcite causes porosity to decrease by about 5 percent (line A in fig. 2-17). It is clear from Figure

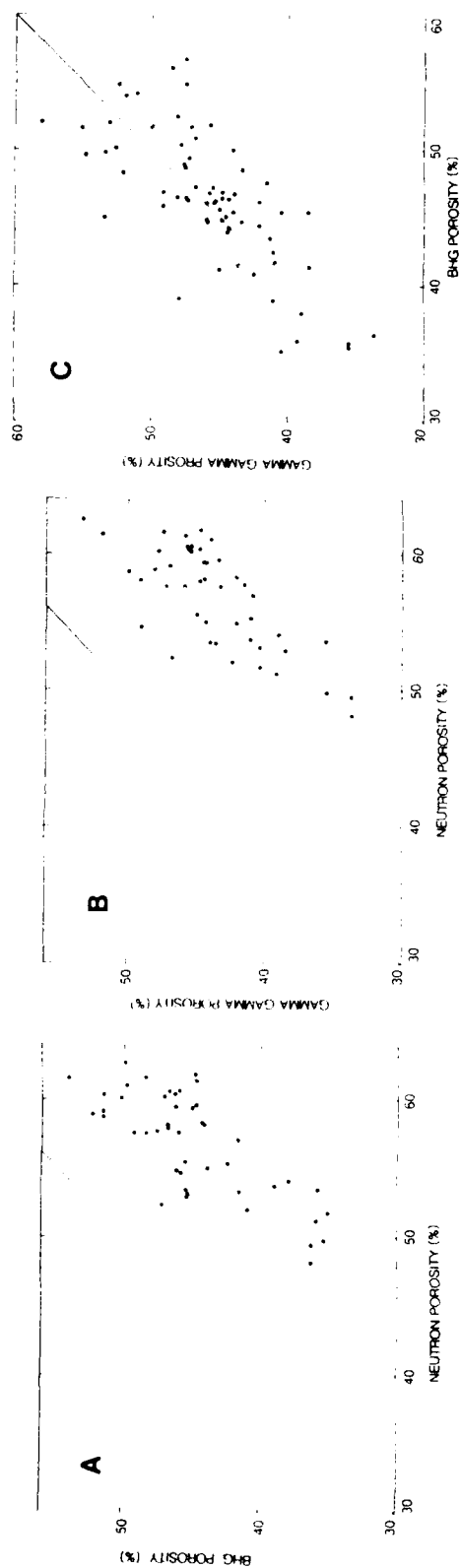


FIGURE 2-15. - Cross plot of BHG porosity and neutron porosity averaged over equivalent depth intervals
 (A). Cross plot of gamma-gamma porosity and neutron porosity, each averaged over BHG depth intervals
 (B). Cross plot of BHG porosity and gamma-gamma porosity averaged over equivalent depth intervals
 (C). Data are from columns 10, 13 and 14, Tables 2-2 through 2-7.

BLANK PAGE

A

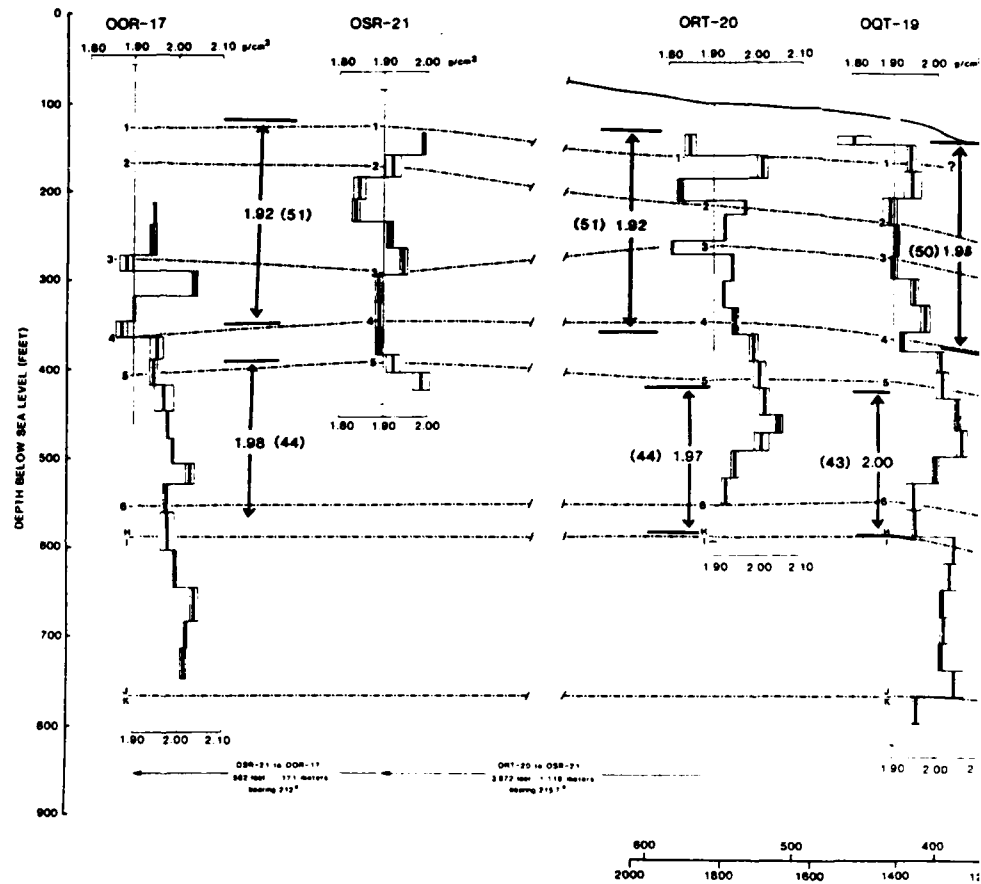


FIGURE 2-16. - Averages of BHG density and porosity fo

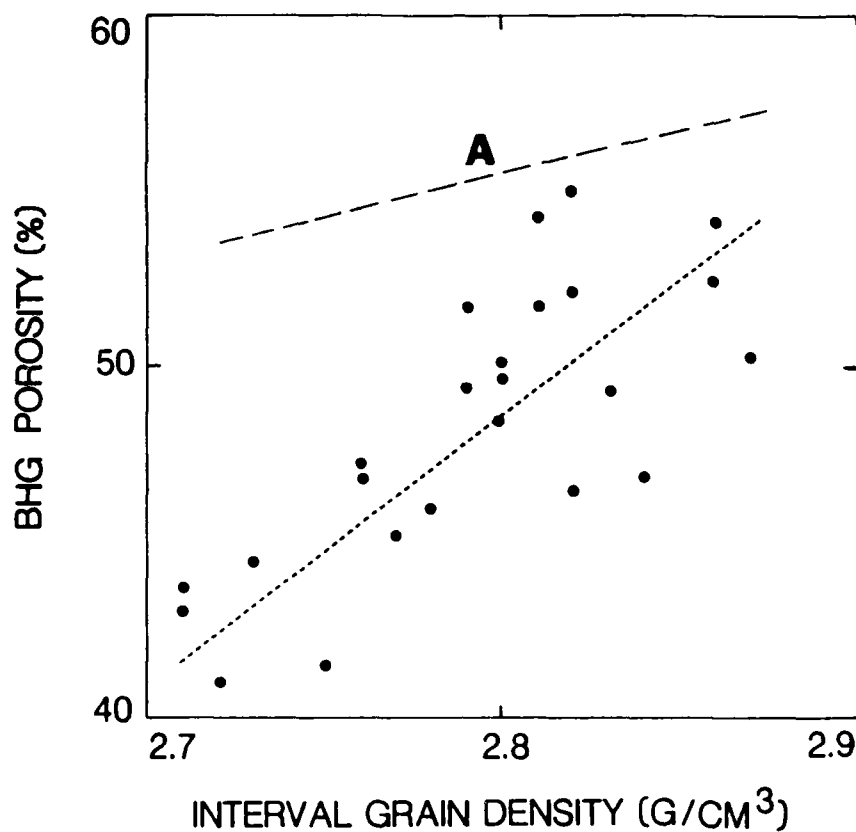


FIGURE 2-17. - Interval grain density versus BHG porosity. Data from reference boreholes OOR-17 and OSR-21. Line A shows decrease in porosity (due only to mineral volume increase) during transformation of an aragonite-bearing sediment to calcite-bearing sediment, assuming 100% aragonite sediment has porosity of 58.5%, and bulk-density is held constant.

2-17 that calcite solution and recrystallization, deposition of externally derived carbonate cement, some compaction, and other processes during well-documented cycles of atoll emergence and submergence (Ristvet and others, 1974; Tracey and Ladd, 1974) also have contributed to porosity loss in the back-reef sediments around OAK crater.

DENSITY, POROSITY, AND MASS CHANGES RELATED TO CRATERING PHENOMENA

A corrected BHG density and porosity model of the south-southwest transect of OAK crater is shown in Figure 2-18. This generalized model closely, but not exactly, follows the disconformity, facies changes, and geologic crater zone correlations defined by Wardlaw and Henry (1986a,b). The density elements of this model are based on the interval divisions of the BHG surveys that were selected during field work prior to knowledge of the exact downhole locations of the geologic boundaries. Intervals of BHG density and porosity have not been divided to correspond to the geologic boundaries because such divisions would be arbitrary in the absence of gravity station readings at the downhole locations of the geologic boundaries. Furthermore, BHG density and porosity are based on mass/volume characteristics that may or may not coincide with divisions based on the geologic characteristics of the sediments. This is clearly seen in Figure 2-5 where a significant number of major BHG density changes occur between, rather than at, the geologic boundaries defined by Wardlaw and Henry (1986a,b). Lack of exact depth correspondence of geologic and density/porosity models does not interfere with comparisons of geologically equivalent intervals between boreholes (figs. 2-16 and 2-19). (Application of the borehole gravity data to the geologic interpretation of OAK crater is expanded in Chapter 7 of the current Open-File report.)

A primary goal of the BHG phase of the PEACE Program was to determine if densification in crater-flank regions could account for observed sea-floor subsidence. BHG surveys were made in transition-zone boreholes OQT-19 and ORT-20 to investigate possible densification. There is considerable variation of BHG density and porosity in the upper parts of these boreholes but averages over larger intervals show that the sediments are not now appreciably denser than in the reference boreholes OOR-17 and OSR-21 (fig. 2-16).

Because documented subsidence of the sea floor at OQT-19 and ORT-20 cannot be explained by densification of the upper few hundred feet of underlying sediments alone, mass displacement from this region and densification of deeper materials probably occurred. Selective removal of finer fractions in this way could be investigated by comparing grain-size distributions of core samples from OQT-19 and the reference boreholes. Slight but definite densification and porosity decreases are present at greater depths in OQT-19 (figs. 2-16 and 2-19).

Unmistakable densification and porosity diminution are inferred in boreholes OTG-23 and beneath 292 ft below sea level in OPZ-18 (figs. 2-16 and 2-19). Independently documented mass transport (Wardlaw and Henry, 1986b) also can be quantified with the BHG density and porosity data. For example, the mass columns at OQT-19 and OPZ-18 are mass deficient by 3 to 5 percent and 6 to 8 percent, respectively, when compared to the mass column at reference

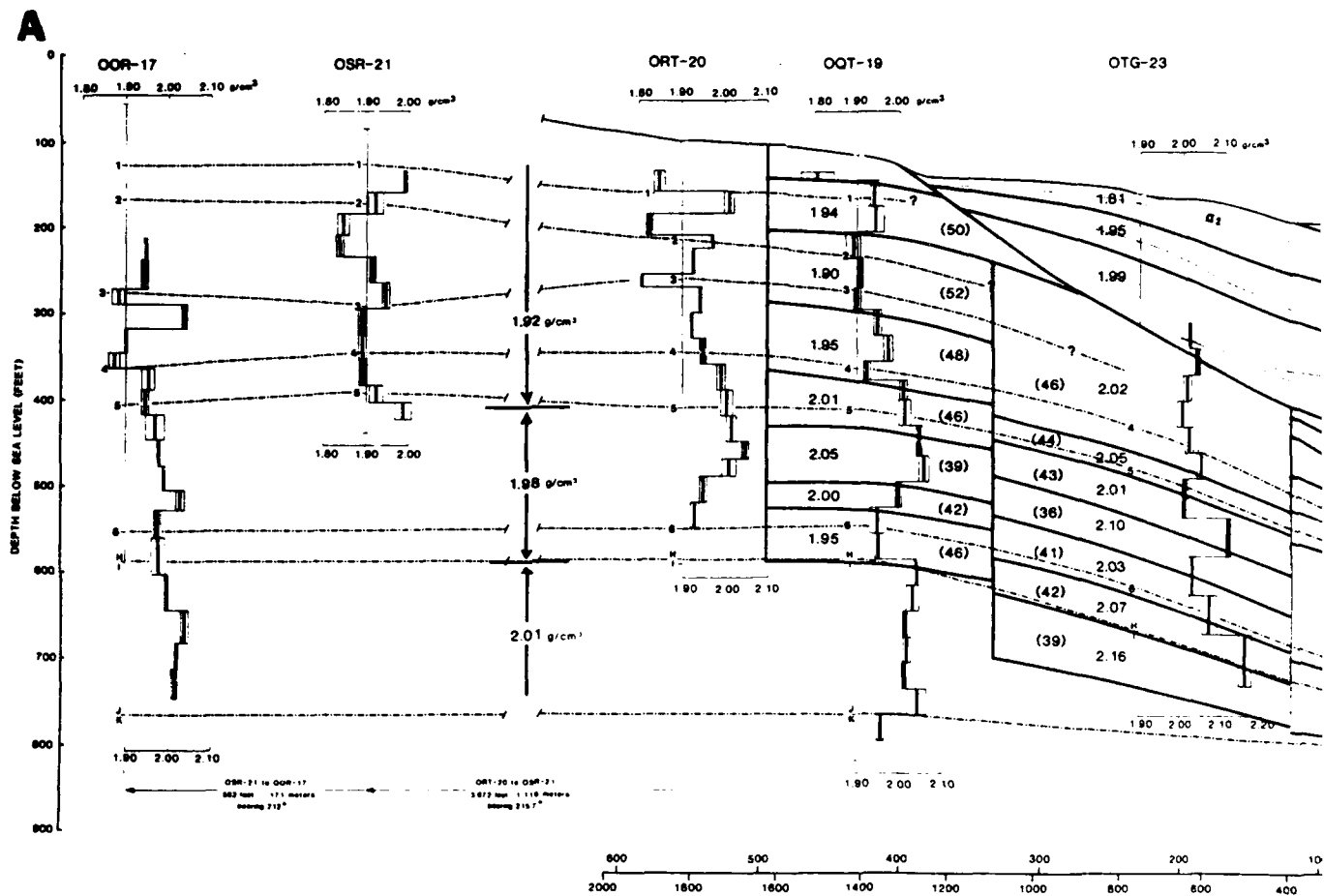
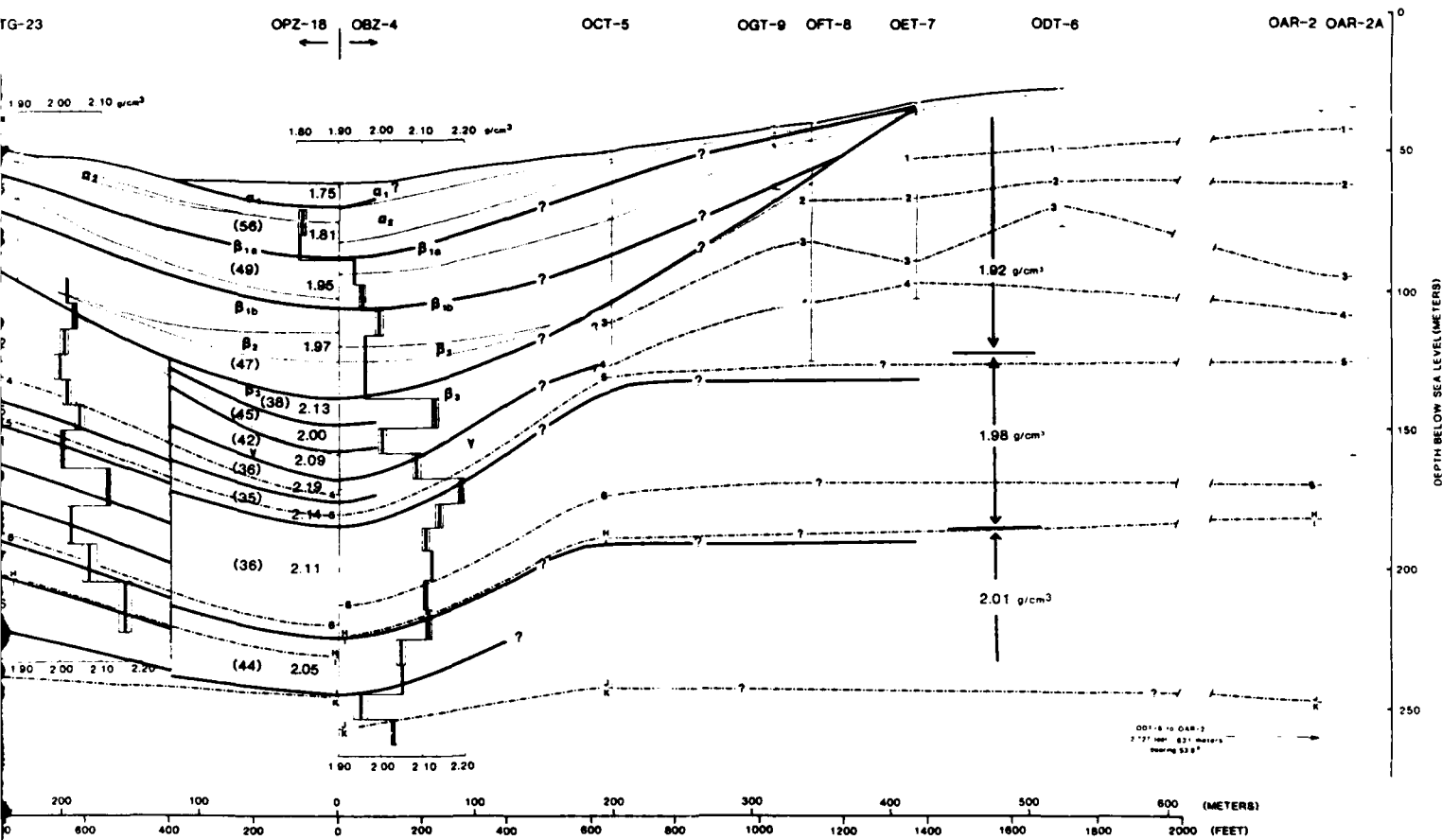


FIGURE 2-18 - BHG density and porosity model for south-southwe

B



south-southwest transect at OAK crater. Porosities are in parentheses.

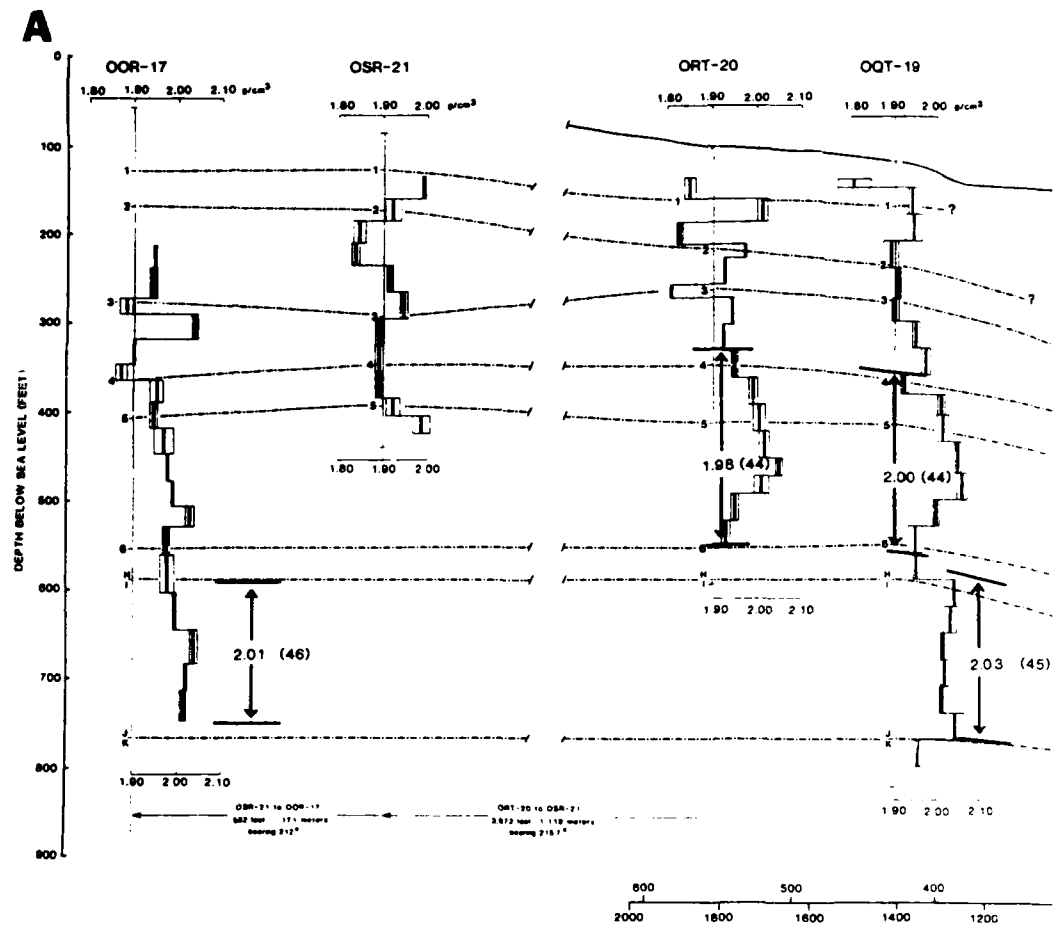
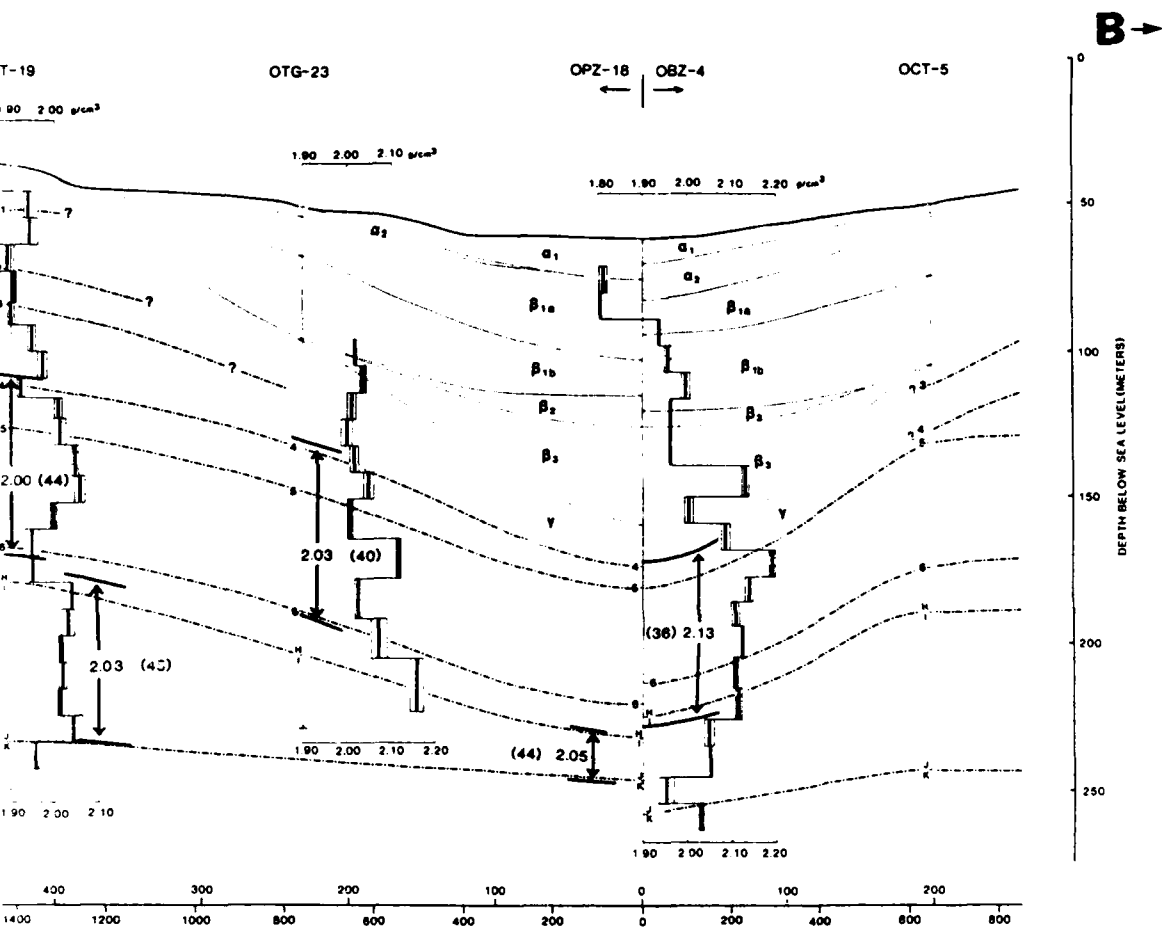


FIGURE 2-19 - Averages of BHG density and porosity for selected wells



ity for selected large intervals. Porosities are in parentheses.

boreholes OOR-17 and OSR-21. Density and porosity changes over the large intervals shown in Figures 2-16 and 2-19 are summarized in Table 2-9.

Many more types of comparisons are possible but are beyond the intent of this paper, which is to provide accurate representative density data and calculated porosity values for atoll materials at the six surveyed boreholes and to present a general density model of the crater.

SUMMARY

Borehole gravity surveys were conducted at OAK crater to obtain accurate large-volume estimates of in situ bulk-density and total porosity of atoll materials beneath and beyond the crater. Reliable density and porosity measurements of undisturbed atoll materials provide important geologic information about these young, loosely consolidated back-reef sediments, and predictions of pre-event material-property conditions for nuclear event calculations. Accurate measurements of differences between the density and porosity of undisturbed atoll materials and the sediment and rock involved in the excavational and apparent OAK craters are crucial to understanding the cratering phenomena at OAK and the mechanics of large crater formation.

Six boreholes were drilled and successfully logged with a borehole gravity meter along a 6,000-foot southwest transect from the bathymetric center of OAK crater (fig. 2-2). Gravity measurements were made in these cased boreholes, generally at spacings of 20 to 35 ft. To obtain reference values for the density and porosity of undisturbed reef-forming material for comparison with material disturbed by cratering processes, gravity surveys were conducted in boreholes OSR-21 and OOR-17, separated by 562 ft, and located approximately 5,500 and 6,050 ft south-southwest of the bathymetric center of OAK crater. Possible densification caused by suspected subsidence on the crater flank just outside the excavational crater was investigated by gravity surveys made in boreholes OQT-19 and ORT-20. These boreholes were separated laterally by 404 ft, and located approximately 1,400 and 1,800 ft south-southwest of the bathymetric center of OAK crater. Gravity surveys were made in borehole OPZ-18 at the bathymetric center of OAK crater, and in OTG-23 located 759 ft south-southwest of OPZ-18 to measure densification beneath the excavational crater and the density of fill within the excavational crater.

The ability of BHG surveys to determine subtle density differences between reef materials located at different locations inside and outside OAK crater depends crucially on the precision of field measurements. Consequently, great effort was devoted to insure that requisite precisions were achieved (Beyer, Ristvet, and Oberste-Lehn, 1986). Repeated measurements show that the precision of BHG densities averages about .01 g/cm³, which is fully adequate for the purposes of the OAK study (fig. 2-3).

BHG measurements permit examination of large volumes of material surrounding the borehole, which means that larger-scale, more distant, lateral density changes are sensed, along with smaller-scale, local density changes that occur within tens to a few hundred feet of the borehole. To obtain BHG density and porosity of atoll materials immediately surrounding each borehole, corrections were calculated and applied for: (1) submarine topography out to a distance of 103 statute miles using bathymetric charts of various scales

(Beyer, Ristvet, and Oberste-Lehn, 1986); (2) generalized two-dimensional density variations associated with large-scale facies changes and diagenesis across the reef margin (fig. 2-4); and (3) generalized three-dimensional density changes due to cratering processes (fig. 2-7). Corrections range from .067 to .156 g/cm³ for submarine topography, .018 to .025 g/cm³ for two-dimensional density variations across the atoll margin, and +.025 to -.021 g/cm³ for generalized three-dimensional density changes due to cratering (tables 2-1 through 2-7).

The following conclusions can be drawn from the corrected BHG densities (fig. 2-5), the derived crater density model (fig. 2-18), and comparisons of corrected BHG density and porosity of geologically equivalent intervals along the south-southwest transect from OOR-17 to OPZ-18 (figs. 2-16 and 2-19):

1. Large natural variations of density and porosity of atoll materials are well-known from numerous geological observations at scales of cubic inches to hundreds of cubic feet. Serious concern was expressed prior to this study that these natural variations of density and porosity would obscure those due to cratering phenomena. The shallow portions of the BHG density profiles from OOR-17, OSR-21, ORT-20, and OQT-19 suggest that this concern may be well-founded when attempting to compare shallow vertical intervals in different boreholes that are on the order of tens of feet thick (fig. 2-5). However, averages of BHG densities over larger vertical intervals show that natural variations of density and porosity tend to average out so that valid lateral comparisons of geologically equivalent intervals can be made (figs. 2-16 and 2-19). Also, over the depths surveyed in OAK boreholes, the range of natural variation of density and porosity appears to decrease slightly with depth, allowing valid comparisons of smaller vertical intervals with increasing depth (fig. 2-5). These results are based solely on BHG surveys made on a trend nearly parallel to the reef along which facies and density changes are believed to be minimal.
2. The shallow section beneath the crater-flank region penetrated by OQT-19 and ORT-20 is not appreciably denser than the equivalent section penetrated by the more distant reference boreholes OOR-17 and OSR-21 (fig. 2-16). Crater-flank subsidence in this area cannot be explained by densification of this shallow section, but probably involved mass removal and densification of a larger vertical interval. Slight densification is evident at greater depth in OQT-19 but cannot be confirmed at greater depth in ORT-20 (figs. 2-16 and 2-19).
3. Atoll material penetrated by OTG-23 within the excavational crater is significantly denser over the surveyed intervals than the geologically equivalent sections penetrated by reference boreholes OPR-17 and OSR-21 and crater flank boreholes ORT-20 and OQT-19 (figs. 2-16, 2-18, and 2-19). Porosity reduction also has occurred as a result of cratering processes.
4. At the bathymetric center of OAK crater, the section penetrated by OPZ-18 is dominated by cratering effects. Major discontinuities of BHG density and porosity occur midway through crater zones β_{1a} and β_3 . Beneath the second discontinuity midway through zone β_3 , and extending at least to the J/K biostratigraphic boundary, a large amount of densification and porosity reduction has resulted from cratering processes (figs. 2-16 and

2-19). In the lower part of this densified interval, the low BHG densities compared to the indicated thinning of geologic units means that major amounts of mass have been removed (fig. 2-19). Densification and/or mass removal appears to extend beneath the depth of the BHG survey in OPZ-18, and may be evaluated by careful study of the lower portions of the gamma-gamma density logs from OAM-1/OAR-2, OBZ-4, OCT-5, and OOR-17.

5. Mass deficiencies of about 3 to 5 percent at OQT-19, and 6 to 8 percent at OPZ-18 are indicated from mass column calculations that utilize BHG densities at OOR-17, OQT-19, and OPZ-18.

Other conclusions of this study are as follows:

1. In reference boreholes OOR-17 and OSR-21, back-reef sediments dominated by aragonite have higher porosities than materials dominated by calcite (fig. 2-17). The mineral volume increase that accompanies the transformation of aragonite to calcite is not sufficient to explain the observed decrease in porosity. Not surprisingly, other diagenetic processes, such as calcite solution and recrystallization and deposition of externally derived carbonate cement, must have contributed to (or dominated) the observed natural decrease of porosity that accompanies the transformation of aragonite to calcite in these back-reef materials.
2. The BHG survey in the E-1 borehole on Medrin (ELMER) Island provided BHG densities of the shallow section that differed only slightly from those measured across Enewetak Atoll at OAK crater (figs. 2-1 and 2-20). BHG densities of the deeper section in the E-1 borehole were important to the construction of the two-dimensional density model of the reef argin (fig. 2-4). The BHG survey in the E-1 borehole also revealed a cyclical pattern of density and porosity that may be due to diagenesis caused by repeated periods of atoll emergence and submergence since middle Miocene (fig. 2-20).
3. BHG measurements permit examination of volumes of materials measured in hundreds of thousands of cubic feet. Unlike conventional, shallow penetration gamma-gamma and neutron logging methods, the large volume of material examined by the BHG method makes it immune to formation damage or borehole rugosity that commonly occurs when drilling through loosely consolidated, highly permeable strata or alternating soft and hard beds. Not unexpectedly, BHG density and porosity in the OAK study are about an order of magnitude more reliable than the next most reliable density or porosity logging method, the gamma-gamma density log, at depths less than about 400 ft below the sea floor in the five OAK boreholes where comparisons were possible (figs. 2-8 through 2-12, 2-14, and 2-15).

This first BHG study of the carbonate deposits of an atoll island and of the materials beneath a large nuclear crater affirms the unique ability of borehole gravimetry to evaluate the density and porosity of heterogeneous and/or loosely consolidated geologic formations.

ACKNOWLEDGEMENTS

I am especially indebted to several key people. D. Oberste-Lehn, of R & D Associates, one of several people who initially recognized the potential value of borehole gravity surveys to the PEACE Program, solicited my involvement and worked closely with me during the past several years. Her persistent questions, stimulating ideas, and material support have been invaluable. Crucial leadership and considerable effort during the difficult field surveys were very ably provided by B. L. Ristvet of S-Cubed, Inc. Early recognition of the value of BHG surveys and strong backing from within the cratering community came from J. G. Trulio of Applied Theory, Inc. I also benefited greatly from information provided at various stages by J. J. Daniels, J. A. Grow, R. B. Halley, J. C. Hampson, T. W. Henry, L. S. Melzer, B. L. Ristvet, E. L. Tremba, J. G. Trulio, and B. R. Wardlaw.

REFERENCES

- Beyer, L. A., 1968, Recent tests of the United States Geological Survey -- La Coste and Romberg borehole gravimeter system (abs.): *Geophysics*, v. 33, no. 6, p. 1030.
- Beyer, L. A., and Corbato, C. E., 1972, A FORTRAN IV computer program for calculating borehole gravity terrain corrections: U.S. Geological Survey Open-File Report, 30 p.; available as report PB-208-679 from National Technical Information Service, Springfield, Virginia.
- Beyer, L. A., Ristvet, B. L., and Oberste-Lehn, D., 1986, Chapter 8: Preliminary density and porosity data and field techniques of borehole gravity surveys, OAK crater: 28 p., 4 figs., 10 tbls.; in Henry, T. W., and Wardlaw, B. R., eds., *Pacific Enewetak Atoll Crater Exploration (PEACE) Program. Enewetak Atoll, Republic of the Marshall Islands; Part 3: Stratigraphic analysis and other geologic and geophysical studies in vicinity of OAK and KOA craters*: U.S. Geological Survey Open-File Report 86-555.
- Black, A. J., and Herring, A. T., 1983, Borehole gravity: Expanded operating limits and performance: Expanded Abstracts with Bibliographies, 1983 Technical Program, 53rd Annual International Society of Economic Geologists Meeting, September 11-15, 1983, Las Vegas, Nevada, p. 21-33.
- Buigues, D., 1985, Principal facies and their distribution at Mururoa Atoll: *Proceedings of the Fifth International Coral Reef Congress*, v. 3, p. 249-255.
- Couch, R. F., Jr., Fetzer, J. A., Goter, E. K., Ristvet, B. L., Tremba, E. L., Walter, D. R., and Wendland, V. P., 1975, Drilling operations on Eniwetok Atoll during Project EXPOE: Air Force Weapons Laboratory Technical Report AFWL-TR-75-216, Kirtland Air Force Base, New Mexico, 270 p., 17 figs., 4 tbls. [Unclassified].

- Folger, D. W., ed., 1986a, Sea-floor observations and subbottom seismic characteristics of OAK and KOA craters, Enewetak Atoll, Marshall Islands: U.S. Geological Survey Bulletin 1678, 301 p., 112 figs., glossary, 2 appendices.
- Henry, T. W., Wardlaw, B. R., Skipp, Betty, Major, R. P., and Tracey, J. I., Jr., 1986, Pacific Enewetak Atoll Crater Exploration (PEACE) Program; Part 1: Drilling operations and descriptions of boreholes in vicinity of KOA and OAK craters: U.S. Geological Survey Open-File Report 86-419, 497 p., 32 figs., 29 pls., 13 tbls., 3 appendices.
- Holloway, G. L., and Young, A. G., 1986, Appendix II: Geotechnical Investigations, Phase II of PEACE Program: 29 p., 16 figs., 36 pls.; in Henry, T. W., Wardlaw, B. R., Skipp, Betty, Major, R. P., and Tracey, J. I., Jr., 1986, Pacific Enewetak Atoll Crater Exploration (PEACE) Program; Part 1: Drilling operations and descriptions of boreholes in vicinity of KOA and OAK craters: U.S. Geological Survey Open-File Report 86-419.
- Ladd, H. S., Ingerson, E., Townsend, R. D., Russell M., and Stephenson, n. K., 1953, Drilling on Eniwetok Atoll, Marshall Islands: Bulletin of the American Association of Petroleum Geologists, v. 37, no. 10, p. 2257-2280.
- Ladd, H. S., and Schlanger, S. O., 1960, Drilling operations on Eniwetok Atoll: U.S. Geological Survey Professional Paper 260-Y, p. 863-903, pls. 255-256, figs. 260-287, 3 tbls.
- Plouff, D., 1976, Gravity and magnetic fields for polygonal prisms and application to magnetic terrain corrections: Geophysics, v. 41, no. 4, p. 727-741.
- Ristvet, B. L., Couch, R. F., Jr., Fetzer, J. D., Goter, E. R., Tremba, E. L., Walter, D. R., and Wendland, V. P., 1974, A Quaternary diagenetic history of Eniwetok Atoll: Geological Society of America Abstracts with Programs, v. 6, p. 928-929.
- Ristvet, B. L. and Tremba, E. L., 1986, Chapter 5: Total organic content of lagoon benthic sediments and of submarine samples from the PEACE drilling program: 9 p., 2 figs., 2 tbls.; in Henry, T. W., and Wardlaw, B. R., eds., Pacific Enewetak Atoll Crater Exploration (PEACE) Program, Enewetak Atoll, Republic of the Marshall Islands; Part 3: Stratigraphic analysis and other geologic and geophysical studies in vicinity of OAK and KOA craters: U.S. Geological Survey Open-File Report 86-555.
- Schmoker, J. W., and Hester, T. C., 1986, Porosity of the Miami Limestone (Late Pleistocene), Lower Florida Keys: Journal of Sedimentary Petrology, v. 56, no. 5, p. 629-634.
- Talwani, M., Worzel, J. L., and Landisman, M., 1959, Rapid gravity computations for two-dimensional bodies with application to the Mendocino submarine fracture zone: Journal of Geophysical Research, v. 64, no. 1, p. 49-59.

Tracey, J. I., Jr., and Ladd, H. S., 1974, Quaternary History of Eniwetok and Bikini Atolls, Marshall Islands: Proceedings of the Second International Symposium on Coral Reefs, Great Barrier Reef Committee, Brisbane, Australia, p. 537-550, 15 figs., 3 tpls.

Tremba, E. L. and Ristvet, B. L., 1986, Chapter 4: X-ray diffraction mineralogy: 49 p., 11 figs., 35 tpls.; in Henry, T. W., and Wardlaw, B. R., eds., Pacific Enewetak Atoll Crater Exploration (PEACE) Program, Enewetak Atoll, Republic of the Marshall Islands; Part 3: Stratigraphic analysis and other geologic and geophysical studies in vicinity of OAK and KOA craters: U.S. Geological Survey Open-File Report 86-555.

Wardlaw, B. R. and Henry, T. W., 1986a, Chapter 2: Physical stratigraphic framework: 36 p., 10 figs., 2 tpls.; in Henry, T. W. and Wardlaw, B. R., eds., Pacific Enewetak Atoll Crater Exploration (PEACE) Program, Enewetak Atoll, Republic of the Marshall Islands; Part 3: Stratigraphic analysis and other geologic and geophysical studies in vicinity of OAK and KOA craters: U.S. Geological Survey Open-File Report 86-555.

Wardlaw, B. R. and Henry, T. W., 1986b, Chapter 14: Geologic interpretation of OAK and KOA craters: 39 p., 21 figs., 2 tpls.; in Henry, T. W. and Wardlaw, B. R., eds., Pacific Enewetak Atoll Crater Exploration (PEACE) Program, Enewetak Atoll, Republic of the Marshall Islands; Part 3: Stratigraphic analysis and other geologic and geophysical studies in vicinity of OAK and KOA craters: U.S. Geological Survey Open-File Report 86-555.

TABLE 2-1. -- Range of corrections for lateral density changes calculated from submarine topography and density models for six BHG surveys at OAK Crater.

Borehole	Range of Corrections Expressed in g/cm ³ Due to		
	Submarine Topography	Large-Scale Lateral Density Changes Across Reef Margin	Smaller-Scale Lateral Density Changes Related to Cratering Processes
OOR-17	.156 to .144	.021 to .019	negligible
OPZ-18	.118 to .067	.025 to .021	.025 to -.021
OQT-19	.145 to .135	.024 to .020	.008 to -.004
ORT-20	.140 to .130	.023 to .020	.005 to -.005
OSR-21	.137 to .126	.020 to .018	negligible
OTG-23	.122 to .108	.022 to .024	.019 to .014

TABLE 2-2.--(on adjacent page) Bulk density, porosity, and grain density obtained from borehole gravity, gamma-gamma, and neutron measurements in borehole OOR-17 and from analysis of cores taken from OOR-17. Gamma-gamma and neutron data averages over depth intervals of BHG survey. Grain densities were calculated by the procedure described in Appendix 2-1 using data from Tremba and Ristvet (1986) and Ristvet and Tremba (1986).




TABLE 2-2.

	1	2	3	4	5	6	7	8	9	10	11	12	13	14
212.-237.		1.772	.003	.156	.019	0.	1.947	2.87	.02	50.2	0.2	1.99	47.8	60.2
237.-271.		1.769	.008	.155	.019	0.	1.943	2.83	.02	49.3	0.4	1.98	47.2	57.6
271.-289.		1.709	.015	.154	.019	0.	1.882	2.79	.02	51.6	0.9	1.91	50.0	58.8
289.-317.		1.864	.006	.153	.019	0.	2.036	2.75	.02	41.5	0.3	2.00	43.6	53.3
317.-345.		1.730	.003	.152	.019	0.	1.901	2.86	.02	52.4	0.2	1.98	48.1	58.9
345.-363.		1.700	.013	.152	.020	0.	1.872	2.86	.02	54.0	0.7	1.91	51.9	61.5
363.-388.		1.780	.015	.151	.020	0.	1.951	2.76	.04	46.8	0.9	1.91	49.1	58.1
388.-417.		1.774	.009	.150	.020	0.	1.944	2.76	.04	47.2	0.5	1.95	46.8	52.3
417.-446.		1.798	.022	.149	.020	0.	1.967	2.76	.04	45.8	1.3	1.91	49.1	54.6
446.-477.		1.807	.003	.149	.020	0.	1.976	2.71	.02	43.7	0.2	0.	0.	0.
477.-505.		1.819	.001	.148	.020	0.	1.987	2.71	.02	43.0	0.1	0.	0.	0.
505.-528.		1.860	.010	.147	.020	0.	2.027	2.72	.02	41.0	0.6	0.	0.	0.
528.-560.		1.807	.008	.147	.020	0.	1.974	2.73	.02	44.5	0.5	0.	0.	0.
560.-603.		1.809	.016	.146	.021	0.	1.976	2.78	.02	45.9	0.9	0.	0.	0.
603.-645.		1.826	.004	.146	.021	0.	1.993	2.84	.02	46.8	0.2	2.03	44.8	58.0
645.-683.		1.870	.009	.145	.021	0.	2.036	2.85	.02	44.7	0.5	2.06	43.4	59.6
683.-713.		1.852	.004	.145	.021	0.	2.018	2.86	.02	46.0	0.2	2.03	45.4	60.6
713.-747.		1.848	.007	.144	.021	0.	2.013	2.86	.02	46.3	0.4	2.05	44.3	59.4

Column 1	Depth interval in feet below sea level
Column 2	Apparent BHG density in g/cm ³ (corrected for instrument calibration and drift and earth tides).
Column 3	Standard deviation of repeated 1g/2z measurements expressed in g/cm ³ .
Column 4	Vertical gravity gradient correction (expressed in g/cm ³) for submarine topography out to a radial distance of 103.5 statute miles (166.7 kilometers). Correction calculated by replacing sea water with density of 1.90 g/cm ³ (see Beyer and Corbato, 1972).
Column 5	Vertical gravity gradient correction expressed in g/cm ³ for lateral density changes (assumed to be two-dimensional) caused by geologic facies changes across the reef (see Figure 2.4).
Column 6	Vertical gravity gradient correction (expressed in g/cm ³) for lateral density changes caused by crater-related processes and assumed to be symmetrical about 0pg-18 (see Figure 2.7).
Column 7	BHG density in g/cm ³ after correction for submarine topography and lateral density variations due to geologic facies changes and cratering processes.
Column 8	Mean grain density for depth interval in g/cm ³ (calculated from mineral and organic content percentages estimated from x-ray diffraction and loss-on-ignition analyses (see Appendix 2.2)).
Column 9	Estimated uncertainty in mean grain density in g/cm ³ .
Column 10	BHG porosity in percent calculated from BHG density (column 7), grain density (column 8) and sea-water density of 1.03 g/cm ³ .
Column 11	Uncertainty in BHG porosity in percent calculated from standard deviation of BHG density (column 4) and uncertainty in mean grain density (column 9).
Column 12	Average gamma-gamma density for depth interval in g/cm ³ .
Column 13	Gamma-gamma porosity in percent calculated from gamma-gamma density (column 12), grain density (column 8) and sea-water density of 1.03 g/cm ³ .
Column 14	Average neutron porosity for depth interval in percent.

TABLE 2-3.--(on adjacent page) Bulk density, porosity, and grain density obtained from borehole gravity, gamma-gamma, and neutron measurements in borehole OPZ-18 and from analysis of cores taken from OPZ-18. Gamma-gamma and neutron data averages over depth intervals of BHG survey. Grain densities were calculated by the procedure described in Appendix 2-1 using data from Tremba and Ristvet (1986) and Ristvet and Tremba (1986).




TABLE 2-3.

1	2	3	4	5	6	7	8	9	10	11	12	13	14
232.-262.	1.729	.009	.067	.021	-.005	1.812	2.81	.02	56.1	0.5	0.	0.	0.
262.-292.	1.719	.001	.073	.021	-.006	1.807	2.83	.02	56.8	0.1	0.	0.	0.
292.-322.	1.844	.001	.077	.021	-.005	1.937	2.84	.02	49.9	0.1	0.	0.	0.
322.-352.	1.861	.008	.080	.021	-.006	1.956	2.83	.02	48.6	0.4	0.	0.	0.
352.-382.	1.892	.010	.084	.022	-.001	1.997	2.82	.02	46.0	0.6	0.	0.	0.
382.-457.	1.871	.	.090	.022	-.021	1.962	2.81	.02	47.6	0.	2.07	41.6	57.8
457.-492.	1.997	.008	.095	.022	0.016	2.130	2.80	.02	37.9	0.5	2.11	39.0	54.0
492.-522.	1.881	.010	.098	.022	0.002	2.003	2.81	.02	45.3	0.6	2.09	40.4	53.1
522.-552.	1.958	.010	.100	.023	0.005	2.086	2.84	.02	41.7	0.6	2.10	40.9	57.0
552.-582.	2.046	.007	.103	.023	0.019	2.191	2.84	.02	35.9	0.4	2.13	39.2	51.2
582.-610.	1.991	.009	.105	.023	0.020	2.139	2.74	.02	35.1	0.5	2.05	40.4	51.7
610.-637.	1.957	.009	.107	.023	0.020	2.107	2.72	.02	36.3	0.5	2.15	33.7	48.1
637.-672.	1.968	.003	.109	.024	0.021	2.122	2.72	.02	35.4	0.2	2.12	35.5	49.8
672.-707.	1.950	.005	.111	.024	0.022	2.107	2.72	.02	36.3	0.3	2.15	33.7	49.5
707.-742.	1.953	.007	.113	.024	0.025	2.115	2.72	.02	35.8	0.4	2.12	35.5	53.5
742.-772.	1.889	.011	.114	.024	0.021	2.048	2.86	.02	44.4	0.6	2.09	42.1	58.3
772.-807.	1.891	.002	.116	.024	0.021	2.052	2.86	.02	44.2	0.1	2.05	44.3	58.1
807.-837.	1.789	.017	.117	.024	0.021	1.951	2.87	.02	49.9	0.9	2.06	44.0	61.1
837.-867.	1.868	.006	.118	.025	0.020	2.031	2.85	.02	45.0	0.3	2.04	44.5	59.4

Column 1	Depth interval in feet below sea level
Column 2	Apparent BHG density in g/cm ³ (corrected for instrument calibration and drift and earth tides).
Column 3	Standard deviation of repeated $\Delta g/\Delta z$ measurements expressed in g/cm ³ .
Column 4	Vertical gravity gradient correction (expressed in g/cm ³) for submarine topography out to a radial distance of 103.5 statute miles (166.7 kilometers). Correction calculated by replacing sea water with density of 1.90 g/cm ³ (see Beyer and Corbato, 1972).
Column 5	Vertical gravity gradient correction expressed in g/cm ³ for lateral density changes (assumed to be two-dimensional) caused by geologic facies changes across the reef (see Figure 2.4).
Column 6	Vertical gravity gradient correction (expressed in g/cm ³) for lateral density changes caused by crater-related processes and assumed to be symmetrical about 082-18 (see Figure 2.7).
Column 7	BHG density in g/cm ³ after correction for submarine topography and lateral density variations due to geologic facies changes and cratering processes.
Column 8	Mean grain density for depth interval in g/cm ³ (calculated from mineral and organic content percentages estimated from x-ray diffraction and loss-on-ignition analyses (see Appendix 2.2)).
Column 9	Estimated uncertainty in mean grain density in g/cm ³ .
Column 10	BHG porosity in percent calculated from BHG density (column 7), grain density (column 8) and sea-water density of 1.03 g/cm ³ .
Column 11	Uncertainty in BHG porosity in porosity percent (calculated from standard deviation of BHG density (column 4) and uncertainty in mean grain density (column 8)).
Column 12	Average gamma-gamma density for depth interval in g/cm ³ .
Column 13	Gamma-gamma porosity in percent calculated from gamma-gamma density (column 12), grain density (column 8) and sea-water density of 1.03 g/cm ³ .
Column 14	Average neutron porosity for depth interval in percent.

TABLE 2-4.--(on adjacent page) Bulk density, porosity, and grain density obtained from borehole gravity, gamma-gamma, and neutron measurements in borehole OQT-19 and from analysis of cores taken from OQT-19. Gamma-gamma and neutron data averages over depth intervals of BHG survey. Grain densities were calculated by the procedure described in Appendix 2-1 using data from Tremba and Ristvet (1986) and Ristvet and Tremba (1986).

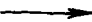


TABLE 2-4.

	1	2	3	4	5	6	7	8	9	10	11	12	13	14
138.-148.		1.646	.038	.145	.020	-.004	1.807	2.84	.02	57.1	2.1	0.	0.	0.
148.-178.		1.777	.010	.140	.020	0.002	1.939	2.85	.02	50.1	0.5	0.	0.	0.
178.-208.		1.787	.020	.134	.021	0.	1.942	2.83	.02	49.3	1.1	0.	0.	0.
208.-238.		1.737	.017	.132	.021	0.	1.890	2.83	.02	52.2	0.9	0.	0.	0.
238.-273.		1.753	.006	.131	.021	0.001	1.906	2.84	.02	51.6	0.3	1.99	47.0	59.1
273.-298.		1.747	.008	.131	.021	0.001	1.900	2.83	.02	51.7	0.4	2.01	45.6	60.4
298.-328.		1.791	.009	.131	.021	0.005	1.948	2.81	.02	48.4	0.5	2.04	43.3	57.6
328.-358.		1.814	.011	.131	.022	0.005	1.972	2.81	.02	47.1	0.6	2.00	45.5	60.2
358.-380.		1.764	.008	.132	.022	0.004	1.922	2.81	.02	49.9	0.4	1.86	53.4	62.6
380.-403.		1.846	.009	.132	.022	0.008	2.008	2.82	.02	45.4	0.5	2.13	38.5	52.8
403.-433.		1.849	.014	.132	.022	0.008	2.011	2.83	.02	45.5	0.8	2.02	45.0	55.4
433.-468.		1.885	.007	.132	.022	0.007	2.046	2.75	.02	40.9	0.4	2.02	42.4	52.0
468.-498.		1.897	.012	.133	.022	0.004	2.056	2.71	.02	38.9	0.7	2.02	41.1	53.7
498.-528.		1.842	.007	.133	.022	0.001	1.998	2.71	.02	42.4	0.4	2.02	41.1	55.3
528.-558.		1.792	.017	.133	.023	0.	1.948	2.71	.02	45.4	1.0	1.97	44.0	53.5
558.-588.		1.793	.008	.134	.023	0.001	1.951	2.74	.02	46.1	0.5	2.02	42.1	54.8
588.-618.		1.882	.002	.134	.023	0.001	2.040	2.83	.02	43.9	0.1	2.03	44.4	54.9
618.-648.		1.874	.015	.134	.023	-.001	2.030	2.84	.02	44.8	0.8	2.01	45.9	61.4
648.-678.		1.858	.005	.134	.023	-.002	2.013	2.86	.02	46.3	0.3	2.04	44.8	60.4
678.-708.		1.861	.009	.135	.024	-.002	2.018	2.86	.02	46.0	0.5	2.02	45.9	57.6
708.-738.		1.854	.005	.135	.024	-.002	2.011	2.87	.02	46.7	0.3	2.03	45.7	60.5
738.-768.		1.884	.022	.135	.024	-.002	2.041	2.86	.02	44.8	1.2	2.04	44.8	61.8
768.-798.		1.799	.008	.135	.024	-.002	1.956	2.84	.02	48.8	0.4	1.98	47.5	61.7

Column 1 Depth interval in feet below sea level

Column 2 Apparent BHG density in g/cm^3 (corrected for instrument calibration and drift and earth tides).

Column 3 Standard deviation of repeated $\Delta g/\Delta z$ measurements expressed in g/cm^3 .

Column 4 Vertical gravity gradient correction (expressed in g/cm^3) for submarine topography out to a radial distance of 103.5 statute miles (166.7 kilometers). Correction calculated by replacing sea water with density of 1.90 g/cm^3 (see Beyer and Corbato, 1972).

Column 5 Vertical gravity gradient correction expressed in g/cm^3 for lateral density changes (assumed to be two-dimensional) caused by geologic facies changes across the reef (see Figure 2.4).

Column 6 Vertical gravity gradient correction (expressed in g/cm^3) for lateral density changes caused by crater-related processes and assumed to be symmetrical about Op2-18 (see Figure 2.7).

Column 7 BHG density in g/cm^3 after correction for submarine topography and lateral density variations due to geologic facies changes and cratering processes.

Column 8 Mean grain density for depth interval in g/cm^3 (calculated from mineral and organic content percentages estimated from x-ray diffraction and loss-on-ignition analyses (see Appendix 2.2)).

Column 9 Estimated uncertainty in mean grain density in g/cm^3 .

Column 10 BHG porosity in percent calculated from BHG density (column 7), grain density (column 8) and sea-water density of 1.03 g/cm^3 .

Column 11 Uncertainty in BHG porosity in percent calculated from standard deviation of BHG density (column 4) and uncertainty in mean grain density (column 8).

Column 12 Average gamma-gamma density for depth interval in g/cm^3 .

Column 13 Gamma-gamma porosity in percent calculated from gamma-gamma density (column 12), grain density (column 8) and sea-water density of 1.03 g/cm^3 .

Column 14 Average neutron porosity for depth interval in percent.

TABLE 2-5 (On opposite page). -- Bulk density, porosity, and grain density obtained from borehole gravity, gamma-gamma, and neutron measurements in borehole ORT-20 and from analysis of cores taken from ORT-20. Gamma-gamma and neutron data averages over depth intervals of BHG survey. Grain densities were calculated by the procedure described in Appendix 2-1 using data from Tremba and Ristvet (1986) and Ristvet and Tremba (1986).




TABLE 2-5.

	1	2	3	4	5	6	7	8	9	10	11	12	13	14
136.-160.		1.693	.013	.130	.020	0.005	1.848	2.84	.02	54.8	0.7	1.98	47.5	0.
160.-186.		1.857	.012	.133	.020	0.	2.010	2.86	.02	46.4	0.7	1.99	47.5	0.
186.-211.		1.673	.007	.134	.021	-.002	1.826	2.84	.02	56.0	0.4	1.96	48.6	0.
211.-226.		1.818	.	.135	.021	-.003	1.971	2.86	.02	48.6	0.	1.99	47.5	0.
226.-256.		1.772	.	.136	.021	-.003	1.926	2.85	.02	50.8	0.	2.00	46.7	0.
256.-271.		1.653	.	.137	.021	-.004	1.807	2.82	.02	56.6	0.	1.97	47.5	0.
271.-301.		1.787	.004	.138	.021	-.004	1.942	2.82	.02	49.1	0.2	0.	0.	0.
301.-331.		1.766	.002	.139	.021	-.004	1.922	2.78	.02	49.0	0.1	0.	0.	0.
331.-361.		1.792	.007	.139	.022	-.005	1.948	2.88	.02	50.4	0.4	0.	0.	0.
361.-391.		1.833	.010	.139	.022	-.005	1.989	2.83	.02	46.7	0.6	2.04	43.9	0.
391.-421.		1.846	.014	.140	.022	-.005	2.003	2.75	.02	43.4	0.8	2.04	41.3	0.
421.-451.		1.857	.012	.140	.022	-.005	2.014	2.70	.02	41.1	0.7	1.95	44.9	0.
451.-471.		1.891	.008	.140	.022	-.005	2.048	2.70	.02	39.0	0.5	1.90	47.9	0.
471.-491.		1.852	.017	.140	.022	-.005	2.009	2.70	.02	41.4	1.0	2.06	38.3	0.
491.-521.		1.792	.009	.140	.022	-.005	1.949	2.69	.02	44.6	0.5	1.93	45.8	0.
521.-551.		1.770	.010	.140	.023	-.004	1.929	2.70	.02	46.2	0.6	1.91	47.3	0.

Column 1 Depth interval in feet below sea level

Column 2 Apparent BHG density in g/cm³ (corrected for instrument calibration and drift and earth tides).

Column 3 Standard deviation of repeated $\Delta g/\Delta z$ measurements expressed in g/cm³.

Column 4 Vertical gravity gradient correction (expressed in g/cm³) for submarine topography out to a radial distance of 103.5 statute miles (166.7 kilometers). Correction calculated by replacing sea water with density of 1.90 g/cm³ (see Beyer and Corbato, 1972).

Column 5 Vertical gravity gradient correction expressed in g/cm³ for lateral density changes (assumed to be two-dimensional) caused by geologic facies changes across the reef (see Figure 2.4).

Column 6 Vertical gravity gradient correction (expressed in g/cm³) for lateral density changes caused by crater-related processes and assumed to be symmetrical about 082-18 (see Figure 2.7).

Column 7 BHG density in g/cm³ after correction for submarine topography and lateral density variations due to geologic facies changes and cratering processes.

Column 8 Mean grain density for depth interval in g/cm³ (calculated from mineral and organic content percentages estimated from x-ray diffraction and loss-on-ignition analyses (see Appendix 2.2)).

Column 9 Estimated uncertainty in mean grain density in g/cm³.

Column 10 BHG porosity in percent calculated from BHG density (column 7), grain density (column 8) and sea-water density of 1.03 g/cm³.

Column 11 Uncertainty in BHG porosity in percent calculated from standard deviation of BHG density (column 4) and uncertainty in mean grain density (column 8).

Column 12 Average gamma-gamma density for depth interval in g/cm³.

Column 13 Gamma-gamma porosity in percent calculated from gamma-gamma density (column 12), grain density (column 8) and sea-water density of 1.03 g/cm³.

Column 14 Average neutron porosity for depth interval in percent.

TABLE 2-6 (On opposite page). -- Bulk density, porosity, and grain density obtained from borehole gravity, gamma-gamma, and neutron measurements in borehole OSR-21 and from analysis of cores taken from OSR-21. Gamma-gamma and neutron data averages over depth intervals of BHG survey. Grain densities were calculated by the procedure described in Appendix 2-1 using data from Tremba and Ristvet (1986) and Ristvet and Tremba (1986).

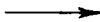


TABLE 2-6.

	1	2	3	4	5	6	7	8	9	10	11	12	13	14
	134.-159.	1.845	.004	.126	.018	0.	1.989	2.82	.02	46.4	0.2	1.96	48.0	0.
	159.-184.	1.776	.018	.126	.018	0.	1.920	2.80	.02	49.7	1.0	1.83	54.8	0.
	184.-209.	1.698	.014	.128	.019	0.	1.845	2.81	.02	54.2	0.8	1.90	51.1	0.
	209.-234.	1.689	.009	.129	.019	0.	1.837	2.82	.02	54.9	0.5	1.88	52.5	0.
	234.-264.	1.763	.007	.131	.019	0.	1.913	2.80	.02	50.1	0.4	1.87	52.5	0.
	264.-294.	1.794	.009	.132	.019	0.	1.945	2.80	.02	48.3	0.5	1.88	52.0	0.
	294.-324.	1.735	.008	.134	.019	0.	1.888	2.82	.02	52.1	0.4	1.87	53.1	0.
	324.-354.	1.736	.009	.135	.019	0.	1.890	2.82	.02	52.0	0.5	1.78	58.1	0.
	354.-384.	1.734	.007	.136	.019	0.	1.889	2.81	.02	51.7	0.4	1.83	55.1	0.
	384.-404.	1.765	.016	.137	.020	0.	1.922	2.79	.02	49.3	0.9	1.72	60.8	0.
	404.-424.	1.829	.020	.137	.020	0.	1.986	2.77	.02	45.1	1.1	1.84	53.4	0.

Column 1 Depth interval in feet below sea level

Column 2 Apparent BHG density in g/cm^3 (corrected for instrument calibration and drift and earth tides).

Column 3 Standard deviation of repeated $\Delta g/z$ measurements expressed in g/cm^3 .

Column 4 Vertical gravity gradient correction (expressed in g/cm^3) for submarine topography out to a radial distance of 103.5 statute miles (166.7 kilometers). Correction calculated by replacing sea water with density of $1.90 g/cm^3$ (see Beyer and Corbato, 1972).

Column 5 Vertical gravity gradient correction expressed in g/cm^3 for lateral density changes (assumed to be two-dimensional) caused by geologic facies changes across the reef (see Figure 2.4).

Column 6 Vertical gravity gradient correction (expressed in g/cm^3) for lateral density changes caused by crater-related processes and assumed to be symmetrical about Op2-18 (see Figure 2.7).

Column 7 BHG density in g/cm^3 after correction for submarine topography and lateral density variations due to geologic facies changes and cratering processes.

Column 8 Mean grain density for depth interval in g/cm^3 (calculated from mineral and organic content percentages estimated from x-ray diffraction and loss-on-ignition analyses (see Appendix 2.2)).

Column 9 Estimated uncertainty in mean grain density in g/cm^3 .

Column 10 BHG porosity in percent calculated from BHG density (column 7), grain density (column 8) and sea-water density of $1.03 g/cm^3$.

Column 11 Uncertainty in BHG porosity in percent calculated from standard deviation of BHG density (column 4) and uncertainty in mean grain density (column 8).

Column 12 Average gamma-gamma density for depth interval in g/cm^3 .

Column 13 Gamma-gamma porosity in percent calculated from gamma-gamma density (column 12), grain density (column 8) and sea-water density of $1.03 g/cm^3$.

Column 14 Average neutron porosity for depth interval in percent.

TABLE 2-7 (On opposite page). -- Bulk density, porosity, and grain density obtained from borehole gravity, gamma-gamma, and neutron measurements in borehole OTG-23 and from analysis of cores taken from OTG-23. Gamma-gamma and neutron data averages over depth intervals of BHG survey. Grain densities were calculated by the procedure described in Appendix 2-1 using data from Tremba and Ristvet (1986) and Ristvet and Tremba (1986).

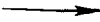


TABLE 2-7.

	1	2	3	4	5	6	7	8	9	10	11	12	13	14
314.-344.		1.869	.003	.108	.022	0.019	2.018	2.85	.04	45.7	0.2	0.	0.	0.
344.-374.		1.888	.007	.109	.022	0.018	2.037	2.85	.04	44.7	0.4	0.	0.	0.
374.-404.		1.860	.010	.111	.022	0.018	2.011	2.85	.04	46.1	0.5	0.	0.	0.
404.-434.		1.848	.013	.112	.022	0.018	2.000	2.85	.04	46.7	0.7	0.	0.	0.
434.-464.		1.864	.010	.113	.022	0.018	2.017	2.85	.02	45.8	0.5	0.	0.	0.
464.-494.		1.895	.012	.114	.022	0.018	2.049	2.84	.02	43.7	0.7	0.	0.	0.
494.-539.		1.855	.006	.116	.022	0.015	2.008	2.74	.02	42.8	0.4	0.	0.	0.
539.-584.		1.958	.005	.117	.023	0.019	2.117	2.72	.02	35.7	0.3	0.	0.	0.
584.-629.		1.867	.008	.119	.023	0.017	2.026	2.73	.02	41.4	0.5	0.	0.	0.
629.-674.		1.915	.018	.120	.023	0.014	2.072	2.81	.02	41.5	1.0	0.	0.	0.
674.-734.		1.991	.015	.122	.024	0.019	2.156	2.88	.02	39.1	0.8	0.	0.	0.

Column 1 Depth interval in feet below sea level

Column 2 Apparent BHG density in g/cm^3 (corrected for instrument calibration and drift and earth tides).

Column 3 Standard deviation of repeated $1g/12$ measurements expressed in g/cm^3 .

Column 4 Vertical gravity gradient correction (expressed in g/cm^3) for submarine topography out to a radial distance of 103.5 statute miles (166.7 kilometers). Correction calculated by replacing sea water with density of $1.90 g/cm^3$ (see Beyer and Corbato, 1972).

Column 5 Vertical gravity gradient correction expressed in g/cm^3 for lateral density changes (assumed to be two-dimensional) caused by geologic facies changes across the reef (see Figure 2.4).

Column 6 Vertical gravity gradient correction (expressed in g/cm^3) for lateral density changes caused by crater-related processes and assumed to be symmetrical about Op2-18 (see Figure 2.7).

Column 7 BHG density in g/cm^3 after correction for submarine topography and lateral density variations due to geologic facies changes and cratering processes.

Column 8 Mean grain density for depth interval in g/cm^3 (calculated from mineral and organic content percentages estimated from x-ray diffraction and loss-on-ignition analyses (see Appendix 2.2)).

Column 9 Estimated uncertainty in mean grain density in g/cm^3 .

Column 10 BHG porosity in percent calculated from BHG density (column 7), grain density (column 8) and sea-water density of $1.03 g/cm^3$.

Column 11 Uncertainty in BHG porosity in percent calculated from standard deviation of BHG density (column 4) and uncertainty in mean grain density (column 8).

Column 12 Average gamma-gamma density for depth interval in g/cm^3 .

Column 13 Gamma-gamma porosity in percent calculated from gamma-gamma density (column 12), grain density (column 8) and sea-water density of $1.03 g/cm^3$.

Column 14 Average neutron porosity for depth interval in percent.

Table 2-8. -- Density model for atoll material surrounding OAK crater. Density layers are averages of BHG densities from OOR-17 and OSR-21 and are contrasted with the crater density model of Figure 2-7. Averaged grain densities and BHG porosities are also shown.

Approximate Depth Interval (feet below sea level)	Averaged BHG Density (g/cm ³)	Averaged Grain Density (g/cm ³)	Averaged BHG Porosity (%)
134 - 410	1.92	2.81	50
410 - 587	1.98	2.73	44
587 - 747	2.01	2.84	46
750 - 962	2.09 \pm .03 (estimate from gamma-gamma log run in OOR-17)		

Table 2-9. -- BHG density and porosity values and their contrasts with respect to reference borehole values (Table 2-8) for the averaged large intervals shown in Figures 2-16 and 2-19.

	<u>OOR-17/OSR-21</u>	<u>OTG-20</u>	<u>OQT-19</u>	<u>OTG-23</u>	<u>OPZ-18</u>
<u>Interval approximately from discontinuity 1 to 4</u>					
Density(contrast) in g/cm ³	1.92	1.92(0)	1.93(+.01)	--	--
Porosity(contrast) in %	50	51(+1)	50(0)	--	--
<u>Interval approximately from discontinuity 4 to 6</u>					
Density(contrast) in g/cm ³	1.97	1.98(+.01)	2.00(+.03)	2.05(+.08)	2.13(+.16)
Porosity(contrast) in %	45	44(-1)	44(-1)	41(-4)	36(-9)
<u>Interval approximately from discontinuity 5 to facies change H/I</u>					
Density(contrast) in g/cm ³	1.98	1.97(-.01)	2.00(+.02)	2.03(+.05)	2.11(+.13)
Porosity(contrast) in %	44	44(0)	43(-1)	40(-4)	37(-7)
<u>Interval approximately from facies change H/I to J/K</u>					
Density(contrast) in g/cm ³	2.01	--	2.03(+.02)	--	2.05(+.04)
Porosity(contrast) in %	46	--	45(-1)	--	44(-2)
<u>Mass columns (%)</u>					
	100		95-97		92-94

APPENDIX 2-1

BOREHOLE GRAVITY SURVEY, BOREHOLE E-1, MEDREN ISLAND

The BHG survey in borehole E-1 on Medren (ELMER) Island (see fig. 2-20) was conducted in April, 1984, by the U.S. Geological Survey to determine if reliable BHG data could be gathered in the microseismic environment of an atoll and to evaluate the range of natural density variations of reef-forming materials. Near-surface vibrations caused by wave action were minimal and the repeatability of BHG measurements generally was excellent. The tabulated data for this survey are given in Beyer, Ristvet, and Oberste-Lehn (1986).

The borehole gravity survey in the E-1 borehole shows that the bulk density of atoll materials to a depth of 1,800 ft ranges from about 1.9 to about 2.3 g/cm³ and averages slightly more than 2.0 g/cm³ at the scale examined by the BHG survey. Several density patterns are evident.

1. Higher densities between 1,140 and about 1,290 ft correspond to harder rocks as indicated by slower drill rates (fig. 2-20).
2. The gravity station at 1,410 ft (point labeled "A" in fig. 2-20) probably is in close proximity to a sizable cavern that has caused measured gravity to be unexpectedly low. This one anomalous gravity reading incorporated into the overlying and underlying density calculations explains the generally high and low densities of the two adjacent intervals.
3. A repeated pattern of density variations (labeled "1" through "5" in fig. 2-20) may be due to facies changes and/or diagenesis associated with relative sea-level changes. These repeated patterns of downward decrease in density (increase in porosity) followed by more abrupt increase in density (decrease in porosity) should be examined for possible correlation with available geologic data.

Densities in the upper 600 ft are slightly higher than the densities over the same depth interval in PEACE Program reference boreholes OOR-17 and OSR-21 at OAK crater. Part of this may be due to the E-1 borehole being much closer to the ocean edge of the reef than are OOR-17 and OSR-21. Boreholes OOR-17 and OSR-21 are more likely to be in a less dense, more lagoonward facies. Corrections for submarine topography are more critical at the E-1 borehole because of its closer proximity to the outer reef slope than the PEACE Program boreholes. Unfortunately, bathymetry is less well known adjacent to the E-1 borehole, and some of the density differences between E-1 and OOR-17 and OSR-21 may be due to errors in corrections for submarine topography at E-1.

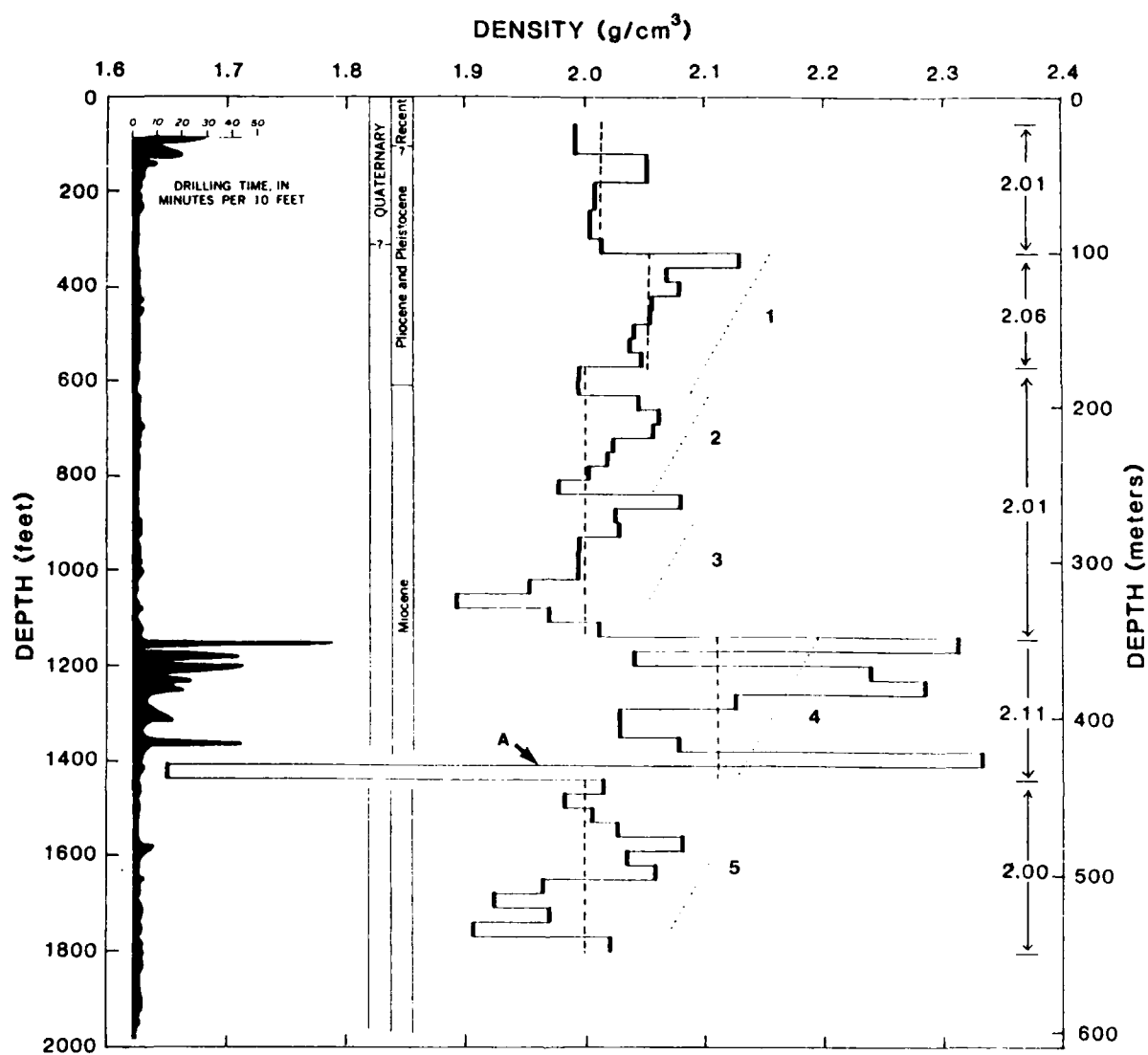


FIGURE 2-20 - BHG density profile for borehole E-1, Medren (ELMER) Island. Drilling time profile and geologic ages are from Ladd and Schlanger (1960). Large interval averages of density along righthand depth scale correspond to vertical dashed lines. Diagonal dotted lines labeled "1" through "5" designate suggested repeated density (porosity?) cycles.

APPENDIX 2-2

DETERMINATION OF INTERVAL GRAIN DENSITY

An estimate of interval grain density is needed before BHG porosity can be calculated from BHG density. Grain densities of individual core samples were estimated from x-ray mineralogy and organic analyses by Tremba and Ristvet (1986) and Ristvet and Tremba (1986) and are shown in Figures 2-8 through 2-13.

An example of how grain density was calculated from x-ray mineralogy and organic analyses follows. Calcite (and magnesium calcite), aragonite, and organic matter were assigned grain densities of 2.72, 2.93, and 1.00 g/cm³ respectively. If organic matter was present and measured in weight percent of dry solids (generally 3 percent or less), the remainder of the dry sample was assumed to consist of inorganic material (generally 97 percent or more). Thus, for a sample with the analysis

Calcite	Aragonite	Organic Matter
(wt %)	(wt %)	(wt %)
<u>29</u>	<u>71</u>	<u>2.5</u>

The grain density is

$$[(.29)(2.72) + (.71)(2.93)](1-.025) + .025 = 2.82 \text{ g/cm}^3$$

If the sample had no measurable organic matter, the grain density is

$$(.29)(2.72) + (.71)(2.93) = 2.87 \text{ g/cm}^3$$

The plots of grain densities of core samples were generalized to average grain densities for BHG intervals as shown in Figures 2-8 through 2-13. Grain densities averaged by sedimentary packages by Tremba and Ristvet (1986) were too generalized for the BHG data. Uncertainties of ± 0.02 or ± 0.04 g/cm³ were assigned in order to estimate errors in porosity calculations (columns 8, 9, 11 of Tables 2-2 through 2-7; also see Appendix 8-2, Beyer, Ristvet, and Oberste-Lehn, 1986).

CHAPTER 3:

PALEONTOLOGIC EVIDENCE FOR SEDIMENTARY MIXING IN OAK CRATER

by

Thomas M. Cronin and Thomas G. Gibson¹

INTRODUCTION

In 1985, during the course of paleontologic studies of OAK and KOA craters, Enewetak Atoll, it was discovered that the analysis of the distribution of microfossils aided the understanding of the dynamic processes involved in the formation and evolution of the nuclear craters (Cronin, Brouwers, and others, 1986; Brouwers, Cronin, and Gibson, 1986; Henry, Wardlaw, and others, 1986; Henry and Wardlaw, 1986; and Wardlaw and Henry, 1986). These paleontologic studies were particularly useful in determining the depth of origin (or provenance) and sedimentologic history of the disturbed and mobilized materials that partially infilled KOA crater after the initial excavation by the detonation of the nuclear device.

The primary purpose of the present study is to determine the composition and provenance of crater-fill materials and the nature of sediment mixing in OAK crater using micropaleontologic data. This study is an extension of the paleontologic component by the U.S. Geological Survey for the PEACE Program (Cronin, Brouwers, and others, 1986; Brouwers, Cronin, and Gibson, 1986). In this study of OAK, we intend to establish the depth limits of mixing of: (1) surficial material, (2) sediment from the uppermost 50 ft of the stratigraphic section, and (3) material from intermediate depths (50 to 300 ft). Furthermore, we intend to determine the pattern of "piping" of deep material emplaced in the crater-fill from horizons 500 to 900 ft below the lagoon bottom or sea floor. Our results are integrated with geologic and geophysical data to form a general model of crater formation in Chapter 7 of this Open-File Report.

MATERIAL AND METHODS

To accomplish our objectives, detailed restudy of samples from reference boreholes OAR-2A and OOR-17 was necessary to refine our zonation of the microfaunal sequence in the upper 400 ft of the stratigraphic section (for discussion of the succession of microfaunal zones used on Enewetak, see Cronin, Brouwers, and others, 1986, and Brouwers, Cronin, and Gibson, 1986). The laboratory and biostratigraphic procedures used herein are the same as those described in the reports cited above. Microfossils were extracted from sediment between 63 and 850 μm in grain size. Samples from two central-crater (ground-zero) boreholes (OBZ-4 and OPZ-18) and three transition boreholes

¹ Branch of Paleontology and Stratigraphy, U.S. Geological Survey,
Reston, VA 22092.

(OCT-5, OFT-8, and OKT-13) were examined in detail for the mixing study of OAK crater. Table 3-1 lists the depths of all 159 samples studied.

Throughout this report, depths of zonal boundaries are occasionally rounded off to whole numbers for convenience. Of course, the accuracy of any particular faunal zone is limited by the resolution of the sampling interval.

STANDARD MICROFAUNAL SEQUENCE

Quantitative data on the occurrence of diagnostic ostracode species (Appendices 3-1 and 3-2) and semiquantitative data on benthic foraminifers (Gibson and Hill, in preparation) from boreholes OAR-2/2A and OOR-17 were used to improve the standard zonation of Cronin, Brouwers, and others (1986) and Brouwers, Cronin, and Gibson (1986), in which 12 faunal zones, designated AA through MM, in descending order, were defined. In addition, the percent of specimens of the ostracode Neonesidea schulzi with preserved setae¹ was used as a new measure to quantify the amount of material mixed downward from the surface. Only living or recently dead specimens of this species found in surficial lagoon sediments have setae preserved (generally 70 to 80%). Ostracode setae normally are degraded and destroyed by natural processes soon after death of the organism and burial of the shell. Therefore, the occurrence of setae in specimens below the sediment surface in the crater-fill materials is taken to indicate mixing of specimens from the surface sediments.

The following zones were used in the quantitative analyses of ostracodes:

<u>Surface:</u>	The percent of <u>Neonesidea schulzi</u> with setae preserved.
<u>Zone AA:</u>	The combined percentages of <u>Hermanites mooneyi</u> and <u>Loxoconchella</u> sp. A.
<u>Zone BB-CC:</u>	The combined percentages of <u>Cletocythereis</u> sp. A and <u>Loxoconcha heronislandensis</u> .
<u>Zone EE-FF:</u>	The combined percentages of <u>Caudites</u> sp. A, <u>Caudites</u> sp. B, <u>Cletocythereis rastromarginata</u> , <u>Loxonconcha labrynthica</u> , and <u>Loxoconchella</u> sp. C.
<u>Zone FF-GG:</u>	The combined percentages of <u>Australimoosella</u> sp. A, <u>Bythoceratina</u> sp. A, <u>Cletocythereis canaliculata</u> , <u>Procythereis</u> sp. A, and <u>Semicytherura</u> sp. A.
<u>Zone II-MM:</u>	The combined percentages of all species restricted to zones II, JJ, KK, LL, and MM as determined by Cronin, Brouwers, and Gibson (1986). In Appendices 3-1 and 3-2 at the end of this Chapter, the totals for these species are given in row 41. <u>Procythereis</u> sp. B generally occurs in zones

¹ Setae are small hairs that occur on the exterior of the valves of some taxa of ostracodes.

TABLE 3-1. — Depth (ft bsf) in boreholes of samples examined during the study of the mixing of crater-fill materials from OAK.

OAR-2A	OBZ-4	OCT-5	OFT-8	OKT-13	OOR-17	OPZ-18
0.25	2.8	0.2	8.75	10.4	0.25	7.0
2.3	11.8	8.8	18.6	18.5	14.15	35.0
6.0	21.1	17.5	27.9	25.4	25.75	44.6
9.3	33.0	39.5	35.1	28.75	38.4	57.85
11.85	40.5	57.55	43.1	36.0	49.7	74.3
14.5	58.5	66.8	48.85	55.65	60.2	89.45
17.1	66.35	76.65	64.0	59.9	66.75	102.0
20.8	75.15	86.15	74.0	68.2	72.8	115.05
22.75	84.15	95.35	-	80.0	83.7	131.0
23.75	93.1	104.25	-	-	89.8	139.7
26.05	104.55	113.15	-	-	100.45	154.2
31.9	112.9	124.0	-	-	101.4	169.35
34.75	121.8	132.8	-	-	110.5	174.95
40.2	130.0	140.9	-	-	119.1	182.3
43.55	144.5	149.65	-	-	125.25	198.0
62.5	151.55	157.6	-	-	131.95	207.3
74.8	166.85	166.4	-	-	137.15	210.4
90.4	178.6	176.25	-	-	146.1	229.95
95.8	186.8	186.0	-	-	154.25	232.1
115.1	193.6	-	-	-	165.6	239.15
127.8	196.5	-	-	-	173.05	-
134.0	205.1	-	-	-	184.25	-
157.45	213.9	-	-	-	193.6	-
171.2	225.65	-	-	-	200.8	-
188.25	-	-	-	-	209.3	-
195.3	-	-	-	-	215.5	-
204.9	-	-	-	-	226.05	-
212.45	-	-	-	-	233.35	-
223.9	-	-	-	-	239.0	-
234.6	-	-	-	-	250.3	-
244.55	-	-	-	-	261.5	-
246.8	-	-	-	-	270.1	-
268.45	-	-	-	-	285.65	-
282.55	-	-	-	-	292.1	-
289.7	-	-	-	-	299.15	-
337.05	-	-	-	-	310.7	-
379.5	-	-	-	-	320.2	-
-	-	-	-	-	331.2	-
-	-	-	-	-	339.0	-
-	-	-	-	-	367.9	-

II-MM; however, it does occur higher in the section in single samples from OOR-17 (331.2 ft bsf) and in OAR-2A (223.9 ft). Specimens of Procythereis sp. B in crater boreholes are considered piped, so that the percent of II-MM species includes species groups 36 and 41 from the appendices.

For the companion analysis of the foraminifers, the zones used are characterized as follows:

- Surface: The presence of chitinous inner linings and original (natural) coloration in several species.
- Zone AA: The presence of Calcarina spengleri and C. hispida. Upper AA is characterized by coloration in specimens of C. spengleri that is not present in specimens in the lower part of this zone, as determined from the reference boreholes.
- Zone BB: The presence of Epistominella tubulosa and Anomolina sp. A.
- Zone CC: The presence of advanced forms of Calcarina rustica.
- Zone EE: The presence of Calcarina delicata and primitive forms of Calcarina rustica.
- Zone FF-GG: The presence of Calcarina calcar and Cibicides sp. A.

The percentages of ostracodes for each category (excluding the Surface¹ and II-MM categories) are plotted for boreholes OAR-2A and OOR-17 in Figures 3-1 and 3-2. These were used for comparison with the mixed faunal sequences in the central crater and transition boreholes. It is noteworthy that the two faunal sequences in OOR-17 and OAR-2A are very similar to each other, enhancing the accuracy of estimates of the original depths of mixed specimens.

A large proportion (generally about 40 to 60% of each sample) consists of long-ranging species not restricted to a particular zone. Some of these non-diagnostic species probably also were mixed during crater filling. Consequently, the percentage values for samples from crater boreholes are, in some cases, minimum values (i.e., if mixed specimens of non-diagnostic species could be identified, the true percentage of an assemblage from any particular zone would be slightly higher).

In many ways, the use in the mixing study of selected species that have acme zones (intervals of greatest abundance) is an exercise in probability. Those species chosen as diagnostic of zones AA, BB-CC, EE-FF, and FF-GG in the upper 400 ft of normal stratigraphic section have a high probability (generally about 80 to 90%) that they originated from within that interval.

¹ Sediments from the lagoon floor or the upper several inches of sediment below the lagoon floor itself are referred hereafter as Surface materials.

OAR-2/2A

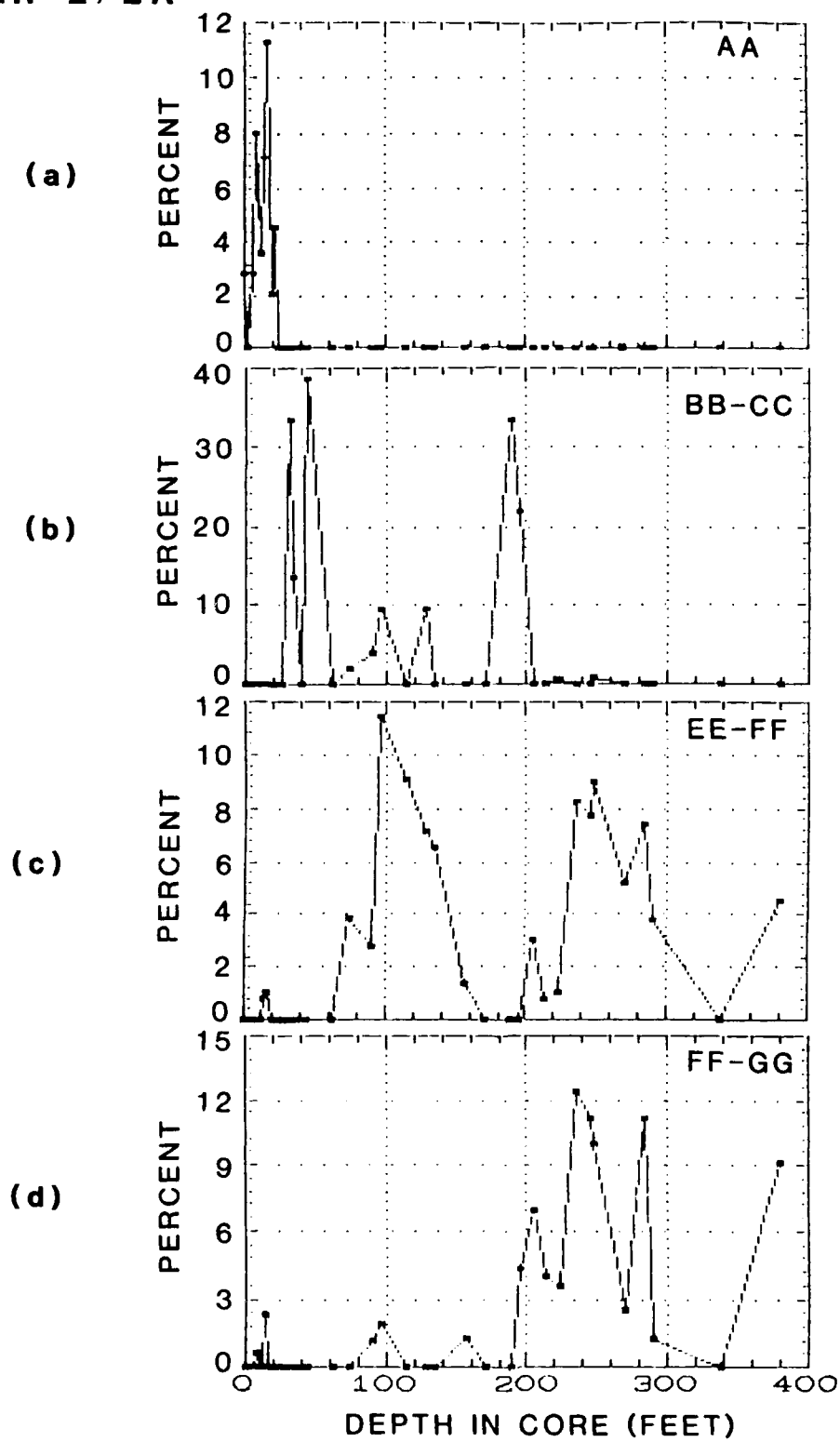


Figure 3-1. -- Borehole OAR-2/2A. Plot of percentages of diagnostic ostracode species. (1a) zone AA; (1b) zones BB-CC; (1c) zones EE-FF; (1d) zones FF-GG.

OOR-17

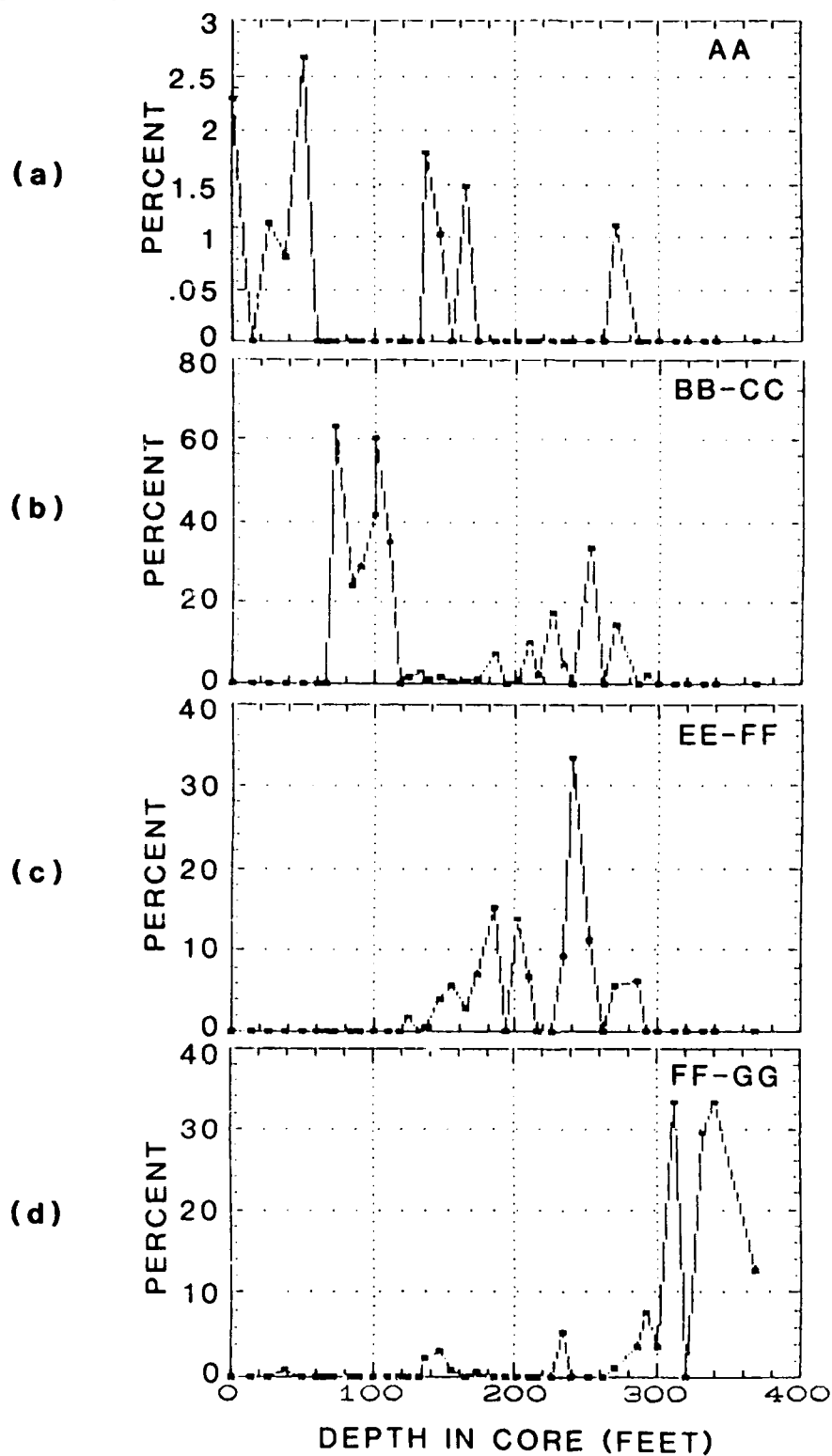


Figure 3-2. --- Borehole OOR-17: Plot of percentages of diagnostic ostracode species. (2a) zone AA; (2b) zones BB-CC; (2c) zones EE-FF; (2d) zones FF-GG.

Confirmation of a zone assignment from both fossil groups increases significantly the probability that the zone assignment is correct.

The use of percentages of specimens from zones II-MM probably underestimates the real percentages by no more than 5 to 10%, because far fewer species from the upper 300 ft of section range downward into these zones. This index of piped specimens is considered an accurate indicator of the proportion of piped material represented in a sample. The percentage piped from a depth interval may be considered representative of the entire sedimentary assemblage at that level if two assumptions are correct. First, we must assume all particles of all sizes behave the same as those between 63 and 850 μm (the size range from which ostracodes were extracted). Second, we must assume sediment particles of different shapes and densities behave the same as the ostracode valves and carapaces. With these assumptions in mind, and given the error margins associated with the limits to microfossils zonations discussed above, these data are useful in making volumetric estimates of the proportion of crater-fill sediments piped from depth.

The percentage of Neonesidea schulzi having setae is a distinct type of index that gives an approximate estimate of the actual percentage of surface material, at least to the extent that it can be determined from using this one common species of ostracodes.

A large proportion of the foraminifer assemblage in most samples is composed of Amphistigina madagascarensis. This species is abundant in the modern reef environments on Enewetak and continues downward into the Miocene strata in the Enewetak boreholes. Therefore, its occurrence alone cannot be used for biostratigraphic determination; however, its preservation state is indicative of its zone of origin or provenance. Translucent specimens of this species occur only in zone AA. Below this zone (i.e., in the Pleistocene section and in older strata), they are opaque. Thus, the occurrence of translucent specimens of A. madagascarensis indicates that their provenance is the Holocene section (zone AA). Many other foraminifer species also have long ranges and cannot be placed definitely. However, the evolutionary changes in the Calcarina lineage are most helpful for determination of the horizons, particularly because they are among the most numerous species in the assemblage.

In some other cases, the preservation of ostracodes and foraminifers also is important in identifying provenance. For example, conspicuous brown specimens of long-ranging species clearly could be identified as originating from deeper zones II-MM. Also, in the injection dikes between 189 and 208 ft bsf and at 233 ft bsf in OPZ-18, the preservation state is almost identical to that of specimens in the upper part of zone AA; therefore, the origin of even non-diagnostic species with the appropriate shell preservation can be shown confidently to be from zone AA.

RESULTS

The following results can be shown from our current studies of samples from OAK crater.

Central Crater (Ground Zero) Boreholes

Boreholes OBZ-4 and OPZ-18 were cored near ground zero in OAK crater; we examined 39 and 21 samples, respectively, from each. The following is an informal zonation of the crater-fill materials based on the characteristics of the mixing of microfossils. The zones of material in the crater-fill from top to bottom are: (1) the **Homogenized Zone**, (2) the **Upwardly Mixed Zone**, (3) the **Maximum Piping Zone**, and (4) the **Basal Mixed Zone**. The boundaries between these zones are gradational and their depths approximate. In addition, we examined material from several injection dikes. The results are based on the ostracode-occurrence data given in Appendices 3-3 and 3-4, many of which are presented graphically in Figures 3-3 and 3-4, and the benthic foraminifer data is summarized in Tables 3-2 through 3-6, located at the end of this Chapter immediately preceeding the Appendices. To appreciate the nature of the mixing described in the next few pages and to see the actual percentage values, it is useful to compare directly the "normal" pattern of ostracodes (figs. 3-1 and 3-2) with that of the mixed sequence (figs. 3-3 and 3-4).

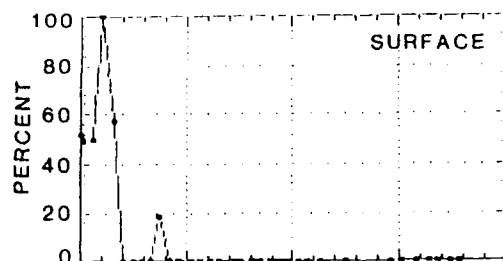
Homogenized Zone (0 to 40 ft). -- In this interval, high percentages (50 to 60%) of Neonesidea schulzi with preserved setae and specimens of Discorbis and Cymbaloporella with chitinous inner linings originated from the Surface. High percentages of AA species, low to moderate numbers of specimens from CC, low to moderate occurrences of EE-GG species, low percentages of presumably piped specimens of II-MM species, and 3 to 6% BB-CC mixed material also characterize the Homogenized Zone. In general, this interval is easily identified by its anomalously high species diversity, resulting from the homogenization of material from virtually all zones with apparently equal contributions from most sub-AA zones. Specimens from the Homogenized Zone are characterized by widely varying preservation states.

Upwardly Mixed Zone (40 to 100 ft). -- This interval contains consistently low percentages of EE-GG ostracodes and greater percentages of piped material from zones II-MM than occur in the upper 40 ft of OAK crater-fill. The absence of surface material is conspicuous (with the exception of a single sample from 84 ft bsf from OBZ-4). Some samples from the Upwardly Mixed Zone contain less AA material than the overlying Homogenized Zone; in others, zone AA foraminifers still predominate. This interval characteristically contains moderate amounts of BB-CC material. The boundary between the Homogenized Zone and the underlying Maximum Piping Zone is not sharp, although this may be due to sample spacing. However, the relative contributions to the Upwardly Mixed Zone of foraminifers and ostracodes from various zones are quite distinct from the rest of the crater-fill. The piped specimens from this zone are from KK-LL and possibly from MM.

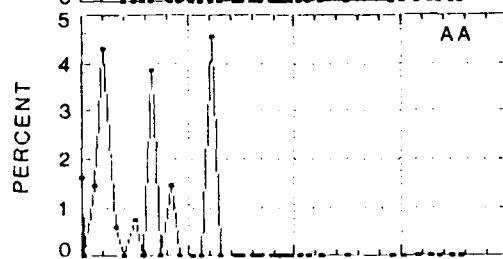
Maximum Piping Zone (100 to 160 ft). -- The highest percentages of piped specimens (9 to 12% in both OBZ-4 and OPZ-18) occur in this zone. LL-MM zone foraminifers and ostracodes are common at 121.8 ft bsf in OBZ-4, where at least eight separate ostracode species were emplaced from depth. Low percentages of AA foraminifers are characteristic of the upper part of the Maximum Piping Zone; however, no definite AA ostracodes or foraminifers are recorded from below about 125 ft in OBZ-4. This interval contains low to moderate numbers of specimens from zones CC and EE-GG. Here, piped foraminifers are not as obvious in OPZ-18 as in OBZ-4. Anomalously large numbers of single ostracode valves and still-articulated carapaces are broken

OBZ-4

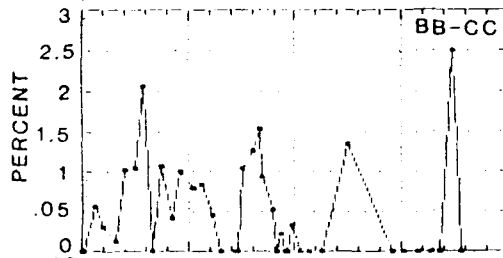
(a)



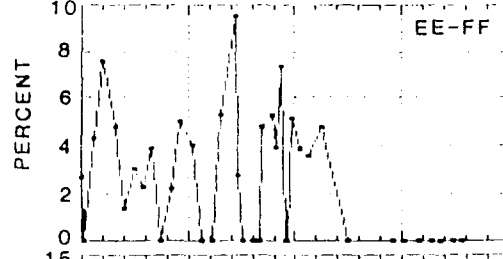
(b)



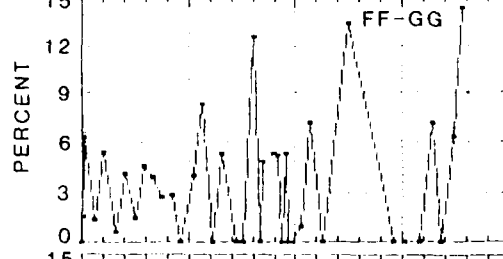
(c)



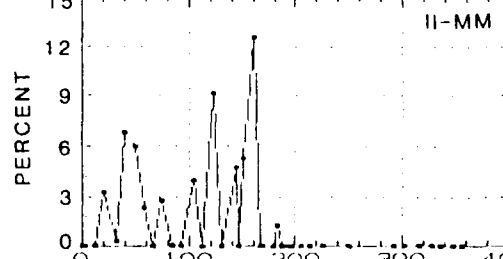
(d)



(e)



(f)



DEPTH IN CORE (FEET)

Figure 3-3. -- Borehole OBZ-4: Plot of percentages of diagnostic ostracode species. (3a) lagoon bottom species; (3b) zone AA; (3c) zones BB-CC; (3d) zones EE-FF; (3e) zones FF-GG; (3f) zones II-MM.

OPZ-18

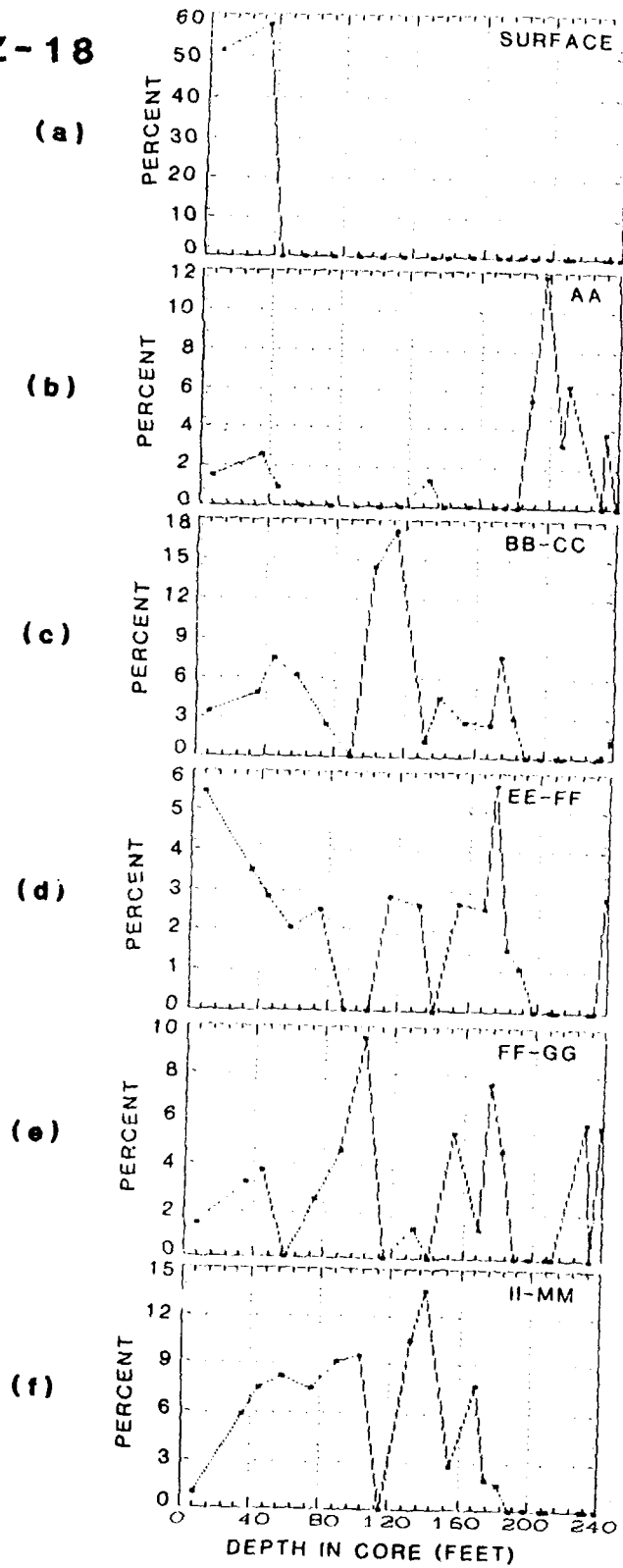


Figure 3-4. -- Borehole OPZ-18: Plot of percentages of diagnostic ostracode species. (4a) species from lagoon floor; (4b) zone AA; (4c) zones BB-CC; (4d) zones EE-FF; (4e) zones FF-GG; (4f) zones II-MM.

in samples from the Maximum Piping Zone, suggesting a kind of shock fracturing. The base of the Maximum Piping Zone is marked by an abrupt drop in the percentage of piped specimens in the samples.

Basal Mixed Zone (160 to 190 ft). -- The Basal Mixed Zone contains low percentages of piped material, low percentages of zone AA foraminifers, and high percentages of zone EE-FF material. Most of the sediment in the Basal Mixed Zone probably originated from zones EE and FF.

Statistical Analysis of Crater-Fill Materials. -- A simple linear-regression analysis of depth versus percentage of piped specimens was performed for samples from the upper 160 ft of OBZ-4 and the upper 145 ft of OPZ-18 (i.e., for all of the samples taken from above the Basal Mixed Zone in both boreholes). This statistical analysis was conducted to further analyze piping in the crater-fill from boreholes OBZ-4 and OPZ-18. Figures 3-5a and 3-5b show this relationship for 20 upper samples from OBZ-4 and 14 samples from OPZ-18. A positive correlation exists with correlation coefficients of $r = 0.46$ and $r = 0.52$, respectively. If samples from these depth intervals containing no piped specimens are excluded (9 samples in OBZ-4, 1 in OPZ-18; see Appendices 3-3 and 3-4), the correlation coefficients are much higher, $r = 0.64$ and $r = 0.93$, respectively (figs. 3-5c and 3-5d). The absence of piped specimens in some samples may be a result of the small number of specimens that could be extracted. Nonetheless, in both boreholes there is a positive correlation, suggesting a diminishing contribution of piped material toward the upper intervals of crater-fill.

Injection Dikes. -- Injection dikes were sampled only in borehole OPZ-18 from 189 to 208 ft and 233 ft bsf. Well-preserved AA foraminifers and ostracodes and many articulated, translucent ostracode carapaces occur in these samples. Bright-red Homotrema is also common. The samples from 189.25, 198.0, and 207.3 ft bsf are composed of almost identical assemblages of species, and the preservation is almost identical also. In these dikes, material from BB-CC is conspicuously missing. All evidence suggests an origin for almost all material between 189 and 208 ft from the upper part of zone AA; however, the lack of Neonesidea schulzi with setae argues against any material originating from the Surface. The sample at 210.4 ft contains recrystallized microfossils, and the samples at 229.95 and 232.1 ft bsf contain zone AA species. These are mixed with zone EE-GG species. No piped II-MM zone material occurs in this dike.

Transition Boreholes

Transition boreholes OCT-5, OFT-8, and OKT-13 were sampled for microfossils for the current mixing study.

OCT-5. -- Samples from borehole OCT-5 were analyzed semiquantitatively for ostracodes (Appendix 3-5) and foraminifers. Both microfossil groups, particularly ostracodes, are much less abundant than in samples from OBZ-4 and OPZ-18, and the following zonation is based more heavily on the foraminifers.

0-9 ft. -- Samples from this interval in OCT-5 have anomalously high diversity, with approximately equal contributions from all mid-upper zones (AA-GG), as was the case in the Homogenized Zone of OBZ-4 and OPZ-18. A few piped foraminifers are found at 8.8 ft bsf.

PIPED SPECIMENS VS DEPTH

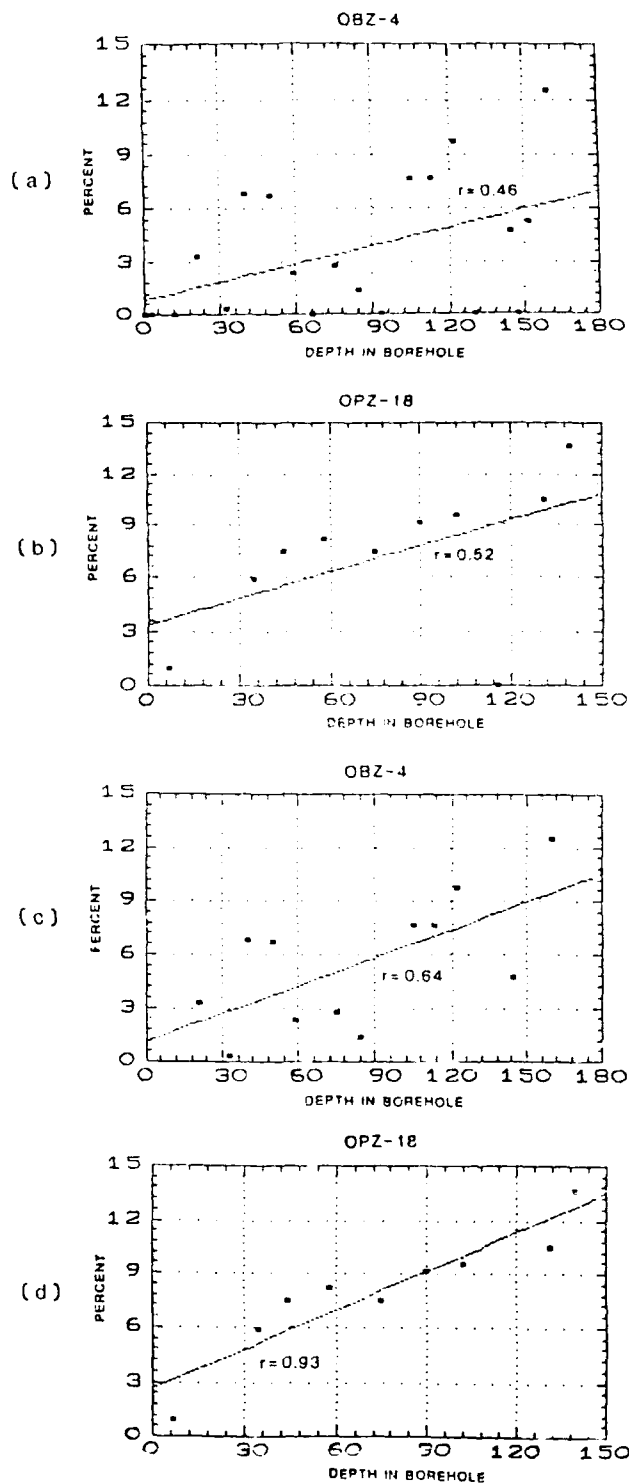


Figure 3-5. -- Plot of percentages of piped specimens versus depth. (5a) borehole OBZ-4, upper 160 ft; (5b) borehole OPZ-18, upper 145 ft; (5c) borehole OBZ-4, upper 160 ft, samples having no piped specimens omitted; (5d) borehole OPZ-18, upper 145 ft, samples having no piped specimens omitted.

39-77 ft. -- Abundant zone AA foraminifers, sparse BB-CC ostracodes, and low percentages of EE-GG material are found in samples from these depths.

86-105 ft. -- Samples from here differ from the overlying ones in lacking zone AA species; this interval has mostly CC-GG foraminifers; however both ostracodes and foraminifers are extremely sparse.

113-140 ft. -- Zone AA species predominate in these samples; preservation of the specimens is similar to specimens from zone AA and bright-red Homotrema (indicative of zone AA) also occurs; samples from here contain low percentages of CC-GG foraminifers.

149-187 ft. -- In this borehole, samples from this interval are almost barren and contain no diagnostic species of either ostracodes or foraminifers. Part of the explanation for the paucity of ostracodes may be that zone EE (normally at roughly comparable depths in the reference boreholes) typically contains few ostracodes in the normal stratigraphic section. However, samples from 149 to 187 ft in OCT-5 also lack even benthic foraminifers, which do occur in zone EE.

OFT-8. -- This borehole has diagnostic microfaunas in all samples examined, allowing a threefold subdivision of the upper 75 ft (Appendix 3-6).

0-19 ft.-- This is a mixed interval containing material from zones AA to probably no deeper than FF. Samples from this interval resemble the Homogenized Zone of the upper parts of other central crater and transitional boreholes. In the uppermost sample at 0.0 to 0.25 ft bsf, a single foraminifer and a single ostracode specimen occur, suggesting piping from zones JJ-MM.

27-50 ft. -- This interval consists almost entirely of material from zone AA, as indicated by the foraminifers. The ostracode species also occur typically in AA and are preserved like those from that zone. There is a noticable absence of zone BB-CC material, also indicating a lack of mixing.

64-75 ft. -- At 64 ft bsf, a mixture of AA and sparse FF-GG foraminifers occurs with typical BB-CC ostracodes. The 74.0-ft sample appears to be from sediment that is essentially in place and consists exclusively of BB-CC material. A detailed sampling across the interval from 50 to 75 ft would be necessary to better document the transition into undisturbed sediments at this borehole site.

OKT-18. -- This borehole contained highly diagnostic ostracodes and foraminifers that allowed a fourfold subdivision of the upper 80 ft (Appendix 3-11). The results from the two fossil groups match each other more consistently, and, thus, these zones are more definitive than in any borehole yet analyzed.

0-19 ft. -- Samples from this interval are noted for their anomalously high species diversity and homogenization of zone AA-GG material. These samples resemble those from the uppermost parts of boreholes OBZ 4, OFZ 13, and OCT-5. No piped specimens are found.

25-37 ft. -- These samples contained almost exclusively material from zone AA; small percentages from EE-GG are noted from the sample at 25.4 ft

bsf. The microfaunas from this interval resemble those from the injection dike in OPZ-18 in both species composition and preservation.

55-66 ft. -- The samples studied contain only material from zones CC-DD. Especially noteworthy is the occurrence of Paracytheridea remanei (which has its acme in DD in all reference boreholes) in OKT-13 at 55.65 (abundant), 59.9, and 68.3 ft. Also, the abundance of Orionina sp. at 59.9 ft is noteworthy. This latter very distinctive species is abundant in OAR-2A at 62 to 75 ft, and a biostratigraphic correlation is probable for strata between 59.9 ft in OKT-13 and 62-75 ft in borehole OAR-2A.

68-81 ft. -- A typical EE-FF assemblage occurs in this interval; there is no obvious mixing from AA or BB.

SUMMARY AND CONCLUSIONS

Our primary conclusions from the mixing study for the OAK crater area follow:

1. Piped material: an inverse relationship exists between sample depth and the percentage of piped material (from zones II-MM) in OBZ-4 between the surface and 160 ft bsf and in OPZ-18 between the surface and 145 ft bsf. Sparse piped specimens occur in the upper 10 ft of OCT-5 and the upper 1 ft of OFT-8; no piped specimens were found in OKT-13.
2. Mixing of abundant Surface material occurs in OBZ-4 and OPZ-18 downward to a depth of 35 ft, although sparse specimens from the Surface occur as deep as 84 ft in OBZ-4.
3. Mixing of abundant material from zone AA is evident in OBZ-4 and OPZ-18 to about 50 to 60 ft bsf; AA material is less common to a depth of about 120 ft bsf in both boreholes.
4. Mixing of moderate amounts of material from zones EE-GG (occurring from 100 to 300 ft bsf in the normal stratigraphic sequence) is encountered in the upper 100 ft of the two central-crater boreholes (OBZ-4 and OPZ-18) and in the upper 20 ft of the transition boreholes. Mixing of BB-CC material is less significant than that of EE-GG material in all boreholes.
5. An apparent injection dike between 189 and 208 ft bsf in OPZ-18 contains almost exclusively AA microfossils. In addition, sediment from these dikes is greenish-gray, like that from the normal AA section. Distinctive microfaunas at 25 to 37 ft in OKT-13 and 27 to 50 ft in OFT-8 are extremely similar to those in this injected OPZ-18 material, although it is not clear if they are genetically related.
6. A Homogenized Mixed Zone containing approximately equal proportions of AA-GG material is a general characteristic of all central-crater (ground-zero) boreholes (down to 40 ft) and in transition boreholes (down to 20 ft).

7. The overall consistency between the ostracodes and foraminifers and our ability to quantitatively revise the standard and mixing zonations to a high degree of resolution gives us confidence that the only limits to our ability to further refine zonations of mixed material, to more accurately identify provenance, and to improve volumetric computations of mixed materials are manpower constraints and sample/core recovery.

REFERENCES

- Brouwers, E.M., Cronin, T.M., and Gibson, T.G., 1986, Chapter 11: Additional paleontologic studies, OAK and KOA Craters: 18 p., 5 figs., 5 tpls., 1 pl.; in Henry, T.W., and Wardlaw, B.R., editors, Pacific Enewetak Atoll Crater Exploration (PEACE) Program, Enewetak Atoll, Republic of the Marshall Islands; Part 3: Stratigraphic analysis and other geologic and geophysical studies in vicinity of OAK and KOA craters: U.S. Geological Survey Open-file Report 86-555.
- Cronin, T.M., Brouwers, E.M., Bybell, L.M., Edwards, L.E., Gibson, T.G., Margerum, R., and Poore, R.Z., 1986, Pacific Enewetak Atoll Crater Exploration (PEACE) Program, Enewetak Atoll, Republic of the Marshall Islands: Part 2; Paleontology and biostratigraphy, application to OAK and KOA craters. U.S. Geological Survey Open-file Report 86-159, 39 p., 20 figs., 12 tpls., 3 appendices.
- Gibson, T.G. and Hill, E.E., in preparation, Late Pliocene to Holocene benthonic Foraminifera from Enewetak Atoll.
- Henry, T.W., and Wardlaw, B.R., 1986, Chapter 1: Introduction: 13 p., 3 figs., 1 tbl.; in Henry, T.W., and Wardlaw, B.R., editors, Pacific Enewetak Crater Exploration (PEACE) Program, Enewetak Atoll, Republic of the Marshall Islands; Part 3: Stratigraphic analysis and other geologic and geophysical studies in vicinity of KOA and OAK craters: U.S. Geological Survey Open-File Report 86-555.
- Henry, T.W., Wardlaw, B.R., Skipp, B., Major, R.P., and Tracy, J.I., Jr., 1986, Pacific Enewetak Atoll Crater Exploration (PEACE) Program, Enewetak Atoll, Republic of the Marshall Islands: Part 1; Drilling operations and descriptions of the boreholes in the vicinity of KOA and OAK craters: U.S. Geological Survey Open-File Report 86-419, 497 p., 32 figs., 29 pls., 13 tpls., 3 appendices.
- Wardlaw, B.R., and Henry, T.W., 1986, Chapter 14: Geologic interpretation of OAK and KOA craters; 39 p., 21 figs., 2 tpls.; in Henry, T.W., and Wardlaw, B.R., editors, Pacific Enewetak Atoll Crater Exploration (PEACE) Program, Enewetak Atoll, Republic of the Marshall Islands; Part 3: Stratigraphic analysis and other geologic and geophysical studies in vicinity of KOA and OAK craters: U.S. Geological Survey Open-File Report 86-555.

Table 3-2.--Summary of foraminifer occurrences in OAK crater borehole OBZ-4.

DEPTH (ft bsf)	FORAMINIFER DATA
2.8-3.05	Mostly AA, some mixing from CC-GG (most likely CC), piping from KK-MM.
11.8-12.05	Mostly AA, moderate amount of CC-GG (most likely CC), piping from JJ-KK.
21.1-21.35	Moderate amount of AA, some CC and EE-GG, piping from II-KK.
33.0-33.25	Mostly AA, mixed with minor CC.
40.05-40.3	Moderate amounts of AA, CC, and EE-GG, moderate amount of piping from II-LL.
58.50-58.75	Mixed AA, CC, and EE-GG, moderate amount of piping from KK-LL.
66.35-66.60	Mixed AA, CC, and EE-GG, more of ?CC or EE-GG than in above sample, some brown specimens presumably from KK-LL.
75.15-75.4	Mixed AA, CC, and EE-GG, more of EE-GG, some brown specimens presumably from KK-LL.
84.15-84.4	Mixed AA, CC, and EE-GG, some piping from KK-LL, possibly MM.
93.1-93.35	Mostly CC and EE-GG, sparse AA, some brown specimens presumably from KK-LL.
104.55-104.8	Mostly CC and EE-GG, sparse AA, piping from KK-LL.
112.9-113.15	No definite AA; some from ?CC, definite EE-GG, piping from KK-LL and possibly from MM.
121.8-122.05	Definite AA and CC and ?EE-GG, some piping from KK-LL.
130.0-130.25	Mostly CC with some EE-GG, sparse brown specimens possibly from deeper zones.
144.5-144.75	?CC and EE-GG.
151.55-151.8	?CC and EE-GG, some brown specimens presumably from deeper zones.
166.85-167.1	?CC and EE-GG.
178.6-178.85	?CC and EE-GG, some brown specimens presumably from deeper zones.
186.8-187.05	?CC and EE-GG.
193.6-193.85	?CC and EE-GG.
196.5-196.75	EE-GG (probably FF) with ?CC.
205.1-205.35	EE-GG (probably FF) with ?CC.
213.9-214.15	EE-GG.
225.65-225.9	EE-GG.

Table 3-3.--Summary of foraminifer occurrences in OAK crater borehole OCT-5.

DEPTH (ft bsf)	FORAMINIFER DATA
0.2-0.45	Specimens from EE-GG, abundant AA, CC; some specimens from II-MM.
8.80-9.05	Mostly specimens from EE-GG, some from AA, some from KK-MM.
17.5-17.75	Some EE-GG, probably BB-CC, no AA.
39.50-39.75	AA and EE-GG with possibly CC and possibly deep zones.
57.55-57.8	Abundant AA and EE-GG.
66.8-67.05	Abundant AA, probable CC and definite EE-GG.
76.65-76.9	Mostly AA, some EE-GG.
86.15-86.4	All from CC-GG, no AA.
95.35-95.6	Same as above sample.
104.25-104.5	Very few specimens, but similar to above sample.
113.15-113.4	Few specimens, definite AA dominant, some from CC.
124.0-124.25	Abundant AA, sparse specimens probably from CC, possibly CC-GG.
132.8-133.05	Almost entirely AA, few specimens from CC or CC-GG.
140.9-141.15	Same as above sample.
149.65-149.9	Barren.
159.6-157.85	Only 1 specimen probably from CC, possibly from BB-GG.
166.4-166.65	Only 1 specimen, provenience uncertain.
176.25-176.5	Only 1 specimen, provenience uncertain, probably CC-GG.
186.0-186.25	Few specimens of CC-GG, probably CC.

Table 3-4.--Summary of foraminifer occurrences in OAK crater borehole OFT-2.

DEPTH (ft bsf)	FORAMINIFER DATA
0.0-0.25	Few specimens, definitely AA (but not uppermost AA), few specimens from EE-GG, scattered light-brown material with 1 immature specimen possibly from JJ-MM, not certain there is deep material.
8.75-9.00	More abundant AA (with more from uppermost AA), sparse specimens from CC, moderate amount from EE-GG, no brown material.
18.60-18.85	Abundant specimens from upper AA, few specimens probably from EE-GG.
27.90-28.15	All specimens from upper part of AA.
35.1-35.35	All specimens from upper part of AA.
43.1-43.35	All specimens from AA, probably slightly lower AA than two samples above.
48.85-49.1	All specimens from AA.
64.0-64.25	Mixture of older part of AA with few from EE-GG.
74.0-74.25	Appears to be unmixed BB-CC.

Table 3-5.--Summary of foraminifer occurrences in OAK crater borehole OKT-13.

DEPTH (ft bsf)	FORAMINIFER DATA
10.4-10.65	Mostly EE-GG, some from lower AA.
18.5-18.75	Mostly CC, some from EE-GG mixed with specimens from AA.
25.4-25.65	Specimens from ?CC mixed with few from EE-GG, more abundant AA than in above two samples
28.75-29.00	All from AA.
36.00-36.25	All from AA.
55.65-55.90	All apparently from CC-DD.
59.5-59.75	All probably from CC-DD.
68.2-68.45	All probably from EE-FF, possibly some CC-DD.
80.00-80.25	All from CC-GG.

Table 3-6.--Summary of foraminifer occurrences in OAK crater borehole OPZ-18.

DEPTH (ft bsf)	FORAMINIFER DATA
7.0-7.25	Mostly AA, with some CC and EE-GG mixed, has light-brown material but no diagnostic specimens.
35.0-35.25	Mostly AA, with some CC and EE-GG mixed, has more light-brown material than above sample but only one probable specimen from KK-MM.
44.6-44.85	AA, with some CC and more EE-GG than above, moderate amount of light-brown material but no diagnostic specimens.
57.85-58.1	More AA than above sample, with EE-GG common, moderate amount of light-brown material but no diagnostic specimens.
74.3-74.55	Mostly AA with some specimens from EE-GG, moderate amount of light-brown but no diagnostic specimens.
89.45-89.7	Mostly AA with some EE-GG, moderate amount of light-brown material with 1 specimen possibly from KK-LL.
102.0-102.25	Few specimens, some AA, some EE-GG, and moderate amount of light-brown material with one specimen questionably from LL-MM.
115.05-115.3	Few specimens, some AA, some EE-GG, moderate amount of light-brown material.
131.0-131.25	Few specimens, some AA, some EE-GG, 1 specimen possibly from KK-MM.
139.7-139.95	Some AA, some EE-GG, some light-brown material.
154.2-154.45	Some AA, some EE-GG, some light-brown material.
169.35-169.6	Some AA and some EE-GG, sparse light-brown material.
174.95-175.1	Some EE-GG, some probably AA, mostly uncertain.
182.3-182.55	Some AA, some EE-GG, very little light brown material.
189.25-189.5	All AA, apparently upper AA.
198.0-198.25	All AA, apparently upper AA.
207.3-207.55	All AA, apparently upper AA.
210.4-210.65	All recrystallized, but no markers??
229.95-230.2	No diagnostic species, most look like ?CC-GG, possibly few AA.
232.1-232.35	Mostly AA, probably upper A, except for 1 specimen from EE-GG.
239.15-239.4	Apparently all EE-GG, probably FF-GG.

BOREHOLE OAR-2/2A

(continued on next page)

BOREHOLE OAR-2/ZA (continued)

DIAGNOSTIC SPECIES	SAMPLE DEPTH (ft bsf)																	TOTAL	
	115.1	127.8	134.0	157.45	171.2	188.25	195.3	204.9	212.45	223.9	234.6	244.55	246.8	268.45	282.55	289.7	337.05	379.5	TOTAL
1. <i>Australimorsella</i> sp.	-	-	-	-	-	-	1	1	1	1	1	2	9	2	3	1	-	-	25
2. <i>Rythoceras</i> sp.	-	-	-	-	-	-	-	1	-	-	-	-	-	-	-	-	-	-	16
3. <i>Callistocythere</i> sp. A	-	-	-	-	-	-	-	-	-	-	-	-	-	-	-	-	-	-	38
4. <i>C. sp. B</i>	2	-	-	1	-	-	-	2	5	13	-	1	-	2	-	-	-	-	5
5. <i>Candohaimia</i> sp.	-	-	-	-	-	-	-	-	-	-	-	-	-	-	-	-	-	-	8
6. <i>Caudites</i> sp. A	-	-	-	-	-	-	-	1	-	2	-	-	2	-	1	-	-	-	10
7. <i>C. sp. B</i>	-	-	-	-	-	-	-	-	-	-	-	4	1	-	-	1	-	-	21
8. <i>Cretocythereis</i> sp. A	-	-	-	1	-	2	5	-	-	1	-	3	1	-	1	-	-	-	12
9. <i>C. canaliculata</i>	-	-	-	-	-	-	-	5	1	-	6	3	-	-	-	-	-	-	9
10. <i>C. rastromarginata</i>	1	1	-	-	-	-	-	-	-	-	-	-	-	-	-	-	-	-	4
11. <i>Cytherelloidea</i> sp.	-	-	-	-	-	-	-	-	-	3	-	1	-	-	-	-	-	-	9
12. <i>Hemicytherura</i> sp.	-	-	-	-	-	-	-	-	-	-	-	-	-	-	-	-	-	-	44
13. <i>Hemicythere</i> sp.	-	-	1	-	-	-	-	4	-	-	-	-	-	-	-	-	-	-	111
14. <i>Hemianites mooneyi</i>	-	-	-	-	-	-	-	-	-	-	-	-	-	5	-	-	-	-	142
15. <i>H. parvifolia</i>	-	-	9	-	-	-	-	16	2	23	1	-	5	-	-	3	-	-	218
16. <i>H. transoceanica</i>	5	8	-	-	-	-	-	4	1	14	3	10	13	7	-	8	-	-	5
17. <i>Jugosocythereis</i> sp.	2	2	4	1	-	-	1	9	7	13	7	9	20	7	-	10	-	-	36
18. <i>Keijia demissa</i>	-	-	-	-	-	-	-	-	-	-	-	-	-	-	-	-	-	-	2
19. <i>Loxococoncha hemorhinalensis</i>	-	4	-	-	-	-	-	-	-	-	-	-	-	-	-	-	-	-	679
20. <i>L. huahinensis</i>	1	18	30	37	-	2	7	82	34	51	8	31	12	15	10	24	-	27	77
21. <i>L. insulariensis</i>	-	-	-	-	-	-	-	13	8	3	7	9	4	3	2	4	-	4	46
22. <i>L. labyrinthica</i>	2	-	5	-	-	-	-	-	-	-	6	5	6	6	3	2	-	1	25
23. <i>L. n. sp. A</i>	-	-	-	-	-	-	-	-	-	-	-	-	-	10	7	6	-	-	8
24. <i>Loxococoncha</i> sp. A	-	-	-	-	-	-	-	-	-	-	-	-	-	-	-	-	-	-	2
25. <i>L. sp. B</i>	-	-	-	1	-	-	-	-	-	-	-	-	-	-	-	-	-	-	12
26. <i>L. sp. C</i>	-	2	-	1	-	-	-	-	-	-	-	-	1	-	-	-	-	-	3
27. <i>Micropridoteis</i> sp.	-	-	-	-	-	-	-	15	14	9	-	-	-	2	4	-	-	1	45
28. <i>Morkhovenia inaequalis</i>	-	-	2	-	-	-	-	4	-	-	-	3	4	1	-	1	-	-	21
29. <i>Neonesidea schulzi</i>	8	-	3	15	1	1	-	10	4	1	2	3	-	-	-	1	-	-	260
30. <i>Oculocythereis</i> sp.	-	-	-	-	-	-	-	-	-	-	-	-	-	-	-	-	-	-	19
31. <i>Orionina</i> sp.	-	-	-	-	-	-	-	-	-	-	-	-	-	-	-	-	-	-	53
32. <i>Ornatoleberis</i> sp.	-	1	5	-	-	-	-	9	-	3	-	-	-	-	-	-	-	-	25
33. <i>Paracytheridea nemani</i>	-	-	-	1	-	-	-	-	-	1	-	-	-	-	-	-	-	-	1
34. <i>Pontocythereis</i> sp.	-	-	-	-	-	-	-	-	-	-	-	-	-	-	-	-	-	-	7
35. <i>Procythereis</i> sp. A	-	-	-	-	-	-	-	13	4	5	-	2	-	-	1	-	-	-	32
36. <i>P. sp. B</i>	-	-	-	-	-	-	-	-	-	11	-	-	-	-	-	-	-	-	11
37. <i>Pterohaimia maddisae</i>	-	-	-	-	-	-	1	-	-	-	1	-	-	-	-	-	-	-	2
38. <i>Semicytherura</i> sp.	-	-	-	-	-	-	-	1	-	1	2	6	2	1	1	-	-	-	19
39. <i>Trieblina senkai</i>	-	-	-	-	-	-	1	1	-	-	-	-	-	-	-	-	-	-	3
40. Other	12	14	9	18	-	1	7	38	44	41	29	28	31	55	21	19	1	34	868
TOTAL	33	42	76	76	1	6	23	230	125	196	73	117	111	116	54	80	1	88	2033

BOREHOLE OOR-17

(continued on next page)

BOREHOLE OOR-17 (continued)

DIAGNOSTIC SPECIES	184.25	193.6	200.9	209.3	215.5	226.05	233.35	239.0	250.3	261.5	270.1	285.65	292.1	299.15	310.7	320.2	331.2	339.0	367.9	TOTAL
1. <i>Australimacella</i> sp.	-	-	-	-	-	-	1	-	-	-	-	-	-	-	-	-	3	2	0	14
2. <i>Bythoseratina</i> sp.	-	-	-	-	-	-	-	-	-	-	1	-	-	-	-	-	-	-	-	1
3. <i>Callistocythere</i> sp. A	5	-	-	-	-	-	-	-	-	-	-	-	-	-	-	-	-	-	-	47
4. <i>C. sp. B</i>	-	-	-	-	-	1	2	-	1	-	-	-	-	1	-	-	-	-	-	25
5. <i>Cardobairdia</i> sp.	-	-	-	-	-	-	-	-	-	-	-	-	-	-	-	-	-	-	-	5
6. <i>Caudites</i> sp. A	1	-	-	-	-	-	4	1	-	-	1	1	-	-	-	-	-	-	-	11
7. <i>C. sp. B</i>	-	-	-	-	-	-	-	-	-	-	4	-	-	-	-	-	-	-	-	5
8. <i>Cletocythereis</i> sp. A	-	-	1	6	1	3	6	-	3	-	13	-	-	1	-	-	1	2	-	113
9. <i>C. canaliculata</i>	-	-	-	-	-	-	3	-	-	-	-	-	-	-	-	-	-	-	-	7
10. <i>C. rastromarginata</i>	2	-	1	1	-	-	1	-	-	-	-	1	-	-	-	-	-	-	-	7
11. <i>Cythereelloidea</i> sp.	-	-	-	-	-	-	-	-	-	-	1	-	-	-	-	-	1	-	-	2
12. <i>Hemicytherura</i> sp.	-	-	-	-	-	-	-	-	-	-	-	-	-	-	-	-	-	-	-	5
13. <i>Hemicythere</i> sp.	-	1	1	-	-	-	-	-	-	-	-	-	-	-	-	-	-	-	-	4
14. <i>Hemantites mooneyi</i>	-	-	-	-	-	-	-	-	-	-	-	-	-	-	-	-	-	-	-	9
15. <i>H. parviflora</i>	1	-	11	5	-	-	-	-	-	-	-	9	-	4	-	-	-	-	-	87
16. <i>H. transoceanica</i>	8	1	9	2	4	-	2	-	1	-	7	4	1	4	-	-	-	-	1	177
17. <i>Jugosocythereis</i> sp.	11	-	6	4	2	-	-	-	-	-	1	1	2	2	1	1	7	2	-	117
18. <i>Katja demissa</i>	-	-	-	-	-	-	-	-	-	-	-	-	-	-	-	-	-	-	-	4
19. <i>Lazocochia heronislanaensis</i>	3	-	-	-	-	-	-	-	-	-	-	-	1	-	-	-	-	-	-	60
20. <i>L. huahinensis</i>	-	3	35	25	14	7	62	-	1	1	16	31	12	26	1	-	3	3	1	475
21. <i>L. theulardaensis</i>	-	-	-	-	3	3	5	-	-	-	5	3	2	2	-	-	2	2	-	79
22. <i>L. labrynthica</i>	3	-	11	3	-	-	7	-	1	-	-	-	-	-	-	-	-	-	-	46
23. <i>L. n. sp. A</i>	-	-	-	-	-	-	-	-	-	-	-	-	-	-	-	-	-	-	2	4
24. <i>Lazocochella</i> sp. A	-	-	-	-	-	-	-	-	-	-	1	-	-	-	-	-	-	-	-	7
25. <i>L. sp. B</i>	-	-	-	-	-	-	4	-	-	-	3	-	-	-	-	-	-	-	-	8
26. <i>L. sp. C</i>	-	-	-	-	-	-	-	-	-	-	-	5	-	-	-	-	-	-	-	6
27. <i>Miocypridea</i> sp.	-	-	-	-	-	-	-	-	-	-	-	-	-	-	-	-	-	-	-	-
28. <i>Morkhovenia inconspicua</i>	-	1	-	-	2	-	2	-	-	-	-	-	3	-	-	-	-	-	-	13
29. <i>Reonesidea schulzei</i>	1	-	5	2	2	2	9	1	-	-	3	-	3	-	-	-	-	-	-	336
30. <i>Oculocythereis</i> sp.	-	-	-	-	-	-	-	-	-	-	-	-	-	-	-	-	-	-	-	-
31. <i>Orionina</i> sp.	-	-	-	-	-	-	-	-	-	-	-	-	-	-	-	-	-	-	-	13
32. <i>Ornatoleberis</i> sp.	-	-	6	-	-	-	1	-	-	-	1	4	-	-	-	-	-	-	-	39
33. <i>Paracytheridea nemani</i>	-	-	-	-	-	1	2	-	-	-	8	2	-	-	-	-	-	-	2	79
34. <i>Pontocythereis</i> sp.	-	-	-	-	-	-	-	-	-	-	-	-	-	-	-	-	-	-	-	1
35. <i>Procythereis</i> sp. A	-	-	-	-	-	-	-	-	-	-	-	-	3	2	1	-	1	-	-	7
36. <i>P. sp. B</i>	-	-	-	-	-	-	-	-	-	-	-	-	-	-	-	-	-	-	-	1
37. <i>Pterohatmia madlockeae</i>	-	-	-	-	-	-	-	-	-	-	-	-	-	-	-	-	-	-	-	1
38. <i>Semicytherura</i> sp.	-	-	-	-	-	-	3	-	-	-	-	-	-	-	-	-	-	-	1	10
39. <i>Trieblina serrata</i>	-	-	-	-	-	-	-	-	-	-	-	-	-	-	-	-	-	-	-	5
40. Other	5	-	2	12	12	-	17	1	2	-	24	47	12	38	-	-	-	1	1	913
TOTAL	40	6	88	60	41	17	131	3	9	1	89	112	39	83	3	1	17	12	8	2743

APPENDIX 3-3

BOREHOLE OBZ-4

DIAGNOSTIC SPECIES	SAMPLE DEPTH (ft bsf)															
	0.0	2.8	11.8	21.1	33.0	40.05	49.7	58.5	66.35	75.15	84.15	93.1	104.55	112.9	121.8	130.0
1. <i>Australimoesella</i> sp.	-	-	-	2	-	1	1	2	1	-	2	-	-	-	1	-
2. <i>Bythoserratina</i> sp.	-	-	-	1	-	-	-	-	-	-	1	-	-	-	-	-
3. <i>Callistocythere</i> sp. A	7	-	-	1	-	1	-	-	-	-	-	-	-	-	-	-
4. <i>C. sp. B</i>	1	-	-	-	4	-	1	-	1	-	2	1	-	1	-	-
5. <i>Cardobairdia</i> sp.	-	-	-	-	-	-	-	-	-	-	-	-	-	-	-	-
6. <i>Caudites</i> sp. A	-	-	-	-	-	-	-	-	-	-	-	-	-	-	-	-
7. <i>C. sp. B</i>	-	-	-	-	-	-	-	-	-	-	-	-	-	-	-	-
8. <i>Cletoocythereis</i> sp. A	-	-	-	3	-	7	3	3	-	1	2	1	-	2	1	-
9. <i>C. canaliculata</i>	-	-	-	-	-	2	-	-	-	-	-	-	-	-	-	-
10. <i>C. rietromarginata</i>	-	-	-	-	-	-	-	-	-	-	-	-	-	-	-	-
11. <i>Cytherelloidea</i> sp.	1	-	-	-	-	1	1	-	-	-	-	-	-	-	-	-
12. <i>Hemicytherura</i> sp.	-	-	-	-	-	2	3	-	-	-	-	-	-	-	-	-
13. <i>Hemicythere</i> sp.	-	-	-	-	-	2	-	-	-	-	-	-	-	-	-	-
14. <i>Hermanites mooneyi</i>	3	-	1	3	2	-	1	-	1	1	2	-	-	-	2	-
15. <i>H. parvifolia</i>	5	-	10	2	2	-	-	-	-	1	7	-	-	-	10	3
16. <i>H. transoceanica</i>	8	2	-	-	25	5	8	-	-	2	3	2	-	1	11	1
17. <i>Jugocythereis</i> sp.	7	3	1	7	6	11	12	4	-	3	10	1	2	1	9	-
18. <i>Ketia demissa</i>	-	-	-	-	1	-	-	-	-	-	1	-	-	-	1	-
19. <i>Loxocoche heronislaniensis</i>	-	-	-	1	2	4	11	6	-	3	4	3	2	1	-	-
20. <i>L. huahinensis</i>	18	9	11	27	25	24	26	5	3	9	31	8	3	4	22	2
21. <i>L. insulariensis</i>	5	1	5	2	7	7	5	1	1	1	4	1	-	6	1	1
22. <i>L. labrynthica</i>	-	-	-	6	1	2	3	1	1	-	3	2	-	-	2	-
23. <i>L. n. sp. A</i>	-	-	-	-	-	-	-	-	-	-	-	-	-	-	-	-
24. <i>Loxococheella</i> sp. A	-	-	-	1	-	-	-	-	-	-	-	-	-	-	-	-
25. <i>L. sp. B</i>	-	-	-	-	-	-	-	-	-	-	-	-	-	-	-	-
26. <i>L. sp. C</i>	5	-	2	1	14	-	-	-	-	-	-	-	-	-	-	-
27. <i>Miocypridea</i> sp.	-	-	-	-	-	3	4	-	-	-	-	-	-	-	-	-
28. <i>Mochoveria inconspicua</i>	1	1	-	-	3	3	1	-	-	-	3	-	2	-	-	-
29. <i>Neonesidea schulzi</i>	33	2	8	2	61	-	13	7	4	5	11	1	-	-	-	-
30. <i>Oculocythereis</i> sp.	-	-	-	-	1	-	-	-	-	-	-	-	-	-	-	-
31. <i>Orionina</i> sp.	-	-	-	-	-	3	1	-	-	-	-	1	-	-	2	-
32. <i>Ornatolabris</i> sp.	4	-	1	-	-	1	3	-	-	-	2	2	-	-	-	-
33. <i>Paracytheridea remani</i>	2	-	-	3	3	6	3	-	-	2	2	-	-	-	8	2
34. <i>Pontocythereis</i> sp.	-	-	-	-	-	-	-	-	-	-	-	-	-	-	-	-
35. <i>Procythereis</i> sp. A	-	-	-	1	-	2	1	-	-	-	-	-	1	1	-	-
36. <i>P. sp. B</i>	-	-	-	-	-	-	2	-	-	-	-	-	-	-	-	-
37. <i>Pterobairdia maddockae</i>	-	-	-	-	-	-	-	-	-	-	-	-	-	-	-	-
38. <i>Semicytherura</i> sp.	-	-	-	1	1	2	1	-	-	-	1	-	-	-	4	-
39. <i>Triebelina serrata</i>	-	-	-	-	-	-	-	-	-	-	-	-	-	-	-	-
40. Other	88	10	23	27	171	47	23	14	13	7	44	17	8	4	37	8
41. "Piped" specimens	-	-	-	3	1	9	7	1	-	-	2	-	1	1	13	-
TOTAL	188	32	70	93	336	147	134	44	26	37	140	40	26	13	133	19
																8

(continued on next page)

BOREHOLE OBZ-4 (continued)

DIAGNOSTIC SPECIES	SAMPLE DEPTH (ft bsf)																			TOTAL
	166.85	169.85	178.6	182.35	186.8	190.3	193.6	196.5	205.1	213.9	225.65	250.05	291.45	300.5	314.75	327.1	336.25	347.15	356.45	
1. <i>Australimorsella</i> sp.	-	1	1	4	-	1	-	-	-	-	-	1	-	-	-	-	-	2	1	21
2. <i>Rythoceratina</i> sp.	-	-	-	-	-	-	-	-	1	1	-	-	-	-	-	-	-	-	-	4
3. <i>Callistocythere</i> sp. A	-	-	-	-	2	-	-	9	6	-	-	-	-	-	-	-	-	1	-	27
4. <i>C. sp. B</i>	-	-	1	-	1	-	-	-	-	1	-	-	-	-	-	-	-	-	-	17
5. <i>Cardobairdia</i> sp.	-	-	-	-	-	-	-	-	-	-	-	-	-	-	-	-	-	1	-	1
6. <i>Caudites</i> sp. A	-	-	-	-	-	-	-	2	-	1	-	-	-	-	-	-	-	-	-	8
7. <i>C. sp. B</i>	-	-	-	-	-	-	-	-	-	-	-	-	-	-	-	-	-	-	-	3
8. <i>Cletocythereis</i> sp. A	1	-	1	-	-	-	-	6	-	-	-	2	-	-	-	-	-	1	-	35
9. <i>C. canaliculata</i>	-	-	-	-	-	-	-	-	-	-	-	-	-	-	-	-	-	-	-	3
10. <i>C. waikamoiensis</i>	-	-	-	-	2	-	-	-	-	-	-	-	-	-	-	-	-	-	-	2
11. <i>Cytherelloidea</i> sp.	-	-	-	-	-	-	-	1	-	-	-	-	-	-	-	-	-	-	-	6
12. <i>Hemicytherura</i> sp.	-	-	-	-	-	-	-	-	-	-	-	-	-	-	-	-	-	-	-	-
13. <i>Hemicythere</i> sp.	-	-	-	-	-	-	-	-	-	-	-	-	-	-	-	-	-	-	-	-
14. <i>Hemantites mooneyi</i>	-	-	-	-	-	-	-	-	-	-	-	-	-	-	-	-	-	-	-	10
15. <i>H. parvifolia</i>	1	-	1	7	5	-	1	6	3	-	1	-	-	-	-	-	-	2	1	15
16. <i>H. transoceanica</i>	-	-	-	2	-	3	-	4	1	-	-	-	-	1	-	-	-	-	-	78
17. <i>Jupanoocythereis</i> sp.	-	1	3	6	4	-	2	17	22	2	8	2	3	-	1	2	-	-	-	82
18. <i>Katja hemia</i>	-	-	-	-	-	-	1	-	-	-	-	-	-	-	-	-	-	-	-	158
19. <i>Loxococoncha heronialandensis</i>	1	2	-	-	-	-	-	-	-	-	-	-	-	-	-	-	-	7	-	5
20. <i>L. huahinensis</i>	2	7	4	17	6	5	4	27	12	14	4	2	-	1	-	3	-	1	-	363
21. <i>L. insularioides</i>	-	-	1	4	1	1	2	11	13	1	1	1	-	-	-	-	-	1	1	88
22. <i>L. labyrinthica</i>	-	1	1	2	1	-	-	7	4	-	1	-	-	-	-	-	-	-	-	42
23. <i>L. n. sp. A</i>	-	-	-	-	-	-	-	-	-	-	-	-	-	-	-	-	-	-	-	-
24. <i>Loxococonchella</i> sp. A	-	-	-	-	-	-	-	-	-	-	-	-	-	-	-	-	-	-	-	1
25. <i>L. sp. B</i>	-	-	-	-	-	-	-	-	-	-	-	-	-	-	-	-	-	-	-	-
26. <i>L. sp. C</i>	-	-	-	1	-	-	-	-	-	-	-	-	-	-	-	-	-	-	-	23
27. <i>Miocyprideis</i> sp.	-	-	-	-	-	-	-	-	-	-	-	-	-	-	-	-	-	-	-	8
28. <i>Monkhouvia inconspicua</i>	-	-	-	2	-	-	-	-	-	-	-	1	-	-	-	-	-	-	-	17
29. <i>Neonesidea schulzei</i>	-	3	1	5	3	-	-	7	4	2	1	-	-	1	-	-	2	-	-	180
30. <i>Oculocythereis</i> sp.	-	-	-	-	-	-	-	-	-	-	-	-	-	-	-	-	-	-	-	-
31. <i>Orionina</i> sp.	-	-	-	-	-	-	-	22	14	-	-	-	-	-	-	-	-	-	-	46
32. <i>Ornatoleberis</i> sp.	-	-	-	-	-	-	-	4	-	-	-	-	-	-	-	1	-	3	-	23
33. <i>Paracytheridea remani</i>	-	1	-	1	2	-	1	-	-	-	-	-	-	-	-	1	-	1	-	39
34. <i>Pontocythereis</i> sp.	-	-	-	-	-	-	-	-	-	-	-	-	-	-	-	-	-	-	-	9
35. <i>Procythereis</i> sp. A	-	-	-	-	-	-	-	-	-	-	-	-	-	-	-	-	-	-	-	6
36. <i>P. sp. B</i>	-	-	-	-	-	-	-	-	-	-	-	-	-	-	-	-	-	-	-	1
37. <i>Pterobairdia madrocare</i>	-	-	-	-	-	-	-	1	-	-	-	-	-	-	-	-	-	-	-	5
38. <i>Semicytherura</i> sp.	-	-	-	-	-	-	-	-	-	1	-	1	-	-	-	-	-	-	-	1
39. <i>Trieblina senhata</i>	-	-	-	-	-	-	-	-	-	-	-	-	-	-	-	-	-	-	-	15
40. Other	8	5	5	25	13	9	7	51	23	5	5	5	2	-	2	5	2	11	3	747
41. "Piped" specimens	-	-	-	1	-	-	-	-	-	-	-	-	-	-	-	-	-	-	-	41
TOTAL	13	21	19	77	41	19	18	175	103	28	21	15	6	3	3	14	2	32	7	2180

APPENDIX 3-4

BOREHOLE OPZ-18

DIAGNOSTIC SPECIES	SAMPLE DEPTH (ft bsf)																					TOTAL
	7.0	35.0	44.6	57.85	74.3	89.45	102.0	115.05	131.0	139.7	154.2	169.35	174.95	182.3	189.25	198.0	207.3	210.4	229.95	232.1	239.15	
1. <i>Australimacella</i> sp.	1	4	1	-	-	-	1	-	1	-	-	-	1	1	-	-	-	-	1	-	1	12
2. <i>Bythoceratina</i> sp.	1	1	1	-	-	-	-	-	-	-	-	1	-	-	-	-	-	-	-	-	-	4
3. <i>Callistocythere</i> sp. A	-	1	-	1	1	-	-	-	-	-	2	-	-	-	-	-	4	-	-	-	-	5
4. <i>C. sp. B</i>	1	2	1	-	-	2	-	1	-	-	-	2	2	2	1	4	4	-	1	1	2	26
5. <i>Cardobairia</i> sp.	-	-	-	-	-	-	-	-	-	-	-	-	-	-	-	-	-	-	-	-	-	-
6. <i>Caudites</i> sp. A	-	6	1	-	-	-	-	-	-	-	-	1	2	-	-	-	-	-	-	-	1	11
7. <i>C. sp. B</i>	-	-	-	-	-	-	-	-	-	-	-	-	-	-	-	-	-	-	-	-	-	-
8. <i>Cleocythereis</i> sp. A	3	14	-	2	-	-	2	-	1	-	-	-	-	-	-	-	-	-	-	1	1	23
9. <i>C. canaliculata</i>	1	2	-	-	-	-	-	-	-	-	-	-	2	-	-	-	-	-	-	-	-	5
10. <i>C. rastrumarginata</i>	-	1	-	-	-	-	-	-	-	-	-	-	-	-	-	-	-	-	-	1	2	2
11. <i>Cytherelloidea</i> sp.	1	1	-	1	-	-	-	-	-	-	-	-	-	-	-	-	-	-	-	1	-	4
12. <i>Hemicytherura</i> sp.	-	-	-	-	-	-	-	-	-	-	1	-	-	-	-	-	-	-	-	-	-	-
13. <i>Hemicythere</i> sp.	2	2	-	-	-	-	-	-	1	-	-	-	-	-	-	-	-	-	-	-	-	-
14. <i>Hemantites mooneyi</i>	1	6	1	-	-	-	-	-	-	-	-	-	-	-	-	-	-	-	-	-	-	-
15. <i>H. parviflora</i>	8	18	10	5	-	-	1	-	3	2	5	-	3	4	-	5	22	3	1	3	3	75
16. <i>H. transoceanica</i>	16	11	8	-	1	-	-	-	2	-	3	3	3	-	14	28	8	2	2	5	6	110
17. <i>Jugosocythereis</i> sp.	8	17	11	5	4	-	-	3	11	-	-	7	-	11	6	2	11	1	-	9	5	111
18. <i>Keijia demissa</i>	-	1	-	-	-	-	-	-	1	1	1	-	1	-	-	-	-	-	-	-	-	6
19. <i>Loxocoche heronialandensis</i>	4	3	8	1	1	-	1	6	-	1	2	2	4	2	-	-	-	-	-	-	-	35
20. <i>L. huatinensis</i>	29	82	17	13	7	4	7	-	11	5	19	23	13	17	33	72	40	3	5	34	13	447
21. <i>L. insulariandensis</i>	6	16	3	1	2	-	-	3	4	-	4	2	2	4	-	1	-	1	1	-	2	52
22. <i>L. labrynthica</i>	4	4	2	1	1	-	-	1	2	-	2	1	1	1	-	-	-	-	-	-	-	20
23. <i>L. n. sp. A</i>	-	-	-	-	-	-	-	-	-	-	-	-	-	-	-	-	-	-	-	-	-	-
24. <i>Loxocoche</i> sp. A	2	3	-	-	-	-	-	-	-	-	-	-	-	-	-	2	-	-	-	1	-	8
25. <i>L. sp. B</i>	-	-	-	-	-	-	-	-	-	-	-	-	1	-	-	-	-	-	-	-	-	1
26. <i>L. sp. C</i>	7	1	-	-	-	-	-	-	-	-	-	-	-	-	1	-	-	-	-	-	-	9
27. <i>Miocyprideis</i> sp.	-	-	-	-	-	-	-	-	-	-	-	-	-	-	-	-	-	-	-	-	-	-
28. <i>Northoventia inconspicua</i>	1	2	1	-	1	-	-	-	-	-	2	2	-	1	-	2	1	-	1	-	1	15
29. <i>Neonastidea echulzi</i>	41	19	-	1	6	-	-	3	-	-	-	-	-	-	-	6	4	-	-	5	-	85
30. <i>Oculocythereis</i> sp.	1	-	-	-	-	-	-	-	-	-	-	-	-	-	-	-	-	-	-	-	-	1
31. <i>Orionina</i> sp.	-	-	-	-	-	-	-	-	-	-	-	-	-	-	-	-	-	-	-	-	-	3
32. <i>Omatoleberis</i> sp.	3	7	1	1	-	1	-	-	1	-	-	-	1	1	-	6	9	2	-	-	-	32
33. <i>Paracytheridea remani</i>	1	22	5	2	2	-	1	-	1	2	10	9	1	3	6	27	5	-	-	2	8	107
34. <i>Pontocythereis</i> sp.	-	-	-	-	-	-	-	-	-	-	-	-	-	-	-	-	-	-	-	-	-	-
35. <i>Procythereis</i> sp. A	-	-	-	-	-	-	-	-	-	-	-	-	-	-	-	-	-	-	-	-	-	-
36. <i>P. sp. B</i>	-	1	-	-	-	-	-	-	-	-	-	-	-	-	-	-	-	-	-	-	-	2
37. <i>Pterobairia maddockensis</i>	1	-	-	-	-	-	-	-	-	-	-	-	-	-	-	-	-	-	-	-	-	1
38. <i>Semicytherura</i> sp.	-	4	2	-	1	1	1	-	-	-	4	-	1	2	-	-	-	-	-	-	3	19
39. <i>Trieblina serrata</i>	-	-	-	-	-	-	-	-	-	-	-	-	-	-	-	-	-	-	-	-	-	-
40. Other	58	73	26	11	10	12	5	17	29	8	17	19	14	13	20	26	15	8	3	41	22	447
41. "Piped" specimens	2	19	8	4	3	2	2	-	8	3	2	6	1	-	-	-	-	-	-	-	-	60
TOTAL	202	343	107	49	40	22	21	35	76	22	74	78	53	65	92	205	95	16	17	106	70	1788

APPENDIX 3-5

BOREHOLE OCT-5

DIAGNOSTIC SPECIES	0.2	8.8	17.5	39.5	48.05	57.55	66.8	76.65	86.15	95.35	104.25	113.15	124.0	132.8	140.9	149.65	157.6	166.4	176.25	186.0	TOTAL
1. <i>Australimoesella</i> sp.	-	-	-	-	-	-	-	-	-	-	-	-	-	-	-	-	-	-	-	-	1
2. <i>Bythoceratina</i> sp.	-	-	-	-	-	-	-	-	-	-	-	-	-	-	-	-	-	-	-	-	4
3. <i>Callistocythere</i> sp. A	4	-	-	-	-	-	-	-	-	-	-	-	-	-	-	-	-	-	-	-	2
4. <i>C. sp. B</i>	1	-	-	-	-	-	-	-	-	-	-	-	-	-	-	-	-	-	-	-	1
5. <i>Cardobairdia</i> sp.	-	-	-	-	-	-	-	-	-	-	-	-	-	-	-	-	-	-	-	-	1
6. <i>Caudites</i> sp. A	1	-	-	-	-	-	-	-	-	-	-	-	-	-	-	-	-	-	-	-	3
7. <i>C. sp. B</i>	3	-	-	-	-	-	-	-	-	-	-	-	-	-	-	-	-	-	-	-	6
8. <i>Cleocythereis</i> sp. A	3	-	-	-	-	-	-	-	-	-	-	-	-	-	-	-	-	-	-	-	1
9. <i>C. canaliculata</i>	1	-	-	-	-	-	-	-	-	-	-	-	-	-	-	-	-	-	-	-	1
10. <i>C. mastromarginata</i>	-	-	-	-	-	-	-	-	-	-	-	-	-	-	-	-	-	-	-	-	-
11. <i>Cythereelloidea</i> sp.	-	-	-	-	-	-	-	-	-	-	-	-	-	-	-	-	-	-	-	-	-
12. <i>Hemicytherura</i> sp.	1	-	-	-	-	-	-	-	-	-	-	-	-	-	-	-	-	-	-	-	5
13. <i>Hemicythere</i> sp.	2	-	-	-	-	-	-	-	-	-	-	-	-	-	-	-	-	-	-	-	2
14. <i>Hemantites mooneyi</i>	4	-	-	-	-	-	-	-	-	-	-	-	-	-	-	-	-	-	-	-	6
15. <i>H. parviloba</i>	13	-	-	-	-	-	-	-	-	-	-	-	-	-	-	-	-	-	-	-	17
16. <i>H. transoceanica</i>	13	1	-	-	-	-	-	-	-	-	-	-	-	-	-	-	-	-	-	-	28
17. <i>Jugosocythereis</i> sp.	2	-	-	-	-	-	-	-	-	-	-	-	-	-	-	-	-	-	-	-	6
18. <i>Katija demissa</i>	5	-	-	-	-	-	-	-	-	-	-	-	-	-	-	-	-	-	-	-	6
19. <i>Loxocoelcha heronialandensis</i>	35	1	1	2	-	-	-	-	-	-	-	-	-	-	-	-	-	-	-	-	61
20. <i>L. huahinensis</i>	6	-	-	-	-	-	-	-	-	-	-	-	-	-	-	-	-	-	-	-	11
21. <i>L. insulariensis</i>	2	-	-	-	-	-	-	-	-	-	-	-	-	-	-	-	-	-	-	-	4
22. <i>L. labrynthica</i>	-	-	-	-	-	-	-	-	-	-	-	-	-	-	-	-	-	-	-	-	-
23. <i>L. n. sp. A</i>	-	-	-	-	-	-	-	-	-	-	-	-	-	-	-	-	-	-	-	-	-
24. <i>Loxocoelcha</i> sp. A	-	-	-	-	-	-	-	-	-	-	-	-	-	-	-	-	-	-	-	-	-
25. <i>L. sp. B</i>	1	-	-	-	-	-	-	-	-	-	-	-	-	-	-	-	-	-	-	-	1
26. <i>L. sp. C</i>	-	-	-	-	-	-	-	-	-	-	-	-	-	-	-	-	-	-	-	-	1
27. <i>Miocypruleis</i> sp.	-	-	-	-	-	-	-	-	-	-	-	-	-	-	-	-	-	-	-	-	5
28. <i>Morhouenia inconspicua</i>	5	-	-	-	-	-	-	-	-	-	-	-	-	-	-	-	-	-	-	-	11
29. <i>Neonestlea schulzi</i>	4	-	-	-	-	-	-	-	-	-	-	-	-	-	-	-	-	-	-	-	1
30. <i>Oeculocythereis</i> sp.	-	-	-	-	-	-	-	-	-	-	-	-	-	-	-	-	-	-	-	-	1
31. <i>Orionina</i> sp.	-	-	-	-	-	-	-	-	-	-	-	-	-	-	-	-	-	-	-	-	1
32. <i>Ornatoleberis</i> sp.	1	-	-	-	-	-	-	-	-	-	-	-	-	-	-	-	-	-	-	-	1
33. <i>Paracytheridea nemani</i>	13	-	-	-	-	-	-	-	-	-	-	-	-	-	-	-	-	-	-	-	13
34. <i>Pontocythereis</i> sp.	-	-	-	-	-	-	-	-	-	-	-	-	-	-	-	-	-	-	-	-	-
35. <i>Procythereis</i> sp. A	-	-	-	-	-	-	-	-	-	-	-	-	-	-	-	-	-	-	-	-	-
36. <i>P. sp. B</i>	2	-	-	-	-	-	-	-	-	-	-	-	-	-	-	-	-	-	-	-	2
37. <i>Pterobairdia madrocarensis</i>	-	-	-	-	-	-	-	-	-	-	-	-	-	-	-	-	-	-	-	-	-
38. <i>Semicytherura</i> sp.	3	-	-	-	-	-	-	-	-	-	-	-	-	-	-	-	-	-	-	-	3
39. <i>Trieblina nemata</i>	-	-	-	-	-	-	-	-	-	-	-	-	-	-	-	-	-	-	-	-	-
40. Other	45	3	3	-	1	15	-	5	1	3	-	4	-	2	3	-	-	-	-	-	88
41. "Piped" specimens	-	-	-	-	-	-	-	-	-	-	-	-	-	-	-	-	-	-	-	-	-
TOTAL	170	2	8	4	1	55	1	10	1	3	-	7	4	3	8	5	1	3	6	-	292

APPENDIX 3-6
BOREHOLE OBT-8

DIAGNOSTIC SPECIES	SAMPLE DEPTH (ft bsf)									TOTAL
	0.0	8.75	18.6	27.9	35.1	43.1	48.85	64.0	74.0	
1. <i>Australimoesella</i> sp.	-	-	-	-	-	-	-	-	-	-
2. <i>Bythoceratina</i> sp.	-	-	-	-	-	-	-	-	-	-
3. <i>Callistocythere</i> sp. A	-	-	-	-	-	1	-	1	-	2
4. <i>C.</i> sp. B	-	-	-	-	-	-	-	-	-	-
5. <i>Cardohairdia</i> sp.	-	-	-	1	-	-	-	-	-	1
6. <i>Caudites</i> sp. A	-	1	-	-	-	-	-	-	-	1
7. <i>C.</i> sp. B	-	-	-	-	-	-	-	-	-	-
8. <i>Cletocythereis</i> sp. A	-	-	1	-	-	-	-	1	-	2
9. <i>C. canaliculata</i>	-	-	-	-	-	-	-	-	-	-
10. <i>C. rastromarginata</i>	-	-	-	-	-	-	-	-	-	-
11. <i>Cytherelloidea</i> sp.	-	-	-	-	-	-	-	-	-	-
12. <i>Hemicytherura</i> sp.	-	-	-	-	-	-	-	-	-	-
13. <i>Hemicythere</i> sp.	-	1	-	-	-	-	-	-	-	1
14. <i>Hermanites mooneyi</i>	-	-	-	1	1	-	-	-	-	2
15. <i>H. parviloba</i>	1	-	-	-	-	-	-	-	-	1
16. <i>H. transoceanica</i>	-	-	-	3	4	-	-	-	-	7
17. <i>Jugosocythereis</i> sp.	-	1	-	-	-	8	-	4	-	13
18. <i>Keijia demissa</i>	-	-	-	-	-	-	-	-	-	-
19. <i>Loxoconcha heronislandensis</i>	-	2	-	-	-	-	-	2	-	4
20. <i>L. huahinensis</i>	1	4	1	5	3	3	1	9	1	28
21. <i>L. insularaensis</i>	-	1	-	-	-	-	-	1	-	2
22. <i>L. labyrinthica</i>	-	-	-	-	-	-	-	-	-	-
23. <i>L. n.</i> sp. A	-	-	-	-	-	-	-	-	-	-
24. <i>Loxoconchella</i> sp. A	-	-	-	-	-	-	-	-	-	-
25. <i>L.</i> sp. B	-	-	-	-	-	-	-	-	-	-
26. <i>L.</i> sp. C	-	-	-	-	-	-	-	-	-	-
27. <i>Miocyprideis</i> sp.	-	-	-	-	-	-	-	-	-	-
28. <i>Morkhovenia inconspicua</i>	-	-	-	-	-	-	-	-	-	-
29. <i>Neonesidea schulzi</i>	-	2	-	-	-	1	-	1	-	4
30. <i>Occultocythereis</i> sp.	-	-	-	-	-	-	-	-	-	-
31. <i>Orionina</i> sp.	-	-	-	-	-	-	-	-	-	-
32. <i>Ornatoleberis</i> sp.	-	1	-	3	-	-	-	-	-	4
33. <i>Paracytheridea remani</i>	-	1	-	2	1	1	-	-	-	5
34. <i>Ponticocythereis</i> sp.	-	-	-	-	-	-	-	-	-	-
35. <i>Procythereis</i> sp. A	-	-	-	-	-	-	-	-	-	-
36. <i>P.</i> sp. B	-	-	-	-	-	-	-	-	-	-
37. <i>Pterohairdia maddockiae</i>	-	-	-	-	-	-	-	-	-	-
38. <i>Semicytherura</i> sp.	-	-	-	-	-	-	-	-	-	-
39. <i>Triebelina sertata</i>	-	-	-	-	-	-	-	-	-	-
40. Other	7	7	2	6	4	4	-	10	-	40
41. "Piped" specimens	1	-	-	-	-	-	-	-	-	1
TOTAL	10	21	4	21	13	18	1	29	1	118

APPENDIX 3-7
BOREHOLE OKT-13

DIAGNOSTIC SPECIES	SAMPLE DEPTH (ft bsf)									
	10.4	18.5	25.4	28.75	36.0	55.65	59.9	68.2	80.0	TOTAL
1. <i>Australimoesella</i> sp.	-	1	-	-	-	-	-	-	-	1
2. <i>Bythoceratina</i> sp.	-	1	-	-	-	-	-	-	-	1
3. <i>Callistocythere</i> sp. A	-	-	-	-	-	-	13	-	3	16
4. <i>C.</i> sp. B	3	2	-	-	-	-	-	-	-	5
5. <i>Carlobairdia</i> sp.	-	-	-	-	-	-	-	-	-	-
6. <i>Caudites</i> sp. A	1	-	-	-	-	-	-	-	-	1
7. <i>C.</i> sp. B	-	-	-	-	-	2	-	-	-	2
8. <i>Cletocythereis</i> sp. A	2	2	2	-	-	2	-	3	3	14
9. <i>C. canaliculata</i>	-	-	-	-	-	-	-	-	-	-
10. <i>C. rastromarginata</i>	-	-	-	-	-	-	-	-	-	-
11. <i>Cytherelloidea</i> sp.	-	1	-	-	-	-	-	-	-	1
12. <i>Hemicytherura</i> sp.	-	-	-	-	-	-	-	-	-	-
13. <i>Hemicythere</i> sp.	-	-	-	-	-	-	-	1	-	1
14. <i>Hermanites mooneyi</i>	-	-	4	5	2	-	-	-	-	11
15. <i>H. parvifolia</i>	2	1	3	8	3	1	-	1	-	19
16. <i>H. transoceanica</i>	3	3	5	6	3	1	5	3	4	33
17. <i>Jugosocythereis</i> sp.	5	7	1	-	3	-	12	3	11	42
18. <i>Keijia demissa</i>	-	1	-	-	-	1	-	-	-	2
19. <i>Loxoconcha heronislaniensis</i>	2	2	-	-	-	-	-	-	-	4
20. <i>L. huahinensis</i>	11	19	17	19	11	12	3	8	12	112
21. <i>L. insulandaensis</i>	-	1	-	-	-	-	2	2	4	9
22. <i>L. labrynthica</i>	-	-	4	-	-	-	2	2	3	11
23. <i>L. n.</i> sp. A	-	-	-	-	-	-	-	-	-	-
24. <i>Loxoconchella</i> sp. A	-	-	1	3	-	-	-	-	-	4
25. <i>L.</i> sp. B	-	-	-	-	-	-	-	-	-	-
26. <i>L.</i> sp. C	1	-	-	-	-	-	-	-	-	1
27. <i>Miocyprideis</i> sp.	-	-	-	-	-	-	-	-	-	-
28. <i>Morkhovenia inconspicua</i>	-	-	-	-	-	-	-	1	-	1
29. <i>Neonesidea schulzei</i>	1	3	1	15	8	1	1	2	-	42
30. <i>Occultocythereis</i> sp.	-	-	-	-	-	-	-	-	-	-
31. <i>Onionina</i> sp.	-	-	1	-	-	-	12	-	1	14
32. <i>Ornatoleberis</i> sp.	-	1	1	1	5	-	-	-	-	8
33. <i>Paracytheridea nemani</i>	4	6	5	-	2	8	1	3	-	29
34. <i>Ponticocythereis</i> sp.	-	-	-	-	-	-	-	-	-	-
35. <i>Procythereis</i> sp. A	-	-	-	-	-	-	-	-	-	-
36. <i>P.</i> sp. B	-	-	-	-	-	-	-	-	-	-
37. <i>Pterobairdia maddocksae</i>	-	-	1	-	-	-	-	-	-	1
38. <i>Semicytherura</i> sp.	1	4	-	2	-	2	-	7	-	16
39. <i>Trieblina serrata</i>	-	-	-	-	-	-	-	-	-	-
40. Other	11	21	29	22	13	7	11	7	26	147
41. "Piped" specimens	-	-	-	-	-	-	-	-	-	-
TOTAL	47	76	84	81	50	37	62	43	67	547

CHAPTER 4:

ELECTRON PARAMAGNETIC RESONANCE STUDIES OF SELECTED BOREHOLE SAMPLES AND DEBRIS MATERIAL FROM OAK CRATER

by

Carol A. Polanskey¹ and Thomas J. Ahrens¹

INTRODUCTION

Electron paramagnetic resonance (EPR) spectrometry was used to measure the peak shock stress experienced by a variety of carbonate samples as a result of the detonation of the OAK nuclear device. The following results are based on EPR spectra from 136 samples taken from six boreholes and 17 debris samples recovered from the crater floor. Shock pressures were determined by comparing the sample spectra with spectra of Enewetak carbonate samples and Solenhofen Limestone that had been shocked to known pressures in the laboratory. Preliminary work on this procedure was developed by Vizgirda and Ahrens (1980) using Enewetak material from CACTUS crater obtained during Project EXPOE. Their work demonstrated a linear relationship between shock pressure and the hyperfine splitting of Mn^{2+} in the calcite component of CACTUS carbonate samples. The current report contains the analysis of the OAK samples and expands upon the previous calibration technique.

EPR ANALYSIS

The EPR spectrum of calcium carbonate, $CaCO_3$, is a result of Mn^{2+} substituting for Ca^{2+} in a single site in the crystal lattice. The theory of Mn^{2+} resonance absorption in single crystal of calcite is described by Hurd and others (1954). The calcite spectrum is dominated by six hyperfine peaks due to the central transitions $M = \pm 1/2$, where M is the electronic magnetic quantum number. The hyperfine splitting results from the coupling between electronic and nuclear magnetic moments (Hurd and others, 1954). The spectrum of a powdered sample of single crystal calcite, Iceland spar, is shown in Figure 4-1. The central transitions are labeled along with the forbidden transitions. Of particular interest to this study are the two outer most peak doublets at the lowest and highest field positions.

Sample Preparation and Spectrometer Settings

The carbonate samples were ground into a coarse powder and placed into Wilmad® 707SQ fused EPR tubes. The spectra were taken at room temperature with a Varian® E-Line Century Series spectrometer. The calcite spectrum is centered near 3,400 Gauss (G), and ranges from approximately 3,150 to 3,650 G.

¹California Institute of Technology, Division of Geological
and Planetary Sciences; Pasadena, California 91125.

CALCITE POWDER SPECTRUM

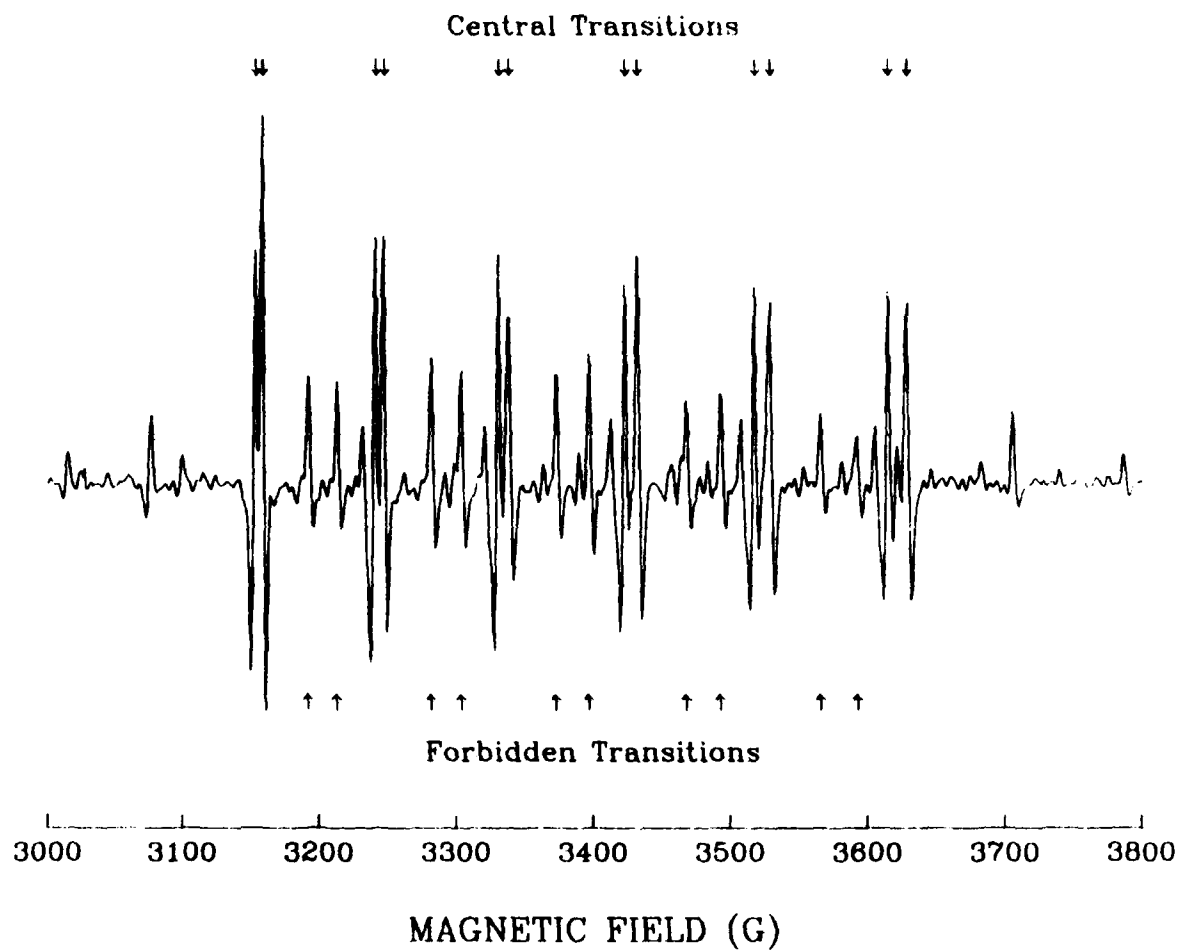


FIGURE 4-1. -- EPR spectrum of powdered single crystal calcite. The central transitions are due to $M = +1/2$, $\Delta m = 0$, where M and m are the electronic and nuclear magnetic quantum numbers, respectively. The forbidden transitions occur when $\Delta m = 1$. G = Gauss.

The spectrometer was set at a microwave frequency of 9.56 GigaHertz (GHz), modulation amplitude of 3.2 G, time constant of 0.25 seconds (sec), and microwave power of 20 milliwatts (mWatt). A scan time of 8 minutes (min) was used to obtain the full spectrum over a 1000-G scan range; however, high-resolution spectra were also recorded for both the extreme lower and higher field components of the spectrum. For these spectra, the magnetic field was swept over 100 G in 4 min. The high resolution spectra provided greater details of the modification of the hyperfine doublets from the shocked samples. As a result, the high-resolution spectra were used in all of the subsequent analyses.

In addition, all spectra were recorded digitally by the spectrometer. Therefore, it was possible to average several scans to improve the signal-to-noise ratio in samples with low signal strength. Signal averaging proved to be extremely useful for the highly shocked samples because there is a definite correlation between decreasing signal strength and increasing shock pressure. Finally, to remove the slope from the spectrum and reduce the line width of the signal, the spectrometer was operated in the second derivative mode. This was accomplished by setting the modulation frequency of the cavity 90 degrees out of phase with the receiver frequency.

SHOCK PRESSURE CALIBRATION OF EPR SPECTRA

Shock-Wave Calibration Experiments

The calibration experiments were a combination of two different data sets. The first set consisted of Enewetak carbonate samples shocked in the laboratory over 10 years ago. The samples were taken from two different depths, 10 ft and 146 ft, from the borehole XRU-3 located outside of CACTUS crater on the eastern side of Enewetak Atoll. These samples and experiments are described in detail by Vizgirda and Ahrens (1980). One reason for reprocessing these samples was to determine if the shock effects observed by Vizgirda and Ahrens (1980) had changed with time. New spectra were taken of each sample and the results confirmed that the effect of shock on the hyperfine splitting had not altered over the time scale of a decade. Secondly, high-resolution spectra were taken from these samples in order to test the pressure-calibration technique; however, these samples were not used for the pressure calibration which is described subsequently in this Chapter.

A series of Solenhofen Limestone samples also were shocked in the laboratory, and these samples became the basis for the pressure calibration. This material was chosen because its EPR spectrum, also due to Mn^{2+} substitution, is orders of magnitude more intense than the Enewetak samples. The Solenhofen is also more chemically homogeneous, although it is still a polycrystalline material. Limestone cores (diameter 0.25 in.) were cut into 0.4-in.-long cylinders and pressed into stainless-steel sample chambers. The sample chambers were sealed in the rear by a stainless-steel plug which was notched to vent any impact generated gases. The sample chamber was then inserted into a large stainless-steel momentum trap and mounted in a 40-mm propellant gun. Projectiles were made of polycarbonate-resin plastic (Lexan) that contained flyer plates of aluminium or Lexan. These impacted the target assembly at velocities between 0.8 and 1.6 km/sec to yield initial shock

pressures of 1.3 to 9.8 Giga Pascals (GPa). Initial shock pressure (rather than final reverberated shock pressure) is reported, because most of the entropy generated by the shock (and hence the shock damage) is associated with the initial shock wave.

Shock pressures were calculated using the projectile velocities and the impedance match technique (Stoffler, 1972). The average bulk density of the limestone samples was 2.61 g/cm^3 , and the Hugoniot for Solenhofen Limestone samples was taken from Tyburczy and Ahrens (1986). The remaining Hugoniots for Lexan® aluminium 2024, and stainless steel 304 are found in Marsh (1980).

Description of Shocked Spectra

Figure 4-2 shows a series of shocked-limestone spectra. The spectra have all been normalized such that the highest peaks (low-resolution spectra) or the highest subpeaks (high-resolution spectra) are of equal height. The shocked-limestone spectra not only reflect in much greater detail the decrease in the hyperfine splitting as a function of increasing pressure, observed previously in the carbonate, but also reveal that the relative signal strength and width of the two subpeaks also varies in a consistent manner with increasing pressure. It is clear from the last two columns in Figure 4-2 that the extreme low-field subpeak in the low-field doublet and the extreme high-field subpeak in the high-field doublet both decrease in relative amplitude and broaden with increasing shock pressure. Because the spectrum of each doublet is the sum of two individual subpeaks, a change in the magnitude or shape of one subpeak can be enough to create the observed decrease in peak separation of the doublet as a whole. In this case, a shift in the actual line position of either subpeak is not required.

The same general trend in peak variation also can be seen in the shocked-carbonate spectra shown in Figure 4-3. Because of the low signal in several samples, these spectra were not uniformly normalized. The specific behavior of the subpeaks in the high-field doublet is less obvious in this series, and the subpeaks are difficult to distinguish at higher shock pressures. The high-field doublet is ultimately lost in the noise (as seen in the sample shocked to 10 GPa). Another factor which complicates the carbonate analysis is that there is also variation between spectra of some of the "unshocked" carbonate samples. Material from two different depths in borehole XRU-3 was used in the calibration experiments of Vizgirda and Ahrens (1980). It appears that the material taken from a depth of 10 ft is not typical of the bulk of the unshocked samples analyzed from Enewetak Atoll. As a result, a systematic difference exists between the spectra taken from these calibration shots and that of the shocked material from 146 ft depth. Both sets of spectra show consistent variation in hyperfine splitting with increasing shock pressure; however, they do differ in the degree to which they are affected by shock deformation.

A second observation, mentioned earlier, is that the amplitude of the entire spectrum tends to decrease with increasing shock pressure. This effect is much more obvious in the Enewetak samples than in the Solenhofen Limestone samples. A loss of signal could be due to a reduction of the Mn^{2+} concentration in the Ca^{2+} lattice sites. The specific mechanism responsible for this reduction has not yet been identified.

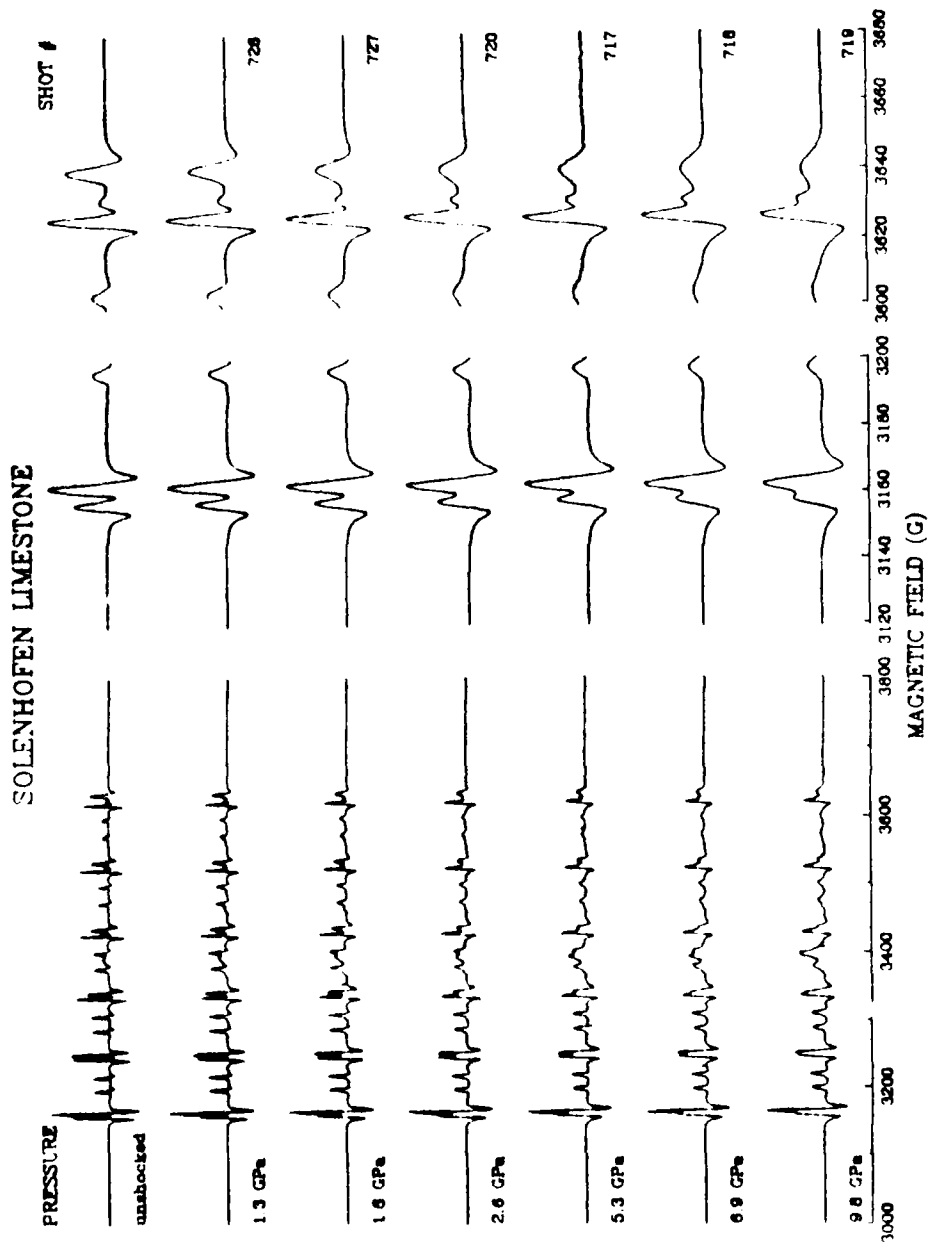


FIGURE 4-2. -- Comparison of limestone spectra shocked in the laboratory. The full spectrum is shown in the first column and centered at 3,400 Gauss (G). High-resolution spectra of the lowest and highest field components are shown in the latter two columns and centered at 3,160 G and 3,630 G, respectively.

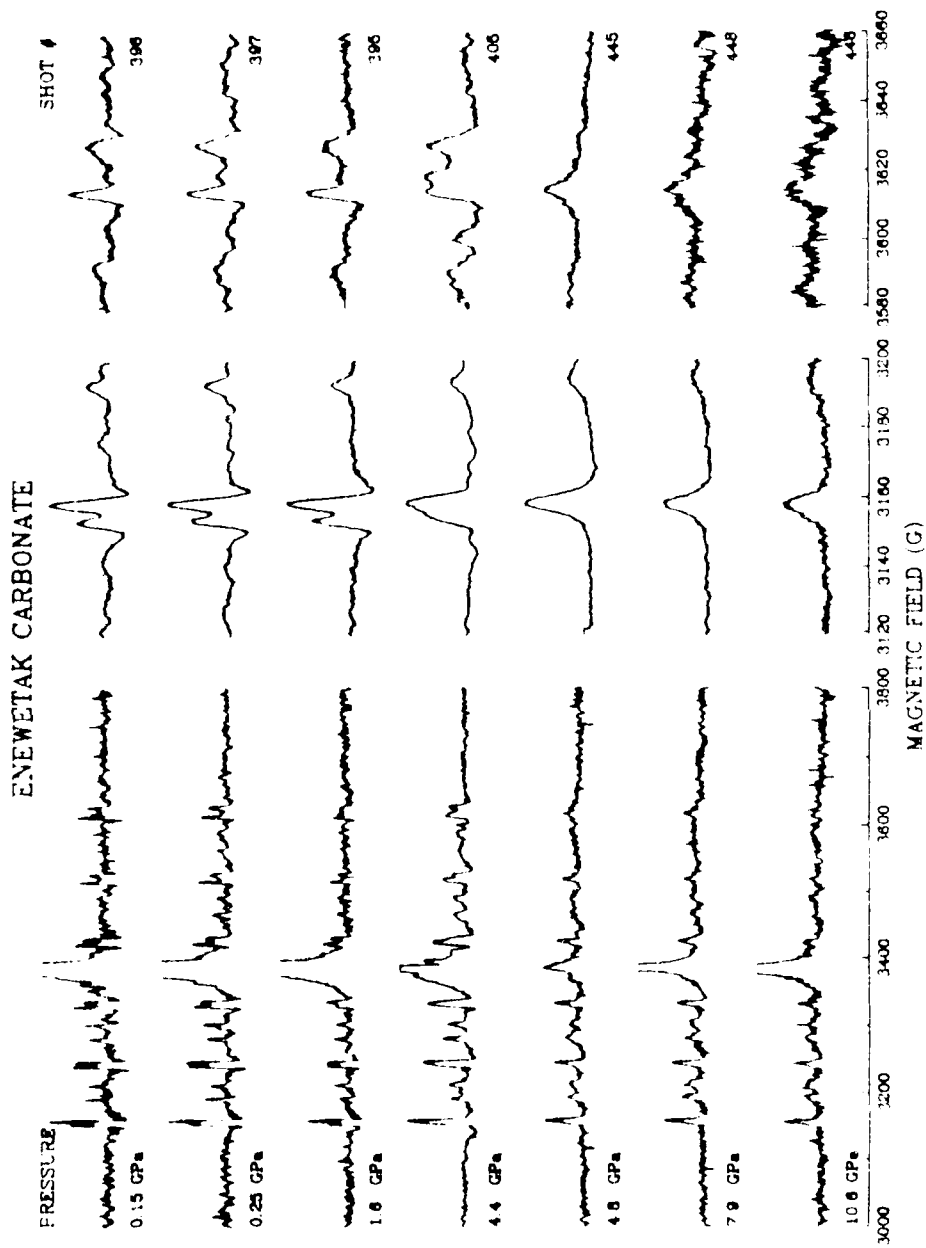


FIGURE 4-3. -- Comparison of coral spectra shocked in the laboratory. The full spectrum is shown in the first column and centered at 3,400 Gauss (G). High-resolution spectra of the lowest and highest field components are shown in the latter two columns and centered at 3,160 G and 3,630 G, respectively.

Pressure Calibration by Differencing Spectra

The previous calibration technique of Vizgirda and Ahrens (1980) relied on measuring the separation, in Gauss (G), of the two subpeaks of the highest field component of each spectrum. The hyperfine peak splitting, HPS, was related to shock pressure, P, by the relationship:

$$\text{HPS(G)} = - 0.60\text{P(GPa)} + 13.85 \quad (\text{high field})$$

Although the decrease in hyperfine splitting is most evident in the high field component, the signal strength of this peak is also the lowest. Therefore, as the signal intensity decreases, the error in measuring hyperfine peak splitting increases. The following technique was developed to incorporate the variations in hyperfine splitting as well as relative peak amplitudes and widths. In addition, the analysis will work equally well for the lowest field component of the spectrum which always has a higher amplitude.

Digital spectra were used to compare each carbonate sample to a pure, single-crystal calcite standard. Both high-resolution spectra from each end of the spectrum were used in the comparison. The digital spectra consisted of 1000 amplitude values evenly spaced over a 100-G field range. Both sample and standard spectra were first normalized by the amplitude of their respective highest subpeaks. The sample spectrum was then translated along the magnetic-field axis until the position of its highest subpeak coincided with that of the standard spectrum. Next the absolute value of the difference in amplitude between the two spectra was calculated for each point over the extent of the doublet. Finally, these individual differences were summed to determine a measure of the "likeness" or "unlikeness" of the sample spectrum to the standard. This number shall be referred to as the integrated difference, or ID, of the sample, which is given analytically by the equation:

$$\text{ID} = \frac{1}{n-n_0} \int_{n=n_0}^{n=400} |Y[\text{standard}] - Y[\text{sample}]| / 40\text{G}$$

where n_0 is the index of the amplitude array corresponding to a magnetic field value 20 G below that of the highest peak of the standard spectrum; $Y[\text{standard}](i)$ and $Y[\text{sample}](i)$ are the normalized amplitudes of the standard and sample spectra, respectively, and N is the number of data points that are integrated. In this case, N is 400. The error in ID is determined by performing a similar calculation, where $Y[\text{sample}](i)$ are points in the flat baseline signal on either side of the Mn^{2+} peak.

Figure 4-4 illustrates this procedure with examples of two spectra from the limestone calibration experiments. The first frame shows an unshocked Solenhofen Limestone spectrum normalized, translated, and plotted over the standard calcite spectrum. The second frame is a plot of the absolute value of the difference between the amplitudes at each point over a 40-G range in magnetic field. The final two frames demonstrate the same technique using a sample which has been shocked to 9.8 GPa. The error is determined by using the same scheme to calculate the integrated difference along a flat portion of the spectrum. This value gives an estimate of the contribution of noise to the ID over the region containing the signal.

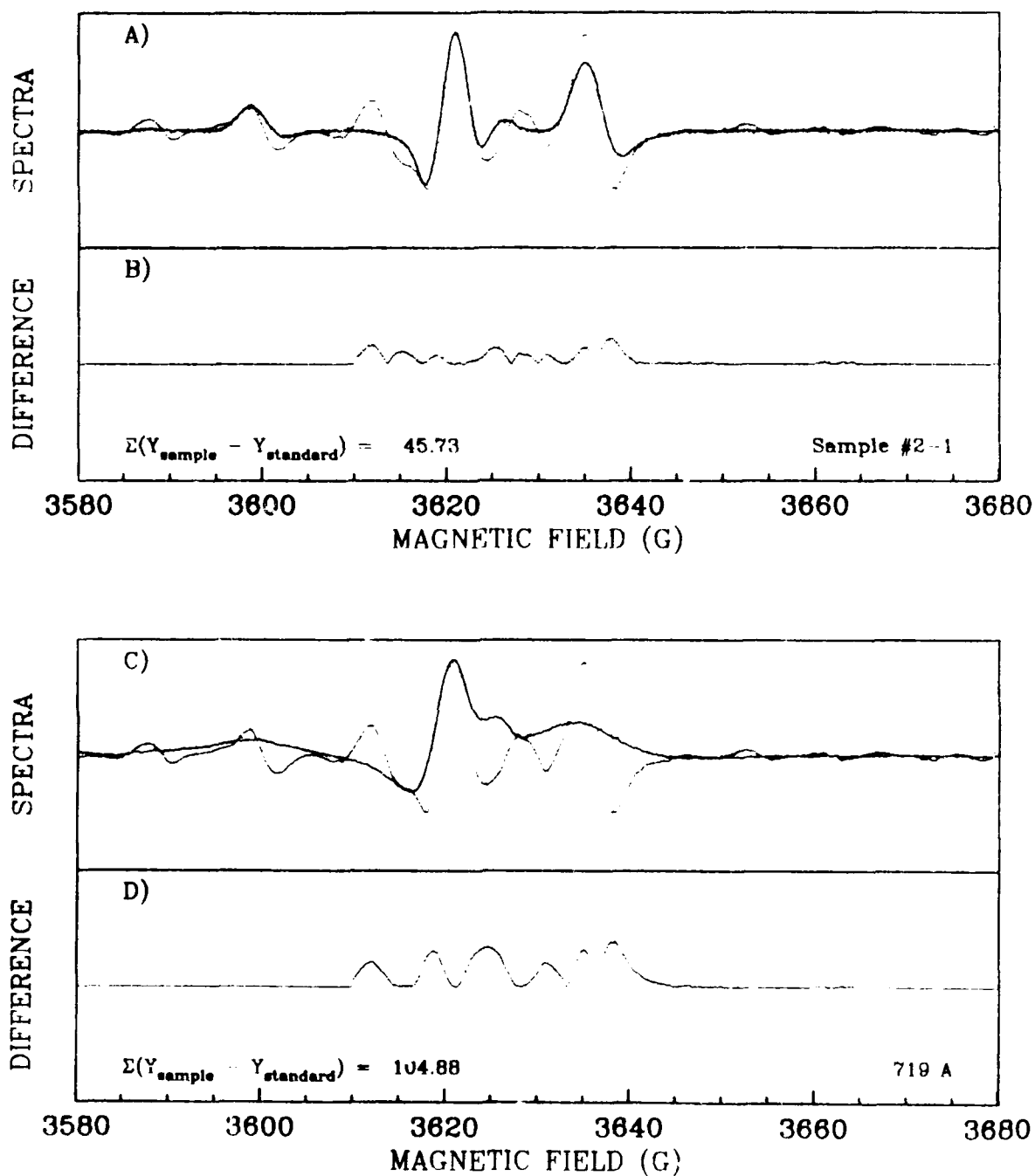


FIGURE 4-4. -- Illustration of the differencing technique showing (A) an overlay of the standard spectra and an unshocked Solenhofen Limestone sample; and (B) a plot of the individual absolute differences at each point along the field. Frames (C) and (D) correspond to (A) and (B) for a limestone sample shocked to 9.8 GigaPascals (GPa).

SOLENHOFEN LIMESTONE

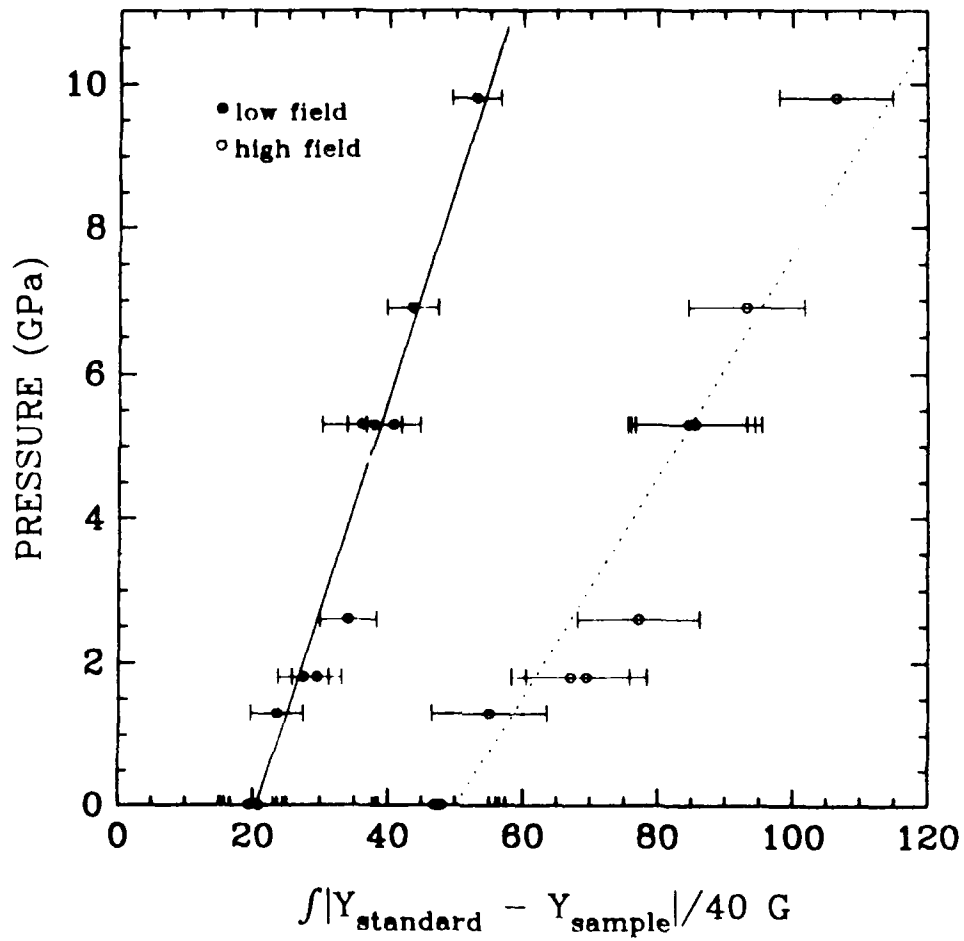


FIGURE 4-5. -- Plot of the summed differences for the low and high field components of the Solenhofen Limestone samples as a function of shock pressure. The ID value is normalized by 40 Gauss (G), the magnetic field range over which the differences were integrated.

TABLE 4-1. Pressure (Giga Pascal) and Integrated Difference (ID) Data for High Resolution Spectra from Samples Shocked in Laboratory Recovery Experiments.

SOLENHOFEN LIMESTONE			
SHOT NUMBER	P (GPa)	ID Low Field	ID High Field
—	0.0	20.79	47.61
717	5.3	38.12	85.13
718	6.9	43.53	93.17
719	9.8	52.99	106.43
720	2.6	34.03	77.16
726	1.3	23.44	55.14
727	1.8	28.42	68.23

ENEWETAK CARBONATES			
SHOT NUMBER	P (GPa)	ID Low Field	ID High Field
394	1.4	37.43	74.68
395	1.6	37.83	84.80
396	0.2	33.67	66.51
397	0.3	33.00	74.79
405	4.4	73.85	146.09
442	1.9	78.25	146.22
443	1.5	68.33	166.97
445	4.8	73.61	165.60
446	10.6	75.70	181.03
448	7.9	70.71	161.79

The results of these calculations for the limestone calibration experiments are plotted in Figure 4-5. The ID values are plotted against pressure for both the low- and high-field components of the spectrum. To determine the pressure to integrated difference calibration, a line was fit to each data set using linear least squares. The resulting equations are listed below:

$$\begin{array}{ll} P \text{ (GPa)} = 0.290(\text{ID}) - 5.97 & \text{(low field)} \\ P \text{ (GPa)} = 0.152(\text{ID}) - 7.59 & \text{(high field)} \end{array}$$

The correlation coefficients for the fit were 0.966 and 0.943, respectively. Table 4-1 contains a list of the ID results for both limestone and Enewetak sample experiments. The average ID values are given for shots where several samples were analyzed.

Using the calibration curves above, shock pressures were then assigned to the OAK carbonate samples. In general, the Enewetak carbonate samples have a much weaker EPR signal than those from the Solenhofen Limestone. Therefore, it was necessary to adjust the intercept of the calibration curves to compensate for the average ID value of the unshocked Enewetak samples. It follows that this method will then assign negative pressures to some samples, because the previous adjustment was made to accomodate the "average" background noise. To avoid this obviously unphysical result, and because this technique is not extremely sensitive for low-shock damage, all samples with shock pressures calculated to be below 2.0 GPa were classified as unshocked. Similarly, the high-pressure cut-off was chosen to be 15 GPa. This is necessary because: (1) no data exist for very high shock pressures, and (2) the intensity of the Enewetak sample spectrum is low even at 10 GPa. Samples with shock pressures calculated to be above 10 GPa were classified as highly shocked.

In most cases, shock pressures were calculated for each sample using both the low- and high-field components of the spectrum. These values were then averaged to determine the final calculated pressure.

OAK DATA

Borehole Sample Selection

The borehole samples consisted of uncemented sediments and carbonate rock clasts from boreholes OAR-2A, OBZ-4, OCT-5, OET-7, OFT-8, and OPZ-18, the locations of which are shown on Figure 4-6. Samples are referred by the appropriate borehole name succeeded by depth in feet below sea level (bsl).

The carbonate material from Enewetak is extremely inhomogeneous and consists of a mixture of both calcite and aragonite. Because aragonite does not have a detectable EPR spectrum (Low and Zeira, 1972), samples were selected, where possible, for their high-calcite content. For example, those samples containing carbonate grains replaced by solution-deposited calcite crystals were preferred because they would yield stronger EPR signals. Choosing good sample material is important because it provides a consistent base for analysis, and because it guards against mistaking a sample with an inherently poor EPR spectrum as being highly shocked. The difference between the two cases generally can be recognized by visual inspection, although it is

more difficult to assess with numerical techniques. As a result, the samples chosen were much less porous than the CACTUS samples used in the earlier shock-wave experiments; consequently, the OAK spectra tended to resemble the Solenhofen Limestone spectra more closely. For each borehole, the majority of samples were taken from depths above the gamma (γ) geologic crater zone, defined by Wardlaw and Henry (1986, p. 3) as that interval of rock and sediment that is fractured and displaced beneath the crater. A more specific description of each sample analyzed is given in Tables 4-2 through 4-7 (located at the end of this Chapter). Detailed descriptions of each borehole are given in Henry, Wardlaw, and others (1986).

Results of Borehole Sample Analysis

The two boreholes drilled almost directly below the position of the explosive device (ground-zero, GZ, and bathymetric-center boreholes OBZ-4 and OPZ-18, respectively) were the most heavily sampled for the EPR study. A very highly shocked layer of uncemented material was found in samples from borehole OPZ-18 between 399.9 ft and 415.9 ft bsl. This layer was distinguished visually by the characteristic greenish color of the muddy carbonate sand. The shocked zone was interrupted at 412.4 ft bsl by a thin zone of lighter-colored material. The location and nature of this shocked material coincides with a zone of Holocene sediments described by Wardlaw and Henry (1986) as a possible example of material that has been injected. The present results are consistent with such an hypothesis since this material most likely originated near the pre-shot sea-floor surface. Three other sand samples above this layer, 386.9 ft, 368.5 ft, and 357.2 ft bsl, were moderately shocked to at most 3.2 GPa. The highly shocked samples were located primarily in the geologic crater zone beta-2 (β_2) --the transition sands-- whereas the moderately shocked material came from zone beta-1b (β_{1b}) (Wardlaw and Henry, 1986; and Chapter 6 of current Report). The remaining 24 of the 31 samples from OPZ-18 appear to be unshocked.

Remarkably, not one of the 26 samples from OBZ-4 showed significant shock damage. Three samples from the β_{1b} zone registered only marginally detectable degrees of shock damage. Sufficient samples were analyzed from the transition sands and vicinity to characterize the core; therefore, it appears that OBZ-4 did not share the same history as OPZ-18.

Thick zones of highly shocked material were found in each of the three northeastern-radial transition boreholes OCT-5, OET-7, and OFT-8. The transition sands have not been identified in any of these boreholes; however, the spectra of the shocked material are similar to those from the shocked material in OPZ-18.

Spectra were taken of 25 samples from borehole OCT-5, drilled 658 ft from GZ. The results of six of these samples define a heavily shocked zone at least 25 ft thick, extending from 285.3 ft to 309.9 ft bsl. This region occurs within zone β_{1b} (early stage collapse rubble), and these samples are also primarily uncemented sands. Aside from the highly shocked material in this region, four widely dispersed samples appear to be moderately shocked. However, two of these samples (368.4 and 464.0 ft bsl in OCT-5) are examples of the aforementioned situation where poor signal quality biases a pressure determination. Simple visual analysis of these spectra suggest that both samples are actually unshocked. The elevated pressures calculated for

OAK CRATER BOREHOLES

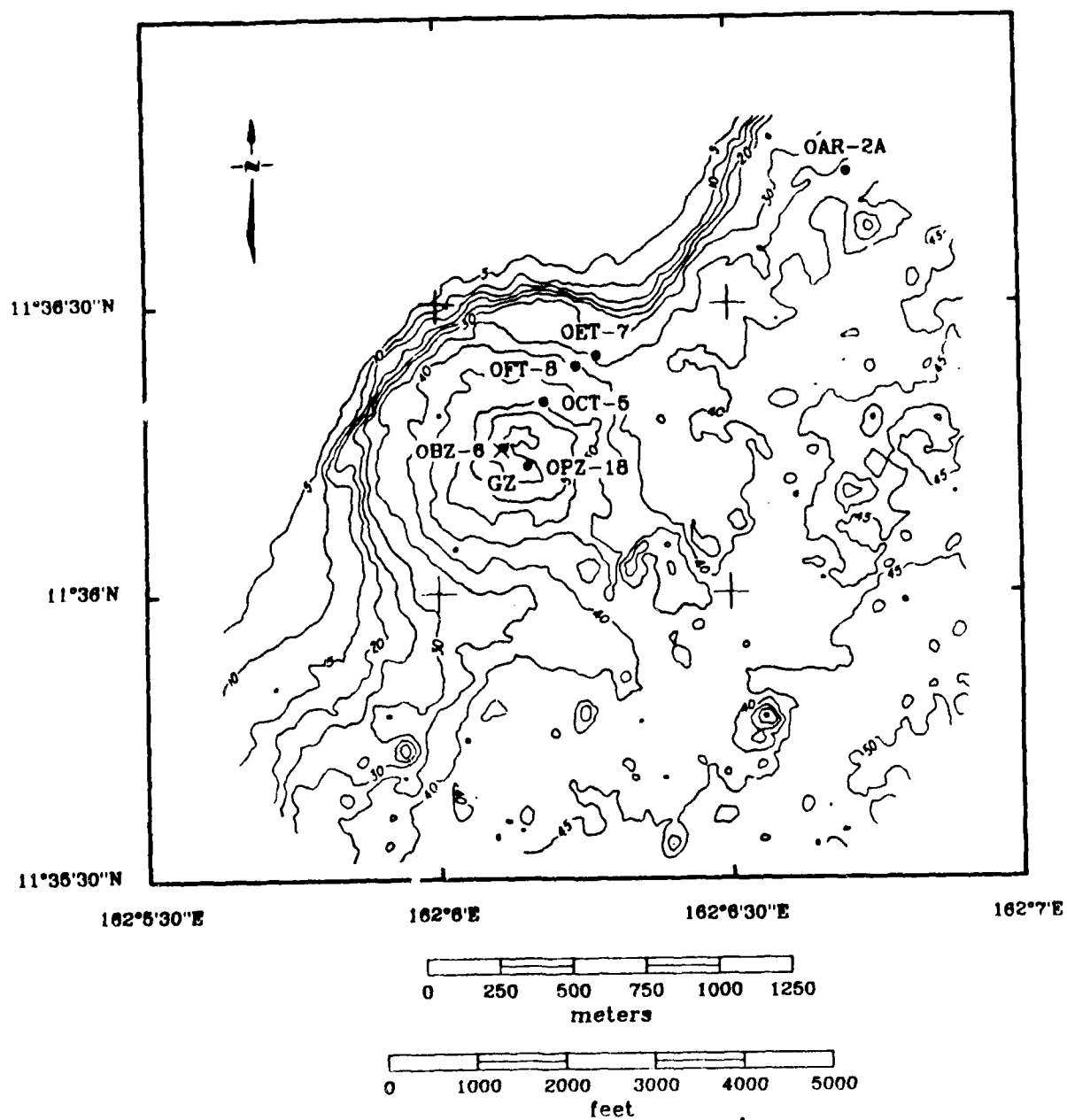


FIGURE 4-6. -- Map of OAK crater showing the location of the boreholes sampled for this study. Bathymetric contours given in 5-meter intervals.

these depths are an artifact of the noisiness of the spectra due to the small fraction of calcite in these samples.

Borehole OFT-8 is located 1,129 ft from GZ, just within the excavational crater (Henry, Wardlaw, and others, 1986). This borehole was sampled at 24 depths. In OFT-8, the region of heavily shocked material begins near the top of the β_{1b} zone and extends downward for approximately 27 ft. Included within this zone were seven heavily shocked samples located between 153.6 ft and 180.9 ft bsl. Bordering this region above and below are zones containing moderately shocked material. Two moderately shocked samples, 149.2 ft and 151.3 ft bsl, were taken at the base of the β_{1a} (late-stage collapse rubble) geologic zone, and three samples deeper in the β_{1b} extending to a depth of 195.3 ft bsl.

The next farthest borehole (OET-7) is 1,374 ft from GZ. Based on seismic-reflection, paleontologic, and lithostatigraphic data, this borehole is thought to be located outside of the excavational crater (Henry, Wardlaw, and others, 1986). The majority of the nine samples were from the GAMMA zone; however, all but the uppermost sample were heavily to moderately shocked. Of the highly shocked samples, six out of seven were uncemented sediment samples. The highly shocked zone extended from 118.9 to 147.5 ft bsl, and a moderately shocked, cemented sample was detected at 173.6 ft bsl.

Borehole OAR-2A, located 4,458 ft from OAK GZ, initially was sampled only as a reference core; however, six of 21 samples from this borehole have been heavily shocked. Two other samples were moderately shocked to pressures of 3.5 and 4.4 GPa. All of the shocked samples were located within the top 39 ft of the core and the most heavily shocked material within the first 24 ft. The proximity of this borehole to the reef may suggest that some highly shocked, fine-grain ejecta was transported from the slope and deposited at the site of OAR-2A.

The combined results from the OAK borehole sample analysis are presented in Figure 4-7. The solid horizontal line in each panel indicates the present sea-floor depth. The depth and thickness of each zone containing highly shocked material ($P > 10$ GPa) as a function of the distance of the borehole from GZ is shown in a simplified manner in Figure 4-8.

Results from Debris Samples

The debris analyzed consists of 14 samples collected throughout the crater by submersible and three samples collected by scuba divers from roughly a single site. The former samples are a subset of a series of debris samples analyzed by Halley, Ludwig, and others (1986). Figure 4-9 shows the locations where each debris sample was recovered. The range values that will be discussed in a subsequent section were measured from this map. Unfortunately, the debris samples included in this study were all taken from roughly the same distance from GZ. Only one sample (OAK 201) was recovered at a significantly different range.

The results of the debris analysis are plotted in Figure 4-10A and listed in Table 4-8 (located at end of Chapter). The majority of the debris samples were relatively unshocked; however, all of the highly shocked debris was found

OAK CRATER BOREHOLE RESULTS

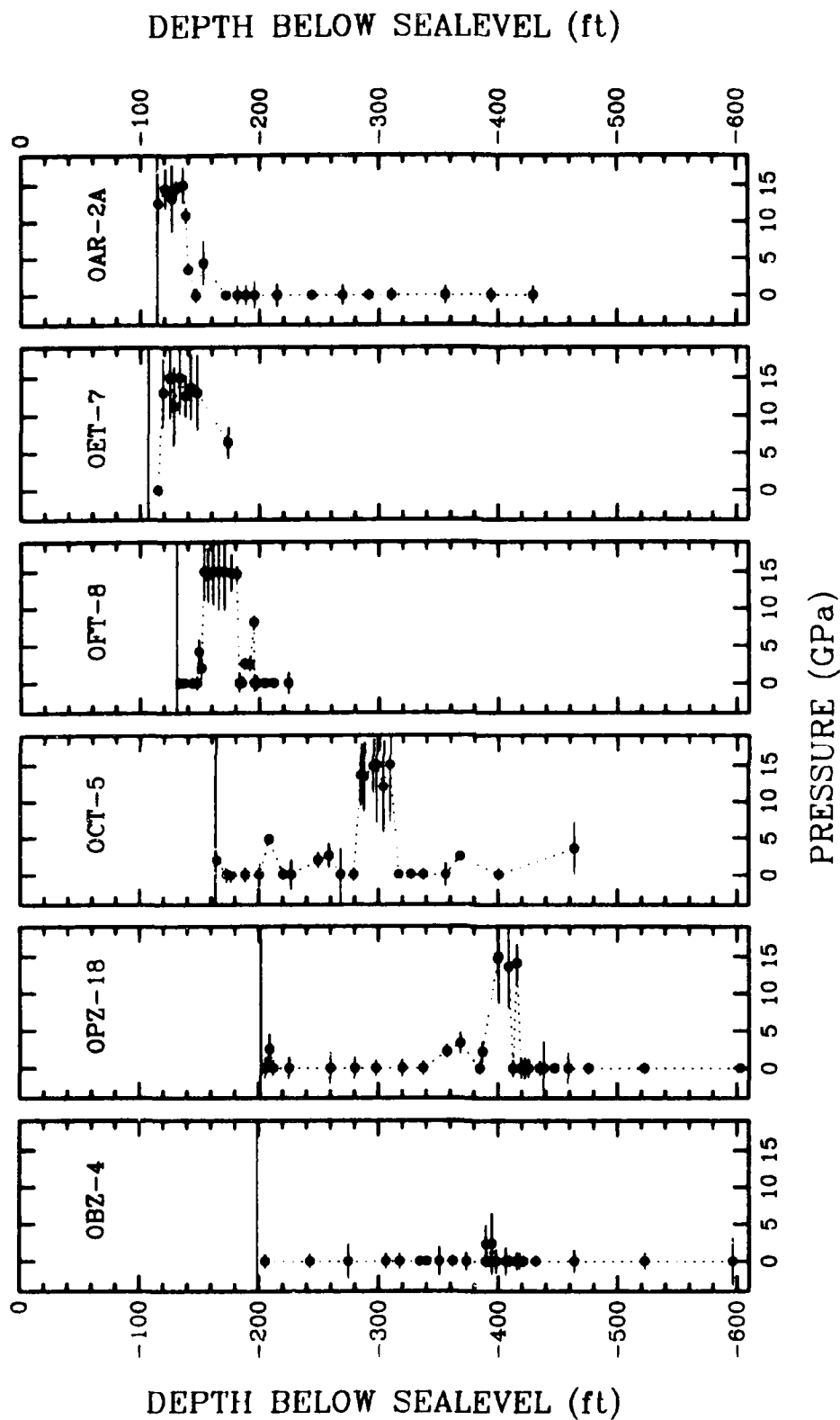


FIGURE 4-7. -- Combined results of the borehole-sample analysis showing the calculated shock pressure in relation to the sample depth in ft below sea level. The boreholes are presented in order of increasing distance from ground zero.

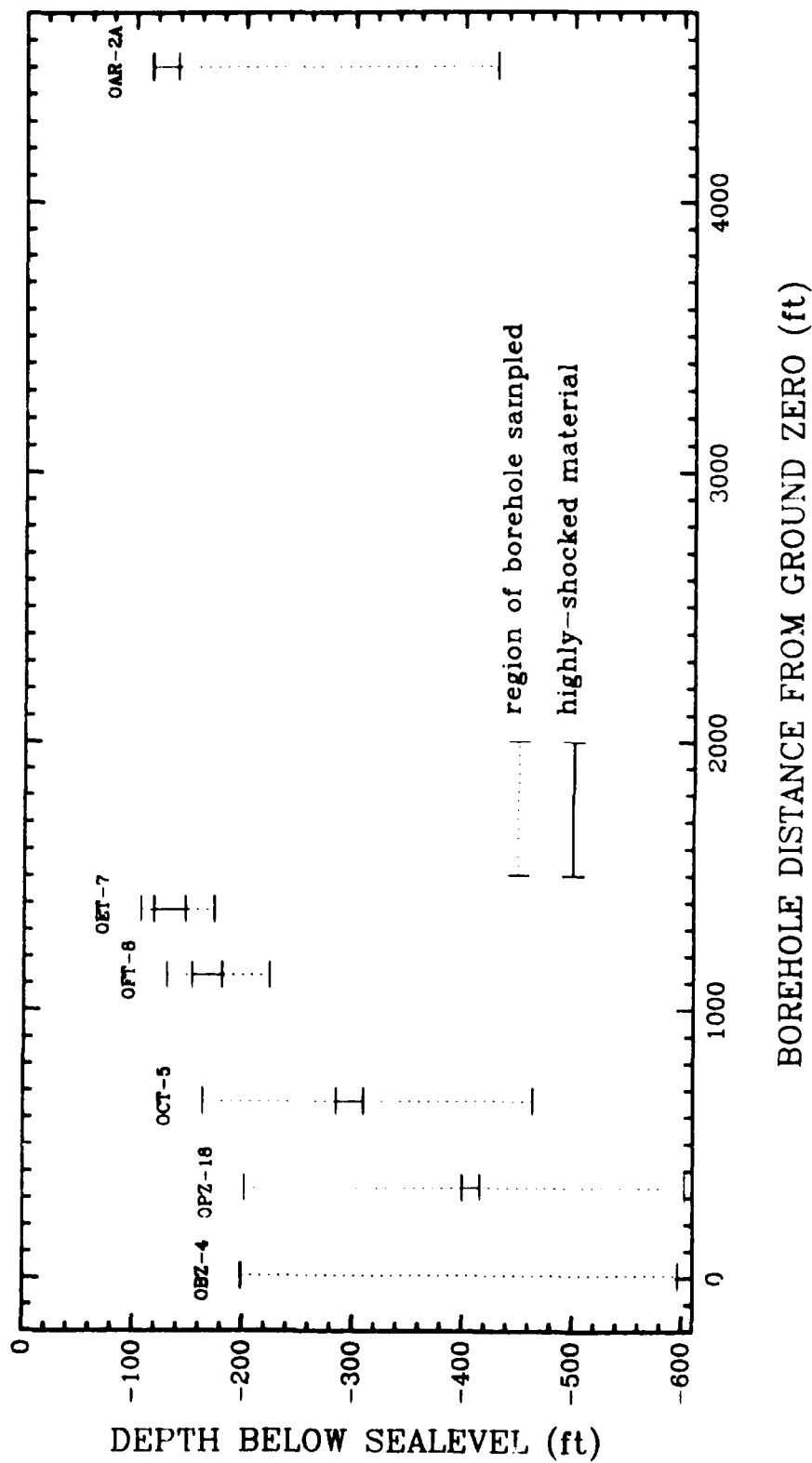


FIGURE 4-8. -- Illustration of the depth and thickness of regions of highly shocked carbonates recovered from each borehole. The dotted line indicates the extent of the borehole sampled, and the solid line defines the highly shocked zone.

OAK CRATER DEBRIS SAMPLES

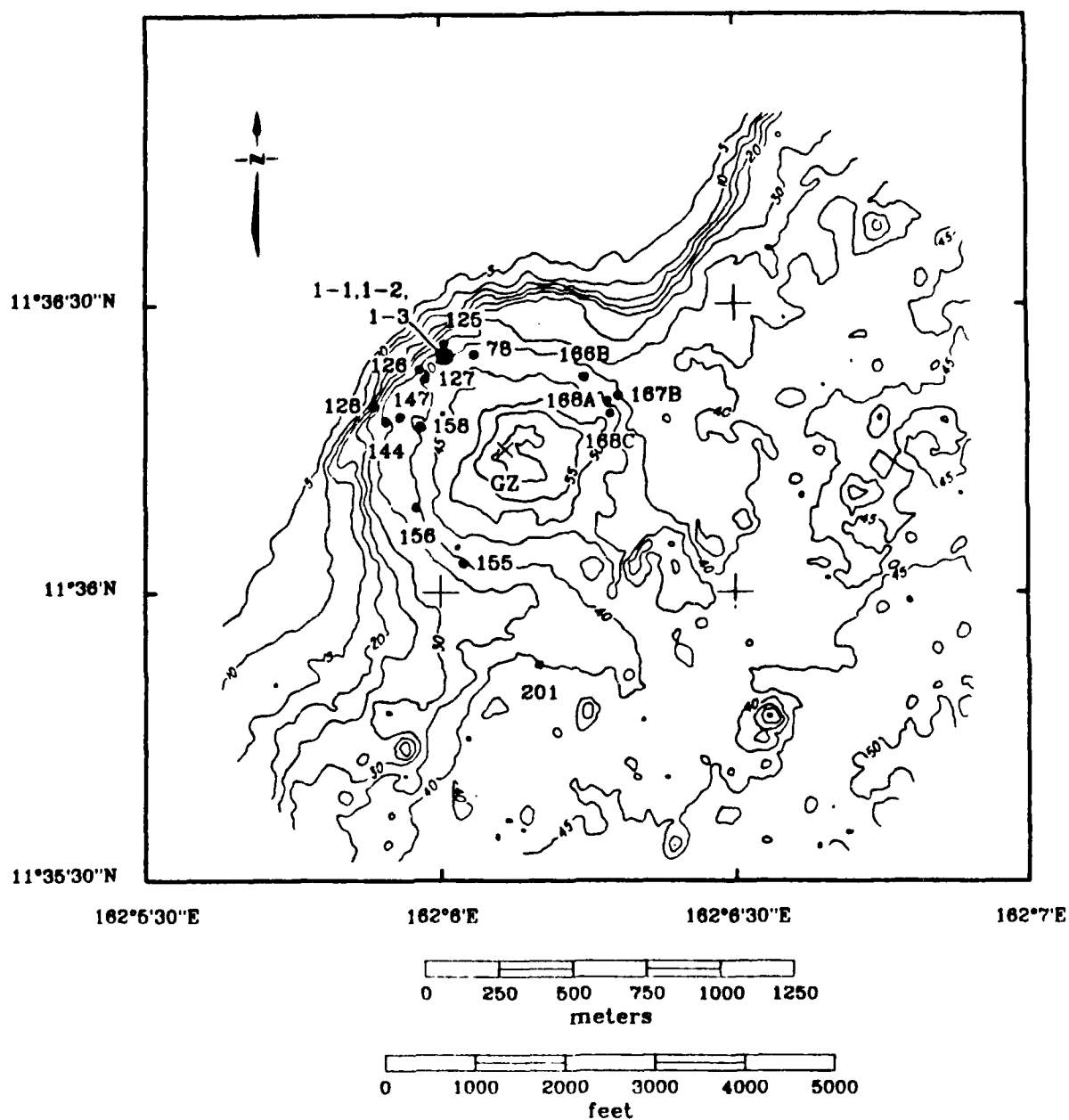
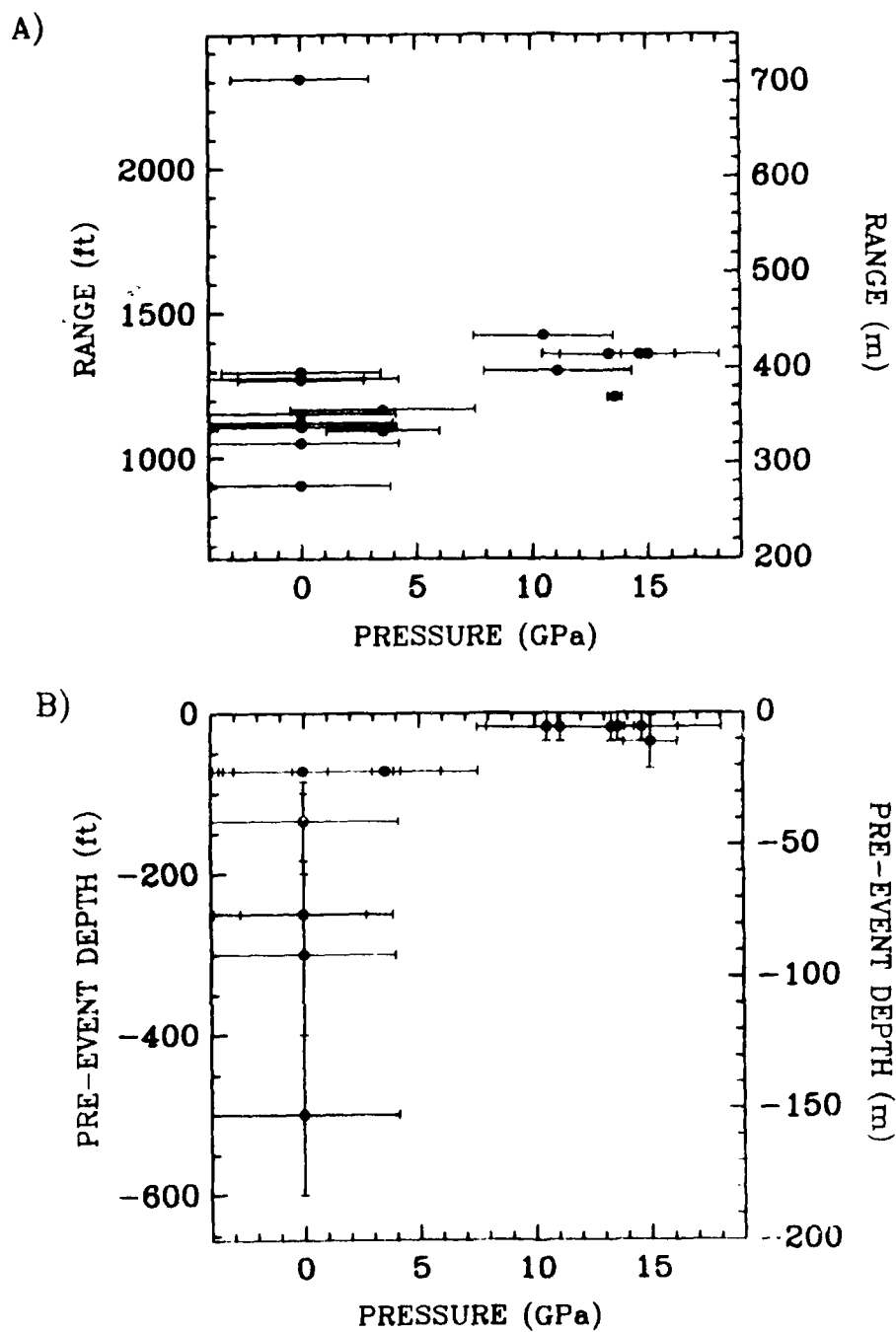


FIGURE 4-9. -- Map of OAK crater showing the debris-sample recovery sites. Bathymetric contours given in 5-meter intervals.

OAK DEBRIS



at the base of the reef slope. The reef may have blocked some of the highly shocked material from leaving the crater as ejecta, or this material (ejected from the crater) could have been transported craterward back down the reef slope some time after the crater was formed.

In addition to the range measurements, the estimated pre-event initial depth of a limited number of the debris samples was available from strontium-isotope analysis (Halley, Major, and others, 1986; and Ludwig, Halley, and others, 1986) and gross paleontologic and petrographic analysis by B.L. Ristvet in 1981 (see Ristvet, 1986) and corroborated by subsequent analysis by USGS personnel. The pre-event depth below sea level is plotted against shock pressure for these samples in Figure 4-10. Although the pre-event depth estimates are crude in some cases, a strong correlation is evident between shock pressure and depth for this limited data set. This correlation is consistent with the assertion that the pre-event surface material near GZ was the most severely shocked.

DISCUSSION

With a few exceptions, the bulk of the samples analyzed can be split into two categories, unshocked and very highly shocked. There were relatively few samples which can be assigned to intermediate pressure categories. This suggests that the majority of the shocked material shares a common origin. Presumably, the material right at or near the surface near GZ received the highest shock pressure from the blast. During the cratering event, some of this material was incorporated in the lining of the transient crater cavity and was then buried almost immediately by the collapse of the crater walls. Subsequent backwash of ejecta and slumping and deformation of the crater would tend to mix this highly shocked material with other rubble and breccia and consequently obscure any stratigraphically discernable zone of highly shocked material.

This hypothesis can be applied to explain the presence of the shocked regions in OPZ-18 and in the transition boreholes. Because slumping and collapse become increasingly more important toward the rim of the crater, it is not unreasonable that OPZ-18 is the only borehole to have the shocked material preserved in a stratigraphically discernable unit such as the transition sands. The thickness of the region of highly shocked material does remain fairly constant throughout the three transition boreholes (Figure 4-8), although the region is located at consistently shallower depths as the distance between the borehole and GZ increases. This is a further indication that these regions were at one time related.

Late-stage debris slumping and the influence of sedimentation also have contributed to borehole stratigraphy. Post-event slumps from the reef have deposited at least 8 ft of unshocked debris at OET-7, and possibly as much as 17 ft at OFT-8. The location of the shocked debris samples collected from the floor of the crater suggest that highly shocked ejecta may also be deposited from the reef slope, and the shocked upper layer of OAR-2A could be the result of accumulated deposition over many years.

ACKNOWLEDGEMENTS

The authors would like to thank the following people: Lt. Col. Robert F. Couch, Jr., for his support of this project; Thomas W. Henry for assistance with sample acquisitions from the boreholes; Robert B. Halley for providing debris samples; Papo Gelle, Mike Long, and Leon Young for preparing the recovery samples for the shock-wave experiments; and Sunney Chan for use of the EPR facilities.

Contribution # 4473, Division of Geological and Planetary Sciences, California Institute of Technology, Pasadena, CA 91125.

REFERENCES CITED

- Blanchard, S.C., and Chasteen, N.D., 1976, Electron paramagnetic resonance spectrum of a sea shell, Mytilus edulis: Journal of Physical Chemistry, v. 80, p. 1362-1367.
- Halley, R.B., Major, R.P., Ludwig, K.R., Peterman, Z.L., and Matthews, R.K., 1986, Preliminary analyses of OAK debris samples; 11 p., 7 figs., 4 tbls.: in Folger, D.W., ed., Sea-floor observations and subbottom seismic characteristics of OAK and KOA craters, Enewetak Atoll, Marshall Islands: U.S. Geological Survey Bulletin 1678.
- Henry, T. W., Wardlaw, B. R., Skipp, B., Major, R.P., and Tracey, J. I., Jr., 1986, Pacific Enewetak Atoll Crater Exploration (PEACE) Program Enewetak Atoll, Republic of the Marshall Islands; Part 1: Drilling operations and descriptions of boreholes in vicinity of KOA and OAK craters: U.S. Geological Survey Open-File Report 86-419, 502 p., 29 figs., 13 tbls., 3 appendices.
- Hurd, F. K., Sachs, M., and Hershberger, W. D., 1954, Paramagnetic resonance absorption of Mn^{++} in single crystals of $CaCO_3$: Physics Review, vol. 93, p. 373-380.
- Low, W. and Zeira, S., 1972, ESR spectra of Mn^{++} in heat-treated aragonite: American Mineralogist, v. 57, p. 1115-1124.
- Ludwig, K.R., Halley, R.B., Simmons, K.R., and Peterman, Z.E., 1986, Sr-isotope stratigraphy of disturbed and undisturbed carbonates: 23 p., 8 figs., 6 tbls.; in Henry, T.W., and Wardlaw, B.R., eds., Pacific Enewetak Atoll Crater Exploration (PEACE) Program Enewetak Atoll, Republic of the Marshall Islands; Part 3: Stratigraphic analysis and other geologic and geophysical studies in vicinity of OAK and KOA craters: U.S. Geological Survey Open-File Report 86-555.
- Marsh, S.P. (Ed.), 1980, LASL Shock Hugoniot Data: University of California Press, Berkeley.
- Ristvet, B.L., 1986, Personal oral communication.

- Stoffler, D., 1972, Deformation and transformation of rock-forming minerals by natural and experimental shock processes: *Fortschrift Mineralogie*, v. 49, p. 50-113.
- Tyburczy, J.A., and Ahrens, T.J., 1986, Dynamic compression and volatile release of carbonates: *Journal of Geophysical Research*, v. 91, p. 4730-4744.
- Vizgirda, J. and Ahrens, T. J., 1980, Shock-induced effects in calcite from Cactus Crater: *Geochimica Cosmochimica Acta*, v. 44, p. 1059-1069.
- Wardlaw, B. R., and Henry, T. W., 1986, Geologic interpretation of OAK and KOA craters; 39 p., 21 figs., 3 tpls., 1 appendix; in *Pacific Enewetak Atoll Crater Exploration (PEACE) Program Enewetak Atoll, Republic of the Marshall Islands; Part 3: Stratigraphic analysis and other geologic and geophysical studies in vicinity of OAK and KOA craters*: U.S. Geological Survey Open-File Report 86-555.

TABLE 4-2. Results for Borehole OAR-2A Samples. The pressures and accompanying errors are given in Giga Pascal (GPa). Depths are provided in both feet below seafloor (ft bsf) and feet below sealevel (ft bsl). For explanation of carbonate petrographic names used under DESCRIPTION column in this and succeeding tables, see Henry, Wardlaw, and others (1986, p. 83-97).

DEPTH (ft bsf) (ft bsl)	P (GPa)	ERROR (GPa)	DESCRIPTION
0.6	111.1	12.5	2.6 uncemented sand
6.6	117.1	14.5	2.7 uncemented wackestone
12.2	122.7	13.2	4.5 uncemented wackestone
15.8	126.3	14.5	1.0 uncemented wackestone
21.4	131.9	15.0	2.4 uncemented packstone
23.8	134.3	10.9	1.0 uncemented wackestone/packstone
25.8	136.3	3.5	0.6 uncemented packstone below AA/BB bndry
32.2	142.7	0.0	1.0 cemented packstone
38.4	148.9	4.4	3.0 poorly-cemented packstone
57.3	167.8	0.0	0.7 cemented packstone
67.1	177.6	0.0	1.2 poorly-cemented wackestone
74.2	184.7	0.0	1.3 uncemented wackestone
81.6	192.1	0.0	1.9 uncemented wackestone
100.3	210.8	0.0	1.6 coral fragment, <i>Astreopora</i>
129.3	239.8	0.0	0.6 cemented wackestone
155.3	265.8	0.0	1.4 spar-replaced coral
177.4	287.9	0.0	0.7 well-cemented mudstone
196.3	306.8	0.0	0.8 cemented wackestone
241.6	352.1	0.0	1.2 uncemented grainstone
280.0	390.5	0.0	0.9 cemented wackestone burrow
315.6	426.1	0.0	1.1 cemented wackestone

TABLE 4-3. Results for Borehole OBZ-4 samples. The pressures and accompanying errors are given in Giga Pascal (GPa). Depths are provided in both feet below seafloor (ft bsf) and feet below sealevel (ft bs!).

CRATER ZONE	DEPTH (ft bsf) (ft bs!)		P (GPa)	ERROR (GPa)	DESCRIPTION
α_1	6.7	205.4	0.0	0.9	mud
α_2	44.0	242.7	0.0	1.0	wackestone
	75.9	274.6	0.0	2.3	coarse-grain packstone
β_{1a}	107.5	306.2	0.0	1.0	cemented
	119.1	317.8	2.3	1.0	cemented packstone
	136.0	334.7	0.0	0.6	cemented packstone
	141.8	340.5	0.0	0.5	cemented
	152.1	350.8	0.0	2.0	cemented
	163.3	362.0	0.0	0.8	cemented
β_{1b}	174.8	373.5	0.0	1.2	spar
	190.8	389.5	0.0	0.7	cemented wackestone burrow
	191.0	389.7	2.3	2.6	lithoclast and spar
	193.2	391.9	0.0	0.6	cemented packstone
	196.1	394.8	2.4	4.2	spar-replaced <i>Favia</i>
	199.6	398.3	0.0	1.6	fine grain muddy sand
β_2	199.9	398.6	0.0	0.7	uncemented wackestone
	207.7	406.4	0.0	1.8	cemented wackestone burrow
	210.9	409.6	0.0	0.7	cemented packstone burrow
	216.6	415.3	0.0	0.7	recrystallized <i>Tridacna</i>
	217.1	415.8	0.0	1.2	well-cemented tea-brown micrite
β_3	219.4	418.1	0.0	1.1	spar-replaced coral
	222.7	421.4	0.0	0.7	cemented packstone
	233.0	431.7	0.0	0.7	uncemented
	265.1	463.8	0.0	1.5	poorly-cemented
	324.0	522.7	0.0	1.1	cemented burrow
γ	397.7	596.4	0.0	3.2	spar-replaced coral

TABLE 4-4. Results for Borehole OCT-5 Samples. The pressures and accompanying errors are given in Giga Pascal (GPa). Depths are provided in both feet below seafloor (ft bsf) and feet below sealevel (ft bsl).

CRATER ZONE	DEPTH (ft bsf) (ft bsl)		P (GPa)	ERROR (GPa)	DESCRIPTION
α_1	0.9	164.6	0.0	1.0	uncemented grainstone
α_2	9.4	173.1	0.0	1.1	coarse-grain packstone
β_{1a}	13.0	176.7	0.0	1.0	uncemented packstone
	25.0	188.7	0.0	0.9	fall-in (?)
	36.7	200.4	0.0	1.5	cemented wackestone burrow
	45.0	208.7	4.8	0.6	echinoid spine
	56.7	220.4	0.0	0.8	cemented packstone lithoclast
	63.4	227.1	0.0	2.0	rounded cemented burrow
	85.8	249.5	0.0	1.0	cemented packstone
	95.1	258.8	2.6	1.6	<i>Cardium</i> with internal filling
	104.7	268.4	0.0	3.5	spar-replaced <i>Cardium</i>
	115.7	279.4	0.0	0.8	cemented wackestone
β_{1b}	121.6	285.3	13.6	4.2	uncemented med-grained grainstone
	124.3	288.0	13.3	4.7	uncemented coarse-grained grainstone
	131.9	295.6	14.8	3.6	uncemented grainstone
	135.1	298.8	15.0	8.0	cemented grainstone
	140.6	304.3	12.0	6.3	uncemented <i>Halimeda</i> packstone
	146.2	309.9	15.0	7.8	uncemented <i>Halimeda</i> packstone
	153.4	317.1	0.0	0.6	cemented burrow
	163.6	327.3	0.0	0.6	cemented packstone
	174.1	337.8	0.0	0.8	cemented packstone
	192.6	356.3	0.0	1.6	cemented packstone
γ	204.7	368.4	2.5	0.4	tea-brown cemented rhizolith
	237.0	400.7	0.0	0.8	tea-brown cemented packstone
	300.3	464.0	3.6	3.5	spar-replaced coral

TABLE 4-5. Results for Borehole OET-7 Samples. The pressures and accompanying errors are given in Giga Pascal (GPa). Depths are provided in both feet below seafloor (ft bsf) and feet below sealevel (ft bsl).

CRATER ZONE	DEPTH (ft bsf) (ft bsl)		P (GPa)	ERROR (GPa)	DESCRIPTION
α_2	8.3	115.2	0.0	0.7	pebble-sized lithoclast
	12.0	118.9	13.0	4.5	uncemented grainstone
	17.8	124.7	15.0	5.5	coral pebble
γ	21.2	128.1	11.2	5.2	uncemented <i>Halimeda</i> grainstone
	25.9	132.8	15.0	4.8	uncemented packstone-grainstone
	30.7	137.6	12.6	2.7	uncemented packstone-grainstone
	35.3	142.2	13.7	4.3	uncemented packstone-grainstone
	40.6	147.5	13.0	5.0	uncemented fine-grain packstone
	66.7	173.6	6.4	2.1	cemented pebble-sized

TABLE 4-6. Results for Borehole OFT-8 Samples. The pressures and accompanying errors are given in Giga Pascal (GPa). Depths are provided in both feet below seafloor (ft bsf) and feet below sealevel (ft bsl).

CRATER ZONE	DEPTH (ft bsf)	DEPTH (ft bsl)	P (GPa)	ERROR (GPa)	DESCRIPTION
α_2	2.7	133.5	0.0	0.6	tea-brown cemented rhizolith
	6.4	137.2	0.0	0.6	tea-brown cemented lithoclast
	13.1	143.9	0.0	0.6	tea-brown cemented packstone
β_{1a}	17.0	147.8	0.0	0.9	cemented packstone
	18.4	149.2	4.2	1.6	cemented matrix within pelecypod
	20.5	151.3	2.0	1.4	partly spar-replaced coral
β_{1b}	22.8	153.6	15.0	4.0	uncemented packstone
	26.0	156.8	14.5	3.7	uncemented grainstone
	30.4	161.2	15.0	4.5	uncemented <i>Halimeda</i>
	35.0	165.8	15.0	5.2	uncemented packstone
	39.8	170.6	15.0	5.3	uncemented packstone
	45.5	176.3	14.8	2.5	partly spar-replaced coral
	50.1	180.9	14.7	1.0	uncemented packstone
	52.3	183.1	0.0	1.2	<i>Cardium</i> with cemented matrix
	52.6	183.4	0.0	0.9	partly spar-replaced coral
	54.4	185.2	0.0	0.6	moderately cemented packstone
	57.0	187.8	2.6	0.7	moderately cemented <i>Halimeda</i>
	61.1	191.9	2.5	0.9	poorly-cemented packstone
	64.5	195.3	8.1	0.8	cemented shell rubble
γ	64.9	195.7	0.0	1.1	spar-replaced <i>Astreopora</i>
	67.0	197.8	0.0	1.0	mudstone filled cemented burrow
	73.8	204.6	0.0	0.4	moderately cemented packstone
	81.2	212.0	0.0	0.5	cemented packstone
	93.5	224.3	0.0	1.4	spar-replaced <i>Porites</i>

TABLE 4-7. Results for Borehole OPZ-18 Samples. The pressures and accompanying errors are given in Giga Pascal (GPa). Depths are provided in both feet below seafloor (ft bsf) and feet below sealevel (ft bsl).

CRATER ZONE	DEPTH (ft bsf) (ft bsl)		P (GPa)	ERROR (GPa)	DESCRIPTION
α_1	3.6	205.5	0.0	1.4	uncemented mudstone
	7.0	208.9	2.5	2.1	uncemented mudstone
	10.0	210.9	0.0	1.0	uncemented mudstone
	23.3	225.2	0.0	1.4	uncemented mudstone
β_{1a}	57.8	259.7	0.0	2.1	uncemented wackestone
	78.2	280.1	0.0	1.4	uncemented grainstone
	95.9	297.8	0.0	1.0	uncemented grainstone
	117.8	319.7	0.0	1.1	uncemented grainstone
	135.3	337.2	0.0	0.9	uncemented grainstone
β_{1b}	155.3	357.2	2.2	0.9	uncemented packstone
	166.6	368.5	3.3	1.4	uncemented packstone
β_2	182.6	384.5	0.0	0.8	spar-cemented grainstone
	185.0	386.9	2.2	1.3	uncemented
	198.0	399.9	14.7	2.5	uncemented
	198.6	400.5	15.0	6.3	green Holocene wackestone mud
	207.0	408.9	13.6	5.4	uncemented
β_3	210.5	412.4	0.0	1.1	cemented packstone burrow
	214.0	415.9	14.1	2.5	uncemented
	217.0	418.9	0.0	0.9	tea-brown cemented packstone
	217.1	419.0	0.0	0.7	cemented wackestone
	217.5	419.4	0.0	1.4	cemented wackestone burrow
	220.4	422.3	0.0	1.3	coarse-grain spar
	220.5	422.4	0.0	0.8	cemented packstone
	223.5	425.4	0.0	1.2	cemented packstone burrow
	232.9	434.8	0.0	0.9	poorly-cemented packstone
	236.3	438.2	0.0	3.5	partially spar-replaced coral
	245.4	447.3	0.0	0.6	cemented wackestone
	256.9	458.8	0.0	2.0	spar-replaced coral
	273.8	475.7	0.0	0.7	spar-cemented packstone burrow
γ	320.5	522.4	0.0	0.7	spar-filled grstropod
	400.5	602.4	0.0	0.6	cemented wackestone

TABLE 4-8. Results for OAK Debris Samples. The pressures and accompanying errors are given in Giga Pascal (GPa). Source-depths are converted to feet below sea level from Ludwig and others (1987) and Ristvet (1981).

SAMPLE	RADIUS (ft)	ERROR (ft)	P (GPa)	ERROR (GPa)	SOURCE- DEPTH (ft bsl)
78	1053	13	0.0	0.9	-
125a	1273	13	0.0	1.8	200-500
126	1211	13	13.6	4.2	105-140
127	1095	13	3.0	2.0	-
128	1421	13	10.5	8.0	105-140
144	1302	13	12.5	2.3	105-140
147	1170	30	2.7	0.9	-
155	1299	13	0.0	1.4	-
156	1109	13	0.0	1.1	-
156b	1109	13	0.0	0.9	-
158	906	13	0.0	1.0	200-500
166B	1109	13	0.0	1.0	500-700
167B	1276	13	0.0	0.6	-
168A	1155	13	0.0	0.8	-
168C	1122	13	0.0	1.4	300-500
201	2310	16	0.0	1.4	420
1-1	1358	157	13.1	1.6	105-140
1-2	1358	157	15.0	3.4	>140
1-3	1358	157	14.6	1.6	105-140

CHAPTER 5:

BATHYMETRIC STUDIES OF OAK CRATER

By

John L. Peterson¹ and Robert W. Henny²

INTRODUCTION

This chapter summarizes recent work done by the Air Force Weapons Laboratory (AFWL) and the New Mexico Engineering Research Institute (NMERI) in a first-order assessment of OAK crater bathymetry (Peterson and Henny, 1987). The starting points for this study were the 1958 pre- and postshot bathymetric maps and a new 1984 bathymetric map of the OAK crater (ALICE reef) area of Enewetak Atoll (fig. 5-1).

Objectives and General Procedures

The primary objectives were to characterize and to quantify changes in bathymetry resulting both from the detonation of the OAK device and from subsequent geologic processes. A secondary objective was to provide a set of working maps at a common scale of 1:2400 for use both by the PEACE Program and future investigations.

The approach was to prepare contour maps by digitizing and reprocessing each of the three bathymetric basemaps and to construct three isopach maps from the contour-map pairs with the aid of a computer. Areas and volumes were computed by contour interval for each of the isopach maps, and planar and cross-sectional features were examined critically on all six maps.

Terminology

The following terms are used in this Chapter. No attempt is made here to correlate the cratering terms with those used in other portions of this Open-File Report; this can only be accomplished after synthesis of the various data sets (see statement 8 of the Conclusions).

Circular crater -- crater region consisting of an inner circular component, as defined by the minus 145-ft closed contour in the postshot contour maps, which is enclosed by an outer-circular component as defined by approximately the minus 50-ft partially closed contour on the same maps.

¹ New Mexico Engineering Research Institute, Albuquerque, NM.

² Air Force Weapons Laboratory, Kirtland Air Force Base, NM.

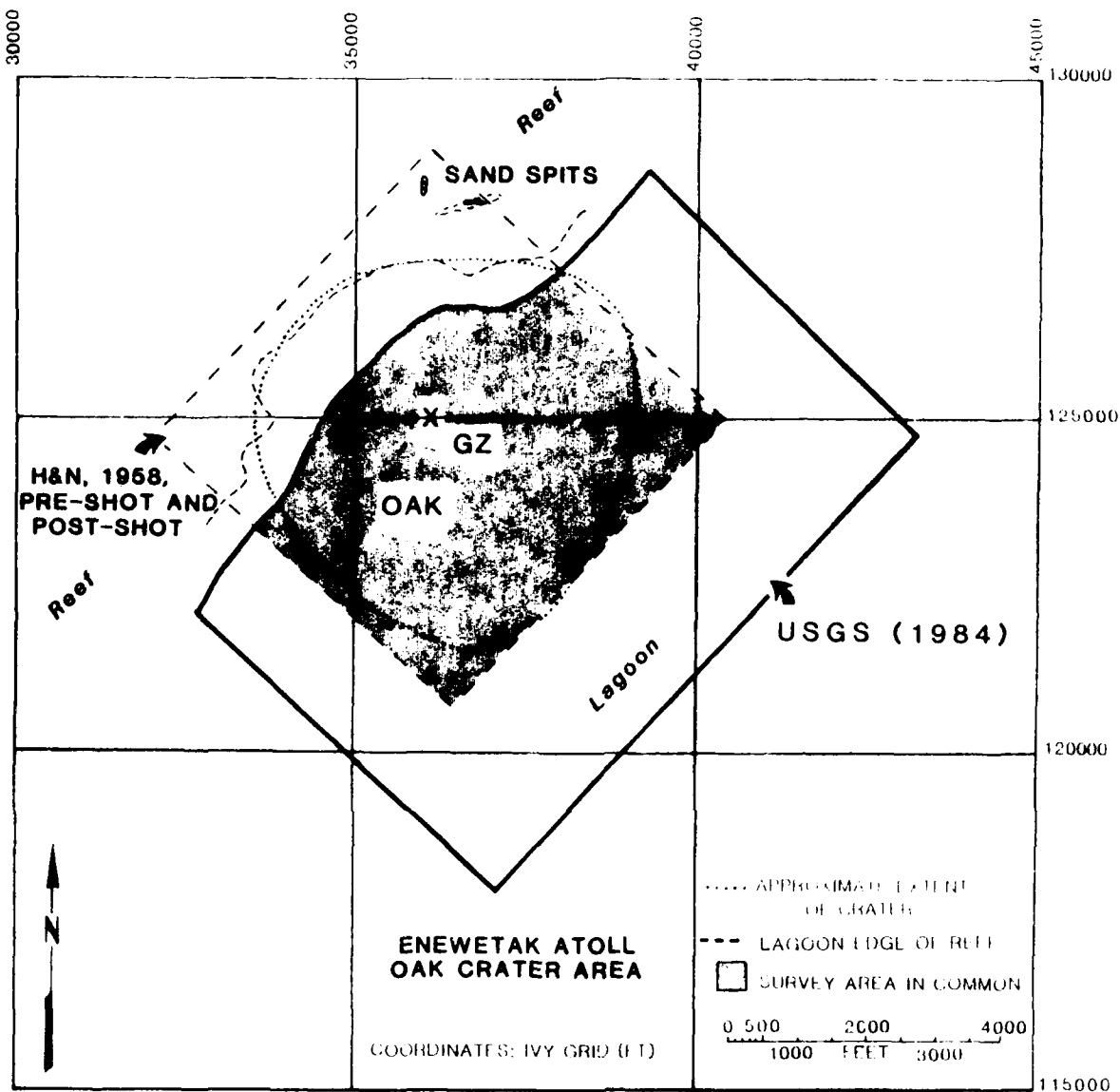


FIGURE 5-1. -- Map showing OAK crater region and areas included in Holmes and Narver pre- and postshot surveys (H&N, 1958a and 1958b) and the U.S. Geological Survey map (USGS, 1984). Area in common to all three basemaps shown in stippled pattern. OAK surface ground zero (SGZ) depicted by "X", and apparent crater shown by dotted line.

Crater wings -- areas primarily within the reef slope and just beyond the boundary of the circular crater.

Elliptical crater -- crater region consisting of the circular crater and portions of the crater wings as defined by the closed minus 20-ft contour of the isopach maps.

Apparent crater -- the final observed crater, composed of the elliptical crater and the encompassing areas of subsidence. Note that the apparent crater boundary extends beyond the mapped areas of this study.

Differential relief (subsequently abbreviated Δ -relief) -- term used in describing the net positive and negative changes in relief of an area with time. This is depicted by isopach maps showing the areas of change of relief derived from comparison of the digitized bathymetric base maps.

Subsidence -- term used to denote an increase in negative Δ -relief without subscribing to any particular mechanism.

Units used in this Chapter are those of the original works; metric for the 1984 bathymetry, engineering for the remainder.

DATA BASE

H&N Preshot Bathymetric Map

Prior to the OAK nuclear event (29 June 1958), a bathymetric survey of the site (ALICE-reef area) was conducted between 3 and 26 June by Holmes and Narver Engineering Company (H&N) for the U.S. Atomic Energy Commission (AEC) using standard rod, fathometer, and lead-line surveying techniques (fig. 5-1). Datum was 0.5 ft below Approximate Mean Low Water Spring (AMLWS). The survey, tied into the Eniwetok Ivy Grid Coordinate System (H&N, 1952; U.S. Army, 1970), originally was planned to cover a 6,000- x 6,000-ft square centered on the OAK surface ground zero (SGZ) and aligned with the oceanward edge of ALICE reef. A baseline approximately 6,000-ft long was established along the highest topographic area of the reef flat (specifically, along a line of sand bars midway on the reef flat) with benchmarks (BMs) placed on 300-ft centers.

A standard rod survey was conducted perpendicular to the baseline at each BM oceanward to near the reef edge and lagoonward to approximately the minus 5-ft elevation. Each survey line was continued lagoonward to 3,000 ft beyond SGZ using an LCM vessel equipped with a Raytheon Recording Fathometer. Vessel course was controlled by theodolite from each BM and at 300-ft intervals by triangulation from the two terminal baseline BMs. Vertical control was provided at these 300-ft intervals by a lead-line sounding. No cross-tie survey lines were run, and a data gap of a few hundred feet at the lagoonward reef edge resulted because of the inability of the LCM-vessel to obtain fathometer readings in water shallower than 10 to 15 ft (H&N, 1958a).

The resultant bathymetric map was hand-contoured with 5-ft intervals (1-ft intervals above the minus 5-ft contour) (pl. 5-1)¹. The map did not include the surveyed ocean side of the reef for reasons discussed below.

H&N Postshot Bathymetric Map

A postshot survey of the OAK crater area, using the same techniques described above, was run between 16 August and 4 September 1958 (D + 47 to 67 days). Numerous major problems were encountered in relocating the baseline along the reef flat opposite the crater because it was significantly disturbed (lowered and covered with debris) by the event. Eventually, the terminal BMs were located and the baseline reconstructed. As in the preshot survey, there was a data gap between rod and fathometer surveys that probably was increased by the difficult postshot conditions. These conditions also resulted in little of the reef oceanward of the baseline being resurveyed. Finally, toward the end of the survey, operationally imposed time constraints may have resulted in only every other line being surveyed in the far eastern quadrant of the grid. The resultant map (H&N, 1958b), contoured at a 5-ft interval, covered the same area as the preshot survey except oceanward of the reef baseline (fig. 5-1), thus giving a common pre-/postshot map area of approximately 6,000 x 5,000 ft or 30 million sqft (pl. 5-2).

Detailed documentation of the H&N surveys does not exist. Most of the information presented here is from B.L. Ristvet (oral communication, 1986) who has reviewed the original field survey books and maps referenced and has conducted extended discussions with several of the original workers.

USGS 1984 Bathymetric Map

The third basemap used in this study was the bathymetric map of the OAK crater and surrounding area prepared from a detailed echo-sounder survey conducted in 1984 (D + 26 years) by the U.S. Geologic Survey (USGS) during the Marine Phase of the PEACE Program (USGS, 1984; see Folger, Hampson, and others, 1986, for details of the survey). This survey also was tied into the Eniwetok Ivy Grid; however, datum was Mean Lower Low Water (MLLW), which is 0.18 m (0.6 ft) below the MLWS established for the earlier H&N surveys. Most of the echo-sounder data were collected along 25-m- (82-ft-) spaced lines oriented parallel to the reef. Perpendicular tie lines were run on the average at 180-m (590-ft) intervals (fig. 5-2). Thus, the USGS survey had a sampling density greater than four times that of the H&N surveys. Although smaller boats provided some data at shallower water depths, nearly all data contoured were obtained from the 41-m R/V Egabrag II, which, because of her draft, effectively excluded data above minus 4 m (minus 13 ft). Therefore, although the greatly increased sample density allowed a 1-m contour interval and the survey extended a 1,000 ft both farther out into the lagoon and along the reef slope (figs. 5-1 and 5-2), no bathymetric data were obtained from

¹ Plates 5-1, 5-2, and 5-3 are digitized, reprocessed versions of the referenced original bathymetric maps; these are located at the end of the Open-File Report in the map pocket.

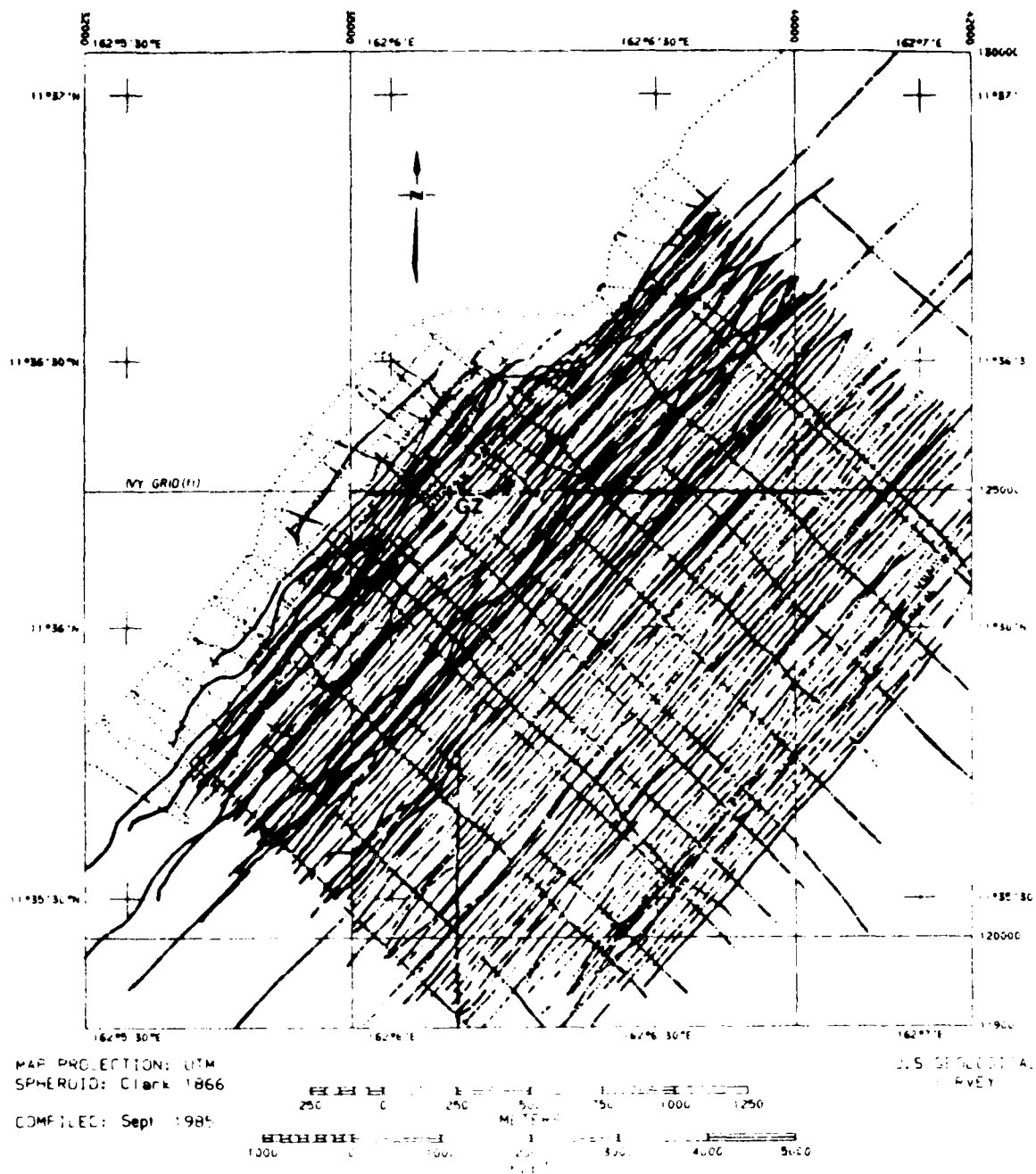


FIGURE 5-2. -- Fathometer lines used in the 1984 USGS study (from Folger, Hampson, and others, 1986, fig 2, p. A-3).

near the reef or on the reef flat itself. This reduced the contoured area common to all three maps to approximately 25.5 million sqft or 85 percent of the digitized H&N maps (see fig. 5-1).

DATA PROCESSING

Digitized Base Contour Maps

All data input and processing were performed using an Arc/Info Geographic Information System software package (ESRI, 1986). Processing was done on a VAX 11/750 computer at the Technology Application Center (TAC), University of New Mexico.

The data-input process for the two H&N maps (pls. 5-1 and 5-2, located in the map pocket at the end of the Report) was complicated because the maps were not on base-stable media. Both were digitized manually from 1:2400-scale bluelines using a 36- x 48-in. Summagraphics Digitizer Tablet operating in the continuous-string sampling mode. All data entered into the system were initialized and recorded in the Eniwetok Ivy Grid Coordinate System.

Digitization of the 1984 USGS basemap (pl. 5-3) required that a photographic enlargement be made from the original mylar map (1:6000). The enlargement was redrafted to separate contour lines along steep slopes within the study area. This redrafted map was photographically enlarged again to increase digitizing accuracy of the contours.

Three minor corrections were required to standardize and update the USGS map. The first was a simple conversion of metric contours to feet. However, since no interpolation was applied to the converted metric units, non-integer engineering-unit contours were generated. The second was a depth correction. This resulted from the comparison of the water-depth values interpolated from the USGS bathymetric map to those measured at each borehole site during the Drilling Phase of the PEACE Program. Linear fits to these data pairs showed that fathometer depths exceeded borehole-site depths by 1 percent down to minus 120 ft, and that borehole-site depths exceeded fathometer depths by 2 percent below minus 120 ft (E.L. Tremba, oral communication, 1986). Third, only those portions of the USGS map that overlaid the H&N map boundaries were digitized.

All digitized basemaps were quality-control checked by interactive zoom editing with a 13-in. Techtronix 4107A Color Graphics Terminal. The maps were scale-corrected by the computer to be compatible for overlaying data sets.

Derived Isopach Maps

Three pairs of isopach maps were computer-generated by digitally subtracting combinations of the three contour maps. The contour-map combinations and descriptions of the resulting three pairs of isopach maps are listed below. The first isopach map of each pair presents negative Δ -relief; the second map shows the positive Δ -relief. All (as plates) are located in the pocket in the back of this Report.

H&N Postshot - H&N Preshot Map Pair: Plates 5-4 and 5-5 display distribution of short-term elevation changes (event to D + 67 days) primarily due to cratering effects.

USGS 1984 - H&N Preshot Map Pair: Plates 5-6 and 5-7 display distribution of long-term elevation changes (event to D + 26 years) primarily due to cratering effects and redistribution of crater-produced and natural debris.

USGS 1984 - H&N Postshot Map Pair: Plates 5-8 and 5-9 display distribution of post-crater long-term elevation changes (from D + 67 days to D + 26 years) primarily due to continued subsidence and redistribution of crater-produced and natural debris.

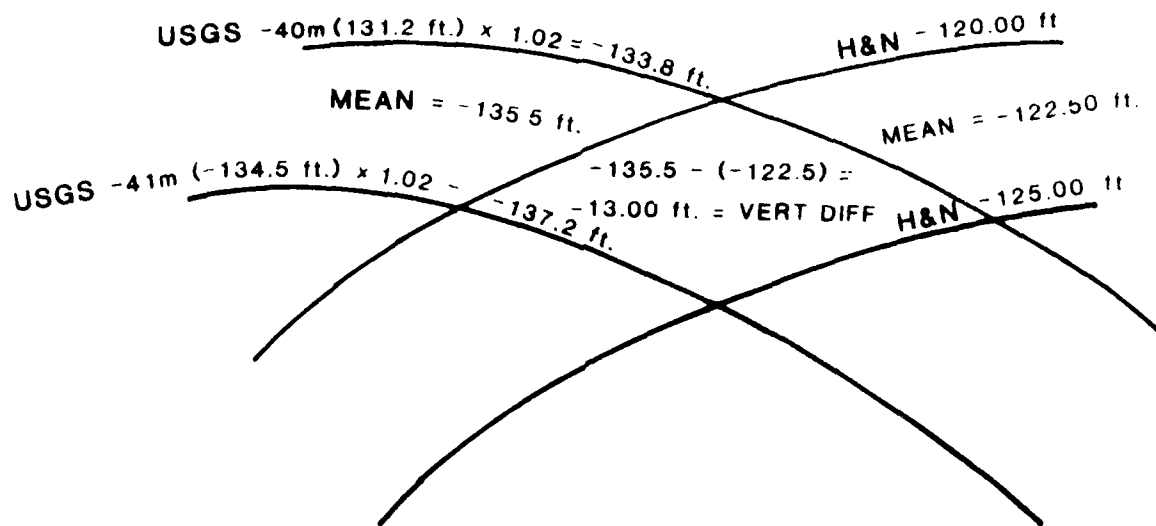
Figure 5-3 illustrates how vertical differences in elevation were calculated within the Arc/Info computer framework. As indicated, a polygon is formed where the two sets of elevation contours, one from each map, intersect. To account for as much of the elevation variance inside the polygon as possible, the mean between the two contours was always used. The vertical difference for each polygon, therefore, is the difference between the means of the two contour sets. In the production of the isopach maps, vertical differences were computed for all polygons formed by the intersection of one map overlaid on another. Typically, five thousand polygons were formed per isopach map. Areas for each polygon were computed in square feet and stored as associated attributes. The vertical-difference files and individual polygons were then sorted into 5-ft increments by a decision rule that grouped polygons with similar vertical differences (i.e.; 0 to 5 ft, 5 to 10 ft, etc.) into the same file.

To reduce required computer memory for the graphic displays, a dissolve module was run on the computer map files that combined adjacent polygons having the same 5-ft increment. Tabular data used to compute areas and volumes for each polygon were saved separately. The final groupings of polygons, representing an increment of 5 ft of positive or negative elevation difference (Δ -relief) between two maps, was then assigned a color and/or symbol for the slides or a shade and/or symbol for the hardcopy maps presented in this Report (pls. 5-4 through 5-9). The jagged appearance of many boundaries on the isopach maps results from the oblique angles formed by intersecting contour sets.

Map Products

Table 5-1 summarizes all maps produced during this study. Each map was produced as a color 35-mm slide, and selected maps were output as hardcopy at a scale of 1:2400 using a 36-in. Versatec Electrostatic Plotter. Because of the large number of contour increments required to fully delineate the crater and disturbed region, the color slides provided the best means to make first-order assessments of the maps. Hardcopy maps were necessary for more detailed analysis and publication. The three digitized contour maps are presented as Plates 5-1 through 5-3, and a positive and a negative display for each of the three derived isopach-map pairs are presented as Plates 5-4 thru 5-9, located in the map pocket of this Report.

EXAMPLE OF VERTICAL DIFFERENCE CALCULATION



VOLUME OF POLYGON = AREA OF POLYGON X VERT DIFF

FIGURE 5-3. -- Diagram showing isopach computational grid.

TABLE 5-1. -- Summary of digitized bathymetric map products for OAK crater for PEACE Program. Note that the 10-ft contour increment is depicted on the negative Δ -relief isopach maps (i.e., pls. 5-4, 5-6, and 5-8) for depth increments greater than minus 20 ft.

MAP PRODUCTS

MAP TYPE	PLATE	MAP TITLE	CONTOUR INTERVAL (ft)				SLIDE SETS	PAPER MAPS	AREA & VOLUME SUMMARY
			3.3	5	10	25			
Contour	5-1	H&N Preshot	-	+	-	-	+	+	-
	5-2	H&N Postshot	-	+	-	-	+	+	-
	5-3	USGS Postshot	+	-	-	-	+	+	-
Overlaid Contour	-	H&N Post- on H&N Pre- Overlay (contours only)	-	+	-	-	+	-	-
	-	USGS on H&N Pre- Overlay (contours only)	-	+	-	-	+	-	-
	-	USGS on H&N Post- Overlay (contours only)	+	+	-	-	+	-	-
Isopach	5-4	H&N Isopach (Pre- & Post-)	Negative Δ -relief	-	+	-	-	+	+
	5-5	H&N Isopach (Pre- & Post-)	Positive Δ -relief	-	+	-	-	+	+
	-	H&N Isopach (Pre- & Post-)	Combined Pos. & Neg. Δ -relief	-	-	-	+	+	+
	5-6	USGS/Pre- H&N Isopach	Negative Δ -relief	-	+	+	-	+	+
	5-7	USGS/Pre- H&N Isopach	Positive Δ -relief	-	+	-	-	+	+
	5-8	USGS/Post- H&N Isopach	Negative Δ -relief	-	+	+	-	+	+
	5-9	USGS/Post- H&N Isopach	Positive Δ -relief	-	+	-	-	+	+

Plus (+) symbol indicates presence of product, minus (-) absence.

ANALYSIS

On comparing the three bathymetric basemaps discussed above (see fig. 5-1) and knowledge of the extent of the apparent crater of OAK, it is obvious that neither the 1958 H&N maps nor the 1984 USGS map continue outward far enough in any direction to fully cover the total area affected by the OAK event. This forms a significant limitation to any bathymetric analysis.

Map Derived Quantities

Several problems are associated with obtaining numerical values from the contour and isopach maps. These are complexly related to the previously discussed survey-sampling differences and deficiencies. They include the following: (1) the differences in areas mapped between surveys; (2) problems with positioning of the survey and drilling ships; and (3) the continuing redistribution of debris with time. The interpretation of the results are further hampered by the fact that both the pileup of debris from the crater (positive Δ -relief) and subsidence after the event (negative Δ -relief) occur over nearly the entire map area yet are inseparable solely from bathymetric data alone. However, even cursory examination of the maps shows clearly recognizable Δ -relief patterns that are easily followed from map to map (i.e., with time). Therefore, in general, the larger the area over which measurements are averaged, the higher the confidence of those values. Below are presented selected point (depths), line (cross sections), and area (area and volumes) estimates.

Water Depths. -- Table 5-2 compares water depths at each borehole drilled during the PEACE Program that are located within the map areas. Borehole depths are those measured in the field at time of drilling and reported in the USGS (Henry, Wardlaw, and others, 1986a), whereas bathymetric water depths are the arithmetic mean of the bounding contours (3.3-ft contour interval). Although the precision of the former are probably to within 0.1 ft, the latter could be in error by up to 1.7 ft. Additional errors probably occur due to borehole location uncertainties (± 10 ft), which could easily translate into several vertical feet in areas of rough postshot terrain.

Because the USGS bathymetry and drilling programs were completed within a year of each other, the differences in water depths provide a measure of the inaccuracies inherent on the USGS contour map. Fourteen of the boreholes exhibit differences ranging from plus 2.9 to minus 1.7 ft, with a mean of only 0.4 ft and an absolute average of 1.6 ft. The other four boreholes (OCT-3, ODT-6, OLT-14, and OUT-24) exhibit differences exceeding 4 ft (range from plus 4.8 to minus 5.8 ft), have a mean difference of 1.9 ft and an absolute average of 4.9 ft. For OLT-14, there was a problem in locating the position of the borehole (see Henry, Wardlaw, and others, 1986b, p. 390-391). For the other three, no trends are obvious nor is the reason for the larger differences known. These differences do illustrate the problem in relying solely on the bathymetric data to obtain point estimates.

Another important observation is that postshot water depths for boreholes located at roughly equal distances, but on opposite sides of SGZ, are similar.

TABLE 5-2. -- Summary of water depths and vertical differences at PEACE Program borehole locations. Water depths are compared between measured values at borehole sites in 1985 (Henry, Wardlaw, and others, 1986, p. 60, tbl. 10) and interpolated values from Holmes and Narver preshot and postshot maps (H&N, 1958a, 1958b) and U.S. Geological Survey postshot map (USGS, 1984), compiled from echo-sounding data from Marine Phase of PEACE Program. All depths given in ft below sea level (bsl); vertical differences are given in ft. Note that the location of borehole OLT-14 is questionable (see Henry, Wardlaw, and others, 1986, p. 390-391).

WATER DEPTHS AND VERTICAL DIFFERENCES

BOREHOLE NUMBER		H&N PRESHOT DEPTH*	USGS DRILL LOG DEPTH** (1985)	USGS MAP DEPTH* (1984)	USGS 1984-85 DIFF.	H&N POSTSHOT DEPTH*	H&N POSTSHOT VS USGS 1984 DIFF.
PARALLEL TO REEF							
1	ORT-20	67.5	101.4	102	-0.9	87.5	-14.8
2	OQT-19	47.5	117.5	115	2.2	107.5	- 7.8
3	OTG-23	47.5	164.0	166	-1.6	152.5	-13.1
4	OPZ-18	47.5	201.9	199	2.8	197.5	- 1.6
5	OBZ-4	12.5	198.7	199	-0.4	197.5	- 1.6
6	OCT-5	17.5	163.7	159	4.8	142.5	-16.4
7	OQT-9	17.5	134.8	136	-0.7	122.5	-13.0
8	OFT-8	17.5	130.8	129	2.0	117.5	-11.3
9	OET-7	17.5	106.9	106	1.4	92.5	-13.0
10	ODT-6	17.5	90.1	86	4.0	72.5	-13.6
PERPENDICULAR TO REEF							
1	OUT-24	1.5	147.0	142	4.8	127.5	-14.7
2	OBZ-4	12.5	198.7	199	-0.4	197.5	- 1.6
3	OPZ-18	47.5	201.9	199	2.8	197.5	- 1.6
4	OKT-13	102.5	164.7	166	-0.9	152.5	-13.1
5	OIT-11	122.5	155.0	152	-2.8	147.5	- 4.7
6	OHT-10	122.5	137.3	139	-1.5	122.5	-16.3
7	OJT-12	112.5	143.8	146	-1.7	132.5	-13.0
8	ONT-16	132.5	135.1	132	2.9	122.5	- 9.7
9	OMT-15	142.5	110.9	112	-1.1	127.5	15.5
10	OLT-14	127.5	139.7	146	-5.8	132.5	-13.0

* From Arc/Info File.

** From Henry, Wardlaw, and others (1986, p. 60, tbl. 10).

regardless of differences in the preshot water depths. For example, at roughly 900 ft from SGZ, preshot differences in water depths between OUT-24 on the reefward side and OKT-13 on the lagoonward side are 101 ft; postshot differences are only 18 ft. At 1,800 ft from SGZ, ODT-6 and ORT-20 differ by 50 ft preshot compared to only 11 ft postshot. Another pair (OQT-19 and OET-20 at 1,400 ft) exhibit preshot and postshot differences of 30 and 10 ft, respectively. These data suggest that the net cratering effects in both the "coral" media and water were about the same.

Except for OMT-15, which lies along the lagoon radial (southwest transect) of a large debris tongue, all 1984 USGS water depths at borehole locations exceed the 1958 H&N postshot depths by 2 to 16 ft (see tbl. 5-2). Although no other trends are obvious, these values represent the minimum net downward displacement (i.e., downward movement of the surface plus any addition of debris that may have occurred between surveys). At OMT-15, there is a 15-ft decrease in water depth which, if valid, can only be explained by a late-time addition of debris possibly from a neighboring high.

Cross Sections. -- Figure 5-4 presents two composite cross sections through the OAK SGZ parallel to (southwest to northeast) and perpendicular to (northwest to southeast) the trend of the reef. Each profile of the composite was prepared by manually digitizing the respective contour maps. Note that a vertical exaggeration of 10:1 results in slopes accordingly out of proportion. The H&N preshot profiles illustrate that the OAK device was placed above a sharp break in slope of the lagoonward edge of the reef. Comparisons of the H&N pre- and postshot profiles show that a large part of the lagoon side of the crater was originally water, and, therefore, most of the ejecta from that side of the crater was water. Within the circular crater, the flat floor is offset lagoonward from SGZ by 300 ft, and sets of terraces on the reefward side of the crater are evident.

The H&N postshot profile, perpendicular to the reef, crosses the most complex portion of the map near the apex of a large debris mass rising over 100 ft above the preshot level near the 1,900-ft mark. A slightly smaller debris mass, 500 ft further out, is some 30 ft above the preshot level and appears to have built up against and engulfed a preshot coral knoll. The cross section parallel to the reef shows the break at the boundary of the circular crater and the crater wings. Several distinct terraces within the crater are visible.

Comparisons of the 1984 USGS and 1958 H&N profiles show that the entire region subsided. Maximum downward displacement is concentrated in the mid- to lower depths of the circular crater and out into the lagoon. Significantly less downward displacement has occurred on the wings of the crater, whereas, on the reefward side, material has moved up and in toward SGZ. In assessing these profiles it is important to consider that redistribution of sediments probably resulted in material moving out of and into the plane of the cross sections.

Areas and Volumes. -- Tabulated areas and volumes for each of the three computed isopach maps are given in Tables 5-3 thru 5-5, located at the end of

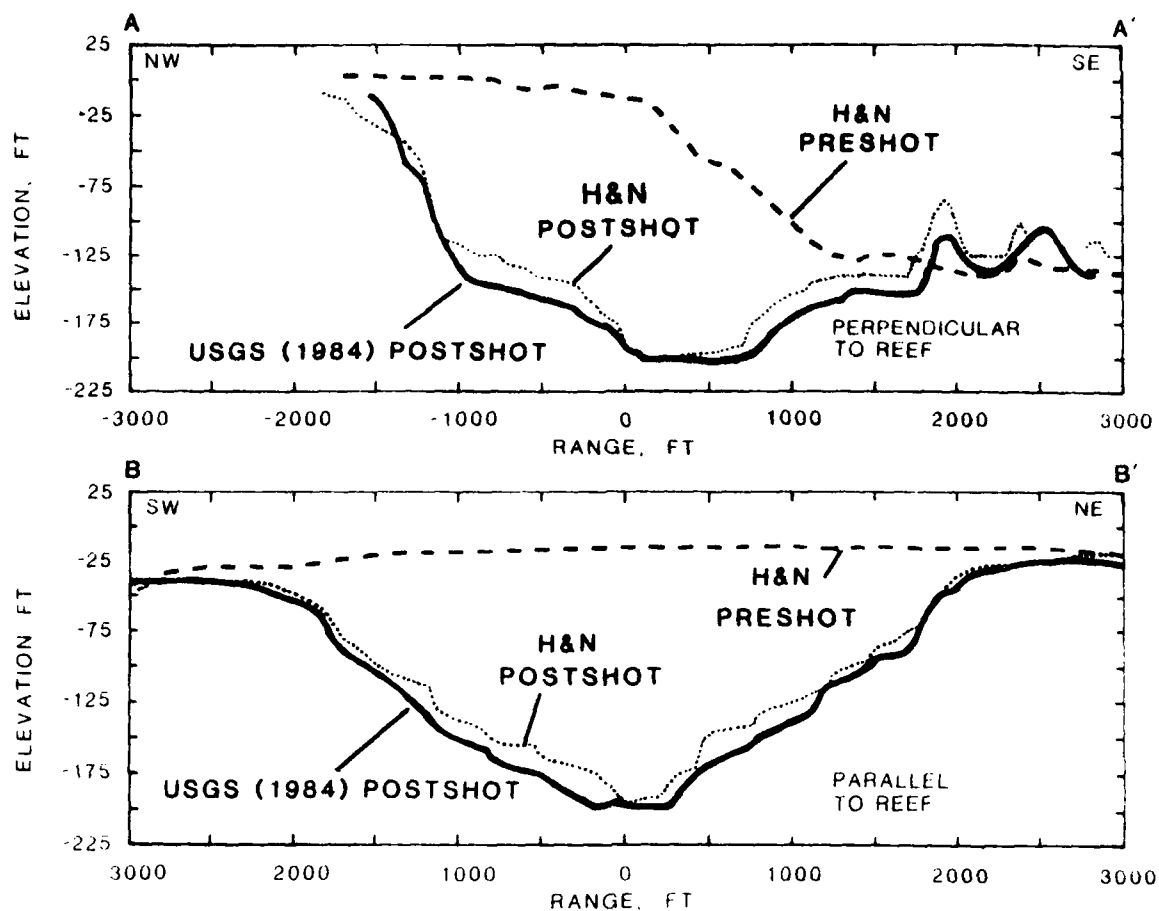


FIGURE 5-4. -- Cross sections through surface ground zero (SGZ) of OAK crater.

the Chapter¹, and summarized in Table 5-6. Volumes were computed in 5-ft increments by multiplying the vertical differences for each polygon by their respective areas and then totaling all of the volumes. Dimensions given are for each map area which, as discussed previously, differ somewhat between maps. The data demonstrate clearly that the entire area subsided an average of 23 ft by D + 67 days and another 12 ft during the next 26 years. As the surface of the crater and surrounding areas dropped, so did the coverage of positive relief, from 27 percent of the area at D + 67 days to only 14 percent of the area after 26 years.

MAP CHARACTERISTICS

The following is a first-order assessment of each contour and isopach map in terms of topographic patterns and characteristics. Because it is difficult to accurately quantify many of the features discussed, dimensions stated are only approximate.

H&N Preshot Contour Map

The northwest one-third (reefward side) of the 1958 H&N preshot map (pl. 5-1) shows the lagoonward side of the reef flat with sand bars along the upper margin. At the wave-break line, there is a well-defined, nearly linear scarp that is distinctly sharper north of SGZ. Approximately 400 ft reefward from SGZ, the scarp is cut by a 400 x 400-ft embayment. Beyond the scarp, a gently sloping shelf, dipping 1.5 degrees into the lagoon, ranges in width from 1,000 ft south of SGZ to less than 500 ft north of SGZ.

The southeast two-thirds of the H&N map (lagoonward side) comprises the reef slope and the lagoon floor, which contains numerous patch reefs. The reef slope, steepest (up to 15 degrees) north and shallowest (up to 5 degrees) south of SGZ, extends 1,000 ft beyond SGZ. Lagoonward from the foot of the reef slope, the lagoon floor slopes very gently (1 degree) toward the lagoon interior. Just south of SGZ is a 75-ft deep, 200-ft wide ravine with a steep, 25-degree headwall. This ravine flattens and widens lagoonward over a distance of about 1,500 ft but retains its identity to at least 2,500 ft as a clear path extending through the patch reefs. On the lagoon floor, numerous patch reefs, roughly aligned in two lineaments parallel to the reef at 1,700 and 2,600 ft lagoonward of SGZ, rise as high as 40 ft above the bottom and range up to several hundred feet in diameter. Their elliptical to triangular shapes on the map are due to the 300-ft H&N-survey spacing. Actually, they are in fact smaller and nearly circular as shown in the 1984 USGS map with its nearly fourfold increase in sampling density.

¹ Tables 5-3 through 5-5, summarizing the data calculated from the computer analysis of the pairs of derivative maps, and Table 5-6, presenting the grand summary of Tables 5-3 through 5-5, are all located at the end of the current Chapter.

Inspection of the H&N Preshot Contour Map (pl. 5-1) shows that the device was placed at a position along the Alice Reef marked by a large embayment. In addition, SGZ was located near the beginning of the lagoonward edge of the reef slope and close to the head of the large ravine that cuts into that slope. Although water depth, interpolated from the preshot map for the OAK SGZ, was almost 13 ft at shot time, according to B.L. Ristvet (oral communication, 1986), it was closer to 14 ft due to a 1.4-ft tide.

H&N Postshot Contour Map

The most striking feature of the OAK crater is its symmetry with respect to the geometric center (GC), which is offset nearly 300 ft lagoonward of SGZ. This is shown clearly in the 1958 H&N postshot map (pl. 5-2). All contours from the bottom of the crater up to the minus 145-ft contour, averaging 850 ft from the GC, are closed. The minus 125-ft contour, averaging 1,200 ft from the GC, closes except for a 45-degree sector on the lagoonward side. Furthermore, on the same side at roughly 1,500 ft from GC, the minus 100-ft contour closes to within 120 degrees. Slopes within the crater are much steeper on the reef side with distinct terraces and slump features evident throughout. Contours in the preshot embayment area are noticeably more distorted than at other locations along the reef.

A second major feature shown by the H&N postshot map is the extension of the debris blanket into the lagoon. This blanket is dominated by a 3,000-ft-long tongue of material, 1,500 ft wide at the crater edge and 55 ft thick at the highest point. Actually, the maximum thickness must be at least 75 ft due to an estimated subsidence in that region of at least 20 ft. The debris tongue is cut radially near the middle by a 400-ft wide channel closely aligned with the preshot ravine. This channel, breaching the crater rim at 1,200 ft from SGZ, passes between two topographic highs at 1,500 ft and bifurcates against another topographic high at 2,700 ft from SGZ.

A third major characteristic is the difference in the preshot to postshot topography in the area of the crater wings along the reef slope. North of SGZ the postshot contours virtually overlay the preshot contours, whereas south of SGZ, the contours have changed considerably and most of the reef slope clearly has been modified by the event.

Many of the patch reefs surveyed preshot do not appear on the H&N postshot map. Some were obviously destroyed, others buried by debris; however, many were probably not mapped in the H&N surveys. Resolution of this issue will require a better understanding of the exact survey lines used by H&N. The 1984 USGS Map (pl. 5-3), with its greater sampling density, adds important information regarding these features and probably could be used as a base to rectify the H&N maps.

USGS 1984 Contour Map

The 1984 USGS map (pl. 5-3) depicts many of the same features shown in the 1958 H&N postshot map (pl. 5-2), except that, with its fourfold increase in sampling density, features such as the coral patch reefs, crater terraces, and slump regions are much more sharply defined. After 26 years, the crater

is larger but retains its basic circular appearance; the crater wings have broadened, especially to the southwest. The inner component of the circular crater, still defined by the minus 145-ft contour, has expanded in radius about the GC from 850 to 1,050 ft. Contours are noticeably smoother, and slopes within the crater are steeper, particularly along the reef where at least two distinct scarps are now present. The debris tongue continues to dominate the lagoonward side, and the preshot ravine is still clearly visible as a remnant feature. Folger, Hampson, and others (1986) discuss the features of the 1984 USGS bathymetric map in terms of "physiographic provinces" and compare them to observations from the submersible, scuba-diving, and sidescan-sonar operations.

H&N Postshot - H&N Preshot Isopach Map

This pair of isopach maps (pls. 5-4 and 5-5) documents the areal distribution of Δ -relief (the net changes in negative and positive elevations), referenced to the preshot datum, resulting from OAK and extending to 67 days after the event.

The most striking feature of the map pair is the nature and distribution of the Δ -relief. Areas of positive Δ -relief, ranging up to 55 ft, cover only 27 percent of the total map of which Δ -relief greater than 5 ft (16 percent of the total map) is restricted to areas lagoonward of the crater. Negative Δ -relief dominates all other areas and covers 63 percent of the map, approximately one-half of that is outside the elliptical crater. The remaining 10 percent of the area shows no change in Δ -relief.

Although it is likely that at least some debris from the crater extends over nearly all of the area covered by the H&N postshot map, most of the reef and large regions on the crater wings and beyond are at a lower elevation than preshot. Therefore, this isopach map grossly understates the amount of debris present because of the unknown amount of event-related subsidence which is very difficult to isolate and measure. In fact, the total amount of debris is further understated because a substantial amount of the debris mass, particularly on the lagoon side, was water. Also, a small amount of ejecta impacted beyond the map area. And finally, an unknown amount of the debris mass may have been transported beyond the confines of the map.

A first-cut estimate of the downward displacement can be obtained by viewing the upper corners of the map (north and west of SGZ) that contain the reef flat. Most distant from SGZ, at 3,000 ft from SGZ, there are areas with a maximum of 5 ft of positive Δ -relief. In contrast at 2,000 ft along the same radials, but still beyond the elliptical crater, there are regions of 5 to 10 ft of negative Δ -relief. Because the positive Δ -relief is probably due to debris, and because debris thickness should increase toward the crater, it is concluded that at least 10 to 15 ft of negative Δ -relief is present at the 2,000 ft range. High-explosive craters in wet media typically display such downwardly displaced profiles, although large azimuthal variations often exist.

A second striking feature of this isopach pair is the elliptically shaped crater, defined by the minus 20-ft contour, which is in sharp contrast to the circular crater of the postshot contour maps (see pls. 5-2 and 5-3). This

elliptical crater, composed of the inner and outer components of the circular crater and the crater wings, has a long axis (4,000 ft) parallel to the reef and a short axis (2,800 ft) perpendicular to the reef.

Difference contours from the deepest point on the crater floor up to the minus 140-ft contour (400-ft radius) are roughly circular and symmetric about the GC of the crater. Above and up to the minus 110-ft contour (1,000-ft radius), the contour lines are roughly circular, but about the SGZ. Above, the largest rates of increasing difference (narrowest contour bands) occur between the minus 60- and minus 20-ft contours and probably represent a series of scarps surrounding the elliptical crater.

The elliptical shape of the crater is primarily due to the crater wings and to the sloping lagoon floor. This suggests that the crater wings, although controlled by the reef structure, are related to the circular crater. The elliptical crater is notably broken along the southeast by a remnant feature of the ravine and its headwall, previously described for the 1958 H&N preshot map. Finally, beyond the crater wings and predominately to the southwest, the en echelon pattern of difference contours suggests successive slumping parallel to the reef and well out into the lagoon.

USGS 1984 - H&N Preshot Isopach Map

This isopach map set (pls. 5-6 and 5-7) documents the distribution of net positive and negative Δ -relief from the preshot datum to 26 years after the detonation of the OAK device. Generally, the same basic difference patterns and features are displayed as at 67 days (previously discussed isopach map), but with some notable changes.

First, the entire area has subsided further so that now 86 percent of the map area exhibits a negative Δ -relief and only 14 percent exhibits a positive Δ -relief. The reef flat in the upper right corner of the map (north of SGZ) indicates an additional 5 to 10 ft of subsidence since the detonation of OAK. At the bottom of the map, 3,300 ft southeast of SGZ, an additional drop of 5 to 10 ft has occurred since the event. The previous maximum high of 55 ft on the ejecta tongue is now only 40 ft, indicating subsidence and possibly some redistribution of debris. Note that the new small circular highs in the bottom right of the map (east of SGZ) are probably artifacts of the higher density sampling by the USGS and were not detected by the earlier H&N surveys.

Second, the elliptical crater, as defined by the minus 20-ft contour, has expanded parallel to the reef in the crater wings and into the lagoon, but has contracted reefward. The net result is an increase of 500 ft in the long axis to 4,500 ft, but only an increase in the short axis of 100 ft to 2,900 ft.

Third, the difference contours near the crater floor have changed from circular to elliptical. However, the contours above that level (i.e., the minus 160- to minus 100-ft contours) have remained circular, expanded considerably, and shifted toward the reef.

USGS 1984 - H&N Postshot Isopach Map

This pair of isopach maps (pls. 5-8 and 5-9) shows the negative and positive changes in Δ -relief relative to the H&N postshot datum (47 to 67 days after the event) caused by redistribution of debris and long-term subsidence. In general, the entire map area is displaced downward increasing from 5 ft at the map boundaries (3,500 ft from SGZ) to 20 ft over much of the lagoon to 30 ft within the crater. Areas of negative Δ -relief now constitute 89 percent of the map area.

Areas of maximum negative Δ -relief are associated with deeper portions of the crater, the debris tongue, and isolated topographic highs in the lagoon. The concentric patterns of increasing negative Δ -relief vary from 5 to 10 ft at the edge of the circular crater (1,700 ft from SGZ) up to 25 to 30 ft just above the crater floor. This indicates that the circular crater has continued to subside with time. The multiple, repeating circumferential patterns in the elliptical-crater walls and along portions of the reef probably represent en echelon slumping of debris.

Beyond the elliptical crater, the debris tongue exhibits 5 to 15 ft greater negative Δ -relief compared with surrounding areas, even at its maximum extent of 3,300 ft, where a negative change of 20 to 25 ft is measured. Localized areas of 30 to 45 ft of negative Δ -relief occur in the lagoon associated with topographic highs. These areas are complex with converging zones of negative and positive Δ -relief probably representing slumping and redistribution of debris.

Areas of positive Δ -relief are associated with the flanks of several topographic highs, suggesting (as mentioned above) movement of debris downslope. The small positive Δ -relief on the floor of the crater is due to infillin and probably masks a 20-ft plus Δ -relief. The positive lineaments along the reef scarp probably reflect movement of reef blocks and washback of debris into the crater. The narrow positive lineaments bordering the extended crater probably represent movement of debris downslope along the crater rim scarps. The positive circular highs on the middle and lower right side of the map are probably artifacts of the previously mentioned bathymetry sampling density. The positive highs in the lower left portion of the map (south of SGZ) are unexplained.

CONCLUSIONS

Based primarily on analysis of the OAK bathymetric data presented herein, the following conclusions are reached:

1. The OAK event produced a circular explosion-type crater with debris distributed outward in all directions, probably continuously, to at least 3,000 ft from SGZ.
2. The circular crater, consisting of an inner circular component on the order of 850 ft in radius, probably formed initially by ejection and outward flow of material. This expanded outward by crater-wall collapse, slumping, and inflow of material to form an outer circular component. By D + 67 days, and probably much sooner, the circular crater had grown to a radius of 1,700 ft and a depth of 200 ft.

3. A very large tongue of debris, 1,500 ft wide at the crater edge and tapering to 500 ft at 3,000 ft from SGZ, was deposited outward onto the lagoon floor. This is cut by a 400-ft-wide channel that closely tracks the preshot ravine.
4. Also by D + 67 days, the entire area out to at least 3,000 ft from SGZ had subsided 5 to 10 ft with crater wings forming and expanding along the reef slope on either side of the circular crater. This resulted in an elliptical crater 4,000 ft parallel to and 2,800 ft perpendicular to the reef.
5. Over the next 26 years, the entire area continued to subside. This subsidence ranged from a minimum of 5 to 10 ft at 3,000 ft from SGZ up to 10 to 20 ft just outside the elliptical crater. Even greater subsidence occurred within the circular crater, particularly the lower portions, and out on the debris tongue. The length of the elliptical crater increased 500 ft (from 4,000 to 4,500 ft), but the width increased only 100 ft (from 2,800 to 2,900 ft).
6. Also, over this 26-year period, debris within the crater, on the debris tongue, and along the crater walls continued to slump. Elsewhere debris was selectively redistributed.
7. In retrospect, preshot topographic features (reef, embayment, ravine, and reef/lagoon slope) had a significant influence on the final size and shape of the crater and on the initial distribution and subsequent reworking of debris.
8. Finally, it is believed that a synthesis of the bathymetric data with the drilling, seismic, side-scan sonar, and gravity data will lead to a significant improvement in the quantification of the postshot topography which, in turn, should provide substantial improvement in the understanding of the cratering mechanics of the OAK event.

ACKNOWLEDGEMENTS

We are indebted to Gar Clark and his staff at the Technology Application Center (TAC), University of New Mexico, for their excellent and painstaking work in digitizing the basemaps and producing the contour and isopach maps. We also greatly appreciate the extended discussions with B.L. Ristvet of S-Cubed on the many details of the 1958 H&N surveying and for providing us the last "originals" of those maps.

This effort was jointly funded by the Defense Nuclear Agency (DNA). Project Officer for DNA was Lt. Col. Robert Couch; the Air Force Systems Command Project Officer was Maj. William Clark.

REFERENCES CITED

- Environmental Systems Research Institute (ESRI), 1986. ARC/INFO Users Manual v. 3.2, April 1986.
- Folger, D.W., Hampson, J.C., Robb, J.M., Woellner, R.A., Foster, D.S., and Tavares, L.A., 1986, Bathymetry of OAK and KOA craters; 32 p., 1 fig., 2 appendices; in Folger, D.W., editor, Sea-floor observations and subbottom seismic characteristics of OAK and KOA craters, Enewetak Atoll, Marshall Islands: U.S. Geological Survey Bulletin 1678.
- Henry, T.W., and Wardlaw, B.R., editors, 1986, Pacific Enewetak Atoll Crater Exploration (PEACE) Program, Enewetak Atoll, Republic of the Marshall Islands; Part 3: Stratigraphic analysis and other geologic and geophysical studies in vicinity of KOA and OAK craters: U.S. Geological Survey Open-File Report 86-555, 486 p., 92 figs., 90 tbls., 34 pls.
- Henry, T.W., Wardlaw, B.R., Skipp, B.A., Major, R.P., and Tracey, J.L., 1986, Pacific Enewetak Atoll Crater Exploration (PEACE) Program, Enewetak Atoll, Republic of the Marshall Islands; Part 1: Drilling operations and descriptions of boreholes in vicinity of KOA and OAK craters: U.S. Geological Survey Open-File Report 86-419, 497 p., 32 figs., 29 pls., 10 tbls., 3 appendices.
- Holmes and Narver Engineering Co. (H&N), 1952, Completion Report, Enewetak Proving Ground Facilities, Operation IVY; v. 1, book 1, p. 2-11 thru 2-25, Los Angeles, CA, 31 December 1952 [Unclassified]. Survey conducted for U.S. Atomic Energy Commission (AEC).
- Holmes and Narver Engineering Co. (H&N), 1958a, OAK preshot topography and hydrography map; Alice Reef Station #25: Field Book # 2-1, p. 2-1 thru 2-26, June 9 through 26, 1958], Map Sheets J/S 03-001-C11 [compiled September 13, 1958]. Survey conducted for U.S. Atomic Energy Commission (AEC).
- Holmes and Narver Engineering Co. (H&N), 1958b, OAK postshot topography and hydrography map; Alice Reef Station #25: Field Book # 2-2, p. 2-1 thru 2-26, August 14 thru September 4, 1958], Map Sheets J/S 03-001-C11 [compiled October 1, 1958]. Survey conducted for U.S. Atomic Energy Commission (AEC).
- Peterson, J.L., and Henny, R.W., 1987, Bathymetric studies of the 1968 OAK nuclear cratering event, Pacific Proving Grounds: New Mexico Geomorphological Research Institute Task Report WA6-16, September 1987, Albuquerque, NM.
- U.S. Army, 1970, Eniwetok Trig List: U.S. Army Topographic Command, Ft. Belvoir, VA.
- U.S. Geological Survey (USGS), 1984 [1985], Bathymetric Map of the OAK Crater Area, Enewetak Atoll [surveyed June 17 thru September 20, 1984, compiled September 1985]. [This is a working-scale map at 1:6000 of the map published as fig. 7, p. A8, of Folger, Hampson, and others, 1986]. Survey conducted for Defense Nuclear Agency (DNA).

TABLE 5-3. -- Summary of areas and volumes calculated from derivative map pair formed by combination of Holmes and Narver (H&N) preshot bathymetric/topographic map (pl. 5-1) and H&N postshot isopach map (pl. 5-2). Corresponding maps are Plates 5-4 for the negative Δ -relief and Plate 5-5 for the positive Δ -relief, respectively.

H&N PRESHOT VS H&N POSTSHOT -- VOLUMES AND AREAS

Δ -RELIEF CATEGORY	CONTOUR INTERVAL (ft)	AREA (sq ft)	TOTAL MAP AREA (%)	VOLUME (cu ft)
Positive Δ -relief	50-55	1,348	0.004	74,160
	45-50	4,176	0.01	208,796
	40-45	6,201	0.02	279,045
	35-40	21,735	0.07	869,194
	30-35	122,071	0.4	4,272,490
	25-30	299,352	1.0	8,480,567
	20-25	317,622	1.1	7,940,551
	15-20	727,271	2.4	14,545,419
	10-15	1,265,755	4.2	18,986,328
	5-10	2,118,996	7.0	21,187,252
	>0-5	<u>3,134,338</u>	<u>10.4</u>	<u>13,788,992</u>
Total Positive Δ -relief		8,018,865	26.6	91,132,994
Total Zero (0) Δ -relief		3,223,946	10.6	0
Negative Δ -relief	>0-5	4,597,830	15.2	19,166,933
	5-10	3,090,431	10.2	29,015,023
	10-15	1,856,139	6.1	27,033,099
	15-20	1,133,271	3.8	22,237,414
	20-25	700,073	2.3	17,178,469
	25-30	454,545	1.5	13,423,574
	30-35	375,716	1.2	12,903,993
	35-40	330,047	1.1	13,017,456
	40-45	276,989	0.9	12,300,535
	45-50	307,840	1.0	15,220,082
	50-55	256,148	0.8	13,975,590
	55-60	294,104	1.0	17,531,655
	60-65	254,941	0.8	16,485,412
	65-70	258,841	0.9	18,033,970
	70-75	264,372	0.9	19,743,284
	75-80	244,716	0.8	19,493,811
	80-85	274,512	0.9	23,247,576
	85-90	269,727	0.9	24,166,199
	90-95	244,963	1.0	27,771,543
	95-100	338,887	1.1	33,472,777
	100-105	291,674	1.0	30,298,728
	105-110	346,830	1.1	37,791,053
	110-115	355,535	1.2	40,539,123
	115-120	320,563	1.1	38,067,852
	120-125	391,098	1.3	48,674,321
	125-130	401,628	1.3	51,943,142
	130-135	324,904	1.1	43,586,633
	135-140	230,240	0.8	31,933,508
	140-145	76,917	0.3	11,138,920
	145-150	61,249	0.2	9,487,333
	150-155	63,632	0.2	9,862,944
	155-160	55,269	0.2	8,843,002
	160-165	41,603	0.1	6,864,333
	165-170	32,152	0.1	5,465,870
	170-175	18,008	0.1	4,901,403
	175-180	22,978	0.1	4,135,995
	180-185	23,807	0.1	4,404,334
	185-190	<u>7,449</u>	<u>0.03</u>	<u>1,415,289</u>
Total Negative Δ -relief		18,951,568	62.8	784,972,178

TABLE 5-4. -- Summary of areas and volumes calculated from derivative map pair formed by combination of U.S. Geological Survey (USGS, 1984) postshot isopach map (pl. 5-3) and Holmes and Narver (H&N) preshot map (pl. 5-1). Corresponding figures are Plates 5-6 for the negative Δ -relief and Plate 5-7 for the positive Δ -relief, respectively

H&N PRESNOT VS USGS POSTSHOT -- AREAS AND VOLUMES				
Δ -RELIEF CATEGORY	CONTOUR INTERVAL (ft)	AREA (sq ft)	TOTAL MAP AREA (%)	VOLUME (cu ft)
Positive Δ -relief	35-40	3,874	0.01	142,848
	30-35	45,563	0.20	1,431,653
	25-30	83,634	0.30	2,269,071
	20-25	222,615	0.9	5,202,429
	15-20	203,841	0.8	3,683,457
	10-15	399,046	1.6	4,865,145
	5-10	897,017	3.5	6,635,921
	0- 5	1,678,303	6.5	3,792,121
Total Positive Δ -relief		3,533,893	13.7	28,022,645
Negative Δ -relief	0- 5	2,933,886	11.4	9,388,814
	5-10	3,826,724	15.0	30,180,137
	10-15	3,220,256	12.5	40,631,938
	15-20	2,359,641	9.2	40,622,228
	20-25	1,191,911	4.6	26,888,750
	25-30	676,404	2.6	18,651,376
	30-35	450,900	1.8	14,686,256
	35-40	371,889	1.5	14,686,256
	40-45	324,188	1.3	13,924,608
	45-50	312,580	1.2	14,938,353
	50-55	302,003	1.2	15,895,082
	55-60	289,656	1.1	16,678,999
	60-65	275,562	1.1	17,264,649
	65-70	253,538	1.0	17,161,796
	70-75	245,220	1.0	17,773,609
	75-80	223,971	0.9	17,366,741
	80-85	252,353	1.0	20,796,354
	85-90	288,305	1.1	25,364,923
	90-95	286,225	1.1	26,602,615
	95-100	270,795	1.1	26,505,055
	100-105	317,440	1.2	32,581,806
	105-110	338,915	1.3	36,342,656
	110-115	292,983	1.1	33,043,380
	115-120	256,188	1.0	30,203,109
	120-125	339,398	1.3	41,854,235
	125-130	306,752	1.2	39,182,244
	130-135	329,502	1.3	43,234,343
	135-140	274,305	1.0	37,836,334
	140-145	285,822	1.1	4,886,445
	145-150	387,055	1.5	57,054,655
	150-155	244,093	1.0	37,287,465
	155-160	127,398	0.5	20,112,575
	160-165	70,272	0.3	11,453,367
	165-170	67,390	0.3	11,340,488
	170-175	54,923	0.2	9,519,263
	175-180	48,496	0.2	8,659,313
	180-185	58,401	0.2	10,717,498
	185-190	41,979	0.2	7,869,618
Total Negative Δ -relief		22,197,319	86.3	935,058,002

TABLE 5-5. -- Summary of areas and volumes calculated from derivative map pairs formed by combination of U.S. Geological Survey postshot map (USGS, 1984) and Holmes and Narver (H&N) postshot isopach map. Corresponding figures are Plates 5-8 for the negative Δ -relief and Plate 5-9 for the positive Δ -relief, respectively.

H&N PRESHOT VS USGS POSTSHOT -- AREAS AND VOLUMES

Δ -RELIEF CATEGORY	CONTOUR INTERVAL (ft)	AREA (sq ft)	TOTAL MAP AREA (%)	VOLUME (cu ft)
Positive Δ -relief	35-40	478	0.002	16,843
	30-35	844	0.003	26,802
	25-30	3,856	0.02	102,241
	20-25	17,189	0.1	378,356
	15-20	112,704	0.4	1,976,824
	0-15	272,512	1.1	3,386,556
	5-10	721,865	2.8	5,217,536
	0- 5	<u>1,820,125</u>	<u>7.1</u>	<u>3,739,364</u>
Total Positive Δ -relief		2,949,573	11.5	14,844,523
Negative Δ -relief	0- 5	4,053,640	15.8	11,485,025
	5-10	6,555,275	25.5	51,868,217
	10-15	7,707,037	30.0	97,957,905
	15-20	3,372,562	13.1	59,101,780
	20-25	857,090	3.3	19,181,484
	25-30	178,053	0.7	4,838,022
	30-35	28,472	0.1	921,606
	35-40	6,822	0.03	257,019
	40-45	3,177	0.01	136,916
	45-50	2,052	0.01	99,545
	50-55	<u>579</u>	<u>0.002</u>	<u>30,640</u>
Total Negative Δ -relief		22,764,759	88.5	245,878,159

TABLE 5-6. -- Grand summary of areas and volumes of negative, zero, and positive Δ -relief for OAK crater area. Summary derived from Tables 5-2 through 5-5. Area given in sq ft, volume in cu ft, net Δ -relief in ft.

TYPE Δ -RELIEF	H&N PRESHOT VS. H&N POSTSHOT		USGS POSTSHOT VS. H&N PRESHOT		USGS POSTSHOT VS. H&N POSTSHOT	
	Value	Percent	Value	Percent	Value	Percent
AREA: (sq ft)						
Positive Δ -relief	8,018,865	26.56	3,533,893	13.73	2,949,573	11.47
Negative Δ -relief	18,951,568	62.77	22,197,319	86.27	22,764,753	88.53
Zero (0) Δ -relief	<u>3,223,337</u>	10.68	<u>-----</u>	---	<u>-----</u>	---
TOTAL	30,193,770 sq ft		25,731,212 sq ft		25,714,302 sq ft	
VOLUME: (cu ft)						
Positive Δ -relief	91,132,994	10.39	28,022,645	2.91	14,844,523	5.69
Negative Δ -relief	<u>789,972,178</u>	89.61	<u>935,058,002</u>	97.09	<u>245,878,159</u>	94.31
NET	(693,809,189) cu ft		(907,035,357) cu ft		(231,033,636) cu ft	
AVERAGE NET Δ -RELIEF:						
	minus 22.99 ft		minus 35.25 ft		minus 8.98 ft	

CHAPTER 6:

CONSTRAINTS ON DENSIFICATION AND PIPING FOR THE OAK EVENT

By

John G. Trulio¹

BACKGROUND AND SUMMARY

PPG (Pacific Proving Grounds) sites differ widely from typical CONUS (Continental U.S.) sites in structure and composition. Hence, plausibly, high-yield near-surface nuclear explosions might dig much different craters in one setting than the other. But do they? The question cannot be answered by direct comparison of craters from such bursts. It therefore raises the kindred one of mechanism: The crater from a given burst could vary greatly from a CONUS site to the PPG, because dominant cratering mechanisms might -- but do they?

A "subsidence hypothesis" proposed in the early 1980's got to the physical nub of this issue:²

Explosive loading causes widespread fracturing of PPG coral, whose parts then settle slowly under gravity to form the outer one-half to three-fourths (in radius) of the apparent crater -- its "wing." By contrast, the inner one-half to one-fourth grows in several ways, including ejection of solid; indeed, virtually all ejecta come from that inner region -- or (hence) "excavation crater."

In sum, the subsidence hypothesis posits cave-in of a "coral" skeleton³ to fill the space left by water flowing out of it. Here, we call that process "simple subsidence." Its hallmark is an increase in coral density, since coral solids are denser than the water they replace [but for that, gravity (its cause) could not drive it]. Hence, alternatively, we speak of simple subsidence as "densification."

¹ Applied Theory, Inc., Los Angeles, CA 90036.

² The basic idea appears to have been suggested independently by S. Blouin, H.L. Brode, and B.L. Ristvet, years before the PEACE Program began. In the form stated here, the simple subsidence hypothesis is credited mainly to K.D. Pyatt and K. Kreyenhagen.

³ The OAK medium is referred to herein simply as coral. Said medium is a mixture of carbonate sediment, carbonate rock, and sea water with small amounts of other substances (see Chapter 7 of this Report for details of composition of the OAK medium). Used as an adjective herein, the meaning of coral is controlled by the noun it modifies; for example, "coral solid" denotes the solid components of the medium just described.

PEACE Program data do tell of excavation craters about one-fourth to one-third as large in radius as present apparent craters, widened by later slumping of their walls to about 0.4 of the latter radii (B.R. Wardlaw, oral communication, November 9, 1987). Thus, if the wings of apparent PPG craters did form by simple subsidence, then, for a given burst, most CONUS craters would have half the radii (or less) seen at the PPG. By the same token, coral under the wings would be denser now than pre-shot. PEACE Program measurements [borehole gravimetry and gamma-gamma (γ - γ) logging], however, disclose only minor changes in density there: Layers of coral (roughly horizontal) from the sea floor to clearly identified interfaces below have thinned much more than the measured densities alone imply. Hence, on the available data, most of the sea-floor lowering had other causes than simple subsidence. Succeeding sections summarize the evidence for and against this last statement; though not airtight, the case for it is strong.

When the mean density of solids in a column grows by a smaller factor than the column's vertical compression, lateral transport must take place. Such transport can occur during plastic flow, as in a tube of toothpaste. Another kind, termed "piping", calls for the flow of slurry (here, water plus coral particles) to the sea floor, where currents may sweep it out of the crater. Signs of piping abound in the OAK crater (Wardlaw and Henry, 1986b, p. 10; Halley and others, 1986, p. 4), but not in its wing, reducing the importance of PEACE measurements as constraints on piping (nonetheless discussed below). Plastic flow, perhaps with some "internal piping" (transport), seems the most likely means whereby the wings of OAK's crater formed. If so, similar wings could form at most CONUS sites -- and early, relative to such gravity-driven processes as slumping and densification. For structures, the wing would still be more benign than the excavation crater, but operating there would be no cinch.

BASIC FACTS AND PARAMETERS

Both the OAK and KOA craters were explored during the PEACE Program, but emphasis fell on OAK because many nearby shots preceded KOA; cratering-mechanism puzzles are made knottier by the effects of prior shots (example: How did MIKE affect KOA coral?). Indeed, even with the focus on OAK, and OAK's relative simplicity, the data base for assessing density changes remains slim. Priority rightly went to OAK.

In the OAK crater area, vital maps of the sea floor were drawn before the event, shortly after, and during the PEACE Program (see Chapter 5 of this Report). The bathymetric maps tell us how far the sea floor has sunk as a result of the shot. That does more than quantify what it is that we have to explain (essential enough). For, PEACE exploration has shown that, in the wing and beyond, the coral is split into layers by clearly identifiable Lagrangian surfaces (termed "horizons" by the geologists) that are critical here; several appear in Figure 6-1.

The horizons' great value lies in knowledge of their undisturbed (hence pre-shot) depths. By geologic means, those depths are reproducible down boreholes to within a few tens of feet, and most often to ± 10 ft, in this part of the atoll. More important still, they can be located generally to within a foot in any one borehole. Thus, the depth of each has been determined in boreholes inside the crater and out. So, therefore, has the shortening of

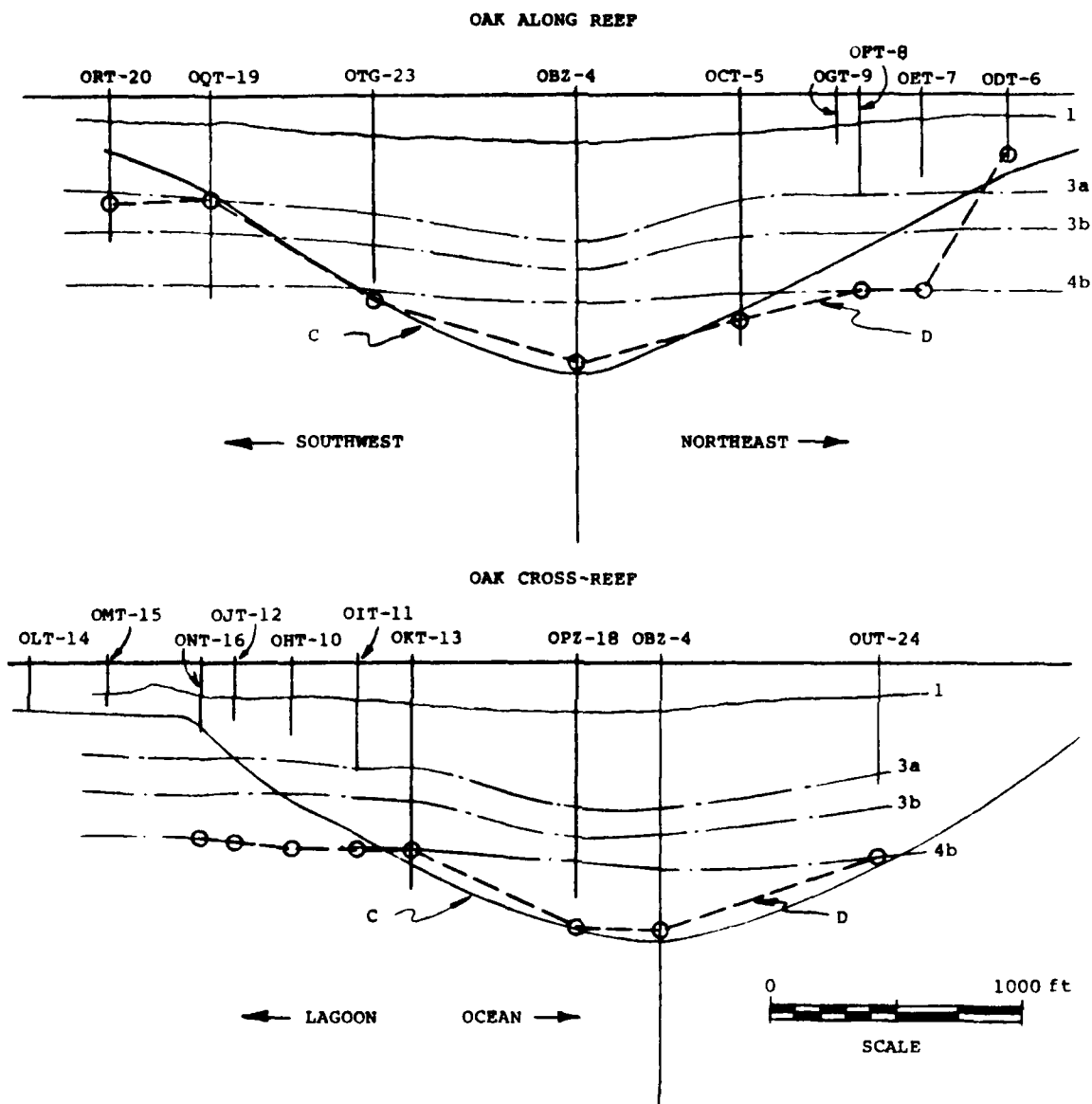


FIGURE 6-1. -- Vertical sections at the OAK site. Contours C and D, respectively, mark the bases of regions of (a) measurable decrease in sonic wavespeed and (b) measurable downward displacement. The SCALE (in ft) applies to all distances.

vertical columns between the sea floor and these horizons.¹ Mapped out too is the base of the region of sensible downward displacement of coral below the crater (contour D; fig. 6-1); its border lies close to the contour (C; fig. 6-1) that marks the limit of the region in which seismic wave-speed has decreased measurably (see Chapter 7 of this Report, particularly tbls. 7-2 and 7-4). Evidently, the shortening of any vertical coral column, flagged by lowering of the sea floor, takes place above the contour D -- and the column's mean vertical shrinkage is given by the ratio of sea-floor lowering at the top of the column, to the column's pre-shot height (current height plus sea-floor drop).

The OAK boreholes lay along two lines through the center of the crater (see Chapter 1, fig. 1-3), one parallel to the reef ("reef-wise") and the other at right angles to it ("cross-reef"). By design, most density logs (and results on densification) came from the reef-wise line (see Chapter 2, fig. 2-2). The reason: We need pre-shot density profiles to compute density changes and their effects. Now -- long after OAK -- those profiles have to come from logging in near-pristine coral outside the crater. For geologic reasons, however, systematic changes in material properties occur along cross-reef lines; on well-chosen reef-wise lines, the medium is subject mainly to smaller, random, local variations. Most actual borehole locations were chosen for OAK by PEACE geologists on that basis. The line those holes form runs close to the crater's center, so that density profiles along it can stand as rough cylindrical crater-averages at their respective reef-wise stations. What "rough" means rests with actual PPG measurements; so does the gut issue of reef-wise fluctuations in natural density profiles (below).

Table 6-1 presents basic PEACE data from the OAK crater, including the mean compressions of coral columns at borehole locations. All OAK boreholes are listed in the table; for reference, so is the estimated peak airblast pressure that acted above each. Of special weight are the table's mean vertical shrinkages $\Delta D/L$. Their average of 13 percent (16-1/2 percent for the reef-wise holes), if achieved via simple subsidence, would entail a mean density increase of $\sim .13$ g/cc (.18 g/cc reef-wise). That is larger by almost a factor of ten than the limit of BHG (and γ - γ) resolution achieved in the PEACE Program (.01 to .02 g/cc). Hence, direct on-site evaluation of the subsidence hypothesis was indeed feasible (not known when the program began). Concern therefore lies instead with systematic error and the natural reef-wise scatter of density/depth profiles. Further, as readily confirmed,

¹ The pre-shot depth of the sea floor is known at borehole locations, as are the depths of some horizons (depth uncertainties and confidence questions are taken up later). For a given borehole and horizon, the difference between horizon depth and sea-floor depth is the pre-shot height of the vertical column between horizon and sea floor. Likewise, for that same borehole and horizon, the post-shot height of the column from horizon to sea floor is also known. Between those two levels (horizon and sea floor), the particles of solid in the column may or may not be the same pre-shot as post-shot. The simple subsidence hypothesis says they are the same. The hypothesis is tested herein by adopting it, and comparing the column shortening it implies (when coupled with measured densities) to the observed shortening.

Hole	Range (ft) from GZ	L I N E	Preshot Depth L, (ft): Sea Floor to C to D	Water Depth (ft) Preshot D ₁ PEACE D ₂	ΔD, ft D ₂ - D ₁	Shrinkage ΔD/L, %; Column to D	Peak Overpressure MPa
JOR-17	6057.8		NA	55.2	0	NA	1.0
OSM-22	5538.6		NA	76.0	0	NA	1.3
OSR-21	5495.3	A	NA	84.0	0	NA	1.3
OPT-20	1845.8	L	144.5	70.0	31.4	8	34
OQT-19	1444.3	O	360.0	46.0	117.5	19	72
OTG-23	804.6	N	796.4	45.6	164.0	15	620
OBZ-4	7.1	G	1125.6	13.1	198.7	17	>690
OCT-5	658.3		841.5	16.2	163.7	17	>690
OGT-9	1043.5	R	-	16.0	134.8	-	228
OFT-8	1129.1	E	598.8	15.4	130.8	15	172
OET-7	1374.8	E	47.7	18.4	106.9	11	85
ODT-6	1714.9	F	291.6	20.0	87.4	32	41
OAM-3	4510.2		NA	-	108.0	NA	2.3
OAR-2A	4500.2		NA	-	110.5	NA	2.3
OAM-11	4458.4		NA	-	114.2	NA	2.4
OAR-21							
OLT-14	2511.2	C	-	132.5	139.7	7.2	13
OMT-15	2203.6	R	-	141.8	110.9	30.9	19
ONT-16	1827.3	O	93.0	130.9	135.1	4.2	34
OJT-12	1695.5	S	257.3	115.0	143.8	28.8	43
OHT-10	1462.2	S	446.5	124.6	137.3	12.7	70
OIT-11	1205.5		568.5	121.6	155.0	33.4	136
OAT-13	988.7	R	730.0	101.7	164.7	63.0	269
OPZ-18	334.8	E	1032.6	46.3	201.9	155.6	>690
OBZ-4	7.1	E	1125.6	13.1	198.7	185.6	>690
OUT-24	858.0	F	828.4	1.6	147.0	145.4	510

TABLE 6-1. -- Column-height changes down boreholes at the OAK site. Contour C is the base of region of decrease in sonic wavespeed; contour D is the base of the region of downward displacement; GZ is ground zero.

Head- ing	Hole	RANGE,ft to OBZ-4	Hole Base	Surface D	PEACE Depth, in ft bsl									
					Horizon									
					2b	2c	2d	3a	3b	4b	5a	5b	5c	
SW ↓ R E E E P W I S E ↓ NE	00R-17	6060.6	1146.3	NA			363.1	405.7	552.4					
	00R-21	5498.2	438.3	NA		290.1	344.2	391.7			765.2	961.2		
	00T-20	1847.8	593.2	445	216.2	262.7	346.7	411.7	552.0		(767.0)	(1013.5)		
	00T-19	1446.1	819.0	426	233.9	274.7	365.3	413.3	548.3		766.5	(1020.1)		
	00T-23	805.5	751.3	(834)			434.0	484.0	610.0		(787.0)	(1000.4)		
	00B-4	0	1803.9	1081				593.0	701.2	847.7	1013.8	1065.1	1114.6	
	00T-5	654.3	1015.2	9074		368.4	417.9	432.7	572.2	799.7	944.6			
	00T-9	1039.6	209.8											
	00T-8	1125.0	414.3	(794)	223.3	272.0	344.6	(419.8)	(565.0)	(794.0)	(925.0)			
	00T-7	1370.5	338.6	(793)	220.6	294.7	320.4	(410.0)	(555.0)	(793.0)	(925.0)			
SE ↓ C R O S S R E E F ↓ NW	00T-6	1710.5	251.6	231	219.0	231.3	(315.0)	(397.0)	(546.0)	(792.0)	(925.0)			
	00R-2A	4495.5	521.0	NA		310.0	355.6	410.6	(556.8)	(812.2)	(918.2)			
	00T-14	2517.3	188.9	(700)	227.0		(341.1)	(383.8)	(534.6)	(700.0)	(1010.2)			
	00T-15	2209.7	187.5	(702)	225.0		(334.6)	(373.9)	(529.7)	(701.9)	(1013.5)			
	00T-16	1833.4	287.4	(715)	238.6		(337.8)	(395.2)	(537.9)	(715.0)	(993.8)			
	00T-12	1701.6	241.1	(732)	238.0		(350.0)	(390.3)	(531.0)	(732.0)	(991.0)			
	00T-10	1456.3	299.8	(751)	213.3		(360.8)	(403.4)	(531.4)	(751.0)	(987.3)			
	00T-11	1199.4	441.5	(758)	274.4		375.0	434.8	(562.0)	(758.0)	(980.0)			
	00T-13	982.7	920.0	766	232.9	326.1	411.6	431.3	564.0	765.8	(974.5)	(1036.5)		
	00P-18	329.1	950.5	(1089)			568.9	593.0	723.5	809.9	(1000.0)	(1063.0)	(1114.0)	
	00B-4	0	1803.9	1081				593.0	701.2	847.7	1013.8	1065.1	1114.6	
	00T-24	864.2	498.1	(784)		373.0	407.0	457.1	(592.0)	784.0	(925.0)	(1025.0)		

TABLE 6-2. -- Uniformity of horizons in OAK area. Parentheses () signifies seismic data because borehole ends above depth shown; cross-hatching covers downward-displacement region; blank spaces signify missing values. Below sea level (given in ft) is abbreviated bsl.

the few tens of feet or less by which horizon depths vary (tbl. 6-2) have scant effect on the values of $\Delta D/\Delta z$ in Table 6-1.

SHORTENING OF CORAL COLUMNS BY DENSIFICATION: BOOKKEEPING

Let subscripts L and S refer, respectively, to the liquid and solid components of saturated coral. In a volume V of the mixture, let V_L and V_S be the volumes of the two components and ρ_L and ρ_S their densities. The mass, m , of the mixture is then equal to the mass of its liquid component ($=\rho_L V_L$) plus the mass of its solid component ($=\rho_S V_S$). Hence, if ρ denotes the density of the mixture, we can write:

$$\rho_L V_L + \rho_S V_S = m = \rho V$$

or

$$\rho_L \alpha_L + \rho_S \alpha_S = \rho \quad \text{Eq. (1)}$$

where α_L and α_S denote the volume-fractions of liquid and solid in the mixture:

$$\alpha_L = V_L/V \quad ; \quad \alpha_S = V_S/V \quad ; \quad \alpha_L + \alpha_S = 1 \quad \text{Eq. (2)}$$

Using the last of Eqs. (2) to eliminate α_L from Eq. (1), and rearranging, we get:

$$\text{Volume Fraction of Solid in Mixture} = \alpha_S = (\rho - \rho_L)/(\rho_S - \rho_L) \quad \text{Eq. (3)}$$

Hence, in volume V of the mixture, we find that:

$$\text{Mass of Solid} = \rho_S V_S = \rho_S \alpha_S V = V \rho_S (\rho - \rho_L)/(\rho_S - \rho_L) \quad \text{Eq. (4)}$$

Now consider a vertical column of coral of unit cross-section. Let the column be divided into short vertical sections. A section of the column of height dh then subtends a volume V , and Eq. (4) -- with dh replacing V -- gives the mass of solid in that section. Summing over all sections of the column from a height z_0 to a greater height z , the total solid mass m_S between those heights is given by:

$$m_S = \rho_S \frac{\rho - \rho_L}{\rho_S - \rho_L} dh \quad \text{Eq. (5)}$$

In Eq. (5), ρ_L , ρ_S , and ρ can all vary with height h in the column. Here however ρ_L (the density of sea water) is constant, while ρ_S can run only from about calcite's density to aragonite's (ρ_S can be set uniformly to the mean of the calcite/aragonite densities, with negligible error in m_S ; below). Thus,

the measured density of the mixture, ρ , holds the key to simple subsidence in the OAK event.

With the key, goes a key assumption: The pre-shot density profile down any crater hole is the same as that found now in holes outside the crater ("control holes"), where the medium is almost unmarred. Then, taking z_0 [Eq. (5)] at a level in the column where coral has not been vertically displaced, the vertical thickness subtended by solid mass m_s [from Eq. (5)] in a control hole, is equal to the pre-shot thickness of mass m_s of solid in the crater hole. On that basis, the hypothesis of simple subsidence can be tested via its mandate to conserve the column's solid mass. For, the present thickness of that mass [also from Eq. (5)], subtracted from its pre-shot thickness, will give the actual change in height of its topmost particle -- if that change is due to simple subsidence.

In particular, if z [Eq. (5)] refers to the crater floor, the change in question should equal the observed sea-floor lowering. Moreover, knowledge of the pre- and post-shot depths of horizons below the crater allows us a stronger result: By letting z_0 and z refer to any two horizons, Eq. (5) should give the same solid mass m_s pre-shot as now -- if the distance between horizons changed by means of simple subsidence. We therefore integrate upward from one and the same horizon R , both pre-shot ($z_0 = z_R^P$) and now ($z_0 = z_R^N$). When that is done (with a control-hole profile taken as "pre-shot"), a given solid mass m_s , reached at $z = z^P$ pre-shot, will be reached at $z = z^N$ now. For that solid (between z_R^P and z^P pre-shot), the difference $(z^N - z_R^N) - (z^P - z_R^P) \equiv \delta z$ specifies the change in thickness implied by the observed density-profile changes, if the solid moved only up or down. Thus, the meaning of measured density profiles for simple subsidence is shown by plotting δz (but with z increasing downward, not upward; i.e., with depth in place of altitude). Such plots tell how coral solid at any depth below the present OAK crater had its depth changed by the shot -- if simple subsidence caused the change.

DENSITY PROFILES, THEIR TREATMENT, AND DOWNWARD DISPLACEMENTS

Logs of back-scattered neutron and γ -ray intensity (see Melzer, 1986), and of gravity-field variations (Beyer, Ristvet, and Oberste-Lehn, 1986) furnished density profiles down boreholes in the OAK crater region ("neutron", " γ - γ ", and "BHG" profiles, respectively). On the reef-wise line (see second section), control-holes OOR-17 and OSR-21 were logged in all three ways, whereas neutron and γ - γ logs were taken in control-hole OAR-2A. There were no cross-reef control holes. On the crater's wing, however, the only reef-wise holes logged close to contour C or D were OQT-19 and ORT-20;¹ that was done by all three methods, save for neutron logging of ORT-20.

¹ That can be seen by comparing (1) the depths listed for contours C and D in Table 6-2 and (2) the density profiles presented in full in Appendix 6-1.

It was known before PEACE operations began at the PPG that we would have to look mainly to BHG for density profiles. Why? Because γ - γ logs tell about the medium only within a few centimeters of our 4-inch-diameter boreholes, where the drilling disturbance is greatest; neutron logs "see" about 4 inches farther out (L.S. Melzer, conversations, summer 1987). By contrast, BHG logs give average densities out to about 10 times the vertical interval between readings (generally an interval of 25 ft for the boreholes in question); BHG densities are thus virtually free of man-made or natural local variations in the medium. It was not known, however, whether BHG logging could be done with useful precision under PPG conditions; doing so was a first, and a major PEACE Program success (see Beyer, Ristvet, and Oberste-Lehn, 1986, and Chapter 2 of this Report).

BHG aside, steel borehole casing that ran downward from the sea floor for 100 to 150 ft, interfered with γ - γ logs; the tool was not calibrated for measurement in coral through such a pipe (L.S. Melzer, conversations, summer 1987). In view of that problem, and of changes to the medium from drilling, γ - γ density profiles are probably reliable only at depths greater than a few hundred feet (where they match BHG profiles fairly well). Further, if neutron logs are to add density profiles to the BHG/ γ - γ set, a way will be needed to calibrate the neutron tool for PPG coral (L.S. Melzer, conversations, early summer 1987). Thus, at present, density changes from the OAK event must be evaluated from BHG density profiles, augmented somewhat by γ - γ profiles.

Copies of all BHG density profiles from OAK's reef-wise line are shown in Figure 6-2, and the γ - γ profiles in Figure 6-3; all profiles appear at full scale in Appendix 6-1. For use in Eq. (5), each profile was fit by a piecewise linear function, an especially simple matter for the BHG step-profiles; the linear coefficients are listed in Appendix 6-1, where the fits are also plotted. At full scale, the fits overlap the measured profiles everywhere, reproducing them about as closely as their finite line width allows. Those fits embody almost all the depth-dependence of the integrand of Eq. (5); the rest stems from the solid component's density ρ_s , whose extremes lie within 4 percent of their mean (see preceding section). As measured, the variation of ρ_s over that small range is also no more than piecewise-linear with depth. Thus, at its worst, Eq. (5) calls only for integrating a ratio of two linear functions [since $\rho_s/(\rho_s - \rho_L) = 1 + \rho_L/(\rho_s - \rho_L)$] -- whence, down a given borehole, the solid mass m_s is easily found in closed form vs. depth. When m_s for a crater hole is equated to m_s for a borehole, however, the resulting equation for z^P in terms of z^n is transcendental. By taking ρ_s as constant over each of the many linear intervals of measured density ρ , we avoid that complication; m_s becomes (at worst) piecewise-quadratic in depth, and $z^n - z^P$ becomes an explicit function of z^n . The results, plotted in Figures 6-4 through 6-7, are identical (when plotted) with those obtained by solving the transcendental equation; indeed, simply replacing ρ_s by its mean (2.821 g/cc), and ignoring its depth-dependence, makes no significant change in the figures. Full equations and details of calculation, including the fits to ρ_s , are presented in Appendix 6-2.

The dotted and dashed curves in our thickness-change figures (figs. 6-4 through 6-7) and in Appendix 6-1 speak to a subtler point in the treatment of density profiles: They make direct use of all horizon-depths measured for a given control-hole/crater-hole pair. Specifically, Eq. (5) was integrated from any one horizon to the next higher one in the given control hole. Starting from the same lower horizon in the crater hole, the z^D -value dictated by equal solid mass m_S in the two holes, was computed from Eq. (5) (in the usual way; above) for each z^D -value. On reaching the next horizon in the control hole, z^D fell above or below -- but not on -- that horizon in the crater hole; the reasons: natural density-profile variations along the reef-wise line, and sources of thickness-change other than simple subsidence. Integration proceeded nonetheless from that horizon in both holes, until the horizon above it was reached in the control hole -- and so on until density data gave out in one hole or the other. A full thickness-change curve was thus developed in sections, with the assurance that integration started for each section from the bottom of the same geologic (bio- or lithostratigraphic) layer -- and hence in as nearly equivalent material as possible in both holes. Dots track that curve in our plots of thickness change. The process was then repeated with the roles of crater hole and control hole reversed (i.e., going from one horizon to the next higher one in the crater hole; dashes limn that curve in our plots of thickness-change. The mean of the dotted and dashed curves -- a solid curve -- also appears in the plots. All three curves are clearly distinguishable on the right half of Figure 6-4 (for example); note the horizontal step on the dotted curve, where integrating the upper surface of a layer in control-hole OQR-17 took us past the corresponding surface in the crater hole (OPZ-18).

As the density profiles show (figs. 6-2, 6-3, and Appendix 6-1), logging began in each hole at a significant depth below the sea floor, not at it. Calculated thickness changes (figs. 6-4 through 6-7 and Appendix 6-1) must therefore be extrapolated up to the sea floor from the smallest depths the logs cover. With OQR-21 as the control hole, the gaps spanned by extrapolation at boreholes OQT-19 and ORT-20, respectively, come to about 5 and 6 percent of the present distance between the sea floor and surface B (downward displacement limit; see preceding section). Using control-hole OQR-17, these figures grow to 23 and 21 percent -- large enough to have three people separately set reasonable upper and lower limits of extrapolation; arrows on Figures 6-6 and 6-7 mark the lines that gave the extremes of the six estimates and their mean.

The downward trend of every BHG-derived curve near its shallow end probably influenced all extrapolations (y-y curves go both ways; Appendix 6-2). If so, the bias can hardly be called a defect, given the trend's persistence. Indeed, it suggests forcibly that, down to 100 to 200 ft below the sea floor, the medium is somewhat less dense now than pre-shot.

CONTRIBUTION OF SIMPLE SUBSIDENCE TO THE OAK CRATER

The solid curves of Figures 6-4 through 6-7 (and Appendix 6-1) present final estimates of thickness change due to densification below Oak Crater. Extrapolating those curves to the sea floor produced the mean values listed as \bar{z} in Table 6-3.

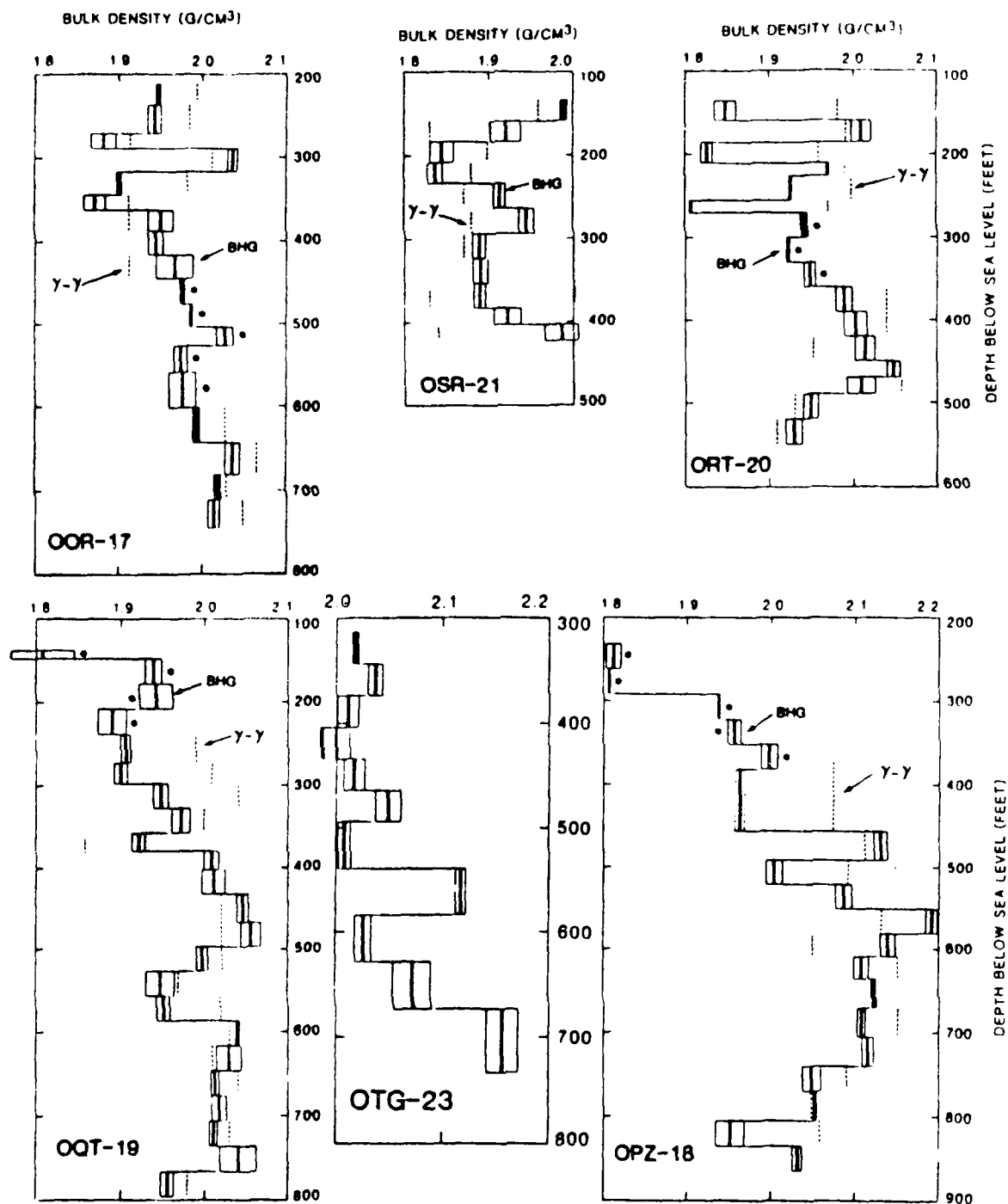


FIGURE 6-2. --Density profiles determined by borehole gravimetry (BHG) in the OAK crater area (Courtesy of L. Beyer, see Chapter 2). Depth below sea level (bsl) given in ft; bulk density in g/cm³. Inferred densities derived from gamma-gamma (Y-Y) logs shown as dotted lines. Asterisks (*) denote intervals where Y-Y logs are not available due to drillpipe.

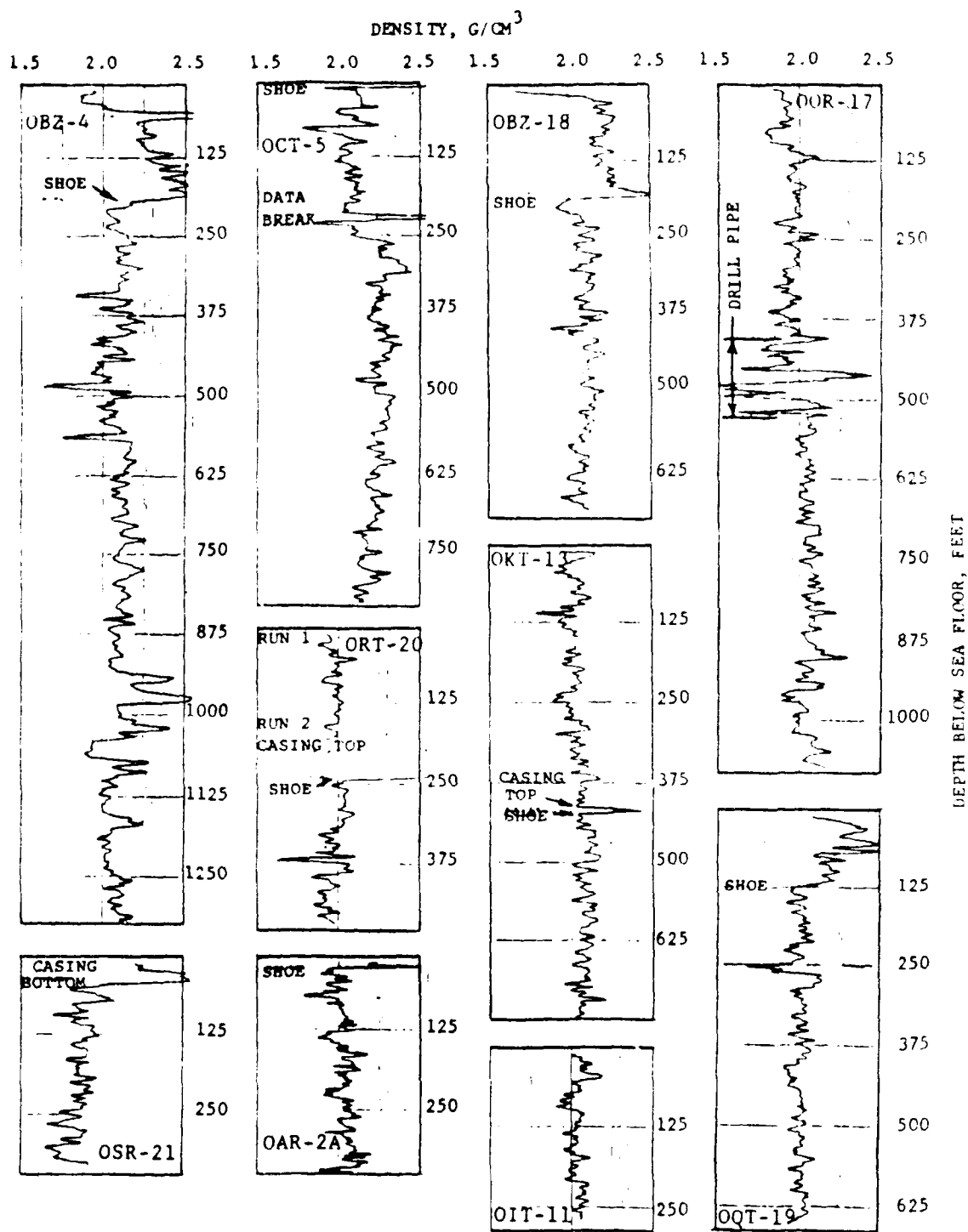


FIGURE 6-3. -- Density profiles from gamma-gamma (Y-Y) logging in OAK crater area (data from Meizer, 1986). Depth below sea floor given in ft.

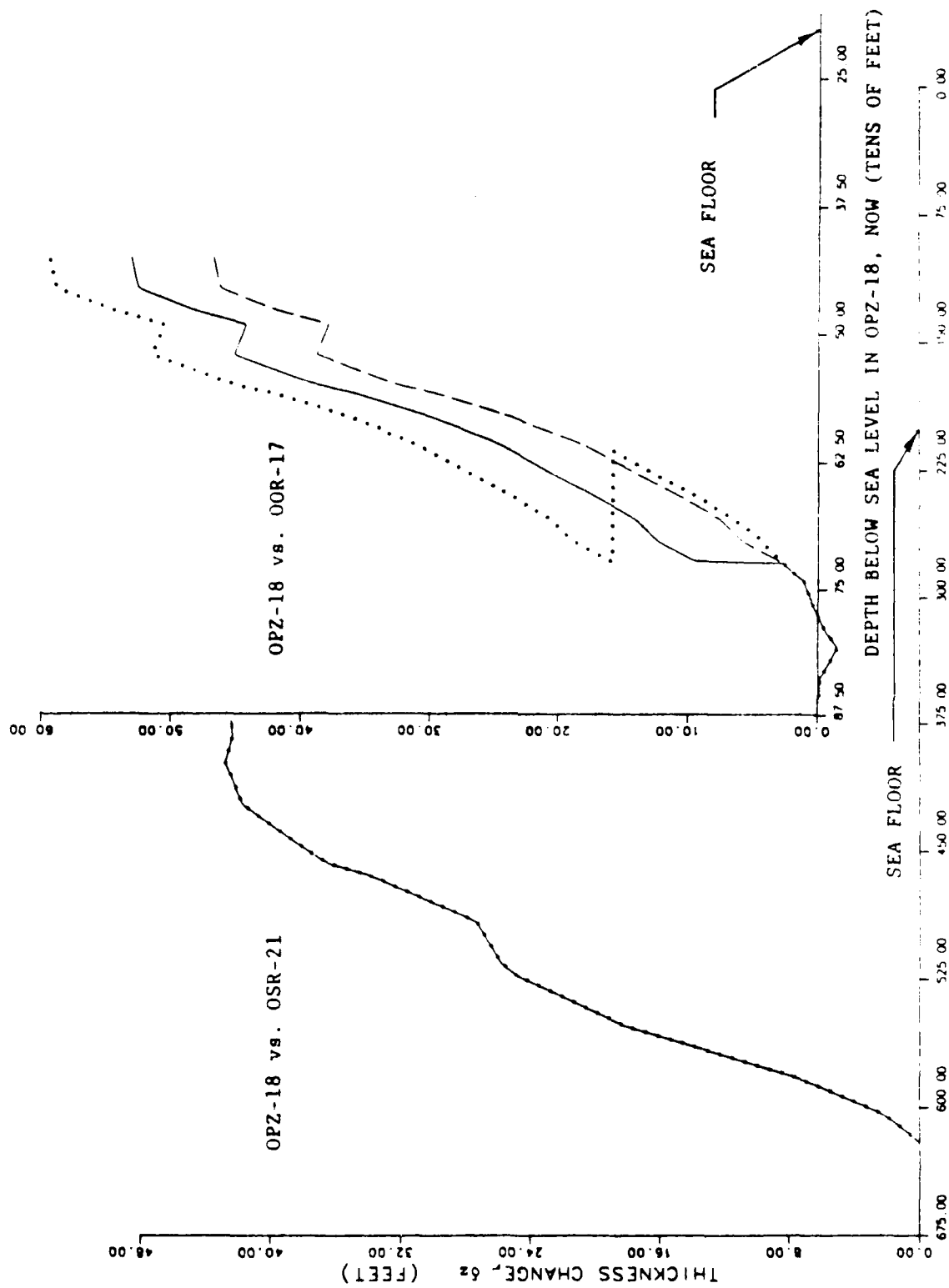


FIGURE 6-4. -- Change in rock thickness from borehole-gravity (BHG) densities, assuming simple subsidence. Boreholes OPZ-18 vs OSR-21 and OPZ-8 vs OOR-17. Strictly speaking, "NOW" refers to December 1984 throughout this Chapter.

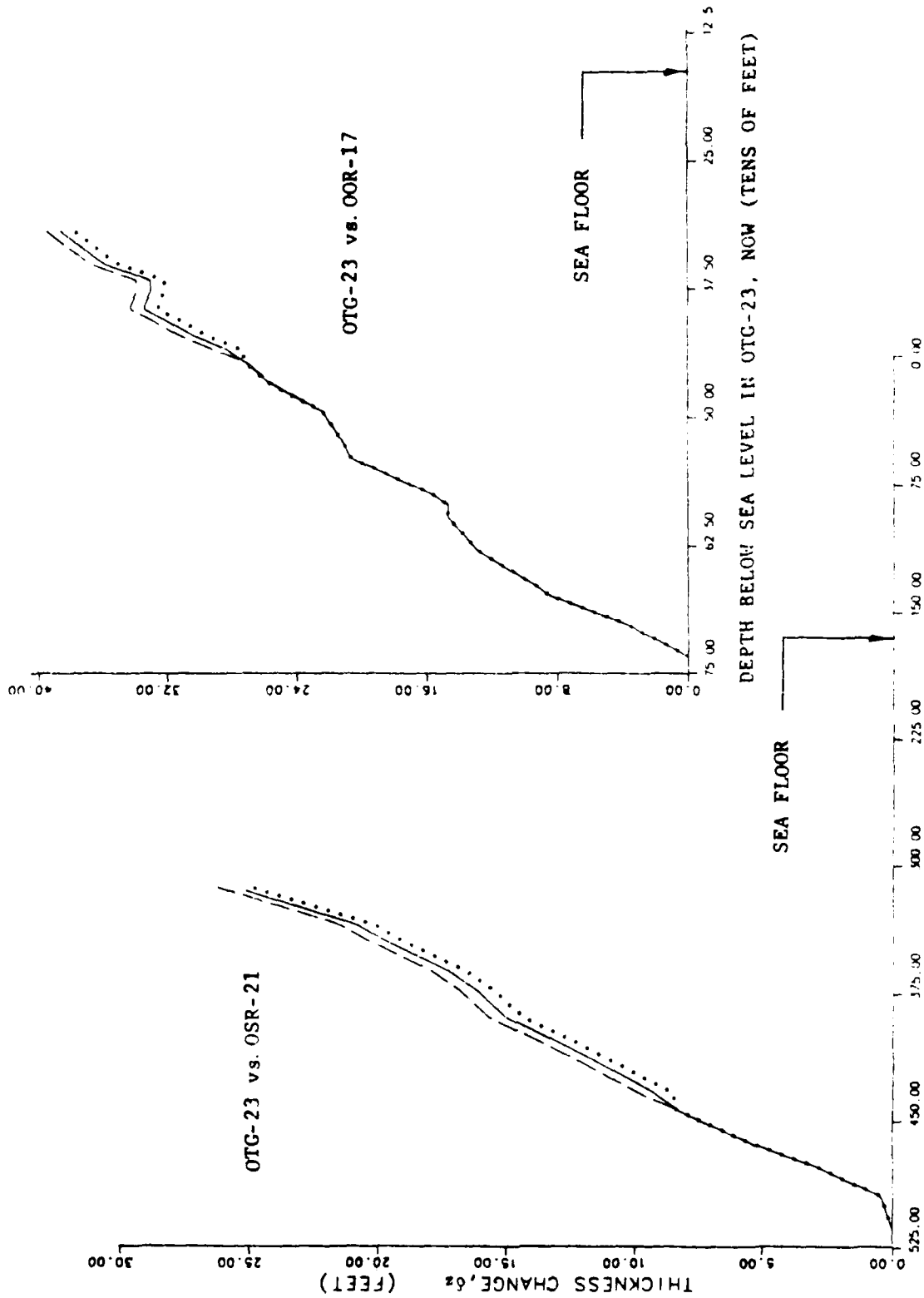


FIGURE 6-5. -- Change in rock thickness from borehole-gravity (BHG) densities, assuming simple subsidence. Boreholes OTG-23 vs. OSR-21 and OTG-23 vs. OOR-17.

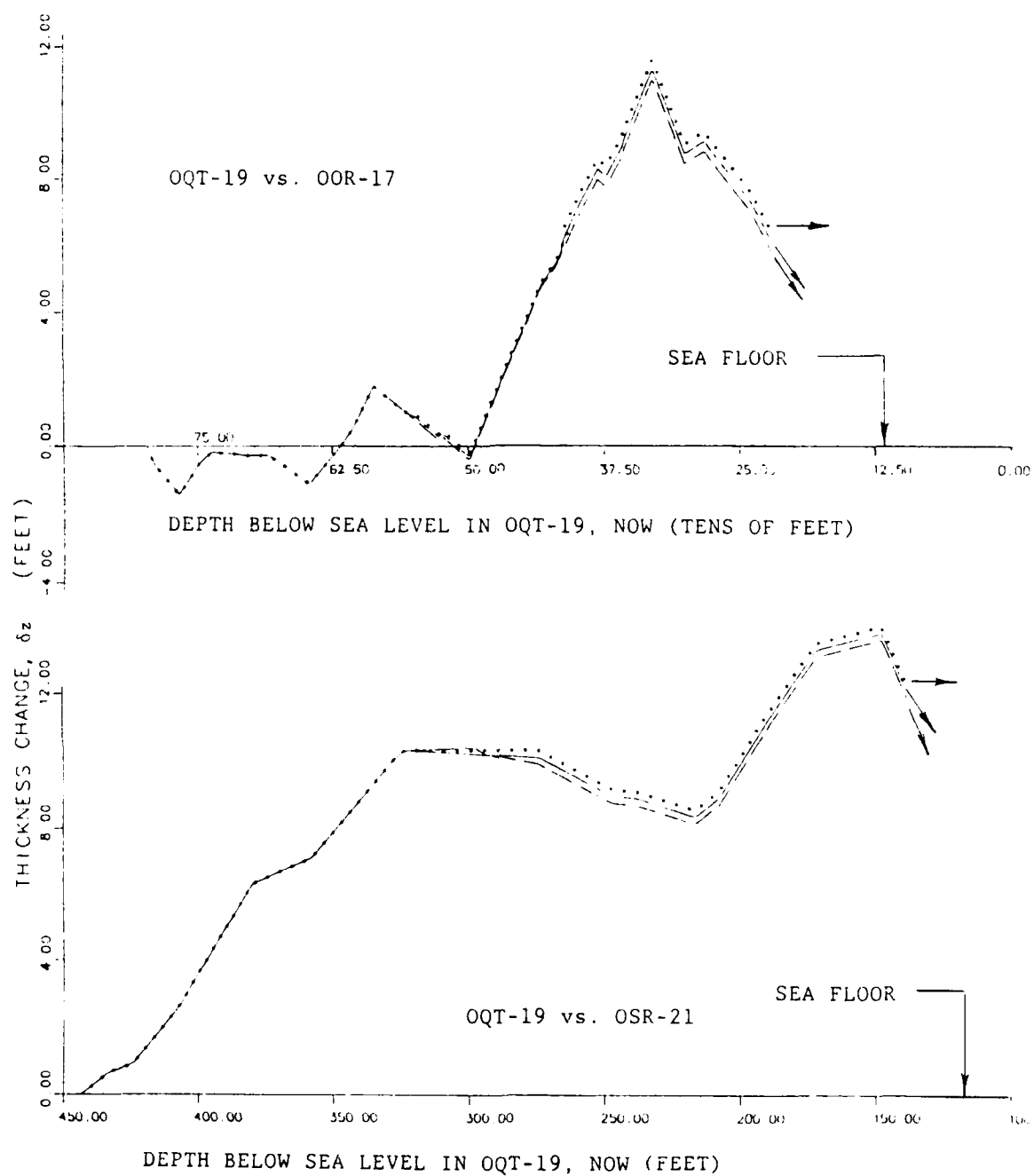


FIGURE 6-6. -- Change in rock thickness from borehole-gravity (BHG) densities, assuming simple subsidence. Boreholes OQT-19 vs OSR-21 and OQT-19 vs OOR-17.

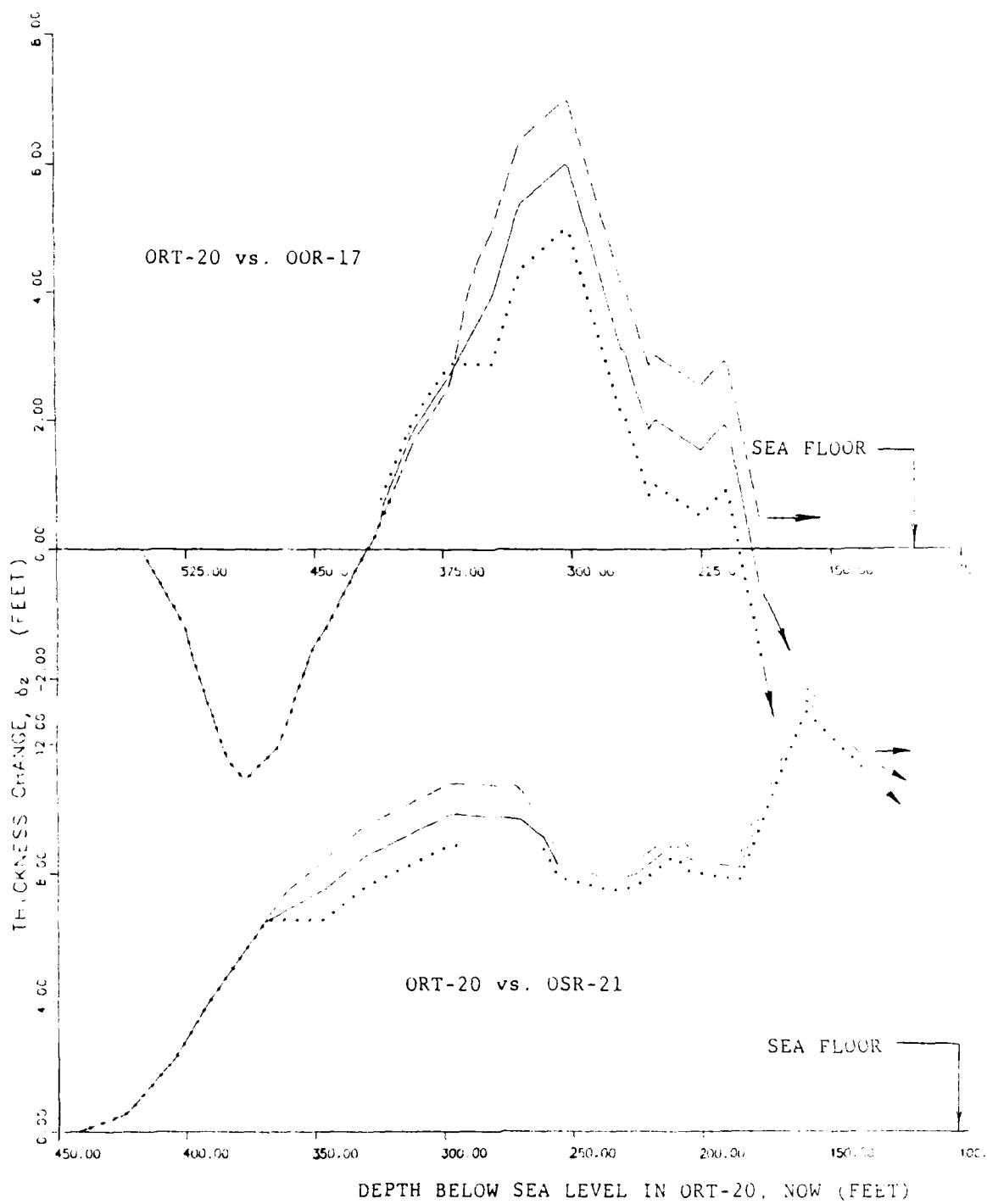


FIGURE 6-7. -- Change in rock thickness from borehole-gravity (BHG) densities, assuming simple subsidence. Boreholes ORT-20 vs. OSR-21 and ORT-20 vs OOR-17.

(Length Unit = 1 ft; $f \equiv \delta z / \Delta z$)

Pairs	Δz	AS MEASURED: D: 423 ft bsl for OQT-19 442 ft bsl for ORT-20			BIASED TO INCREASE f: D: 498 ft bsl for OQT-19 $\delta z = 3$ ft at D for ORT-20		
		δz	f	σ_3	δz	f	σ_3
19/17	71.5	1.6	.02	.17	7.0	.10	.17
19/21	71.5	11.4	.16	.20	16.8	.23	.20
20/17	31.4	1.6	.05	.18	4.6	.15	.19
20/21	31.4	11.9	.38	.07	14.9	.47	.07
							High Estimate $\langle f \rangle = \begin{cases} .153, \text{ no bias} \\ .238, \text{ bias up} \end{cases}$
19/17	71.5	-3.6	-.05	.24	1.8	.03	.24
19/21	71.5	8.6	.12	.25	14.0	.20	.25
20/17	31.4	-4.7	-.15	.19	-1.7	-.05	.20
20/21	31.4	10.1	.32	.14	13.1	.42	.13
							Best Estimate $\langle f \rangle = \begin{cases} .060, \text{ no bias} \\ .146, \text{ bias up} \end{cases}$
19/17	71.5	-4.2	-.06	.30	1.2	.02	.30
19/21	71.5	6.5	.09	.29	11.9	.17	.30
20/17	31.4	-10.3	-.32	.16	-7.3	-.23	.17
20/21	31.4	8.2	.26	.21	11.2	.36	.20
							Low Estimate $\langle f \rangle = \begin{cases} -.079, \text{ no bias} \\ .077, \text{ bias up} \end{cases}$

TABLE 6-3. -- Column-height changes (in ft) due to densification. Borehole pairs shown in left-hand column; f denotes the fraction $\delta z / \Delta z$.

If a column of material between D and the sea floor changed thickness via simple subsidence, then the thickness change δz computed from density profiles measured pre-shot (under our key assumption, see p. 6-8 above) and post-shot should equal the observed sea-floor lowering at the top of the column. The latter lowering is the column's actual thickness-change Δz (tbl. 6-3), whereas δz is the virtual change which densification provides, as computed from measured density profiles. For each control-hole/crater-hole pair, the ratio $\delta z/\Delta z$ appears in Table 6-3 as the fraction "f" of the sea-floor drop due to simple subsidence. On the wing of the OAK crater, the BHG profiles at hand (crater-holes OQT-19, ORT-20; control-holes OOR-17, OSR-21) tell a clear story: Only a small part of the sea-floor drop can be laid to simple subsidence. The highlights, subsumed in the f-values of Table 6-3, follow:

- (1). For the sea-floor drop, best estimates of the fraction (f) due to densification run from -.15 to .32, with a mean of .06.
- (2). With each variable (some not yet discussed) pushed to a reasonable extreme so as to increase f, the minimum, maximum, and mean of f are .02, .38, and .15.
- (3). With each variable pushed to a reasonable extreme to decrease f, the least, greatest, and mean f-values are -.32, .26, and .01.
- (4). With further possible but unlikely increases in all δz -values (right side of tbl. 6-3), the best-estimate values of f [(1), above] increase by .10, .10, and .09, respectively; the f-values in (2) and (3), above, also increase by about those amounts.

Items (1) through (4) above cover systematic errors in determining the fractions by which densification changed column-heights. A major question remains, however, especially with so small a data-set: What confidence can be placed in these results?

CONFIDENCE ASSESSMENT

To fix levels of confidence, we look first at "thickness-changes" caused not by the OAK shot but by natural density-profile variations from one reef-wise borehole to another. To that end, the profile from OSR-21 has been used as a crater profile with the one from control-hole OOR-17 (fig. 6-8) -- and vice versa (fig. 6-9). With OSR-21 as crater hole, extrapolation to the sea floor gives "thickness-change" extremes of -16.3 and -22.5 ft; with OOR-17 as the crater hole, the extremes become 19.8 and 30.4 ft. These are thickness-changes that the two profiles would imply if simple subsidence, in a single coral column down to about 400 ft below sea level (bsl), turned one profile into the other. Thus, not only is density steadily higher in OOR-17 than OSR-21 to about 442 ft bsl, but, as forseen,¹ the "changes" in question are a good deal larger than those due to the burst (the measured δz 's in tbl. 6-3

¹ Letters of July 12, 1984, and April 21, 1985, from author to Dean Oberste-Lehn, Research and Development Associates (RDA), and to Maj. Robert F. Couch, Defense Nuclear Agency (DNA), respectively.

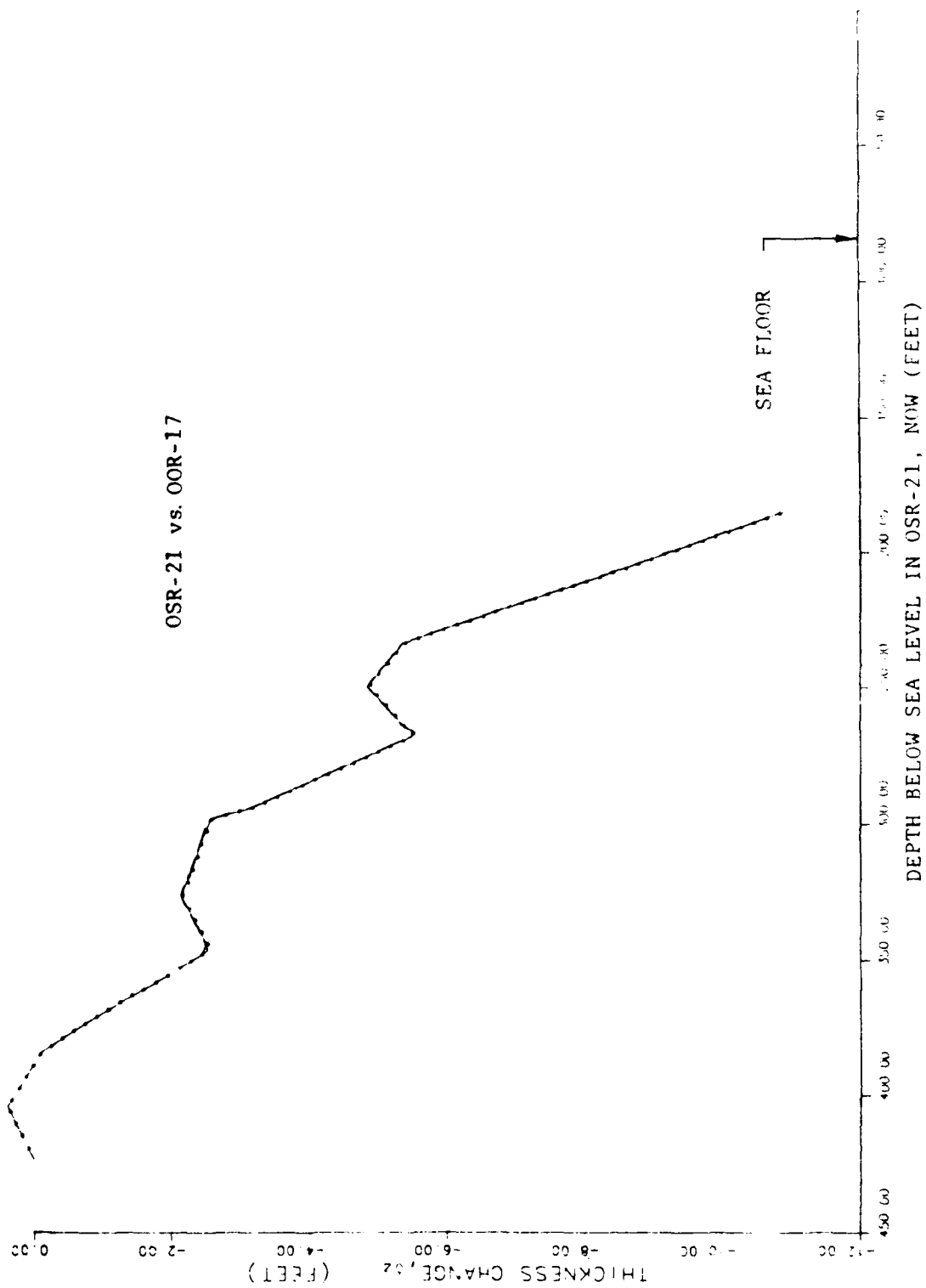


FIGURE 6-8. -- Change in rock thickness from borehole-gravity (BHG) densities, assuming simple subsidence. Boreholes OSR-21 vs OOR-17.

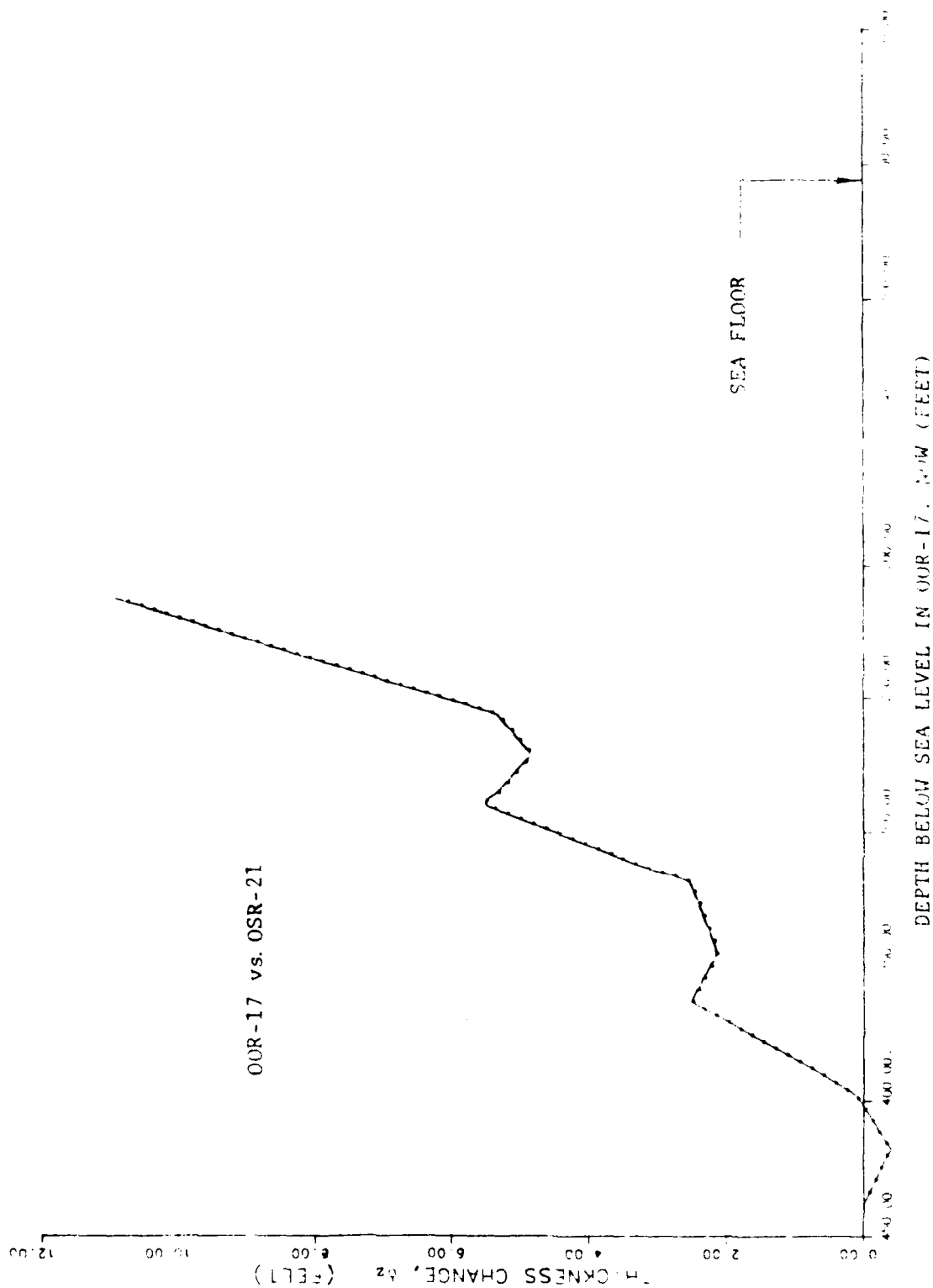


FIGURE 6-9. -- Change in rock thickness from borehole-gravity (BHG) densities, assuming simple subsidence. Boreholes 00R-17 vs. OSR-21.

are ≤ 12.4 ft and average 3.0, 6.1, and .1 ft, respectively, for our best, high, and low extrapolations). With nature causing so much variation (presumably at random) in our calculated thickness-change δz , natural density variations dominate the δz -values. Indeed, for equal depths (442 ft) and the same control hole, absolute differences in δz between OQT-19 and ORT-20 come to < 4 ft and average only 1.8 ft. Hence, treating all four of the resulting f-values as randomly distributed about a mean appears, at the least, a fair approximation (actually, three sets of four must be dealt with, owing to uncertainty in extrapolating δz to the sea floor). On that basis, the question of confidence turns to one of confidence in the estimated mean of a distributed random variable, and can be answered for a data-set of any size by standard statistical methods.

By reason of central tendency, and lacking data that would establish a precise distribution, we assume (as usual) that f-values are normally distributed. In each case (best, highest, and lowest extrapolation), the data of Table 6-3 then supply both a sample mean of f and a sample standard deviation. In computing the latter, however, it must be recognized that only three of the four f-values are independent. For example, given z in both OQT-19 and ORT-20, vs. z in OOR-17, we know z in OQT-19 vs. z in ORT-20; z in OQT-19 vs. z in OSR-21, then yields z in ORT-20 vs z in OSR-21. Since any three of the four f-values can be taken as independent, four estimates emerge of the standard deviation σ_3 ; two degrees of freedom enter the calculation of each (par for the standard deviation of three independent measurements). For each mode of extrapolation (high, best, low), every one of the four σ_3 -estimates is listed in Table 6-3 alongside the f-value omitted in its calculation; also listed are the drop Δz of the sea floor, and the part (δz) of the sea-floor drop due to densification.

For each estimate in Table 6-3 (high, best, and low) the mean $\langle f \rangle$ and a standard deviation imply a distribution of the true mean of the densification-fraction f. In its cumulative form, that "t-distribution" states the probability $\text{Prob}(f > v)$ that the true mean of f (denoted f) lies above any stated value v. Since $\text{Prob}(f > v)$ increases monotonically with σ_3 for a given sample mean $\langle f \rangle$, the largest of the four pertinent σ_3 -values was chosen to get a high estimate of $\text{Prob}(f > v)$, and the smallest σ_3 -value for a low estimate; for the best estimate, the four σ_3 -values were averaged. With those respective values of the standard deviation σ_3 , we computed $\text{Prob}(f > .5)$ and $\text{Prob}(f > 1)$ for each estimate of $\langle f \rangle$ [high, low, and best; a value of about 1/2 would be expected for $\text{Prob}(f > 1)$ if densification accounted for all of the sea-floor drop]. The net result -- fundamental to the whole study -- is that every case $\text{Prob}(f > .5) \leq .05$, with much smaller values for $\text{Prob}(f > 1)$. That is, the odds against densification having caused as much as half the observed sea-floor drop are at least 20-to-1. The left side of Table 6-4 presents a detailed, though brief, summary of all key quantities. As for the right sides of Tables 6-3 and 6-4, the following applies.

The thickness-change curve for OQT-19 vs OOR-17 rises at its greatest rate at a depth of about 426 ft, from a minimum at 498 ft (fig. 6-6). The rise between 498 and 426 ft, and the curve's wiggles below 498 ft, may well stem from the medium's random reef-wise variations, rather than any error in estimating the depth of D at OQT-19. In addition, at ORT-20 (and elsewhere), non-zero downward displacement of a few feet might have been missed at D. Both hypothetical errors would act to decrease f; errors of opposite sign -- about as likely -- would make our f-values too large. Nonetheless, to bias f

Estimate	AS MEASURED: D: 423 ft bsl for OQT-19 442 ft bsl for OQT-20						BIASED TO INCREASE \bar{f} D: 498 ft bsl for OQT-19 $\Delta z = 3$ ft at D for OQT-20					
	$\bar{f} > .5$			$\bar{f} > 1$			$\bar{f} > .5$			$\bar{f} > 1$		
	$\langle f \rangle$	σ_3	t	Prob	t	Prob	$\langle f \rangle$	σ_3	t	Prob	t	Prob
High	.153	.07	8.31	.007	20.29	.001	.238	.07	6.52	.011	18.98	.001
	.153	.15	3.89	.030	9.50	.005	.238	.16	2.85	.052	8.31	.007
	.153	.20	3.03	.047	7.40	.009	.238	.20	2.21	.079	6.44	.012
Best.	.060	.14	5.58	.015	11.92	.003	.146	.13	4.80	.020	11.58	.004
	.060	.20	3.77	.032	8.06	.008	.146	.20	3.02	.047	7.28	.009
	.060	.25	3.06	.046	6.55	.011	.146	.25	2.43	.068	5.86	.014
Low	-.009	.16	5.50	.016	10.92	.004	.077	.17	4.30	.025	9.39	.006
	-.009	.24	3.63	.034	7.20	.009	.077	.24	3.03	.047	6.61	.011
	-.009	.30	2.91	.050	5.76	.014	.077	.30	2.44	.068	5.32	.017

TABLE 6-4. -- Likelihood that true mean \bar{f} exceeds .5 or 1, given a sample mean $\langle f \rangle$. Symbol f denotes the fraction of column-height change due to densification. For each estimate (high, best, low), the three standard deviations shown are the greatest, mean, and least of the four values of Table 6-3.

as far toward higher values as common sense allows, we have assumed on the right of Tables 6-3 and 6-4 that: (a) the depth of D at OQT-19 is 498 ft, causing δz to increase by 5.4 ft (vs. OOR-17); (b) δz is also greater by 5.4 ft at D for OQT-19 vs OSR-21; (c) for ORT-20, the downward displacement is 3 ft (not zero) at 442 ft bsl, where the geologist's horizons place D; and (d) the 3-ft drop at D for ORT-20 is due entirely to densification at greater depths (contrary to all evidence above D). These assumptions lead to the values of f on the right of Figures 6-2 and 6-3, under the heading "BIASED TO INCREASE f ". The main result (besides raising $\langle f \rangle$ -values by $\sim .10$): $\text{Prob}(f > .5) \leq .08$. Strengthened, therefore, is our central conclusion: Densification accounts for just a small part of the wing of OAK's crater.

LONG-TERM SETTLING

Within 67 days of the OAK shot (viz., B+67 days), the sea floor had been re-surveyed to $\sim 3,000$ ft from ground zero (GZ). Coupling that survey with PEACE bathymetry has brought to light notable changes in sea-floor depth between August 1958 and December 1984 (see Chapter 5 of this Report). Specifically, in that period, the sea floor sank by ~ 12 ft at ORT-20, 11 ft at OQT-19, and $4\frac{1}{2}$ ft outside the crater (3,000 ft southwest of GZ on the reef-wise line). That cuts the respective sea-floor drops at ORT-20 and OQT-19 to ~ 20 and 60 ft seven to ten weeks after the event; i.e., "early". What those results mean for densification -- still our working hypothesis -- is perhaps plainest in terms of ORT-20.

Suppose first that the 1958 to 1984 sea-floor drop was caused by vertical settling of coral from the floor down to surface D; such densification is both simple and credible (any net settling below D, for example, would entail an error in present estimates of D's depth). The early sea-floor drop of ~ 20 ft at ORT-20 would take less densification to produce than the drop from pre-shot time to now (31.4 ft) -- but the column between D and the sea floor would have been 12 ft taller in 1958 than now, lowering its mean density. More precisely, the sea-floor drop δz due to densification would be less by 12 ft than in 1984 (see tbl. 6-3); the high, best, and low estimates of its value would all fall by that amount, making negative every f on Table 6-3 but one (for ORT-20). The opposite, less likely scenario has contour D move downward by the same amount as the sea floor above it. Above D, density profiles (and hence δz) are then unaffected; mean densification there stays in the small positive range shown in Tables 6-3 and 6-4 [$f = \delta z / (\Delta z - \Delta z_D)$; δz unaffected; equal changes in Δz and in the drop Δz_D at D] -- even if the drop Δz_D has other causes than densification.

Both extremes (D-depth unchanged vs. equal change at D and at sea floor) lead to the same fraction f of the sea-floor drop due to densification. For, if h_D is the increase in D-depth due to slow densification below D, then δz_D (the part of Δz_D due to densification) evolved to zero in 1984 from $-h_D$ at B+67 days (48 to 67 days after the OAK burst); similarly, if h denotes the increase in sea-floor depth due to slow densification above D, then (for coral above D) δz in 1984 becomes $\delta z - h$ at B+67 days. On the densification hypothesis, we have $h + h_D = 11.8$ ft (the total sea-floor drop at ORT-20 from B+67 to 1984) for any value of h_D ; at OQT-19, $h + h_D = 11.2$ ft. Hence δz (densification's part of the total sea-floor drop by 1984) becomes $\delta z - h - h_D$ at day B+67 -- i.e., $\delta z - 11.8$ ft for ORT-20 and $\delta z - 11.2$ ft for OQT-19. Likewise,

the sea-floor drop Δz (in 1984) becomes $\Delta z - 11.8$ ft for ORT-20 at day B+67, and $\Delta z - 11.2$ ft for OQT-19. The f 's, reckoned as $\delta z / \Delta z$ for 1984, change to $(\delta z - h - h_D) / (\Delta z - h - h_D)$ for day B+67. Thus, with the 1958 to 1984 sea-floor drop $h + h_D$ fixed (no matter how it is split into parts h and h_D due to densification above and below D), the change in f during that period is also fixed. Accordingly, at B+67, the f - and σ_3 -values of Table 6-3, and the probabilities of Table 6-4, becomes those of Table 6-5 below.

Table 6-5, like Tables 6-3 and 6-4, tells a clear and simple tale: As in 1984, the odds against densification having caused half or more of the sea-floor drop measured at B+67, are ≥ 18 -to-1 in all cases; biased to favor densification, the odds remain ≥ 16 -to-1. At B+67, however, all values of $\langle f \rangle$ are negative, with a best estimate of $-.30$ (vs. $.06$ in 1984). Hence, had f -values been as precise for B+67 as for 1984, $\text{Prob}(f > .5)$ would have been a good deal smaller than $.05$; higher σ_3 's at B+67 blocked that (the largest were almost twice as big at B+67). Still, simple subsidence points to negative densification at B+67 (f -values < 0), and it may actually have been negative then (dilatancy). More likely, though, the simple subsidence hypothesis is at fault; it is hard to believe that a medium with 40 to 60 percent porosity, even though fully saturated, would show sizable volume increases on loading and unloading either in uniaxial strain [peak overpressures: ~ 30 to 78 MegaPascals (MPa) (Table 6-1)] or thereafter.

Larger σ_3 's, and the increased scatter of f -values they reflect, take some explaining. They stem primarily from the reduced value, for ORT-20, of the column-height change that forms the denominator of f (a factor of 1.6 smaller at B+67 than 1984). Physically, small column-height changes can flag a breakdown of the f -criterion for measuring the part densification played in forming the crater. That measure makes sense only if the column-height change ($\Delta z - h - h_D$ in this case) is large compared to random ups and downs (standard deviation) in the part densification contributes to the change. Otherwise values of f for columns with small changes in height (changes adding little to the sea-floor drop and crater volume) will dominate the mean value $\langle f \rangle$ used to characterize the whole set of f 's (including f 's for holes with much larger changes in height). The problem can perhaps be finessed (below, last section), but the true cure lies in computing f as a fraction of crater volume due to densification -- given axial symmetry, a sum (over all crater holes) of products $R\delta z$, divided by a sum of products $R\Delta z$ (R = horizontal range at a given crater hole). That fraction, after all, is the ultimate object sought. On present knowledge, its uncertainty would come mostly from its dependence on the choice of control hole for computing each δz . Here, however, we have density profiles from just two crater holes and two control holes. They yield too small a sample (2 ratios) to make such a criterion practical; the one adopted here, despite the drawback under discussion, permits more efficient use of those data (3 independent f 's). Given profiles from a half-dozen or more holes of each kind, the volume criterion appears the better choice.

As for slow settling beyond the presently defined crater, pre-shot and 1984 contour maps show ~ 4 to 6 ft of it. So do the maps for B+67. The drop appears widespread as to direction, occurring (for example) at both 2-to-4 o'clock relative to GZ (north = 12 o'clock), and 6-to-8 o'clock. Here, however, it matters only if it means that the shot appreciably disturbed control-hole material. That is not at all likely for the following reasons:

Pairs	Δz	AS MEASURED			BIASED TO INCREASE \bar{f}		
		$\delta z - (h+h_p)$	f	σ_3	$\delta z - (h+h_p)$	f	σ_3
19/17	60.3	1.6-11.2	-.16	.30	7.0-11.2	-.07	.29
19/21	60.3	11.4-11.2	.00	.27	16.8-11.2	.09	.26
20/17	19.6	1.6-11.8	-.52	.09	4.6-11.8	-.37	.12
20/21	19.6	11.9-11.8	.01	.27	14.9-11.8	.16	.23
19/17	60.3	-3.6-11.2	-.25	.45	1.8-11.2	-.16	.43
19/21	60.3	8.6-11.2	-.04	.40	14.0-11.2	.05	.39
20/17	19.6	-4.7-11.8	-.84	.11	-1.7-11.8	-.69	.12
20/21	19.6	10.1-11.8	-.09	.42	13.1-11.8	.07	.38
19/17	60.3	-4.2-11.2	-.26	.58	1.2-11.2	-.17	.56
19/21	60.3	6.5-11.2	-.08	.53	11.9-11.2	.01	.51
20/17	19.6	-10.3-11.8	-1.13	.09	-7.3-11.8	-.97	.09
20/21	19.6	8.2-11.8	-.18	.56	11.2-11.8	-.03	.53

LIKELIHOOD THAT THE TRUE MEAN \bar{f} EXCEEDS .5 OR 1, GIVEN A SAMPLE MEAN $\langle f \rangle$

Estimate	$\langle f \rangle$	AS MEASURED:			BIASED TO INCREASE \bar{f}		
		σ_3	$\bar{f} > .5$	$\bar{f} > 1$	σ_3	$\bar{f} > .5$	$\bar{f} > 1$
			t	Prob	t	Prob	Prob
High	-.17	.09	12.26	.003	21.44	.001	.001
	-.17	.23	4.95	.019	8.66	.007	.008
	-.17	.30	3.81	.031	6.68	.011	.012
Best	-.30	.11	13.08	.003	21.22	.001	.002
	-.30	.34	4.07	.028	6.60	.011	.013
	-.30	.45	3.10	.045	5.03	.019	.021
Low	-.41	.09	17.68	.002	27.38	.001	.001
	-.41	.44	3.60	.035	5.57	.015	.017
	-.41	.58	2.73	.056	4.23	.026	.029

TABLE 6-5. -- Column-height changes due to densification in OAK crater 48 to 67 days after burst. Borehole pairs given in left-hand column.

- (1). Whereas 4-to-6 ft of subsidence appears to have occurred around most of the crater, the pre-shot map runs only about 1.2 crater radii; there, peak overpressure was greater by a factor of 5-to-10 than at control-holes OSR-21 and OOR-17.
- (2). As horizontal range increases, a steady decrease occurs in the sea-floor drop observed between 1958 (pre-shot) and 1984. On the reef-wise line of BHG logging, those drops run from ~120 ft one-fourth of the way to the crater's edge, to ~64 ft halfway there, to ~5 ft at the edge itself. They and their rapid decrease with range were doubtless both caused by the explosive loads the medium bore -- loads which also decreased rapidly with range. Like those loads, the sea-floor drop should be a good deal smaller at two crater radii than one -- and the drop of 5 ft at the crater's edge is already small, whether it came about by densification or not.
- (3). Uncemented layers were breached in the crater's central region, opening new routes for leakage of water to the surface from great ranges; at a speed of only 1 cm/hr, water would have flowed ~7,500 ft by 1984. Driving such flow, however, would be gravity, just as it has tended over geologic ages to force water upward through the local fissures and passages present in coral. Balancing gravity over that time has been the ability of the solid skeleton to support vertical loads without transferring them to interstitial water; owing to those very loads, the strength of uncemented sand is >0. Gravity and strength act no differently now than in the past -- and the absence of detectable change in the separation of horizons in control holes argues that the balance between them remains where it was struck ages ago.

PIPING

During simple subsidence, skeletal coral replaces water that flows from it; since coral solids are denser than water, the medium then densifies, in accord with Eqs. (1)-(5). Yet, as discussed above, applying Eqs. (1)-(5) to the observed density profiles accounts for only some of the observed sea-floor drop; in material below the crater floor, density has increased by only a small fraction of the requisite amount. However, the finding that material hundreds of feet below the excavation crater had risen to the crater floor (see Wardlaw and Henry, 1986b; and Chapters 3 and 7 of this Report), suggests a way out -- namely, transport of solid particles by upwelling water. Any observed changes in density and column-height can be brought about by such "piping", given the right ratio of solid to liquid in piped slurry; for example, no density changes will be seen if the density of the slurry equals that of the pre-shot medium. In addition, of course, the right amount of material must be piped. On that point, the idea founders; evidence of

substantial piping is limited to the central crater region.¹ There is also an implicit demand that piped solid be transported not just to the sea floor, but out of the apparent crater; that puts direct measurement of the amount of piped material beyond reach now. Nevertheless, piping was noted at OAK; some of its properties follow.

Eqs. (1)-(5) remain valid, but it is no longer useful to ask what pre- and post-shot heights are subtended in a column by a given solid mass m_s . Rather, with solid leaving the column, the mass of solid between two coral particles that remain in it will be different before the shot than after; moreover, the distance between them changes as both solids and liquid are lost. To compute the effects of both losses, let V denote a pre-shot control volume of the medium in which the following definitions apply:

α = pre-shot volume-fraction of liquid in V

β = pre-shot volume fraction of solid in $V = 1 - \alpha$

ρ_L = density of liquid component

ρ_S = density of solid component

ρ = mean pre-shot density of mixture in V .

As on page 6-7 of this Chapter, it then follows that:

$$\alpha\rho_L + \beta\rho_S = \rho \quad \text{Eq. (6)}$$

To describe the post-shot state of the same material, let

γ = piped-out fraction (volume or mass) of the liquid within V

$k\gamma$ = piped-out fraction (volume or mass) of the solid within V

$\bar{\rho}$ = present mean density of mixture not piped from V .

¹ For a cratering mechanism, a useful measure of significance lies in the fraction of the apparent crater's volume that can be laid to it. The piping observed at OAK crater occurred only within ~ 4 apparent radii from GZ -- the central crater -- whereas the main PEACE problem is to account for the wing beyond the central crater. Piping will merit great attention if it can be shown, by tight quantitative arguments, to have produced something like half the wing's volume. By that standard, the fact that piping occurred can only suggest it as a possibly significant mechanism. The same holds for other observations as well, applying (for example) to any sand boils outside the apparent KOA crater; what their quantitative relation might be to the volume of KOA crater (let alone OAK's) is not at all obvious [mud boils also appeared above the Tatum salt dome after the SALMON event (Werth and Randolph, 1966, p. 3409) -- clear proof of piping, but piping played no role in forming SALMON's cavity].

Since αV and βV are the respective pre-shot volumes of liquid and solid, the volumes of liquid and solid piped out of V equal $\gamma\alpha V$ and $k\gamma\beta V$. Hence, of the volume V , the piped-out fraction ϕ is given by:

$$\phi = \frac{\text{Volume of Mixture Piped}}{\text{Pre-shot Volume, } V} = (\gamma\alpha V + k\gamma\beta V)/V = \gamma(\alpha + k\beta) \quad \text{Eq. (7)}$$

Likewise, the mean density of the remaining mixture becomes:

$$\begin{aligned} \bar{\rho} &= [(1-\gamma)\alpha V\rho_L + (1-k\gamma)\beta V\rho_S]/[(1-\phi)V] \\ &= [(\alpha\rho_L + \beta\rho_S) - \gamma(\alpha\rho_L + k\beta\rho_S)]/(1-\phi) - [\rho - \gamma(\alpha\rho_L + k\beta\rho_S)]/(1-\phi) \end{aligned} \quad \text{Eq. (8)}$$

Using Eq. (7) to eliminate γ from Eq. (8), the direct result is:

$$\bar{\rho} = [\rho - (\alpha\rho_L + k\beta\rho_S)\phi/(\alpha + k\beta)]/(1-\phi)$$

Slight rearrangement of this last equation makes it linear in $k\beta/\alpha$, whence

$$\begin{aligned} k\beta/\alpha &= [(\bar{\rho} - \rho_L)\phi - (\bar{\rho} - \rho)\phi + (\bar{\rho} - \rho)] \\ &= \frac{k\gamma\beta V}{\gamma\alpha V} = \frac{\text{Volume of Solid Piped}}{\text{Volume of Liquid Piped}} \equiv \frac{V_{SP}}{V_{LP}} \end{aligned} \quad \text{Eq. (9)}$$

The sludge density, $\bar{\rho}_{SL}$, follows from the ratio V_{SP}/V_{LP} :

$$\bar{\rho}_{SL} = (\rho_L V_{LP} + \rho_S V_{SP})/(V_{LP} + V_{SP}) = [\rho_L + \rho_S (V_{SP}/V_{LP})]/[1 + (V_{SP}/V_{LP})] \quad \text{Eq. (10)}$$

Values for the mean densities ρ and $\bar{\rho}$ come from density profiles measured, respectively, in control holes and crater holes. Also, for a vertical column of OAK coral, the fraction ϕ is just the change in column-height, divided by the column's pre-shot height. Hence, from PEACE observations, Eq. (9) allows us to compute the ratio of solid and liquid volumes in piped material, and Eq. (10) its density, if piping caused the changes observed. Perforce, then, those quantities constrain the piping process, whereas γ and $k\gamma$ simply fix the unmeasurable total amount piped. For example, if no density changes occur ($\bar{\rho} = \rho$), then the volume and mass ratios implied by Eq. (9) will be those of pre-shot material, and piped sludge will have the same density as the rest of the medium -- in which case, gravity cannot cause it to be piped. However, if a shot raises the medium's density a bit (as the PEACE logs indicate for OAK), the resulting small pressure head can push sludge upward. To help quantify that push, estimates of the density of piped material have been made from PEACE measurements using Eqs. (7), (9), and (10).

In Table 6-6 below are recorded: (a) the mean densities (ρ and $\bar{\rho}$) measured for OOR-17, OSR-21, OQT-19, and ORT-20 from their shallowest common horizon, down to each of three others (the deepest at base D of the downward-displacement region); (b) the depths z and z_0 , respectively, of the top and bottom of the column to which each mean density refers; (c) the measured

column shrinkage, ϕ , between z and z_0 for OQT-19 and ORT-20¹ (together with the changes in depth Δz and Δz_0 at z and z_0)²; (d) volume ratios implied by those data and Eq. (9), for the four control-hole/crater-hole pairs; (e) a mean density of piped material (also listed) follows from each volume ratio by Eq. (10), and with it (f) a "density decrement" $\rho_{SL} - \bar{\rho}$ (the difference between the densities of piped and remaining material). Evidently, subsidence by piping would require extruded material to have a bit lower density than that not piped. Note, however, that the residue's density $\bar{\rho}$ runs from slightly greater than that of the supposed sludge, to $\sim .45$ g/cc less. That wide spread reflects sensitivity of the volume ratio [Eq. (9)] to random differences among borehole density profiles, when column shrinkages (ϕ) are $\ll 1$. Thus, the most consistent sludge densities and density decrements are obtained for the longest columns (third quartet of tbl. 6-6, running down to D at ~ 443 ft bsl for OQT-19 and ORT-20).

From the decrements in Table 6-6, it appears that slurry would be driven upward by pressures of about a tenth of the lithostatic head (mean decrement $\sim .2$ g/cc), though the standard deviation of decrements is also that large (.21 and .26 g/cc; second and third quartets). At an upward acceleration of .1 g (decrement $\sim .2$ g/cc), sludge would take ~ 11 sec to rise 200 ft in a wide, unobstructed pipe -- but there's more to piping than that.

OTHER CONSTRAINTS; HORIZONTAL PIPING

The densities in Table 6-6 apply to vertical columns 200 to 300 ft in height. Within such a column, single layers could have been driven by a density decrement as large as 1/3 g/cc. However, the path of sludge piped from the crater's wing leads first to the central crater, where lie nearly all the vents known to have guided solids from depth to the sea floor. That first path-leg has its pitfalls. For one, all horizons grow in depth along it; the horizons crossed by contour D at boreholes OQT-19 and ORT-20 (roughly 3a in fig. 6-1) run ~ 70 ft deeper at OTG-23, 800 ft from GZ (tbl. 6-2), and the sea floor lies ~ 55 ft deeper. Adding 55 ft of sea water and 15 ft (70 minus 55 ft) of coral makes the overburden ~ 11 percent greater than at the intersection of D with OQT-19 (or ORT-20). Along the horizon in question (H, say), the resulting overburden gradient opposes inward flow to the vents -- and while 11

¹ The "Volume of Mixture Piped", needed to calculate ϕ by Eq. (7), is equal to the change in depth Δz_0 of the column's bottom end, minus the change in depth Δz of its top end. The column's "Pre-shot Volume, V" is equal to the pre-shot depth $z_0 - \Delta z_0$ of its bottom end minus the pre-shot depth $z - \Delta z$ of its top end, where z_0 and z are the current (1984) depths of its bottom and top ends, respectively.

² Values of z , z_0 , Δz and Δz_0 were obtained for Table 6-6 from Table 7-4 of the present Report. For several horizons, the latter table lists both 1984 depths measured in crater holes, and estimates of pre-shot depth based on the full set of 1984 measurements (including horizon depths in control holes). Given a 1984 depth, the pre-shot depth of the same horizon was obtained for Table 6-6 by linear interpolation in Table 7-4 -- with the change in its depth equal to the difference between the 1984 and pre-shot values.

Pair	z_0	z	Δz_0	Δz	ϕ	$\bar{\rho}$	ρ	V_{SP}/V_{LP}	$\bar{\rho}_{SL}$	$\bar{\rho}_{SL} - \bar{\rho}$
19/17	309	220	35.0	38.9	.042	1.91	1.96	<0	> ρ	>0
19/21	309	220	35.0	38.9	.042	1.91	1.89	.36	1.50	-.40
20/17	300	192	19.7	29.7	.085	1.91	1.96	4.66	> ρ	>0
20/21	300	192	19.7	29.7	.085	1.91	1.89	.62	1.71	-.19
19/17	410	220	9.2	38.9	.135	1.94	1.94	1.04	1.94	.00
19/21	410	220	9.2	38.9	.135	1.94	1.89	.44	1.57	-.37
20/17	408	192	6.0	29.7	.099	1.94	1.94	1.14	1.98	.04
20/21	408	192	6.0	29.7	.099	1.94	1.89	.34	1.48	-.46
19/17	444	220	0	38.9	.148	1.95	1.94	.92	1.89	-.06
19/21	444	220	0	38.9	.148	1.95	1.90	.47	1.60	-.35
20/17	442	192	0	29.7	.106	1.95	1.94	.97	1.91	-.04
20/21	442	192	0	29.7	.106	1.95	1.90	.37	1.51	-.44

TABLE 6-6. -- Piping hypothesis. Symbol $\bar{\rho}_{SL}$ denotes density of piped material; densities in g/cm³; lengths in ft.

percent of overburden may be a small pressure, it is two-thirds or more of the total head available to pipe sludge from H. That head acts at the vents; slurry near them can, of course, be piped upward. At bigger ranges, however, their influence weakens relative to that of overburden. Hence, if we are dealing with a liquefied layer (all sludge), the denser layers above probably settle soonest near the vents, replacing piped material but pinching off the flow. Note also that slurry converges cylindrically as it moves inward, slowing its passage to the vents. The "aperture" available to it (proportional to horizontal radius) decreases by a factor of 2-1/2, for example, as slurry goes from 2,000 ft of radius to 800.

An unliquefied layer presents added bars to piping. For, in a layer with strength, unpiped material bears at least part of the overburden; the pressure that drives piping is smaller than the head that the density decrement would otherwise supply. Indeed, the slurry pressure may simply equal its own head, as in any drained unit; then no piping occurs. More generally, creep of the layer's strong component, like weakening induced by the blast, provides some impetus for piping -- but reduced from that which the full density decrement could furnish, and on a wholly different time-scale. Indeed, creep can be so slow that almost no solid particles are entrained by piped water (simple subsidence), which may well have been the mechanism for settling between B+67 and 1984 (see preceding section). In addition, members with strength physically block piping; sludge has to flow between and around those solid parts. Such flow -- through a porous solid -- is described in simplest quantitative terms as diffusion, in accord with D'Arcy's Law, with flow rates set mainly by the medium's permeability. The lower the rates, however, the more solid settles out (under gravity) on its way to the crater's floor; further, at any given rate, entrained particles will not accelerate upward unless the drag on them exceeds their submerged weight.

These remarks suggest detailed calculations of upward/inward diffusion that have not been made, partly because the medium's post-shot permeability is poorly known, but more because PEACE disclosed no piping of note on the crater's wing.

Once at the surface, slurry particles would have to ride out of the crater on reef-wise currents of perhaps 1 knot (~1.5 ft/sec) (Halley and others, 1986, p. 5). During that half-hour trip, gravity would cause particles to settle; those with diameters $>1/8$ mm would drop an estimated 100 ft or more along the way (Stokes flow), and hence would leave the crater, if at all, only by other, slower means. The same forces of drag, weight and buoyancy also act on the particles during their rise to the crater's floor; treating them again as isolated spheres, the buoyancy and drag of water rising 200 ft in one hour (1/18 ft/sec) can move them only if their diameters are $<1/8$ mm, while for 10 and 100 hours of rise, respectively, the critical diameters are $3/80$ and $1/80$ mm. These estimates are rough, since the particles are not spheres (nor do spheres bound drag \pm mass), they and their wakes overlap [increasing drag \pm mass if they do not clump (Soo, 1967, Ch. 5)], and they rise in ragged, twisty channels (not straight, free streams) that may be <10 diameters wide in places.

Fissures, and cones of debris containing coral fragments raised hundreds of feet, were seen in the central region, where coral was most damaged (Halley and others, 1986; Slater, and others, 1986). Piping accounts neatly for that, and much of it could have occurred in a few seconds or less. For, with

overpressure at the .1-MPa level, burst-induced sub-crater pressures up to ~100 MPa would furnish the required vertical stress gradients. Relief of those pressures would be rapid, requiring a volume increase of <1/2 percent for decay to .1 MPa (from 100 MPa). Though slight in relation to crater volume, enough material would be extruded in such an expansion to make impressive deposits on the sea floor, and cloud the reef currents that cross the crater.

DENSIFICATION: SUMMARY AND CRITIQUE

Borehole cores have let geologists fix the depths of many layer interfaces ("horizons") below and outside the OAK crater. Further, in two holes on the crater's wing, gravimetry has furnished density profiles down to horizons not moved by the OAK burst; to the same horizons, but well outside the crater, borehole gravimetry (BHG) also has given two density profiles. All four holes lie on a curve roughly parallel to the reef. There, in pristine coral, geology argues for random density-profile variations about some mean. The present coral medium formed in about the same way at different points on any one of a set of curves roughly parallel to the reef. Moreover, PEACE cores and density profiles support the idea of such variations about a mean. Treating the far-field pair as pristine profiles then yields density changes due to the burst, from depth to 20-100 ft below the crater floor. From those changes come the downward displacements that densification implies for sub-crater coral, vs. depth, and for the crater floor itself. Comparing the latter displacements to actual sea-floor drops yields the result that densification played but a small role in forming the crater's wing.

Except for converting density profiles to downward displacements, significant uncertainty attends each step noted:

1. The general increase of coral density from lagoon to ocean is a source of systematic error in the measured profiles. Specifically, prior to OAK, departures from the mean density profile would have been random along the curve on which boreholes were supposed to lie. That curve is not known precisely. Actual boreholes therefore depart from it, but are about as likely to fall on one side of it as the other. Hence, given the oceanward density gradient, the general effect of such misplacement is to increase the differences among measured profiles. The unlikely opposite result, however, is more apt to have occurred in our four-profile set than in a large set. The scatter of profiles would then have been underestimated.
2. A horizon's drop (or rise) by a few feet could have escaped notice. That holds for the "unmoved" horizons above which we reckoned density-change effects in the two crater-wing holes.
3. From the shallowest point of BHG logging in a given borehole to the sea floor, horizon-depth changes due to densification were estimated by extrapolation from below.
4. Limits of precision render BHG-measured densities uncertain, but by $< \pm .02$ g/cc. Further, BHG densities are averages over such large regions that the effects of them of local site inhomogeneities (vugs, etc.) are believed negligible (for PEACE, a great advantage of BHG over other methods).

5. The sea-floor drop δz implied by density changes down a borehole, divided by the actual sea-floor drop at the hole (Δz), measures the contribution of densification to the crater. That ratio (f), however, gives too much weight to holes where the actual drop is small. Further, though f is a random variable, its distribution may not be near-normal (as assumed).
6. The largest values of δz (vs. depth) come from pairing the two wells outside the crater, just 560 ft apart ("control-holes," ~5,500 and 6,000 ft from GZ). Moreover, paired with the same control hole, the two holes 400 ft apart in the crater's wing (~4,000 ft from the control holes) have much the same curve of δz -vs.-depth. Nature, not the OAK burst, thus appears the chief source of variation among the four density profiles; our signals (density changes due to OAK) were buried in noise (random natural differences in density). As a result, the likelihood that the crater wing formed by simple subsidence could be assessed using three independent values of δz (the maximum from four profiles) -- despite our having just two profiles from the wing. Strictly, that can be correct only as f , divided by its standard deviation, approaches zero. The crater-wing profiles show some densification ($f > 0$), however, and may differ systematically therein owing to their different ranges.

Caveats 1 through 6 forced us to assess confidence in the overall finding of low densification ($\delta z < .1 \Delta z$). To that end, our data base and calculations were altered (within reason) to maximize f :

i) Since oceanward density gradients could have acted to reduce differences among our f -values [caveat 1 above], the standard deviation of f was assigned the largest value found from the data (of the four deviations at hand when three of four f 's are independent).

ii) For each borehole, δz was set at the sea floor to the highest δz -value found by extrapolating δz -vs.-depth to the floor [point 2 above].

iii) Unseen displacement of the shallowest "unmoved horizon" D in a given borehole would probably have been downward. Each δz -value from item (ii) above was increased by 3 ft or more to offset such an error [caveat 3 above].

iv) Adding offsets (iii) directly to δz -values credits the unseen drop of D entirely to densification below D -- even though densification accounted for just a small part of the horizon-drops observed above D (in the crater's wing).

v) On the PEACE data, the tendency of f to place undue weight on holes with small sea-floor drops [point 5 above] led to high -- but accepted -- values of both f and its standard deviation (ORT-20 has smaller Δz -values than OQT-19 and higher f -values).

The overstatement of f flagged by item (v) looks correctible (next section). That correction would probably be cancelled, and then some, if no appeal were made to the limit where f , divided by its standard deviation, tends to zero (item 6 above). How to avoid that limit without giving f another strong ad hoc lift is not clear. As it is, each upward bias lent to f appears within reason. Having them all act at once to make high f -values likely does not. But even so, only minor densification results.

CONCLUSIONS

If the wing of the OAK crater resulted from densification, then the sea-floor drop at a wing-station, W, can be computed exactly from density profiles before and after the shot in a vertical column below W. No such profiles were measured pre-shot. That heightens the problem of reading density increases due to OAK through the noise of random natural variations in density. Below the crater's wing, those variations were found to dominate shot-driven changes in density. More important, however, the noise level proved low enough to admit a clear answer to the main question posed -- **on the wing of OAK's crater, most of the sea-floor drop had causes other than densification.**

As a best estimate, 6 percent of the sea-floor drop on the crater's wing can be laid to density increases caused by the burst. That figure follows from profiles down two crater holes and down two control holes outside the crater -- profiles that yield four estimates (3 independent) of the fraction, f , contributed by densification to the sea-floor drop. Each of the four has a high, best, and low value, depending on how a gap in data just below the sea floor is bridged (fig. 6-10). To be sure, the sample is small, but its size has been taken into account in assessing confidence in the mean of f . The results: The probability that densification caused half or more of the sea-floor drop is $<.1$. That result holds even if the main parameters of the calculation are all varied at once (each within reasonable limits) so as to increase f . The PEACE density profiles could be of course atypical, but, at most, that observation only supports measuring more profiles; with the data at hand, the results are as stated.

Extant maps show that, in the crater wing, the sea floor sank appreciably between August 1958 (a few months after OAK) and December 1984 (PEACE). The crater was therefore significantly shallower in 1958 than now. By the same token, given simple subsidence, the medium was notably less dense (on average), from the base of the region of downward displacement to the crater floor. Combining that slow sea-floor drop with the PEACE density profiles leads to a best estimate of $\sim -.2$ for f at August 1958 -- and again (by chance) the probability that densification caused half or more of the sea-floor drop at that date is $<.1$.

The same data base of sea-floor maps and PEACE density profiles also yields mean values for the density of materials piped up to the sea floor, if the piping hypothesis is correct. From those values, the densities of piped and residual material differ by an average of $\sim .2$ g/cc, but with a standard deviation at least that large. A density difference of $.2$ g/cc can drive piping, but weakly -- and the chain of events leading to transport of piped material out of the crater has many weak links (e.g., it appears that particles $>.1$ mm in diameter will settle before they can exit).

The statistical grounds for assessing densification probably can be strengthened, using only extant data. Given the cost of the data, that should be done. Specifically, both the sea-floor drop (Δz) and the part of it due to density changes (δz) can be expressed as fractions of the pre-shot depth to D. The probability that the latter fraction exceeds half (say) of the former can then be computed, using standard deviations supplied by PEACE data. A BHG profile from the central region could also be added to the present set, but not without giving a further strong upward bias to the estimated extent of

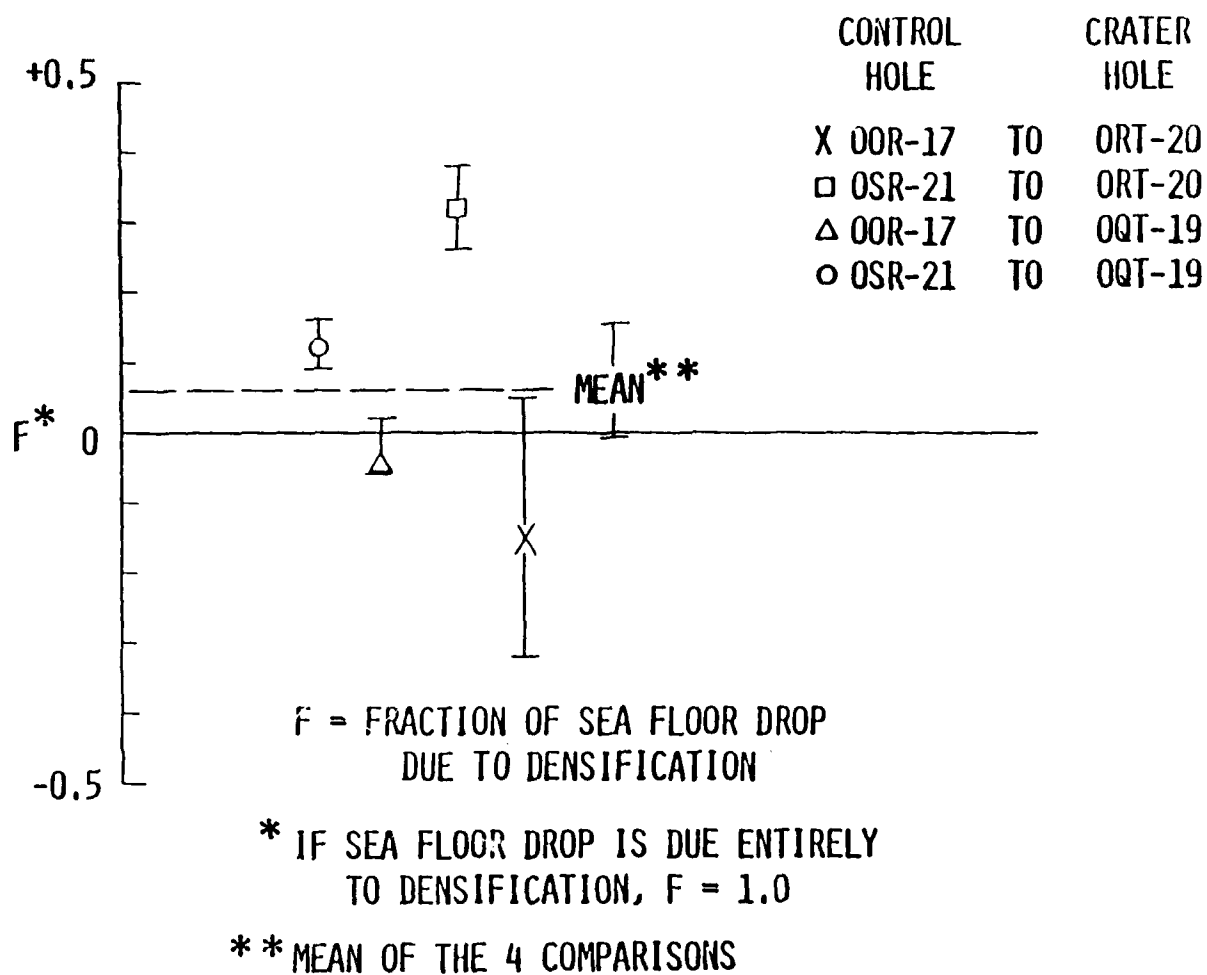


FIGURE 6-10. -- High, low, and best estimates of the fraction contributed to sea-floor drop by densification at boreholes OQT-19 and ORT-20.

densification. In addition, the plausibility of the piping hypothesis should be examined further. With densification as an unlikely mechanism for forming OAK's crater-wing, however, plastic flow appears to offer the simplest and most plausible explanation for it. Whether that explanation will withstand close scrutiny is unclear; flow is well understood in principle, but not much is known about the displacement field around a flow crater.

ACKNOWLEDGEMENTS

For the PEACE Program data herein, and much kind assistance besides, my sincere thanks go to Larry Beyer, Scott Blouin, Bob Henny, Woody Henry, Steve Melzer, Dean Oberste-Lehn, John Peterson, Byron Ristvet, Ed Tremba, and Bruce Wardlaw. Larry, John, Woody, and Byron, and (above all) Steve and Bruce are due special thanks for extended discussions of both the data and its implications; so are my co-workers Neil Perl, Jim Workman, and Ken Burrell, for reducing PEACE data to forms from which conclusions more readily follow.

REFERENCES CITED

- Beyer, L.A., Ristvet, B.L., and Oberste-Lehn, D., Chapter 8, Preliminary density and porosity data and field techniques of borehole gravity surveys, OAK crater; 28 p., 4 figs. 10 tpls; in Henry, T.W., and Wardlaw, B.R., eds., Pacific Enewetak Atoll Crater Exploration (PEACE) Program, Enewetak Atoll, Republic of the Marshall Islands; Part 3: Stratigraphic analysis and other geologic and geophysical studies in vicinity of KOA and OAK craters: U.S. Geological Survey Open-File Report 86-555.
- Halley, R.B., Slater, R.A., Shinn, E.A., Folger, D.W., Hudson, J.H., Kindinger, J.L., and Roddy, D.J., 1986, Observations of OAK and KOA craters from the submersible; 32 p., 13 figs., 1 appendix; in Folger, D.W., ed., Sea-floor observations and subbottom seismic characteristics of OAK and KOA craters, Enewetak Atoll, Marshall Islands: U.S. Geological Survey Bulletin 1678.
- Melzer, L.S., 1986, Chapter 7, Downhole geophysical logs; 32 p., 16 figs., 7 tpls., in Henry, T.W., and Wardlaw, B.R., eds., Pacific Enewetak Atoll Crater Exploration (PEACE) Program, Enewetak Atoll, Republic of the Marshall Islands; Part 3: Stratigraphic analysis and other geologic and geophysical studies in vicinity of KOA and OAK craters: U.S. Geological Survey Open-File Report 86-555.
- Pierce, B.O., 1929, A Short Table of Integrals; Third Revised Edition, Ginn and Company, Boston, New York (etc.).
- Slater, R.A., Roddy, D.J., Folger, D.W., Halley, R.B., and Shinn, E.A., 1986, Chapter 13; Additional submersible studies; detailed observations of the sea floor of OAK, KOA, and MIKE craters; 153 p., 2 tpls., 4 pls.; in Henry, T.W., and Wardlaw, B.R., eds., Pacific Enewetak Atoll Crater Exploration (PEACE) Program, Enewetak Atoll, Republic of the Marshall Islands; Part 3: Stratigraphic analysis and other geologic and geophysical studies in vicinity of KOA and OAK craters: U.S. Geological Survey Open-File Report 86-555.
- Soo, S.L., 1967, Chapter 5; in Fluid Dynamics of Multiphase Systems; Blaisdell Publishing Company, Division of Ginn and Company, Waltham, Massachusetts, Toronto, London.
- Tremba, E.L., and Ristvet, B.L., 1986, Chapter 4; X-ray diffraction mineralogy; 49 p., 11 figs., 35 tpls., in Henry, T.W., and Wardlaw, B.R., eds., Pacific Enewetak Atoll Crater Exploration (PEACE) Program, Enewetak Atoll, Republic of the Marshall Islands; Part 3: Stratigraphic analysis and other geologic and geophysical studies in vicinity of KOA and OAK craters: U.S. Geological Survey Open-File Report 86-555.

Wardlaw, B.R., and Henry, T.W., 1986b, Chapter 14; Geologic interpretation of OAK and KOA craters; 39 p., 21 figs., 2 tbls.; in Henry, T.W., and Wardlaw, B.R., eds., Pacific Enewetak Atoll Crater Exploration (PEACE) Program, Enewetak Atoll, Republic of the Marshall Islands; Part 3: Stratigraphic analysis and other geologic and geophysical studies in vicinity of KOA and OAK craters: U.S. Geological Survey Open-File Report 86-555.

Werth, G., and Randolph, P., 1966, The Salmon seismic experiment: Journal of Geophysical Research, v. 71, no. 14, p. 3405-3413.

APPENDIX 6-1

This appendix contains (1) all PEACE density profiles measured in the OAK area, with (2) plots of the fits made to those profiles as part of the work reported here. Also presented are (3) tables of coefficients for the piecewise linear function used to fit all profiles. That function is defined as follows:

$$\rho = [(z-z_j) \rho_{j+1}^- + (z_{j+1}-z) \rho_j^+] / (z_{j+1} - z_j); j = 1, 2, \dots, J \quad \text{Eq. (11)}$$

where ρ and z denote density and depth, respectively. For the BHG profiles [received as step-functions from L.A. Beyer, written communication, May 15, 1987]; see Chapter 2, this Report], ρ_j^+ and ρ_{j+1}^- have the same value $\rho_{j+1/2}$. Otherwise, $\rho_j^- = \rho_j^+ = \rho_j$, and (p_j, z_j) gives the coordinates of an endpoint of either two or one straight-line segments of the complete function. Specifically, for $j \neq 1$ or J , a segment runs from (ρ_{j-1}, z_{j-1}) to (ρ_j, z_j) , and another from (ρ_j, z_j) to (ρ_{j+1}, z_{j+1}) ; the single segment for $j=1$ runs from (ρ_1, z_1) to (ρ_2, z_2) , and the single segment for $j=J$ connects (ρ_J, z_J) to (ρ_{J+1}, z_{J+1}) .

The measured BHG profiles, in graphic form, comprise the first exhibit below (figs. 6-11 to 6-16). In each case, for ready comparison, a graph of the density-function fit to a given profile [Eq. (11)] is shown next to it, with the pair on identical scales. Then, in exactly the same format, a set of figures (6-17 to 6-26) follows in which appear all the profiles derived from γ - γ logging, together with the density function fit to each. Next, on a single page (tbl. 6-7), come all the (ρ_j, z_j) -points that specify the functions fit to BHG profiles (points supplied by the tables of Chapter 2 of this report). A corresponding table for fits to all the γ - γ profiles comes last (tbl. 6-8). The latter table was compiled by measuring coordinates from the profiles themselves, having overlain them with thin graph paper; thus, at the outset, our measures of density and depth, denoted "DIV" in the tables, were a pair of coordinates read off graph paper. Conversion was made from DIV to g/cc, and from DIV to ft, by means of the following formulas:

$$\text{density (g/cc)} = Q + (\text{DIV} - Y_0)/S; \quad \text{depth (ft)} = A + B(\text{DIV} - X_0)/C \quad \text{Eq. (12)}$$

Values of Q , Y_0 , S , A , B , X_0 , and C are given for each profile in Table 6-8.

BOREHOLE CAVITY SURVEY: HOLE OOR-17

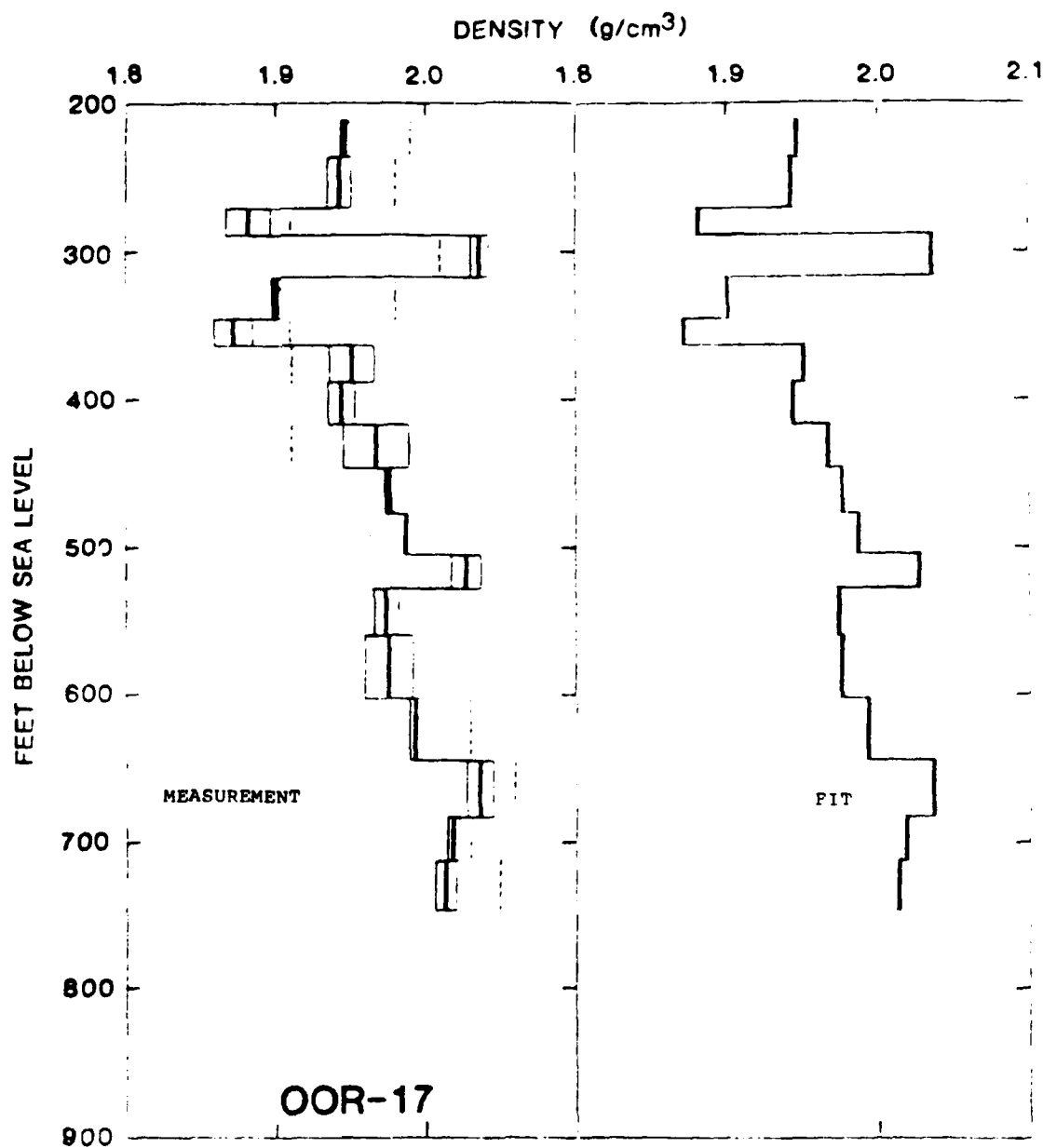


FIGURE 6-11. -- Left: profile of density vs. depth from BHG logging in control hole OOR-17, as received. Right: plot of broken-straight-line fit [Eq. (11)] to profile at left. The left- and right-hand plot scales are identical.

BOREHOLE GRAVITY SURVEY: HOLE OSR-21

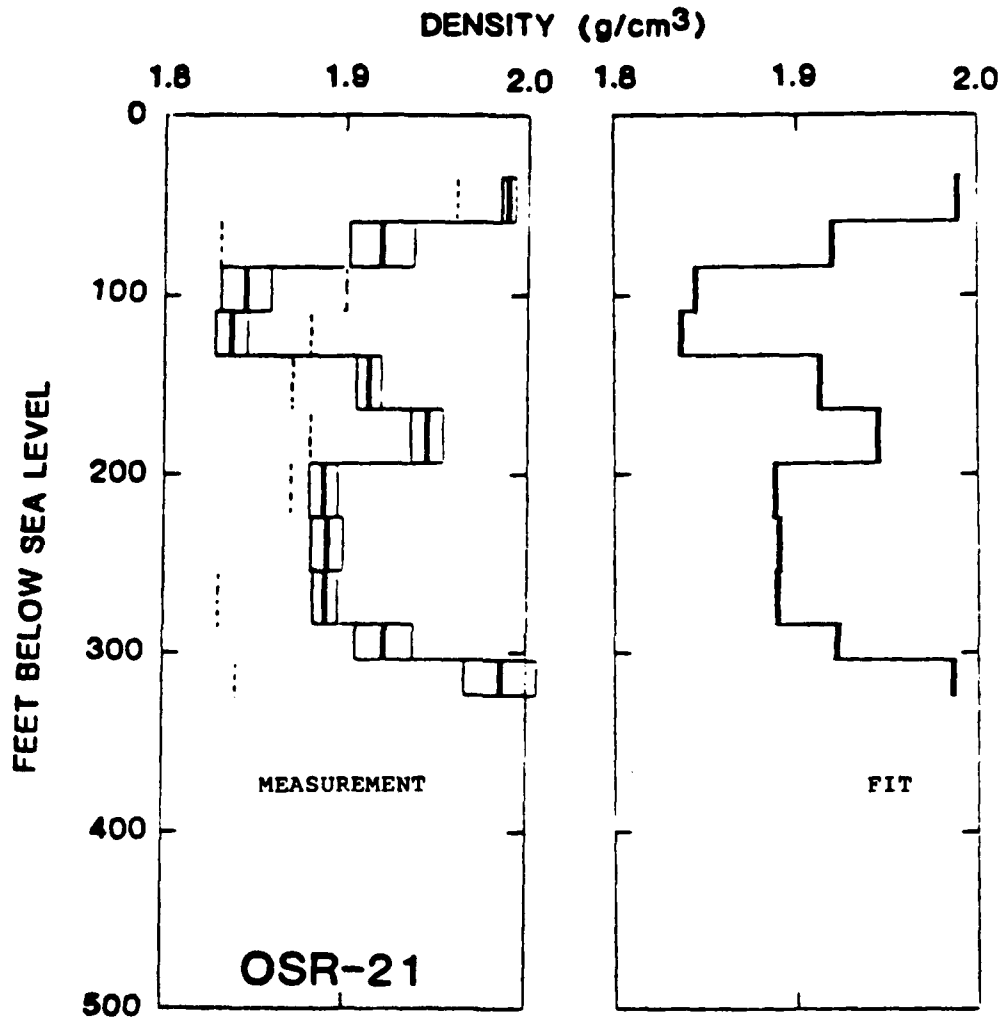


FIGURE 6-12. -- Left: profile of density vs. depth from BHG logging in control hole OSR-21, as received. Right: plot of broken-straight-line fit [Eq. (11)] to profile at left. The left- and right-hand plot scales are identical.

BOREHOLE GRAVITY SURVEY: HOLE ORT-20

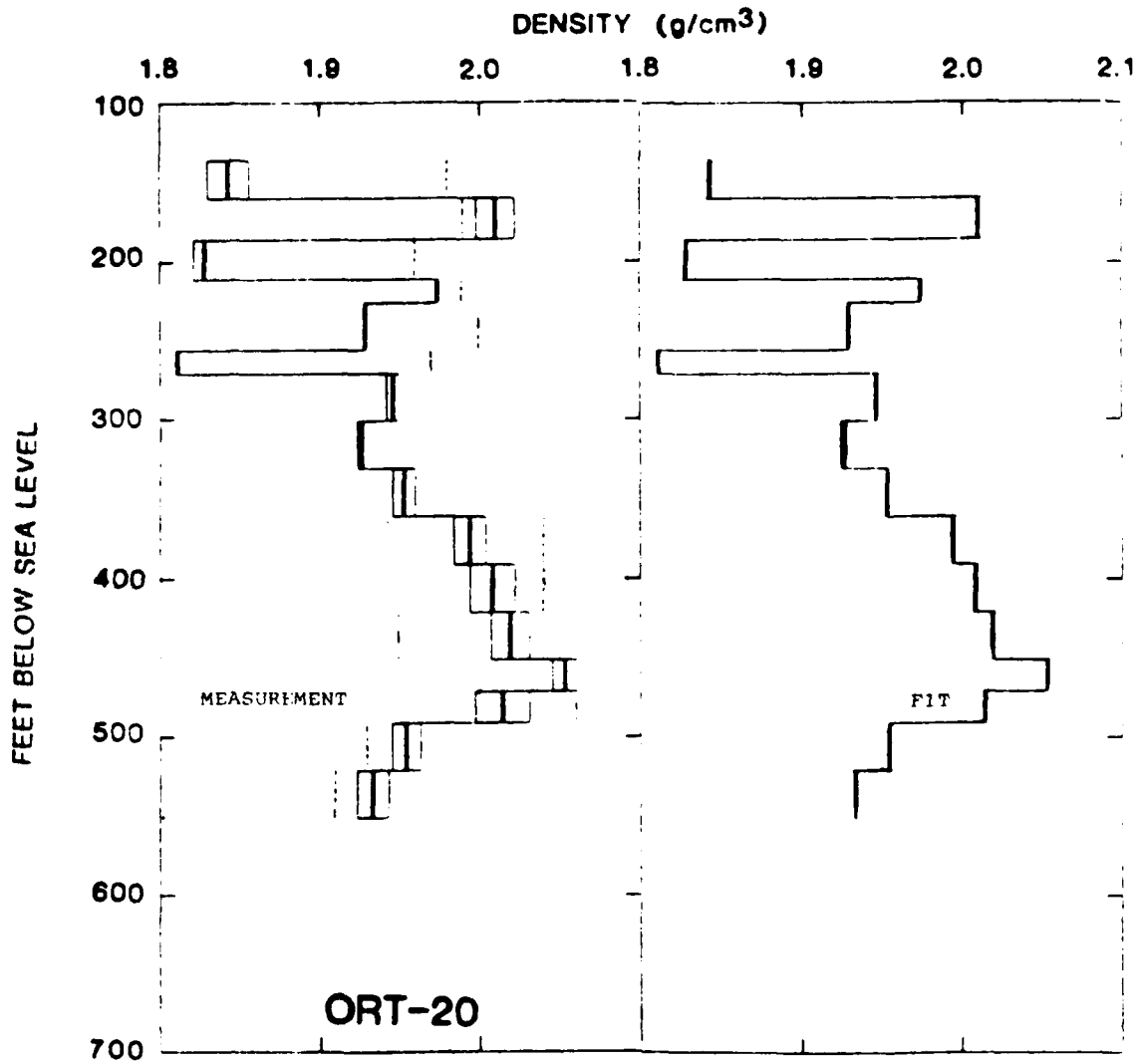


FIGURE 6-13. -- Left: profile of density vs. depth from BHG logging in crater hole ORT-20, as received. Right: plot of broken-straight-line fit [Eq. (11)] to profile at left. The left- and right-hand plot scales are identical.

BOREHOLE GRAVITY SURVEY: HOLE OQT-19

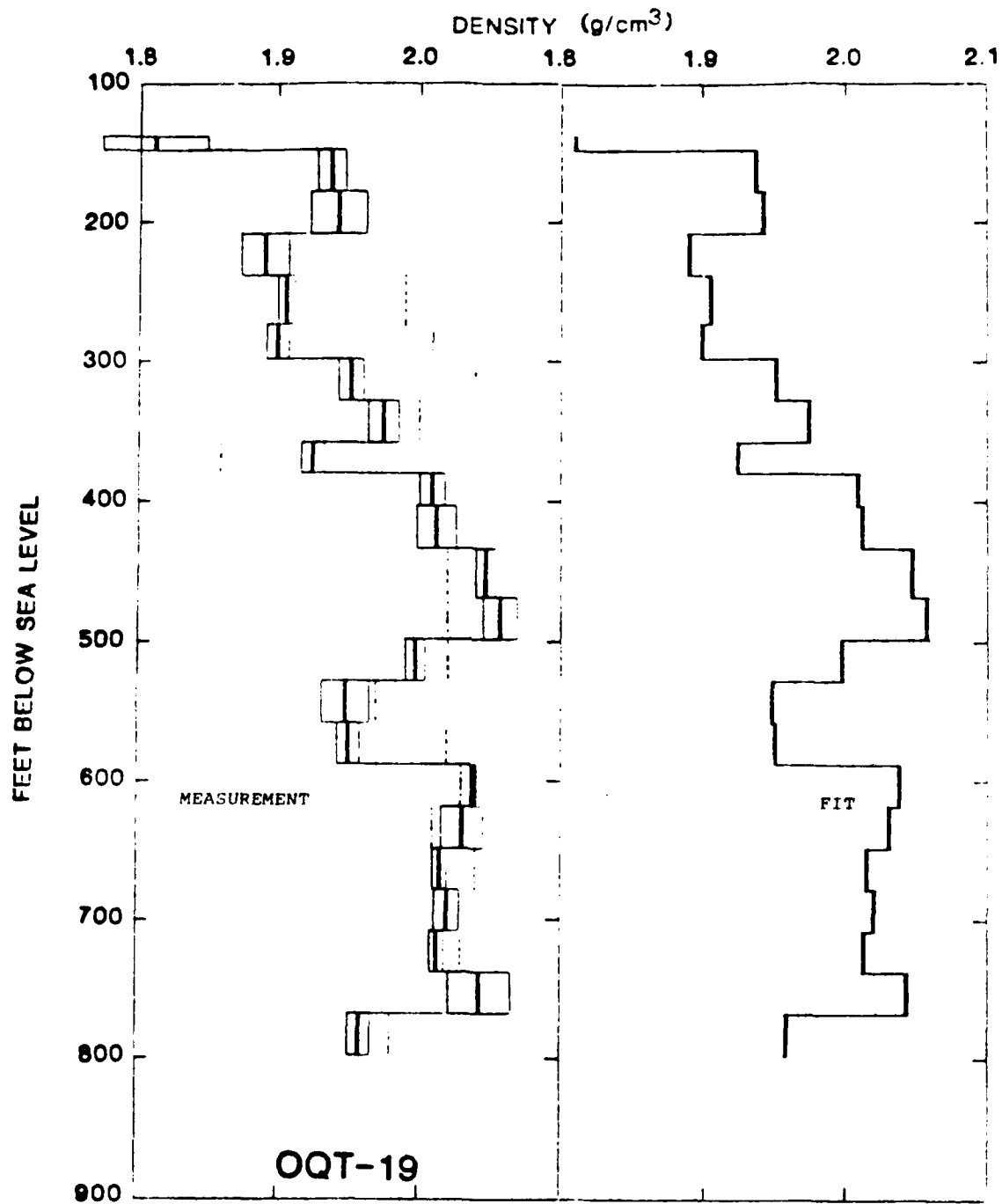


FIGURE 6-14. -- Left: profile of density vs. depth from BHG logging in crater hole OQT-19, as received. Right: plot of broken-straight-line fit [Eq. (11)] to profile at left. The left- and right-hand plot scales are identical.

BOREHOLE GRAVITY SURVEY: HOLE OTG-23

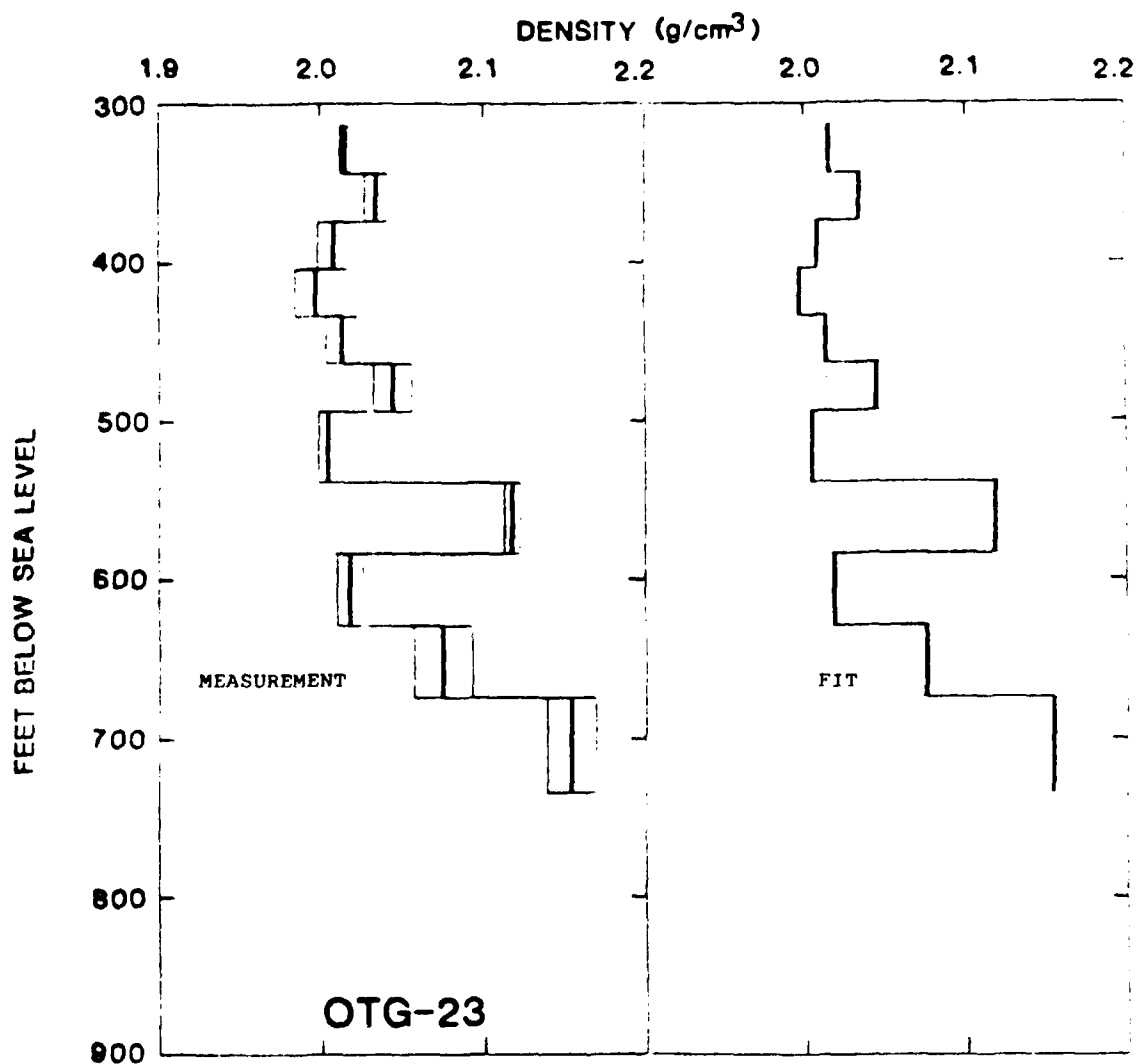


FIGURE 6-15. -- Left: profile of density vs. depth from BHG logging in crater hole OTG-23, as received. Right: plot of broken-straight-line fit [Eq. (11)] to profile at left. The left- and right-hand plot scales are identical.

BOREHOLE GRAVITY SURVEY: HOLE OPZ-18

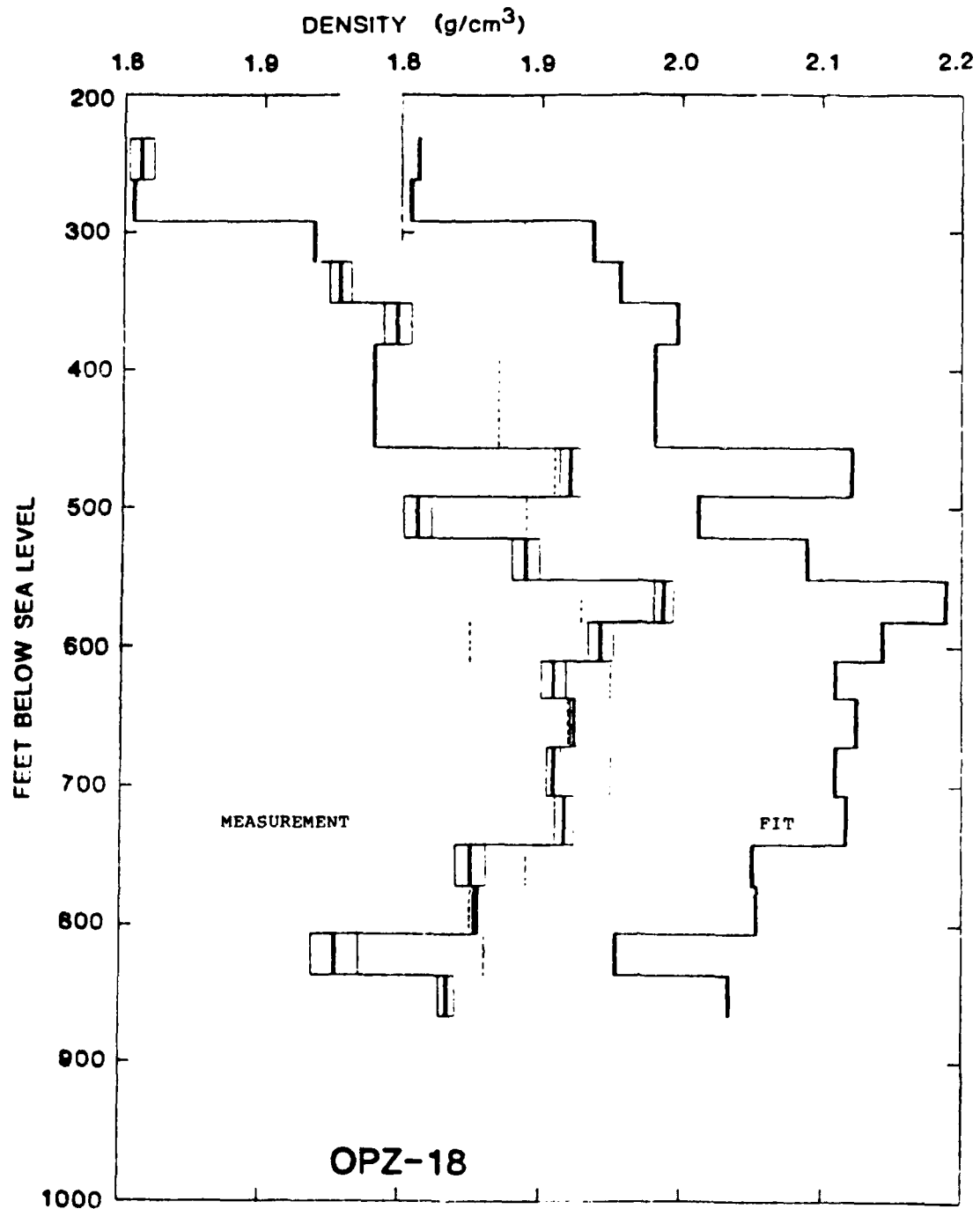


FIGURE 6-16. -- Left: profile of density vs. depth from BHG logging in crater hole OPZ-18, as received. Right: plot of broken-straight-line fit [Eq. (11)] to profile at left. The left- and right-hand plot scales are identical.

BOREHOLE OOR-17: GAMMA-GAMMA LOGGING

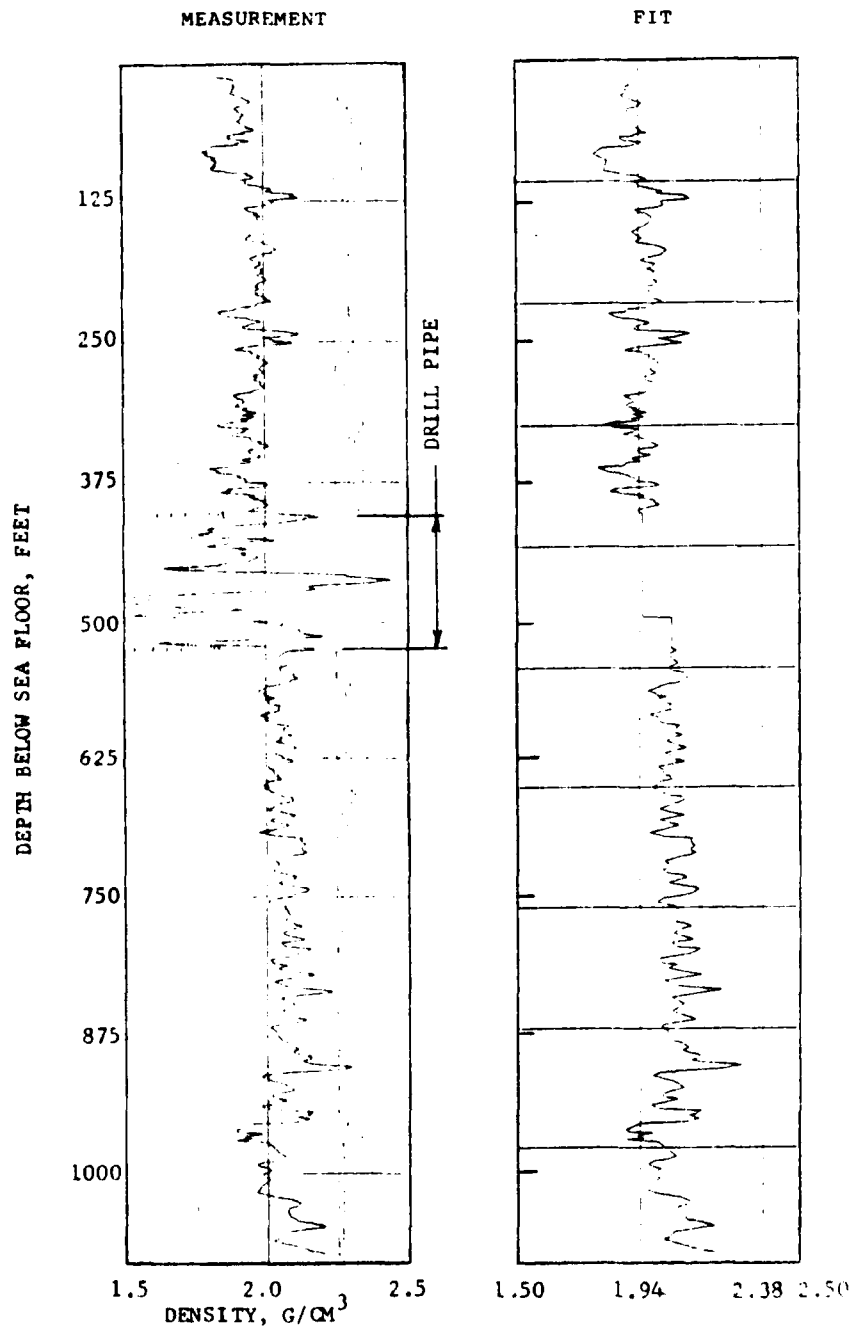


FIGURE 6-17. -- Left: profile of density vs. depth from γ - γ logging in control hole OOR-17, at .70 times the scale of the plot as received. Right: plot of broken-straight-line fit [Eq. (11)] to profile at left. The left- and right-hand plot scales are identical.

BOREHOLE OSR-21: GAMMA-GAMMA LOGGING

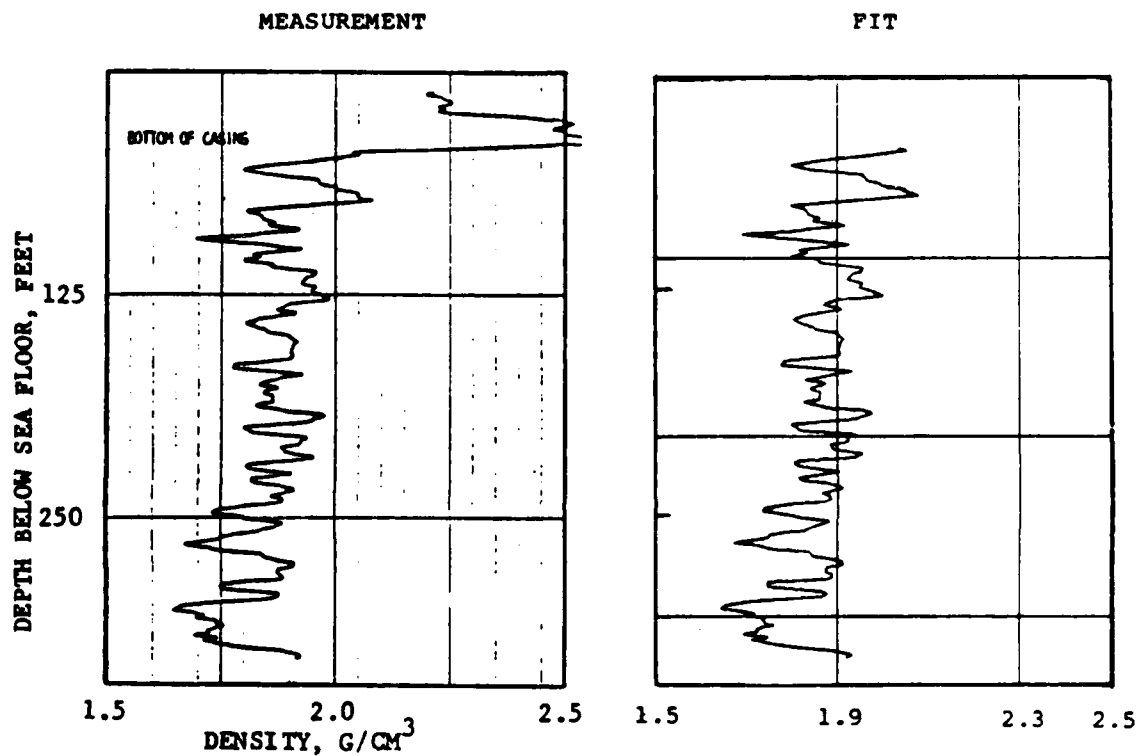


FIGURE 6-18. -- Left: profile of density vs. depth from γ - γ logging in control hole OSR-21, at 1.0 times the scale of the plot as received. Right: plot of broken-straight-line fit [Eq. (11)] to profile at left. The left- and right-hand plot scales are identical.

BOREHOLE ORT-20: GAMMA-GAMMA LOGGING

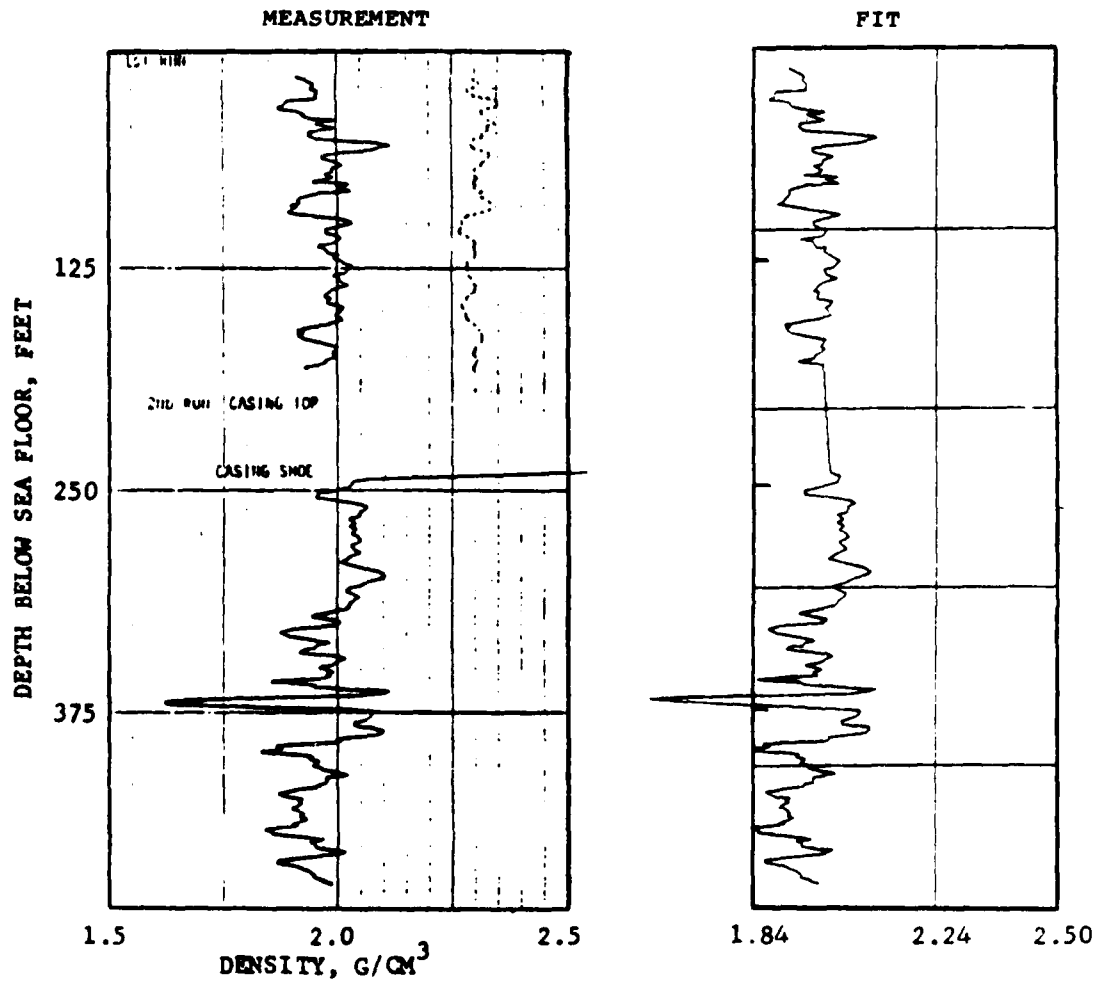


FIGURE 6-19. -- Left: profile of density vs. depth from γ - γ logging in crater hole ORT-20 at 1.0 times the scale of the plot as received. Right: plot of broken-straight-line fit [Eq. (11)] to profile at left. The left- and right-hand plot scales are identical.

BOREHOLE OQT-19: GAMMA-GAMMA LOGGING

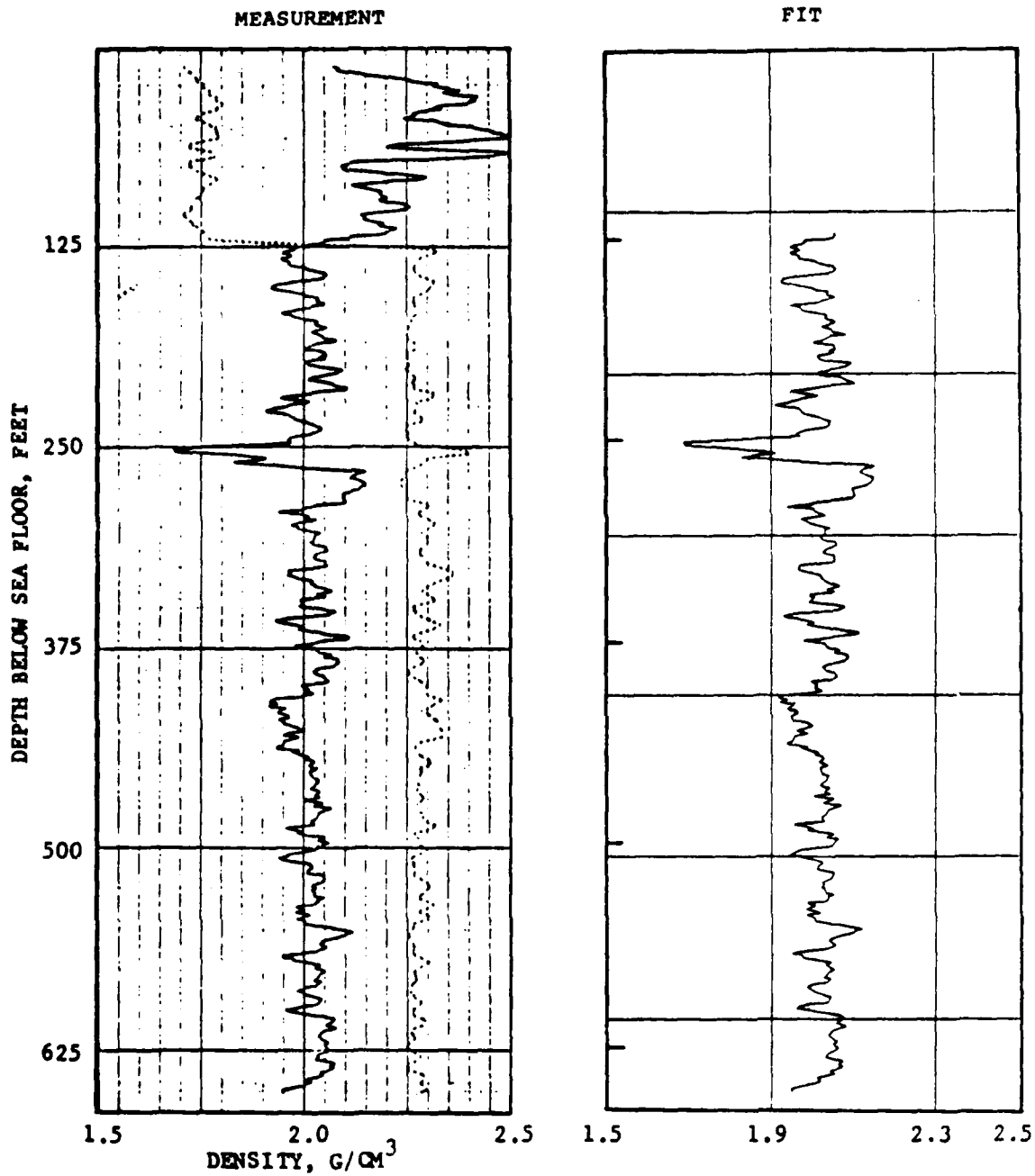


FIGURE 6-20. -- Left: profile of density vs. depth from γ - γ logging in crater hole OQT-19, at 1.0 times the scale of the plot as received. Right: plot of broken-straight-line fit [Eq. (11)] to profile at left. The left- and right-hand plot scales are identical.

BOREHOLE OBZ-4: GAMMA-GAMMA LOGGING

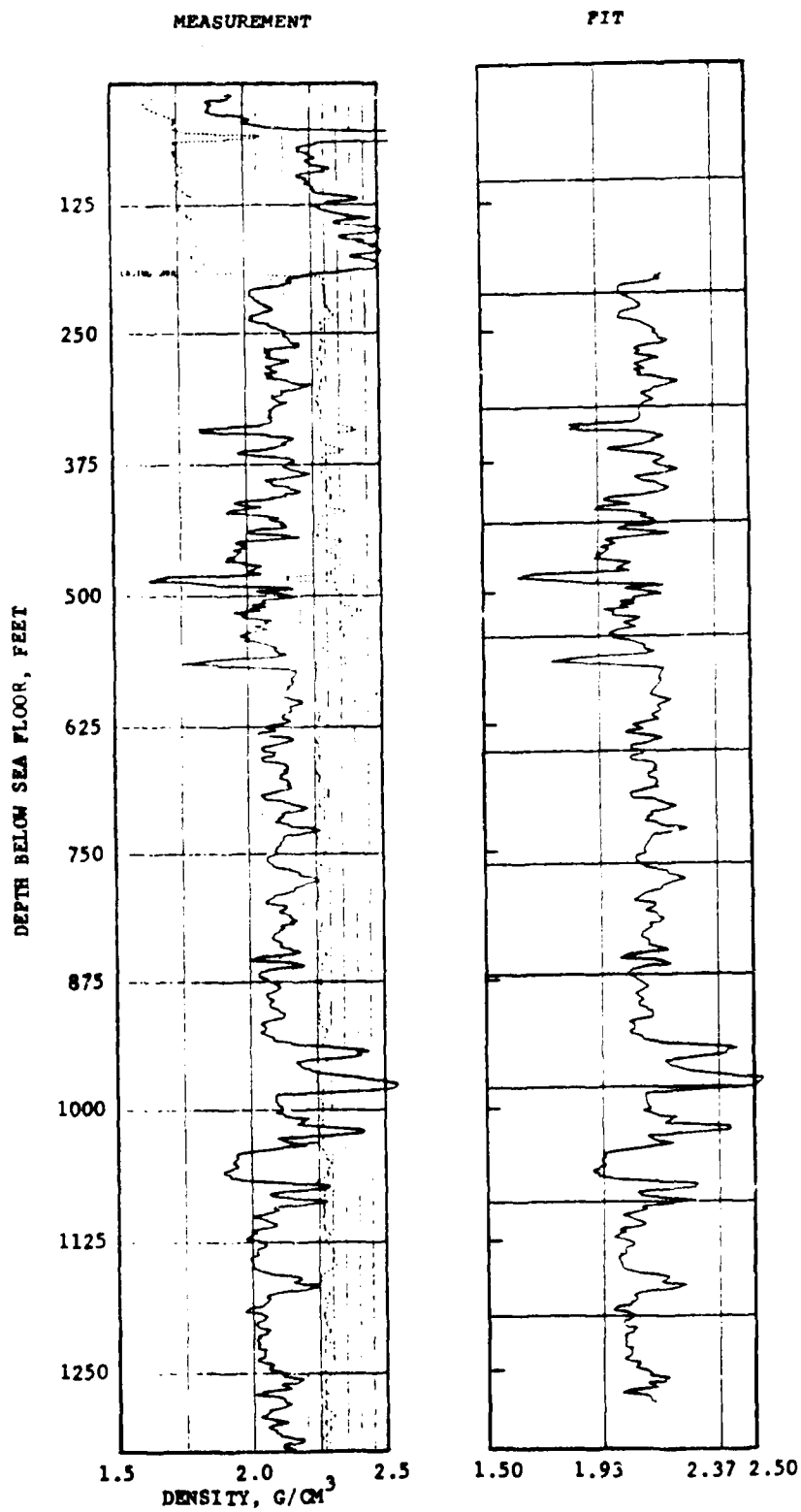


FIGURE 6-21. -- Left: profile of density vs. depth from γ - γ logging in crater hole OBZ-4, at .70 times the scale of the plot as received.
Right: plot of broken-straight-line fit [Eq. (11)] to profile at left. The left- and right-hand plot scales are identical.

BOREHOLE OCT-5: GAMMA-GAMMA LOGGING

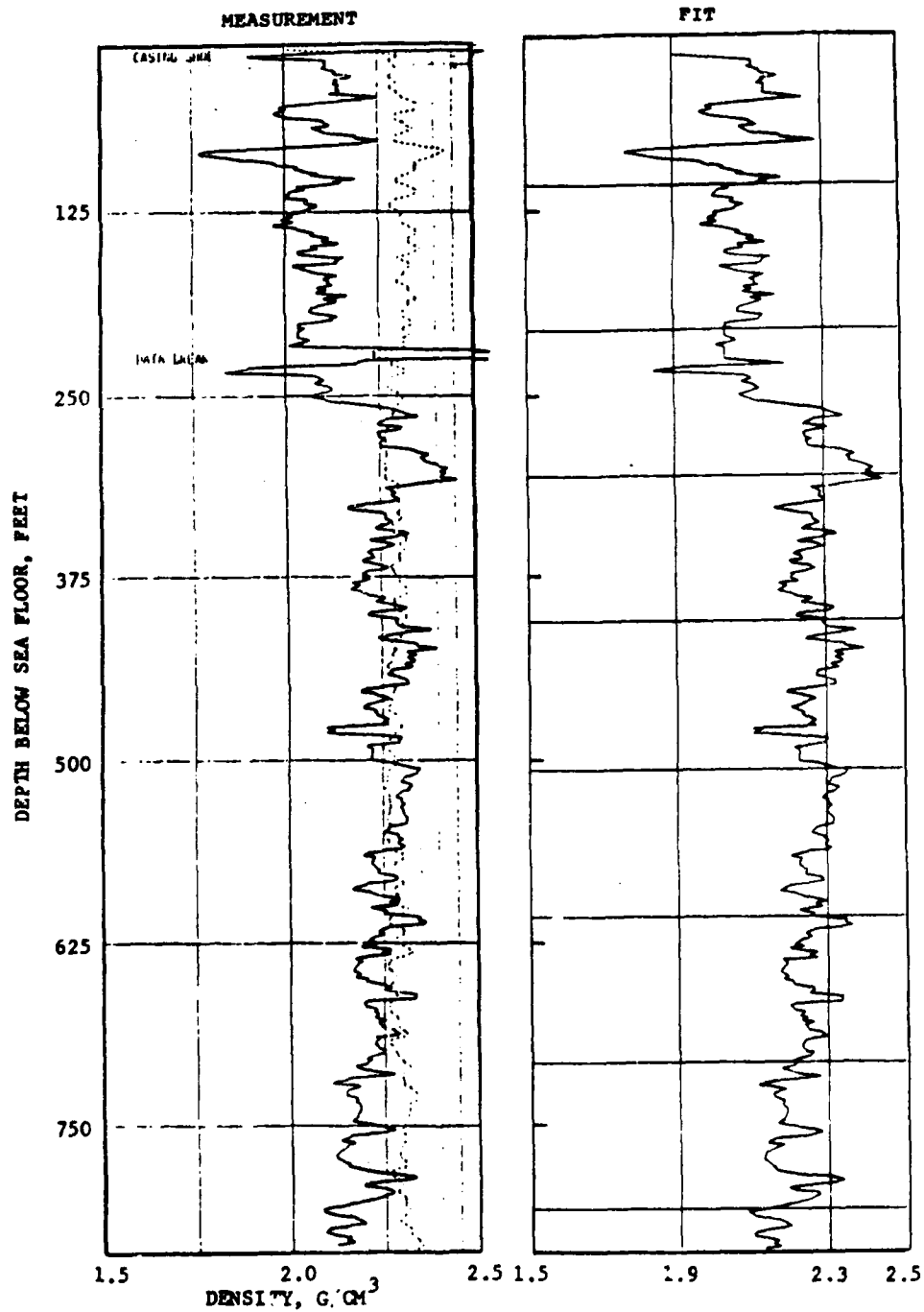


FIGURE 6-22. -- Left: profile of density vs. depth from γ - γ logging in crater hole OCT-5, at 1.0 times the scale of the plot as received. Right: plot of broken-straight-line fit [Eq. (11)] to profile at left. The left- and right-hand plot scales are identical.

BOREHOLE OAR-2A: GAMMA-GAMMA LOGGING

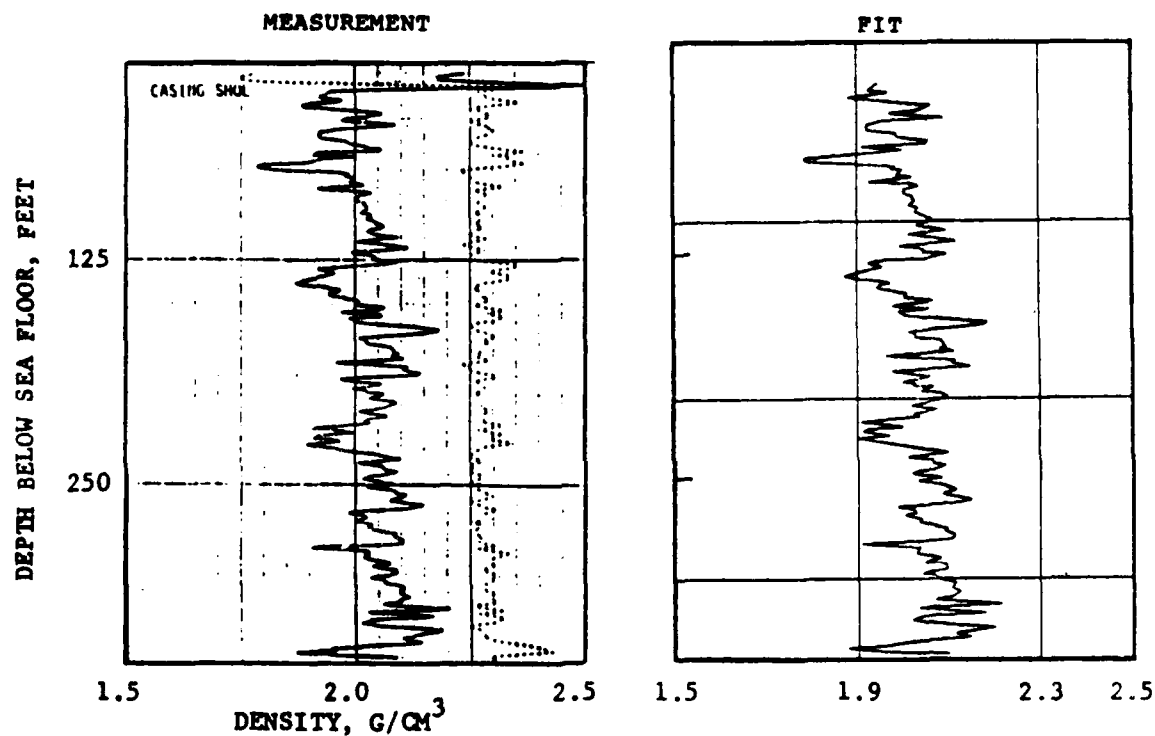


FIGURE 6-23. -- Left: profile of density vs. depth from γ - γ logging in control hole OAR-2A, at 1.0 times the scale of the plot as received. Right: plot of broken-straight-line fit [Eq. (11)] to profile at left. The left- and right-hand plot scales are identical.

BOREHOLE OIT-11: GAMMA-GAMMA LOGGING

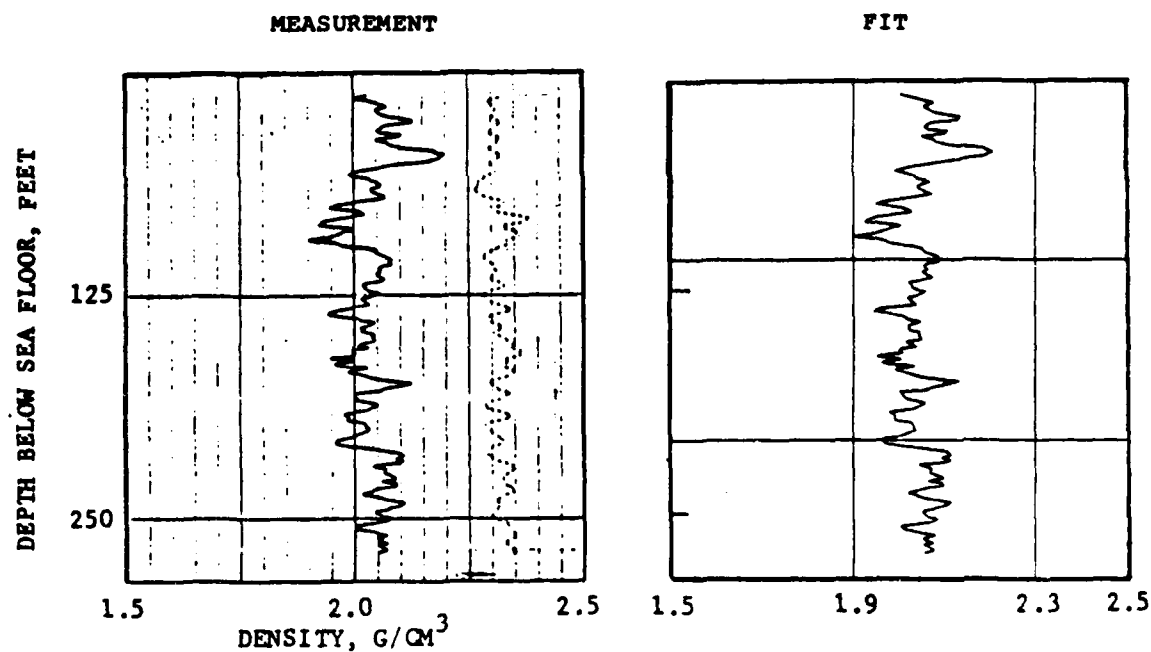


FIGURE 6-24. -- Left: profile of density vs. depth from γ - γ logging in crater hole OIT-11, at 1.0 times the scale of the plot as received. Right: plot of broken-straight-line fit [Eq. (11)] to profile at left. The left- and right-hand plot scales are identical.

BOREHOLE OKT-13: GAMMA-GAMMA LOGGING

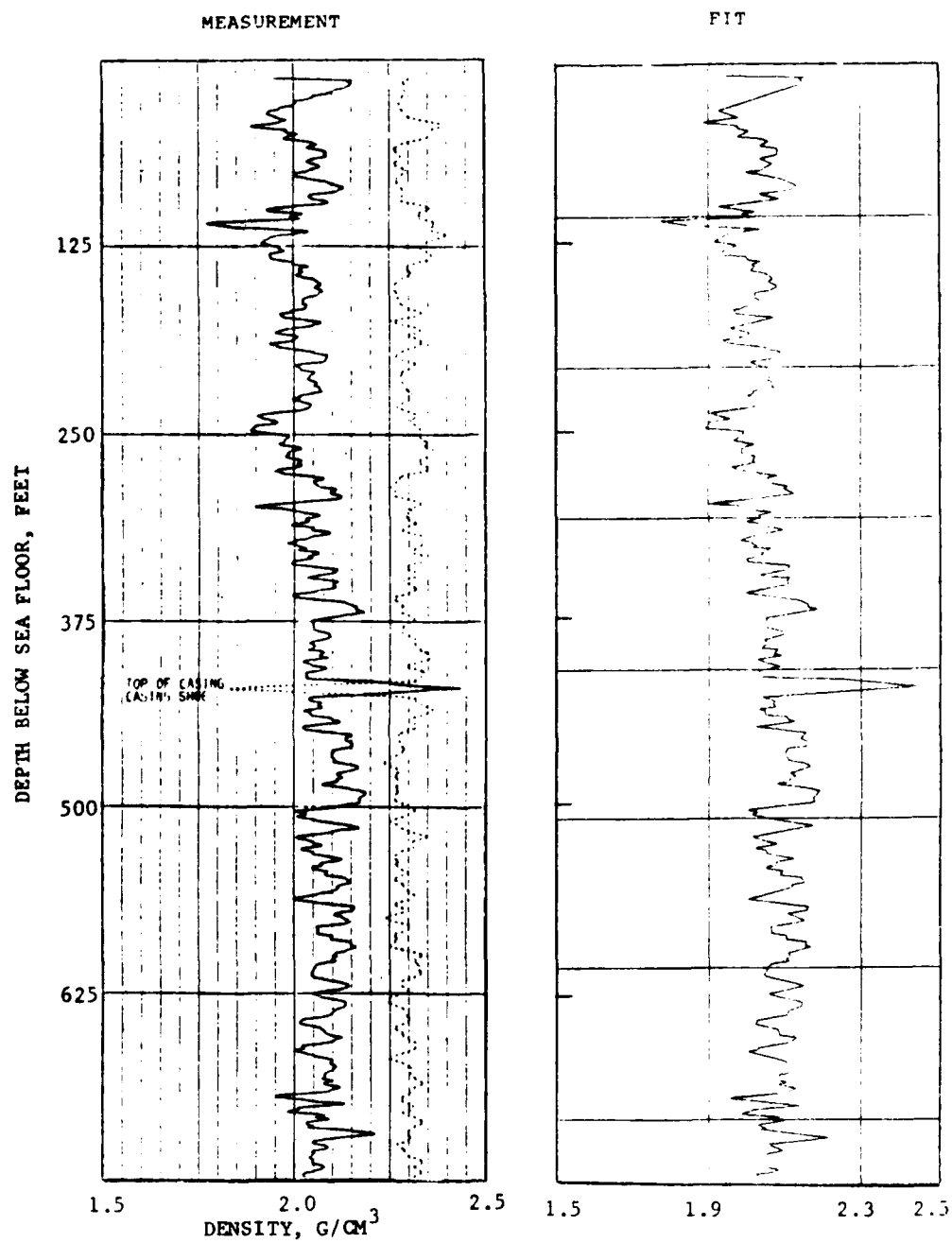


FIGURE 6-25. -- Left: profile of density vs. depth from γ - γ logging in crater hole OKT-13, at 1.0 times the scale of the plot as received. Right: plot of broken-straight-line fit [Eq. (11)] to profile at left. The left- and right-hand plot scales are identical.

BOREHOLE OPZ-18: GAMMA-GAMMA LOGGING

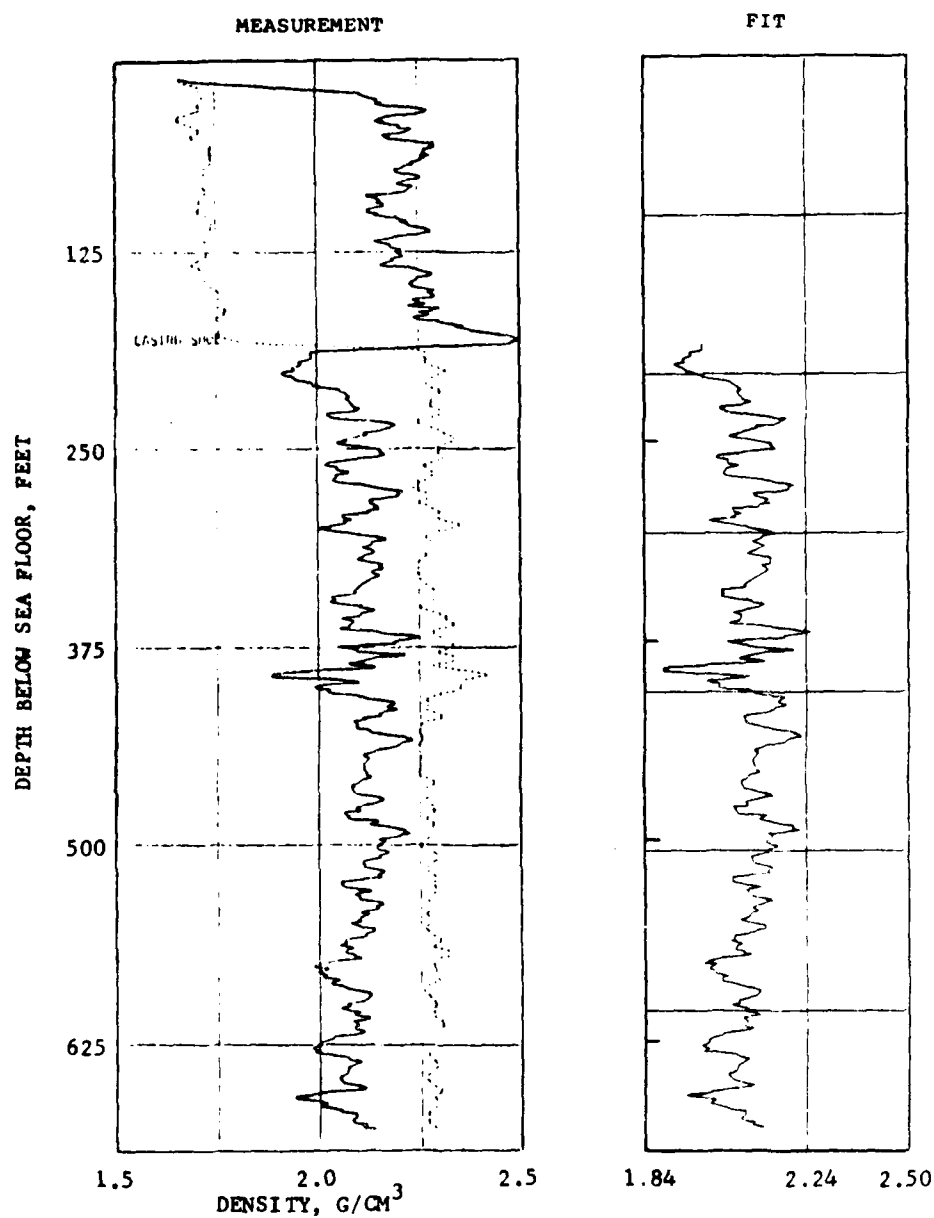


FIGURE 6-26. -- Left: profile of density vs. depth from γ - γ logging in crater hole OPZ-18, at 1.0 times the scale of the plot as received. Right: plot of broken-straight-line fit [Eq. (11)] to profile at left. The left- and right-hand plot scales are identical.

PEACE BOREHOLE UOR-17				PEACE BOREHOLE 0PZ-18				PEACE BOREHOLE 0JF-19				PEACE BOREHOLE 0SH-21				PEACE BOREHOLE 075-23			
J	DEPTH (FT)	DENSITY (GM/CC)		J	DEPTH (FT)	DENSITY (GM/CC)		J	DEPTH (FT)	DENSITY (GM/CC)		J	DEPTH (FT)	DENSITY (GM/CC)		J	DEPTH (FT)	DENSITY (GM/CC)	
1	412	1.987		1	252	1.912		1	138	1.907		1	134	1.949		1	314	2.012	
2	437	1.987		2	262	1.912		2	149	1.907		2	159	1.949		2	344	2.012	
3	457	1.983		3	262	1.907		3	149	1.907		3	159	1.920		3	344	2.012	
4	471	1.983		4	292	1.907		4	179	1.907		4	189	1.920		4	374	2.012	
5	471	1.983		5	292	1.907		5	179	1.907		5	189	1.920		5	374	2.012	
6	489	1.982		6	342	1.917		6	209	1.902		6	209	1.945		6	404	2.012	
7	489	1.982		7	342	1.917		7	209	1.902		7	209	1.945		7	404	2.012	
8	517	1.981		8	352	1.916		8	239	1.900		8	239	1.947		8	434	2.012	
9	517	1.981		9	352	1.916		9	239	1.900		9	239	1.947		9	434	2.012	
10	545	1.972		10	382	1.917		10	279	1.900		10	279	1.947		10	464	2.012	
11	545	1.972		11	382	1.917		11	279	1.900		11	279	1.947		11	464	2.012	
12	563	1.972		12	432	1.962		12	329	1.900		12	329	1.947		12	494	2.012	
13	563	1.972		13	432	1.962		13	329	1.900		13	329	1.947		13	494	2.012	
14	588	1.971		14	472	2.130		14	359	1.904		14	359	1.944		14	524	2.012	
15	588	1.971		15	472	2.130		15	359	1.904		15	359	1.944		15	524	2.012	
16	617	1.969		16	542	2.003		16	389	1.972		16	389	1.944		16	554	2.012	
17	617	1.969		17	542	2.003		17	389	1.972		17	389	1.944		17	554	2.012	
18	646	1.967		18	542	2.086		18	359	1.922		18	359	1.944		18	584	2.012	
19	646	1.967		19	542	2.086		19	359	1.922		19	359	1.944		19	584	2.012	
20	676	1.976		20	592	2.191		20	389	2.009		20	389	1.944		20	614	2.012	
21	676	1.976		21	592	2.191		21	389	2.009		21	389	1.944		21	614	2.012	
22	707	1.967		22	642	2.139		22	403	2.011		22	403	1.922		22	644	2.012	
23	707	1.967		23	642	2.139		23	403	2.011		23	403	1.922		23	644	2.012	
24	735	1.977		24	610	2.107		24	433	2.011		24	433	1.922		24	674	2.012	
25	735	1.977		25	610	2.107		25	433	2.011		25	433	1.922		25	674	2.012	
26	767	1.987		26	637	2.107		26	463	2.011		26	463	1.922		26	704	2.012	
27	767	1.987		27	637	2.107		27	463	2.011		27	463	1.922		27	704	2.012	
28	797	1.976		28	672	2.122		28	493	2.011		28	493	1.922		28	734	2.012	
29	797	1.976		29	672	2.122		29	493	2.011		29	493	1.922		29	734	2.012	
30	827	1.976		30	707	2.107		30	523	2.011		30	523	1.922		30	764	2.012	
31	827	1.976		31	707	2.107		31	523	2.011		31	523	1.922		31	764	2.012	
32	857	1.992		32	742	2.113		32	553	1.945		32	553	1.945		32	794	2.012	
33	857	1.992		33	742	2.113		33	553	1.945		33	553	1.945		33	794	2.012	
34	887	2.036		34	772	2.048		34	583	1.951		34	583	1.929		34	824	2.012	
35	887	2.036		35	772	2.048		35	583	1.951		35	583	1.929		35	824	2.012	
36	913	2.016		36	807	2.052		36	613	2.047		36	613	1.929		36	854	2.012	
37	913	2.016		37	807	2.052		37	613	2.047		37	613	1.929		37	854	2.012	
38	947	2.013		38	837	1.951		38	643	2.030		38	643	1.929		38	884	2.012	
39	947	2.013		39	837	1.951		39	643	2.030		39	643	1.929		39	884	2.012	
40	977	2.013		40	867	2.031		40	673	2.013		40	673	1.929		40	914	2.012	

TABLE 6-7. -- Endpoints of segments of piecewise linear fits [Eq. (11)] to density profiles from borehole gravity surveys.

PEACE BOREHOLE OOR-17					PEACE BOREHOLE OOR-17				
J	DENSITY DEPTH (G/CM ³)	DENSITY DEPTH (G/CM ³)	COMPUTER DEPTH (FT)	COMPUTER DENSITY (G/CM ³)	J	DENSITY DEPTH (G/CM ³)	DENSITY DEPTH (G/CM ³)	COMPUTER DEPTH (FT)	COMPUTER DENSITY (G/CM ³)
1	5.00	23.30	72.72	1.903	101	76.00	42.00	352.17	1.881
2	5.10	23.50	74.74	1.907	102	76.00	42.10	356.84	1.913
3	5.20	23.50	75.75	1.889	103	71.50	42.00	358.19	1.920
4	5.30	23.80	76.31	1.890	104	71.50	42.20	358.62	1.901
5	5.70	22.40	88.83	1.888	105	74.20	42.50	361.65	1.889
6	7.50	22.50	88.61	1.889	106	72.60	42.90	363.35	1.931
7	7.60	23.60	88.90	1.872	107	76.00	44.00	365.07	1.917
8	9.20	46.00	90.76	1.920	108	73.50	47.00	367.22	1.967
9	10.00	46.00	94.22	1.929	109	73.80	48.00	368.51	1.915
10	10.20	23.20	95.06	1.901	110	74.40	36.50	371.00	1.958
11	10.80	22.80	97.65	1.894	111	74.70	43.80	372.30	1.912
12	12.00	24.90	102.81	1.931	112	75.20	25.00	374.55	1.933
13	12.00	46.20	106.75	1.919	113	75.50	40.30	375.81	1.851
14	12.40	23.40	108.43	1.905	114	76.00	16.70	377.84	1.894
15	12.00	46.20	111.41	1.914	115	76.50	20.00	380.11	1.894
16	14.70	25.00	114.42	1.906	116	76.70	45.10	380.97	1.934
17	15.00	45.20	115.71	1.936	117	77.50	24.20	384.41	1.914
18	15.40	27.10	117.45	1.904	118	78.00	21.80	386.54	1.877
19	15.40	27.70	118.74	1.927	119	78.50	25.30	389.71	1.904
20	16.00	26.40	120.01	1.922	120	80.40	49.50	394.44	2.017
21	16.20	41.50	120.87	1.872	121	80.80	26.30	396.16	1.997
22	16.90	41.70	123.88	1.875	122	81.00	26.00	399.46	1.950
23	17.30	26.00	125.60	1.959	123	81.40	45.05	401.17	1.935
24	18.20	23.30	129.87	1.985	124	87.10	25.80	404.13	1.944
25	18.50	17.00	138.76	1.888	125	82.80	28.00	405.48	1.984
26	19.70	16.00	135.92	1.777	126	85.20	21.75	404.46	1.917
27	21.20	18.80	142.37	1.825	127	85.70	25.80	411.07	1.944
28	23.20	18.20	150.97	1.815	128	84.00	45.00	412.36	1.898
29	24.00	42.20	154.40	1.884	129	84.70	22.00	415.37	1.881
30	24.10	25.00	154.83	1.923	130	85.00	16.00	416.66	1.791
31	25.00	27.10	156.70	1.969	131	86.00	19.00	420.96	1.829
32	25.00	160.42	160.42	1.915	132	86.20	22.00	421.82	1.881
33	25.60	25.20	161.28	1.936	133	87.30	44.50	426.55	1.922
34	26.30	25.30	164.29	1.930	134	87.90	24.70	429.15	1.927
35	27.50	30.30	169.45	2.024	135	88.10	28.80	429.99	1.990
36	27.90	29.00	171.17	2.082	136	88.60	29.50	432.13	2.017
37	28.30	34.80	172.89	2.102	137	89.00	27.80	433.85	1.981
38	28.10	36.10	176.35	2.125	138	89.50	21.20	435.14	1.867
39	29.60	38.00	178.46	2.019	139	90.00	19.30	438.15	1.854
40	30.40	38.70	181.92	2.031	140	90.80	26.50	441.59	1.958
41	30.80	39.50	183.64	2.010	141	91.20	25.20	443.31	1.936
42	31.30	24.70	185.79	1.927	142	92.80	46.70	446.75	1.997
43	31.80	25.30	187.96	1.938	143	92.30	48.40	448.84	1.991
44	34.10	27.20	189.25	1.971	144	92.80	49.60	450.19	2.012
45	35.00	48.20	193.10	1.988	145	93.80	46.30	453.63	1.955
46	34.20	27.30	198.26	1.976	146	94.00	25.80	455.85	1.935
47	36.00	24.00	206.00	1.915	147	94.70	46.00	458.36	1.957
48	37.20	26.10	211.15	1.952	148	116.40	26.00	451.65	1.950
49	38.00	26.80	214.54	1.928	149	116.50	32.00	452.04	2.054
50	39.20	49.00	218.44	2.016	150	123.00	32.00	460.01	2.051
51	39.00	31.20	222.44	2.040	151	123.50	35.00	462.18	2.071
52	40.80	30.00	226.43	2.019	152	124.00	31.80	464.35	2.052
53	41.20	47.20	228.78	1.971	153	124.70	31.70	467.34	2.048
54	41.70	25.80	231.36	1.966	154	124.00	33.40	469.93	2.078
55	42.70	26.80	234.80	1.990	155	126.70	31.60	469.94	2.047
56	43.00	48.00	238.24	1.984	156	127.50	32.00	469.87	2.054
57	44.60	46.00	238.67	1.964	157	128.00	34.80	461.52	2.182
58	44.80	48.00	241.25	1.998	158	129.00	35.80	465.82	2.111
59	46.70	48.00	243.40	1.984	159	130.00	43.40	461.12	2.076
60	48.00	47.30	245.55	1.972	160	130.80	31.00	461.41	2.056
61	46.80	89.20	250.28	2.085	161	131.80	37.00	467.84	1.967
62	47.00	88.50	251.89	1.993	162	132.30	78.80	462.01	1.998
63	47.10	87.60	253.72	1.978	163	132.80	48.00	462.14	2.080
64	47.50	46.90	255.44	1.964	164	133.00	31.00	462.02	2.036
65	48.20	27.70	258.45	1.974	165	133.40	49.80	464.74	2.007
66	48.70	87.00	260.60	1.967	166	134.10	49.30	467.75	2.087
67	49.70	87.20	264.89	1.971	167	134.60	82.00	469.90	2.094
68	50.00	89.20	266.18	2.005	168	135.00	31.60	461.62	2.047
69	50.60	30.40	268.76	2.026	169	135.50	31.60	463.77	2.047
70	51.00	84.00	270.44	1.964	170	135.70	32.00	464.63	2.054
71	51.00	27.00	273.72	1.967	171	136.40	49.00	467.64	2.082
72	52.00	45.50	276.76	1.907	172	137.00	47.80	464.22	1.978
73	54.70	42.30	277.79	1.884	173	137.50	29.30	464.37	2.007
74	53.00	19.20	279.08	1.832	174	138.00	49.00	464.52	2.082
75	53.90	40.80	282.95	1.866	175	138.70	30.80	467.53	2.019
76	54.10	24.20	283.81	1.919	176	139.30	33.70	460.11	2.083
77	55.80	48.00	287.60	1.984	177	140.00	42.60	463.11	2.067
78	55.50	25.50	289.83	1.930	178	140.00	52.80	464.55	2.067
79	56.20	24.20	292.84	1.919	179	141.20	34.30	468.27	2.091
80	56.50	26.00	294.13	1.970	180	141.80	32.00	468.85	2.054
81	56.90	34.00	295.85	2.088	181	142.60	31.00	464.29	2.036
82	57.30	36.00	297.57	2.123	182	144.00	35.00	470.31	2.104
83	58.00	22.40	300.58	2.061	183	145.20	30.50	473.47	2.028
84	58.20	29.30	301.44	2.007	184	145.80	32.20	478.90	2.057
85	59.20	34.30	305.74	2.093	185	146.80	31.80	480.20	2.050
86	60.00	29.00	309.18	1.935	186	147.00	34.70	483.21	2.100
87	60.60	22.40	311.76	1.888	187	148.20	49.00	488.37	2.002
88	61.00	46.00	313.48	1.950	188	148.90	30.30	491.38	2.024
89	61.50	26.40	315.43	1.957	189	149.60	30.30	495.25	2.024
90	61.60	27.70	316.06	1.979	190	150.00	31.50	496.11	2.045
91	62.30	27.30	319.07	1.972	191	150.80	32.80	499.55	2.054
92	62.50	28.80	319.92	1.990	192	151.30	49.30	501.70	2.007
93	63.40	28.50	323.79	2.010	193	152.70	48.20	507.72	1.988
94	64.60	27.50	326.95	1.978	194	154.20	31.80	514.16	2.050
95	65.30	29.00	331.96	2.000	195	154.30	34.00	514.59	2.088
96	66.00	26.50	334.97	1.950	196	155.10	34.50	518.03	2.097
97	66.90	26.80	338.84	1.964	197	157.00	29.50	526.20	2.007
98	67.00	46.10	339.27	1.986	198	158.30	30.60	531.79	2.099
99	68.30	48.60	344.86	1.995	199	159.20	49.30	535.46	2.007
100	69.50	26.00	350.02	1.950	200	160.40	33.50	540.82	2.080

TABLE 6-8. -- Endpoints of segments of piecewise linear fits [Eq. (11)] to density profiles from gamma-gamma logging. Table continues on succeeding pages. Data given for boreholes OOR-17, OSR-21, ORT-20, OQT-19, ORZ-4, OCT-5, OAR-2A, OIT-11, OKT-13, and OPZ-18 in OAK crater and KAR-1 in KOA crater.

TABLE 6-8 (Continued)

PEACE BOREHOLE				PEACE BOREHOLE			
DEPTH, ft		DEPTH, ft		DEPTH, ft		DEPTH, ft	
DENSITY (DMV)	DENSITY (DMV)	COMPUTED DENSITY (DMV)	COMPUTED DENSITY (DMV)	DENSITY (DMV)	DENSITY (DMV)	COMPUTED DENSITY (DMV)	COMPUTED DENSITY (DMV)
201 164.00	27.30	747.70	1.972	301 241.00	35.70	1083.04	2.110
202 162.00	26.40	751.14	2.024	302 241.70	34.90	1084.25	2.104
203 163.20	26.20	752.06	2.124	303 241.31	33.30	1087.77	2.074
204 164.00	25.00	754.38	2.114	304 242.00	33.00	1091.64	2.071
205 165.00	26.70	759.74	2.135	305 242.20	33.50	1092.51	2.074
206 165.00	26.00	761.04	2.123	306 243.10	34.90	1096.37	2.080
207 166.00	26.00	764.89	2.123	307 243.51	34.90	1098.08	2.104
208 166.30	27.00	766.16	2.140	308 243.60	35.40	1099.37	2.106
209 166.70	25.70	767.50	2.110	309 243.90	36.10	1099.80	2.125
210 167.00	26.00	769.19	2.085	310 244.20	36.10	1101.00	2.134
211 168.00	26.00	773.40	2.026	311 244.50	36.90	1102.81	2.173
212 168.50	21.30	775.64	2.042	312 244.80	40.20	1103.67	2.196
213 169.00	21.50	779.53	2.042	313 245.10	40.60	1104.34	2.202
214 169.00	20.00	781.23	2.019	314 245.30	37.70	1106.68	2.126
215 170.00	21.00	784.67	2.034	315 245.70	36.30	1109.69	2.045
216 171.00	20.00	786.94	2.008	316 246.20	32.70	1110.98	2.061
217 171.50	25.00	788.54	2.106	317 246.50	32.40	1111.41	2.054
218 172.60	21.10	793.27	2.038	318 246.60	31.90	1112.77	2.047
219 173.00	26.70	797.57	2.135	319 246.80	31.60	1114.56	2.045
220 174.00	27.40	799.24	2.117	320 247.10	31.50	1116.28	2.024
221 174.10	26.40	802.30	2.022	321 247.50	30.30	1117.43	2.022
222 175.00	25.00	804.84	2.046	322 247.80	32.00	1119.15	2.034
223 176.00	20.20	807.05	2.022	323 248.00	33.90	1121.73	2.087
224 176.00	20.00	810.67	2.002	324 248.10	34.20	1122.16	2.092
225 177.00	22.70	814.34	2.066	325 248.40	35.40	1124.74	2.116
226 179.00	23.00	822.50	2.067	326 249.70	37.10	1126.40	2.142
227 180.00	24.30	829.30	2.093	327 250.20	40.70	1129.04	2.204
228 181.00	26.00	832.02	2.120				
229 181.00	26.00	834.81	2.085				
230 182.30	22.20	838.41	2.130				
231 183.10	26.00	844.43	2.040				
232 184.50	21.70	846.54	2.071				
233 185.00	23.00	850.80	2.114				
234 186.00	23.50	852.60	2.114				
235 186.00	23.50	854.33	2.019				
236 187.50	23.50	855.93	2.071				
237 188.00	23.50	857.22	2.036				
238 189.50	23.00	858.84	2.157				
239 189.50	23.00	860.97	2.067				
240 190.00	22.00	864.19	2.067				
241 191.00	22.00	866.00	2.227				
242 191.00	21.70	868.45	2.046				
243 192.00	21.70	868.45	2.094				
244 193.00	22.30	872.63	2.059				
245 193.00	22.30	874.16	2.040				
246 194.00	22.30	876.00	2.039				
247 194.00	22.30	878.15	2.032				
248 195.00	22.30	880.45	2.030				
249 195.00	22.30	882.16	2.037				
250 196.00	22.30	884.02	2.148				
251 197.00	22.30	887.77	2.123				
252 197.00	22.30	890.42	2.137				
253 198.00	22.30	892.77	2.235				
254 198.00	22.30	894.01	2.010				
255 199.00	22.30	896.02	1.901				
256 199.00	22.30	897.41	2.061				
257 200.00	22.30	899.00	2.059				
258 200.00	22.30	900.16	2.019				
259 201.00	22.30	901.36	2.021				
260 201.00	22.30	902.51	2.071				
261 202.00	22.30	903.75	2.019				
262 202.00	22.30	905.00	1.976				
263 203.00	22.30	907.01	1.990				
264 203.00	22.30	908.06	2.157				
265 203.00	22.30	909.07	2.140				
266 204.00	22.30	910.79	2.104				
267 204.00	22.30	912.31	2.149				
268 205.00	22.30	913.95	2.087				
269 205.00	22.30	915.67	1.991				
270 205.00	22.30	917.43	1.986				
271 206.00	22.30	919.24	1.986				
272 206.00	22.30	921.07	1.986				
273 207.00	22.30	922.89	1.927				
274 207.00	22.30	924.73	1.950				
275 208.00	22.30	926.59	1.888				
276 208.00	22.30	928.44	2.002				
277 209.00	22.30	930.31	2.049				
278 209.00	22.30	932.16	2.033				
279 210.00	22.30	934.02	1.995				
280 210.00	22.30	935.89	1.967				
281 211.00	22.30	937.75	1.984				
282 211.00	22.30	939.61	1.984				
283 212.00	22.30	941.47	1.984				
284 212.00	22.30	943.31	1.984				
285 213.00	22.30	945.16	1.984				
286 213.00	22.30	947.00	1.984				
287 214.00	22.30	948.84	1.984				
288 214.00	22.30	950.67	1.984				
289 215.00	22.30	952.51	1.984				
290 215.00	22.30	954.34	1.984				
291 216.00	22.30	956.16	1.984				
292 216.00	22.30	957.99	1.984				
293 217.00	22.30	959.81	1.984				
294 217.00	22.30	961.64	1.984				
295 218.00	22.30	963.46	1.984				
296 218.00	22.30	965.28	1.984				
297 219.00	22.30	967.09	1.984				
298 219.00	22.30	968.91	1.984				
299 220.00	22.30	970.72	1.984				
300 220.00	22.30	972.54	1.984				

YU = 0.51
 XU = 0.51
 1.00 1.30 57.60
 30.00 100.20 500.00 116.30

TABLE 6-8 (Continued)

PEACE FORMHOLE OSR-21					PEACE FORMHOLE OSR-21				
J	DIGITIZED DEPTH, A (DIV)	DIGITIZED DENSITY, Y (DIV)	COMPUTED DEPTH (FT)	COMPUTED DENSITY (GM/CC)	J	DIGITIZED DEPTH, A (DIV)	DIGITIZED DENSITY, Y (DIV)	COMPUTED DEPTH (FT)	COMPUTED DENSITY (GM/CC)
1	10.00	30.70	130.64	1.833	101	61.90	19.00	333.92	1.798
2	10.30	30.00	131.44	1.809	102	62.10	19.30	334.71	1.806
3	11.00	29.00	134.50	1.939	103	62.60	20.00	336.47	1.876
4	11.60	28.70	136.94	1.871	104	63.00	20.30	337.45	1.881
5	12.30	19.00	139.69	1.798	105	63.50	22.00	340.19	1.805
6	12.90	21.60	142.03	1.839	106	64.00	21.00	342.15	1.829
7	13.60	20.00	144.74	1.955	107	64.30	18.00	343.32	1.782
8	14.30	20.60	148.30	1.964	108	64.60	16.00	344.50	1.751
9	14.90	31.00	149.67	1.992	109	65.00	15.00	346.06	1.748
10	15.20	31.00	151.04	1.998	110	65.00	11.00	349.20	1.672
11	15.60	24.90	152.61	2.047	111	66.00	14.50	350.76	1.727
12	15.90	24.60	153.59	2.042	112	66.70	16.00	352.72	1.751
13	16.70	26.00	156.92	2.077	113	67.10	21.70	354.24	1.840
14	17.20	30.00	158.07	1.970	114	67.70	21.90	356.44	1.843
15	18.00	19.00	167.01	1.794	115	68.00	23.00	357.81	1.875
16	18.30	21.00	165.96	1.829	116	68.00	26.20	359.38	1.911
17	18.30	21.90	167.10	1.857	117	69.00	26.20	361.73	1.911
18	19.00	23.00	169.06	1.861	118	69.20	24.00	362.51	1.876
19	20.20	22.00	170.62	1.845	119	70.00	23.70	364.44	1.871
20	21.00	24.50	172.97	1.911	120	70.20	24.60	366.43	1.886
21	21.30	21.20	174.93	1.832	121	70.70	24.60	368.39	1.881
22	21.60	20.00	176.10	1.815	122	71.00	23.00	369.56	1.875
23	22.10	17.20	178.04	1.691	123	71.20	18.00	370.34	1.782
24	23.00	22.00	181.59	1.845	124	71.40	15.00	371.13	1.748
25	23.40	27.00	183.55	1.925	125	72.00	15.70	373.48	1.746
26	24.20	20.20	186.29	1.817	126	72.70	23.00	376.22	1.861
27	24.60	21.20	187.45	1.832	127	73.00	24.00	377.34	1.876
28	25.20	19.00	190.20	1.784	128	73.40	23.10	378.96	1.865
29	25.50	22.70	191.38	1.856	129	74.10	13.70	381.70	1.715
30	26.10	22.40	193.73	1.854	130	74.50	10.20	383.27	1.660
31	26.00	29.00	196.44	1.955	131	75.00	9.10	385.23	1.643
32	27.30	28.30	199.45	1.951	132	75.40	12.00	386.74	1.688
33	27.60	27.70	197.60	1.954	133	75.80	13.00	388.36	1.716
34	28.40	26.00	202.73	1.920	134	76.10	12.60	389.53	1.697
35	29.00	29.00	205.06	1.955	135	76.50	15.20	391.10	1.738
36	29.40	28.70	207.43	1.947	136	77.10	15.40	394.25	1.741
37	30.00	30.70	209.00	1.970	137	77.40	16.50	396.62	1.759
38	31.70	31.00	211.74	1.994	138	78.00	14.20	398.97	1.723
39	32.00	30.00	212.92	1.970	139	78.40	14.40	399.56	1.726
40	32.30	25.50	214.09	1.908	140	78.70	12.30	399.72	1.693
41	32.70	25.30	216.83	1.868	141	79.10	15.00	401.80	1.748
42	32.70	26.00	219.57	1.908	142	79.90	13.60	403.05	1.713
43	33.30	28.00	222.71	1.926	143	79.90	15.40	404.41	1.741
44	34.30	19.30	225.06	1.803	144	80.50	19.00	406.76	1.798
45	34.90	20.80	226.19	1.826	145	81.00	24.50	408.72	1.884
46	35.00	28.00	228.70	1.845	146	81.60	27.40	411.07	1.929
47	35.90	22.40	230.15	1.851	147	82.10	26.70	413.83	1.918
48	36.90	25.30	232.11	1.897					
49	36.00	26.30	236.02	1.912					
50	37.30	26.00	238.00	1.908					
51	38.20	29.70	241.11	1.903					
52	39.20	25.00	245.03	1.904					
53	39.80	20.00	247.35	1.826					
54	40.00	18.00	248.16	1.782					
55	40.60	17.00	250.51	1.779					
56	41.00	22.00	252.00	1.845					
57	41.50	27.30	254.00	1.928					
58	42.00	24.70	255.99	1.887					
59	42.60	21.00	259.13	1.829					
60	43.10	23.00	266.30	1.861					
61	43.30	23.00	261.80	1.873					
62	44.00	21.70	263.61	1.840					
63	44.20	21.80	264.61	1.842					
64	44.50	23.00	265.78	1.861					
65	45.60	23.00	270.89	1.861					
66	46.00	29.70	271.66	1.824					
67	46.70	24.00	274.40	1.876					
68	46.90	24.00	275.18	1.869					
69	47.00	29.00	274.57	1.955					
70	47.50	30.20	277.53	1.975					
71	48.00	29.00	278.64	1.954					
72	48.40	28.00	281.06	1.940					
73	49.00	20.00	285.43	1.820					
74	49.20	19.00	284.14	1.798					
75	50.00	20.30	287.32	1.810					
76	50.40	27.00	288.04	1.923					
77	50.60	28.00	289.67	1.937					
78	50.90	26.00	290.85	1.922					
79	51.60	26.90	293.59	1.922					
80	51.90	24.50	294.76	1.864					
81	52.60	24.40	297.50	1.869					
82	53.20	28.00	299.85	1.951					
83	53.70	28.00	301.81	1.939					
84	54.20	28.20	303.77	1.917					
85	54.60	19.40	305.34	1.804					
86	55.00	20.00	304.90	1.813					
87	55.70	25.70	309.44	1.903					
88	56.60	20.00	313.17	1.813					
89	57.20	20.40	314.74	1.820					
90	57.30	23.30	315.91	1.866					
91	57.80	25.30	317.87	1.900					
92	58.10	26.00	319.04	1.908					
93	58.80	23.20	321.70	1.864					
94	59.10	24.30	322.96	1.881					
95	59.60	24.50	324.92	1.884					
96	60.00	23.30	326.48	1.864					
97	60.20	19.50	327.87	1.804					
98	60.70	16.00	329.22	1.751					
99	60.90	15.00	330.01	1.735					
100	61.20	15.00	331.18	1.735					

TOTAL: S: .00 1.50 63.40
 TOTAL: A: B: C: 30.00 209.00 1.00 .25535467

TABLE 6-8 (Continued)

PEACE BOMB-COLE CRT-20					PEACE BOMB-COLE CRT-20				
Y	DIGITIZED DEPTH, X (DIV)	DIGITIZED DENSITY, Y (DIV)	COMPUTED DEPTH (FT)	CUMMUL DENSITY (LB/CC)	Y	DIGITIZED DEPTH, X (DIV)	DIGITIZED DENSITY, Y (DIV)	COMPUTED DEPTH (FT)	CUMMUL DENSITY (LB/CC)
1	2.00	4.70	119.82	1.917	191	75.80	11.70	409.87	2.027
2	3.00	6.90	123.74	1.951	192	76.20	11.10	407.43	2.017
3	4.50	6.70	126.08	1.968	193	77.10	12.90	410.96	2.046
4	4.90	7.30	128.05	1.958	194	78.80	11.20	417.62	2.019
5	5.90	7.30	131.96	1.958	195	79.00	10.00	418.41	2.000
6	6.10	3.10	132.75	1.892	196	79.90	6.40	421.95	1.943
7	6.90	2.70	135.80	1.885	197	80.40	8.50	423.84	1.976
8	7.20	2.00	137.06	1.874	198	80.60	10.00	426.14	2.000
9	7.50	4.70	138.23	1.917	199	81.60	10.30	429.96	2.005
10	8.20	5.30	140.98	1.926	200	81.20	9.90	427.05	1.998
11	9.00	9.00	144.11	1.997	201	81.60	3.50	428.59	1.898
12	9.30	7.30	145.29	1.958	202	84.10	2.00	430.45	1.874
13	10.10	9.00	148.42	1.997	203	84.70	3.30	432.70	1.895
14	10.80	6.30	144.49	1.942	204	85.30	7.00	436.02	1.948
15	11.00	6.80	151.95	1.940	205	85.70	8.70	438.00	1.956
16	11.50	7.00	154.91	1.953	206	86.00	7.20	439.77	1.951
17	12.20	15.00	156.65	2.079	207	86.40	6.90	439.96	1.929
18	12.60	17.00	158.29	2.113	208	86.50	5.50	439.96	1.912
19	13.20	15.00	160.57	2.079	209	86.50	4.40	440.27	2.000
20	14.00	8.00	163.70	1.969	210	86.50	10.00	445.84	2.016
21	14.20	8.00	165.66	1.969	211	86.50	9.60	448.14	1.994
22	15.20	10.00	168.91	2.014	212	86.50	9.30	449.36	1.987
23	15.70	9.30	170.37	1.992	213	87.20	7.30	450.94	1.958
24	16.30	9.30	172.72	1.992	214	87.90	4.30	453.28	1.932
25	16.50	8.30	173.50	1.973	215	88.30	6.40	454.85	1.977
26	17.10	4.50	175.85	1.992	216	88.60	9.00	456.02	1.988
27	17.40	8.30	177.81	1.973	217	89.30	6.00	458.77	1.855
28	17.70	6.80	178.20	1.950	218	89.80	4.70	460.73	1.948
29	18.00	11.60	179.58	2.025	219	90.10	7.00	461.90	1.953
30	18.40	10.00	180.95	2.000	220	90.60	17.10	464.44	2.112
31	19.00	11.80	183.30	2.028	221	91.40	15.00	467.00	2.087
32	19.20	7.20	184.08	1.956	222	91.70	-12.00	468.17	1.853
33	19.50	4.00	187.82	1.938	223	92.00	-14.20	469.35	1.619
34	20.00	9.90	189.17	1.920	224	93.00	2.00	473.27	1.876
35	21.00	3.70	194.27	1.901	225	93.50	18.00	476.01	2.075
36	21.90	3.20	194.66	1.893	226	94.30	14.70	478.56	2.074
37	22.50	7.00	197.01	1.953	227	94.80	15.00	480.32	2.060
38	23.00	10.00	198.97	2.000	228	95.20	12.30	481.88	2.036
39	23.30	12.10	200.36	2.033	229	95.70	12.40	483.85	2.038
40	23.80	10.00	202.50	2.000	230	96.00	16.00	485.02	2.094
41	24.20	8.30	203.67	1.973	231	96.50	16.30	486.54	2.094
42	24.80	8.30	206.82	1.973	232	96.50	15.00	488.55	2.091
43	25.60	10.20	209.16	2.003	233	97.50	10.50	490.90	2.004
44	26.30	9.50	211.90	1.992	234	98.00	10.40	492.86	2.006
45	26.80	6.30	213.86	1.944	235	98.40	1.40	494.93	1.865
46	26.90	8.00	214.25	1.969	236	98.80	2.20	495.99	1.877
47	27.90	0.70	218.17	1.980	237	99.30	-1.80	497.95	1.830
48	28.00	10.00	218.56	2.000	238	100.00	6.40	500.49	1.943
49	28.50	9.70	220.52	1.995	239	100.30	6.00	501.87	1.937
50	29.00	12.00	225.27	2.031	240	100.70	7.30	503.44	1.958
51	29.80	11.00	229.14	1.997	241	101.90	6.50	505.74	1.945
52	31.00	9.00	235.45	1.983	242	101.30	7.50	506.57	1.941
53	31.80	11.50	235.41	2.024	243	102.70	7.70	508.53	1.966
54	33.00	9.20	238.16	1.987	244	103.70	11.40	511.77	2.022
55	34.00	8.20	242.87	1.972	245	103.20	8.40	513.78	1.975
56	34.80	9.10	242.86	1.986	246	104.00	8.40	516.37	1.975
57	35.20	4.60	245.99	1.978	247	104.20	7.30	517.15	1.958
58	35.50	10.90	247.95	2.014	248	104.50	7.00	518.45	1.953
59	36.20	10.50	250.69	2.000	249	105.30	1.60	521.46	1.868
60	36.50	9.90	251.87	1.998	250	106.00	8.50	524.71	1.895
61	36.50	10.00	255.76	2.013	251	106.20	5.10	524.99	1.823
62	37.30	9.00	257.75	1.964	252	106.50	4.30	526.16	1.914
63	38.00	4.10	260.84	1.910	253	106.80	5.00	527.34	1.921
64	38.10	5.00	262.06	1.921	254	107.30	8.30	528.78	1.968
65	39.10	4.30	262.04	1.919	255	107.70	8.30	530.81	1.914
66	40.00	8.00	269.58	1.981	256	108.30	5.00	533.72	1.895
67	40.00	10.00	269.58	2.000	257	108.60	4.70	534.59	1.917
68	41.00	9.30	273.81	1.989	258	109.00	5.60	535.96	1.931
69	42.00	9.00	274.49	1.990	259	109.50	4.50	537.92	1.914
70	42.00	8.50	277.34	1.976	260	110.30	4.60	538.70	1.899
71	43.50	8.00	279.30	1.975	261	110.70	4.40	539.49	1.912
72	44.10	5.00	281.65	1.934	262	110.40	-3.30	541.45	1.838
73	44.50	9.70	283.22	1.995	263	110.50	.70	541.84	1.854
74	46.00	10.50	283.22	1.995	264	111.00	.70	543.80	1.854
75	46.00	12.00	285.91	2.031	265	112.00	8.00	547.72	1.965
76	46.50	11.50	289.44	2.024	266	112.30	4.00	548.80	1.957
77	47.50	7.00	293.75	1.953	267	114.30	6.70	549.68	1.988
78	48.50	7.00	295.32	1.953	268	114.50	6.70	551.64	1.988
79	49.00	10.00	296.87	2.000	269	115.00	6.70	553.20	1.988
80	49.50	13.50	298.87	2.055	270	115.40	9.00	555.20	1.988
81	50.00	13.50	300.24	2.055	271	115.60	11.00	557.99	2.016
82	50.30	14.10	300.89	2.064	272	116.10	10.00	559.48	2.000
83	50.80	13.10	302.76	2.049	273	116.90	1.70	564.08	1.884
84	50.50	12.90	305.51	2.064	274	117.30	6.50	567.48	1.945
85	50.50	12.50	307.07	2.049	275	117.70	7.90	570.05	1.967
86	50.50	12.50	309.45	2.059	276	118.00	8.00	571.23	1.969
87	50.50	11.60	311.50	2.025	277	118.30	9.10	572.40	1.986
88	50.50	12.60	312.95	2.041					
89	50.50	11.80	315.69	2.028					
90	50.50	12.70	317.26	2.042					
91	50.50	13.20	319.61	2.050					
92	50.50	11.00	321.96	2.028					
93	50.50	13.00	323.80	2.047					
94	50.50	11.70	327.84	2.027					
95	50.50	10.30	331.37	2.003					
96	50.50	15.00	336.07	2.079					
97	50.50	16.30	339.25	2.091					
98	50.50	16.30	339.25	2.091					
99	50.50	13.60	342.73	2.057					
100	50.50	13.00	344.69	2.047					

Y0 = 0.01 10.00 2.00 63.80
 Y0 = 0.01 30.00 226.40 250.00 63.80

TABLE 6-8 (Continued)

PEACE BOREHOLE COT-14					PEACE BOREHOLE COT-14				
J	DISTILLED DEPTH, ft (DIV)	DISTILLED DENSITY, g (DIV)	COMPUTED DEPTH (FT)	COMPUTED DENSITY (GM/CC)	J	DISTILLED DEPTH, ft (DIV)	DISTILLED DENSITY, g (DIV)	COMPUTED DEPTH (FT)	COMPUTED DENSITY (GM/CC)
1	29.00	35.40	238.57	2.057	101	77.90	35.60	430.71	2.060
2	29.70	35.00	241.32	2.050	102	78.40	34.80	432.73	2.045
3	30.00	30.70	242.50	1.983	103	79.00	33.40	435.04	2.020
4	30.50	30.60	244.47	1.981	104	79.50	33.10	437.06	2.032
5	31.00	28.50	246.43	1.948	105	80.00	33.20	440.99	2.054
6	31.50	36.00	248.40	1.972	106	81.00	29.80	442.95	1.964
7	32.00	48.50	250.36	1.944	107	81.80	29.60	444.10	1.965
8	32.40	49.80	251.93	1.969	108	82.50	33.00	448.05	2.019
9	32.90	49.00	253.90	1.970	109	83.00	33.20	450.01	2.022
10	33.20	42.00	255.08	2.083	110	83.70	34.00	453.97	2.035
11	33.70	35.20	257.04	1.975	111	84.00	46.00	455.92	2.064
12	34.10	35.28	258.61	2.055	112	84.90	34.60	458.28	2.035
13	34.50	35.60	260.18	2.060	113	85.20	35.20	459.46	2.057
14	35.00	35.10	262.15	4.052	114	85.60	31.50	461.01	1.995
15	35.50	36.60	264.12	1.981	115	85.90	31.20	462.71	1.991
16	36.00	27.10	266.08	1.929	116	86.00	48.00	462.61	2.083
17	36.40	47.80	268.44	1.975	117	86.40	41.20	464.75	1.991
18	37.00	41.80	271.59	2.000	118	87.10	34.70	466.93	2.044
19	37.80	32.50	273.16	2.011	119	87.60	36.70	468.84	2.077
20	38.00	34.30	273.94	4.039	120	88.10	35.80	470.81	2.063
21	38.50	44.10	275.91	2.036	121	88.70	49.00	473.27	1.956
22	39.00	45.30	277.47	2.055	122	89.00	47.30	474.40	1.929
23	39.40	33.60	279.45	2.028	123	89.00	32.00	478.31	2.001
24	39.70	32.90	280.43	2.017	124	90.00	31.00	479.50	1.987
25	40.30	28.50	282.99	1.948	125	91.00	34.80	482.26	2.047
26	40.60	30.00	283.38	1.972	126	91.70	39.00	485.01	2.114
27	41.00	30.30	285.74	1.976	127	92.00	36.70	486.17	2.102
28	41.70	34.00	288.44	2.035	128	92.80	45.00	487.37	2.050
29	42.10	33.60	290.06	2.028	129	93.60	43.70	488.55	2.030
30	42.80	33.30	292.81	2.055	130	94.00	30.50	490.12	1.980
31	43.40	33.30	295.17	2.024	131	94.40	33.60	491.69	2.028
32	43.80	34.50	296.74	2.042	132	94.00	34.00	494.05	2.035
33	44.40	35.00	299.10	2.050	133	94.50	36.00	494.01	2.066
34	44.80	37.00	300.67	2.082	134	94.90	35.00	497.58	2.050
35	45.00	34.70	301.46	2.046	135	95.10	47.00	498.37	2.082
36	45.70	33.00	304.21	2.019	136	95.60	47.40	500.34	2.086
37	46.00	32.00	305.34	2.005	137	96.10	46.70	503.09	2.077
38	46.40	35.00	306.96	2.050	138	96.70	46.30	504.66	2.039
39	47.00	45.40	309.32	2.057	139	97.20	33.00	506.43	2.027
40	47.30	34.40	310.50	2.041	140	97.50	33.00	507.81	2.031
41	47.50	49.20	311.28	2.055	141	97.80	34.00	508.98	2.054
42	48.00	32.50	313.24	2.011	142	97.90	35.00	509.28	2.050
43	48.50	32.90	315.21	2.017	143	98.10	35.60	512.32	2.060
44	48.80	44.10	316.39	2.036	144	99.00	35.00	513.70	2.050
45	49.20	37.40	317.74	2.096	145	99.40	31.60	515.27	1.999
46	49.70	47.10	319.93	2.083	146	100.00	32.50	517.63	2.011
47	50.50	42.80	323.07	2.016	147	100.30	32.00	518.81	2.003
48	51.00	43.00	325.04	2.019	148	100.90	33.30	520.78	2.028
49	51.30	35.90	326.22	2.064	149	101.30	31.20	522.74	1.991
50	51.80	46.70	328.18	2.080	150	101.60	47.00	523.92	1.925
51	52.30	38.40	330.15	2.038	151	102.00	46.50	525.49	1.937
52	52.70	44.20	331.72	2.038	152	102.30	47.90	526.67	1.954
53	53.20	41.40	333.69	1.994	153	102.70	46.80	529.24	1.921
54	53.60	40.50	335.26	1.948	154	103.00	49.10	529.42	1.958
55	54.00	32.60	337.62	2.013	155	103.60	48.00	532.57	1.940
56	54.70	40.00	339.50	1.972	156	104.00	49.30	535.35	1.961
57	55.00	49.30	340.74	1.961	157	104.40	29.60	534.93	1.965
58	55.70	44.00	343.51	1.947	158	104.90	44.40	536.44	1.944
59	56.30	49.70	345.87	1.967	159	105.40	48.70	539.64	1.951
60	57.00	30.30	348.62	1.974	160	106.00	41.00	541.21	1.987
61	57.50	32.50	350.59	2.011	161	106.60	31.80	543.57	2.000
62	58.00	39.70	353.74	2.046	162	107.30	29.20	546.32	1.959
63	59.00	34.00	356.48	4.035	163	107.70	51.00	547.90	1.997
64	59.70	30.50	359.24	1.980	164	108.20	49.00	549.86	1.986
65	60.30	29.40	361.59	1.962	165	108.90	28.70	552.61	1.951
66	60.60	49.90	362.77	1.970	166	109.40	47.80	554.58	1.937
67	61.50	12.00	366.31	1.689	167	109.90	31.00	556.54	1.987
68	62.00	12.00	368.27	1.692	168	110.00	40.00	558.94	1.972
69	62.50	20.00	370.24	1.814	169	110.70	32.60	559.69	2.015
70	63.20	46.00	372.98	1.909	170	111.00	32.00	560.87	2.003
71	63.90	41.00	375.74	1.830	171	111.20	33.00	561.69	2.014
72	64.00	47.90	377.71	1.939	172	111.60	33.50	563.73	2.027
73	64.90	35.50	379.67	2.027	173	112.00	32.00	565.19	2.016
74	65.00	49.80	381.07	2.126	174	112.80	34.00	567.94	2.055
75	65.40	41.40	381.84	2.151	175	113.00	32.90	568.75	2.017
76	65.70	40.00	383.82	2.127	176	114.00	33.50	572.66	2.024
77	66.30	35.30	385.18	2.118	177	114.50	34.20	573.84	2.034
78	67.00	40.00	386.75	2.129	178	115.00	34.10	576.59	2.036
79	67.20	41.30	388.71	2.144	179	115.80	35.00	579.73	2.019
80	67.50	41.20	389.88	2.148	180	116.20	34.40	581.31	2.041
81	68.30	40.30	393.04	2.134	181	116.90	33.70	584.04	2.030
82	68.80	40.00	395.00	2.097	182	117.20	34.40	585.24	2.041
83	69.00	38.40	399.72	2.104	183	117.60	32.00	586.81	2.003
84	70.00	48.00	400.90	2.097	184	118.00	35.00	588.38	2.050
85	70.70	34.00	402.47	2.014	185	118.60	36.20	590.74	2.025
86	71.00	32.00	405.45	2.005	186	119.00	34.00	592.70	2.069
87	71.30	32.00	404.83	2.003	187	119.80	35.20	595.44	2.036
88	71.80	48.10	406.79	1.942	188	120.00	33.90	597.81	2.051
89	72.00	42.00	407.59	2.003	189	120.90	33.20	599.76	2.022
90	72.50	32.40	409.54	2.004	190	121.30	33.60	602.14	2.020
91	73.00	33.70	411.51	2.030	191	122.00	29.00	604.18	1.956
92	73.70	30.00	414.26	1.972	192	122.40	31.00	605.67	1.944
93	74.00	31.00	415.44	1.947	193	122.80	32.00	607.25	2.001
94	74.30	31.20	416.62	1.941	194	122.90	31.00	607.44	1.987
95	75.00	34.40	419.37	2.041	195	123.50	35.70	610.00	2.050
96	75.30	35.60	421.16	2.024	196	124.00	34.00	611.98	2.035
97	76.00	33.00	423.30	2.028	197	124.50	45.00	613.14	2.061
98	76.60	33.00	425.64	2.014	198	124.80	45.00	615.11	2.050
99	77.00	33.40	427.71	2.025	199	125.30	34.80	617.07	2.047
100	77.20	35.20	428.72	2.055	200	126.00	30.60	619.02	1.972

TABLE 6-8 (Continued)

PEACE BUREAU HOLE NO. 19					PEACE BUREAU HOLE NO. 20				
DEPTH (DIV.)	DENSITY (DIV.)	COMPUTED DEPTH (FT.)	COMPUTED DENSITY (G/CC)		DEPTH (DIV.)	DENSITY (DIV.)	COMPUTED DEPTH (FT.)	COMPUTED DENSITY (G/CC)	
403	126.60	48.30	622.97	1.944	1	96.30	40.00	387.66	1.944
404	127.70	49.00	624.31	2.014	2	97.20	39.30	387.52	2.055
405	128.00	49.40	624.65	2.014	3	97.50	39.60	388.81	2.177
406	128.50	49.70	631.42	2.011	4	98.40	39.00	392.67	2.132
407	129.00	50.00	633.58	2.050	5	99.30	38.00	395.25	2.030
408	130.00	50.70	637.12	2.046	6	99.50	38.30	397.39	2.018
409	131.00	51.50	639.48	2.024	7	100.60	38.40	402.11	2.020
410	131.50	51.80	641.25	2.027	8	101.00	38.40	403.81	2.037
411	132.00	52.10	642.42	2.020	9	101.50	38.30	405.97	2.035
412	132.50	52.40	643.41	2.028	10	101.70	38.40	406.03	2.054
413	133.00	52.70	644.16	2.031	11	102.20	38.20	407.77	2.102
414	133.50	53.00	647.34	2.050	12	102.40	38.20	407.70	2.102
415	134.00	53.30	648.12	2.039	13	102.10	38.50	407.45	2.021
416	134.50	53.60	649.48	2.039	14	102.50	38.90	407.18	2.028
417	135.00	53.90	649.41	2.025	15	102.20	39.10	406.15	2.017
418	135.50	54.20	652.44	1.987	16	102.00	39.50	409.48	2.090
419	136.00	54.50	654.41	2.006	17	102.00	39.50	408.16	2.150
420	136.50	54.80	655.48	1.986	18	102.00	39.70	408.17	2.154
421	137.00	55.10	657.44	2.014	19	102.20	39.00	408.31	2.107
422	137.50	55.40	659.41	1.986	20	102.00	39.00	408.74	2.167
423	138.00	55.70	661.09	2.009	21	101.50	39.10	408.84	2.201
424	138.50	56.00	662.06	2.003	22	102.00	39.00	408.04	2.184
425	139.00	56.30	666.20	2.071	23	102.70	39.00	408.04	2.090
426	139.50	56.60	668.17	2.118	24	103.00	39.70	408.62	2.076
427	140.00	56.90	668.95	2.102	25	103.70	39.00	408.34	2.094
428	140.50	57.20	670.13	2.087	26	104.00	39.00	408.77	2.076
429	141.00	57.50	673.47	2.050	27	104.30	39.00	408.20	2.167
430	141.50	57.80	675.24	2.039	28	104.70	39.70	408.21	2.076
431	142.00	58.10	677.99	2.052	29	105.00	39.00	408.50	2.114
432	142.50	58.40	679.46	2.035	30	105.00	39.50	408.74	2.073
433	143.00	58.70	683.17	1.950	31	105.00	39.00	409.77	2.089
434	143.50	59.00	684.28	1.972	32	105.20	39.00	409.74	2.081
435	144.00	59.30	686.25	1.978	33	105.50	39.00	408.23	2.150
436	144.50	59.60	687.43	2.019	34	106.00	39.00	407.45	2.214
437	145.00	59.90	688.51	2.042	35	106.00	39.70	408.96	2.148
438	145.50	60.20	689.18	2.031	36	106.70	39.70	409.04	2.130
439	146.00	60.50	692.93	2.050	37	107.00	39.00	409.74	2.098
440	146.50	60.80	694.30	2.039	38	107.00	39.00	409.74	2.144
441	147.00	61.10	698.04	2.027	39	107.00	39.00	409.74	2.111
442	147.50	61.40	698.83	2.044	40	107.20	39.70	409.74	2.093
443	148.00	61.70	701.18	2.035	41	107.50	39.00	409.74	2.094
444	148.50	62.00	702.36	2.003	42	107.50	39.00	409.74	2.064
445	149.00	62.30	704.33	1.987	43	108.00	39.00	409.74	2.064
446	149.50	62.60	707.08	2.004	44	108.00	39.00	409.74	2.064
447	150.00	62.90	710.22	2.042	45	108.00	39.00	409.74	2.064
448	150.50	63.20	712.98	2.035	46	108.00	39.00	409.74	2.064
449	151.00	63.50	714.15	1.992	47	108.00	39.00	409.74	2.064
450	151.50	63.80	716.91	1.959	48	108.00	39.00	409.74	2.064
451	152.00	64.10	720.84	2.050	49	108.00	39.00	409.74	2.064
452	152.50	64.40	722.02	2.074	50	108.00	39.00	409.74	2.064
453	153.00	64.70	724.37	2.069	51	108.00	39.00	409.74	2.064
454	153.50	65.00	725.94	2.047	52	108.00	39.00	409.74	2.064
455	154.00	65.30	728.30	2.280	53	108.00	39.00	409.74	2.064
456	154.50	65.60	728.30	2.059	54	108.00	39.00	409.74	2.064
457	155.00	65.90	731.81	2.038	55	108.00	39.00	409.74	2.064
458	155.50	66.20	737.34	2.160	56	108.00	39.00	409.74	2.064
459	156.00	66.50	738.52	2.049	57	108.00	39.00	409.74	2.064
460	156.50	66.80	741.67	2.061	58	108.00	39.00	409.74	2.064
461	157.00	67.10	744.42	2.039	59	108.00	39.00	409.74	2.064
462	157.50	67.40	747.17	2.031	60	108.00	39.00	409.74	2.064
463	158.00	67.70	749.53	2.072	61	108.00	39.00	409.74	2.064
464	158.50	68.00	751.44	2.063	62	108.00	39.00	409.74	2.064
465	159.00	68.30	753.07	2.074	63	108.00	39.00	409.74	2.064
466	159.50	68.60	755.42	2.052	64	108.00	39.00	409.74	2.064
467	160.00	68.90	757.00	2.052	65	108.00	39.00	409.74	2.064
468	160.50	69.20	759.36	2.011	66	108.00	39.00	409.74	2.064
469	161.00	69.50	761.34	2.019	67	108.00	39.00	409.74	2.064
470	161.50	69.80	762.89	2.075	68	108.00	39.00	409.74	2.064
471	162.00	70.10	764.04	1.947	69	108.00	39.00	409.74	2.064
472	162.50	70.40	767.61	1.950	70	108.00	39.00	409.74	2.064
Total 51					71	108.00	39.00	409.74	2.064
Total 52					72	108.00	39.00	409.74	2.064
Total 53					73	108.00	39.00	409.74	2.064
Total 54					74	108.00	39.00	409.74	2.064
Total 55					75	108.00	39.00	409.74	2.064
Total 56					76	108.00	39.00	409.74	2.064
Total 57					77	108.00	39.00	409.74	2.064
Total 58					78	108.00	39.00	409.74	2.064
Total 59					79	108.00	39.00	409.74	2.064
Total 60					80	108.00	39.00	409.74	2.064
Total 61					81	108.00	39.00	409.74	2.064
Total 62					82	108.00	39.00	409.74	2.064
Total 63					83	108.00	39.00	409.74	2.064
Total 64					84	108.00	39.00	409.74	2.064
Total 65					85	108.00	39.00	409.74	2.064
Total 66					86	108.00	39.00	409.74	2.064
Total 67					87	108.00	39.00	409.74	2.064
Total 68					88	108.00	39.00	409.74	2.064
Total 69					89	108.00	39.00	409.74	2.064
Total 70					90	108.00	39.00	409.74	2.064
Total 71					91	108.00	39.00	409.74	2.064
Total 72					92	108.00	39.00	409.74	2.064
Total 73					93	108.00	39.00	409.74	2.064
Total 74					94	108.00	39.00	409.74	2.064
Total 75					95	108.00	39.00	409.74	2.064
Total 76					96	108.00	39.00	409.74	2.064
Total 77					97	108.00	39.00	409.74	2.064
Total 78					98	108.00	39.00	409.74	2.064
Total 79					99	108.00	39.00	409.74	2.064
Total 80					100	108.00	39.00	409.74	2.064

TABLE 6-8 (Continued)

PLACE BOREHOLE DBZ-04				PLACE BOREHOLE DBZ-04			
DIGITIZED DEPTH, F (U/I)	DIGITIZED DENSITY, g (U/I)	COMPUTER DEPTH (FT)	COMPUTER DENSITY (GM/CC)	DIGITIZED DEPTH, F (U/I)	DIGITIZED DENSITY, g (U/I)	COMPUTER DEPTH (FT)	COMPUTER DENSITY (GM/CC)
101	120.60	32.30	712.50	401	209.70	33.30	1094.00
102	121.00	34.50	714.26	402	210.50	33.70	1098.30
103	121.50	40.00	716.40	403	210.80	35.20	1099.67
104	122.50	48.30	719.00	404	211.50	35.30	1102.67
105	122.80	50.70	721.44	405	211.80	36.30	1103.10
106	123.50	53.50	724.44	406	213.00	36.00	1109.11
107	124.00	57.70	727.11	407	213.30	35.80	1110.40
108	125.00	59.70	731.41	408	214.00	31.30	1113.00
109	125.50	60.07	733.97	409	214.60	32.50	1115.97
110	126.00	67.50	737.43	410	215.70	32.50	1120.70
111	126.90	69.70	739.50	411	216.80	31.20	1123.27
112	127.50	68.50	742.15	412	217.50	30.20	1127.56
113	127.80	62.00	745.44	413	218.00	34.30	1130.57
114	128.00	59.50	748.50	414	219.00	39.80	1134.86
115	129.00	65.30	752.03	415	220.00	35.00	1139.15
116	130.00	57.60	754.60	416	220.50	32.80	1141.50
117	131.00	65.50	757.19	417	221.00	32.50	1145.16
118	131.50	63.00	759.32	418	221.80	39.00	1151.80
119	132.00	68.67	763.61	419	222.00	40.70	1156.52
120	132.50	74.00	765.74	420	223.00	40.70	1161.47
121	133.00	59.50	770.00	421	223.50	41.30	1164.14
122	133.50	58.20	770.97	422	224.00	40.00	1170.63
123	134.50	59.20	780.70	423	225.00	38.70	1182.07
124	135.00	56.50	785.57	424	226.50	35.00	1191.94
125	135.10	61.10	800.52	425	228.00	36.00	1197.09
126	135.20	58.00	805.24	426	230.00	34.00	1199.24
127	135.10	59.00	809.11	427	230.00	36.00	1200.95
128	136.50	56.70	815.12	428	230.00	37.00	1203.53
129	136.50	58.50	818.55	429	230.00	41.50	1205.25
130	136.50	52.50	823.70	430	230.70	39.00	1210.82
131	137.00	55.00	827.04	431	231.50	33.50	1214.26
132	137.00	52.00	829.28	432	230.50	35.40	1217.69
133	138.20	51.00	831.00	433	230.50	35.00	1222.84
134	139.00	59.10	836.15	434	230.50	36.80	1227.15
135	139.70	55.30	841.73	435	231.00	40.80	1229.28
136	139.10	52.20	845.44	436	231.00	36.20	1232.71
137	139.00	52.20	847.31	437	231.00	35.10	1233.57
138	139.00	55.00	849.01	438	232.00	47.70	1237.43
139	139.00	55.00	851.60	439	232.00	45.80	1239.50
140	139.50	62.20	853.74	440	232.00	46.10	1242.58
141	139.50	62.20	857.61	441	232.00	45.10	1246.52
142	139.50	67.00	860.18	442	230.00	45.00	1248.02
143	139.50	60.00	864.07	443	230.00	45.20	1248.14
144	139.50	67.00	866.19	444	230.70	45.80	1249.45
145	139.50	57.00	868.34	445	230.00	46.10	1250.74
146	139.50	56.00	870.41	446	230.00	45.80	1251.60
147	139.50	60.00	874.77	447	230.00	48.70	1252.03
148	139.50	57.50	875.20	448	230.00	44.00	1253.74
149	139.20	58.10	878.21	449	230.00	43.30	1254.60
150	139.50	57.50	881.21	450	230.50	23.00	1256.32
151	140.00	58.50	882.93	451	231.50	43.20	1257.19
152	141.00	51.00	889.37	452	231.50	44.40	1258.03
153	141.00	52.00	891.52	453	230.00	29.30	1261.04
154	141.00	60.00	894.04	454	230.70	46.30	1262.53
155	141.00	62.00	902.24	455	230.10	27.70	1264.04
156	141.00	66.30	908.25	456	230.10	45.20	1268.34
157	141.00	67.00	911.24	457	230.00	46.10	1269.19
158	141.00	65.30	912.54	458	230.00	45.50	1270.05
159	141.00	66.00	915.12	459	230.00	45.30	1271.77
160	140.50	65.00	916.88	460	231.50	46.90	1274.34
161	140.50	67.30	918.12	461	232.00	42.70	1276.49
162	140.50	60.50	920.27	462	232.00	43.80	1277.35
163	140.00	64.30	924.56	463	232.00	43.30	1279.06
164	141.00	56.80	930.14	464	232.00	45.10	1279.92
165	141.50	64.80	938.87	465	233.00	45.00	1284.22
166	142.00	65.30	947.73	466	234.70	46.90	1288.08
167	142.00	65.00	950.31	467	235.00	46.10	1289.57
168	142.00	65.00	954.60	468	235.00	46.30	1290.65
169	142.00	65.00	961.04	469	235.00	46.90	1291.94
170	142.00	60.00	964.90	470	236.20	35.20	1294.52
171	142.00	60.00	967.91	471	237.00	49.00	1297.75
172	141.20	64.00	972.63	472	237.00	30.90	1299.67
173	142.00	59.00	974.49	473	238.70	46.30	1305.25
174	143.00	58.20	983.74	474	239.10	46.50	1306.96
175	144.00	56.80	987.22	475	239.60	52.90	1309.11
176	144.50	52.50	994.52	476	240.10	29.10	1311.25
177	147.00	57.30	997.52	477	240.30	46.80	1312.11
178	147.00	57.30	1000.09	478	240.50	49.10	1312.97
179	148.00	55.00	1004.59	479	240.80	40.30	1314.76
180	149.00	57.50	1006.10	480	241.00	49.10	1315.12
181	150.00	56.00	1010.40	481	241.10	46.80	1315.55
182	150.00	59.20	1012.11	482	241.50	49.00	1316.40
183	151.30	58.00	1015.97	483	242.00	27.60	1319.41
184	151.70	55.80	1017.69	484	242.30	49.50	1320.70
185	152.30	66.60	1020.27	485	243.00	31.50	1323.70
186	153.50	64.00	1025.42	486	243.40	32.10	1325.42
187	154.00	58.00	1030.14	487	244.00	31.90	1327.13
188	155.50	56.00	1034.70	488	244.14	30.40	1328.42
189	156.50	55.50	1038.24	489	245.60	30.10	1330.57
190	157.00	60.00	1044.01	490	245.80	30.20	1333.57
191	158.70	61.00	1047.73	491	246.00	30.40	1335.00
192	159.50	49.30	1051.17	492	246.00	29.20	1336.50
193	160.00	58.50	1055.31	493	246.20	29.00	1337.43
194	160.00	60.50	1057.18	494	246.40	28.00	1338.99
195	161.30	55.40	1059.69	495	246.60	28.70	1339.15
196	162.20	61.00	1062.76	496	246.90	28.70	1340.44
197	163.00	51.00	1066.19	497	247.50	29.30	1343.01
198	164.00	55.60	1070.04	498	248.00	28.90	1344.73
199	167.00	52.70	1085.70	499	248.00	29.40	1345.16
200	209.00	54.50	1091.94	500	248.00	29.40	1346.88

TABLE 6-8 (Continued)

PLATE BOREHOLE 052-04					PLATE BOREHOLE 052-04				
DEPTH (FEET)	DENSIFIED DENSITY (G/CC)	DENSIFIED DENSITY (G/CC)	COMPUTED DENSITY (G/CC)	COMPUTED DENSITY (G/CC)	DEPTH (FEET)	DENSIFIED DENSITY (G/CC)	DENSIFIED DENSITY (G/CC)	COMPUTED DENSITY (G/CC)	COMPUTED DENSITY (G/CC)
291	269.40	31.40	1351.17	2.057	1	0.00	45.60	182.40	2.174
292	269.50	32.50	1351.40	2.056	2	0.00	39.00	186.34	2.174
293	269.90	33.20	1353.31	2.060	3	0.00	39.10	186.20	2.174
294	270.40	34.70	1355.46	2.162	4	0.20	38.4	181.74	2.103
295	270.80	35.40	1356.72	2.174	5	0.30	40.30	183.74	2.174
296	271.00	36.20	1357.18	2.180	6	0.30	40.40	183.74	2.174
297	271.40	36.70	1358.08	2.180	7	0.30	40.40	183.74	2.174
298	271.60	37.00	1358.61	2.184	8	0.30	40.40	183.74	2.174
299	271.80	37.60	1359.47	2.184	9	0.30	40.40	183.74	2.174
300	272.00	38.00	1360.18	2.184	10	0.00	40.00	200.12	2.184
301	272.20	38.40	1360.72	2.184	11	0.20	41.00	202.09	2.184
302	272.40	38.80	1361.18	2.184	12	0.30	41.10	204.84	2.184
303	272.60	39.20	1361.64	2.184	13	0.40	40.40	209.17	2.184
304	272.80	39.60	1362.10	2.184	14	0.40	40.40	211.93	2.184
305	273.00	40.00	1362.56	2.184	15	0.40	40.40	214.68	2.184
306	273.20	40.40	1363.02	2.184	16	0.40	40.40	217.44	2.184
307	273.40	40.80	1363.48	2.184	17	0.40	40.40	220.19	2.184
308	273.60	41.20	1363.94	2.184	18	0.40	40.40	222.95	2.184
309	273.80	41.60	1364.40	2.184	19	0.40	40.40	225.70	2.184
310	274.00	42.00	1364.86	2.184	20	0.40	40.40	228.46	2.184
311	274.20	42.40	1365.32	2.184	21	0.40	40.40	231.21	2.184
312	274.40	42.80	1365.78	2.184	22	0.40	40.40	233.97	2.184
313	274.60	43.20	1366.24	2.184	23	0.40	40.40	236.72	2.184
314	274.80	43.60	1366.70	2.184	24	0.40	40.40	239.48	2.184
315	275.00	44.00	1367.16	2.184	25	0.40	40.40	242.23	2.184
316	275.20	44.40	1367.62	2.184	26	0.40	40.40	245.00	2.184
317	275.40	44.80	1368.08	2.184	27	0.40	40.40	247.75	2.184
318	275.60	45.20	1368.54	2.184	28	0.40	40.40	250.51	2.184
319	275.80	45.60	1369.00	2.184	29	0.40	40.40	253.26	2.184
320	276.00	46.00	1369.46	2.184	30	0.40	40.40	256.02	2.184
321	276.20	46.40	1369.92	2.184	31	0.40	40.40	258.77	2.184
322	276.40	46.80	1370.38	2.184	32	0.40	40.40	261.53	2.184
323	276.60	47.20	1370.84	2.184	33	0.40	40.40	264.28	2.184
324	276.80	47.60	1371.30	2.184	34	0.40	40.40	267.04	2.184
325	277.00	48.00	1371.76	2.184	35	0.40	40.40	269.79	2.184
326	277.20	48.40	1372.22	2.184	36	0.40	40.40	272.55	2.184
327	277.40	48.80	1372.68	2.184	37	0.40	40.40	275.30	2.184
328	277.60	49.20	1373.14	2.184	38	0.40	40.40	278.06	2.184
329	277.80	49.60	1373.60	2.184	39	0.40	40.40	280.81	2.184
330	278.00	50.00	1374.06	2.184	40	0.40	40.40	283.57	2.184
331	278.20	50.40	1374.52	2.184	41	0.40	40.40	286.32	2.184
332	278.40	50.80	1374.98	2.184	42	0.40	40.40	289.08	2.184
333	278.60	51.20	1375.44	2.184	43	0.40	40.40	291.83	2.184
334	278.80	51.60	1375.90	2.184	44	0.40	40.40	294.59	2.184
335	279.00	52.00	1376.36	2.184	45	0.40	40.40	297.34	2.184
336	279.20	52.40	1376.82	2.184	46	0.40	40.40	300.10	2.184
337	279.40	52.80	1377.28	2.184	47	0.40	40.40	302.85	2.184
338	279.60	53.20	1377.74	2.184	48	0.40	40.40	305.61	2.184
339	279.80	53.60	1378.20	2.184	49	0.40	40.40	308.36	2.184
340	280.00	54.00	1378.66	2.184	50	0.40	40.40	311.12	2.184
341	280.20	54.40	1379.12	2.184	51	0.40	40.40	313.87	2.184
342	280.40	54.80	1379.58	2.184	52	0.40	40.40	316.63	2.184
343	280.60	55.20	1380.04	2.184	53	0.40	40.40	319.38	2.184
344	280.80	55.60	1380.50	2.184	54	0.40	40.40	322.14	2.184
345	281.00	56.00	1380.96	2.184	55	0.40	40.40	324.89	2.184
346	281.20	56.40	1381.42	2.184	56	0.40	40.40	327.65	2.184
347	281.40	56.80	1381.88	2.184	57	0.40	40.40	330.40	2.184
348	281.60	57.20	1382.34	2.184	58	0.40	40.40	333.16	2.184
349	281.80	57.60	1382.80	2.184	59	0.40	40.40	335.91	2.184
350	282.00	58.00	1383.26	2.184	60	0.40	40.40	338.67	2.184
351	282.20	58.40	1383.72	2.184	61	0.40	40.40	341.42	2.184
352	282.40	58.80	1384.18	2.184	62	0.40	40.40	344.18	2.184
353	282.60	59.20	1384.64	2.184	63	0.40	40.40	346.93	2.184
354	282.80	59.60	1385.10	2.184	64	0.40	40.40	349.69	2.184
355	283.00	60.00	1385.56	2.184	65	0.40	40.40	352.44	2.184
356	283.20	60.40	1386.02	2.184	66	0.40	40.40	355.20	2.184
357	283.40	60.80	1386.48	2.184	67	0.40	40.40	357.95	2.184
358	283.60	61.20	1386.94	2.184	68	0.40	40.40	360.71	2.184
359	283.80	61.60	1387.40	2.184	69	0.40	40.40	363.46	2.184
360	284.00	62.00	1387.86	2.184	70	0.40	40.40	366.22	2.184
361	284.20	62.40	1388.32	2.184	71	0.40	40.40	368.97	2.184
362	284.40	62.80	1388.78	2.184	72	0.40	40.40	371.73	2.184
363	284.60	63.20	1389.24	2.184	73	0.40	40.40	374.48	2.184
364	284.80	63.60	1389.70	2.184	74	0.40	40.40	377.24	2.184
365	285.00	64.00	1390.16	2.184	75	0.40	40.40	380.00	2.184
366	285.20	64.40	1390.62	2.184	76	0.40	40.40	382.75	2.184
367	285.40	64.80	1391.08	2.184	77	0.40	40.40	385.51	2.184
368	285.60	65.20	1391.54	2.184	78	0.40	40.40	388.26	2.184
369	285.80	65.60	1392.00	2.184	79	0.40	40.40	391.02	2.184
370	286.00	66.00	1392.46	2.184	80	0.40	40.40	393.77	2.184
371	286.20	66.40	1392.92	2.184	81	0.40	40.40	396.53	2.184
372	286.40	66.80	1393.38	2.184	82	0.40	40.40	399.28	2.184
373	286.60	67.20	1393.84	2.184	83	0.40	40.40	402.04	2.184
374	286.80	67.60	1394.30	2.184	84	0.40	40.40	404.79	2.184
375	287.00	68.00	1394.76	2.184	85	0.40	40.40	407.55	2.184
376	287.20	68.40	1395.22	2.184	86	0.40	40.40	410.30	2.184
377	287.40	68.80	1395.68	2.184	87	0.40	40.40	413.06	2.184
378	287.60	69.20	1396.14	2.184	88	0.40	40.40	415.81	2.184
379	287.80	69.60	1396.60	2.184	89	0.40	40.40	418.57	2.184
380	288.00	70.00	1397.06	2.184	90	0.40	40.40	421.32	2.184
381	288.20	70.40	1397.52	2.184	91	0.40	40.40	424.08	2.184
382	288.40	70.80	1397.98	2.184	92	0.40	40.40	426.83	2.184
383	288.60	71.20	1398.44	2.184	93	0.40	40.40	429.59	2.184
384	288.80	71.60	1398.90	2.184	94	0.40	40.40	432.34	2.184
385	289.00	72.00	1399.36	2.184	95	0.40	40.40	435.10	2.184
386	289.20	72.40	1399.82	2.184	96	0.40	40.40	437.85	2.184
387	289.40	72.80	1400.28	2.184	97	0.40	40.40	440.61	2.184
388	289.60	73.20	1400.74	2.184	98	0.40	40.40	443.36	2.184
389	289.80	73.60	1401.20	2.184	99	0.40	40.40	446.12	2.184
390	290.00	74.00	1401.66	2.184	100	0.40	40.40	448.87	2.184
391	290.20	74.40	1402.12	2.184					
392	290.40	74.80	1402.58	2.184					
393	290.60	75.20	1403.04	2.184					
394	290.80	75.60	1403.50	2.184					
395	291.00	76.00	1403.96	2.184					
396	291.20	76.40	1404.42	2.184					
397	291.40	76.80	1404.88	2.184					
398	291.60	77.20	1405.34	2.184					
399	291.80	77.60	1405.80	2.184					
400	292.00	78.00	1406.26	2.184					
401	292.20	78.40	1406.72	2.184					
402	292.40	78.80	1407.18	2.184					
403	292.60	79.20	1407.64	2.184					
404	292.80	79.60	1408.10	2.184					
405	293.00	80.00	1408.56	2.184					
406	293.20	80.40	1409.02	2.184					
407	293.40	80.80	1409.48	2.184					
408	293.60	81.20	1409.94	2.184					
409	293.80	81.60	1410.40	2.184					
410	294.00	82.00	1410.86	2.184					
411	294.20	82.40	1411.32	2.184					
412	294.40	82.80	1411.78	2.184					
413	294.60	83.20	1412.24	2.184		</			

TABLE 6-8 (Continued)

PEACE MOREHOUSE OCT-08					PEACE MOREHOUSE OCT-08				
J	DIGITIZED DEPTH (FATH)	DIGITIZED DENSITY (LB/CC)	COMPUTED DEPTH (FT)	COMPUTED DENSITY (LB/CC)	J	DIGITIZED DEPTH (FATH)	DIGITIZED DENSITY (LB/CC)	COMPUTED DEPTH (FT)	COMPUTED DENSITY (LB/CC)
101	58.00	82.00	398.94	1.845	401	115.00	84.00	619.01	2.191
102	58.00	87.50	402.04	2.086	402	115.00	87.00	620.94	2.250
103	59.00	88.00	404.84	2.106	403	115.00	88.00	623.74	2.260
104	59.00	87.00	406.81	2.081	404	115.00	89.00	625.25	2.203
105	59.00	89.00	408.78	2.112	405	117.00	87.00	629.00	2.250
106	62.00	90.00	411.14	2.128	406	117.00	88.00	632.90	2.284
107	62.00	86.00	415.47	2.075	407	117.00	89.00	637.91	2.264
108	62.00	89.00	419.41	2.119	408	117.00	90.00	639.68	2.254
109	62.00	90.00	425.11	2.209	409	119.00	89.00	641.46	2.264
110	66.00	84.00	430.43	2.108	410	119.00	90.00	643.03	2.101
111	66.00	89.00	432.01	2.274	411	120.00	88.00	643.82	2.123
112	67.00	87.00	435.55	2.204	412	120.00	89.00	646.18	2.105
113	68.00	91.00	438.51	2.308	413	120.00	90.00	647.54	2.244
114	68.00	87.00	441.44	2.104	414	121.00	87.00	647.54	2.244
115	68.00	87.00	445.39	2.204	415	121.00	90.00	649.00	2.274
116	70.00	88.00	446.18	2.264	416	121.00	90.00	650.12	2.201
117	70.00	87.00	447.76	2.250	417	121.00	90.00	653.27	2.274
118	71.00	88.00	450.90	2.257	418	121.00	90.00	656.02	2.213
119	71.00	90.00	453.30	2.337	419	121.00	90.00	657.60	2.274
120	74.00	84.00	454.42	2.301	420	121.00	90.00	660.00	2.274
121	73.00	84.00	457.93	2.336	421	121.00	90.00	661.45	2.274
122	73.00	90.00	459.17	2.360	422	121.00	90.00	662.59	2.327
123	73.00	90.00	461.14	2.365	423	121.00	90.00	667.96	2.296
124	74.00	87.00	463.11	2.301	424	121.00	90.00	670.98	2.301
125	74.00	90.00	465.47	2.331	425	121.00	90.00	674.25	2.301
126	75.00	88.00	468.62	2.311	426	121.00	90.00	676.90	2.308
127	75.00	89.00	469.89	2.326	427	121.00	90.00	678.46	2.310
128	76.00	88.00	471.77	2.314	428	121.00	90.00	680.43	2.301
129	76.00	88.00	475.74	2.356	429	121.00	90.00	682.40	2.301
130	76.00	90.00	477.71	2.356	430	121.00	90.00	685.55	2.318
131	78.00	88.00	478.44	2.301	431	121.00	90.00	686.34	2.301
132	78.00	90.00	479.25	2.265	432	121.00	90.00	687.89	2.297
133	78.00	90.00	480.04	2.277	433	121.00	90.00	689.88	2.285
134	79.00	90.00	482.79	2.290	434	121.00	90.00	691.46	2.301
135	79.00	90.00	485.14	2.282	435	121.00	90.00	693.21	2.317
136	80.00	90.00	487.52	2.301	436	121.00	90.00	695.00	2.297
137	80.00	90.00	488.70	2.285	437	121.00	90.00	700.49	2.307
138	81.00	90.00	491.06	2.282	438	121.00	90.00	703.66	2.314
139	81.00	90.00	493.03	2.164	439	121.00	90.00	707.60	2.315
140	83.00	90.00	497.36	2.265	440	121.00	90.00	709.96	2.272
141	84.00	90.00	501.30	2.266	441	121.00	90.00	713.50	2.250
142	84.00	90.00	502.87	2.285	442	121.00	90.00	715.87	2.291
143	84.00	90.00	504.84	2.272	443	121.00	90.00	717.83	2.293
144	85.00	90.00	506.02	2.274	444	121.00	90.00	719.01	2.304
145	85.00	90.00	507.60	2.210	445	121.00	90.00	721.77	2.291
146	86.00	90.00	509.57	2.313	446	121.00	90.00	723.34	2.312
147	86.00	90.00	511.14	2.324	447	121.00	90.00	725.31	2.297
148	86.00	90.00	511.93	2.301	448	121.00	90.00	727.71	2.294
149	87.00	90.00	513.11	2.297	449	121.00	90.00	729.70	2.282
150	87.00	90.00	514.76	2.225	450	121.00	90.00	730.43	2.230
151	88.00	90.00	517.83	2.271	451	121.00	90.00	731.16	2.222
152	88.00	90.00	519.41	2.281	452	121.00	90.00	732.70	2.291
153	89.00	90.00	521.77	2.290	453	121.00	90.00	734.46	2.238
154	89.00	90.00	523.56	2.283	454	121.00	90.00	736.43	2.279
155	89.00	90.00	525.35	2.285	455	121.00	90.00	738.43	2.284
156	89.00	90.00	527.99	2.235	456	121.00	90.00	740.43	2.284
157	90.00	90.00	529.84	2.206	457	121.00	90.00	742.43	2.284
158	91.00	90.00	530.84	2.206	458	121.00	90.00	744.43	2.284
159	91.00	90.00	532.79	2.206	459	121.00	90.00	746.43	2.284
160	92.00	90.00	534.76	2.272	460	121.00	90.00	748.43	2.284
161	92.00	90.00	535.94	2.284	461	121.00	90.00	750.43	2.284
162	92.00	90.00	537.91	2.206	462	121.00	90.00	752.43	2.284
163	93.00	90.00	538.76	2.214	463	121.00	90.00	754.43	2.284
164	93.00	90.00	540.06	2.206	464	121.00	90.00	756.43	2.284
165	93.00	90.00	541.06	2.206	465	121.00	90.00	758.43	2.284
166	93.00	90.00	543.03	2.227	466	121.00	90.00	760.43	2.284
167	93.00	90.00	544.61	2.175	467	121.00	90.00	762.43	2.284
168	93.00	90.00	546.72	2.172	468	121.00	90.00	764.43	2.284
169	93.00	90.00	548.72	2.172	469	121.00	90.00	766.43	2.284
170	93.00	90.00	551.37	2.201	470	121.00	90.00	768.43	2.284
171	93.00	90.00	553.66	2.224	471	121.00	90.00	770.43	2.284
172	93.00	90.00	555.63	2.265	472	121.00	90.00	772.43	2.284
173	94.00	90.00	557.99	2.235	473	121.00	90.00	774.43	2.284
174	94.00	90.00	560.35	2.297	474	121.00	90.00	776.43	2.284
175	94.00	90.00	562.32	2.321	475	121.00	90.00	778.43	2.284
176	100.00	90.00	564.24	2.307	476	121.00	90.00	780.43	2.284
177	100.00	90.00	565.47	2.230	477	121.00	90.00	782.43	2.284
178	100.00	90.00	567.44	2.214	478	121.00	90.00	784.43	2.284
179	101.00	90.00	570.20	2.301	479	121.00	90.00	786.43	2.284
180	102.00	90.00	572.14	2.290	480	121.00	90.00	788.43	2.284
181	102.00	90.00	574.42	2.301	481	121.00	90.00	790.43	2.284
182	103.00	90.00	577.69	2.379	482	121.00	90.00	792.43	2.284
183	104.00	90.00	581.22	2.274	483	121.00	90.00	794.43	2.284
184	104.00	90.00	583.13	2.244	484	121.00	90.00	796.43	2.284
185	105.00	90.00	586.75	2.304	485	121.00	90.00	798.43	2.284
186	106.00	90.00	587.91	2.304	486	121.00	90.00	800.43	2.284
187	106.00	90.00	590.27	2.400	487	121.00	90.00	802.43	2.284
188	107.00	90.00	591.85	2.314	488	121.00	90.00	804.43	2.284
189	107.00	90.00	594.61	2.345	489	121.00	90.00	806.43	2.284
190	108.00	90.00	595.79	2.321	490	121.00	90.00	808.43	2.284
191	108.00	90.00	597.76	2.301	491	121.00	90.00	810.43	2.284
192	108.00	90.00	599.33	2.301	492	121.00	90.00	812.43	2.284
193	109.00	90.00	600.51	2.314	493	121.00	90.00	814.43	2.284
194	109.00	90.00	602.44	2.334	494	121.00	90.00	816.43	2.284
195	110.00	90.00	604.84	2.277	495	121.00	90.00	818.43	2.284
196	111.00	90.00	607.99	2.272	496	121.00	90.00	820.43	2.284
197	112.00	90.00	611.53	2.321	497	121.00	90.00	822.43	2.284
198	112.00	90.00	614.29	2.323	498	121.00	90.00	824.43	2.284
199	113.00	90.00	616.43	2.274	499	121.00	90.00	826.43	2.284
200	113.00	90.00	617.83	2.204	500	121.00	90.00	828.43	2.284

TABLE 6-8 (Continued)

PEACE BOATHOLE OCT-93					PEACE BOATHOLE CHAS. 7				
J	DIGITIZED DEPTH (F)	DIGITIZED DENSITY (LB/CC)	COMPUTED DEPTH (FT)	COMPUTED DENSITY (LB/CC)	J	DIGITIZED DEPTH (F)	DIGITIZED DENSITY (LB/CC)	COMPUTED DEPTH (FT)	COMPUTED DENSITY (LB/CC)
301	172.30	47.60	848.94	2.247	1	5.30	48.30	141.87	1.449
302	172.60	49.40	850.12	2.276	2	6.80	47.00	145.36	1.927
303	173.00	50.50	853.27	2.293	3	7.10	44.70	144.53	1.970
304	174.00	46.80	845.63	2.255	4	7.40	24.30	149.64	1.866
305	175.00	46.30	849.57	2.277	5	9.00	35.70	153.91	1.865
306	176.00	47.00	863.50	2.250	6	9.40	35.50	146.24	1.810
307	176.20	48.10	844.29	2.255	7	10.00	30.00	147.40	1.974
308	176.70	47.90	846.24	2.252	8	10.40	37.30	140.87	1.897
309	177.20	46.00	848.24	2.272	9	11.20	49.00	142.44	1.954
310	177.70	44.70	870.20	2.204	10	11.80	46.00	144.74	1.924
311	178.00	44.40	871.58	2.215	11	12.60	46.00	147.40	1.924
312	178.20	45.00	873.34	2.204	12	13.00	30.00	147.40	1.967
313	178.00	42.40	875.31	2.172	13	13.40	31.00	171.00	1.891
314	179.40	45.80	878.46	2.219	14	14.70	33.20	172.17	2.027
315	180.30	49.50	880.43	2.277	15	14.70	35.10	173.34	2.059
316	181.00	41.80	883.19	2.156	16	14.30	30.00	174.44	2.054
317	181.80	38.90	899.72	2.113	17	14.90	46.20	174.44	1.917
318	184.50	43.50	889.04	2.183	18	15.20	31.80	176.57	2.007
319	183.20	41.80	891.85	2.150	19	15.70	47.00	178.44	1.927
320	183.00	41.50	894.61	2.151	20	16.00	44.00	181.11	1.881
321	184.50	43.50	896.47	2.180	21	16.50	18.00	183.50	1.787
322	185.20	42.00	899.72	2.173	22	17.00	18.50	184.44	1.787
323	186.00	43.80	902.47	2.188	23	17.40	46.80	174.17	1.924
324	187.00	43.70	906.81	2.186	24	17.60	30.70	187.33	1.983
325	187.80	43.20	909.96	2.177	25	18.00	30.20	188.44	1.774
326	188.50	42.20	912.72	2.162	26	18.20	31.80	189.17	2.024
327	189.50	48.00	916.61	2.254	27	18.40	31.00	192.17	1.771
328	190.00	49.60	918.62	2.274	28	18.40	31.00	193.17	2.022
329	190.50	47.90	920.59	2.252	29	18.90	47.00	194.74	1.927
330	191.00	42.00	922.46	2.159	30	20.10	42.80	197.04	2.019
331	191.90	40.30	926.10	2.133	31	20.40	34.00	199.20	2.038
332	192.20	43.00	927.28	2.175	32	21.00	32.00	200.43	2.006
333	192.60	41.70	928.84	2.155	33	21.40	34.00	202.44	2.006
334	193.60	40.00	932.74	2.118	34	21.00	35.20	203.64	2.129
335	194.50	49.60	936.34	2.182	35	22.50	206.75	2.037	
336	196.20	41.70	943.03	2.133	36	23.20	52.80	209.04	2.019
337	196.60	41.80	944.61	2.156	37	23.50	34.10	210.27	2.020
338	197.00	46.00	947.76	2.222	38	24.10	43.50	212.54	2.050
339	197.80	51.20	944.31	2.304	39	25.10	45.80	216.44	2.064
340	198.30	53.20	951.30	2.335	40	26.00	33.80	219.96	2.024
341	198.80	51.40	953.27	2.308	41	26.80	37.70	225.17	2.077
342	199.30	46.00	955.24	2.222	42	27.30	32.70	225.17	2.077
343	199.60	44.00	946.42	2.191	43	28.30	39.30	224.44	2.124
344	200.10	45.00	957.99	2.206	44	29.00	31.40	231.60	1.947
345	200.10	46.40	959.17	2.240	45	29.20	34.10	232.34	2.040
346	200.70	47.20	960.75	2.272	46	29.60	34.80	234.45	2.051
347	201.60	47.50	964.29	2.246	47	29.90	34.60	235.11	2.047
348	202.90	42.00	969.41	2.159	48	30.10	37.90	235.99	2.100
349	203.70	37.00	972.56	2.081	49	30.40	45.00	238.61	2.054
350	204.50	38.20	975.71	2.100	50	31.00	29.40	243.39	1.945
351	205.28	48.10	978.46	2.170	51	31.50	47.00	241.11	1.977
352	206.50	46.80	982.78	2.145	52	32.80	47.00	246.27	1.959
353	207.10	38.50	985.44	2.104	53	33.40	43.80	248.71	1.877
354	207.80	37.80	988.70	2.093	54	33.80	45.00	250.24	1.896
355	208.70	48.00	992.24	2.154	55	34.80	48.80	251.04	1.975
356	209.20	41.20	994.21	2.117	56	34.50	50.00	252.59	1.975
357	209.70	42.50	996.18	2.144	57	34.50	49.00	252.59	1.959
358	210.00	39.70	997.34	2.123	58	35.00	46.20	254.43	1.976
					59	35.30	49.00	254.74	1.959
					60	36.00	32.40	254.81	2.014
					61	36.40	32.00	260.17	2.006
					62	37.40	46.00	262.70	2.070
					63	37.70	30.50	265.42	1.983
					64	38.10	35.50	266.97	2.062
					65	38.50	41.30	268.52	1.995
					66	39.00	42.00	270.47	2.066
					67	40.00	46.30	274.34	2.190
					68	40.40	46.00	275.91	2.180
					69	41.40	42.70	279.74	2.077
					70	41.50	38.50	280.14	2.050
					71	42.20	33.50	282.90	2.030
					72	42.50	37.00	284.07	2.084
					73	43.80	37.00	287.44	2.097
					74	43.80	37.60	289.12	2.085
					75	44.20	38.80	290.47	2.114
					76	44.80	49.50	293.00	1.967
					77	45.50	39.00	295.72	2.117
					78	45.80	40.60	296.87	2.111
					79	46.30	41.00	298.83	2.140
					80	47.00	30.80	301.54	1.979
					81	47.60	33.40	304.64	2.060
					82	48.30	35.00	306.60	2.022
					83	48.50	31.80	307.34	2.081
					84	48.70	33.40	308.15	2.028
					85	49.00	34.30	309.52	2.097
					86	49.20	36.00	310.10	2.070
					87	49.40	34.30	312.43	2.043
					88	50.10	37.00	313.54	2.085
					89	50.40	37.40	314.74	2.094
					90	51.00	36.50	317.04	2.078
					91	51.60	33.00	320.70	2.024
					92	52.30	36.40	322.14	2.074
					93	53.00	33.30	324.46	2.027
					94	53.30	34.00	326.03	2.048
					95	54.10	46.00	329.13	1.911
					96	54.80	51.80	331.85	2.005
					97	55.00	77.00	332.43	1.927
					98	55.40	46.10	334.18	1.916
					99	56.00	29.80	336.52	1.972
					100	56.40	25.50	338.07	1.903

FOR M. S. .80 1.50 45.70

FOR M. B. C. 37.00 284.70 1.00 .254

TABLE 6-8 (Continued)

PEACE BOMBHOLE OAR-2A					PEACE BOMBHOLE OIT-11				
J	DIGITIZED DEPTH, z (101V)	DIGITIZED DENSITY, y (101V)	COMPUTED DEPTH (FT)	COMPUTED DENSITY (GM/CC)	J	DIGITIZED DEPTH, z (101V)	DIGITIZED DENSITY, y (101V)	COMPUTED DEPTH (FT)	COMPUTED DENSITY (GM/CC)
101	58.40	38.00	345.84	2.181	1	1.90	22.00	169.37	2.002
102	59.00	38.50	349.17	2.014	2	3.00	26.60	175.70	2.074
103	59.40	39.00	350.11	2.066	3	4.60	35.20	176.04	2.052
104	60.00	39.00	352.06	2.066	4	6.40	46.70	179.21	2.075
105	60.20	37.50	352.83	2.093	5	8.00	59.10	180.79	2.114
106	60.40	36.00	355.16	2.070	6	9.00	60.80	181.57	2.132
107	61.00	34.00	355.94	2.088	7	9.40	60.00	183.15	2.127
108	61.50	34.00	357.11	2.022	8	9.60	58.50	185.94	2.103
109	62.00	37.00	359.03	2.085	9	9.60	56.20	184.72	2.067
110	62.40	33.00	361.38	2.035	10	6.50	45.60	187.00	2.055
111	63.00	37.40	363.71	2.092	11	6.80	36.00	188.66	2.064
112	63.40	39.00	366.04	2.117	12	7.00	38.60	189.65	2.105
113	64.00	37.20	368.76	2.084	13	7.30	38.20	190.63	2.099
114	65.00	41.20	371.48	2.152	14	7.80	35.00	192.60	2.044
115	65.40	39.40	373.04	2.150	15	6.50	36.80	194.57	2.077
116	66.00	31.00	375.57	1.991	16	8.50	37.00	195.35	2.080
117	66.40	33.40	376.54	2.022	17	9.00	39.00	197.32	2.111
118	66.80	33.50	378.44	2.030	18	9.40	33.40	198.90	2.180
119	67.00	32.00	379.33	2.006	19	10.00	45.00	201.26	2.205
120	67.40	34.50	381.97	2.043	20	10.60	43.40	203.62	2.168
121	68.00	34.40	383.53	2.034	21	11.30	38.00	206.38	2.094
122	68.40	37.00	387.02	2.094	22	12.20	33.00	209.92	2.017
123	68.80	37.00	388.19	2.093	23	12.70	31.40	211.84	1.992
124	69.40	38.40	390.52	2.114	24	13.30	34.00	214.25	2.033
125	70.00	38.70	392.07	2.112	25	13.60	34.20	215.43	2.134
126	70.40	38.00	393.24	2.101	26	13.80	35.00	216.72	2.044
127	71.00	40.00	395.57	1.911	27	14.20	36.00	217.80	2.064
128	71.40	40.00	397.51	1.938	28	14.80	44.30	220.16	2.038
129	72.00	38.50	398.42	2.030	29	15.30	44.50	222.13	2.041
130	72.40	37.00	398.78	2.005	30	16.00	46.30	224.88	2.068
131	73.00	34.00	400.06	2.051	31	17.00	30.00	226.82	1.970
132	73.40	37.70	407.23	2.097	32	17.40	48.70	230.34	1.950
133	74.00	37.00	409.46	2.098	33	18.00	32.60	232.76	2.011
134	74.40	34.40	411.89	2.044	34	18.60	33.50	235.12	2.025
135	75.00	36.00	412.67	2.070	35	19.80	48.30	237.87	1.944
136	75.40	37.00	415.58	2.085	36	20.00	27.00	240.63	1.923
137	76.00	39.00	416.94	2.117	37	20.50	31.00	241.81	1.966
138	77.00	38.00	420.05	2.104	38	24.50	32.00	242.60	2.002
139	78.00	39.40	421.99	2.127	39	21.00	30.40	244.57	1.976
140	78.40	38.30	424.71	2.106	40	21.50	29.00	246.54	1.955
141	79.00	36.20	426.26	2.075	41	22.10	25.00	248.90	1.904
142	79.40	35.20	428.98	2.215	42	22.50	24.40	250.47	1.941
143	80.00	34.60	430.93	2.036	43	23.00	30.70	252.44	1.975
144	81.00	34.00	433.65	2.107	44	24.70	35.00	255.20	2.044
145	81.40	34.50	435.20	2.046	45	24.20	34.20	257.17	2.052
146	82.00	33.00	437.53	2.022	46	25.00	37.30	260.31	2.085
147	82.40	35.00	438.70	2.054	47	25.80	37.20	263.46	2.083
148	83.00	40.40	441.42	2.203	48	26.60	35.60	266.25	2.058
149	83.40	39.00	443.50	2.117	49	26.40	35.20	268.83	2.052
150	84.00	41.00	447.24	2.149	50	26.80	35.80	267.40	2.061
151	85.00	33.00	449.57	2.022	51	27.20	35.70	268.98	2.044
152	85.40	44.00	451.91	1.959	52	28.00	36.10	272.13	2.064
153	86.00	44.00	453.77	1.980	53	28.50	35.10	273.11	2.044
154	86.40	40.00	455.01	1.959	54	28.70	35.10	274.88	2.014
155	86.80	38.00	456.14	2.101	55	29.40	34.70	275.67	2.025
156					56	29.50	33.50	277.24	2.025
157					57	29.70	34.50	278.82	2.038
158					58	30.00	35.40	280.00	2.055
159					59	30.50	34.40	281.97	2.037
160					60	30.80	35.80	283.15	2.017
161					61	31.70	34.20	284.64	2.036
162					62	32.80	39.50	289.06	1.962
163					63	34.70	40.30	290.63	1.944
164					64	33.40	42.50	293.39	2.009
165					65	34.80	42.80	294.96	2.014
166					66	34.10	40.70	296.14	2.044
167					67	34.70	43.00	298.50	2.017
168					68	34.90	33.20	299.29	2.020
169					69	35.30	33.20	300.87	2.020
170					70	35.60	34.60	302.05	2.042
171					71	36.10	34.50	304.02	2.041
172					72	36.60	34.90	305.98	2.047
173					73	37.00	42.80	307.56	2.014
174					74	37.60	34.00	309.92	2.033
175					75	38.00	31.80	311.50	1.998
176					76	38.50	32.20	313.46	2.005
177					77	39.00	48.70	315.43	1.944
178					78	39.40	32.00	317.01	2.004
179					79	39.90	29.30	318.98	1.954
180					80	40.10	40.50	319.76	1.978
181					81	40.40	33.90	320.94	2.031
182					82	40.90	31.30	322.91	1.991
183					83	42.00	35.00	327.24	2.044
184					84	42.60	40.80	329.61	2.127
185					85	43.30	34.40	332.56	2.071
186					86	43.80	35.30	334.31	2.053
187					87	44.00	32.00	335.12	2.002
188					88	45.00	32.60	339.06	2.011
189					89	45.40	35.40	341.42	2.055
190					90	46.40	34.70	344.57	2.035
191					91	46.40	40.50	346.54	1.978
192					92	47.20	31.30	347.72	1.991
193					93	48.00	31.50	350.87	1.991
194					94	48.50	33.50	352.05	2.025
195					95	49.40	34.20	356.38	2.036
196					96	50.20	32.00	359.55	2.102
197					97	50.70	29.60	361.50	1.964
198					98	51.30	29.70	363.46	1.966
199					99	51.70	32.40	365.43	2.004
200					100	52.50	38.50	368.58	2.103

T.D. 51 1.00 1.50 63.23

SUM A. B. C. 30.60 355.90 1.00 .25734667

TABLE 6-8 (Continued)

PEACE BOREHOLE URT-11					PEACE BOREHOLE URT-11				
J	DIGITIZED DEPTH, F (DIV)	DIGITIZED DENSITY, g (DIV)	COMPUTED DEPTH, (FT)	COMPUTED DENSITY (GM/CC)	J	DIGITIZED DEPTH, F (DIV)	DIGITIZED DENSITY, g (DIV)	COMPUTED DEPTH, (FT)	COMPUTED DENSITY (GM/CC)
101	55.00	29.00	570.55	2.111	1	1.00	28.50	180.55	1.907
102	55.00	27.00	572.13	2.092	2	2.00	21.50	181.52	2.150
103	55.70	29.00	573.31	2.111	3	2.20	20.60	182.12	2.136
104	56.00	30.50	574.40	2.103	4	3.00	21.10	185.26	2.144
105	56.20	30.90	575.20	2.063	5	3.60	27.20	203.47	1.926
106	56.40	24.70	576.06	2.044	6	4.20	20.50	207.71	1.978
107	56.60	26.30	576.03	2.064	7	4.80	24.70	210.86	1.887
108	56.50	26.10	580.39	2.066	8	10.40	30.40	213.61	1.974
109	57.00	27.20	581.97	2.083	9	10.60	30.40	215.19	1.976
110	56.50	30.00	583.50	2.096	10	11.00	32.30	216.76	2.006
111	56.60	25.90	584.72	2.063	11	11.50	30.20	220.51	1.975
112	56.90	27.90	585.91	2.094	12	12.50	34.50	221.88	2.036
113	57.30	28.00	587.40	2.096	13	12.60	35.60	223.85	2.058
114	57.60	25.30	588.66	2.053	14	13.40	34.10	226.22	2.034
115	58.50	23.20	591.42	2.020	15	14.00	37.00	228.56	2.080
116	58.90	28.40	593.78	2.055	16	15.00	37.00	232.47	2.080
117	59.60	29.80	596.54	2.121	17	15.60	34.00	236.08	2.033
118	60.00	30.70	598.11	2.107	18	16.50	36.20	238.40	2.067
119	60.00	37.00	599.69	2.080	19	17.50	34.00	242.36	2.033
120	60.00	25.00	601.65	2.044	20	17.80	31.70	243.54	1.997
121	61.70	26.00	604.00	2.054	21	19.00	37.60	248.27	2.009
122	62.00	27.20	605.90	2.081	22	20.20	40.20	253.00	2.130
123	62.30	26.50	607.17	2.077	23	20.40	34.00	255.75	2.111
124	63.00	32.00	609.52	2.082	24	21.60	34.00	258.41	2.033
125	63.40	32.80	611.50	2.006	25	22.50	37.40	262.04	2.084
126	64.00	33.20	613.86	2.052	26	23.80	47.20	267.17	1.926
127	64.30	36.00	615.94	2.077	27	24.60	33.20	270.32	2.020
128	64.00	35.00	617.01	2.049	28	25.00	31.00	271.40	1.986
129	65.40	26.60	619.37	2.074	29	25.50	38.00	275.87	2.017
130	65.70	25.20	620.55	2.052	30	26.00	17.50	275.84	1.774
131	66.30	26.60	622.91	2.074	31	26.80	21.80	278.94	1.842
132	66.60	26.40	624.04	2.071	32	27.50	34.20	281.74	2.036
133	66.80	25.30	624.84	2.053	33	28.30	29.00	284.90	1.955
					34	28.60	26.40	290.02	1.914
					35	30.00	29.00	291.59	1.935
					36	30.40	40.20	293.17	1.973
					37	31.20	27.80	296.32	1.936
					38	32.00	28.00	297.47	1.939
					39	32.10	31.80	299.86	1.998
					40	32.60	32.00	302.62	2.002
					41	33.00	33.30	303.91	2.038
					42	34.50	32.60	305.37	2.014
					43	35.90	33.20	306.95	2.020
					44	36.50	32.50	309.31	2.009
					45	37.00	35.00	311.28	2.049
					46	38.00	36.20	313.82	2.067
					47	38.50	35.40	317.19	2.055
					48	37.20	36.90	319.95	2.078
					49	37.90	35.80	322.77	2.061
					50	38.40	43.20	324.67	2.078
					51	39.30	38.20	326.22	2.028
					52	39.80	45.90	329.00	2.081
					53	40.10	45.80	331.37	2.030
					54	40.70	41.30	333.75	1.991
					55	40.90	41.00	334.52	1.986
					56	41.10	49.60	335.30	1.964
					57	41.60	40.00	338.06	1.970
					58	42.40	36.30	340.42	2.069
					59	44.20	49.00	347.51	1.955
					60	45.00	32.20	350.66	2.005
					61	45.60	31.60	353.05	1.995
					62	46.20	47.80	355.59	1.936
					63	46.70	49.00	357.36	1.955
					64	47.50	35.00	360.51	2.049
					65	48.00	36.00	362.48	2.064
					66	48.10	37.40	362.87	2.086
					67	49.10	47.00	366.41	2.080
					68	49.90	36.40	368.97	2.005
					69	50.50	53.00	371.54	2.017
					70	50.90	35.20	373.97	2.054
					71	51.10	35.20	374.64	2.054
					72	52.10	34.20	378.63	2.036
					73	54.50	35.60	380.27	2.058
					74	55.00	35.60	382.17	2.058
					75	55.10	35.10	382.56	2.050
					76	55.20	36.00	382.96	2.064
					77	56.00	36.00	384.11	2.064
					78	56.60	36.50	386.90	2.072
					79	56.70	32.90	388.67	2.076
					80	56.20	32.90	390.83	2.016
					81	55.50	31.70	392.02	1.997
					82	55.80	31.80	393.20	2.017
					83	56.10	34.30	394.58	2.058
					84	56.50	34.00	395.94	2.045
					85	57.00	44.30	397.52	2.058
					86	57.50	42.80	399.49	2.082
					87	56.40	25.70	401.44	1.983
					88	59.40	49.10	407.37	1.956
					89	60.00	25.50	409.74	1.900
					90	60.90	24.90	413.28	1.890
					91	61.50	21.20	415.47	1.889
					92	62.00	21.20	417.61	1.989
					93	63.10	29.70	421.94	1.966
					94	63.80	22.20	424.70	2.020
					95	64.10	21.70	425.86	1.997
					96	64.50	21.00	427.46	1.986
					97	65.00	21.00	429.45	1.986
					98	65.20	20.80	430.22	1.983
					99	65.80	45.80	432.58	2.022
					100	66.50	37.80	434.54	2.014

YUR G. S: .00 1.50 63.40
 YUR G. R. C: 30.00 280.00 1.00 .254

TABLE 6-8 (Continued)

PEACE BOREHOLE DKT-13					PEACE BOREHOLE DKT-13				
J	DIGITIZED DEPTH, X (DIV)	DIGITIZED DENSITY, Y (DIV)	COMPUTED DEPTH (FT)	COMPUTED DENSITY (GM/CC)	J	DIGITIZED DEPTH, X (DIV)	DIGITIZED DENSITY, Y (DIV)	COMPUTED DEPTH (FT)	COMPUTED DENSITY (GM/CC)
101	66.80	33.30	436.52	2.022	201	132.80	45.10	696.07	2.050
102	67.60	29.30	439.67	1.959	202	133.80	35.10	697.23	2.050
103	68.10	30.30	441.64	1.978	203	133.80	39.70	700.38	2.122
104	69.00	37.00	445.14	2.000	204	134.00	36.70	702.74	2.075
105	69.40	45.20	446.76	2.032	205	135.00	46.70	705.11	2.075
106	70.30	36.00	450.38	2.064	206	135.20	35.80	705.89	2.049
107	70.80	36.00	452.27	2.100	207	135.30	35.00	707.00	2.049
108	71.30	36.00	454.20	2.096	208	135.90	37.70	708.65	2.091
109	72.10	39.00	457.39	2.124	209	136.70	37.20	711.80	2.083
110	73.80	25.50	464.09	1.908	210	137.00	40.80	712.98	2.139
111	74.00	48.00	464.87	1.970	211	137.00	31.40	714.15	2.149
112	75.00	34.00	468.81	2.033	212	138.30	39.30	718.10	2.114
113	75.20	46.20	469.60	2.067	213	138.60	39.30	720.07	2.114
114	75.80	33.00	471.96	2.030	214	140.80	32.00	727.45	2.002
115	76.20	44.20	473.54	2.084	215	142.10	42.00	733.07	2.150
116	76.80	31.50	475.09	2.045	216	142.80	41.80	735.82	2.155
117	77.20	34.80	477.44	2.045	217	143.30	38.50	737.74	2.103
118	77.60	34.80	479.05	2.045	218	143.80	40.00	739.74	2.127
119	78.20	38.00	481.81	2.094	219	144.50	41.40	742.52	2.149
120	78.60	34.00	484.56	2.033	220	145.50	35.70	746.46	2.060
121	79.50	32.00	486.54	2.002	221	146.60	36.00	748.43	2.044
122	80.00	30.70	488.50	1.991	222	146.50	45.80	750.40	2.061
123	80.00	32.00	488.90	2.004	223	147.00	38.30	752.37	2.100
124	80.80	33.50	491.65	2.025	224	147.60	38.30	754.75	2.100
125	81.10	32.80	492.83	2.014	225	148.00	41.50	756.30	2.150
126	81.50	35.90	493.62	2.063	226	148.70	41.60	759.06	2.154
127	82.20	34.20	497.17	2.036	227	149.00	42.00	759.85	2.165
128	82.00	46.00	497.05	2.047	228	149.00	38.00	763.74	2.108
129	83.00	32.00	498.32	2.082	229	150.40	49.00	765.76	2.111
130	83.90	31.00	501.11	1.990	230	151.00	46.20	768.12	2.099
131	83.60	32.00	502.68	2.002	231	151.20	38.00	768.91	2.108
132	84.20	39.00	505.04	2.111	232	151.00	45.70	771.27	2.080
133	85.00	46.50	508.19	2.103	233	153.50	44.50	777.96	2.091
134	85.10	34.10	510.95	2.030	234	153.90	35.00	779.54	2.049
135	86.10	35.20	512.53	2.032	235	155.30	41.20	785.85	2.144
136	86.30	39.00	513.81	2.121	236	156.90	45.40	791.35	2.055
137	86.50	38.50	515.20	2.103	237	157.00	46.00	791.75	2.064
138	87.60	48.70	517.65	2.107	238	157.10	46.20	792.14	2.067
139	88.00	45.50	519.01	2.086	239	158.10	40.90	796.88	2.101
140	88.00	41.60	523.16	1.990	240	158.00	40.90	798.08	2.102
141	90.00	40.50	527.09	2.135	241	159.60	48.60	801.99	2.103
142	90.00	42.10	531.04	2.160	242	160.50	48.50	804.74	2.103
143	91.20	41.90	532.61	2.157	243	161.10	53.50	807.89	2.025
144	91.60	33.50	534.19	2.182	244	161.80	43.10	810.65	2.019
145	93.00	35.00	539.70	2.049	245	162.00	47.00	814.70	2.080
146	94.50	35.80	545.61	2.049	246	163.70	57.20	818.13	2.085
147	95.10	37.60	547.97	2.089	247	164.10	40.10	819.71	2.179
148	95.80	38.00	550.73	2.096	248	165.00	48.70	823.25	2.107
149	96.70	36.70	554.27	2.064	249	165.80	51.70	826.40	2.028
150	97.00	35.50	556.22	2.053	250	166.10	51.70	827.39	2.028
151	98.00	34.30	559.59	2.030	251	166.50	52.00	829.16	2.002
152	98.20	36.90	560.18	2.078	252	167.30	45.30	832.51	2.053
153	99.00	36.30	563.33	2.069	253	168.10	48.30	835.46	2.100
154	99.20	37.70	564.12	2.091	254	168.80	48.20	836.22	2.099
155	100.00	48.70	567.87	2.028	255	169.20	49.00	839.79	2.111
156	100.00	35.00	569.84	2.049	256	169.50	38.60	840.98	2.108
157	101.10	47.40	571.68	2.086	257	170.00	48.00	842.95	2.108
158	101.90	43.80	574.75	2.030	258	170.30	47.20	844.13	2.083
159	102.00	36.00	578.69	2.033	259	171.20	46.80	847.67	2.071
160	102.00	40.00	579.87	2.052	260	171.60	46.50	849.95	2.103
161	103.50	40.00	580.99	2.040	261	172.00	47.00	850.92	2.080
162	104.20	40.00	591.68	2.039	262	172.60	44.00	853.18	2.127
163	106.00	36.40	596.05	2.071	263	173.20	46.30	855.35	2.100
164	107.00	36.10	596.02	2.066	264	173.30	46.00	855.94	2.096
165	107.00	46.70	597.99	2.079	265	174.20	45.00	859.49	1.953
166	108.00	33.60	599.56	2.027	266	175.50	40.60	864.61	2.106
167	108.50	40.00	600.74	2.045	267	176.20	45.00	867.36	2.017
168	109.20	40.00	603.50	2.005	268	176.90	41.00	870.18	1.986
169	109.50	38.40	604.68	2.102	269	177.40	37.20	872.04	2.083
170	110.00	30.00	606.65	2.108	270	177.80	35.00	873.66	2.061
171	110.30	49.00	607.03	2.102	271	178.10	36.00	874.84	2.076
172	111.20	33.00	611.58	2.024	272	178.70	45.70	877.21	2.020
173	112.30	41.70	615.71	2.154	273	179.30	35.00	879.57	2.049
174	113.00	40.70	619.65	2.138	274	179.50	34.00	880.36	2.033
175	113.80	41.70	621.62	2.154	275	180.00	45.40	885.48	2.212
176	114.50	41.70	624.57	2.154	276	184.00	35.50	890.20	2.056
177	115.00	36.30	626.54	2.103	277	185.00	37.00	894.14	2.092
178	116.00	38.00	630.28	2.096	278	185.50	35.20	896.11	2.052
179	117.10	40.70	634.61	2.107	279	186.50	34.00	900.05	2.045
180	117.50	41.30	636.19	2.147	280	187.80	35.50	905.17	2.056
181	118.10	42.30	638.55	2.163	281	188.20	37.20	906.74	2.085
182	119.20	39.00	642.88	2.111	282	190.70	36.00	908.71	2.064
183	119.90	39.90	645.25	2.125	283	187.00	35.50	909.70	2.025
184	120.20	39.00	646.82	2.111	284	187.50	35.50	911.86	2.025
185	120.60	40.60	649.18	2.093					
186	121.10	46.70	650.36	2.075					
187	121.70	41.00	652.73	2.143					
188	122.40	43.00	655.09	2.167					
189	123.00	42.90	659.42	2.172					
190	124.20	43.10	662.57	2.176					
191	125.60	42.00	668.09	2.004					
192	126.00	31.00	669.66	2.030					
193	126.50	42.70	670.84	2.013					
194	127.00	35.20	673.60	2.032					
195	128.50	42.80	678.72	2.171					
196	129.10	38.20	681.87	2.099					
197	130.20	32.00	684.20	2.014					
198	130.90	35.00	688.74	2.049					
199	131.40	36.00	690.71	2.077					
200	132.10	35.10	693.64	2.019					
								</	

TOTAL S: .00 1.50 63.80
 TOTAL B. C: 29.54 289.70 1.00 .29399

TABLE 6-8 (Continued)

PEACE BOREHOLE OPZ-18				PEACE BOREHOLE OPZ-18			
J	DIGITIZED DEPTH (DIY)	DIGITIZED DEPTH (DIY)	COMPUTED DEPTH (DIY)	J	DIGITIZED DEPTH (DIY)	DIGITIZED DEPTH (DIY)	COMPUTED DEPTH (DIY)
1	46.00	9.00	387.89	101	104.00	17.00	610.56
2	47.00	9.00	393.83	102	102.00	40.00	611.94
3	47.00	7.10	395.00	103	102.10	20.00	614.70
4	47.00	7.40	397.37	104	102.60	22.20	616.66
5	48.00	6.10	399.34	105	104.00	20.00	618.74
6	48.00	6.30	401.31	106	104.00	19.00	621.39
7	49.00	6.60	402.00	107	105.10	17.00	622.57
8	49.00	6.20	405.24	108	105.00	19.50	623.74
9	50.00	6.50	406.82	109	106.70	16.00	626.87
10	51.00	9.30	409.50	110	107.00	10.00	630.05
11	51.00	9.30	411.55	111	107.20	10.20	630.24
12	52.00	13.30	413.51	112	108.00	23.30	633.99
13	53.00	15.20	418.63	113	108.70	24.70	636.74
14	53.00	14.90	419.81	114	109.00	25.30	637.92
15	55.10	15.70	425.72	115	109.60	22.00	640.29
16	55.00	16.70	426.51	116	110.10	19.30	642.25
17	55.00	15.00	429.67	117	111.00	17.00	645.00
18	56.00	12.00	429.24	118	111.00	17.00	647.37
19	56.30	11.70	430.44	119	112.00	17.00	649.10
20	56.00	13.00	432.01	120	112.20	17.70	651.40
21	56.00	12.30	437.14	121	112.60	10.20	654.97
22	57.00	17.60	441.07	122	113.00	16.90	661.55
23	57.20	17.60	441.07	123	113.60	16.20	663.91
24	57.50	17.90	443.07	124	113.00	15.20	665.09
25	60.00	13.30	448.16	125	113.00	15.60	668.81
26	61.50	17.20	450.92	126	114.20	20.10	671.14
27	62.00	20.00	452.00	127	114.30	15.90	674.47
28	62.00	19.00	454.07	128	114.00	16.30	680.84
29	62.00	18.60	455.67	129	120.00	14.00	681.23
30	63.00	11.60	460.34	130	121.10	16.70	685.56
31	64.30	11.30	461.94	131	121.00	19.20	686.74
32	64.50	13.20	462.73	132	124.10	18.00	689.50
33	65.20	15.20	465.00	133	123.10	23.30	693.94
34	65.00	15.00	466.27	134	123.60	23.30	695.00
35	65.00	13.00	468.24	135	124.70	19.20	695.00
36	66.00	12.60	471.78	136	124.00	19.30	698.16
37	67.10	13.20	472.96	137	124.00	20.20	698.95
38	67.50	17.40	474.54	138	125.70	16.90	701.67
39	68.00	20.00	476.51	139	126.20	20.90	705.64
40	68.00	23.60	478.07	140	126.70	19.50	707.61
41	68.70	22.90	479.26	141	127.20	19.30	709.58
42	69.30	22.70	481.62	142	127.00	16.00	712.33
43	70.00	17.20	484.38	143	127.00	17.10	714.66
44	70.00	17.40	485.96	144	129.60	20.00	714.05
45	70.00	19.40	487.92	145	130.10	19.70	720.99
46	71.00	18.90	489.10	146	130.60	19.60	722.96
47	71.50	19.70	490.10	147	131.20	18.70	725.35
48	72.00	16.20	490.68	148	132.00	14.70	728.47
49	72.10	17.90	492.65	149	132.00	16.10	732.02
50	72.20	15.90	495.04	150	133.20	15.00	733.20
51	73.00	15.20	495.40	151	133.00	16.20	735.99
52	73.00	15.30	496.14	152	134.10	16.20	736.74
53	73.20	14.40	496.94	153	134.00	20.00	739.04
54	73.60	14.20	498.55	154	135.20	18.00	741.07
55	74.00	10.00	501.31	155	135.30	19.10	741.07
56	75.00	15.50	504.07	156	136.20	16.70	745.03
57	75.50	16.50	506.05	157	136.00	17.00	746.59
58	76.00	20.70	508.74	158	136.00	16.70	747.77
59	76.70	10.60	510.74	159	137.00	16.40	750.52
60	77.10	10.40	512.33	160	138.00	15.00	752.10
61	77.60	17.00	514.30	161	138.00	16.70	754.87
62	78.20	10.90	516.64	162	139.00	16.90	756.03
63	79.50	16.30	521.76	163	139.00	16.90	757.63
64	80.10	19.00	524.14	164	139.70	17.30	758.79
65	82.10	19.00	528.08	165	140.00	17.90	759.97
66	81.30	10.40	529.87	166	140.00	10.10	762.33
67	82.10	10.60	532.02	167	141.00	20.10	765.09
68	82.00	10.00	535.36	168	141.00	18.00	765.06
69	82.00	15.70	541.47	169	141.90	15.20	767.95
70	84.00	10.00	543.04	170	142.00	14.60	767.04
71	85.00	12.10	545.81	171	142.70	14.10	770.60
72	85.00	12.00	546.59	172	143.00	15.50	771.78
73	86.30	11.00	548.55	173	143.00	25.70	773.36
74	87.00	16.60	551.31	174	143.50	16.60	775.75
75	87.00	16.70	552.10	175	144.00	12.30	775.72
76	87.00	10.00	553.67	176	144.00	9.20	776.87
77	87.20	17.70	556.03	177	145.10	11.20	780.05
78	88.00	13.00	558.79	178	145.20	9.00	782.41
79	89.10	15.00	559.50	179	146.20	10.90	784.38
80	89.00	15.30	560.76	180	146.00	10.00	785.17
81	90.00	14.00	563.91	181	146.90	13.00	787.14
82	90.50	15.30	565.99	182	147.10	12.20	787.92
83	91.00	19.70	567.06	183	147.70	11.90	790.24
84	92.00	16.00	570.99	184	148.10	14.00	791.86
85	92.60	28.00	573.36	185	148.20	14.00	794.19
86	92.90	22.00	574.34	186	150.00	17.00	795.34
87	93.50	13.00	576.90	187	150.00	14.70	802.44
88	94.10	16.10	579.36	188	151.20	14.70	804.07
89	94.10	16.20	580.05	189	151.00	13.50	804.85
90	94.90	43.50	582.41	190	152.00	16.20	807.21
91	95.20	19.00	583.59	191	152.00	19.50	808.74
92	96.70	14.90	587.53	192	152.00	10.00	811.15
93	96.00	3.10	594.09	193	153.50	15.20	813.12
94	96.00	2.90	595.89	194	154.10	16.00	815.48
95	97.20	16.40	599.34	195	154.00	15.50	818.24
96	97.00	9.60	602.10	196	154.00	16.00	819.81
97	98.20	11.70	603.88	197	154.00	12.00	822.96
98	100.00	11.00	606.93	198	156.00	12.00	823.75
99	101.00	12.00	607.21	199	156.90	10.00	826.51
100	101.00	12.00	607.21	200	157.50	10.00	828.08

TABLE 6-8 (Continued)

PEACE BOREHOLE OPZ-18					PEACE BOREHOLE WAR-01				
	DEPTH, ft (DIV)	DENSITY, g/cm ³ (DIV)	COMPUTED DENSITY (g/cm ³)	COMPUTED DENSITY (g/cm ³)		DEPTH, ft (DIV)	DENSITY, g/cm ³ (DIV)	COMPUTED DENSITY (g/cm ³)	COMPUTED DENSITY (g/cm ³)
201	157.00	8.96	838.44	1.983	1	20.00	46.00	189.94	1.921
202	158.00	10.00	832.41	1.980	2	20.20	46.20	192.74	1.960
203	159.00	8.10	835.50	1.986	3	21.20	46.00	194.75	1.955
204	159.20	14.30	835.54	2.000	4	21.40	46.00	195.50	1.978
205	159.60	14.70	837.14	2.074	5	21.60	47.00	197.14	1.931
206	160.00	16.30	838.71	2.099	6	22.20	10.00	198.76	1.659
207	161.00	14.60	842.65	2.072	7	22.40	1.00	199.57	1.516
208	162.00	19.20	846.30	2.066	8	23.40	7.00	201.90	1.612
209	162.60	18.00	848.95	2.047	9	23.30	4.10	203.10	1.644
210	163.50	18.00	852.49	2.060	10	23.70	7.70	204.79	1.623
211	164.00	16.00	854.46	2.094	11	24.10	10.00	206.40	1.639
212	164.30	17.00	855.64	2.119	12	24.30	17.00	208.00	1.704
213	165.00	6.30	861.55	1.942	13	24.60	16.00	209.21	1.755
214	166.00	10.00	863.91	2.000	14	24.90	15.20	209.61	1.742
215	166.80	11.00	865.48	2.016	15	25.10	15.10	210.41	1.761
216	167.20	10.00	867.04	2.000	16	25.20	14.00	210.82	1.723
217	168.00	13.20	870.21	2.050	17	25.40	14.00	211.62	1.760
218	168.20	13.20	870.99	2.050	18	26.00	10.00	214.03	1.659
219	169.00	15.00	871.78	2.091	19	26.40	2.10	215.64	1.532
220	169.30	15.70	874.54	2.090	20	26.80	3.00	217.65	1.568
221	169.60	15.00	876.51	2.079	21	27.20	13.00	218.85	1.707
222	169.80	15.10	877.29	2.083	22	27.50	45.60	220.06	1.900
223	170.20	17.20	878.07	2.113	23	28.00	4.30	223.28	1.569
224	170.60	16.91	880.44	2.100	24	29.30	10.40	227.24	1.666
225	171.00	18.50	882.02	2.134	25	29.80	10.60	229.30	1.669
					26	30.10	17.70	230.50	1.782
					27	31.00	1.20	234.10	1.519
					28	31.50	4.00	236.11	1.564
					29	31.60	3.90	236.53	1.561
					30	31.90	5.10	237.73	1.581
					31	32.40	3.00	239.74	1.548
					32	32.50	4.70	240.14	1.511
					33	33.20	12.70	242.44	1.703
					34	33.40	13.20	243.76	1.711
					35	33.70	16.80	244.96	1.800
					36	34.20	11.90	246.97	1.690
					37	34.60	11.00	248.58	1.675
					38	34.90	8.90	249.74	1.628
					39	35.60	16.00	252.67	1.755
					40	36.00	19.00	254.26	1.730
					41	36.60	16.70	256.62	1.764
					42	37.00	17.00	258.22	1.771
					43	37.30	40.50	259.43	1.827
					44	37.70	41.30	261.03	1.840
					45	37.90	20.00	261.84	1.819
					46	38.20	19.00	263.04	1.803
					47	38.30	18.80	263.44	1.787
					48	38.70	17.90	265.05	1.785
					49	39.40	13.20	267.86	1.711
					50	39.70	15.00	269.24	1.739
					51	40.10	45.20	270.48	1.902
					52	40.60	42.60	272.68	1.860
					53	41.00	42.50	274.24	1.859
					54	41.20	42.00	275.10	1.851
					55	41.60	43.20	276.73	1.870
					56	42.10	43.20	278.73	1.870
					57	42.50	44.00	279.51	1.883
					58	42.70	46.20	281.12	1.910
					59	43.50	43.20	284.34	1.870
					60	43.80	25.00	285.54	1.899
					61	44.30	43.80	287.55	1.880
					62	44.70	44.70	289.16	1.894
					63	44.90	43.60	289.76	1.874
					64	45.20	17.40	291.17	1.778
					65	45.60	24.20	293.58	1.806
					66	46.70	10.00	297.19	1.639
					67	47.30	45.70	299.60	1.910
					68	47.50	45.00	300.41	1.867
					69	47.60	42.90	300.81	1.885
					70	47.70	41.20	301.21	1.870
					71	48.20	30.80	303.22	1.991
					72	48.30	48.20	305.62	1.930
					73	48.40	30.80	304.02	1.991
					74	48.80	40.00	305.63	1.819
					75	49.20	45.90	307.23	1.915
					76	49.80	42.10	309.65	1.852
					77	50.10	44.10	310.85	1.884
					78	50.50	40.30	312.46	1.824
					79	51.10	49.60	314.87	1.972
					80	51.50	49.70	316.48	1.974
					81	52.00	42.00	318.48	1.910
					82	52.20	41.00	319.29	1.894
					83	52.80	41.90	321.70	1.849
					84	53.60	40.80	324.91	1.831
					85	54.10	40.00	326.92	1.978
					86	54.30	46.80	328.53	1.919
					87	54.90	49.90	330.15	1.977
					88	55.50	15.00	332.54	1.734
					89	55.80	12.90	333.75	1.704
					90	56.40	18.00	336.16	1.787
					91	56.70	19.50	337.87	1.811
					92	57.10	18.20	338.97	1.771
					93	57.80	19.90	341.79	1.817
					94	58.00	20.60	343.80	1.829
					95	58.00	42.80	346.61	1.864
					96	58.00	43.60	348.21	1.876
					97	59.00	40.90	349.82	1.783
					98	60.50	16.40	352.63	1.762
					99	61.00	25.00	355.44	1.849
					100	61.60	26.60	357.55	1.924

YU = 5: 10.00 1.00 63.40
 XJ = A, B, C: 30.00 32.90 1.00 1.254

TABLE 6-8 (Continued)

PEACE BUREAU HOLE 444-01					PEACE BUREAU HOLE 444-01				
J	DISTILLED DEPTH, ft (DIY)	DISTILLED DEPTH, ft (DIY)	COMPUTED DEPTH, ft (DY)	COMPUTED DEPTH, ft (DY)	J	DISTILLED DEPTH, ft (DIY)	DISTILLED DEPTH, ft (DIY)	COMPUTED DEPTH, ft (DY)	COMPUTED DEPTH, ft (DY)
191	67.50	66.60	379.95	1.924	201	121.70	90.00	598.50	2.138
192	68.50	67.70	382.76	1.974	202	122.50	90.60	600.91	2.227
193	69.50	68.80	385.97	2.022	203	123.50	91.20	603.92	2.317
194	69.70	69.00	386.78	2.067	204	124.50	91.80	606.12	2.359
195	69.70	69.00	389.54	2.138	205	125.50	92.40	607.74	2.402
196	70.50	69.80	392.80	2.234	206	126.50	93.00	609.35	2.469
197	70.50	69.80	394.41	2.308	207	127.50	93.60	610.95	2.474
198	71.50	70.80	397.23	2.354	208	128.50	94.20	613.56	2.498
199	72.50	71.80	398.83	2.438	209	129.50	94.80	615.77	2.487
200	72.50	71.80	402.05	2.499	210	130.50	95.40	617.78	2.496
201	73.50	72.80	403.65	2.522	211	131.50	96.00	618.98	2.490
202	73.50	72.80	406.86	2.588	212	132.50	96.60	620.60	2.490
203	74.50	73.80	408.07	2.642	213	133.50	97.20	622.60	2.474
204	74.50	73.80	408.07	2.692	214	134.50	97.80	624.21	2.474
205	75.50	74.80	411.29	2.758	215	135.50	98.40	626.62	2.474
206	75.50	74.80	414.90	2.800	216	136.50	99.00	628.65	2.461
207	76.50	75.80	415.71	2.830	217	137.50	99.60	630.24	2.461
208	77.50	76.80	418.92	2.884	218	138.50	100.20	631.04	2.462
209	77.50	76.80	421.33	2.854	219	139.50	100.80	632.65	2.462
210	78.50	77.80	423.74	2.884	220	140.50	101.40	635.96	2.462
211	78.50	77.80	426.15	2.934	221	141.50	102.00	638.67	2.451
212	79.50	78.80	428.96	2.982	222	142.50	102.60	642.64	2.444
213	80.50	79.80	432.18	3.034	223	143.50	103.20	643.92	2.417
214	80.50	79.80	433.78	3.099	224	144.50	103.80	647.51	2.425
215	81.50	80.80	436.70	3.149	225	145.50	104.40	649.57	2.487
216	82.50	81.80	439.51	3.199	226	146.50	105.00	651.13	2.484
217	82.50	81.80	441.82	3.249	227	147.50	105.60	652.74	2.487
218	83.50	82.80	444.63	3.299	228	148.50	106.20	655.98	2.484
219	84.50	83.80	448.05	3.352	229	149.50	106.80	658.35	2.487
220	84.50	83.80	449.04	3.399	230	150.50	107.40	659.76	2.425
221	85.50	84.80	452.46	3.452	231	151.50	108.00	662.57	2.425
222	85.50	84.80	454.06	3.502	232	152.50	108.60	664.57	2.425
223	86.50	85.80	457.48	3.554	233	153.50	109.20	667.51	2.425
224	86.50	85.80	459.08	3.604	234	154.50	109.80	669.51	2.425
225	87.50	86.80	462.50	3.657	235	155.50	110.40	671.62	2.425
226	87.50	86.80	464.10	3.707	236	156.50	111.00	673.22	2.425
227	88.50	87.80	467.52	3.760	237	157.50	111.60	675.22	2.425
228	88.50	87.80	469.12	3.810	238	158.50	112.20	677.22	2.425
229	89.50	88.80	472.54	3.863	239	159.50	112.80	679.22	2.425
230	89.50	88.80	474.14	3.913	240	160.50	113.40	680.86	2.425
231	90.50	89.80	477.56	3.966	241	161.50	114.00	682.86	2.425
232	90.50	89.80	479.16	4.016	242	162.50	114.60	684.86	2.425
233	91.50	90.80	482.58	4.069	243	163.50	115.20	686.86	2.425
234	91.50	90.80	484.18	4.119	244	164.50	115.80	688.86	2.425
235	92.50	91.80	487.60	4.172	245	165.50	116.40	690.86	2.425
236	92.50	91.80	489.20	4.222	246	166.50	117.00	692.86	2.425
237	93.50	92.80	492.62	4.275	247	167.50	117.60	694.86	2.425
238	93.50	92.80	494.22	4.325	248	168.50	118.20	696.86	2.425
239	94.50	93.80	497.64	4.378	249	169.50	118.80	698.86	2.425
240	94.50	93.80	500.24	4.431	250	170.50	119.40	700.86	2.425
241	95.50	94.80	503.66	4.484	251	171.50	120.00	702.86	2.425
242	95.50	94.80	505.26	4.534	252	172.50	120.60	704.86	2.425
243	96.50	95.80	508.68	4.587	253	173.50	121.20	706.86	2.425
244	96.50	95.80	510.28	4.637	254	174.50	121.80	708.86	2.425
245	97.50	96.80	513.70	4.690	255	175.50	122.40	710.86	2.425
246	97.50	96.80	515.30	4.740	256	176.50	123.00	712.86	2.425
247	98.50	97.80	518.72	4.793	257	177.50	123.60	714.86	2.425
248	98.50	97.80	520.32	4.843	258	178.50	124.20	716.86	2.425
249	99.50	98.80	523.74	4.896	259	179.50	124.80	718.86	2.425
250	99.50	98.80	525.34	4.946	260	180.50	125.40	720.86	2.425
251	100.50	99.80	528.76	4.999	261	181.50	126.00	722.86	2.425
252	100.50	99.80	530.36	5.049	262	182.50	126.60	724.86	2.425
253	101.50	100.80	533.78	5.102	263	183.50	127.20	726.86	2.425
254	101.50	100.80	535.38	5.152	264	184.50	127.80	728.86	2.425
255	102.50	101.80	538.80	5.205	265	185.50	128.40	730.86	2.425
256	102.50	101.80	540.40	5.255	266	186.50	129.00	732.86	2.425
257	103.50	102.80	543.82	5.308	267	187.50	129.60	734.86	2.425
258	103.50	102.80	545.42	5.358	268	188.50	130.20	736.86	2.425
259	104.50	103.80	548.84	5.411	269	189.50	130.80	738.86	2.425
260	104.50	103.80	550.44	5.461	270	190.50	131.40	740.86	2.425
261	105.50	104.80	553.86	5.514	271	191.50	132.00	742.86	2.425
262	105.50	104.80	555.46	5.564	272	192.50	132.60	744.86	2.425
263	106.50	105.80	558.88	5.617	273	193.50	133.20	746.86	2.425
264	106.50	105.80	560.48	5.667	274	194.50	133.80	748.86	2.425
265	107.50	106.80	563.90	5.720	275	195.50	134.40	750.86	2.425
266	107.50	106.80	565.50	5.770	276	196.50	135.00	752.86	2.425
267	108.50	107.80	568.92	5.823	277	197.50	135.60	754.86	2.425
268	108.50	107.80	570.52	5.873	278	198.50	136.20	756.86	2.425
269	109.50	108.80	573.94	5.926	279	199.50	136.80	758.86	2.425
270	109.50	108.80	575.54	5.976	280	200.50	137.40	760.86	2.425
271	110.50	109.80	578.96	6.029	281	201.50	138.00	762.86	2.425
272	110.50	109.80	580.56	6.079	282	202.50	138.60	764.86	2.425
273	111.50	110.80	583.98	6.132	283	203.50	139.20	766.86	2.425
274	111.50	110.80	585.58	6.182	284	204.50	139.80	768.86	2.425
275	112.50	111.80	589.00	6.235	285	205.50	140.40	770.86	2.425
276	112.50	111.80	590.60	6.285	286	206.50	141.00	772.86	2.425
277	113.50	112.80	594.02	6.338	287	207.50	141.60	774.86	2.425
278	113.50	112.80	595.62	6.388	288	208.50	142.20	776.86	2.425
279	114.50	113.80	599.04	6.441	289	209.50	142.80	778.86	2.425
280	114.50	113.80	600.64	6.491	290	210.50	143.40	780.86	2.425
281	115.50	114.80	604.06	6.544	291	211.50	144.00	782.86	2.425
282	115.50	114.80	605.66	6.594	292	212.50	144.60	784.86	2.425
283	116.50	115.80	609.08	6.647	293	213.50	145.20	786.86	2.425
284	116.50	115.80	610.68	6.697	294	214.50	145.80	788.86	2.425
285	117.50	116.80	614.10	6.750	295	215.50	146.40	790.86	2.425
286	117.50	116.80	615.70	6.800	296	216.50	147.00	792.86	2.425
287	118.50	117.80	619.12	6.853	297	217.50	147.60	794.86	2.425
288	118.50	117.80	620.72	6.903	298	218.50	148.20	796.86	2.425
289	119.50	118.80	624.14	6.956	299	219.50	148.80	798.86	2.425
290	119.50	118.80	625.74	7.006	300	220.50	149.40	800.86	2.425

TABLE 6-8 (Continued)

PEACE BORERHOLE KAN-01					PEACE BORERHOLE KAN-01				
W	DIGITIZED DEPTH, Z (DIV)	DIGITIZED DENSITY, Y (DIV)	COMPUTED DEPTH (FT)	COMPUTED DENSITY (G/CC)	J	DIGITIZED DEPTH, Z (DIV)	DIGITIZED DENSITY, Y (DIV)	COMPUTED DEPTH (FT)	COMPUTED DENSITY (G/CC)
201	175.50	29.00	805.80	2.122	401	230.00	30.00	1037.21	1.978
202	175.50	28.00	807.01	2.106	402	231.00	30.50	1037.61	1.986
203	176.10	30.00	809.01	2.049	403	231.00	30.50	1041.22	1.986
204	176.70	31.00	811.02	2.007	404	232.50	30.00	1043.65	2.074
205	175.40	35.00	816.28	2.038	405	233.00	35.00	1045.64	2.058
206	176.00	36.20	816.45	2.005	406	233.20	35.50	1046.45	2.054
207	176.20	32.20	817.45	2.014	407	233.60	32.90	1048.05	2.027
208	176.50	32.00	818.46	2.010	408	234.50	34.10	1050.86	2.044
209	176.90	30.00	820.26	1.983	409	234.70	32.50	1052.87	2.018
210	177.50	30.10	822.67	1.998	410	235.00	32.50	1053.68	1.970
211	176.00	30.10	824.68	2.008	411	236.00	32.00	1057.69	2.014
212	178.70	30.00	827.99	2.002	412	236.00	32.00	1060.10	2.010
213	179.20	30.30	829.50	2.103	413	237.00	31.10	1061.51	2.060
214	180.10	31.30	833.12	1.999	414	238.20	31.10	1064.53	1.994
215	180.60	37.00	835.93	2.090	415	238.80	32.50	1068.94	2.014
216	181.00	37.30	836.71	2.095	416	239.20	32.40	1070.55	2.017
217	181.50	36.00	837.94	2.074	417	240.00	30.00	1073.76	1.104
218	181.00	31.00	844.95	2.007	418	240.20	33.50	1074.57	2.194
219	184.50	36.50	841.06	4.082	419	240.70	34.00	1074.78	2.229
220	184.90	36.70	844.37	2.117	420	241.00	34.00	1075.74	2.102
221	184.10	31.30	849.14	1.999	421	241.40	31.40	1076.54	2.102
222	184.70	35.00	851.60	4.058	422	241.90	31.40	1076.54	2.102
223	185.30	37.30	855.01	2.095	423	242.50	31.70	1076.54	2.126
224	185.70	36.00	855.62	2.074	424	242.50	31.40	1076.54	2.081
225	186.00	36.20	856.82	2.045	425	242.50	31.40	1076.54	2.081
226	186.00	32.90	858.03	2.025	426	242.50	31.50	1076.54	2.098
227	187.30	39.00	862.0	2.128	427	242.50	31.60	1076.54	2.074
228	187.30	37.70	864.05	2.101	428	242.50	31.60	1076.54	2.049
229	188.20	38.40	865.66	2.112	429	242.50	31.60	1076.54	2.085
230	188.50	37.60	867.87	2.100	430	242.50	31.60	1076.54	2.082
231	188.90	34.20	868.47	2.045	431	242.50	31.60	1076.54	2.082
232	189.50	35.50	870.88	2.066	432	242.50	31.60	1076.54	2.082
233	190.00	32.30	872.89	2.015	433	242.50	31.60	1076.54	2.082
234	190.50	32.30	874.90	2.015	434	242.50	31.60	1076.54	2.082
235	190.60	31.20	875.30	1.998	435	242.50	31.60	1076.54	2.082
236	191.20	30.00	877.71	1.995	436	242.50	31.60	1076.54	2.082
237	192.00	30.00	880.93	2.106	437	242.50	31.60	1076.54	2.082
238	192.60	35.40	883.34	2.065	438	242.50	31.60	1076.54	2.082
239	193.20	33.70	885.75	2.037	439	242.50	31.60	1076.54	2.082
240	194.80	30.30	889.97	2.111	440	242.50	31.60	1076.54	2.082
241	194.50	37.50	890.97	2.098	441	242.50	31.60	1076.54	2.082
242	195.10	34.00	893.38	2.042	442	242.50	31.60	1076.54	2.082
243	195.70	38.10	895.79	2.100	443	242.50	31.60	1076.54	2.082
244	196.10	30.00	897.40	2.104	444	242.50	31.60	1076.54	2.082
245	197.00	40.00	901.01	2.202	445	242.50	31.60	1076.54	2.082
246	197.30	41.50	902.22	2.162	446	242.50	31.60	1076.54	2.082
247	197.60	40.80	904.23	2.151	447	242.50	31.60	1076.54	2.082
248	198.00	39.30	905.03	2.127	448	242.50	31.60	1076.54	2.082
249	198.60	40.50	907.44	2.130	449	242.50	31.60	1076.54	2.082
250	199.20	40.80	909.85	2.109	450	242.50	31.60	1076.54	2.082
251	199.50	35.50	911.06	2.066	451	242.50	31.60	1076.54	2.082
252	199.90	35.50	912.46	2.063	452	242.50	31.60	1076.54	2.082
253	200.40	38.00	914.67	2.104	453	242.50	31.60	1076.54	2.082
254	200.60	42.00	915.46	2.170	454	242.50	31.60	1076.54	2.082
255	201.00	42.00	917.88	2.174	455	242.50	31.60	1076.54	2.082
256	201.30	41.00	918.79	2.154	456	242.50	31.60	1076.54	2.082
257	201.50	38.90	921.10	2.089	457	242.50	31.60	1076.54	2.082
258	202.40	38.00	922.71	2.130	458	242.50	31.60	1076.54	2.082
259	202.80	40.10	924.72	2.124	459	242.50	31.60	1076.54	2.082
260	203.00	43.10	928.73	2.187	460	242.50	31.60	1076.54	2.082
261	204.00	41.00	929.14	2.154	461	242.50	31.60	1076.54	2.082
262	204.60	37.00	931.35	2.096	462	242.50	31.60	1076.54	2.082
263	204.10	40.70	933.56	2.149	463	242.50	31.60	1076.54	2.082
264	205.70	37.70	935.97	2.101	464	242.50	31.60	1076.54	2.082
265	206.10	40.50	937.57	2.146	465	242.50	31.60	1076.54	2.082
266	206.60	39.80	940.80	2.127	466	242.50	31.60	1076.54	2.082
267	207.20	41.00	941.99	2.152	467	242.50	31.60	1076.54	2.082
268	207.80	41.20	942.80	2.157	468	242.50	31.60	1076.54	2.082
269	208.10	40.60	945.61	2.211	469	242.50	31.60	1076.54	2.082
270	208.80	40.50	948.42	2.186	470	242.50	31.60	1076.54	2.082
271	209.00	36.50	949.22	2.082	471	242.50	31.60	1076.54	2.082
272	209.50	38.10	951.23	2.044	472	242.50	31.60	1076.54	2.082
273	210.00	40.80	953.65	2.151	473	242.50	31.60	1076.54	2.082
274	211.00	38.90	958.06	1.983	474	242.50	31.60	1076.54	2.082
275	212.20	36.90	962.08	2.089	475	242.50	31.60	1076.54	2.082
276	213.50	36.40	967.30	2.081	476	242.50	31.60	1076.54	2.082
277	214.00	37.30	969.51	2.095	477	242.50	31.60	1076.54	2.082
278	214.70	30.30	972.12	2.047	478	242.50	31.60	1076.54	2.082
279	215.50	36.00	975.34	2.074					
280	216.00	39.50	976.44	2.130					
281	216.50	38.70	979.35	2.117					
282	218.20	37.50	984.18	2.098					
283	219.00	39.30	989.40	2.127					
284	219.50	40.00	990.60	2.130					
285	220.40	38.00	995.02	2.106					
286	222.30	38.00	1002.66	1.947					
287	224.10	36.60	1008.27	2.004					
288	224.70	35.00	1008.27	2.026					
289	224.90	42.50	1009.48	2.018					
290	225.50	40.00	1011.49	2.130					
291	226.00	40.60	1013.50	2.148					
292	225.40	40.50	1015.11	2.111					
293	226.00	40.70	1017.52	1.980					
294	226.70	35.50	1020.33	2.034					
295	227.10	37.90	1021.94	2.104					
296	228.00	36.10	1023.55	2.044					
297	228.70	37.00	1026.37	2.090					
298	229.20	40.30	1030.58	2.145					
299	231.00	32.40	1033.49	2.018					
300	231.50	32.40	1035.60	2.017					
					YOU MAY SEE	1.00	1.50	62.90	
					YOU MAY SEE	30.00	250.10	875.60	217.80

YU M S: .00 1.50 62.90
 YU A B C: 30.00 230.10 875.00 217.80

APPENDIX 6-2

DENSITIES OF "CORAL" AND ITS SOLID COMPONENT AS CONTINUOUS FUNCTIONS OF DEPTH

Data on the composition of coral solids¹ place its density ρ_S in a narrow range of values (2.71 to 2.93 g/cc; see Tremba and Ristvet, 1986). Within that range, however, ρ_S varies erratically over the discrete set of borehole depths for which solid composition has been measured. Hence, in a given borehole, straight-line connections between measured (ρ_S, z) -points embody virtually all the extant information on the continuous change of ρ_S with depth (or altitude) z . At that level of description, we have:

$$\rho_S = [(z - z_m) \rho_S^{m+1} + (z_{m+1} - z) \rho_S^m] / (z_{m+1} - z_m) \quad ; m=1, 2, \dots, M \quad \text{Eq. (13)}$$

with (ρ_S^m, z_m) denoting point m of the set measured for a given borehole, and with the points so ordered that depth decreases as m increases.

For the same borehole, let the z_j -points of Eq. (11) also be ordered so that depth decreases as j increases. Now, merge the two sets of z -values, and number different z 's of the combined set in the order of decreasing depth (again), obtaining thereby the values z_k ($k=1, 2, \dots, K+1$). The z -interval between z_k and z_{k+1} ($k=1, 2, \dots, K$) must then lie entirely within one of the z -intervals on which ρ (the density of coral) has the linear depth-dependence specified by Eq. (11); it must also lie entirely within one of the z -intervals of linear variation of ρ_S (the density of the coral solid) specified by Eq. (13). However, a given z_k -value need not appear among the z_j 's of Eq. (11); if not, then, at $z=z_k$, the value of ρ ($=\rho_k$) is obtained from Eq. (11) for the z_j -interval in which $z=z_k$ falls. Likewise, for a z_k -value not among the z_m 's of Eq. (13), we find the z_m -interval in which z_k falls, and use Eq. (13) to compute ρ_S at z_k ($\rho_S = \rho_S^k$). Eqs. (11) and (13) can then be replaced by the following equivalent relations:

$$\begin{aligned} \rho &= [(z - z_k) \rho_{k+1}^- + (z_{k+1} - z) \rho_k^+] / (z_{k+1} - z_k) \\ \rho_S &= [(z - z_k) \rho_S^{k+1} + (z_{k+1} - z) \rho_S^k] / (z_{k+1} - z_k) \end{aligned} \quad ; k=1, 2, \dots, K \quad \text{Eq. (14)}$$

In accord with Appendix 6-1, $\rho_k^- = \rho_k^+ = \rho_k$ for the γ - γ profiles; for the BHG profiles, $\rho_k^+ = \rho_{k+1}^- = \rho_{k+1/2}$ where $\rho_{k+1/2} = \rho_{j+1/2}$ -- the value of j being set by the requirement that the interval from z_k to z_{k+1} lie on the interval of Table 6-7 from z_j to z_{j+1} .

For each borehole included in the BHG survey, Table 6-9 (located in this Appendix) presents the depths z_k ($k=1, 2, \dots, K+1$) that mark the endpoints of

¹ See footnote 3 on page 6-1 for explanation of use of "coral" in this text.

the depth-intervals on which both ρ and ρ_S are simple linear functions of z [Eq. (14)]. For each depth z_k , the density of either coral or its solid component is also shown (third and fourth columns of table). Where blank spaces appear between two listed values of coral density ρ (called "BHG DENSITY" in tbl. 6-9), those two ρ 's are identical; that same value applies everywhere between them. Also, where values of ρ appear, the density ρ_S of coral's solid component does not; the value of ρ_S at that blank spot is given by Eq. (13) with z equal to the depth listed (or to its negative, if z denotes height).

MASS OF SOLID AS A CONTINUOUS FUNCTION OF DEPTH IN A BOREHOLE

Table 6-9 (in this Appendix 6-2) and Eqs. (13) allow ρ and ρ_S to be computed for any depth and borehole covered by the BHG survey. Hence, the mass m_S of coral solid can also be computed from Eq. (5). In fact, given piecewise linear dependence of ρ and ρ_S on z [Eq. (14)], m_S can be expressed in terms of z using only elementary functions. In particular, if z lies between z_k and z_{k+1} , then:

$$m_S = m_S^k + \int_{z_k}^z \rho_S \left(\frac{\rho - \rho_L}{\rho_S - \rho_L} \right) dh \quad ; \quad k = 1, 2, \dots, K \quad \text{Eq. (15)}$$

where $m_S^1 = 0$ and

$$m_S^k = m_S^{k-1} + \int_{z_{k-1}}^{z_k} \rho_S \left(\frac{\rho - \rho_L}{\rho_S - \rho_L} \right) dh \quad ; \quad k = 2, 3, \dots, K+1 \quad \text{Eq. (16)}$$

Next, observing that $\rho_S / (\rho_S - \rho_L) = (\rho_S - \rho_L + \rho_L) / (\rho_S - \rho_L)$, we can write Eq. (15) as follows:

$$m_S = m_S^k + \int_{z_k}^z \left[(\rho - \rho_L) + \rho_L \left(\frac{\rho - \rho_L}{\rho_S - \rho_L} \right) \right] dh \quad \text{Eq. (17)}$$

Replacing ρ and ρ_S in Eq. (17) by their linear equivalents in terms of z [Eq. (14)], we obtain

$$m_S = m_S^k + \int_{z_k}^z \left\{ a_k + b_k(h - z_k) + \rho_L \left[\frac{a_k + b_k(h - z_k)}{a_k' + b_k'(h - z_k)} \right] \right\} dh \quad \text{Eq. (18)}$$

where

$$a_k = \rho_k - \rho_L, \quad b_k = (\rho_{k+1} - \rho_k) / (z_{k+1} - z_k); \quad a_k' = \rho_S - \rho_L, \quad b_k' = (\rho_S^{k+1} - \rho_S^k) / (z_{k+1} - z_k) \quad \text{Eq. (19)}$$

The integral of Eq. (17) is readily found as an explicit function of z (Pierce, 1929)

$$m_S = m_S^k + a_k x + b_k x^2 + \rho_L \left[\frac{b_k x}{b_k'} + \frac{(a_k b_k' - a_k' b_k)}{(b_k')^2} \cdot \ln \left(\frac{a_k' + b_k' x}{a_k'} \right) \right] \quad \text{Eq. (20)}$$

where $x = z - z_k$.

From Eq. (16), it follows that $m_S = m_S^{k+1}$, when z is set equal to z_{k+1} in Eq. (20); with m_S^{k+1} known, a similar computation then gives m_S^{k+2} , etc. Thus, using the depths and densities of Table 6-9, the m_S^k -values ($k=2, \dots, K+1$) can be computed in sequence from Eq. (20). For each borehole of the BHG survey, the resulting values of m_S^2, m_S^3, m_S^{K+1} appear in the seventh column of Table 6-9, starting at the greatest depth logged in that hole. Listed in the sixth column is an approximation to m^k -- \underline{m}_S , say -- obtained by setting ρ_S equal to its mid-value $\underline{\rho}_S^k \equiv 1/2(\rho_S^{k+1} + \rho_S^k)$, the mean of ρ_S on the z -interval from z_k to z_{k+1} . Using that value for ρ_S in the integral of Eq. (15), but with ρ still related to z by Eq. (14), we can write

$$m_S \approx \underline{m}_S = \underline{m}_S^k + \frac{\underline{\rho}_S^k}{\underline{\rho}_S^k - \rho_L} \int_{z_k}^z (\rho - \rho_L) dh = \underline{m}_S^k + (a_k x + b_k x^2) \underline{\rho}_S^k / (\underline{\rho}_S^k - \rho_L) \quad \text{Eq. (21)}$$

where $\underline{m}_S^1 = 0$, and \underline{m}_S^{k+1} is the value obtained for \underline{m}_S by setting z equal to z_{k+1} in Eq. (21) (or $x = z_{k+1} - z_k$). Replacing the $\underline{\rho}_S^k$ ($k=1, 2, \dots, K$) of Eq. (21), for all k , by the single value 2.821 g/cc (half the sum of aragonite and calcite densities) yields yet a coarser estimate of m_S , and the approximate values of m_S^k listed in the fifth column of Table 6-9.

Table 6-10 (also located in Appendix 6-2), identical in format and derivation to Table 6-9, differs from Table 6-9 only in that the density profiles on which it rests came from γ - γ logging (not from BHG surveys).

DENSIFICATION: THICKNESS CHANGES AS CONTINUOUS FUNCTIONS OF DEPTH IN CRATER HOLES

Eq. (20) allows us to compute the solid mass per unit cross-section, m_S^a , from the greatest depth logged to the depth at $z = z_a$ in a given borehole. The horizon at z_a in the given borehole -- horizon "a" -- will generally have somewhat different depth in a second borehole¹. Let $z = z_a^*$ at that horizon in the latter hole, with m_S^{a*} denoting solid mass (per unit cross-section) in the second hole, from the greatest depth logged therein to horizon "a". For any

¹ As needed, the depths to a given horizon in different boreholes have been found herein by linear interpolation among the horizon-depths fixed by PEACE Program geologists (see Chapter 7 of the current Report, particularly tbls. 7-2 and 7-4).

depth above "a" in the first borehole, the solid mass between "a" and that depth is equal to $m_S - m_S^a (\equiv \Delta m_S)$, where m_S is computed to the depth in question from Eq. (20), using the a_k - and b_k -values for that first borehole. Likewise, in the second borehole, the solid mass from "a" to a given depth above "a" is equal to $m_S - m_S^{a*} (\equiv \Delta m_S^*)$, with m_S computed from Eq. (20) using a_k - and b_k -values appropriate to that borehole. For each choice of z in the second hole -- $z=z^*$, say -- Δm_S^* can be computed simply by evaluating the right-hand member of Eq. (20) and subtracting m_S^{a*} from the result. However, in the first hole, finding the value of z at which the solid mass Δm_S above "a" is equal to Δm_S^* , plainly requires equating Δm_S to Δm_S^* . The relation determining z is therefore the following:

$$\Delta m_S^* + m_S^a = m_S^k + a_k x + b_k x^2 + \rho_L \left[\frac{b_k x}{b_k'} + \frac{(a_k b_k' - a_k' b_k)}{(b_k')^2} \ln \left(\frac{a_k' + b_k' x}{a_k'} \right) \right] \quad \text{Eq. (22)}$$

where $x = z - z_k$.

Eq. (22), which is transcendental, can be solved for x (hence z) by numerical means. Exactly one value of x satisfies it because m_S [Eq. (20)] increases monotonically as depth decreases, and the mass Δm_S^* above horizon "a" in the second borehole is ≥ 0 . Solution of Eq. (22) for x is greatly expedited by foreknowledge of m_k ($k=1,2,\dots,K$): As k is increased from $k=1$, it reaches a level at which positive values of $\Delta m_S^* + m_S^a - m_S^k$ turn negative; the root of Eq. (21) must lie on the z_k -interval over which that change of sign occurs. With the root of Eq. (22) so bounded, it can be found easily by search or iteration. Repeating the process for a series of ever-shallower z 's gives a set of (z^*, z) pairs for which the solid mass between horizon "a" ($z=z_a^*$) and level z^* in the second hole is equal to that between "a" ($z=z_a$) and level z in the first. The height of the column between z_a and z is $z - z_a$ (or its negative if z denotes depth); $z^* - z_a^*$ gives the corresponding height in the second hole (for equal mass above "a"). If the two holes are actually the same, but with pre- and post-shot density profiles representing the "second" and "first" holes, respectively, then $z - z_a$ and $z^* - z_a^*$ (or their negatives) give the post- and pre-shot thicknesses of a column above "a" that contains the same mass of solid at both times. The change in that column's thickness due to shot-induced changes in density is just $(z^* - z_a^*) - (z - z_a)$ (or its negative).

Under the key assumption given previously on pages 6-7 and 6-8, the pre-shot profiles are found today in control holes -- whence, we do in fact compute (z^*, z) pairs from profiles in different holes. A detail of the calculation (noted previously on pages 6-8 through 6-10) lies in redefining horizon "a" at each successive geologic horizon met along the stepwise march in z^* (from depth toward the sea floor). With z^* referring to the control hole, z is then allowed to shift suddenly to its value, in the crater hole, at a newly encountered geologic horizon. Geologic horizons are thereby strictly retained as Lagrangian surfaces, regardless of departures from the ideal of simple subsidence, or of actual differences between pre-shot density profiles

and control-hole profiles. In addition (see p.6-8 through 6-10), differences in column height are thereby computed from densities in materials that are (as nearly as possible) the same.¹

Curves of thickness-change vs. depth are plotted as a series of dots when z^* refers to a control hole (jumps in z can then occur, marking shifts to geologic crater-hole horizons). When z^* refers to a crater hole, curves of thickness-change vs. depth are drawn with dashes (jumps in z then mark shifts to geologic horizons in control holes). The mean of a dotted and dashed curve is also drawn, as a continuous line.

As functions of present crater-hole depth, the thickness changes computed from profiles of the BHG survey were presented in preceeding sections (p. 6-7 and 6-8 and 6-8 through 6-10) (see figs. 6-4 through 6-9). Corresponding curves, deduced from γ - γ density profiles, appear on succeeding pages as Figures 6-27 through 6-53.

REFERENCES CITED

See pages 6-35 and 6-36 for references cited in this Appendix.

¹ Thickness-change curves were first computed with horizon "a" fixed near Contour D. Except for larger gaps between end-of-data and the sea floor, there are no appreciable differences between those curves and the ones presented in this report -- and no change at all in conclusions drawn from them (conclusions first reached, in fact, with horizon "a" fixed).

H	PEACE (EWT) DIFF	RMS DENSITY (G/CC)	BUREHOLE DGR-17				H	PEACE (EWT) DIFF	RMS DENSITY (G/CC)	BUREHOLE DGR-17			
			DENSITY OF SOLID COMPONENT (G/CC)	CUMULATIVE RHO2.F21	NO. TO MASS RHO2.F21	SP. LINE FOR RHO				DENSITY OF SOLID COMPONENT (G/CC)	CUMULATIVE RHO2.F21	NO. TO MASS RHO2.F21	SP. LINE FOR RHO
1	1000.00		2.0210				101	209.00	2.036		27013.	27734.	27734.
2	1100.00		2.0210				102	209.00	1.992		27013.	27734.	27734.
3	1100.00		2.0262				103	209.00		2.7461	27013.	27734.	27734.
4	1100.00		2.0349				104	211.00	1.992	2.8341	27013.	27734.	27734.
5	1100.00		2.0360				105	211.00	1.992		27013.	27734.	27734.
6	1100.00		2.0360				106	211.00	1.993		27013.	27734.	27734.
7	1092.00		2.0291				107	209.00		2.8341	27013.	27734.	27734.
8	1080.00		2.0242				108	209.00		2.8404	27013.	27734.	27734.
9	1065.00		2.0262				109	209.00	1.993		27013.	27734.	27734.
10	1049.00		2.0242				110	209.00	1.997		27013.	27734.	27734.
11	1042.00		2.0304				111	211.00		2.8655	27013.	27734.	27734.
12	1035.00		2.0304				112	211.00		2.8652	27013.	27734.	27734.
13	1025.00		2.0301				113	211.00	1.997		27013.	27734.	27734.
14	1018.00		2.0301				114	211.00		2.8652	27013.	27734.	27734.
15	1008.00		2.0242				115	211.00		2.8652	27013.	27734.	27734.
16	998.00		2.0242				116	211.00		2.8652	27013.	27734.	27734.
17	990.00		2.0242				117	211.00		2.8652	27013.	27734.	27734.
18	975.00		2.0242				118	211.00		2.8652	27013.	27734.	27734.
19	962.00		2.0242				119	211.00		2.8652	27013.	27734.	27734.
20	949.00		2.0242				120	211.00		2.8652	27013.	27734.	27734.
21	921.00		2.0242				121	211.00		2.8652	27013.	27734.	27734.
22	912.00		2.0242				122	211.00		2.8652	27013.	27734.	27734.
23	895.00	2.013					123	211.00		2.8652	27013.	27734.	27734.
24	887.00		2.0183				124	211.00		2.8652	27013.	27734.	27734.
25	870.00		2.0159				125	211.00		2.8652	27013.	27734.	27734.
26	857.00	2.013					126	211.00		2.8652	27013.	27734.	27734.
27	857.00	2.010					127	211.00		2.8652	27013.	27734.	27734.
28	852.00		2.9206				128	211.00		2.8652	27013.	27734.	27734.
29	840.00		2.9272				129	211.00		2.8652	27013.	27734.	27734.
30	827.00	2.010					130	211.00		2.8652	27013.	27734.	27734.
31	827.00	2.036											
32	826.00		2.9252										
33	812.00		2.9241										
34	798.00		2.9146										
35	789.00	2.036											
36	789.00	1.993											
37	785.00		2.9002										
38	782.00		2.9206										
39	751.00		2.9130										
40	747.00	1.993											
41	747.00	2.013											
42	737.00		2.9103										
43	725.00		2.8886										
44	713.00	2.013											
45	713.00	2.010											
46	700.00		2.8948										
47	683.00	2.010											
48	683.00	2.036											
49	668.00		2.8948										
50	652.00		2.8768										
51	645.00	2.036											
52	645.00	1.993											
53	628.00		2.8580										
54	618.00		2.8610										
55	605.00	1.993											
56	605.00	1.976											
57	602.00		2.8997										
58	588.00		2.8752										
59	578.00		2.7792										
60	560.00	1.976											
61	560.00	1.976											
62	550.00		2.7242										
63	533.00		2.7405										
64	520.00	1.976											
65	520.00	2.047											
66	525.00		2.7304										
67	508.00		2.7289										
68	505.00	2.027											
69	505.00	1.977											
70	502.00		2.7308										
71	502.00		2.7308										
72	493.00		2.7342										
73	481.00												
74	477.00	1.987											
75	477.00	1.976											
76	470.00		2.7702										
77	456.00		2.7241										
78	446.00	1.976											
79	446.00	1.967											
80	441.00		2.7181										
81	426.00		2.6777										
82	420.00		2.7749										
83	417.00	1.967											
84	417.00	1.964											
85	411.00		2.7202										
86	400.00		2.7406										
87	386.00		2.6755										
88	380.00	1.964											
89	380.00	1.951											
90	376.00		2.7467										
91	363.00	1.951											
92	363.00	1.872											
93	350.00		2.9116										
94	340.00	1.872											
95	335.00	1.901											
96	334.00		2.9206										
97	325.00		2.8765										
98	317.00	1.901											
99	317.00	2.036											
100	297.00		2.7932										

TABLE 6-9. -- Mass of solid in vertical columns of unit cross-section, from BHG-survey data (continued on next 3 pages).

SOREHOLE DHT-20						SOREHOLE DHT-19					
A	PEACE DEPTH (FT)	BHG DENSITY (G/CC)	DENSITY OF SOLID COMPONENT (G/CC)	CUMULATIVE SOLID MASS RHO=2.021 RHO=CRMO	LINEAR SP. LINE FOR RHO	A	PEACE DEPTH (FT)	BHG DENSITY (G/CC)	DENSITY OF SOLID COMPONENT (G/CC)	CUMULATIVE SOLID MASS RHO=2.021 RHO=CRMO	LINEAR SP. LINE FOR RHO
0	1000.00		2.0210			0	1000.00		2.0210		
1	591.41		2.0210			1	818.51		2.0210		
2	591.00		2.0670			2	818.50		2.0096		
3	591.00	1.929		0.	0.	3	808.50		2.9191		
4	572.00		2.7571	872.	875.	4	798.10		2.9052		
5	551.00		2.7242	1468.	1278.	5	798.00	1.956		0.	0.
6	551.00	1.929		1899.	1314.	6	783.30		2.9198	647.	635.
7	537.00		2.7242	1888.	1919.	7	760.00		2.9237	1311.	1287.
8	527.00		2.7241	2021.	2361.	8	760.00	1.956		1338.	1313.
9	521.00	1.909		2598.	2644.	9	760.00	2.001		1538.	1515.
10	521.00	1.949		2598.	2644.	10	760.00		2.001	1710.	1710.
11	511.00		2.7100	3014.	3064.	11	759.10		2.9148	1771.	1758.
12	491.00	1.949		3926.	4080.	12	730.00	2.001	2.9113	2000.	2216.
13	491.00	2.009		3926.	4080.	13	730.00	2.711		2700.	2747.
14	481.00		2.7242	4369.	4653.	14	729.00		2.9159	2704.	2747.
15	471.00	2.009		4860.	4963.	15	700.00	2.011		3199.	3161.
16	471.00	2.048		4860.	4963.	16	700.00	2.010		4210.	4159.
17	460.00		2.7241	5172.	5273.	17	700.00		2.8974	4590.	4590.
18	451.00	2.048		5868.	5964.	18	678.00	2.018		5601.	5544.
19	451.00	2.014		5868.	5964.	19	678.00	2.013		5601.	5544.
20	442.00		2.7101	6457.	6561.	20	670.00		2.9066	6070.	5916.
21	432.10		2.7140	6745.	6879.	21	659.00		2.8951	6518.	6405.
22	421.00	2.014		7269.	7416.	22	648.00	2.013		7061.	6905.
23	421.00	2.003		7269.	7416.	23	648.00	2.030		7061.	6905.
24	416.00		2.7344	7961.	7617.	24	629.00		2.7242	7566.	7409.
25	401.00		2.7146	8161.	8371.	25	618.00	2.030		8055.	8007.
26	391.00	2.003		8674.	8829.	26	618.00	2.040		8055.	8007.
27	391.00	1.974		8674.	8829.	27	598.00		2.8001	8960.	8958.
28	387.00		2.9974	9027.	9300.	28	588.00	2.040		9763.	9873.
29	367.00		2.8341	9766.	9989.	29	588.00	1.991		9763.	9873.
30	361.00	1.989		10068.	10203.	30	578.00		2.8343	10300.	10290.
31	361.00	1.948		10068.	10203.	31	558.00	1.951		11290.	11208.
32	351.00		2.9098	10604.	10622.	32	558.00	1.940		11290.	11208.
33	351.00		2.8882	11324.	11449.	33	558.00		2.7241	11901.	11615.
34	331.00	1.948		11806.	11510.	34	548.00		2.7140	12047.	12047.
35	331.00	1.922		11806.	11510.	35	528.00	1.948		12047.	12047.
36	318.00		2.7844	12106.	12106.	36	528.00	1.999		12047.	12047.
37	303.00		2.8231	12706.	12706.	37	515.00		2.7140	12047.	12047.
38	301.00	1.922		12675.	12799.	38	508.00	1.998		12047.	12047.
39	301.00	1.942		12675.	12799.	39	498.00	2.056		12047.	12047.
40	288.00		2.8277	13030.	13354.	40	485.00		2.7101	12734.	12725.
41	272.00		2.8565	13981.	14052.	41	468.00	2.056		13499.	13495.
42	271.00	1.948		13981.	14052.	42	468.00	2.046		13499.	13495.
43	271.00	1.887		13981.	14052.	43	468.00		2.4002	13499.	13495.
44	256.00	1.887		14030.	14073.	44	438.00	2.046		16477.	16474.
45	256.00	1.926		14030.	14073.	45	438.00	2.011		17811.	17821.
46	256.00		2.8341	14623.	14749.	46	409.00		2.7995	18335.	18346.
47	233.00		2.8643	15521.	15635.	47	403.00	2.011		18335.	18346.
48	226.00	1.926		15800.	15959.	48	403.00	2.008		18335.	18346.
49	226.00	1.971		15800.	15959.	49	399.00		2.8905	18335.	18346.
50	222.00		2.8951	16021.	16129.	50	380.00		2.9040	18335.	18346.
51	211.00		2.8859	16511.	16612.	51	380.00	2.008		18335.	18346.
52	211.00	1.971		16529.	16630.	52	370.00	1.922		18335.	18346.
53	211.00	1.886		16529.	16630.	53	358.00	1.922		18335.	18346.
54	200.00		2.8836	16916.	17012.	54	358.00	1.972		18335.	18346.
55	190.00		2.7844	17119.	17114.	55	355.00		2.9040	18335.	18346.
56	186.00	1.826		17489.	17584.	56	350.00		2.8365	18335.	18346.
57	186.00	2.010		17489.	17584.	57	328.00	1.972		18335.	18346.
58	178.10		2.9090	17661.	17953.	58	328.00	1.946		18335.	18346.
59	165.00		2.8799	18056.	18325.	59	311.10		2.7473	18335.	18346.
60	161.10		2.9178	18663.	18747.	60	298.00	1.908		18335.	18346.
61	160.00	2.010		18715.	18798.	61	298.00	1.900		18335.	18346.
62	160.00	1.840		18715.	18798.	62	296.00		2.8233	18335.	18346.
63	146.00		2.9297	19243.	19316.	63	273.00	1.900		18335.	18346.
64	146.00	1.840		19661.	19726.	64	273.00	1.906		18335.	18346.
65	131.00		2.9096			65	251.00		2.8768	18335.	18346.
66	131.00		2.8210			66	238.00	1.906		18335.	18346.
67	131.00		2.8210			67	238.00	1.890		18335.	18346.
						68	226.00		2.8788	18335.	18346.
						69	216.00		2.8541	18335.	18346.
						70	208.00	1.898		18335.	18346.
						71	208.00	1.942		18335.	18346.
						72	196.00		2.8059	18335.	18346.
						73	189.00		2.6474	18335.	18346.
						74	178.00	1.942		18335.	18346.
						75	178.00	1.989		18335.	18346.
						76	171.00		2.8307	18335.	18346.
						77	168.00		2.9139	18335.	18346.
						78	163.00		2.9133	18335.	18346.
						79	148.00	1.942		18335.	18346.
						80	148.00	1.989		18335.	18346.
						81	148.00		1.939	18335.	18346.
						82	148.00	1.807		18335.	18346.
						83	148.00	1.807		18335.	18346.
						84	127.00		2.9291	18335.	18346.
						85	124.00		2.9165	18335.	18346.
						86	118.00		2.9197	18335.	18346.
						87	117.00		2.8210	18335.	18346.
										18335.	18346.

TABLE 6-9 (page 2 of 3 pages). -- Mass of solid in vertical columns of unit cross-section, from BHG-survey data.

BUREHOLE 076-23							BUREHOLE 072-16						
A	DEPTH FEET	BHG DENSITY (GM/CC)	DENSITY OF SOLID COMPONENT (GM/CC)	CUMULATIVE SOLID MASS KG/CC	CO-10 MASS KG/CC	CO-10 MASS KG/CC	A	DEPTH FEET	BHG DENSITY (GM/CC)	DENSITY OF SOLID COMPONENT (GM/CC)	CUMULATIVE SOLID MASS KG/CC	CO-10 MASS KG/CC	CO-10 MASS KG/CC
0	1000.00		2.8210	0.	0.	0.	0	1000.00		2.8210	0.	0.	0.
1	750.00	2.156		750.	750.	750.	1	1062.00	2.031		1062.	1062.	1062.
2	720.00		2.8210	750.	750.	750.	2	1052.00	2.031		1052.	1052.	1052.
3	720.00		2.8253	750.	750.	750.	3	1052.00	1.951		1052.	1052.	1052.
4	690.00	2.156	2.8779	2021.	5395.	5395.	4	1002.00	1.951		2776.	2776.	2776.
5	670.00	2.072		3250.	5214.	5214.	5	1002.00	2.052		4776.	4776.	4776.
6	670.00			3250.	5214.	5214.	6	967.00	2.052		4488.	4488.	4488.
7	650.00		2.8059	3972.	5927.	5927.	7	967.00	2.048		4488.	4488.	4488.
8	650.00	2.072		5006.	4489.	5006.	8	937.00	2.048		5967.	5967.	5967.
9	620.00	2.026		5506.	4489.	5506.	9	937.00	2.115		5967.	5967.	5967.
10	600.00	2.026		7064.	7615.	7615.	10	902.00	2.115		7704.	7704.	7704.
11	580.00	2.117		7664.	7615.	7615.	11	902.00	2.107		7704.	7704.	7704.
12	560.00		2.1305	8779.	8779.	8779.	12	871.00		2.9710	9874.	9874.	9874.
13	560.00	2.117		10017.	10006.	10006.	13	871.00		2.9253	9274.	9274.	9274.
14	530.00	2.008		10017.	10006.	10006.	14	867.00	2.107		9608.	9608.	9608.
15	525.00		2.7047	10386.	10170.	10170.	15	867.00	2.031		9608.	9608.	9608.
16	505.00		2.7973	11698.	11695.	11695.	16	866.00		2.9189	9618.	9618.	9618.
17	490.00	2.008		12150.	12145.	12145.	17	852.00		2.9156	10821.	10821.	10821.
18	490.00	2.008		12150.	12145.	12145.	18	851.00	2.081		11055.	11055.	11055.
19	470.00		2.7134	13145.	13142.	13142.	19	851.00	1.951		11055.	11055.	11055.
20	460.00	2.700		13607.	13597.	13597.	20	852.00		2.9252	11235.	11235.	11235.
21	460.00	2.017		13607.	13597.	13597.	21	823.00		2.9206	11666.	11666.	11666.
22	440.00		2.8005	14751.	14706.	14706.	22	815.00		2.9185	12193.	12193.	12193.
23	440.00	2.3217		14751.	14706.	14706.	23	809.00		2.9043	12495.	12495.	12495.
24	430.00	2.617		15012.	14705.	15005.	24	807.00	1.951		12544.	12544.	12544.
25	430.00	2.000		15012.	14705.	15005.	25	807.00	2.152		12544.	12544.	12544.
26	400.00	2.000		16433.	16406.	16406.	26	799.00		2.9185	13023.	13023.	13023.
27	400.00	2.011		16433.	16406.	16406.	27	772.00	2.052		13106.	13106.	13106.
28	370.00	2.011		17850.	17823.	17823.	28	772.00	2.048		13106.	13106.	13106.
29	370.00	2.037		17850.	17823.	17823.	29	766.00		2.9206	13684.	13684.	13684.
30	360.00	2.857		19300.	19277.	19277.	30	762.00	2.048		13684.	13684.	13684.
31	360.00	2.810		19300.	19277.	19277.	31	762.00	2.115		13684.	13684.	13684.
32	310.00	2.710		20751.	20705.	20705.	32	757.00		2.8059	15000.	15000.	15000.
33			2.9210				33	757.00	2.7241		16729.	16617.	16617.
							34	709.00	2.7303		17808.	17180.	17180.
							35	707.00	2.115		17402.	17304.	17304.
							36	707.00	2.107		17402.	17304.	17304.
							37	672.00	2.7241		19190.	19127.	19127.
							38	672.00	2.107		19216.	19154.	19154.
							39	672.00	2.122		19216.	19154.	19154.
							40	660.00		2.9146	19800.	19380.	19380.
							41	651.00	2.7303		20283.	20241.	20241.
							42	647.00	2.122		21055.	21019.	21019.
							43	647.00	2.107		21055.	21019.	21019.
							44	631.00	2.7241		21555.	21509.	21509.
							45	610.00	2.7241		22122.	22108.	22108.
							46	610.00	2.187		22444.	22408.	22408.
							47	610.00	2.139		22444.	22408.	22408.
							48	602.00	2.7140		22854.	22857.	22857.
							49	590.00	2.7613		23334.	23306.	23306.
							50	582.00	2.139		23908.	23859.	23859.
							51	582.00	2.151		23908.	23859.	23859.
							52	570.00	2.9146		24121.	24110.	24110.
							53	550.00	2.871		25257.	25211.	25211.
							54	552.00	2.191		25628.	25612.	25612.
							55	552.00	2.066		25628.	25612.	25612.
							56	555.00		2.8882	26505.	26561.	26561.
							57	522.00	2.008		27147.	27119.	27119.
							58	522.00	2.004		27147.	27119.	27119.
							59	517.00		2.8633	27349.	27318.	27318.
							60	492.00	2.008		28552.	28515.	28515.
							61	492.00	2.150		28552.	28515.	28515.
							62	491.00		2.8059	28552.	28515.	28515.
							63	470.00	2.9070		29400.	29365.	29365.
							64	457.00	2.180		30405.	30352.	30352.
							65	457.00	1.962		30405.	30352.	30352.
							66	452.00		2.8541	30509.	30455.	30455.
							67	435.00	2.9166		31449.	31445.	31445.
							68	410.00	2.8081		32119.	32045.	32045.
							69	395.00	2.9665		32236.	32159.	32159.
							70	382.00	1.962		33770.	33686.	33686.
							71	382.00	1.997		33770.	33686.	33686.
							72	376.00		2.8098	34031.	33945.	33945.
							73	361.00	2.8585		34704.	34615.	34615.
							74	352.00	1.997		35167.	35172.	35172.
							75	352.00	1.956		35167.	35172.	35172.
							76	347.00		2.8768	35272.	35175.	35175.
							77	331.00	2.8765		36099.	35994.	35994.
							78	322.00	1.956		36505.	36396.	36396.
							79	322.00	1.967		36505.	36396.	36396.
							80	313.00		2.8765	36859.	36746.	36746.
							81	290.00	2.8882		37669.	37564.	37564.
							82	292.00	1.937		37815.	37691.	37691.
							83	292.00	1.807		37815.	37691.	37691.
							84	277.00		2.8005	38244.	38212.	38212.
							85	266.00	2.8059		38778.	38641.	38641.
							86	262.00	1.807		38949.	38800.	38800.
							87	262.00	1.812		38949.	38800.	38800.
							88	240.00		2.8814	39345.	39251.	39251.
							89	233.00	2.8683		40033.	39882.	39882.
							90	232.00	2.8210		40033.	39882.	39882.
							91	224.00	1.812		40070.	39919.	39919.
							92			2.8210			

TABLE 6-9 (page 3 of 3 pages). -- Mass of solid in vertical columns of unit cross-section, from BHG-survey data.

B REMOTE						B REMOTE					
Y-Y SURVEY DATA						Y-Y SURVEY DATA					
PLATE	DATE	DENSITY	CUMULATIVE	SOLID MASS	INTEGRATED	PLATE	DATE	DENSITY	CUMULATIVE	SOLID MASS	INTEGRATED
(L IN)	(L IN)	(G/CC)	(G/CC)	(G/CC)	(G/CC)	(L IN)	(L IN)	(G/CC)	(G/CC)	(G/CC)	(G/CC)
DIFF	DIFF	DIFF	DIFF	DIFF	DIFF	DIFF	DIFF	DIFF	DIFF	DIFF	DIFF
0	1000.00	2.0210				101	999.00	2.020	9925.	9758.	9758.
1	1100.01	2.0210				102	992.00	2.114	9733.	9668.	9668.
2	1100.00	2.7262				103	939.00		2.8965	9901.	10034.
3	1100.00	2.704	0.	0.	0.	104	930.00	2.092	9955.	10087.	10087.
4	1136.70	2.145	110.	121.	121.	105	930.00	2.059	10063.	10117.	10117.
5	1136.70	2.145	187.	192.	192.	106	932.00	2.048	10235.	10260.	10260.
6	1136.70	2.116	233.	238.	238.	107	926.00	2.033	10344.	10368.	10368.
7	1136.70		240.	245.	245.	108	928.00	2.016	10490.	10510.	10510.
8	1136.70	2.112	300.	307.	307.	109	921.00		2.9101	10781.	10899.
9	1136.70	2.092	367.	375.	375.	110	920.00	2.024	10793.	10911.	10911.
10	1136.70	2.087	389.	397.	397.	111	918.00	2.140	10793.	10911.	10911.
11	1136.70	2.104	507.	539.	539.	112	912.00		2.8948	11243.	11353.
12	1136.70	2.145	645.	649.	649.	113	909.00	2.059	11364.	11473.	11473.
13	1136.70	2.142	714.	730.	730.	114	907.00	2.059	11471.	11570.	11570.
14	1136.70	2.116	760.	776.	776.	115	908.00	2.049	11731.	11834.	11834.
15	1136.70	2.112	827.	843.	843.	116	898.00	2.048	12043.	12132.	12132.
16	1136.70	2.092	844.	852.	852.	117	898.00	2.227	12171.	12269.	12269.
17	1136.70	2.087	914.	918.	918.	118	898.00		2.9101	12425.	12514.
18	1136.70		918.	928.	928.	119	898.00	2.267	12505.	12673.	12673.
19	1136.70	2.134	1045.	1066.	1066.	120	898.00	2.024	12557.	12921.	12921.
20	1136.70	2.022	1120.	1151.	1151.	121	876.00	2.157	13000.	13150.	13150.
21	1136.70	2.024	1169.	1199.	1199.	122	876.00	2.036	13000.	13150.	13150.
22	1136.70	2.045	1472.	1527.	1527.	123	870.00		2.9109	13309.	13462.
23	1136.70	2.047	1524.	1592.	1592.	124	867.00	2.071	13536.	13607.	13607.
24	1136.70	2.052	1558.	1595.	1595.	125	865.00	2.014	13599.	13668.	13668.
25	1136.70	2.074	1621.	1650.	1650.	126	861.00	2.010	13603.	13664.	13664.
26	1136.70	2.063	1643.	1672.	1672.	127	857.00	2.134	14018.	14078.	14078.
27	1136.70		1677.	1686.	1686.	128	852.00		2.9206	14467.	14528.
28	1136.70	2.066	1687.	1697.	1697.	129	852.00	2.154	14671.	14728.	14728.
29	1136.70	2.120	1617.	1649.	1649.	130	850.00	2.071	14671.	14728.	14728.
30	1136.70	2.152	1663.	1696.	1696.	131	846.00	2.048	14671.	14728.	14728.
31	1136.70	2.104	1750.	1793.	1793.	132	844.00	2.130	14671.	14728.	14728.
32	1136.70	2.116	1830.	1867.	1867.	133	840.00		2.9252	14698.	14793.
33	1136.70	2.173	1878.	1915.	1915.	134	838.00	2.057	14698.	14793.	14793.
34	1136.70		1912.	1950.	1950.	135	834.00	2.085	14698.	14793.	14793.
35	1136.70	2.154	1972.	2011.	2011.	136	832.00	2.125	14698.	14793.	14793.
36	1136.70	2.125	2041.	2081.	2081.	137	829.00	2.093	14698.	14793.	14793.
37	1136.70	2.106	2064.	2104.	2104.	138	828.00	2.067	14698.	14793.	14793.
38	1136.70	2.104	2130.	2172.	2172.	139	826.00		2.9252	14698.	14793.
39	1136.70	2.090	2130.	2172.	2172.	140	822.00	2.085	14698.	14793.	14793.
40	1136.70		2218.	2262.	2262.	141	814.00	2.066	14698.	14793.	14793.
41	1136.70	2.7201	2413.	2461.	2461.	142	812.00		2.9241	14698.	14793.
42	1136.70	2.071	2456.	2505.	2505.	143	810.00	2.002	14698.	14793.	14793.
43	1136.70	2.076	2551.	2604.	2604.	144	807.00	2.022	14698.	14793.	14793.
44	1136.70	2.104	2738.	2793.	2793.	145	804.00	2.058	14698.	14793.	14793.
45	1136.70	2.110	2805.	2853.	2853.	146	802.00	2.128	14698.	14793.	14793.
46	1136.70		2826.	2877.	2877.	147	799.00	2.147	14698.	14793.	14793.
47	1136.70	2.080	3072.	3134.	3134.	148	797.00	2.135	14698.	14793.	14793.
48	1136.70	1.967	3261.	3329.	3329.	149	795.00		2.9106	14698.	14793.
49	1136.70	1.961	3674.	3748.	3748.	150	793.00	2.058	14698.	14793.	14793.
50	1136.70		3789.	3869.	3869.	151	788.00	2.156	14698.	14793.	14793.
51	1136.70	2.010	3814.	3893.	3893.	152	786.00	2.088	14698.	14793.	14793.
52	1136.70	1.986	4054.	4146.	4146.	153	785.00		2.9082	14698.	14793.
53	1136.70	1.988	4173.	4277.	4277.	154	784.00	2.036	14698.	14793.	14793.
54	1136.70	2.014	4314.	4431.	4431.	155	781.00	2.017	14698.	14793.	14793.
55	1136.70	1.984	4416.	4553.	4553.	156	778.00	2.044	14698.	14793.	14793.
56	1136.70		4464.	4604.	4604.	157	775.00	2.074	14698.	14793.	14793.
57	1136.70	1.967	4512.	4653.	4653.	158	773.00	2.046	14698.	14793.	14793.
58	1136.70	1.995	4650.	4794.	4794.	159	769.00	2.085	14698.	14793.	14793.
59	1136.70	2.038	4711.	4866.	4866.	160	767.00	2.110	14698.	14793.	14793.
60	1136.70	2.069	4786.	4953.	4953.	161	764.00	2.140	14698.	14793.	14793.
61	1136.70		4838.	5015.	5015.	162	764.00	2.123	14698.	14793.	14793.
62	1136.70	2.022	5161.	5348.	5348.	163	762.00		2.9206	14698.	14793.
63	1136.70	1.880	5377.	5592.	5592.	164	761.00	2.125	14698.	14793.	14793.
64	1136.70	1.930	5577.	5809.	5809.	165	759.00	2.135	14698.	14793.	14793.
65	1136.70		5614.	5856.	5856.	166	756.00	2.119	14698.	14793.	14793.
66	1136.70	1.927	5661.	5915.	5915.	167	752.00	2.126	14698.	14793.	14793.
67	1136.70	1.908	5727.	6002.	6002.	168	751.00		2.9190	14698.	14793.
68	1136.70	1.880	5842.	6199.	6199.	169	751.00	2.026	14698.	14793.	14793.
69	1136.70	1.890	5861.	6278.	6278.	170	747.00	1.972	14698.	14793.	14793.
70	1136.70	1.886	5966.	6486.	6486.	171	740.00	2.080	14698.	14793.	14793.
71	1136.70		6130.	6704.	6704.	172	737.00		2.9183	14698.	14793.
72	1136.70	1.991	6205.	6831.	6831.	173	735.00	2.007	14698.	14793.	14793.
73	1136.70	2.007	6267.	6965.	6965.	174	731.00	2.044	14698.	14793.	14793.
74	1136.70	2.140	6464.	7199.	7199.	175	726.00	2.007	14698.	14793.	14793.
75	1136.70	2.116	6559.	7427.	7427.	176	723.00		2.8036	14698.	14793.
76	1136.70	2.140	6649.	7684.	7684.	177	718.00	2.097	14698.	14793.	14793.
77	1136.70		6669.	7905.	7905.	178	714.00	2.088	14698.	14793.	14793.
78	1136.70	2.137	6811.	8150.	8150.	179	714.00	2.050	14698.	14793.	14793.
79	1136.70	1.990	6920.	8400.	8400.	180	707.00	1.908	14698.	14793.	14793.
80	1136.70	1.976	7098.	8652.	8652.	181	701.00	1.907	14698.	14793.	14793.
81	1136.70		7137.	8902.	8902.	182	700.00		2.8948	14698.	14793.
82	1136.70	2.019	7150.	9104.	9104.	183	699.00	2.054	14698.	14793.	14793.
83	1136.70		7240.	9393.	9393.	184	696.00	2.045	14698.	14793.	14793.
84	1136.70	2.071	7266.	9671.	9671.	185	698.00	2.024	14698.	14793.	14793.
85	1136.70	2.021	7322.	9952.	9952.	186	691.00	2.044	14698.	14793.	14793.
86	1136.70	2.019	7375.	10237.	10237.	187	688.00	2.004	14698.	14793.	14793.
87	1136.70	2.045	7430.	10520.	10520.	188	683.00	2.100	14698.	14793.	14793.
88	1136.70		8022.	11211.	11211.	189	680.00	2.050	14698.	14793.	14793.
89	1136.70	2.061	8122.	11904.	11904.	190	678.00	2.057	14698.	14793.	14793.
90	1136.70	1.961	8170.	12600.	12600.	191	675.00	2.028	14698.	14793.	14793.
91	1136.70	2.010	8510.	13300.	13300.	192	670.00	2.106	14698.	14793.	14793.
92	1136.70		8614.	14004.	14004.	193	666.00		2.8948	14698.	14793.
93	1136.70	2.233	8699.	14723.	14723.	194	664.00	2.036	14698.	14793.	14793.
94	1136.70	2.209	8870.	15454.	15454.	195	660.00	2.054	14698.	14793.	14793.
95	1136.70	2.197	9052.	16197.	16197.	196	658.00	2.049	14698.	14793.	14793.
96	1136.70	1.988	9140.	16942.	16942.	197	656.00	2.067	14698.	14793.	14793.
97	1136.70	2.140	9180.	17692.	17692.	198	653.00	2.067	14698.	14793.	14793.
98	1136.70	2.186	9305.	18448.	18448.	199	652.00		2.8768	14698.	14793.
99	1136.70	2.147	9440.	19209.	19209.	200	650.00	2.063	14698.	14793.	14793.
100</											

TABLE 6-10 (Continued)

J	PEAK DENSITY (G/CC)	W - S DENSITY (G/CC)	BURHOLE DENSITY OF SOLID COMPONENT (G/CC)	DNR-17 CUMULATIVE SOLID MASS (MG/2.52)	DNR-17 RHO (G/CC)	RHO (G/CC)	J	PEAK DENSITY (G/CC)	W - S DENSITY (G/CC)	BURHOLE DENSITY OF SOLID COMPONENT (G/CC)	DNR-17 CUMULATIVE SOLID MASS (MG/2.52)	DNR-17 RHO (G/CC)	RHO (G/CC)
201	647.39	2.019	2.019	24463.	24452.	24452.	801	644.40			24463.	24452.	24452.
202	644.37	2.002	2.002	24405.	24442.	24442.	802	639.47	1.986	2.9908	24405.	24442.	24442.
203	642.37	2.007	2.007	24706.	24492.	24492.	803	638.49	1.964		24706.	24492.	24492.
204	640.44	1.974	1.974	24808.	24691.	24691.	804	634.47	1.938		24808.	24691.	24691.
205	637.46	2.002	2.002	24929.	24809.	24809.	805	631.46	2.002		24929.	24809.	24809.
206	636.43	2.038	2.038	25049.	24992.	24992.	806	628.43	1.974	2.8545	25049.	24992.	24992.
207	634.47	2.047	2.047	25111.	24994.	24994.	807	628.43			25111.	24994.	24994.
208	631.46	2.047	2.047	25117.	24998.	24998.	808	625.47	2.010		25117.	24998.	24998.
209	629.49	2.034	2.034	25301.	24982.	24982.	809	619.42	1.998		25301.	24982.	24982.
210	628.40		2.0408	25376.	24944.	24944.	810	619.42	1.972		25376.	24944.	24944.
211	627.45	2.007		25400.	24924.	24924.	811	616.46	1.979		25400.	24924.	24924.
212	624.46	2.007		25546.	24924.	24924.	812	613.43	1.957		25546.	24924.	24924.
213	623.46	2.036		25628.	24907.	24907.	813	613.43	1.950		25628.	24907.	24907.
214	622.49	2.000		25649.	24947.	24947.	814	611.46	1.974		25649.	24947.	24947.
215	621.43	1.944		25744.	24947.	24947.	815	609.49	1.931		25744.	24947.	24947.
216	618.46		2.0408	25744.	24911.	24911.	816	605.44	2.003		25744.	24911.	24911.
217	617.48	1.947		25844.	24944.	24944.	817	601.44	2.007		25844.	24944.	24944.
218	611.43	1.974		26177.	24944.	24944.	818	600.44	2.004		26177.	24944.	24944.
219	610.47	2.070		26233.	24906.	24906.	819	597.47	1.973		26233.	24906.	24906.
220	605.44	2.111		26453.	24924.	24924.	820	597.47		2.7477	26453.	24924.	24924.
221	602.49		2.0977	26605.	24975.	24975.	821	595.49	2.088		26605.	24975.	24975.
222	601.49	2.102		26676.	24943.	24943.	822	594.49	1.950		26676.	24943.	24943.
223	599.47	2.034		26705.	24955.	24955.	823	592.49	1.919		26705.	24955.	24955.
224	595.49	2.047		26705.	24917.	24917.	824	589.49	1.938		26705.	24917.	24917.
225	592.43	2.074		27103.	24964.	24964.	825	587.49	1.904		27103.	24964.	24964.
226	587.49	2.058		27381.	24920.	24920.	826	584.49		2.7447	27381.	24920.	24920.
227	586.49		2.0408	27437.	24925.	24925.	827	583.49	1.919		27437.	24925.	24925.
228	584.49	2.050		27528.	24907.	24907.	828	582.49	1.880		27528.	24907.	24907.
229	582.49	2.071		27635.	24948.	24948.	829	579.49	1.832		27635.	24948.	24948.
230	580.49	2.054		27742.	24902.	24902.	830	577.49	1.886		27742.	24902.	24902.
231	578.49		2.7202	27817.	24978.	24978.	831	575.49		4.9341	27817.	24978.	24978.
232	576.49	2.054		27943.	24975.	24975.	832	574.49	1.907		27943.	24975.	24975.
233	572.49	2.050		28119.	24906.	24906.	833	573.49	1.867		28119.	24906.	24906.
234	571.49	1.950		28138.	24927.	24927.	834	570.49	1.884		28138.	24927.	24927.
235	569.49		2.7305	28258.	24982.	24982.	835	568.49	2.024		28258.	24982.	24982.
236	565.49	2.7364		30479.	24906.	24906.	836	566.49	2.005		30479.	24906.	24906.
237	560.49	2.7202		31063.	24906.	24906.	837	564.49	1.971		31063.	24906.	24906.
238	560.49	2.7202		31212.	24941.	24941.	838	560.49	1.967	2.8451	31212.	24941.	24941.
239	552.49	2.7364		31429.	24955.	24955.	839	558.49	1.974		31429.	24955.	24955.
240	551.49	2.7364		31587.	24955.	24955.	840	555.49	1.974		31587.	24955.	24955.
241	548.49	2.7202		32259.	24906.	24906.	841	553.49	1.965		32259.	24906.	24906.
242	547.49	2.7202		32447.	24906.	24906.	842	552.49		2.8454	32447.	24906.	24906.
243	540.49	1.950		32711.	24906.	24906.	843	552.49	1.978		32711.	24906.	24906.
244	536.49	2.7241		33366.	24937.	24937.	844	551.49	1.963		33366.	24937.	24937.
245	535.49	1.953		33503.	24937.	24937.	845	550.49	2.005		33503.	24937.	24937.
246	533.49	1.953		33779.	24937.	24937.	846	549.49	1.972		33779.	24937.	24937.
247	530.49	2.014		33647.	24937.	24937.	847	548.49	1.984		33647.	24937.	24937.
248	528.49	1.971		33747.	24937.	24937.	848	541.49	1.994		33747.	24937.	24937.
249	526.49	1.971		33747.	24937.	24937.	849	540.49	1.964		33747.	24937.	24937.
250	523.49	1.971		33747.	24937.	24937.	850	538.49	1.984		33747.	24937.	24937.
251	521.49	1.950		33747.	24937.	24937.	851	534.49	1.998		33747.	24937.	24937.
252	521.49	1.950		33747.	24937.	24937.	852	533.49	1.998		33747.	24937.	24937.
253	520.49	1.950		33747.	24937.	24937.	853	531.49	1.998	2.8625	33747.	24937.	24937.
254	518.49	1.950		33747.	24937.	24937.	854	529.49	1.994		33747.	24937.	24937.
255	518.49	1.950		33747.	24937.	24937.	855	528.49	1.971		33747.	24937.	24937.
256	518.49	1.950		33747.	24937.	24937.	856	526.49	1.971		33747.	24937.	24937.
257	518.49	1.950		33747.	24937.	24937.	857	524.49	2.019	2.8482	33747.	24937.	24937.
258	518.49	1.950		33747.	24937.	24937.	858	524.49	2.000		33747.	24937.	24937.
259	518.49	1.950		33747.	24937.	24937.	859	521.49	2.016		33747.	24937.	24937.
260	518.49	1.950		33747.	24937.	24937.	860	518.49	1.929		33747.	24937.	24937.
261	518.49	1.950		33747.	24937.	24937.	861	517.49	1.932	2.8638	33747.	24937.	24937.
262	518.49	1.950		33747.	24937.	24937.	862	516.49	1.974		33747.	24937.	24937.
263	518.49	1.950		33747.	24937.	24937.	863	516.49	1.933		33747.	24937.	24937.
264	518.49	1.950		33747.	24937.	24937.	864	516.49	1.974		33747.	24937.	24937.
265	518.49	1.950		33747.	24937.	24937.	865	516.49	1.960	2.8299	33747.	24937.	24937.
266	518.49	1.950		33747.	24937.	24937.	866	516.49	1.971		33747.	24937.	24937.
267	518.49	1.950		33747.	24937.	24937.	867	516.49	1.930		33747.	24937.	24937.
268	518.49	1.950		33747.	24937.	24937.	868	516.49	1.927	2.8344	33747.	24937.	24937.
269	518.49	1.950		33747.	24937.	24937.	869	516.49	1.927		33747.	24937.	24937.
270	518.49	1.950		33747.	24937.	24937.	870	516.49	1.927		33747.	24937.	24937.
271	518.49	1.950		33747.	24937.	24937.	871	516.49	1.927		33747.	24937.	24937.
272	518.49	1.950		33747.	24937.	24937.	872	516.49	1.927	2.8548	33747.	24937.	24937.
273	518.49	1.950		33747.	24937.	24937.	873	516.49	1.927		33747.	24937.	24937.
274	518.49	1.950		33747.	24937.	24937.	874	516.49	1.927		33747.	24937.	24937.
275	518.49	1.950		33747.	24937.	24937.	875	516.49	1.927		33747.	24937.	24937.
276	518.49	1.950		33747.	24937.	24937.	876	516.49	1.927		33747.	24937.	24937.
277	518.49	1.950		33747.	24937.	24937.	877	516.49	1.927	2.8625	33747.	24937.	24937.
278	518.49	1.950		33747.	24937.	24937.	878	516.49	1.927		33747.	24937.	24937.
279	518.49	1.950		33747.	24937.	24937.	879	516.49	1.927		33747.	24937.	24937.
280	518.49	1.950		33747.	24937.	24937.	880	516.49	1.927		33747.	24937.	24937.
281	518.49	1.950		33747.	24937.	24937.	881	516.49	1.927		33747.	24937.	24937.
282	518.49	1.950		33747.	24937.	24937.	882	516.49	1.927		33747.	24937.	24937.
283	518.49	1.950		33747.	24937.	24937.	883	516.49	1.927	2.8638	33747.	24937.	24937.
284	518.49	1.950		33747.	24937.	24937.	884	516.49	1.927		33747.	24937.	24937.
285	518.49	1.950		33747.	24937.	24937.	885	516.49	1.927		33747.	24937.	24937.
286	518.49	1.950		33747.	24937.	24937.	886	516.49	1.927		33747.	24937.	24937.
287	518.49	1.950		33747.	24937.	24937.	887	516.49	1.927	2.8638	33747.	24937.	24937.
288	518.49	1.950		33747.	24937.	24937.	888	516.49	1.927		33747.	24937.	24937.
289	518.49	1.950		33747.	24937.	24937.	889	516.49	1.927		33747.	24937.	24937.
290	518.49	1.950		33747.									

TABLE 6-10 (Continued)

PEACE DEPTH (FT)	6 - 5 DENSITY (G/CC)	BUREHOLE OF BULLIO COMPONENT (IN/CC)	BUREHOLE COR-17			PEACE DEPTH (FT)	6 - 5 DENSITY (G/CC)	BUREHOLE OF BULLIO COMPONENT (IN/CC)	BUREHOLE COR-21		
			CUMULATIVE RHO=2.821	SOLID MASS RHO=2.821	100%CH=21 LINEAR SP. LINE FOR RHO				CUMULATIVE RHO=2.821	SOLID MASS RHO=2.821	100%CH=21 LINEAR SP. LINE FOR RHO
404	119.71	1.996	40405.	40567.	40367.	0	1000.00		2.8210		
402	119.47	1.996	40461.	40623.	40423.	1	432.71		2.8210		
403	118.00		40469.	40649.	40449.	2	432.70		2.8432		
404	111.41	1.919	40502.	40551.	40551.	3	421.50		2.7202		
405	100.09	1.905	40702.	40650.	40650.	4	412.05	1.910			
406	107.49		40711.	40726.	40726.	5	411.00		2.8144	0.	0.
407	106.45	1.919	40811.	40765.	40765.	6	411.07	1.929		70.	70.
408	102.01	1.931	40959.	40911.	40911.	7	408.74	1.904		84.	84.
409	97.65	1.894	40179.	40125.	40125.	8	406.76	1.790		104.	104.
410	95.00	1.901	40207.	40281.	40281.	9	404.41	1.761		124.	124.
411	94.44	1.929	40223.	40267.	40267.	10	402.85	1.715		144.	144.
412	90.78	1.950	40474.	40415.	40415.	11	401.60		2.7740	459.	459.
413	86.40		40671.	40608.	40608.	12	401.48	1.748		472.	472.
414	85.90	1.874	40766.	40701.	40701.	13	399.74	1.693		502.	504.
415	82.61	1.884	40819.	40753.	40753.	14	398.34	1.726		540.	543.
416	80.40	1.888	40926.	40857.	40857.	15	396.97	1.723		593.	596.
417	78.51	1.898	40967.	40928.	40927.	16	394.66	1.759		675.	677.
418	75.75	1.884	40105.	50035.	50035.	17	394.43	1.741		687.	691.
419	74.44	1.907	40159.	50086.	50086.	18	391.10	1.738		704.	704.
420	72.74	1.905	50231.	50157.	50157.	19	389.53	1.697		844.	851.
421	66.40					20	388.26	1.716		885.	890.
422	56.50	2.9252				21	386.79	1.608		935.	941.
423	56.49	2.8210				22	385.25	1.643		985.	989.
424		2.8210				23	383.70	1.660		1042.	1048.
						24	381.10	1.715		1092.	1098.
						25	378.96	1.665		1142.	1149.
						26	377.34	1.676		1192.	1199.
						27	376.44	1.661		1246.	1252.
						28	373.40	1.746		1305.	1310.
						29	371.15	1.740		1365.	1370.
						30	370.34	1.762		1427.	1432.
						31	369.49	1.755		1487.	1494.
						32	369.54	1.673		1551.	1551.
						33	368.57	1.886		1617.	1621.
						34	366.40	1.886		1685.	1688.
						35	365.00	1.671	2.8307	1705.	1711.
						36	363.50			1813.	1819.
						37	362.21	1.876		1855.	1858.
						38	361.73	1.911		1905.	1911.
						39	359.38	1.911		1965.	1970.
						40	357.81	1.873		2030.	2035.
						41	356.66	1.888		2077.	2082.
						42	354.49	1.880		2149.	2153.
						43	354.74	1.751		2227.	2231.
						44	350.76	1.727		2294.	2297.
						45	349.20	1.672		2344.	2348.
						46	346.80		2.8545	2422.	2425.
						47	346.06	1.740		2407.	2450.
						48	344.50	1.751		2502.	2504.
						49	343.46	1.782		2545.	2545.
						50	342.11	1.829		2587.	2589.
						51	340.19	1.845		2661.	2664.
						52	337.45	1.891		2772.	2774.
						53	336.47	1.874	2.8508	2805.	2805.
						54	336.00			2832.	2832.
						55	334.71	1.806		2882.	2881.
						56	333.94	1.790		2911.	2910.
						57	331.18	1.755		3009.	3007.
						58	330.01	1.755		3048.	3047.
						59	329.44	1.751		3095.	3094.
						60	327.47	1.806		3146.	3144.
						61	326.48	1.806		3177.	3174.
						62	324.92	1.884		3240.	3238.
						63	322.96	1.884		3321.	3318.
						64	321.78	1.864	2.8545	3369.	3365.
						65	320.90			3404.	3401.
						66	319.04	1.908		3482.	3478.
						67	317.87	1.900		3551.	3547.
						68	315.91	1.868		3612.	3608.
						69	314.74	1.870		3658.	3655.
						70	313.17	1.813		3717.	3715.
						71	309.64	1.903		3850.	3853.
						72	306.90	1.813		3967.	3962.
						73	305.34	1.804	2.8476	4026.	4020.
						74	304.20			4069.	4063.
						75	303.77	1.617		4085.	4079.
						76	301.01	1.444		4165.	4158.
						77	299.45	1.451		4251.	4245.
						78	297.20	1.880		4352.	4345.
						79	294.74	1.884		4465.	4459.
						80	293.59	1.922		4514.	4507.
						81	291.00		2.7718	4624.	4621.
						82	290.45	1.422		4632.	4627.
						83	289.67	1.954		4685.	4679.
						84	288.89	1.925		4757.	4753.
						85	287.52	1.818		4780.	4777.
						86	284.19	1.798		4890.	4886.
						87	283.41	1.820		4927.	4925.
						88	281.06	1.939		5024.	5022.
						89	279.44	1.955		5093.	5092.
						90	277.53	1.873		5161.	5160.
						91	275.57	1.955		5249.	5249.
						92	275.18	1.889		5286.	5285.
						93	274.40	1.876		5310.	5314.
						94	271.66	1.824	2.8146	5376.	5376.
						95	270.70			5443.	5443.
						96	270.49	1.861		5468.	5468.
						97	264.41	1.842		5706.	5706.
						98	263.83	1.840		5737.	5737.
						99	261.40	1.875	2.8635	5846.	5845.
						100	260.50			5970.	5969.

TABLE 6-10 (Continued)

J	PEACE DEPTH (FEET)	S + S DENSITY (LB/CC)	BOREHOLE DENSITY OF SOLID COMPONENT (LB/CC)	05H-21			PEACE DEPTH (FEET)	S + S DENSITY (LB/CC)	BOREHOLE DENSITY OF SOLID COMPONENT (LB/CC)	05H-22		
				CUMULATIVE AND 21	SOLID MASS AND 21	SP. GR. FOR AND 21				CUMULATIVE AND 22	SOLID MASS AND 22	SP. GR. FOR AND 22
101	260.30	1.861		5878.	4877.	5877.	0	1800.00		4.8210		
104	259.10	1.829		5929.	4922.	5922.	1	51.91				
105	258.99	1.807		6046.	6046.	6046.	4	591.00		2.8210		
106	257.04	1.828		6132.	6129.	6129.	3	572.00	1.986	2.8678		
107	256.51	1.845		6219.	6209.	6209.	4	572.00				
108	255.40	1.779		6272.	6267.	6267.	7	571.00		2.7471		
109	254.40		2.8506	6296.	6289.	6289.	7	571.00	1.969			
110	253.40	1.782		6397.	6352.	6352.	6	570.00	1.967			
111	252.40	1.826		6508.	6501.	6501.	6	569.00	1.965			
112	251.40	1.808		6600.	6600.	6600.	9	567.51	1.968			
113	250.40	1.803		6645.	6645.	6645.	9	569.70	1.957			
114	249.40	1.808		6687.	6688.	6688.	13	568.61	1.918			
115	248.40	1.812		6727.	6727.	6727.	13	568.61	1.915			
116	247.40	1.812		6860.	6852.	6852.	14	568.26	1.966			
117	246.40	1.812		7025.	7015.	7015.	15	568.90	1.969			
118	245.40	1.803		7105.	7095.	7095.	16	568.90	1.968			
119	244.40	1.826		7166.	7156.	7156.	17	568.90	2.716			
120	243.40	1.803		7182.	7171.	7171.	18	568.90	1.968			
121	242.40	1.826		7300.	7289.	7289.	17	568.90	1.968	2.7402		
122	241.40	1.808		7389.	7377.	7377.	18	568.90	1.968			
123	240.40		2.8541	7515.	7502.	7502.	19	568.90	1.968			
124	239.40	1.868		7588.	7581.	7581.	20	568.90	1.968			
125	238.40	1.800		7625.	7615.	7615.	21	568.90	1.968			
126	237.40	1.870		7793.	7777.	7777.	24	568.90	1.854			
127	236.40	1.899		7847.	7831.	7831.	25	568.90	1.854			
128	235.40	1.899		7972.	7956.	7956.	29	568.90	1.854			
129	234.40	1.897	2.8631	7986.	7970.	7970.	26	568.90	1.912			
130	233.40	1.855		8043.	8026.	8026.	27	568.90	1.912			
131	232.40	1.920		8129.	8129.	8129.	28	568.90	1.912	2.7282		
132	231.40	1.934		8251.	8251.	8251.	29	568.90	1.931			
133	230.40	1.931		8346.	8346.	8346.	30	568.90	1.931			
134	229.40	1.931		8436.	8417.	8417.	31	568.90	1.925			
135	228.40	1.931		8523.	8504.	8504.	32	568.90	1.925			
136	227.40	1.934		8639.	8619.	8619.	33	568.90	1.925			
137	226.40	1.934		8733.	8713.	8713.	34	568.90	1.925	2.7241		
138	225.40	1.934		8778.	8758.	8758.	35	568.90	1.925			
139	224.40	1.934	2.8341	8867.	8846.	8846.	36	568.90	1.925			
140	223.40	1.934		8927.	8906.	8906.	38	568.90	1.925			
141	222.40	1.945		9038.	9017.	9017.	39	568.90	1.925			
142	221.40	1.931		9118.	9098.	9098.	40	568.90	1.925			
143	220.40	1.931		9244.	9223.	9223.	41	568.90	1.925			
144	219.40	1.931		9312.	9291.	9291.	42	568.90	1.925			
145	218.40	1.934	2.8368	9314.	9293.	9293.	43	568.90	1.925			
146	217.40	1.934		9357.	9336.	9336.	44	568.90	1.925			
147	216.40	1.934		9435.	9414.	9414.	45	568.90	1.925	2.7160		
148	215.40	1.934		9535.	9514.	9514.	46	568.90	1.925			
149	214.40	1.934		9672.	9651.	9651.	47	568.90	1.925			
150	213.40	1.934		9744.	9723.	9723.	48	568.90	1.925			
151	212.40	1.934		9846.	9825.	9825.	49	568.90	1.925			
152	211.40	1.934		9946.	9925.	9925.	50	568.90	1.925			
153	210.40	2.071		10090.	10069.	10069.	51	568.90	1.925			
154	209.40	2.042		10265.	10243.	10243.	52	568.90	1.925			
155	208.40	2.042		10303.	10281.	10281.	53	568.90	1.925			
156	207.40	1.998		10378.	10356.	10356.	54	568.90	1.925			
157	206.40	1.992		10478.	10456.	10456.	55	568.90	2.008			
158	205.40	1.944		10551.	10529.	10529.	56	568.90	2.008			
159	204.40		2.8499	10607.	10585.	10585.	57	568.90	2.008			
160	203.40	1.955		10662.	10640.	10640.	58	568.90	2.008			
161	202.40	1.955		10775.	10753.	10753.	59	568.90	2.008			
162	201.40	1.955		10866.	10844.	10844.	60	568.90	2.008			
163	200.40	1.955		10972.	10950.	10950.	61	568.90	2.008			
164	199.40	2.049		11077.	11055.	11055.	62	568.90	2.008	2.7292		
165	198.40		2.9866	11200.	11178.	11178.	63	568.90	2.008			
166	197.40	2.883		11242.	11220.	11220.	64	568.90	2.008			
167	196.40		2.9288	11287.	11265.	11265.	65	568.90	2.008			
168	195.40	2.9288					66	568.90	2.008			
169	194.40	2.9288					67	568.90	2.008			
170	193.40	2.9288					68	568.90	2.008			
171	192.40	2.9288					69	568.90	2.008			
172	191.40						70	568.90	2.008			
173	190.40						71	568.90	2.008			
174	189.40						72	568.90	2.008			
175	188.40						73	568.90	2.008			
176	187.40						74	568.90	2.008			
177	186.40						75	568.90	2.008			
178	185.40						76	568.90	2.008			
179	184.40						77	568.90	2.008			
180	183.40						78	568.90	2.008			
181	182.40						79	568.90	2.008			
182	181.40						80	568.90	2.008			
183	180.40						81	568.90	2.008			
184	179.40						82	568.90	2.008			
185	178.40						83	568.90	2.008			
186	177.40						84	568.90	2.008			
187	176.40						85	568.90	2.008			
188	175.40						86	568.90	2.008			
189	174.40						87	568.90	2.008			
190	173.40						88	568.90	2.008			
191	172.40						89	568.90	2.008			
192	171.40						90	568.90	2.008			
193	170.40						91	568.90	2.008			
194	169.40						92	568.90	2.008			
195	168.40						93	568.90	2.008			
196	167.40						94	568.90	2.008			
197	166.40						95	568.90	2.008			
198	165.40						96	568.90	2.008			
199	164.40						97	568.90	2.008			
200	163.40						98	568.90	2.008			
201	162.40						99	568.90	2.008			
202	161.40						100	568.90	2.008			

TABLE 6-10 (Continued)

J	PEACE DEPTH DIP (°)	G + G DENSITY (G/CC)	DENSITY OF SOLID COMPONENT (G/CC)	BOTH HOLE DRT-20 CUMULATIVE RHO2-021	SOLID MASS RHO2-021 RHO2-021	ISPC/CM2 LINEAR SP. INT FOR RHO	J	PEACE DEPTH DIP (°)	G + G DENSITY (G/CC)	DENSITY OF SOLID COMPONENT (G/CC)	BOTH HOLE DRT-20 CUMULATIVE RHO2-021	SOLID MASS RHO2-021 RHO2-021	ISPC/CM2 LINEAR SP. INT FOR RHO
101	416.90		2.1344	6078.	7020.	7828.	201	165.66	1.969		10622.	10697.	10697.
102	418.96	2.046		7164.	7312.	7512.	202	163.70	1.969		10710.	10765.	10765.
103	407.58	2.017		7334.	7483.	7683.	203	161.15		2.9198	10804.	10876.	10876.
104	405.27	2.027		7409.	7559.	7759.	204	159.57	2.079		10860.	10932.	10932.
105	406.89	2.047		7466.	7616.	7816.	205	158.26	2.113		10901.	10950.	10950.
106	402.73	2.057		7563.	7712.	7912.	206	156.45	2.079		10961.	11029.	11029.
107	401.90		2.8146	7604.	7754.	7954.	207	153.91	1.953		11011.	11057.	11057.
108	399.21	2.059		7749.	7899.	8099.	208	151.93	1.940		11078.	11142.	11142.
109	397.23	2.091		7841.	7991.	8191.	209	149.99	1.942		11144.	11206.	11206.
110	396.37	2.079		7901.	8050.	8250.	210	148.92	1.997		11193.	11255.	11255.
111	391.27	2.005		8130.	8277.	8477.	211	146.40		2.9297	11258.	11317.	11317.
112	387.84	2.047		8297.	8442.	8642.	212	143.29	1.958		11317.	11375.	11375.
113	387.70		4.8974	8304.	8449.	8649.	213	140.13	1.997		11361.	11418.	11418.
114	385.88	2.091		8392.	8536.	8736.	214	138.98	1.926		11411.	11468.	11468.
115	381.90	2.026		8582.	8723.	8923.	215	136.20	1.917		11469.	11521.	11521.
116	375.61	2.050		8796.	8934.	9134.	216	137.06	1.874		11538.	11593.	11593.
117	377.20	2.042		8811.	8950.	9150.	217	135.00	1.885		11597.	11653.	11653.
118	375.69	2.026		8867.	9004.	9204.	218	132.75	1.892		11656.	11714.	11714.
119	372.95	2.041		9028.	9157.	9357.	219	131.96	1.958		11716.	11777.	11777.
120	371.98	2.024		9095.	9233.	9433.	220	131.94		2.9096	11777.	11838.	11838.
121	369.78	2.059		9198.	9327.	9527.	221	121.89		2.8210	11838.	11900.	11900.
122	367.40		2.8341	9287.	9424.	9624.	222	120.05	1.958		11899.	11962.	11962.
123	367.07	2.024		9303.	9440.	9640.	223	116.40	1.946		11960.	12024.	12024.
124	365.51	2.046		9379.	9515.	9715.	224	123.74	1.951		12021.	12086.	12086.
125	362.76	2.044		9513.	9649.	9849.	225	119.62	1.917		12082.	12148.	12148.
126	360.00	2.044		9610.	9746.	9946.	226			2.8916	12143.	12210.	12210.
127	359.00	1.955		9648.	9782.	9982.					12204.	12272.	12272.
128	356.89	2.000		9801.	9934.	10134.					12265.	12334.	12334.
129	355.32	1.953		9872.	10004.	10204.					12326.	12396.	12396.
130	353.75	1.953		9942.	10073.	10273.					12387.	12458.	12458.
131	351.40		2.9040	10048.	10178.	10378.					12448.	12520.	12520.
132	349.90	2.024		10140.	10268.	10468.					12509.	12582.	12582.
133	349.91	2.031		10210.	10335.	10535.					12569.	12643.	12643.
134	348.93	2.008		10303.	10423.	10623.					12629.	12704.	12704.
135	342.40		2.8802	10396.	10512.	10712.					12689.	12765.	12765.
136	343.00		2.7824	10482.	10595.	10795.					12750.	12827.	12827.
137	340.30		2.8235	10569.	10674.	10874.					12810.	12888.	12888.
138	339.00		2.8277	10657.	10753.	10953.					12870.	12949.	12949.
139	338.22	1.995		10744.	10838.	11038.					12930.	13010.	13010.
140	331.65	1.955		10831.	10923.	11123.					13000.	13081.	13081.
141	329.30	1.975		10919.	11009.	11209.					13060.	13142.	13142.
142	327.35	1.976		11008.	11097.	11297.					13120.	13203.	13203.
143	324.99	1.999		11097.	11184.	11384.					13180.	13264.	13264.
144	324.00	1.989		11186.	11271.	11471.					13240.	13325.	13325.
145	322.40		2.8545	11275.	11358.	11558.					13300.	13386.	13386.
146	320.30	2.000		11364.	11445.	11645.					13360.	13447.	13447.
147	318.50	1.941		11453.	11532.	11732.					13420.	13508.	13508.
148	316.80	1.921		11542.	11619.	11819.					13480.	13569.	13569.
149	315.00	1.910		11631.	11707.	11907.					13540.	13631.	13631.
150	313.20	1.900		11720.	11804.	12004.					13600.	13693.	13693.
151	311.40	1.900		11809.	11891.	12101.					13660.	13756.	13756.
152	309.60	2.013		11898.	11978.	12201.					13720.	13820.	13820.
153	307.80	1.990		11987.	12065.	12295.					13780.	13883.	13883.
154	306.00	2.014		12076.	12151.	12381.					13840.	13947.	13947.
155	304.20	1.970		12165.	12238.	12468.					13900.	14006.	14006.
156	302.40	1.966		12254.	12325.	12555.					13960.	14066.	14066.
157	300.60	2.004		12343.	12412.	12642.					14020.	14127.	14127.
158	300.00	2.004		12432.	12500.	12730.					14080.	14189.	14189.
159	298.20	2.004		12521.	12588.	12818.					14140.	14252.	14252.
160	296.40	2.004		12610.	12676.	12896.					14200.	14315.	14315.
161	294.60	2.004		12699.	12764.	12974.					14260.	14379.	14379.
162	292.80	2.004		12788.	12852.	13052.					14320.	14443.	14443.
163	291.00	2.004		12877.	12944.	13144.					14380.	14508.	14508.
164	289.20	2.004		12966.	13032.	13232.					14440.	14573.	14573.
165	287.40	2.004		13055.	13120.	13320.					14500.	14639.	14639.
166	285.60	2.004		13144.	13208.	13408.					14560.	14705.	14705.
167	283.80	2.004		13233.	13296.	13506.					14620.	14771.	14771.
168	282.00	2.004		13322.	13384.	13604.					14680.	14838.	14838.
169	280.20	2.004		13411.	13472.	13704.					14740.	14905.	14905.
170	278.40	2.004		13500.	13560.	13804.					14800.	14972.	14972.
171	276.60	2.004		13589.	13648.	13904.					14860.	15040.	15040.
172	274.80	2.004		13678.	13736.	14004.					14920.	15108.	15108.
173	273.00	2.004		13767.	13824.	14104.					14980.	15176.	15176.
174	271.20	2.004		13856.	13912.	14204.					15040.	15245.	15245.
175	269.40	2.004		13945.	14000.	14304.					15100.	15314.	15314.
176	267.60	2.004		14034.	14098.	14404.					15160.	15384.	15384.
177	265.80	2.004		14123.	14186.	14504.					15220.	15454.	15454.
178	264.00	2.004		14212.	14274.	14604.					15280.	15525.	15525.
179	262.20	2.004		14301.	14362.	14704.					15340.	15596.	15596.
180	260.40	2.004		14390.	14450.	14804.					15400.	15667.	15667.
181	258.60	2.004		14479.	14538.	14904.					15460.	15738.	15738.
182	256.80	2.004		14568.	14626.	15004.					15520.	15809.	15809.
183	255.00	2.004		14657.	14714.	15104.					15580.	15880.	15880.
184	253.20	2.004		14746.	14802.	15204.					15640.	15951.	15951.
185	251.40	2.004		14835.	14890.	15304.					15700.	16022.	16022.
186	249.60	2.004		14924.	14978.	15404.					15760.	16093.	16093.
187	247.80	2.004		15013.	15066.	15504.					15820.	16164.	16164.
188	246.00	2.004		15102.	15154.	15604.					15880.	16235.	16235.
189	244.20	2.004		15191.	15242.	15704.					15940.	16306.	16306.
190	242.40	2.004		15280.	15330.	15804.					16000.	16377.	16377.
191	240.60	2.004		15369.	15418.	15904.					16060.	16448.	16448.
192	238.80	2.004		15458.	15506.	16004.					16120.	16519.	16519.
193	237.00	2.004		15547.	15594.	16104.					16180.	16590.	16590.
194	235.20	2.004		15636.	15682.	16204.					16240.	16661.	16661.
195	233.40	2.004		15725.	15770.	16304.					16300.	16732.	16732.
196	231.60	2.004		15814.	15858.	16404.					16360.	16803.	16803.
197	229.80	2.004		15903.	15946.	16504.					16420.	16874.	16874.
198	228.00	2.004		15992.	16034.	16604.					16480.	16945.	16945.
199	226.20	2.004		16081.	16124.	16704.					16540.	17016.	17016.
200	22												

TABLE 6-10 (Continued)

U	PLACE (DEPTH DIFF)	G - S DENSITY (G/CC)	BUREHOLE CUT-19				U	PLACE (DEPTH DIFF)	G - S DENSITY (G/CC)	BUREHOLE CUT-19			
			DENSITY OF SOLID COMPONENT (G/CC)	CUMULATIVE RHOx2.821	SOLID MASS RHOxCMPO	LINEAR SPINALE FOR RHO				DENSITY OF SOLID COMPONENT (G/CC)	CUMULATIVE RHOx2.821	SOLID MASS RHOxCMPO	LINEAR SPINALE FOR RHO
1	1800.00		2.0216				101	597.74	2.0225	8996.	8930.	8997.	
2	810.51		2.0210				102	598.33	2.0230	8911.	8845.	8977.	
3	810.50		2.0096				103	598.81	2.003	8806.	8720.	8872.	
4	808.50		2.0131				104	599.24	2.041	8761.	8695.	8825.	
5	798.10		2.0042				105	599.70	2.030	8719.	8752.	8772.	
6	788.50		2.0198				106	591.31	2.041	8655.	8685.	8744.	
7	788.60		2.0237				107	579.73	2.019	8661.	8761.	8761.	
8	767.50	1.950		0.	0.	0.	108	578.20		2.0343	9086.	9019.	9049.
9	766.80	1.947		70.	68.	68.	109	576.39	2.036		9170.	9111.	9131.
10	761.34	2.003		213.	209.	209.	110	571.84	2.038		9311.	9245.	9265.
11	759.10	2.011		281.	281.	281.	111	572.66	2.024		9368.	9301.	9321.
12	759.10		2.011	300.	375.	375.	112	568.73	2.017		9355.	9289.	9309.
13	759.10			362.	385.	385.	113	567.94	2.035		9393.	9327.	9347.
14	755.47	2.052	2.9148	404.	485.	485.	114	565.19	2.016		9720.	9660.	9680.
15	753.07	2.042		571.	560.	560.	115	565.45	2.027		9819.	9755.	9775.
16	751.99	2.043		687.	675.	675.	116	561.63	2.019		9894.	9830.	9850.
17	749.10	2.072		766.	742.	742.	117	560.87	2.003		9931.	9867.	9887.
18	749.10		2.9113	864.	848.	848.	118	559.00			9966.	9902.	9922.
19	747.17	2.071		885.	870.	870.	119	558.44	1.812		10110.	10053.	10073.
20	744.42	2.039		980.	962.	962.	120	558.74	1.481		10152.	10071.	10071.
21	741.67	2.041		1113.	1093.	1093.	121	554.50	1.937		10220.	10163.	10183.
22	738.54	2.049		1248.	1226.	1226.	122	552.41	1.951		10307.	10249.	10249.
23	738.54			1403.	1378.	1378.	123	549.88	1.956		10379.	10324.	10344.
24	737.34	2.042		1461.	1455.	1455.	124	549.00		2.7241	10468.	10413.	10433.
25	735.81	2.071		1606.	1606.	1606.	125	547.90	1.987		10518.	10465.	10485.
26	729.80	2.071		1827.	1794.	1794.	126	546.34	1.959		10589.	10534.	10554.
27	728.34	2.082	2.9159	1845.	1812.	1812.	127	543.57	2.000		10715.	10664.	10684.
28	725.95	2.057		1905.	1871.	1871.	128	541.41	1.987		10825.	10778.	10798.
29	724.57	2.064		2023.	1987.	1987.	129	539.64	1.951		10886.	10831.	10851.
30	722.44	2.074		2101.	2065.	2065.	130	538.67		2.7140	10929.	10874.	10894.
31	720.94	2.050		2219.	2180.	2180.	131	536.89	1.945		11017.	10975.	10995.
32	716.91	1.999		2278.	2257.	2257.	132	534.93	1.965		11105.	11065.	11085.
33	714.15	1.992		2462.	2418.	2418.	133	533.30	1.961		11176.	11137.	11157.
34	712.98	2.035		2508.	2542.	2542.	134	531.57	1.990		11210.	11173.	11193.
35	710.22	2.042		2643.	2597.	2597.	135	529.44	1.958		11350.	11315.	11335.
36	707.00	2.036		2777.	2728.	2728.	136	528.44	1.921		11401.	11368.	11388.
37	704.33	1.987		2927.	2876.	2876.	137	526.67	1.939		11469.	11438.	11458.
38	702.40	2.014		3055.	3022.	3022.	138	525.49	1.917		11520.	11490.	11510.
39	701.10	2.035		3147.	3082.	3082.	139	523.92	1.925		11588.	11559.	11579.
40	700.10		2.8974	3217.	3147.	3147.	140	522.74	1.971		11640.	11613.	11633.
41	698.10	2.044		3255.	3199.	3199.	141	520.78	2.044		11735.	11707.	11727.
42	696.10	2.042		3317.	3260.	3260.	142	518.81	2.003		11826.	11803.	11823.
43	694.10	2.034		3355.	3298.	3298.	143	517.43	2.011		11881.	11858.	11878.
44	692.94	2.070		3526.	3466.	3466.	144	515.70		2.7140	11991.	11962.	11982.
45	690.10	2.031		3603.	3541.	3541.	145	513.27	1.997		11992.	11973.	11993.
46	688.10	2.042		3737.	3673.	3673.	146	513.70	2.050		12067.	12049.	12069.
47	687.93	2.039		3813.	3748.	3748.	147	512.52	2.080		12125.	12107.	12127.
48	686.10	2.078		3870.	3809.	3809.	148	509.38	2.050		12247.	12248.	12268.
49	684.28	1.973		3925.	3868.	3868.	149	508.44	2.035		12300.	12287.	12307.
50	682.10	1.950		4014.	3946.	3946.	150	507.81	2.031		12377.	12346.	12366.
51	679.98	2.035		4067.	3988.	3988.	151	506.63	2.025		12413.	12404.	12424.
52	677.94	2.055		4113.	4042.	4042.	152	504.44	2.039		12468.	12451.	12471.
53	675.98	2.055		4159.	4083.	4083.	153	503.09	2.077		12508.	12500.	12520.
54	673.67	2.050		4206.	4144.	4144.	154	500.34	2.088		12572.	12573.	12593.
55	670.34	2.077		4278.	4200.	4200.	155	498.37	2.082		12625.	12625.	12645.
56	670.00		2.9046	4378.	4260.	4260.	156	497.59	2.050		12646.	12665.	12685.
57	668.95	2.110		4405.	4266.	4266.	157	496.01	2.066		12742.	12744.	12764.
58	668.17	2.110		4459.	4279.	4279.	158	494.75	2.035		12836.	12843.	12863.
59	666.20	2.071		4501.	4318.	4318.	159	491.69	2.068		12912.	12915.	12935.
60	663.00	2.003		4553.	4380.	4380.	160	490.10	1.980		12966.	12966.	12986.
61	661.00	2.003		4615.	4468.	4468.	161	488.30	2.030		13000.	13110.	13130.
62	659.91	1.984		4659.	4509.	4509.	162	487.17	2.030		13057.	13169.	13189.
63	657.90	2.019	2.8921	4700.	4513.	4513.	163	486.19	2.102		13116.	13229.	13249.
64	655.90	1.984		4749.	4520.	4520.	164	485.01	2.113		13177.	13292.	13312.
65	654.91	2.006		4798.	4529.	4529.	165	483.30		2.7181	13255.	13371.	13391.
66	652.43	1.987		4857.	4537.	4537.	166	482.44	2.047		13316.	13434.	13454.
67	651.66	2.025		4906.	4548.	4548.	167	479.90	1.987		13379.	13498.	13518.
68	649.48	2.038		4955.	4558.	4558.	168	478.33	2.003		13402.	13522.	13542.
69	648.14	2.049		5004.	4565.	4565.	169	474.40	1.924		13479.	13600.	13620.
70	647.14	2.050		5053.	4571.	4571.	170	473.47	1.986		13501.	13651.	13671.
71	647.14	2.050		5102.	4578.	4578.	171	470.86	2.065		13562.	13682.	13702.
72	644.10	2.081		5151.	4584.	4584.	172	468.89	2.077		13620.	13740.	13760.
73	644.10	2.081		5200.	4591.	4591.	173	468.00		2.8892	13685.	13804.	13824.
74	641.91	2.028		5249.	4598.	4598.	174	466.93	2.046		13742.	13856.	13876.
75	642.64	2.020		5298.	4607.	4607.	175	465.75	1.991		13800.	13911.	13931.
76	641.05	2.027		5347.	4615.	4615.	176	465.75	2.003		13858.	13963.	13983.
77	639.10	2.049		5396.	4622.	4622.	177	462.41	2.005		13916.	14015.	14035.
78	637.10	2.046		5445.	4629.	4629.	178	461.03	1.995		13974.	14073.	14093.
79	635.30	2.050		5494.	4637.	4637.	179	459.44	2.033		14032.	14131.	14151.
80	631.67	2.011		5543.	4640.	4640.	180	458.28	1.035		14090.	14189.	14209.
81	629.65	2.011	2.7242	5592.	4648.	4648.	181	455.94	2.066		14148.	14247.	14267.
82	627.65	2.014		5641.	4657.	4657.	182	453.97	2.035		14206.	14305.	14325.
83	626.51	2.014		5690.	4660.	4660.	183	450.81	2.022		14264.	14363.	14383.
84	624.77	1.995		5739.	4671.	4671.	184	448.85	2.019		14322.	14421.	14441.
85	624.77	1.972		5788.	4682.	4682.	185	448.00		2.7201	14380.	14479.	14499.
86	621.07	2.047		5837.	4693.	4693.	186	446.10	1.965		14438.	14537.	14557.
87	619.10	2.030		5886.	4704.	4704.	187	442.99	1.969		14496.	14595.	14615.
88	615.10	2.030		5935.	4715.	4715.	188	440.99	2.003		14554.	14653.	14673.
89	613.10	2.030		5984.	4726.	4726.	189	437.06	2.032		14612.	14711.	14731.
90	610.00	2.050		6033.	4737.	4737.	190	435.09	2.025		14670.	14769.	14789.
91	607.64	1.987		6082.	4748.	4748.	191	432.74	2.035		14728.	14827.	14847.
92	607.64	2.003		6131.	4759.	4759.	192	430.77	2.060		14786.	14885.	14905.
93	605.67	1.987		6180.	4770.	4770.	193	428.04	2.003		14844.	14943.	14963.
94	604.10	1.996		6229.	4781.	4781.	194	427.43	2.023		14902.	15001.	15021.
95	602.10	2.028		6278.	4793.	4793.	195	425.06	2.019		14960.	15059.	15079.
96													

TABLE 6-10 (Continued)

J	PEACH DEPTH DIFF)	G - E DENSITY (GM/CC)	BOREHOLE DGT-19				J	PEACH DEPTH DIFF)	G - E DENSITY (GM/CC)	BOREHOLE DGT-14			
			DENSITY OF SOLID COMPONENT (GM/CC)	CUMULATIVE RHO=2.82	SOLID MASS RHO=(RHO)	16W/CH=2 LINEAR SPLINE FOR RHO				DENSITY OF SOLID COMPONENT (GM/CC)	CUMULATIVE RHO=2.82	SOLID MASS RHO=(RHO)	16W/CH=2 LINEAR SPLINE FOR RHO
203	414.46	1.972		16894.	16899.	16899.	301	226.90		2.0700			
204	411.51	2.030		16903.	17020.	17020.	302	216.30		2.0541			
205	409.54	2.009		17076.	17122.	17122.	303	196.90		2.0039			
206	409.40		2.1995	17092.	17139.	17139.	304	189.00		2.0074			
207	407.50	2.003		17169.	17215.	17215.	305	171.00		2.0307			
208	406.79	1.962		17204.	17251.	17251.	306	160.00		2.0159			
209	404.00	2.003		17203.	17300.	17300.	307	163.00		2.0153			
210	403.00	2.003		17349.	17395.	17395.	308	148.70		2.0213			
211	402.07	2.005		17405.	17450.	17450.	309	128.00		2.0201			
212	400.00	2.007		17403.	17520.	17520.	310	122.90		2.0130			
213	399.14	2.104		17544.	17580.	17580.	311	110.00		2.1107			
214	399.50		2.0005	17545.	17595.	17595.	312	117.99		2.0210			
215	395.00	2.091		17677.	17620.	17620.							
216	393.00	2.134		17690.	17620.	17620.							
217	389.00	2.140		18050.	18090.	18090.							
218	388.71	2.149		18121.	18157.	18157.							
219	386.75	2.129		18226.	18460.	18460.							
220	385.10	2.138		18309.	18502.	18502.							
221	382.84	2.129		18453.	18464.	18464.							
222	381.64	2.151		18490.	18526.	18526.							
223	380.50		2.0040	18556.	18506.	18506.							
224	380.07	2.146		18579.	18608.	18608.							
225	379.67	2.037		18599.	18626.	18626.							
226	377.71	1.959		18689.	18717.	18717.							
227	375.74	1.830		18770.	18796.	18796.							
228	372.93	1.909		18802.	18906.	18906.							
229	370.44	1.814		18992.	19014.	19014.							
230	368.27	1.692		19060.	19082.	19082.							
231	366.81	1.889		19123.	19190.	19190.							
232	362.77	1.970		19259.	19289.	19289.							
233	361.53	1.962		19312.	19337.	19337.							
234	359.40	1.980		19419.	19435.	19435.							
235	356.40	2.035		19469.	19463.	19463.							
236	355.30		2.0040	19506.	19609.	19609.							
237	353.73	2.046		19602.	19640.	19640.							
238	350.50	2.011		19834.	19845.	19845.							
239	348.04	1.976		19925.	19930.	19930.							
240	345.07	1.967		20050.	20057.	20057.							
241	343.51	1.909		20155.	20159.	20159.							
242	340.76	1.961		20273.	20279.	20279.							
243	339.50	1.978		20324.	20330.	20330.							
244	338.70		2.0045	20366.	20372.	20372.							
245	337.64	2.013		20411.	20422.	20422.							
246	335.46	1.940		20525.	20530.	20530.							
247	333.09	1.990		20596.	20601.	20601.							
248	331.78	2.000		20649.	20650.	20650.							
249	330.15	2.000		20760.	20775.	20775.							
250	328.18	2.000		20860.	20873.	20873.							
251	326.44	2.044		20967.	20972.	20972.							
252	325.00	2.019		21070.	21079.	21079.							
253	323.07	2.016		21130.	21125.	21125.							
254	321.90	2.068		21272.	21277.	21277.							
255	317.90	2.096		21372.	21370.	21370.							
256	316.49	2.036		21451.	21456.	21456.							
257	315.21	2.017		21507.	21513.	21513.							
258	313.45	2.011		21600.	21607.	21607.							
259	311.40	2.053		21695.	21708.	21708.							
260	310.50		2.1973	21790.	21731.	21731.							
261	309.40	2.041		21735.	21741.	21741.							
262	309.40	2.057		21791.	21799.	21799.							
263	308.90	2.050		21907.	21915.	21915.							
264	308.00	2.001		21983.	21991.	21991.							
265	306.41	2.019		22089.	22087.	22087.							
266	301.00	2.046		22171.	22180.	22180.							
267	300.07	2.002		22210.	22219.	22219.							
268	299.10	2.000		22269.	22297.	22297.							
269	298.70	2.002		22400.	22413.	22413.							
270	296.90		2.0733	22416.	22420.	22420.							
271	295.17	2.024		22440.	22480.	22480.							
272	292.01	2.055		22595.	22603.	22603.							
273	290.06	2.020		22720.	22737.	22737.							
274	288.49	2.035		22804.	22812.	22812.							
275	285.74	1.976		22939.	22941.	22941.							
276	283.00	1.972		23041.	23040.	23040.							
277	282.90	1.940		23050.	23065.	23065.							
278	280.60	2.017		23167.	23173.	23173.							
279	279.49	2.040		23223.	23229.	23229.							
280	277.41	2.055		23299.	23305.	23305.							
281	275.91	2.036		23395.	23401.	23401.							
282	273.94	2.039		23491.	23496.	23496.							
283	273.10	2.011		23520.	23533.	23533.							
284	271.50	2.000		23602.	23607.	23607.							
285	268.00	1.925		23703.	23707.	23707.							
286	266.00	1.929		23803.	23808.	23808.							
287	264.14	1.901		23933.	23935.	23935.							
288	262.15	2.057		24024.	24027.	24027.							
289	260.15	2.060		24124.	24124.	24124.							
290	258.01	2.053		24201.	24201.	24201.							
291	257.00	2.022		24277.	24276.	24276.							
292	255.00	2.003		24370.	24360.	24360.							
293	253.00	1.970		24424.	24422.	24422.							
294	251.00	1.969		24510.	24510.	24510.							
295	251.00		2.4748	24515.	24511.	24511.							
296	250.00	1.944		24584.	24579.	24579.							
297	248.00	1.972		24672.	24666.	24666.							
298	246.00	1.940		24740.	24733.	24733.							
299	244.00	1.901		24840.	24841.	24841.							
300	242.00	1.883		24930.	24930.	24930.							
301	241.50	2.050		24994.	24985.	24985.							
302	240.00	2.057		25130.	25120.	25120.							

TABLE 6-10 (Continued)

PEARL OCEAN CITY	6 - 6 DENSITY (G/CC)	BOREHOLE DENSITY OF SOLID COMPONENT (G/CC)	BOREHOLE 002-04			PEARL OCEAN CITY	6 - 6 DENSITY (G/CC)	BOREHOLE DENSITY OF SOLID COMPONENT (G/CC)	BOREHOLE 007-04		
			CUMULATIVE SOLID MASS (G/CM ²)	LINEAR MASS (G/CM)	FOR BMD				CUMULATIVE SOLID MASS (G/CM ²)	LINEAR MASS (G/CM)	FOR BMD
1	1000.00	2.8210				101	1375.00				
2	1000.00	2.8210				102	1375.00				
3	1000.00	2.8210				103	1375.00				
4	1000.00	2.8210				104	1375.00				
5	1000.00	2.8210				105	1375.00				
6	1000.00	2.8210				106	1375.00				
7	1000.00	2.8210				107	1375.00				
8	1000.00	2.8210				108	1375.00				
9	1000.00	2.8210				109	1375.00				
10	1000.00	2.8210				110	1375.00				
11	1000.00	2.8210				111	1375.00				
12	1000.00	2.8210				112	1375.00				
13	1000.00	2.8210				113	1375.00				
14	1000.00	2.8210				114	1375.00				
15	1000.00	2.8210				115	1375.00				
16	1000.00	2.8210				116	1375.00				
17	1000.00	2.8210				117	1375.00				
18	1000.00	2.8210				118	1375.00				
19	1000.00	2.8210				119	1375.00				
20	1000.00	2.8210				120	1375.00				
21	1000.00	2.8210				121	1375.00				
22	1000.00	2.8210				122	1375.00				
23	1000.00	2.8210				123	1375.00				
24	1000.00	2.8210				124	1375.00				
25	1000.00	2.8210				125	1375.00				
26	1000.00	2.8210				126	1375.00				
27	1000.00	2.8210				127	1375.00				
28	1000.00	2.8210				128	1375.00				
29	1000.00	2.8210				129	1375.00				
30	1000.00	2.8210				130	1375.00				
31	1000.00	2.8210				131	1375.00				
32	1000.00	2.8210				132	1375.00				
33	1000.00	2.8210				133	1375.00				
34	1000.00	2.8210				134	1375.00				
35	1000.00	2.8210				135	1375.00				
36	1000.00	2.8210				136	1375.00				
37	1000.00	2.8210				137	1375.00				
38	1000.00	2.8210				138	1375.00				
39	1000.00	2.8210				139	1375.00				
40	1000.00	2.8210				140	1375.00				
41	1000.00	2.8210				141	1375.00				
42	1000.00	2.8210				142	1375.00				
43	1000.00	2.8210				143	1375.00				
44	1000.00	2.8210				144	1375.00				
45	1000.00	2.8210				145	1375.00				
46	1000.00	2.8210				146	1375.00				
47	1000.00	2.8210				147	1375.00				
48	1000.00	2.8210				148	1375.00				
49	1000.00	2.8210				149	1375.00				
50	1000.00	2.8210				150	1375.00				
51	1000.00	2.8210				151	1375.00				
52	1000.00	2.8210				152	1375.00				
53	1000.00	2.8210				153	1375.00				
54	1000.00	2.8210				154	1375.00				
55	1000.00	2.8210				155	1375.00				
56	1000.00	2.8210				156	1375.00				
57	1000.00	2.8210				157	1375.00				
58	1000.00	2.8210				158	1375.00				
59	1000.00	2.8210				159	1375.00				
60	1000.00	2.8210				160	1375.00				
61	1000.00	2.8210				161	1375.00				
62	1000.00	2.8210				162	1375.00				
63	1000.00	2.8210				163	1375.00				
64	1000.00	2.8210				164	1375.00				
65	1000.00	2.8210				165	1375.00				
66	1000.00	2.8210				166	1375.00				
67	1000.00	2.8210				167	1375.00				
68	1000.00	2.8210				168	1375.00				
69	1000.00	2.8210				169	1375.00				
70	1000.00	2.8210				170	1375.00				
71	1000.00	2.8210				171	1375.00				
72	1000.00	2.8210				172	1375.00				
73	1000.00	2.8210				173	1375.00				
74	1000.00	2.8210				174	1375.00				
75	1000.00	2.8210				175	1375.00				
76	1000.00	2.8210				176	1375.00				
77	1000.00	2.8210				177	1375.00				
78	1000.00	2.8210				178	1375.00				
79	1000.00	2.8210				179	1375.00				
80	1000.00	2.8210				180	1375.00				
81	1000.00	2.8210				181	1375.00				
82	1000.00	2.8210				182	1375.00				
83	1000.00	2.8210				183	1375.00				
84	1000.00	2.8210				184	1375.00				
85	1000.00	2.8210				185	1375.00				
86	1000.00	2.8210				186	1375.00				
87	1000.00	2.8210				187	1375.00				
88	1000.00	2.8210				188	1375.00				
89	1000.00	2.8210				189	1375.00				
90	1000.00	2.8210				190	1375.00				
91	1000.00	2.8210				191	1375.00				
92	1000.00	2.8210				192	1375.00				
93	1000.00	2.8210				193	1375.00				
94	1000.00	2.8210				194	1375.00				
95	1000.00	2.8210				195	1375.00				
96	1000.00	2.8210				196	1375.00				
97	1000.00	2.8210				197	1375.00				
98	1000.00	2.8210				198	1375.00				
99	1000.00	2.8210				199	1375.00				
100	1000.00	2.8210				200	1375.00				

TABLE 6-10 (Continued)

BOREHOLE DR-04						BOREHOLE DR-04					
PLACED DEPTH DIFF	G - G DENSITY (GM/CC)	DENSITY OF SOLID COMPONENT (GM/CC)	CUMULATIVE RHO2-821	SOLID MASS RHO2-821	SP LINE FOR RHO	PLACED DEPTH DIFF	G - G DENSITY (GM/CC)	DENSITY OF SOLID COMPONENT (GM/CC)	CUMULATIVE RHO2-821	SOLID MASS RHO2-821	SP LINE FOR RHO
204	1149.19	2.548	17864.	14251.	18251.	301	180.78	2.170	38473.	36923.	38924.
206	1151.47	2.548	18075.	14475.	18475.	302	179.72	2.158	38652.	37144.	39144.
208	1153.81	2.548	18287.	14700.	18700.	303	178.85	2.175	38830.	37368.	39368.
210	1156.10	2.547	18503.	14926.	18926.	304	178.01	1.910	39007.	37593.	39593.
212	1158.44	2.547	18721.	15153.	19153.	305	177.16	1.750	39184.	37819.	39819.
214	1160.80	2.548	18941.	15381.	19381.	306	176.32	1.895	39360.	38046.	40046.
216	1163.19	2.548	19163.	15610.	19610.	307	175.48	2.107	39536.	38274.	40274.
218	1165.60	2.548	19387.	15840.	19840.	308	174.64	2.143	39711.	38503.	40503.
220	1168.03	2.548	19613.	16071.	20071.	309	173.80	2.188	39886.	38733.	40733.
222	1170.47	2.548	19841.	16303.	20303.	310	172.96	2.197	40060.	38964.	40964.
224	1172.93	2.548	20071.	16536.	20536.	311	172.12	2.047	40234.	39195.	41195.
226	1175.40	2.548	20303.	16770.	20770.	312	171.28	1.987	40408.	39426.	41426.
228	1177.89	2.548	20536.	17005.	21005.	313	170.44	2.008	40582.	39657.	41657.
230	1180.39	2.548	20771.	17241.	21241.	314	169.60	2.070	40756.	39888.	41888.
232	1182.90	2.548	21007.	17478.	21478.	315	168.76	2.013	40930.	40119.	42119.
234	1185.42	2.548	21244.	17716.	21716.	316	167.92	2.076	41104.	40350.	42350.
236	1187.95	2.548	21482.	17955.	21955.	317	167.08	2.025	41278.	40581.	42581.
238	1190.49	2.548	21721.	18195.	22195.	318	166.24	2.075	41452.	40812.	42812.
240	1193.04	2.548	21961.	18436.	22436.	319	165.40	2.098	41626.	41043.	43043.
242	1195.60	2.548	22203.	18678.	22678.	320	164.56	2.061	41800.	41274.	43274.
244	1198.17	2.548	22446.	18921.	22921.	321	163.72	2.034	41974.	41505.	43505.
246	1200.75	2.548	22690.	19165.	23165.	322	162.88	2.017	42148.	41736.	43736.
248	1203.34	2.548	22935.	19410.	23410.	323	162.04	2.000	42322.	41967.	43967.
250	1205.94	2.548	23181.	19656.	23656.	324	161.20	1.983	42496.	42198.	44198.
252	1208.55	2.548	23428.	19903.	23903.	325	160.36	1.966	42670.	42429.	44429.
254	1211.17	2.548	23676.	20151.	24151.	326	159.52	1.949	42844.	42660.	44660.
256	1213.80	2.548	23925.	20400.	24400.	327	158.68	1.932	43018.	42891.	44891.
258	1216.44	2.548	24175.	20650.	24650.	328	157.84	1.915	43192.	43122.	45122.
260	1219.09	2.548	24426.	20901.	24901.	329	157.00	1.898	43366.	43353.	45353.
262	1221.75	2.548	24678.	21153.	25153.	330	156.16	1.881	43540.	43584.	45584.
264	1224.42	2.548	24931.	21406.	25406.	331	155.32	1.864	43714.	43815.	45815.
266	1227.10	2.548	25185.	21660.	25660.	332	154.48	1.847	43888.	44046.	46046.
268	1229.79	2.548	25440.	21915.	25915.	333	153.64	1.830	44062.	44277.	46277.
270	1232.49	2.548	25696.	22171.	26171.	334	152.80	1.813	44236.	44508.	46508.
272	1235.20	2.548	25953.	22428.	26428.	335	151.96	1.796	44410.	44739.	46739.
274	1237.92	2.548	26211.	22686.	26686.	336	151.12	1.779	44584.	44970.	46970.
276	1240.65	2.548	26470.	22945.	26945.	337	150.28	1.762	44758.	45201.	47201.
278	1243.39	2.548	26730.	23205.	27205.	338	149.44	1.745	44932.	45432.	47432.
280	1246.14	2.548	26991.	23466.	27466.	339	148.60	1.728	45106.	45663.	47663.
282	1248.90	2.548	27253.	23728.	27728.	340	147.76	1.711	45280.	45894.	47894.
284	1251.67	2.548	27516.	23991.	27991.	341	146.92	1.694	45454.	46125.	48125.
286	1254.45	2.548	27780.	24255.	28255.	342	146.08	1.677	45628.	46356.	48356.
288	1257.24	2.548	28045.	24520.	28520.	343	145.24	1.660	45802.	46587.	48587.
290	1260.04	2.548	28311.	24786.	28786.	344	144.40	1.643	45976.	46818.	48818.
292	1262.85	2.548	28578.	25053.	29053.	345	143.56	1.626	46150.	47049.	49049.
294	1265.67	2.548	28846.	25321.	29321.	346	142.72	1.609	46324.	47280.	49280.
296	1268.50	2.548	29115.	25590.	29590.	347	141.88	1.592	46498.	47511.	49511.
298	1271.34	2.548	29385.	25860.	29860.	348	141.04	1.575	46672.	47742.	49742.
300	1274.19	2.548	29656.	26131.	30131.	349	140.20	1.558	46846.	47973.	49973.
302	1277.05	2.548	29928.	26403.	30403.	350	139.36	1.541	47020.	48204.	50204.
304	1279.92	2.548	30201.	26676.	30676.	351	138.52	1.524	47194.	48435.	50435.
306	1282.80	2.548	30475.	26950.	30950.	352	137.68	1.507	47368.	48666.	50666.
308	1285.69	2.548	30750.	27225.	31225.	353	136.84	1.490	47542.	48897.	50897.
310	1288.59	2.548	31026.	27501.	31501.	354	136.00	1.473	47716.	49128.	51128.
312	1291.50	2.548	31303.	27778.	31778.	355	135.16	1.456	47890.	49359.	51359.
314	1294.42	2.548	31581.	28056.	32056.	356	134.32	1.439	48064.	49590.	51590.
316	1297.35	2.548	31860.	28335.	32335.	357	133.48	1.422	48238.	49821.	51821.
318	1300.29	2.548	32140.	28615.	32615.	358	132.64	1.405	48412.	50052.	52052.
320	1303.24	2.548	32421.	28896.	32896.	359	131.80	1.388	48586.	50283.	52283.
322	1306.20	2.548	32703.	29178.	33178.	360	130.96	1.371	48760.	50514.	52514.
324	1309.17	2.548	32986.	29461.	33461.	361	130.12	1.354	48934.	50745.	52745.
326	1312.15	2.548	33270.	29745.	33745.	362	129.28	1.337	49108.	50976.	52976.
328	1315.14	2.548	33555.	30030.	34030.	363	128.44	1.320	49282.	51207.	53207.
330	1318.14	2.548	33841.	30316.	34316.	364	127.60	1.303	49456.	51438.	53438.
332	1321.15	2.548	34128.	30603.	34603.	365	126.76	1.286	49630.	51669.	53669.
334	1324.17	2.548	34416.	30891.	34891.	366	125.92	1.269	49804.	51900.	53900.
336	1327.20	2.548	34705.	31180.	35180.	367	125.08	1.252	49978.	52131.	54131.
338	1330.24	2.548	35000.	31470.	35470.	368	124.24	1.235	50152.	52362.	54362.
340	1333.29	2.548	35300.	31761.	35761.	369	123.40	1.218	50326.	52593.	54593.
342	1336.35	2.548	35605.	32053.	36053.	370	122.56	1.201	50500.	52824.	54824.
344	1339.42	2.548	35916.	32346.	36346.	371	121.72	1.184	50674.	53055.	55055.
346	1342.50	2.548	36233.	32640.	36640.	372	120.88	1.167	50848.	53286.	55286.
348	1345.59	2.548	36556.	32935.	36935.	373	120.04	1.150	51022.	53517.	55517.
350	1348.69	2.548	36885.	33231.	37231.	374	119.20	1.133	51196.	53748.	55748.
352	1351.80	2.548	37220.	33528.	37528.	375	118.36	1.116	51370.	53979.	55979.
354	1354.92	2.548	37561.	33826.	37826.	376	117.52	1.099	51544.	54210.	56210.
356	1358.05	2.548	37908.	34125.	38125.	377	116.68	1.082	51718.	54441.	56441.
358	1361.19	2.548	38261.	34425.	38425.	378	115.84	1.065	51892.	54672.	56672.
360	1364.34	2.548	38620.	34726.	38726.	379	115.00	1.048	52066.	54903.	56903.
362	1367.50	2.548	39000.	35028.	39028.	380	114.16	1.031	52240.	55134.	57134.
364	1370.67	2.548	39391.	35331.	39331.	381	113.32	1.014	52414.	55365.	57365.
366	1373.85	2.548	39794.	35635.	39635.	382	112.48	0.997	52588.	55596.	57596.
368	1377.04	2.548	40209.	35940.	39940.	383	111.64	0.980	52762.	55827.	57827.
370	1380.24	2.548	40636.	36246.	40246.	384	110.80	0.963	52936.	56058.	58058.
372	1383.45	2.548	41075.	36553.	40553.	385	110.00	0.946	53110.	56289.	58289.
374	1386.67	2.548	41526.	36861.	40861.	386	109.16	0.929	53284.	56520.	58520.
376	1389.90	2.548	41989.	37170.	41170.	387	108.32	0.912	53458.	56751.	58751.
378	1393.14	2.548	42464.	37480.	41480.	388	107.48	0.895	53632.	56982.	58982.
380	1396.39	2.548	42951.	37791.	41791.	389	106.64	0.878	53806.	57213.	59213.
382	1400.65	2.548	43450.	38103.	42103.	390	105.80	0.861	53980.	57444.	59444.
384	1404.92	2.548	43961.	38416.	42416.	391	104.96	0.844	54154.	57675.	59675.
386	1409.20	2.548	44484.	38730.	42730.	392	104.12	0.827	54328.	57906.	59906.
388	1413.49	2.548	45019.	39045.	43045.	393	103.28	0.810	54502.	58137.	60137.
390	1417.79	2.548	45566.	39361.	43361.	394	102.44	0.793	54676.	58368.	60368.
392	1422.10	2.548	46125.	39678.	43678.	395	101.60	0.776	54850.	58599.	60599.
394	1426.42	2.548	46696.	40000.	43990.	396	100.76	0.759	55024.	58830.	60830.
396	1430.75	2.548	47279.	40323.	44303.	397	99.92				

TABLE 6-10 (Continued)

J	PLATE DEPTH DIPT	K - G DENSITY G/CM ³	BOREHOLE 082-09			J	PLATE DEPTH DIPT	K - G DENSITY G/CM ³	BOREHOLE 081-09		
			ULSIVITY OF SOLID COMPONENT (G/CM ³)	CUMULATIVE HMDU2.871	SOLID MASS HMDU2.871				DENSITY OF SOLID COMPONENT G/CM ³	CUMULATIVE HMDU2.871	SOLID MASS HMDU2.871
401	404.00	2.098		54211.	54661.	4	1800.00	2.125	2.8210	0.	0.
402	401.00	2.104		54872.	54822.	5	997.36	2.125		65.	65.
403	408.09	2.103		54902.	54942.	6	996.10	2.124		170.	170.
404	406.72	2.107		54611.	54661.	7	994.41	2.127		276.	276.
405	403.81	2.107		54799.	54808.	8	992.40	2.129		463.	463.
406	401.17	2.104		54935.	54865.	9	988.70	2.093		605.	605.
407	400.10	2.105		54877.	54527.	10	985.94	2.104		776.	776.
408	409.30	2.090		54529.	54578.	11	982.77	2.105		1015.	1015.
409	406.10	2.015		54697.	54107.	12	978.46	2.100		1461.	1461.
410	403.14	2.028		54841.	54291.	13	975.71	2.100		1922.	1922.
411	401.93	2.021		54923.	54373.	14	972.30	2.081		2322.	2322.
412	406.70	2.102		54157.	54607.	15	969.41	2.109		2767.	2767.
413	423.47	2.102		54654.	54784.	16	964.29	2.246		3176.	3176.
414	418.93	2.034		54655.	54509.	17	960.70	2.272		3540.	3540.
415	413.97	2.035		54701.	54551.	18	958.31	2.260		3857.	3857.
416	413.00	2.037		54805.	54705.	19	956.94	2.197		4197.	4197.
417	412.11	2.032		54807.	54757.	20	955.27	2.308		4519.	4519.
418	407.39	2.018		54807.	54757.	21	951.32	2.355		4841.	4841.
419	403.45	2.030		54807.	54757.	22	948.31	2.308		5163.	5163.
420	402.07	2.132		54807.	54757.	23	947.76	2.222		5485.	5485.
421	398.01	2.177		54807.	54757.	24	944.61	2.156		5807.	5807.
422	397.36	2.155		54807.	54757.	25	943.03	2.155		6129.	6129.
423	393.66	2.109	2.8710	54807.	54757.	26	938.34	2.122		6451.	6451.
						27	932.79	2.128		6773.	6773.
						28	928.00	2.135		7095.	7095.
						29	927.40	2.175		7417.	7417.
						30	926.10	2.151		7739.	7739.
						31	922.56	2.159		8061.	8061.
						32	920.77	2.252		8383.	8383.
						33	918.62	2.274		8705.	8705.
						34	916.47	2.254		9027.	9027.
						35	912.72	2.194		9349.	9349.
						36	909.70	2.174		9671.	9671.
						37	906.61	2.186		9993.	9993.
						38	902.67	2.188		10315.	10315.
						39	899.74	2.173		10637.	10637.
						40	896.87	2.180		10959.	10959.
						41	894.41	2.151		11281.	11281.
						42	891.80	2.150		11603.	11603.
						43	889.09	2.183		11925.	11925.
						44	886.34	2.131		12247.	12247.
						45	883.19	2.156		12569.	12569.
						46	880.42	2.277		12891.	12891.
						47	878.40	2.219		13213.	13213.
						48	875.32	2.174		13535.	13535.
						49	873.35	2.206		13857.	13857.
						50	871.30	2.213		14179.	14179.
						51	870.49	2.282		14501.	14501.
						52	868.49	2.222		14823.	14823.
						53	866.49	2.252		15145.	15145.
						54	864.49	2.255		15467.	15467.
						55	863.50	2.230		15789.	15789.
						56	861.57	2.227		16111.	16111.
						57	859.60	2.254		16433.	16433.
						58	857.67	2.293		16755.	16755.
						59	855.64	2.276		17077.	17077.
						60	853.94	2.247		17399.	17399.
						61	851.90	2.235		17721.	17721.
						62	849.90	2.260		18043.	18043.
						63	847.45	2.227		18365.	18365.
						64	845.40	2.243		18687.	18687.
						65	843.40	2.244		19009.	19009.
						66	841.40	2.235		19331.	19331.
						67	839.40	2.210		19653.	19653.
						68	837.40	2.197		19975.	19975.
						69	835.40	2.211		20297.	20297.
						70	833.40	2.235		20619.	20619.
						71	831.40	2.210		20941.	20941.
						72	829.40	2.235		21263.	21263.
						73	827.40	2.255		21585.	21585.
						74	825.40	2.235		21907.	21907.
						75	823.40	2.260		22229.	22229.
						76	821.40	2.230		22551.	22551.
						77	819.40	2.255		22873.	22873.
						78	817.40	2.230		23195.	23195.
						79	815.40	2.255		23517.	23517.
						80	813.40	2.230		23839.	23839.
						81	811.40	2.255		24161.	24161.
						82	809.40	2.230		24483.	24483.
						83	807.40	2.255		24805.	24805.
						84	805.40	2.230		25127.	25127.
						85	803.40	2.255		25449.	25449.
						86	801.40	2.230		25771.	25771.
						87	799.40	2.255		26093.	26093.
						88	797.40	2.230		26415.	26415.
						89	795.40	2.255		26737.	26737.
						90	793.40	2.230		27059.	27059.
						91	791.40	2.255		27381.	27381.
						92	789.40	2.230		27703.	27703.
						93	787.40	2.255		28025.	28025.
						94	785.40	2.230		28347.	28347.
						95	783.40	2.255		28669.	28669.
						96	781.40	2.230		28991.	28991.
						97	779.40	2.255		29313.	29313.
						98	777.40	2.230		29635.	29635.
						99	775.40	2.255		29957.	29957.
						100	773.40	2.230		30279.	30279.

TABLE 6-10 (Continued)

BDRMOLC 0.1-05					BDRMOLC 0.1-05								
J	PEACE DEPTH DFT	6 - 6 DENSITY 164/CC	DENSITY OF SOLID COMPONENT 164/CC	CUMULATIVE RHO=2.821	SOLIC MASS RHO=CRMO	16P/CM=21 LINEAR SP. LINE FOR RMC	J	PEACE DEPTH DFT	6 - 6 DENSITY 164/CC	DENSITY OF SOLID COMPONENT 164/CC	CUMULATIVE RHO=2.821	SOLIC MASS RHO=CRMO	16P/CM=21 LINEAR SP. LINE FOR RMC
101	759.96	2.293		13466.	13466.	13466.	201	528.99	2.266		27210.	27210.	27210.
102	757.20	2.255		13630.	13630.	13640.	202	528.07	2.228		27255.	27255.	27255.
104	759.44	2.213		13765.	13765.	13765.	204	528.73	2.255		27395.	27395.	27395.
106	752.40	2.170		13897.	13897.	13897.	206	528.55	2.216		27466.	27466.	27466.
108	748.13	2.200		14072.	14072.	14072.	208	522.39	2.233		27575.	27575.	27575.
109	747.76	2.259		14163.	14163.	14163.	209	521.77	2.250		27619.	27619.	27619.
107	746.19	2.296		14247.	14247.	14247.	206	519.74	2.291		27761.	27761.	27761.
100	743.46	2.279		14275.	14275.	14275.	210	517.89	2.277		27866.	27866.	27866.
109	741.46	2.268		14399.	14399.	14399.	209	516.47	2.245		27996.	27996.	27996.
110	736.70	2.291		14449.	14449.	14449.	210	513.14	2.297		28135.	28135.	28135.
112	735.22	2.262		14504.	14504.	14504.	211	511.79	2.301		28207.	28207.	28207.
114	730.49	2.230		15155.	15155.	15155.	214	511.14	2.329		28255.	28255.	28255.
119	729.49	2.202		15243.	15243.	15243.	213	509.57	2.313		28351.	28351.	28351.
114	725.11	2.259		15467.	15467.	15467.	210	507.40	2.258		28455.	28455.	28455.
119	725.81	2.297		15471.	15471.	15471.	213	506.06	2.254		28471.	28471.	28471.
119	723.89	2.332		15591.	15591.	15591.	210	504.08	2.272		28563.	28563.	28563.
117	721.77	2.291		15687.	15687.	15687.	211	502.87	2.245		28653.	28653.	28653.
118	715.01	2.294		15859.	15859.	15859.	210	501.39	2.244		28719.	28719.	28719.
119	717.89	2.293		15927.	15927.	15927.	211	497.36	2.265		28846.	28846.	28846.
120	715.87	2.291		16047.	16047.	16047.	210	493.03	2.316		28979.	28979.	28979.
121	713.76	2.299		16108.	16108.	16108.	221	491.06	2.202		29326.	29326.	29326.
124	701.96	2.272		16999.	16999.	16999.	222	488.70	2.285		29455.	29455.	29455.
124	707.84	2.315		16942.	16942.	16942.	223	487.54	2.301		29455.	29455.	29455.
126	703.86	2.316		16785.	16785.	16785.	224	485.31	2.282		29748.	29748.	29748.
125	702.09	2.307		16882.	16882.	16882.	222	482.79	2.290		29931.	29931.	29931.
126	697.36	2.297		17171.	17171.	17171.	220	480.01	2.277		30097.	30097.	30097.
127	695.00	2.332		17316.	17316.	17316.	221	477.49	2.285		30144.	30144.	30144.
128	694.41	2.301		17664.	17664.	17664.	220	476.40	2.304		30191.	30191.	30191.
130	691.40	2.301		17933.	17933.	17933.	229	475.71	2.307		30365.	30365.	30365.
136	681.86	2.285		18295.	18295.	18295.	230	473.76	2.256		30497.	30497.	30497.
131	686.36	2.301		17845.	17845.	17845.	231	471.77	2.216		30630.	30630.	30630.
134	685.39	2.318		17892.	17892.	17892.	234	469.50	2.226		30761.	30761.	30761.
139	682.40	2.369		18088.	18088.	18088.	235	468.92	2.211		30865.	30865.	30865.
136	680.46	2.301		18209.	18209.	18209.	235	465.87	2.243		30970.	30970.	30970.
139	678.46	2.310		18330.	18330.	18330.	235	463.11	2.201		31074.	31074.	31074.
136	676.30	2.308		18551.	18551.	18551.	230	461.14	2.363		31208.	31208.	31208.
137	674.39	2.293		18579.	18579.	18579.	237	459.17	2.368		31356.	31356.	31356.
139	670.99	2.356		18798.	18798.	18798.	238	457.99	2.356		31462.	31462.	31462.
139	670.59	2.327		18823.	18823.	18823.	238	456.77	2.381		31530.	31530.	31530.
140	666.00	2.274		19064.	19064.	19064.	240	453.47	2.257		31639.	31639.	31639.
141	665.00	2.228		19156.	19156.	19156.	241	458.19	2.257		31845.	31845.	31845.
142	657.46	2.225		19266.	19266.	19266.	242	457.76	2.250		31984.	31984.	31984.
143	656.06	2.213		19476.	19476.	19476.	243	456.19	2.266		32167.	32167.	32167.
144	655.47	2.279		19818.	19818.	19818.	244	455.39	2.249		32262.	32262.	32262.
149	650.14	2.301		20250.	20250.	20250.	244	451.58	2.249		32309.	32309.	32309.
148	648.56	2.296		20124.	20124.	20124.	240	448.51	2.309		32559.	32559.	32559.
147	646.18	2.103		20256.	20256.	20256.	241	455.55	2.294		32728.	32728.	32728.
148	643.84	2.123		20377.	20377.	20377.	240	452.01	2.274		32893.	32893.	32893.
149	645.50	2.301		20518.	20518.	20518.	240	448.43	2.348		33102.	33102.	33102.
150	641.96	2.296		20505.	20505.	20505.	241	445.51	2.285		33199.	33199.	33199.
151	639.88	2.259		20549.	20549.	20549.	251	425.31	2.205		33516.	33516.	33516.
152	637.91	2.269		20715.	20715.	20715.	251	419.91	2.219		33846.	33846.	33846.
154	635.90	2.232		20946.	20946.	20946.	252	415.77	2.075		34050.	34050.	34050.
156	632.49	2.238		21037.	21037.	21037.	254	411.14	2.148		34274.	34274.	34274.
157	629.03	2.203		21108.	21108.	21108.	255	408.78	2.112		34366.	34366.	34366.
159	623.79	2.268		21537.	21537.	21537.	255	406.81	2.081		34499.	34499.	34499.
159	620.90	2.238		21649.	21649.	21649.	259	404.86	2.106		34599.	34599.	34599.
159	619.01	2.191		21811.	21811.	21811.	257	402.97	2.086		34741.	34741.	34741.
159	617.00	2.206		21878.	21878.	21878.	250	398.76	2.144		34822.	34822.	34822.
160	616.83	2.259		21966.	21966.	21966.	260	394.61	2.194		34979.	34979.	34979.
161	614.86	2.283		22089.	22089.	22089.	261	391.06	2.034		35074.	35074.	35074.
164	611.96	2.241		22440.	22440.	22440.	264	388.19	2.034		35260.	35260.	35260.
164	607.99	2.272		22476.	22476.	22476.	264	381.61	2.213		35601.	35601.	35601.
164	604.46	2.277		22666.	22666.	22666.	264	378.07	2.065		35716.	35716.	35716.
169	602.40	2.284		22809.	22809.	22809.	264	375.42	2.084		35888.	35888.	35888.
169	600.91	2.318		22931.	22931.	22931.	260	370.99	2.039		36023.	36023.	36023.
169	599.46	2.381		23005.	23005.	23005.	260	369.80	2.053		36233.	36233.	36233.
169	597.76	2.391		23109.	23109.	23109.	260	369.41	2.035		36280.	36280.	36280.
169	595.71	2.321		23227.	23227.	23227.	260	369.41	2.035		36310.	36310.	36310.
170	594.41	2.345		23301.	23301.	23301.	260	366.85	2.057		36443.	36443.	36443.
174	591.00	2.819		23974.	23974.	23974.	271	365.90	2.145		36582.	36582.	36582.
174	590.87	2.408		23974.	23974.	23974.	271	361.19	2.148		36729.	36729.	36729.
174	587.99	2.389		23974.	23974.	23974.	274	358.49	2.080		36871.	36871.	36871.
174	586.79	2.398		23974.	23974.	23974.	274	355.43	2.076		37008.	37008.	37008.
175	583.19	2.294		24017.	24017.	24017.	279	350.70	2.139		37294.	37294.	37294.
175	581.48	2.274		24154.	24154.	24154.	279	348.99	2.106		37358.	37358.	37358.
177	577.00	2.379		24355.	24355.	24355.	277	349.00	2.087		37442.	37442.	37442.
179	574.98	2.301		24528.	24528.	24528.	278	343.02	2.112		37566.	37566.	37566.
179	572.80	2.390		24666.	24666.	24666.	279	341.96	2.089		37668.	37668.	37668.
180	570.20	2.301		24815.	24815.	24815.	280	339.00	2.128		37744.	37744.	37744.
181	567.41	2.219		24978.	24978.	24978.	280	339.00	2.128		37851.	37851.	37851.
182	565.47	2.230		25092.	25092.	25092.	281	339.49	2.119		37851.	37851.	37851.
184	564.89	2.307		25162.	25162.	25162.	284	336.73	2.119		37996.	37996.	37996.
184	564.86	2.341		25283.	25283.	25283.	289	335.19	2.192		38037.	38037.	38037.
184	564.86	2.297		25404.	25404.	25404.	289	331.44	2.078		38182.	38182.	38182.
184	563.99	2.295		25545.	25545.	25545.	286	329.45	2.049		38280.	38280.	38280.
187	555.86	2.295		25683.	25683.	25683.	287	326.89	2.024		38366.	38366.	38366.
188	553.40	2.282		25790.	25790.	25790.	288	326.89	2.024		38496.	38496.	38496.
189	551.40	2.203		25933.	25933.	25933.	288	326.55	2.139		38616.	38616.	38616.
191	549.79	2.178		26020.	26020.	26020.	290	321.77	2.184		38763.	38763.	38763.
191	548.86	2.199		26195.	26195.	26195.	291	319.01	2.046		38805.	38805.	38805.
191	548.11	2.175		26305.	26305.	26305.	291	317.44	2.034		38947.	38947.	38947.
193	543.04	2.227		26381.	26381.	26381.	292	314.46	2.043		39083.	39083.	39083.

TABLE 6-10 (Continued)

PLACED DEPTH (FT)	G - 6 DENSITY (G/CC)	DENSITY OF SOLID COMPONENT (G/CC)	BOREHOLE OCT-85		CUMULATIVE SOLID MASS (G/CM ²)*2	GPR/CMH2 SP. LINE FOR RHM	PLACED DEPTH (FT)	G - 6 DENSITY (G/CC)	DENSITY OF SOLID COMPONENT (G/CC)	BOREHOLE DAR-28		CUMULATIVE SOLID MASS (G/CM ²)*2	GPR/CMH2 SP. LINE FOR RHM
			RMH2.02	RMH2.02						RMH2.02	RMH2.02		
301	1.00,31	2.007	39840.	39840.	39840.	1	1000.00			2.0210			
302	1.00,34	2.007	39932.	39932.	39932.	2	993.21			2.0210			
303	1.00,37	2.011	40024.	40024.	40024.	3	986.30			2.0210			
304	1.00,41	2.014	40116.	40116.	40116.	4	979.40			2.0210			
305	1.00,44	2.017	40208.	40208.	40208.	5	972.50			2.0210			
306	1.00,47	2.020	40300.	40300.	40300.	6	965.60			2.0210			
307	1.00,50	2.023	40392.	40392.	40392.	7	958.70			2.0210			
308	1.00,53	2.026	40484.	40484.	40484.	8	951.80			2.0210			
309	1.00,56	2.029	40576.	40576.	40576.	9	944.90			2.0210			
310	1.00,59	2.032	40668.	40668.	40668.	10	938.00			2.0210			
311	1.00,62	2.035	40760.	40760.	40760.	11	931.10			2.0210			
312	1.00,65	2.038	40852.	40852.	40852.	12	924.20			2.0210			
313	1.00,68	2.041	40944.	40944.	40944.	13	917.30			2.0210			
314	1.00,71	2.044	41036.	41036.	41036.	14	910.40			2.0210			
315	1.00,74	2.047	41128.	41128.	41128.	15	903.50			2.0210			
316	1.00,77	2.050	41220.	41220.	41220.	16	896.60			2.0210			
317	1.00,80	2.053	41312.	41312.	41312.	17	889.70			2.0210			
318	1.00,83	2.056	41404.	41404.	41404.	18	882.80			2.0210			
319	1.00,86	2.059	41496.	41496.	41496.	19	875.90			2.0210			
320	1.00,89	2.062	41588.	41588.	41588.	20	869.00			2.0210			
321	1.00,92	2.065	41680.	41680.	41680.	21	862.10			2.0210			
322	1.00,95	2.068	41772.	41772.	41772.	22	855.20			2.0210			
323	1.00,98	2.071	41864.	41864.	41864.	23	848.30			2.0210			
324	1.01,01	2.074	41956.	41956.	41956.	24	841.40			2.0210			
325	1.01,04	2.077	42048.	42048.	42048.	25	834.50			2.0210			
326	1.01,07	2.080	42140.	42140.	42140.	26	827.60			2.0210			
327	1.01,10	2.083	42232.	42232.	42232.	27	820.70			2.0210			
328	1.01,13	2.086	42324.	42324.	42324.	28	813.80			2.0210			
329	1.01,16	2.089	42416.	42416.	42416.	29	806.90			2.0210			
330	1.01,19	2.092	42508.	42508.	42508.	30	800.00			2.0210			
331	1.01,22	2.095	42600.	42600.	42600.	31	793.10			2.0210			
332	1.01,25	2.098	42692.	42692.	42692.	32	786.20			2.0210			
333	1.01,28	2.101	42784.	42784.	42784.	33	779.30			2.0210			
334	1.01,31	2.104	42876.	42876.	42876.	34	772.40			2.0210			
335	1.01,34	2.107	42968.	42968.	42968.	35	765.50			2.0210			
336	1.01,37	2.110	43060.	43060.	43060.	36	758.60			2.0210			
337	1.01,40	2.113	43152.	43152.	43152.	37	751.70			2.0210			
338	1.01,43	2.116	43244.	43244.	43244.	38	744.80			2.0210			
339	1.01,46	2.119	43336.	43336.	43336.	39	737.90			2.0210			
340	1.01,49	2.122	43428.	43428.	43428.	40	731.00			2.0210			
341	1.01,52	2.125	43520.	43520.	43520.	41	724.10			2.0210			
342	1.01,55	2.128	43612.	43612.	43612.	42	717.20			2.0210			
343	1.01,58	2.131	43704.	43704.	43704.	43	710.30			2.0210			
344	1.01,61	2.134	43796.	43796.	43796.	44	703.40			2.0210			
345	1.01,64	2.137	43888.	43888.	43888.	45	696.50			2.0210			
346	1.01,67	2.140	43980.	43980.	43980.	46	689.60			2.0210			
347	1.01,70	2.143	44072.	44072.	44072.	47	682.70			2.0210			
348	1.01,73	2.146	44164.	44164.	44164.	48	675.80			2.0210			
349	1.01,76	2.149	44256.	44256.	44256.	49	668.90			2.0210			
350	1.01,79	2.152	44348.	44348.	44348.	50	662.00			2.0210			
351	1.01,82	2.155	44440.	44440.	44440.	51	655.10			2.0210			
352	1.01,85	2.158	44532.	44532.	44532.	52	648.20			2.0210			
353	1.01,88	2.161	44624.	44624.	44624.	53	641.30			2.0210			
354	1.01,91	2.164	44716.	44716.	44716.	54	634.40			2.0210			
355	1.01,94	2.167	44808.	44808.	44808.	55	627.50			2.0210			
356	1.01,97	2.170	44900.	44900.	44900.	56	620.60			2.0210			
357	1.02,00	2.173	44992.	44992.	44992.	57	613.70			2.0210			
358	1.02,03	2.176	45084.	45084.	45084.	58	606.80			2.0210			
359	1.02,06	2.179	45176.	45176.	45176.	59	600.00			2.0210			
360	1.02,09	2.182	45268.	45268.	45268.	60	593.10			2.0210			
361	1.02,12	2.185	45360.	45360.	45360.	61	586.20			2.0210			
362	1.02,15	2.188	45452.	45452.	45452.	62	579.30			2.0210			
363	1.02,18	2.191	45544.	45544.	45544.	63	572.40			2.0210			
364	1.02,21	2.194	45636.	45636.	45636.	64	565.50			2.0210			
365	1.02,24	2.197	45728.	45728.	45728.	65	558.60			2.0210			
366	1.02,27	2.200	45820.	45820.	45820.	66	551.70			2.0210			
367	1.02,30	2.203	45912.	45912.	45912.	67	544.80			2.0210			
368	1.02,33	2.206	46004.	46004.	46004.	68	537.90			2.0210			
369	1.02,36	2.209	46096.	46096.	46096.	69	531.00			2.0210			
370	1.02,39	2.212	46188.	46188.	46188.	70	524.10			2.0210			
371	1.02,42	2.215	46280.	46280.	46280.	71	517.20			2.0210			
372	1.02,45	2.218	46372.	46372.	46372.	72	510.30			2.0210			
373	1.02,48	2.221	46464.	46464.	46464.	73	503.40			2.0210			
374	1.02,51	2.224	46556.	46556.	46556.	74	496.50			2.0210			
375	1.02,54	2.227	46648.	46648.	46648.	75	489.60			2.0210			
376	1.02,57	2.230	46740.	46740.	46740.	76	482.70			2.0210			
377	1.02,60	2.233	46832.	46832.	46832.	77	475.80			2.0210			
378	1.02,63	2.236	46924.	46924.	46924.	78	468.90			2.0210			
379	1.02,66	2.239	47016.	47016.	47016.	79	462.00			2.0210			
380	1.02,69	2.242	47108.	47108.	47108.	80	455.10			2.0210			
381	1.02,72	2.245	47200.	47200.	47200.	81	448.20			2.0210			
382	1.02,75	2.248	47292.	47292.	47292.	82	441.30			2.0210			
383	1.02,78	2.251	47384.	47384.	47384.	83	434.40			2.0210			
384	1.02,81	2.254	47476.	47476.	47476.	84	427.50			2.0210			
385	1.02,84	2.257	47568.	47568.	47568.	85	420.60			2.0210			
386	1.02,87	2.260	47660.	47660.	47660.	86	413.70			2.0210			
387	1.02,90	2.263	47752.	47752.	47752.	87	406.80			2.0210			
388	1.02,93	2.266	47844.	47844.	47844.	88	400.00			2.0210			
389	1.02,96	2.269	47936.	47936.	47936.	89	393.10			2.0210			
390	1.02,99	2.272	48028.	48028.	48028.	90	386.20			2.0210			
391	1.03,02	2.275	48120.	48120.	48120.	91	379.30			2.0210			
392	1.03,05	2.278	48212.	48212.	48212.	92	372.40			2.0210			
393	1.03,08	2.281	48304.	48304.	48304.	93	365.50			2.0210			
394	1.03,11	2.284	48396.	48396.	48396.	94	358.60			2.0210			
395	1.03,14	2.287	48488.	48488.	48488.	95	351.70			2.0210			
396	1.03,17	2.290	48580.	48580.	48580.	96	344.80			2.0210			
397	1.03,20	2.293	48672.	48672.	48672.	97	337.90			2.0210			
398	1.03,23	2.296	48764.	48764.	48764.	98	331.00			2.0210			
399	1.03,26	2.299	48856.	48856.	48856.	99	324.10			2.0210			
400	1.03,29	2.302	48948.	48948.	48948.	100	317.20			2.0210			

TABLE 6-10 (Continued)

BURE HOLE DASH-2A							BURE HOLE DASH-2A						
J	PLACED DEPTH DIFF	G - G DENSITY (G/CC)	DENSITY OF SOLID COMPONENT (G/CC)	CUMULATIVE RHO2-0.021 RHO2-CRHO2	SOLID MASS RHO2-CRHO2	(G/CM2) LINEAR SCALE FOR RHO	J	PLACED DEPTH DIFF	G - G DENSITY (G/CC)	DENSITY OF SOLID COMPONENT (G/CC)	CUMULATIVE RHO2-0.021 RHO2-CRHO2	SOLID MASS RHO2-CRHO2	(G/CM2) LINEAR SCALE FOR RHO
101	393.44	2.101		3167.	3190.	3190.	201	285.84	2.100		10796.	10890.	10880.
102	392.10		2.0255	3226.	3249.	3249.	202	285.11	2.097		10875.	10899.	10899.
103	392.07	2.112		3227.	3250.	3250.	203	285.95	2.091		10892.	10896.	10896.
104	390.34	2.116		3308.	3331.	3331.	204	282.89	2.090		10908.	10912.	10912.
105	388.19	2.093	2.0974	3412.	3434.	3434.	205	281.61	1.997		10925.	10929.	10929.
106	387.02	2.098		3429.	3450.	3450.	206	278.90	2.122		11000.	11004.	11004.
107	385.90		2.0974	3498.	3519.	3519.	207	275.30		2.0168	11020.	11024.	11024.
108	383.38	2.036		3563.	3581.	3581.	208	275.01	2.017		11034.	11038.	11038.
109	381.97	2.043		3748.	3755.	3755.	209	270.94	2.035		11050.	11054.	11054.
110	380.67	2.004		3747.	3847.	3847.	210	276.44	2.066		11074.	11078.	11078.
111	378.48	2.070		3721.	3921.	3921.	211	272.38	2.030		11094.	11098.	11098.
112	376.33	2.027		3809.	4012.	4012.	212	271.50		2.0474	11099.	11103.	11103.
113	375.37	1.994		4035.	4035.	4035.	213	269.08	2.040		11100.	11104.	11104.
114	373.04	2.130	2.0760	4129.	4181.	4181.	214	268.75	2.038		11116.	11120.	11120.
115	371.04	2.132		4169.	4180.	4180.	215	268.75	2.038		11116.	11120.	11120.
116	368.76	2.069		4252.	4262.	4262.	216	263.64	2.025		11228.	11232.	11232.
117	366.04	2.117		4304.	4304.	4304.	217	262.66	2.004		11237.	11241.	11241.
118	363.71	2.092		4335.	4344.	4344.	218	262.66		2.7613	11241.	11245.	11245.
119	361.38	2.035		4355.	4365.	4365.	219	262.66			11241.	11245.	11245.
120	359.04		2.7866	4771.	4781.	4781.	220	262.66	2.004		11241.	11245.	11245.
121	356.70		2.6565	4780.	4790.	4790.	221	262.66	2.004		11241.	11245.	11245.
122	354.37	2.085	2.8700	4859.	4859.	4859.	222	197.04	2.019		11241.	11245.	11245.
123	352.04			4859.	4859.	4859.	223	196.26	1.927		11241.	11245.	11245.
124	350.04	2.085		4859.	4859.	4859.	224	193.34	2.024		11241.	11245.	11245.
125	347.71	2.082		4859.	4859.	4859.	225	192.37	1.991		11241.	11245.	11245.
126	345.38	2.040	2.7760	4859.	4859.	4859.	226	188.95	2.003		11241.	11245.	11245.
127	343.04			4859.	4859.	4859.	227	188.95	2.003		11241.	11245.	11245.
128	340.71	2.014		4859.	4859.	4859.	228	187.34	1.986		11241.	11245.	11245.
129	338.38	2.070		4859.	4859.	4859.	229	186.35	1.974		11241.	11245.	11245.
130	336.04	2.093		4859.	4859.	4859.	230	186.35	1.974		11241.	11245.	11245.
131	333.71	2.101	2.9144	4859.	4859.	4859.	231	186.35	1.974		11241.	11245.	11245.
132	331.38	2.103		4859.	4859.	4859.	232	186.35	1.974		11241.	11245.	11245.
133	329.04	2.103		4859.	4859.	4859.	233	186.35	1.974		11241.	11245.	11245.
134	326.71	2.103		4859.	4859.	4859.	234	186.35	1.974		11241.	11245.	11245.
135	324.38	2.103		4859.	4859.	4859.	235	186.35	1.974		11241.	11245.	11245.
136	322.04	2.103		4859.	4859.	4859.	236	186.35	1.974		11241.	11245.	11245.
137	319.71	2.103		4859.	4859.	4859.	237	186.35	1.974		11241.	11245.	11245.
138	317.38	2.103		4859.	4859.	4859.	238	186.35	1.974		11241.	11245.	11245.
139	315.04	2.103		4859.	4859.	4859.	239	186.35	1.974		11241.	11245.	11245.
140	312.71	2.103		4859.	4859.	4859.	240	186.35	1.974		11241.	11245.	11245.
141	310.38	2.103		4859.	4859.	4859.	241	186.35	1.974		11241.	11245.	11245.
142	308.04	2.103		4859.	4859.	4859.	242	186.35	1.974		11241.	11245.	11245.
143	305.71	2.103		4859.	4859.	4859.	243	186.35	1.974		11241.	11245.	11245.
144	303.38	2.103		4859.	4859.	4859.	244	186.35	1.974		11241.	11245.	11245.
145	301.04	2.103		4859.	4859.	4859.	245	186.35	1.974		11241.	11245.	11245.
146	298.71	2.103		4859.	4859.	4859.	246	186.35	1.974		11241.	11245.	11245.
147	296.38	2.103		4859.	4859.	4859.	247	186.35	1.974		11241.	11245.	11245.
148	294.04	2.103		4859.	4859.	4859.	248	186.35	1.974		11241.	11245.	11245.
149	291.71	2.103		4859.	4859.	4859.	249	186.35	1.974		11241.	11245.	11245.
150	289.38	2.103		4859.	4859.	4859.	250	186.35	1.974		11241.	11245.	11245.
151	287.04	2.103		4859.	4859.	4859.	251	186.35	1.974		11241.	11245.	11245.
152	284.71	2.103		4859.	4859.	4859.	252	186.35	1.974		11241.	11245.	11245.
153	282.38	2.103		4859.	4859.	4859.	253	186.35	1.974		11241.	11245.	11245.
154	280.04	2.103		4859.	4859.	4859.	254	186.35	1.974		11241.	11245.	11245.
155	277.71	2.017		4859.	4859.	4859.	255	186.35	1.974		11241.	11245.	11245.
156	275.38	2.100		4859.	4859.	4859.	256	186.35	1.974		11241.	11245.	11245.
157	273.04	2.190		4859.	4859.	4859.	257	186.35	1.974		11241.	11245.	11245.
158	270.71	2.006		4859.	4859.	4859.	258	186.35	1.974		11241.	11245.	11245.
159	268.38	1.995		4859.	4859.	4859.	259	186.35	1.974		11241.	11245.	11245.
160	266.04	2.034		4859.	4859.	4859.	260	186.35	1.974		11241.	11245.	11245.
161	263.71	2.062		4859.	4859.	4859.	261	186.35	1.974		11241.	11245.	11245.
162	261.38	1.985		4859.	4859.	4859.	262	186.35	1.974		11241.	11245.	11245.
163	259.04	2.070		4859.	4859.	4859.	263	186.35	1.974		11241.	11245.	11245.
164	256.71	2.006		4859.	4859.	4859.	264	186.35	1.974		11241.	11245.	11245.
165	254.38	2.015		4859.	4859.	4859.	265	186.35	1.974		11241.	11245.	11245.
166	252.04	1.959		4859.	4859.	4859.	266	186.35	1.974		11241.	11245.	11245.
167	249.71	1.996		4859.	4859.	4859.	267	186.35	1.974		11241.	11245.	11245.
168	247.38	1.959		4859.	4859.	4859.	268	186.35	1.974		11241.	11245.	11245.
169	245.04	1.975		4859.	4859.	4859.	269	186.35	1.974		11241.	11245.	11245.
170	242.71	1.996		4859.	4859.	4859.	270	186.35	1.974		11241.	11245.	11245.
171	240.38	1.877		4859.	4859.	4859.	271	186.35	1.974		11241.	11245.	11245.
172	238.04	1.959		4859.	4859.	4859.	272	186.35	1.974		11241.	11245.	11245.
173	235.71	1.977		4859.	4859.	4859.	273	186.35	1.974		11241.	11245.	11245.
174	233.38	1.977		4859.	4859.	4859.	274	186.35	1.974		11241.	11245.	11245.
175	231.04	1.977		4859.	4859.	4859.	275	186.35	1.974		11241.	11245.	11245.
176	228.71	1.977		4859.	4859.	4859.	276	186.35	1.974		11241.	11245.	11245.
177	226.38	1.977		4859.	4859.	4859.	277	186.35	1.974		11241.	11245.	11245.
178	224.04	1.977		4859.	4859.	4859.	278	186.35	1.974		11241.	11245.	11245.
179	221.71	1.977		4859.	4859.	4859.	279	186.35	1.974		11241.	11245.	11245.
180	219.38	1.977		4859.	4859.	4859.	280	186.35	1.974		11241.	11245.	11245.
181	217.04	1.977		4859.	4859.	4859.	281	186.35	1.974		11241.	11245.	11245.
182	214.71	1.977		4859.	4859.	4859.	282	186.35	1.974		11241.	11245.	11245.
183	212.38	1.977		4859.	4859.	4859.	283	186.35	1.974		11241.	11245.	11245.
184	210.04	1.977		4859.	4859.	4859.	284	186.35	1.974		11241.	11245.	11245.
185	207.71	1.977		4859.	4859.	4859.	285	186.35	1.974		11241.	11245.	11245.
186	205.38	1.977		4859.	4859.	4859.	286	186.35	1.974		11241.	11245.	11245.
187	203.04	1.977		4859.	4859.	4859.	287	186.35	1.974		11241.	11245.	11245.
188	200.71	1.977		4859.	4859.	4859.	288	186.35	1.974		11241.	11245.	11245.
189	198.38	1.977		4859.	4859.	4859.	289	186.35	1.974		11241.	11245.	11245.
190	196.04	1.977		4859.	4859.	4859.	290	186.35	1.974		11241.	11245.	11245.
191	193.71	1.977		4859.	4859.	4859.	291	186.35	1.974		11241.	11245.	11245.
192	191.38	1.977		4859.	4859.	4859.	292	186.35	1.974		11241.	11245.	11245.
193	189.04	1.977		4859.	4859.	4859.	293	186.35	1.974		11241.	11245.</	

TABLE 6-10 (Continued)

Borehole 017-11						Borehole 017-11					
PEACE DEPTH DIT-1	4 - 5 DENSITY (G/CC)	DENSITY OF SOLID COMPONENT (G/CC)	CUMULATIVE SOLID MASS RHOx2.021	SP. GRAV. RHOxCRHO2	SP. GRAV. RHOxCRHO2	PEACE DEPTH DIT-1	4 - 5 DENSITY (G/CC)	DENSITY OF SOLID COMPONENT (G/CC)	CUMULATIVE SOLID MASS RHOx2.021	SP. GRAV. RHOxCRHO2	SP. GRAV. RHOxCRHO2
1000.00	2.030	2.0210	0.	0.	0.	101	2.031	2.0210	9265.	9265.	9265.
1001.00	2.031		39.	39.	39.	102	2.031	2.0210	9275.	9275.	9275.
1002.00	2.031		78.	78.	78.	103	2.031	2.0210	9285.	9285.	9285.
1003.00	2.031		117.	117.	117.	104	2.031	2.0210	9295.	9295.	9295.
1004.00	2.031		156.	156.	156.	105	2.031	2.0210	9305.	9305.	9305.
1005.00	2.031		195.	195.	195.	106	2.031	2.0210	9315.	9315.	9315.
1006.00	2.031		234.	234.	234.	107	2.031	2.0210	9325.	9325.	9325.
1007.00	2.031		273.	273.	273.	108	2.031	2.0210	9335.	9335.	9335.
1008.00	2.031		312.	312.	312.	109	2.031	2.0210	9345.	9345.	9345.
1009.00	2.031		351.	351.	351.	110	2.031	2.0210	9355.	9355.	9355.
1010.00	2.031		390.	390.	390.	111	2.031	2.0210	9365.	9365.	9365.
1011.00	2.031		429.	429.	429.	112	2.031	2.0210	9375.	9375.	9375.
1012.00	2.031		468.	468.	468.	113	2.031	2.0210	9385.	9385.	9385.
1013.00	2.031		507.	507.	507.	114	2.031	2.0210	9395.	9395.	9395.
1014.00	2.031		546.	546.	546.	115	2.031	2.0210	9405.	9405.	9405.
1015.00	2.031		585.	585.	585.	116	2.031	2.0210	9415.	9415.	9415.
1016.00	2.031		624.	624.	624.	117	2.031	2.0210	9425.	9425.	9425.
1017.00	2.031		663.	663.	663.	118	2.031	2.0210	9435.	9435.	9435.
1018.00	2.031		702.	702.	702.	119	2.031	2.0210	9445.	9445.	9445.
1019.00	2.031		741.	741.	741.	120	2.031	2.0210	9455.	9455.	9455.
1020.00	2.031		780.	780.	780.	121	2.031	2.0210	9465.	9465.	9465.
1021.00	2.031		819.	819.	819.	122	2.031	2.0210	9475.	9475.	9475.
1022.00	2.031		858.	858.	858.	123	2.031	2.0210	9485.	9485.	9485.
1023.00	2.031		897.	897.	897.	124	2.031	2.0210	9495.	9495.	9495.
1024.00	2.031		936.	936.	936.	125	2.031	2.0210	9505.	9505.	9505.
1025.00	2.031		975.	975.	975.	126	2.031	2.0210	9515.	9515.	9515.
1026.00	2.031		1014.	1014.	1014.	127	2.031	2.0210	9525.	9525.	9525.
1027.00	2.031		1053.	1053.	1053.	128	2.031	2.0210	9535.	9535.	9535.
1028.00	2.031		1092.	1092.	1092.	129	2.031	2.0210	9545.	9545.	9545.
1029.00	2.031		1131.	1131.	1131.	130	2.031	2.0210	9555.	9555.	9555.
1030.00	2.031		1170.	1170.	1170.	131	2.031	2.0210	9565.	9565.	9565.
1031.00	2.031		1209.	1209.	1209.	132	2.031	2.0210	9575.	9575.	9575.
1032.00	2.031		1248.	1248.	1248.	133	2.031	2.0210	9585.	9585.	9585.
1033.00	2.031		1287.	1287.	1287.	134	2.031	2.0210	9595.	9595.	9595.
1034.00	2.031		1326.	1326.	1326.	135	2.031	2.0210	9605.	9605.	9605.
1035.00	2.031		1365.	1365.	1365.	136	2.031	2.0210	9615.	9615.	9615.
1036.00	2.031		1404.	1404.	1404.	137	2.031	2.0210	9625.	9625.	9625.
1037.00	2.031		1443.	1443.	1443.	138	2.031	2.0210	9635.	9635.	9635.
1038.00	2.031		1482.	1482.	1482.	139	2.031	2.0210	9645.	9645.	9645.
1039.00	2.031		1521.	1521.	1521.	140	2.031	2.0210	9655.	9655.	9655.
1040.00	2.031		1560.	1560.	1560.	141	2.031	2.0210	9665.	9665.	9665.
1041.00	2.031		1599.	1599.	1599.	142	2.031	2.0210	9675.	9675.	9675.
1042.00	2.031		1638.	1638.	1638.	143	2.031	2.0210	9685.	9685.	9685.
1043.00	2.031		1677.	1677.	1677.	144	2.031	2.0210	9695.	9695.	9695.
1044.00	2.031		1716.	1716.	1716.	145	2.031	2.0210	9705.	9705.	9705.
1045.00	2.031		1755.	1755.	1755.	146	2.031	2.0210	9715.	9715.	9715.
1046.00	2.031		1794.	1794.	1794.	147	2.031	2.0210	9725.	9725.	9725.
1047.00	2.031		1833.	1833.	1833.	148	2.031	2.0210	9735.	9735.	9735.
1048.00	2.031		1872.	1872.	1872.	149	2.031	2.0210	9745.	9745.	9745.
1049.00	2.031		1911.	1911.	1911.	150	2.031	2.0210	9755.	9755.	9755.
1050.00	2.031		1950.	1950.	1950.	151	2.031	2.0210	9765.	9765.	9765.
1051.00	2.031		1989.	1989.	1989.	152	2.031	2.0210	9775.	9775.	9775.
1052.00	2.031		2028.	2028.	2028.	153	2.031	2.0210	9785.	9785.	9785.
1053.00	2.031		2067.	2067.	2067.	154	2.031	2.0210	9795.	9795.	9795.
1054.00	2.031		2106.	2106.	2106.	155	2.031	2.0210	9805.	9805.	9805.
1055.00	2.031		2145.	2145.	2145.	156	2.031	2.0210	9815.	9815.	9815.
1056.00	2.031		2184.	2184.	2184.	157	2.031	2.0210	9825.	9825.	9825.
1057.00	2.031		2223.	2223.	2223.	158	2.031	2.0210	9835.	9835.	9835.
1058.00	2.031		2262.	2262.	2262.	159	2.031	2.0210	9845.	9845.	9845.
1059.00	2.031		2301.	2301.	2301.	160	2.031	2.0210	9855.	9855.	9855.
1060.00	2.031		2340.	2340.	2340.	161	2.031	2.0210	9865.	9865.	9865.
1061.00	2.031		2379.	2379.	2379.	162	2.031	2.0210	9875.	9875.	9875.
1062.00	2.031		2418.	2418.	2418.	163	2.031	2.0210	9885.	9885.	9885.
1063.00	2.031		2457.	2457.	2457.	164	2.031	2.0210	9895.	9895.	9895.
1064.00	2.031		2496.	2496.	2496.	165	2.031	2.0210	9905.	9905.	9905.
1065.00	2.031		2535.	2535.	2535.	166	2.031	2.0210	9915.	9915.	9915.
1066.00	2.031		2574.	2574.	2574.	167	2.031	2.0210	9925.	9925.	9925.
1067.00	2.031		2613.	2613.	2613.	168	2.031	2.0210	9935.	9935.	9935.
1068.00	2.031		2652.	2652.	2652.	169	2.031	2.0210	9945.	9945.	9945.
1069.00	2.031		2691.	2691.	2691.	170	2.031	2.0210	9955.	9955.	9955.
1070.00	2.031		2730.	2730.	2730.	171	2.031	2.0210	9965.	9965.	9965.
1071.00	2.031		2769.	2769.	2769.	172	2.031	2.0210	9975.	9975.	9975.
1072.00	2.031		2808.	2808.	2808.	173	2.031	2.0210	9985.	9985.	9985.
1073.00	2.031		2847.	2847.	2847.	174	2.031	2.0210	9995.	9995.	9995.
1074.00	2.031		2886.	2886.	2886.	175	2.031	2.0210	10005.	10005.	10005.
1075.00	2.031		2925.	2925.	2925.	176	2.031	2.0210	10015.	10015.	10015.
1076.00	2.031		2964.	2964.	2964.	177	2.031	2.0210	10025.	10025.	10025.
1077.00	2.031		3003.	3003.	3003.	178	2.031	2.0210	10035.	10035.	10035.
1078.00	2.031		3042.	3042.	3042.	179	2.031	2.0210	10045.	10045.	10045.
1079.00	2.031		3081.	3081.	3081.	180	2.031	2.0210	10055.	10055.	10055.
1080.00	2.031		3120.	3120.	3120.	181	2.031	2.0210	10065.	10065.	10065.
1081.00	2.031		3159.	3159.	3159.	182	2.031	2.0210	10075.	10075.	10075.
1082.00	2.031		3198.	3198.	3198.	183	2.031	2.0210	10085.	10085.	10085.
1083.00	2.031		3237.	3237.	3237.	184	2.031	2.0210	10095.	10095.	10095.
1084.00	2.031		3276.	3276.	3276.	185	2.031	2.0210	10105.	10105.	10105.
1085.00	2.031		3315.	3315.	3315.	186	2.031	2.0210	10115.	10115.	10115.
1086.00	2.031		3354.	3354.	3354.	187	2.031	2.0210	10125.	10125.	10125.
1087.00	2.031		3393.	3393.	3393.	188	2.031	2.0210	10135.	10135.	10135.
1088.00	2.031		3432.	3432.	3432.	189	2.031	2.0210	10145.	10145.	10145.
1089.00	2.031		3471.	3471.	3471.	190	2.031	2.0210	10155.	10155.	10155.
1090.00	2.031		3510.	3510.	3510.	191	2.031	2.0210	10165.	10165.	10165.
1091.00	2.031		3549.	3549.	3549.	192	2.031	2.0210	10175.	10175.	10175.
1092.00	2.031		3588.	3588.	3588.	193	2.031	2.0210	10185.	10185.	10185.
1093.00	2.031		3627.	3627.	3627.	194	2.031	2.0210	10195.	10195.	10195.
1094.00	2.031		3666.	3666.	3666.	195	2.031	2.0210	10205.	10205.	10205.
1095.00	2.031		3705.	3705.	3705.	196	2.031	2.0210	10215.	10215.	10215.
1096.00	2.031		3744.	3744.	3744.	197	2.031	2.0210	10225.	10225.	10225.
1097.00	2.031		3783.	3783.	3783.	198	2.031	2.0210	10235.	10235.	10235.
1098.00	2.031		3822.	3822.	3822.	199	2.031	2.0210	10245.	10245.	10245.
1099.00	2.031		3861.	3861.	3861.	200	2.031	2.0210	10255.	10255.	10255.
1100.00	2.031		3900.	3900.	3900.						

TABLE 6-10 (Continued)

J	PEACK DEPTH (FT)	G + G DENSITY (GM/CC)	BOREHOLE DWT-13			J	PEACK DEPTH (FT)	G + G DENSITY (GM/CC)	BOREHOLE DWT-13		
			DENSITY OF SOLID COMPONENT (GM/CC)	CUMULATIVE RHO22.821	SOLID MASS RHO22.821 (GM/CC)				DENSITY OF SOLID COMPONENT (GM/CC)	CUMULATIVE RHO22.821	SOLID MASS RHO22.821 (GM/CC)
0	1800.00		2.8210	0.	0.	191	646.00	2.111	13469.	14469.	13469.
1	911.00	2.025		0.	0.	192	645.00	2.125	13552.	14552.	13552.
2	909.00	2.025		94.	94.	193	644.00	2.111	13675.	14675.	13675.
3	908.10	2.025		192.	192.	194	643.00	2.165	13806.	14806.	13806.
4	907.10	2.025		251.	251.	195	642.00	2.187	14034.	15034.	14034.
5	906.00	2.025		330.	330.	196	641.00	2.107	14117.	15117.	14117.
6	905.00	2.025		401.	401.	197	640.00	2.076	14300.	15300.	14300.
7	904.10	2.025		474.	474.	198	639.00	2.103	14543.	15543.	14543.
8	903.00	2.025		551.	551.	199	638.00	2.134	14847.	15847.	14847.
9	902.00	2.025		630.	630.	200	637.00	2.134	15196.	16196.	15196.
10	901.00	2.025		711.	711.	201	636.00	2.130	15592.	16592.	15592.
11	900.00	2.025		794.	794.	202	635.00	2.134	16037.	16937.	16037.
12	899.00	2.025		879.	879.	203	634.00	2.124	16532.	17432.	16532.
13	898.00	2.025		966.	966.	204	633.00	2.108	17076.	17976.	17076.
14	897.00	2.025		1055.	1055.	205	632.00	2.102	17670.	18570.	17670.
15	896.00	2.025		1146.	1146.	206	631.00	2.045	18314.	19214.	18314.
16	895.00	2.025		1239.	1239.	207	630.00	2.045	19008.	19908.	19008.
17	894.00	2.025		1334.	1334.	208	629.00	2.045	19752.	20652.	19752.
18	893.00	2.025		1431.	1431.	209	628.00	2.045	20546.	21446.	20546.
19	892.00	2.025		1530.	1530.	210	627.00	2.045	21390.	22290.	21390.
20	891.00	2.025		1631.	1631.	211	626.00	2.045	22284.	23184.	22284.
21	890.00	2.025		1734.	1734.	212	625.00	2.045	23228.	24128.	23228.
22	889.00	2.025		1839.	1839.	213	624.00	2.045	24222.	25122.	24222.
23	888.00	2.025		1946.	1946.	214	623.00	2.045	25266.	26166.	25266.
24	887.00	2.025		2055.	2055.	215	622.00	2.045	26360.	27260.	26360.
25	886.00	2.025		2166.	2166.	216	621.00	2.045	27504.	28404.	27504.
26	885.00	2.025		2279.	2279.	217	620.00	2.045	28698.	29598.	28698.
27	884.00	2.025		2394.	2394.	218	619.00	2.045	29942.	30842.	29942.
28	883.00	2.025		2511.	2511.	219	618.00	2.045	31236.	32136.	31236.
29	882.00	2.025		2630.	2630.	220	617.00	2.045	32580.	33480.	32580.
30	881.00	2.025		2751.	2751.	221	616.00	2.045	33974.	34874.	33974.
31	880.00	2.025		2874.	2874.	222	615.00	2.045	35418.	36318.	35418.
32	879.00	2.025		3000.	3000.	223	614.00	2.045	36912.	37812.	36912.
33	878.00	2.025		3129.	3129.	224	613.00	2.045	38456.	39356.	38456.
34	877.00	2.025		3261.	3261.	225	612.00	2.045	40050.	40950.	40050.
35	876.00	2.025		3396.	3396.	226	611.00	2.045	41694.	42594.	41694.
36	875.00	2.025		3534.	3534.	227	610.00	2.045	43388.	44288.	43388.
37	874.00	2.025		3675.	3675.	228	609.00	2.045	45132.	45932.	45132.
38	873.00	2.025		3819.	3819.	229	608.00	2.045	46926.	47726.	46926.
39	872.00	2.025		3966.	3966.	230	607.00	2.045	48770.	49570.	48770.
40	871.00	2.025		4116.	4116.	231	606.00	2.045	50664.	51464.	50664.
41	870.00	2.025		4269.	4269.	232	605.00	2.045	52608.	53408.	52608.
42	869.00	2.025		4425.	4425.	233	604.00	2.045	54602.	55402.	54602.
43	868.00	2.025		4584.	4584.	234	603.00	2.045	56646.	57446.	56646.
44	867.00	2.025		4746.	4746.	235	602.00	2.045	58740.	59540.	58740.
45	866.00	2.025		4911.	4911.	236	601.00	2.045	60884.	61684.	60884.
46	865.00	2.025		5079.	5079.	237	600.00	2.045	63078.	63878.	63078.
47	864.00	2.025		5250.	5250.	238	599.00	2.045	65322.	66122.	65322.
48	863.00	2.025		5424.	5424.	239	598.00	2.045	67616.	68416.	67616.
49	862.00	2.025		5601.	5601.	240	597.00	2.045	69960.	70260.	69960.
50	861.00	2.025		5781.	5781.	241	596.00	2.045	72354.	72654.	72354.
51	860.00	2.025		5964.	5964.	242	595.00	2.045	74798.	75098.	74798.
52	859.00	2.025		6150.	6150.	243	594.00	2.045	77292.	77592.	77292.
53	858.00	2.025		6339.	6339.	244	593.00	2.045	79836.	80136.	79836.
54	857.00	2.025		6531.	6531.	245	592.00	2.045	82430.	82730.	82430.
55	856.00	2.025		6726.	6726.	246	591.00	2.045	85074.	85374.	85074.
56	855.00	2.025		6924.	6924.	247	590.00	2.045	87768.	88068.	87768.
57	854.00	2.025		7125.	7125.	248	589.00	2.045	90512.	90812.	90512.
58	853.00	2.025		7329.	7329.	249	588.00	2.045	93306.	93606.	93306.
59	852.00	2.025		7536.	7536.	250	587.00	2.045	96150.	96450.	96150.
60	851.00	2.025		7746.	7746.	251	586.00	2.045	99044.	99344.	99044.
61	850.00	2.025		7959.	7959.	252	585.00	2.045	101988.	102288.	101988.
62	849.00	2.025		8175.	8175.	253	584.00	2.045	104582.	104882.	104582.
63	848.00	2.025		8394.	8394.	254	583.00	2.045	107226.	107526.	107226.
64	847.00	2.025		8616.	8616.	255	582.00	2.045	109920.	110220.	109920.
65	846.00	2.025		8841.	8841.	256	581.00	2.045	112664.	112964.	112664.
66	845.00	2.025		9069.	9069.	257	580.00	2.045	115458.	115758.	115458.
67	844.00	2.025		9300.	9300.	258	579.00	2.045	118302.	118602.	118302.
68	843.00	2.025		9534.	9534.	259	578.00	2.045	121196.	121496.	121196.
69	842.00	2.025		9771.	9771.	260	577.00	2.045	124140.	124440.	124140.
70	841.00	2.025		10011.	10011.	261	576.00	2.045	127134.	127434.	127134.
71	840.00	2.025		10254.	10254.	262	575.00	2.045	130178.	130478.	130178.
72	839.00	2.025		10500.	10500.	263	574.00	2.045	133272.	133572.	133272.
73	838.00	2.025		10749.	10749.	264	573.00	2.045	136416.	136716.	136416.
74	837.00	2.025		11001.	11001.	265	572.00	2.045	139610.	140010.	139610.
75	836.00	2.025		11256.	11256.	266	571.00	2.045	142854.	143254.	142854.
76	835.00	2.025		11514.	11514.	267	570.00	2.045	146148.	146548.	146148.
77	834.00	2.025		11775.	11775.	268	569.00	2.045	149492.	149892.	149492.
78	833.00	2.025		12039.	12039.	269	568.00	2.045	152886.	153286.	152886.
79	832.00	2.025		12306.	12306.	270	567.00	2.045	156330.	156730.	156330.
80	831.00	2.025		12576.	12576.	271	566.00	2.045	159824.	160224.	159824.
81	830.00	2.025		12849.	12849.	272	565.00	2.045	163368.	163768.	163368.
82	829.00	2.025		13125.	13125.	273	564.00	2.045	166962.	167362.	166962.
83	828.00	2.025		13404.	13404.	274	563.00	2.045	170606.	171006.	170606.
84	827.00	2.025		13686.	13686.	275	562.00	2.045	174300.	174700.	174300.
85	826.00	2.025		13971.	13971.	276	561.00	2.045	178044.	178444.	178044.
86	825.00	2.025		14259.	14259.	277	560.00	2.045	181838.	182238.	181838.
87	824.00	2.025		14550.	14550.	278	559.00	2.045	185682.	186082.	185682.
88	823.00	2.025		14844.	14844.	279	558.00	2.045	189576.	189976.	189576.
89	822.00	2.025		15141.	15141.	280	557.00	2.045	193520.	193920.	193520.
90	821.00	2.025		15441.	15441.	281	556.00	2.045	197514.	197914.	197514.
91	820.00	2.025		15744.	15744.	282	555.00	2.045	201558.	201958.	201558.
92	819.00	2.025		16050.	16050.	283	554.00	2.045	205652.	206052.	205652.
93	818.00	2.025		16359.	16359.	284	553.00	2.045	209796.	210196.	209796.
94	817.00	2.025		16671.	16671.	285	552.00	2.045	213990.	214390.	213990.
95	816.00	2.025		16986.	16986.	286	551.00	2.045	218234.	218634.	218234.
96	815.00	2.025		17304.	17304.	287	550.00	2.045	222528.	222928.	222528.
97	814.00	2.025		17625.	17625.	288	549.00	2.045	226872.	227272.	226872.
98	813.00	2.025		17949.	17949.	289	548.00	2.045	231266.	231666.	231266.
99	812.00	2.025		18276.	18276.	290	547.00	2.045	235710.	236110.	235710.
100	811.00	2.025		18606.	18606.	291	546.00	2.045	240204.	240604.	240204.

TABLE 6-10 (Continued)

BENCHMOUNT DWT-13					BENCHMOUNT DWT-16				
PLACE DEPTH DIFT	G + S DENSITY (GM/CC)	DENSITY OF SOLID COMPONENT (GM/CC)	CUMULATIVE SOLID MASS RHO22.821 RHO22.821	FOR (CROSS-2) LINEAR SP. INC FOR RHO	PLACE DEPTH DIFT	G + S DENSITY (GM/CC)	DENSITY OF SOLID COMPONENT (GM/CC)	CUMULATIVE SOLID MASS RHO22.821 RHO22.821	FOR (CROSS-2) LINEAR SP. INC FOR RHO
201	395.75	2.045	25940.	25940.	25940.	4	1000.00	2.0210	0.
202	395.75	2.045	26027.	26027.	26027.	5	1000.00	2.0210	0.
203	395.75	2.045	26083.	26083.	26083.	6	1000.00	2.0210	0.
204	395.75	2.045	26139.	26139.	26139.	7	1000.00	2.0210	0.
205	395.75	2.045	26195.	26195.	26195.	8	1000.00	2.0210	0.
206	395.75	2.045	26251.	26251.	26251.	9	1000.00	2.0210	0.
207	395.75	2.045	26307.	26307.	26307.	10	1000.00	2.0210	0.
208	395.75	2.045	26363.	26363.	26363.	11	1000.00	2.0210	0.
209	395.75	2.045	26419.	26419.	26419.	12	1000.00	2.0210	0.
210	395.75	2.045	26475.	26475.	26475.	13	1000.00	2.0210	0.
211	395.75	2.045	26531.	26531.	26531.	14	1000.00	2.0210	0.
212	395.75	2.045	26587.	26587.	26587.	15	1000.00	2.0210	0.
213	395.75	2.045	26643.	26643.	26643.	16	1000.00	2.0210	0.
214	395.75	2.045	26699.	26699.	26699.	17	1000.00	2.0210	0.
215	395.75	2.045	26755.	26755.	26755.	18	1000.00	2.0210	0.
216	395.75	2.045	26811.	26811.	26811.	19	1000.00	2.0210	0.
217	395.75	2.045	26867.	26867.	26867.	20	1000.00	2.0210	0.
218	395.75	2.045	26923.	26923.	26923.	21	1000.00	2.0210	0.
219	395.75	2.045	26979.	26979.	26979.	22	1000.00	2.0210	0.
220	395.75	2.045	27035.	27035.	27035.	23	1000.00	2.0210	0.
221	395.75	2.045	27091.	27091.	27091.	24	1000.00	2.0210	0.
222	395.75	2.045	27147.	27147.	27147.	25	1000.00	2.0210	0.
223	395.75	2.045	27203.	27203.	27203.	26	1000.00	2.0210	0.
224	395.75	2.045	27259.	27259.	27259.	27	1000.00	2.0210	0.
225	395.75	2.045	27315.	27315.	27315.	28	1000.00	2.0210	0.
226	395.75	2.045	27371.	27371.	27371.	29	1000.00	2.0210	0.
227	395.75	2.045	27427.	27427.	27427.	30	1000.00	2.0210	0.
228	395.75	2.045	27483.	27483.	27483.	31	1000.00	2.0210	0.
229	395.75	2.045	27539.	27539.	27539.	32	1000.00	2.0210	0.
230	395.75	2.045	27595.	27595.	27595.	33	1000.00	2.0210	0.
231	395.75	2.045	27651.	27651.	27651.	34	1000.00	2.0210	0.
232	395.75	2.045	27707.	27707.	27707.	35	1000.00	2.0210	0.
233	395.75	2.045	27763.	27763.	27763.	36	1000.00	2.0210	0.
234	395.75	2.045	27819.	27819.	27819.	37	1000.00	2.0210	0.
235	395.75	2.045	27875.	27875.	27875.	38	1000.00	2.0210	0.
236	395.75	2.045	27931.	27931.	27931.	39	1000.00	2.0210	0.
237	395.75	2.045	27987.	27987.	27987.	40	1000.00	2.0210	0.
238	395.75	2.045	28043.	28043.	28043.	41	1000.00	2.0210	0.
239	395.75	2.045	28099.	28099.	28099.	42	1000.00	2.0210	0.
240	395.75	2.045	28155.	28155.	28155.	43	1000.00	2.0210	0.
241	395.75	2.045	28211.	28211.	28211.	44	1000.00	2.0210	0.
242	395.75	2.045	28267.	28267.	28267.	45	1000.00	2.0210	0.
243	395.75	2.045	28323.	28323.	28323.	46	1000.00	2.0210	0.
244	395.75	2.045	28379.	28379.	28379.	47	1000.00	2.0210	0.
245	395.75	2.045	28435.	28435.	28435.	48	1000.00	2.0210	0.
246	395.75	2.045	28491.	28491.	28491.	49	1000.00	2.0210	0.
247	395.75	2.045	28547.	28547.	28547.	50	1000.00	2.0210	0.
248	395.75	2.045	28603.	28603.	28603.	51	1000.00	2.0210	0.
249	395.75	2.045	28659.	28659.	28659.	52	1000.00	2.0210	0.
250	395.75	2.045	28715.	28715.	28715.	53	1000.00	2.0210	0.
251	395.75	2.045	28771.	28771.	28771.	54	1000.00	2.0210	0.
252	395.75	2.045	28827.	28827.	28827.	55	1000.00	2.0210	0.
253	395.75	2.045	28883.	28883.	28883.	56	1000.00	2.0210	0.
254	395.75	2.045	28939.	28939.	28939.	57	1000.00	2.0210	0.
255	395.75	2.045	28995.	28995.	28995.	58	1000.00	2.0210	0.
256	395.75	2.045	29051.	29051.	29051.	59	1000.00	2.0210	0.
257	395.75	2.045	29107.	29107.	29107.	60	1000.00	2.0210	0.
258	395.75	2.045	29163.	29163.	29163.	61	1000.00	2.0210	0.
259	395.75	2.045	29219.	29219.	29219.	62	1000.00	2.0210	0.
260	395.75	2.045	29275.	29275.	29275.	63	1000.00	2.0210	0.
261	395.75	2.045	29331.	29331.	29331.	64	1000.00	2.0210	0.
262	395.75	2.045	29387.	29387.	29387.	65	1000.00	2.0210	0.
263	395.75	2.045	29443.	29443.	29443.	66	1000.00	2.0210	0.
264	395.75	2.045	29499.	29499.	29499.	67	1000.00	2.0210	0.
265	395.75	2.045	29555.	29555.	29555.	68	1000.00	2.0210	0.
266	395.75	2.045	29611.	29611.	29611.	69	1000.00	2.0210	0.
267	395.75	2.045	29667.	29667.	29667.	70	1000.00	2.0210	0.
268	395.75	2.045	29723.	29723.	29723.	71	1000.00	2.0210	0.
269	395.75	2.045	29779.	29779.	29779.	72	1000.00	2.0210	0.
270	395.75	2.045	29835.	29835.	29835.	73	1000.00	2.0210	0.
271	395.75	2.045	29891.	29891.	29891.	74	1000.00	2.0210	0.
272	395.75	2.045	29947.	29947.	29947.	75	1000.00	2.0210	0.
273	395.75	2.045	30003.	30003.	30003.	76	1000.00	2.0210	0.
274	395.75	2.045	30059.	30059.	30059.	77	1000.00	2.0210	0.
275	395.75	2.045	30115.	30115.	30115.	78	1000.00	2.0210	0.
276	395.75	2.045	30171.	30171.	30171.	79	1000.00	2.0210	0.
277	395.75	2.045	30227.	30227.	30227.	80	1000.00	2.0210	0.
278	395.75	2.045	30283.	30283.	30283.	81	1000.00	2.0210	0.
279	395.75	2.045	30339.	30339.	30339.	82	1000.00	2.0210	0.
280	395.75	2.045	30395.	30395.	30395.	83	1000.00	2.0210	0.
281	395.75	2.045	30451.	30451.	30451.	84	1000.00	2.0210	0.
282	395.75	2.045	30507.	30507.	30507.	85	1000.00	2.0210	0.
283	395.75	2.045	30563.	30563.	30563.	86	1000.00	2.0210	0.
284	395.75	2.045	30619.	30619.	30619.	87	1000.00	2.0210	0.
285	395.75	2.045	30675.	30675.	30675.	88	1000.00	2.0210	0.
286	395.75	2.045	30731.	30731.	30731.	89	1000.00	2.0210	0.
287	395.75	2.045	30787.	30787.	30787.	90	1000.00	2.0210	0.
288	395.75	2.045	30843.	30843.	30843.	91	1000.00	2.0210	0.
289	395.75	2.045	30899.	30899.	30899.	92	1000.00	2.0210	0.
290	395.75	2.045	30955.	30955.	30955.	93	1000.00	2.0210	0.
291	395.75	2.045	31011.	31011.	31011.	94	1000.00	2.0210	0.
292	395.75	2.045	31067.	31067.	31067.	95	1000.00	2.0210	0.
293	395.75	2.045	31123.	31123.	31123.	96	1000.00	2.0210	0.
294	395.75	2.045	31179.	31179.	31179.	97	1000.00	2.0210	0.
295	395.75	2.045	31235.	31235.	31235.	98	1000.00	2.0210	0.
296	395.75	2.045	31291.	31291.	31291.	99	1000.00	2.0210	0.
297	395.75	2.045	31347.	31347.	31347.	100	1000.00	2.0210	0.
298	395.75	2.045	31403.	31403.	31403.				
299	395.75	2.045	31459.	31459.	31459.				
300	395.75	2.045	31515.	31515.	31515.				
301	395.75	2.045	31571.	31571.	31571.				
302	395.75	2.045	31627.	31627.	31627.				
303	395.75	2.045	31683.	31683.	31683.				
304	395.75	2.045	31739.	31739.	31739.				
305	395.75	2.045	31795.	31795.	31795.				
306	395.75	2.045	31851.	31851.	31851.				
307	395.75	2.045	31907.	31907.	31907.				
308	395.75	2.045	31963.	31963.	31963.				
309	395.75	2.045	32019.	32019.	32019.				
310	395.75	2.045	32075.	32075.	32075.				
311	395.75	2.045	32131.	32131.	32131.				
312	395.75	2.045	32187.	32187.	32187.				
313	395.75	2.045	32243.	32243.	32243.				
314	395.75	2.045	32299.	32299.	32299.				
315	395.75	2.045	32355.	32355.	32355.				
316	395.75	2.045	32411.	32411.	32411.				
317	395.75	2.045	32467.	32467.	32467.				
318	395.75	2.045	32523.	32523.	32523.				
319	395.75	2.045	32579.	32579.	32579.				
320	395.75	2.045	32635.	32635.	32635.				
321	395.75	2.045	32691.	32691.	32691.				
322	395.75	2.045	32747.	32747.	32747.				
323	395.75	2.045	32803.	32803.	32803.				
324	395.75	2.045	32859.	32859.	32859.				

TABLE 6-10 (Continued)

J	PLATE DEPTH DIFT	G - G DENSITY OF SOLID COMPONENT (GM/CC)	BOREHOLE DENSITY OF SOLID COMPONENT (GM/CC)	OPZ-18			J	PLATE DEPTH DIFT	G - G DENSITY OF SOLID COMPONENT (GM/CC)	BOREHOLE DENSITY OF SOLID COMPONENT (GM/CC)	OPZ-18		
				CUMULATIVE RHOZ-2.821	SOLID MASS RHOZ-2.821	(G/CM ³) LINEAR DENSITY FOR RHO					CUMULATIVE RHOZ-2.821	SOLID MASS RHOZ-2.821	(G/CM ³) LINEAR DENSITY FOR RHO
101	832.20		2.9130	7600.	9623.	9623.	201	699.97	2.129	19465.	19403.	19403.	
102	848.95	2.897		7801.	9740.	9740.	202	658.97	2.141	19546.	19484.	19484.	
103	848.95	2.896		7917.	9858.	9858.	203	652.10	2.110	19677.	19623.	19623.	
104	842.83	2.873		10114.	10098.	10098.	204	651.70		19808.	19844.	19844.	
105	838.74	2.899		10314.	1024.	10244.	205	647.67	2.124	20124.	20075.	20075.	
106	837.14	2.876		10399.	10363.	10363.	206	645.80	2.119	20207.	20159.	20159.	
107	835.26	2.868		10473.	10440.	10440.	207	648.25	2.144	20308.	20349.	20349.	
108	842.25	1.986		10546.	10533.	10533.	208	649.27	2.149	20402.	20459.	20459.	
109	832.90		2.9282	10607.	10564.	10564.	209	637.98	2.104	20544.	20595.	20595.	
110	832.41	2.800		10711.	10596.	10596.	210	636.74	2.231	20702.	20663.	20663.	
111	830.44	1.985		10717.	10676.	10676.	211	633.99	2.709	20859.	20824.	20824.	
112	828.21	2.000		10815.	10783.	10783.	212	631.60		20991.	20959.	20959.	
113	828.21	2.000		10846.	10859.	10859.	213	630.84	2.129	21032.	21001.	21001.	
114	823.70	2.035		11027.	10983.	10983.	214	630.05	2.144	21073.	21043.	21043.	
115	823.40		2.9206	11054.	11010.	11010.	215	628.87	2.094	21135.	21106.	21106.	
116	822.94	2.035		11065.	11021.	11021.	216	623.73	2.086	21294.	21372.	21372.	
117	819.81	2.108		11229.	11176.	11176.	217	622.57	2.110	21457.	21434.	21434.	
118	815.24	2.086		11309.	11255.	11255.	218	621.49	2.151	21598.	21580.	21580.	
119	815.44	1.994		11445.	11345.	11345.	219	618.45	2.144	21690.	21674.	21674.	
120	813.60		2.9183	11541.	11487.	11487.	220	616.66	2.192	21777.	21747.	21747.	
121	813.12	2.082		11565.	11511.	11511.	221	616.66		21792.	21777.	21777.	
122	811.15	2.126		11667.	11611.	11611.	222	614.70	2.170	21886.	21873.	21873.	
123	809.00		2.9043	11778.	11721.	11721.	223	611.94	2.184	21988.	21979.	21979.	
124	808.17	2.086		11780.	11741.	11741.	224	610.36	2.114	22023.	22014.	22014.	
125	807.41	2.097		11869.	11810.	11810.	225	607.41	2.094	22266.	22262.	22262.	
126	804.05	2.055		11980.	11927.	11927.	226	606.05	2.025	22345.	22342.	22342.	
127	804.67	2.074		12024.	11966.	11966.	227	603.40	2.027	22477.	22477.	22477.	
128	802.99	2.074		12107.	12044.	12044.	228	602.50		22514.	22514.	22514.	
129	798.34	2.118		12288.	12282.	12282.	229	604.14	1.994	22633.	22634.	22634.	
130	798.14	2.124		12355.	12365.	12365.	230	599.34	2.101	22648.	22672.	22672.	
131	794.80		2.9183	12547.	12476.	12476.	231	595.80	1.888	22832.	22840.	22840.	
132	791.86	2.064		12655.	12582.	12582.	232	593.62	1.892	22914.	22922.	22922.	
133	790.49	2.030		12732.	12658.	12658.	233	593.50		22928.	22936.	22936.	
134	787.92	2.035		12846.	12770.	12770.	234	589.49	2.140	23101.	23111.	23111.	
135	787.14	2.047		12888.	12807.	12807.	235	587.33	2.077	23223.	23234.	23234.	
136	785.17	2.013		12979.	12900.	12900.	236	585.39	2.142	23328.	23337.	23337.	
137	784.34	2.014		13017.	12937.	12937.	237	582.41	2.212	23443.	23502.	23502.	
138	782.41	1.993		13109.	13028.	13028.	238	580.95	2.097	23521.	23628.	23628.	
139	780.05	2.014		13221.	13137.	13137.	239	579.26	2.096	23641.	23667.	23667.	
140	778.87	1.987		13276.	13191.	13191.	240	578.90		23680.	23684.	23684.	
141	775.78	2.036		13399.	13337.	13337.	241	574.30	2.047	23717.	23744.	23744.	
142	774.75	2.104		13523.	13434.	13434.	242	574.34	2.189	23703.	23705.	23705.	
143	773.86	2.090		13545.	13454.	13454.	243	573.36	2.189	23769.	23770.	23770.	
144	771.70	2.086		13624.	13532.	13532.	244	570.99	2.252	23804.	23810.	23810.	
145	770.80	2.086		13683.	13591.	13591.	245	567.86	2.155	23826.	23822.	23822.	
146	767.80	2.072		13821.	13726.	13726.	246	564.30	2.032	23928.	23922.	23922.	
147	767.45	2.082		13861.	13745.	13745.	247	563.91	2.078	23968.	23968.	23968.	
148	766.80		2.9704	13861.	13772.	13772.	248	560.76	2.083	24045.	24038.	24038.	
149	765.40	2.053		13939.	13847.	13847.	249	559.30	2.074	24105.	24077.	24077.	
150	763.09	2.044		13958.	13861.	13861.	250	556.90		24139.	24130.	24130.	
151	762.34	2.044		14096.	13995.	13995.	251	558.74	2.060	24144.	24136.	24136.	
152	758.97	2.118		14146.	14114.	14114.	252	556.13	2.141	24280.	24275.	24275.	
153	758.70	2.118		14278.	14174.	14174.	253	553.67	2.118	24368.	24368.	24368.	
154	757.81	2.190		14340.	14256.	14256.	254	552.10	2.105	24503.	24500.	24500.	
155	756.04	2.190		14425.	14319.	14319.	255	551.41	2.104	24533.	24522.	24522.	
156	754.87	2.105		14528.	14420.	14420.	256	548.35	2.030	24571.	24547.	24547.	
157	752.14	2.079		14629.	14519.	14519.	257	546.30	2.038	24566.	24551.	24551.	
158	750.74	2.101		14708.	14589.	14589.	258	543.00	2.053	24562.	24546.	24546.	
159	747.77	2.105		14851.	14739.	14739.	259	544.04	2.081	24542.	24523.	24523.	
160	746.34	2.123		14913.	14799.	14799.	260	541.43	2.090	24521.	24502.	24502.	
161	745.01	2.105		14995.	14860.	14860.	261	543.86	2.124	24527.	24504.	24504.	
162	741.47	2.105		15181.	14964.	14964.	262	543.10		24508.	24504.	24504.	
163	741.07	2.190		15282.	15089.	15089.	263	542.00	2.151	24516.	24501.	24501.	
164	739.80	2.197		15468.	15184.	15184.	264	538.87	2.132	24528.	24527.	24527.	
165	737.70		2.8859	15683.	15263.	15263.	265	538.87	2.154	24526.	24509.	24509.	
166	736.74	2.097		15822.	15312.	15312.	266	524.14	2.154	24539.	24509.	24509.	
167	733.89	2.097		15974.	15452.	15452.	267	521.78	2.099	24644.	24633.	24633.	
168	733.40	2.091		16014.	15492.	15492.	268	517.70		24677.	24644.	24644.	
169	732.94	2.147		16079.	15555.	15555.	269	514.86	2.140	24732.	24699.	24699.	
170	748.47	2.058		16047.	15594.	15594.	270	514.30	2.110	24756.	24702.	24702.	
171	725.45	2.058		16013.	15692.	15692.	271	512.33	2.132	24760.	24725.	24725.	
172	722.96	2.151		16135.	16015.	16015.	272	510.74	2.135	24743.	24708.	24708.	
173	720.99	2.145		16241.	16124.	16124.	273	408.79	2.168	24740.	24714.	24714.	
174	719.99		2.7241	16249.	16183.	16183.	274	406.05	2.102	24746.	24740.	24740.	
175	719.00			16347.	16211.	16211.	275	404.97	2.086	24747.	24740.	24740.	
176	716.46	2.112		16477.	16344.	16344.	276	401.31	2.000	24731.	24744.	24744.	
177	712.43	2.107		16447.	16389.	16389.	277	400.55	2.044	24744.	24727.	24727.	
178	709.49	2.149		16843.	16737.	16737.	278	406.98	2.049	24793.	24766.	24766.	
179	709.49		2.7505	16963.	16758.	16758.	279	406.17	2.083	24783.	24766.	24766.	
180	707.44	2.149		16949.	16809.	16809.	280	405.30	2.048	24822.	24783.	24783.	
181	705.80	2.171		17056.	16934.	16934.	281	405.04	2.081	24840.	24805.	24805.	
182	703.87	2.190		17162.	17063.	17063.	282	402.65	2.124	24860.	24823.	24823.	
183	698.90	2.180		17317.	17323.	17323.	283	401.00		24899.	24813.	24813.	
184	698.10	2.196		17459.	17366.	17366.	284	400.80	2.129	24864.	24827.	24827.	
185	695.40	2.223		17591.	17500.	17500.	285	400.27	2.155	24885.	24848.	24848.	
186	695.40	2.209		17613.	17523.	17523.	286	405.10	2.140	24940.	24912.	24912.	
187	693.44	2.209		17725.	17637.	17637.	287	407.74	2.148	24911.	24875.	24875.	
188	689.30	2.126		17940.	17856.	17856.	288	405.94	2.116	24916.	24879.	24879.	
189	686.74	2.145		18087.	18006.	18006.	289	404.80	2.113	24908.	24861.	24861.	
190	685.96	2.076		18146.	18068.	18068.	290	401.64	2.200	24947.	24909.	24909.	
191	681.28	2.063		18368.	18289.	18289.	291	409.26	2.205	24980.	24940.	24940.	
192	680.40	2.094		18510.	18504.	18504.	292	408.87	2.087	24953.	24901.	24901.	
193	678.47	2.093		18509.	18453.	18453.	293	406.31	2.157	24954.	24902.	24902.	
194	674.14	2.159		18754.	18666.	186							

TABLE 6-10 (Continued)

J	PEACK DEPTH (FT)	S - G DENSITY (GM/CC)	BOREHOLE OP2-18			J	PEACK DEPTH (FT)	S - G DENSITY (GM/CC)	BOREHOLE KAR-01		
			DENSITY OF SOLID COMPONENT (GM/CC)	CUMULATIVE RHO2-221	SP. MASS RHO<RHO> LINEAR SPLINE FOR RHO				DENSITY OF SOLID COMPONENT (GM/CC)	CUMULATIVE RHO2-221	SP. MASS RHO<RHO> LINEAR SPLINE FOR RHO
301	462.78	2.030		29722.	29670.	29670.	0	1800.00	2.000	0.	0.
302	461.90	2.020		29760.	29707.	29707.	1	1105.00	2.005	0.	0.
303	460.36	2.020		29835.	29782.	29782.	2	1103.80	2.001	61.	61.
304	459.04	2.167		30077.	30022.	30022.	3	1102.40	2.057	140.	140.
305	458.07	2.130		30163.	30107.	30107.	4	1101.45	2.030	210.	210.
306	458.00			30206.	30170.	30170.	5	1115.80	2.000	297.	297.
307	452.00	2.157	2.0541	30227.	30171.	30171.	6	1117.01	2.050	375.	375.
308	450.74	2.113		30232.	30274.	30274.	7	1115.01	2.000	445.	445.
309	449.16	2.052		30471.	30413.	30413.	8	1114.40	2.042	530.	530.
310	449.04	2.120		30732.	30671.	30671.	9	1112.19	2.000	632.	632.
311	441.00	2.119		30794.	30732.	30732.	10	1104.70	1.990	746.	746.
312	441.01	2.151		30836.	30774.	30774.	11	1104.17	2.002	810.	810.
313	437.10	2.193		31053.	30907.	30907.	12	1104.10	2.025	1014.	1014.
314	433.50		2.9166	31446.	31177.	31177.	13	1101.30	2.120	1157.	1157.
315	432.92	2.047		31300.	31231.	31231.	14	1159.30	2.005	1299.	1299.
316	430.50	2.027		31396.	31325.	31325.	15	1158.13	2.017	1317.	1317.
317	429.40	2.031		31453.	31381.	31381.	16	1155.30	2.005	1452.	1452.
318	426.97	2.070		31491.	31419.	31419.	17	1152.90	1.990	1567.	1567.
319	426.31	2.105		31542.	31519.	31519.	18	1150.90	2.020	1663.	1663.
320	425.74	2.090		31632.	31559.	31559.	19	1149.40	2.000	1740.	1740.
321	419.01	2.071		31931.	31856.	31856.	20	1140.00	2.050	1804.	1804.
322	418.90		2.0001	31977.	31902.	31902.	21	1140.00	1.915	1897.	1897.
323	418.62	2.002		31990.	31916.	31916.	22	1143.67	2.070	2009.	2009.
324	413.21	2.072		32206.	32131.	32131.	23	1142.00	2.002	2049.	2049.
325	411.50	1.900		32440.	32365.	32365.	24	1142.00	2.070	2080.	2080.
326	409.30	1.900		32511.	32355.	32355.	25	1140.00	2.010	2149.	2149.
327	408.00	1.900		32555.	32470.	32470.	26	1140.00	2.010	2202.	2202.
328	405.40	1.900		32620.	32500.	32500.	27	1136.00	1.970	2257.	2257.
329	402.00	1.915		32728.	32609.	32609.	28	1130.00	2.001	2340.	2340.
330	401.51	1.902		32790.	32716.	32716.	29	1132.00	1.990	2405.	2405.
331	399.30	1.930		32901.	32802.	32802.	30	1130.01	2.030	2467.	2467.
332	397.40	1.900		32960.	32800.	32800.	31	1126.00	1.970	2508.	2508.
333	395.00	1.930		33030.	32970.	32970.	32	1123.00	2.030	2591.	2591.
334	393.90		2.9065	33120.	33041.	33041.	33	1121.97	2.055	2641.	2641.
335	393.03	1.900		33127.	33040.	33040.	34	1120.37	2.020	2677.	2677.
336	389.09	1.900		33308.	33227.	33227.	35	1118.70	2.010	2715.	2715.
337	376.00		2.0490				36	1116.70	1.990	3209.	3209.
338	361.90	2.050					37	1115.90	2.030	3423.	3423.
339	367.00	2.0760					38	1112.30	1.980	3499.	3499.
340	361.10	2.0700					39	1110.30	1.900	3591.	3591.
341	313.90	2.0700					40	1105.10	1.900	3645.	3645.
342	290.90	2.0002					41	1107.91	2.035	3701.	3701.
343	277.90	2.0900					42	1106.71	2.007	3760.	3760.
344	266.30	2.0059					43	1100.00	2.070	3861.	3861.
345	249.90	2.0010					44	1101.00	1.967	3996.	3996.
346	233.00	2.0623					45	1099.07	1.965	4223.	4223.
347	232.90	2.0210					46	1098.47	1.966	4359.	4359.
348			2.0210				47	1097.07	1.970	4496.	4496.
							48	1096.40	1.900	4631.	4631.
							49	1095.00	1.990	4806.	4806.
							50	1094.20	2.002	4945.	4945.
							51	1093.00	2.005	5080.	5080.
							52	1090.00	2.000	5225.	5225.
							53	1087.00	2.070	5380.	5380.
							54	1085.00	2.070	5540.	5540.
							55	1083.01	2.001	5690.	5690.
							56	1082.00	2.005	5840.	5840.
							57	1081.00	2.120	5990.	5990.
							58	1079.30	2.162	6140.	6140.
							59	1077.70	2.202	6290.	6290.
							60	1076.30	2.229	6440.	6440.
							61	1074.07	2.170	6590.	6590.
							62	1073.70	2.100	6740.	6740.
							63	1070.30	2.037	6890.	6890.
							64	1060.00	2.010	7040.	7040.
							65	1060.30	2.010	7190.	7190.
							66	1057.00	2.030	7340.	7340.
							67	1050.00	1.970	7490.	7490.
							68	1053.00	1.970	7640.	7640.
							69	1052.07	2.030	7790.	7790.
							70	1050.00	2.000	7940.	7940.
							71	1048.00	2.000	8090.	8090.
							72	1040.00	2.025	8240.	8240.
							73	1040.00	2.030	8390.	8390.
							74	1040.00	2.050	8540.	8540.
							75	1040.00	2.070	8690.	8690.
							76	1041.00	1.980	8840.	8840.
							77	1040.00	1.980	8990.	8990.
							78	1037.00	1.970	9140.	9140.
							79	1040.00	2.017	9290.	9290.
							80	1033.30	2.010	9440.	9440.
							81	1030.00	2.145	9590.	9590.
							82	1028.37	2.090	9740.	9740.
							83	1025.00	2.000	9890.	9890.
							84	1021.00	2.100	10040.	10040.
							85	1020.00	2.030	10190.	10190.
							86	1017.00	1.990	10340.	10340.
							87	1015.11	2.111	10490.	10490.
							88	1013.30	2.100	10640.	10640.
							89	1011.00	2.130	10790.	10790.
							90	1009.00	2.010	10940.	10940.
							91	1008.00	2.000	11090.	11090.
							92	1005.00	2.000	11240.	11240.
							93	1002.00	1.990	11390.	11390.
							94	999.00	2.100	11540.	11540.
							95	990.00	2.180	11690.	11690.
							96	989.00	2.127	11840.	11840.
							97	986.10	2.250	11990.	11990.
							98	979.00	2.117	12140.	12140.
							99	970.00	2.130	12290.	12290.
							100	970.00	2.070	12440.	12440.

TABLE 6-10 (Continued)

J	PLATE DEPTH (FT)	W - S DENSITY (G/CC)	DENSITY OF SOLID COMPONENT (G/CC)	BUREHOLE RAR-01			J	PLATE DEPTH (FT)	W - S DENSITY (G/CC)	DENSITY OF SOLID COMPONENT (G/CC)	BUREHOLE RAR-01		
				CUMULATIVE RHO2.821	SOLID MASS RHO2.821	IGF/CH22 LINEAR SLOPE FOR RHO					CUMULATIVE RHO2.821	SOLID MASS RHO2.821	IGF/CH22 LINEAR SLOPE FOR RHO
101	972.14	2.097		10466.	10466.	10466.	201	749.96	2.071		21756.	21756.	21756.
102	969.31	2.095		10606.	10606.	10606.	202	747.13	2.109		21896.	21896.	21896.
103	967.39	2.091		10709.	10709.	10709.	203	745.39	2.099		21962.	21962.	21962.
104	962.00	2.089		10974.	10974.	10974.	204	743.92	2.065		22045.	22045.	22045.
105	958.06	2.191		11120.	11120.	11120.	205	742.72	2.060		22103.	22103.	22103.
106	955.69	2.191		11206.	11206.	11206.	206	741.14	2.051		22184.	22184.	22184.
107	951.49	2.094		11513.	11513.	11513.	207	739.11	2.074		22285.	22285.	22285.
108	949.44	2.082		11613.	11613.	11613.	208	737.09	2.133		22372.	22372.	22372.
109	948.44	2.146		11655.	11655.	11655.	209	735.60	2.101		22472.	22472.	22472.
110	945.61	2.211		11810.	11810.	11810.	210	734.47	2.130		22572.	22572.	22572.
111	942.09	2.157		11966.	11966.	11966.	211	732.86	2.122		22672.	22672.	22672.
112	941.99	2.159		12010.	12010.	12010.	212	731.05	2.127		22772.	22772.	22772.
113	940.30	2.147		12096.	12096.	12096.	213	729.05	2.122		22872.	22872.	22872.
114	937.37	2.196		12245.	12245.	12245.	214	727.04	2.124		22972.	22972.	22972.
115	935.97	2.101		12330.	12330.	12330.	215	725.04	2.096		23072.	23072.	23072.
116	933.36	2.149		12457.	12457.	12457.	216	723.04	2.077		23172.	23172.	23172.
117	931.35	2.196		12563.	12563.	12563.	217	721.04	2.090		23272.	23272.	23272.
118	929.19	2.154		12699.	12699.	12699.	218	719.04	2.133		23372.	23372.	23372.
119	928.75	2.197		12712.	12712.	12712.	219	717.04	2.124		23472.	23472.	23472.
120	924.74	2.124		12929.	12929.	12929.	220	715.04	2.130		23572.	23572.	23572.
121	922.71	2.140		13035.	13035.	13035.	221	713.04	2.130		23672.	23672.	23672.
122	921.19	2.089		13118.	13118.	13118.	222	711.04	2.115		23772.	23772.	23772.
123	918.49	2.154		13265.	13265.	13265.	223	709.04	2.114		23872.	23872.	23872.
124	917.00	2.114		13351.	13351.	13351.	224	707.04	2.106		23972.	23972.	23972.
125	915.40	2.114		13419.	13419.	13419.	225	705.04	2.085		24072.	24072.	24072.
126	914.67	2.106		13462.	13462.	13462.	226	703.04	2.100		24172.	24172.	24172.
127	912.66	2.083		13564.	13564.	13564.	227	701.04	2.106		24272.	24272.	24272.
128	911.06	2.066		13644.	13644.	13644.	228	699.04	2.106		24372.	24372.	24372.
129	909.05	2.108		13706.	13706.	13706.	229	697.04	2.104		24472.	24472.	24472.
130	907.44	2.130		13832.	13832.	13832.	230	695.04	2.074		24572.	24572.	24572.
131	905.03	2.127		13959.	13959.	13959.	231	693.04	2.062		24672.	24672.	24672.
132	904.49	2.151		14002.	14002.	14002.	232	691.04	2.015		24772.	24772.	24772.
133	902.44	2.162		14111.	14111.	14111.	233	689.04	2.019		24872.	24872.	24872.
134	901.01	2.202		14170.	14170.	14170.	234	687.04	2.049		24972.	24972.	24972.
135	897.40	2.186		14273.	14273.	14273.	235	685.04	2.033		25072.	25072.	25072.
136	895.79	2.108		14356.	14356.	14356.	236	683.04	2.025		25172.	25172.	25172.
137	893.20	2.042		14378.	14378.	14378.	237	681.04	2.096		25272.	25272.	25272.
138	890.97	2.298		14490.	14490.	14490.	238	679.04	2.090		25372.	25372.	25372.
139	889.76	2.111		14761.	14761.	14761.	239	677.04	2.050		25472.	25472.	25472.
140	889.75	2.037		14963.	14963.	14963.	240	675.04	2.030		25572.	25572.	25572.
141	885.40	2.265		15081.	15081.	15081.	241	673.04	2.069		25672.	25672.	25672.
142	880.92	2.106		15203.	15203.	15203.	242	671.04	2.082		25772.	25772.	25772.
143	877.71	1.995		15461.	15461.	15461.	243	669.04	2.058		25872.	25872.	25872.
144	875.00	1.998		15473.	15473.	15473.	244	667.04	2.058		25972.	25972.	25972.
145	874.98	2.015		15492.	15492.	15492.	245	665.04	2.042		26072.	26072.	26072.
146	872.09	2.015		15507.	15507.	15507.	246	663.04	2.047		26172.	26172.	26172.
147	870.00	2.264		15509.	15509.	15509.	247	661.04	2.028		26272.	26272.	26272.
148	868.47	2.045		15609.	15609.	15609.	248	659.04	2.028		26372.	26372.	26372.
149	864.87	2.100		15685.	15685.	15685.	249	657.04	2.025		26472.	26472.	26472.
150	865.66	2.114		15647.	15647.	15647.	250	655.04	2.047		26572.	26572.	26572.
151	864.05	2.101		16030.	16030.	16030.	251	653.04	2.042		26672.	26672.	26672.
152	862.45	2.128		16135.	16135.	16135.	252	651.04	2.047		26772.	26772.	26772.
153	858.42	2.025		16337.	16337.	16337.	253	649.04	1.985		26872.	26872.	26872.
154	856.82	2.045		16396.	16396.	16396.	254	647.04	2.002		26972.	26972.	26972.
155	855.82	2.074		16435.	16435.	16435.	255	645.04	2.045		27072.	27072.	27072.
156	854.91	2.095		16537.	16537.	16537.	256	643.04	2.017		27172.	27172.	27172.
157	851.00	2.058		16650.	16650.	16650.	257	641.04	1.974		27272.	27272.	27272.
158	849.19	1.999		16774.	16774.	16774.	258	639.04	2.023		27372.	27372.	27372.
159	848.07	2.117		17013.	17013.	17013.	259	637.04	2.002		27472.	27472.	27472.
160	847.96	2.002		17137.	17137.	17137.	260	635.04	2.025		27572.	27572.	27572.
161	845.98	2.007		17235.	17235.	17235.	261	633.04	2.002		27672.	27672.	27672.
162	843.94	2.074		17333.	17333.	17333.	262	631.04	2.010		27772.	27772.	27772.
163	841.79	2.095		17399.	17399.	17399.	263	629.04	2.041		27872.	27872.	27872.
164	839.93	2.090		17535.	17535.	17535.	264	627.04	2.017		27972.	27972.	27972.
165	835.12	1.999		17575.	17575.	17575.	265	625.04	2.017		28072.	28072.	28072.
166	829.00	2.143		17755.	17755.	17755.	266	623.04	2.074		28172.	28172.	28172.
167	827.89	2.042		17846.	17846.	17846.	267	621.04	2.090		28272.	28272.	28272.
168	824.00	1.946		17987.	17987.	17987.	268	619.04	2.090		28372.	28372.	28372.
169	824.07	1.980		18077.	18077.	18077.	269	617.04	2.096		28472.	28472.	28472.
170	820.46	1.965		18100.	18100.	18100.	270	615.04	2.087		28572.	28572.	28572.
171	818.00	2.010		18268.	18268.	18268.	271	613.04	2.098		28672.	28672.	28672.
172	817.05	2.014		18319.	18319.	18319.	272	611.04	2.070		28772.	28772.	28772.
173	816.05	2.045		18350.	18350.	18350.	273	609.04	2.069		28872.	28872.	28872.
174	814.24	2.038		18477.	18477.	18477.	274	607.04	2.042		28972.	28972.	28972.
175	811.00	2.007		18612.	18612.	18612.	275	605.04	2.050		29072.	29072.	29072.
176	809.01	2.099		18728.	18728.	18728.	276	603.04	2.170		29172.	29172.	29172.
177	807.01	2.136		18789.	18789.	18789.	277	601.04	2.188		29272.	29272.	29272.
178	805.00	2.124		18894.	18894.	18894.	278	599.04	2.188		29372.	29372.	29372.
179	802.59	2.100		19061.	19061.	19061.	279	597.04	2.140		29472.	29472.	29472.
180	799.77	2.114		19206.	19206.	19206.	280	595.04	2.133		29572.	29572.	29572.
181	797.77	2.108		19311.	19311.	19311.	281	593.04	1.911		29672.	29672.	29672.
182	795.62	2.111		19356.	19356.	19356.	282	591.04	1.949		29772.	29772.	29772.
183	793.75	2.089		19519.	19519.	19519.	283	589.04	1.978		29872.	29872.	29872.
184	791.74	2.098		19621.	19621.	19621.	284	587.04	2.058		29972.	29972.	29972.
185	788.93	2.087		19765.	19765.	19765.	285	585.04	2.100		30072.	30072.	30072.
186	786.92	2.045		19865.	19865.	19865.	286	583.04	2.071		30172.	30172.	30172.
187	785.31	2.077		19945.	19945.	19945.	287	581.04	2.089		30272.	30272.	30272.
188	779.09	2.149		20233.	20233.	20233.	288	579.04	2.075		30372.	30372.	30372.
189	775.27	2.030		20456.	20456.	20456.	289	577.04	2.095		30472.	30472.	30472.
190	775.26	2.023		20553.	20553.	20553.	290	575.04	2.075		30572.	30572.	30572.
191	772.05	2.031		20611.	20611.	20611.	291	573.04	1.878		3		

TABLE 6-10 (Continued)

HOLE DEPTH DIAMETER	W - 6 DENSITY (G/CC)	DENSITY OF SOLID COMPONENT (G/CC)	BOREHOLE HAR-01			HOLE DEPTH DIAMETER	W - 6 DENSITY (G/CC)	DENSITY OF SOLID COMPONENT (G/CC)	BOREHOLE HAR-01		
			CUMULATIVE HOLE-2, 021	SOLID MASS HOLE-2, 021	SP/CMHOLE-2 1 INCH 1.00 RHO				CUMULATIVE HOLE-2, 021	SOLID MASS HOLE-2, 021	SP/CMHOLE-2 1 INCH 1.00 RHO
301	347.93	2.050	32264.	32264.	32264.	401	312.44	1.724	42507.	42507.	42507.
302	325.02	2.012	32342.	32342.	32342.	402	310.87	1.704	42711.	42711.	42711.
303	334.44	2.010	32399.	32399.	32399.	403	309.12	1.672	42820.	42820.	42820.
304	333.41	1.996	32443.	32443.	32443.	404	307.49	1.613	42719.	42719.	42719.
305	331.91	1.999	32449.	32449.	32449.	405	305.63	1.619	42784.	42784.	42784.
306	329.90	1.996	32442.	32442.	32442.	406	304.02	1.601	42851.	42851.	42851.
307	328.17	1.999	32449.	32449.	32449.	407	303.64	1.570	42870.	42870.	42870.
308	327.37	2.020	32734.	32734.	32734.	408	303.22	1.591	42888.	42888.	42888.
309	326.17	1.978	32743.	32743.	32743.	409	301.41	1.638	42973.	42973.	42973.
310	324.90	1.915	32863.	32863.	32863.	410	300.81	1.605	42989.	42989.	42989.
311	323.27	1.931	32916.	32916.	32916.	411	300.41	1.667	43005.	43005.	43005.
312	322.17	2.042	32910.	32910.	32910.	412	299.40	1.910	43059.	43059.	43059.
313	320.19	2.054	33065.	33065.	33065.	413	297.17	1.679	43124.	43124.	43124.
314	318.97	2.001	33123.	33123.	33123.	414	295.70	1.604	43256.	43256.	43256.
315	316.75	2.114	33222.	33222.	33222.	415	291.17	1.778	43300.	43300.	43300.
316	316.14	2.120	33244.	33244.	33244.	416	289.90	1.676	43395.	43395.	43395.
317	315.72	2.038	33307.	33307.	33307.	417	289.16	1.604	43429.	43429.	43429.
318	309.21	1.951	33504.	33504.	33504.	418	287.75	1.907	43485.	43485.	43485.
319	305.19	1.996	33759.	33759.	33759.	419	287.34	1.644	43570.	43570.	43570.
320	304.49	1.950	33793.	33793.	33793.	420	284.34	1.674	43620.	43620.	43620.
321	302.00	1.671	33825.	33825.	33825.	421	281.14	1.910	43761.	43761.	43761.
322	299.67	1.796	33968.	33968.	33968.	422	279.21	1.681	43829.	43829.	43829.
323	298.00	1.698	34024.	34024.	34024.	423	278.71	1.739	43862.	43862.	43862.
324	295.82	1.774	34106.	34106.	34106.	424	278.70	1.917	43951.	43951.	43951.
325	292.04	1.932	34215.	34215.	34215.	425	275.10	1.651	44007.	44007.	44007.
326	290.03	1.870	34280.	34280.	34280.	426	274.49	1.909	44059.	44059.	44059.
327	288.84	1.824	34327.	34327.	34327.	427	272.80	1.660	44103.	44103.	44103.
328	286.71	1.899	34420.	34420.	34420.	428	270.60	1.902	44160.	44160.	44160.
329	285.30	2.218	34463.	34463.	34463.	429	269.16	1.704	44247.	44247.	44247.
330	281.99	2.079	34649.	34649.	34649.	430	267.86	1.711	44287.	44287.	44287.
331	279.30	2.162	34776.	34776.	34776.	431	265.07	1.705	44385.	44385.	44385.
332	277.70	2.290	34861.	34861.	34861.	432	263.44	1.707	44443.	44443.	44443.
333	275.97	2.010	34959.	34959.	34959.	433	263.40	1.805	44458.	44458.	44458.
334	273.96	2.170	35062.	35062.	35062.	434	261.05	1.619	44504.	44504.	44504.
335	272.30	2.242	35151.	35151.	35151.	435	261.40	1.910	44551.	44551.	44551.
336	271.15	2.154	35218.	35218.	35218.	436	259.43	1.877	44597.	44597.	44597.
337	268.74	1.707	35327.	35327.	35327.	437	258.44	1.771	44641.	44641.	44641.
338	267.13	1.899	35390.	35390.	35390.	438	256.64	1.766	44699.	44699.	44699.
339	264.33	1.835	35422.	35422.	35422.	439	254.49	1.759	44783.	44783.	44783.
340	263.74	2.084	35467.	35467.	35467.	440	252.64	1.755	44838.	44838.	44838.
341	262.71	2.044	35508.	35508.	35508.	441	249.79	1.648	44924.	44924.	44924.
342	260.30	2.074	35707.	35707.	35707.	442	248.30	1.675	44964.	44964.	44964.
343	258.47	2.007	35805.	35805.	35805.	443	246.77	1.690	45014.	45014.	45014.
344	257.09	2.034	35863.	35863.	35863.	444	244.70	1.800	45044.	45044.	45044.
345	255.08	2.034	35960.	35960.	35960.	445	244.76	1.711	45126.	45126.	45126.
346	252.67	2.090	36070.	36070.	36070.	446	242.96	1.704	45193.	45193.	45193.
347	251.06	2.100	36167.	36167.	36167.	447	240.14	1.511	45231.	45231.	45231.
348	249.45	2.076	36244.	36244.	36244.	448	239.74	1.598	45241.	45241.	45241.
349	247.04	2.090	36364.	36364.	36364.	449	237.74	1.501	45291.	45291.	45291.
350	245.03	2.054	36466.	36466.	36466.	450	236.22	1.561	45324.	45324.	45324.
351	243.43	2.048	36545.	36545.	36545.	451	234.13	1.584	45337.	45337.	45337.
352	241.84	2.090	36628.	36628.	36628.	452	234.12	1.719	45384.	45384.	45384.
353	239.94	1.996	36763.	36763.	36763.	453	230.20	1.782	45493.	45493.	45493.
354	238.49	1.695	36873.	36873.	36873.	454	229.34	1.667	45533.	45533.	45533.
355	235.70	1.999	36968.	36968.	36968.	455	227.49	1.644	45549.	45549.	45549.
356	232.10	1.846	37057.	37057.	37057.	456	225.40	1.569	45652.	45652.	45652.
357	228.96	2.202	37191.	37191.	37191.	457	224.04	1.908	45731.	45731.	45731.
358	226.19	2.018	37330.	37330.	37330.	458	218.95	1.707	45776.	45776.	45776.
359	223.74	2.082	37457.	37457.	37457.	459	217.65	1.548	45811.	45811.	45811.
360	221.33	1.804	37566.	37566.	37566.	460	215.59	1.552	45904.	45904.	45904.
361	218.74	2.186	37651.	37651.	37651.	461	214.03	1.659	46004.	46004.	46004.
362	215.71	2.030	37840.	37840.	37840.	462	211.62	1.708	46044.	46044.	46044.
363	214.70	2.090	37907.	37907.	37907.	463	210.08	1.725	46111.	46111.	46111.
364	211.74	2.138	38076.	38076.	38076.	464	210.41	1.741	46125.	46125.	46125.
365	208.07	2.022	38238.	38238.	38238.	465	209.61	1.742	46159.	46159.	46159.
366	206.87	2.042	38296.	38296.	38296.	466	209.41	1.735	46167.	46167.	46167.
367	204.86	2.198	38399.	38399.	38399.	467	208.00	1.780	46210.	46210.	46210.
368	203.35	2.122	38463.	38463.	38463.	468	206.40	1.659	46263.	46263.	46263.
369	202.00	1.899	38539.	38539.	38539.	469	204.79	1.625	46311.	46311.	46311.
370	198.82	2.158	38692.	38692.	38692.	470	203.18	1.645	46350.	46350.	46350.
371	197.44	2.339	38786.	38786.	38786.	471	201.98	1.612	46392.	46392.	46392.
372	195.41	2.108	38947.	38947.	38947.	472	199.57	1.516	46455.	46455.	46455.
373	194.00	2.334	39085.	39085.	39085.	473	198.76	1.699	46476.	46476.	46476.
374	189.59	2.138	39225.	39225.	39225.	474	197.19	1.931	46536.	46536.	46536.
375	186.70	2.007	39366.	39366.	39366.	475	195.55	1.978	46607.	46607.	46607.
376	184.97	2.122	39504.	39504.	39504.	476	194.72	1.915	46643.	46643.	46643.
377	182.74	1.978	39665.	39665.	39665.	477	192.74	1.760	46721.	46721.	46721.
378	179.95	1.924	39809.	39809.	39809.	478	189.93	1.921	46831.	46831.	46831.
379	177.02	1.924	40076.	40076.	40076.	479	187.00				
380	175.44	1.899	40740.	40740.	40740.						
381	172.84	1.762	40852.	40852.	40852.						
382	174.44	1.905	40967.	40967.	40967.						
383	174.41	1.876	41036.	41036.	41036.						
384	174.01	1.864	41101.	41101.	41101.						
385	174.00	1.829	41138.	41138.	41138.						
386	171.79	1.817	41206.	41206.	41206.						
387	168.97	1.711	41266.	41266.	41266.						
388	167.37	1.911	41343.	41343.	41343.						
389	166.16	1.707	41487.	41487.	41487.						
390	163.73	1.706	41571.	41571.	41571.						
391	161.50	1.759	41611.	41611.	41611.						
392	160.11	1.877	41707.	41707.	41707.						
393	158.55	1.919	41778.	41778.	41778.						
394	156.94	1.979	41849.	41849.	41849.						
395	154.91	2.151	41949.	41949.	41949.						
396	152.70	1.849	42099.	42099.	42099.						
397	151.49	1.996	42203.	42203.	42203.						
398	149.48	2.010	42261.	42261.	42261.						
399	148.48	1.974	42334.	42334.	42334.						
400	146.87	1.972	42407.	42407.	42407.						

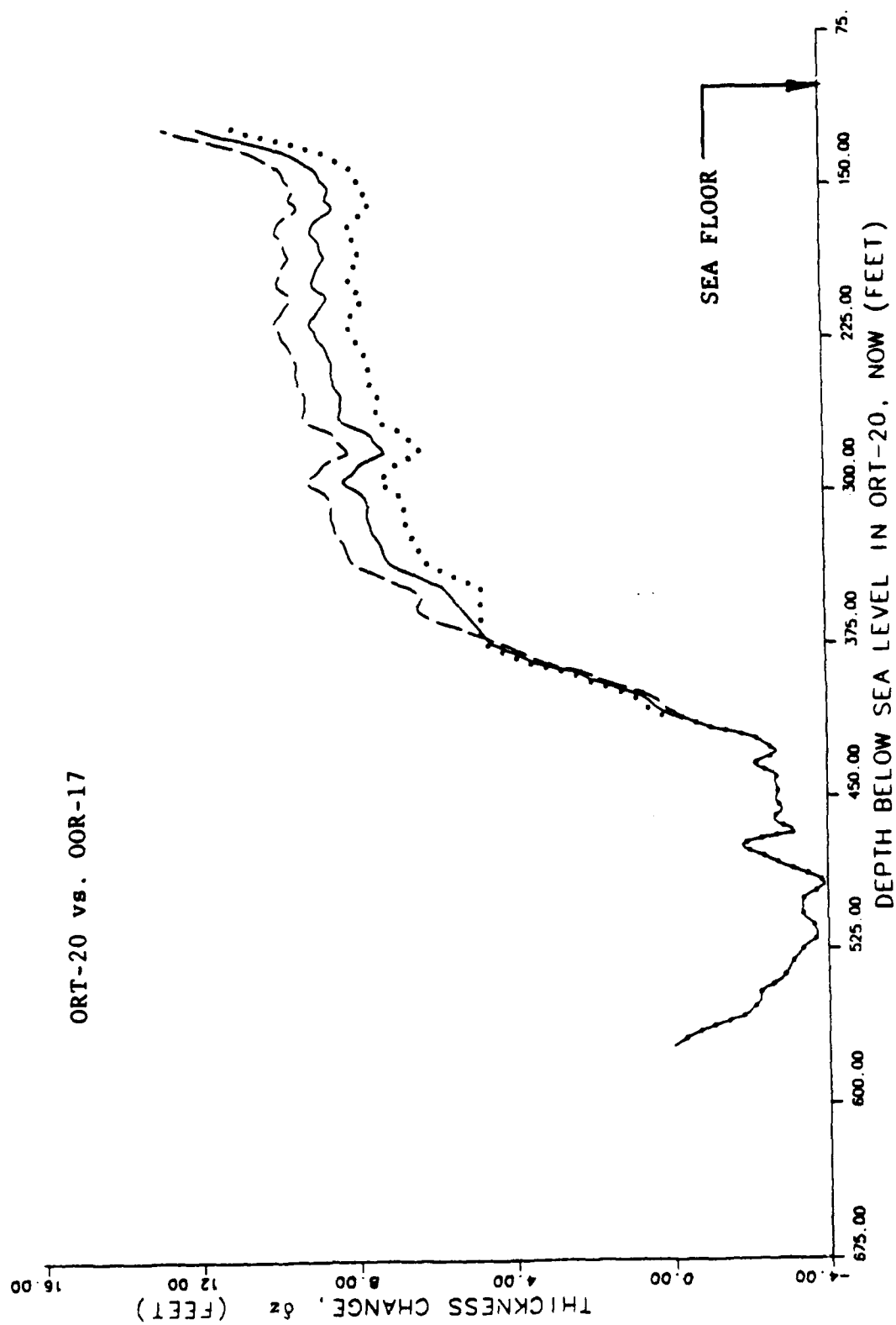


FIGURE 6-27. -- Change in rock thickness from γ - γ densities, assuming simple subsidence. Borehole ORT-20 vs. OOR-17.

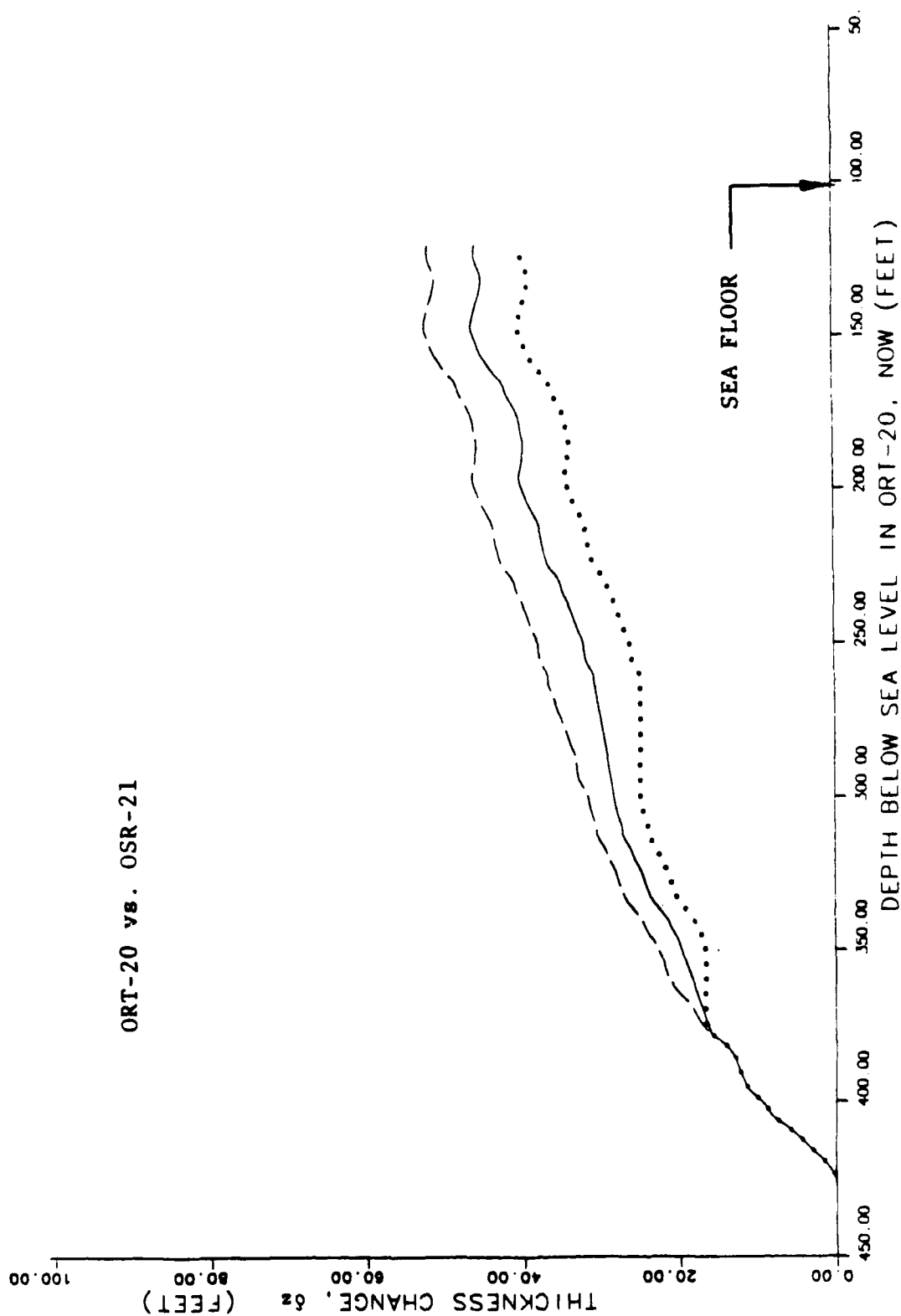


FIGURE 6-28. -- Change in rock thickness from Y-Y densities, assuming simple subsidence. Borehole ORT-20 vs. OSR-21.

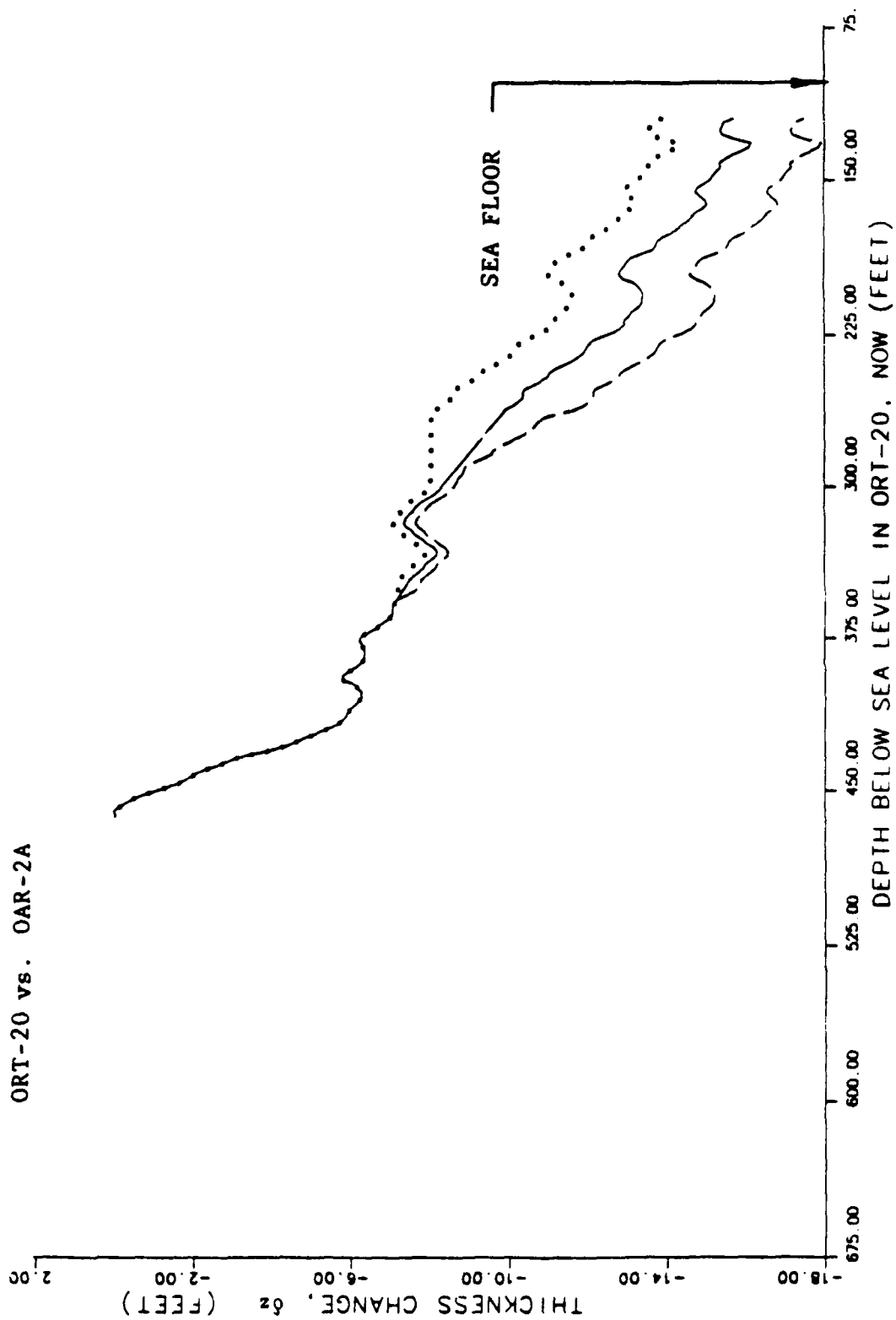


FIGURE 6-29. -- Change in rock thickness from γ - γ densities, assuming simple subsidence. Borehole ORT-20 vs. OAR-2A.

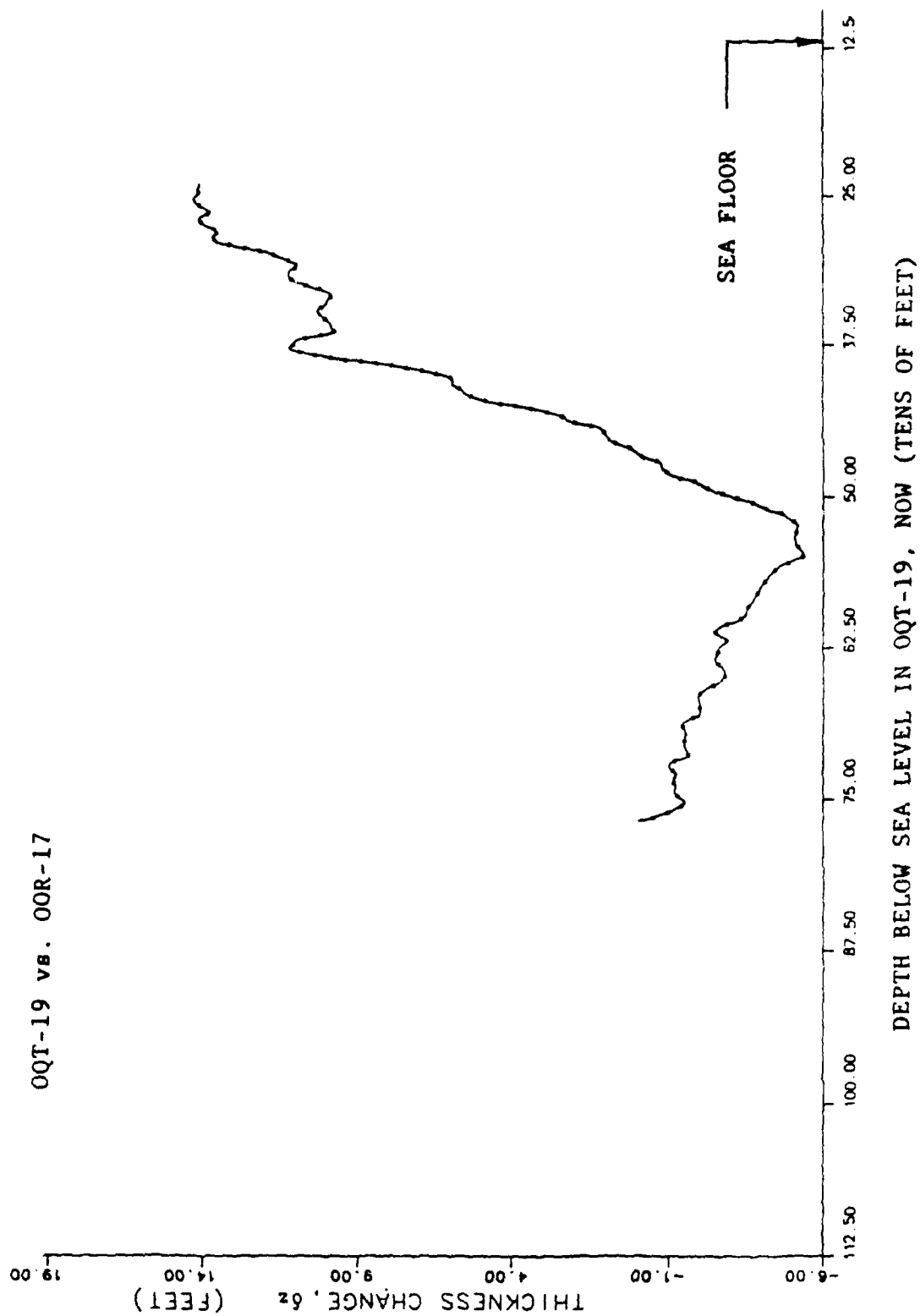


FIGURE 6-30. -- Change in rock thickness from γ - γ densities, assuming simple subsidence. Borehole OQT-19 vs. OOR-17.

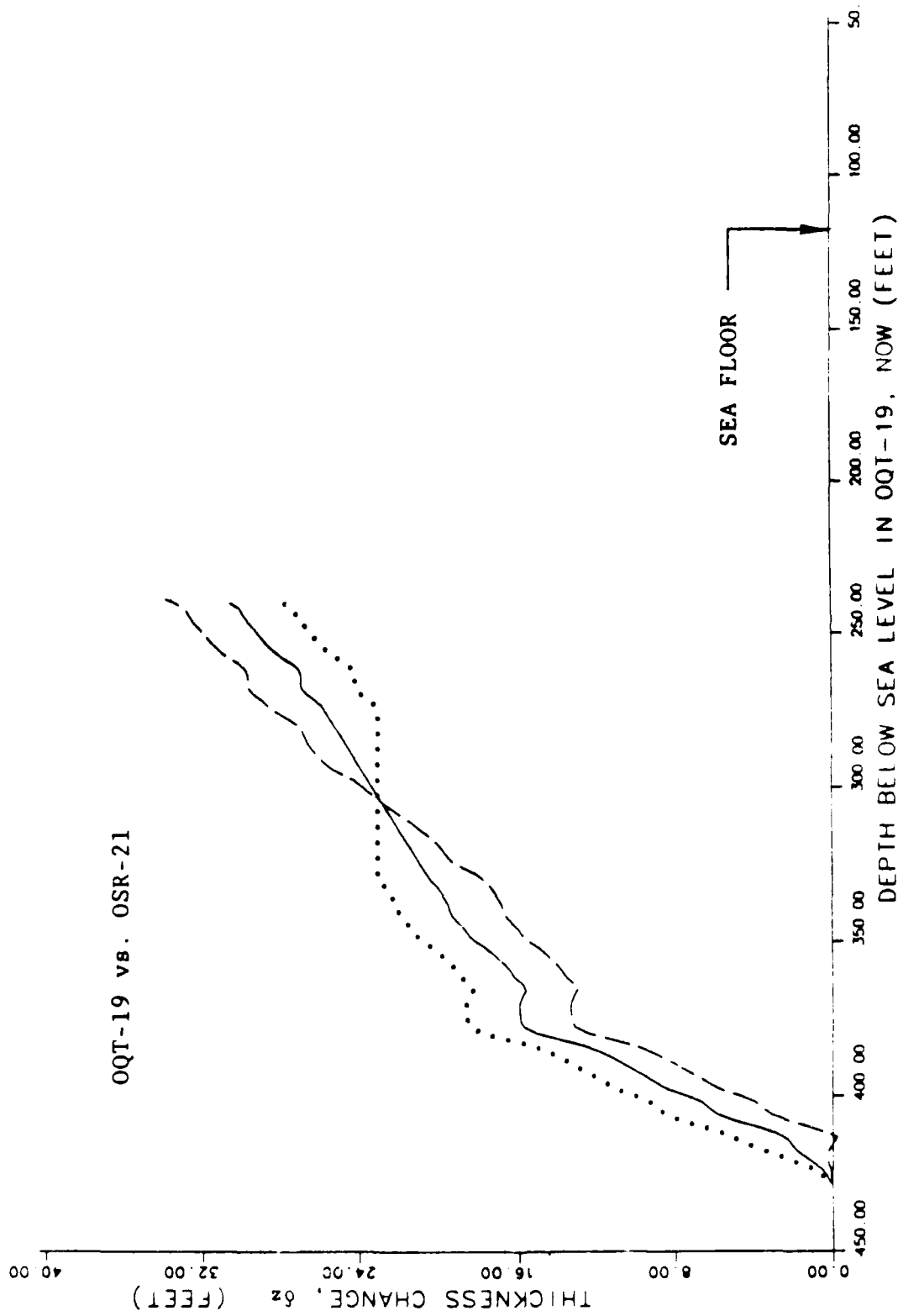


FIGURE 6-31. -- Change in rock thickness from γ - γ densities, assuming simple subsidence. Borehole QQT-19 vs. OSR-21.

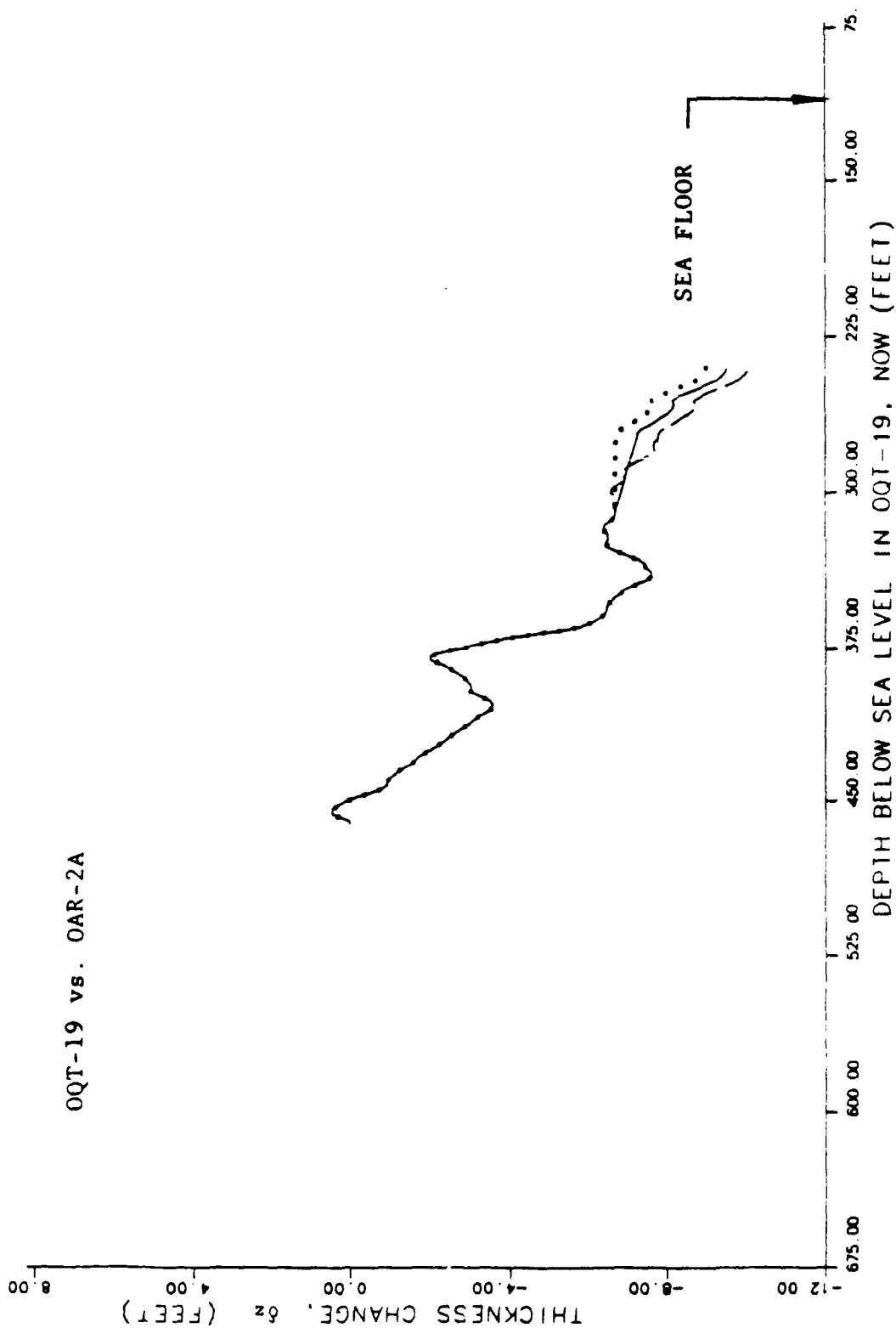


FIGURE 6-32. -- Change in rock thickness from γ - γ densities, assuming simple subsidence. Borehole OQT-19 vs. OAR-2A.

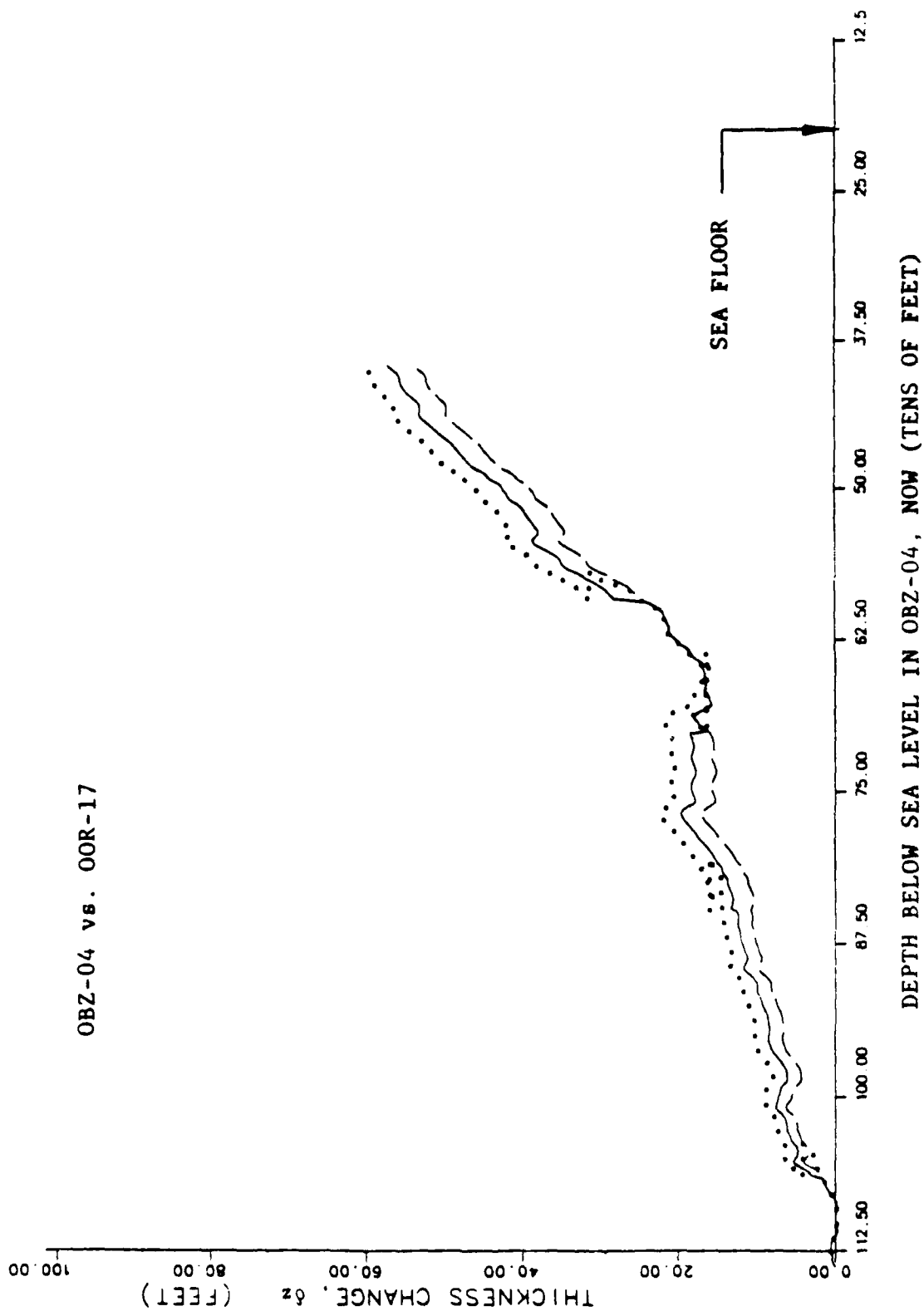


FIGURE 6-33. -- Change in rock thickness from γ - γ densities, assuming simple subsidence. Borehole OBZ-04 vs. OOR-17.

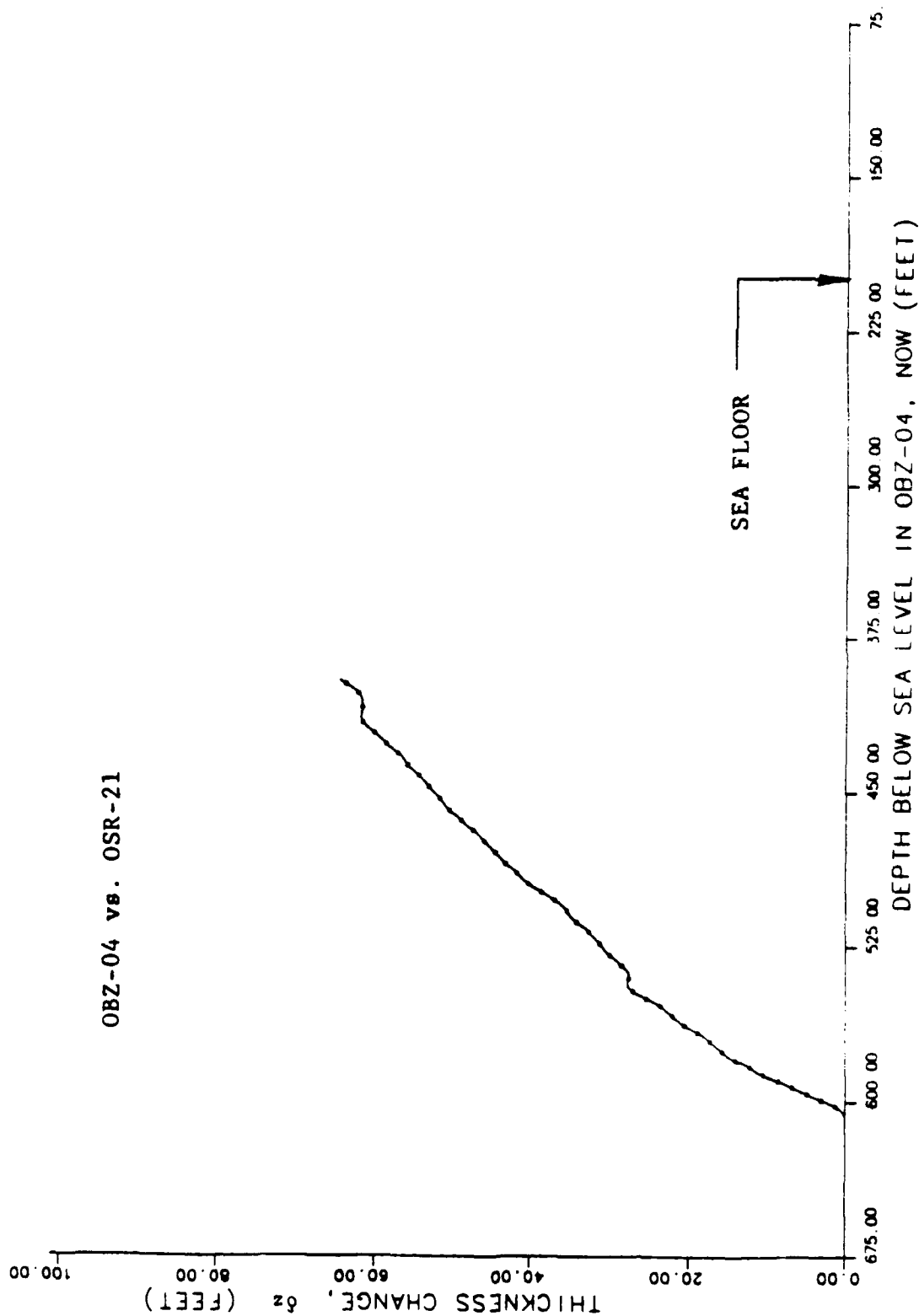


FIGURE 6-3+. -- Change in rock thickness from γ - γ densities, assuming simple subsidence. Borehole OBZ-04 vs. OSR-21.

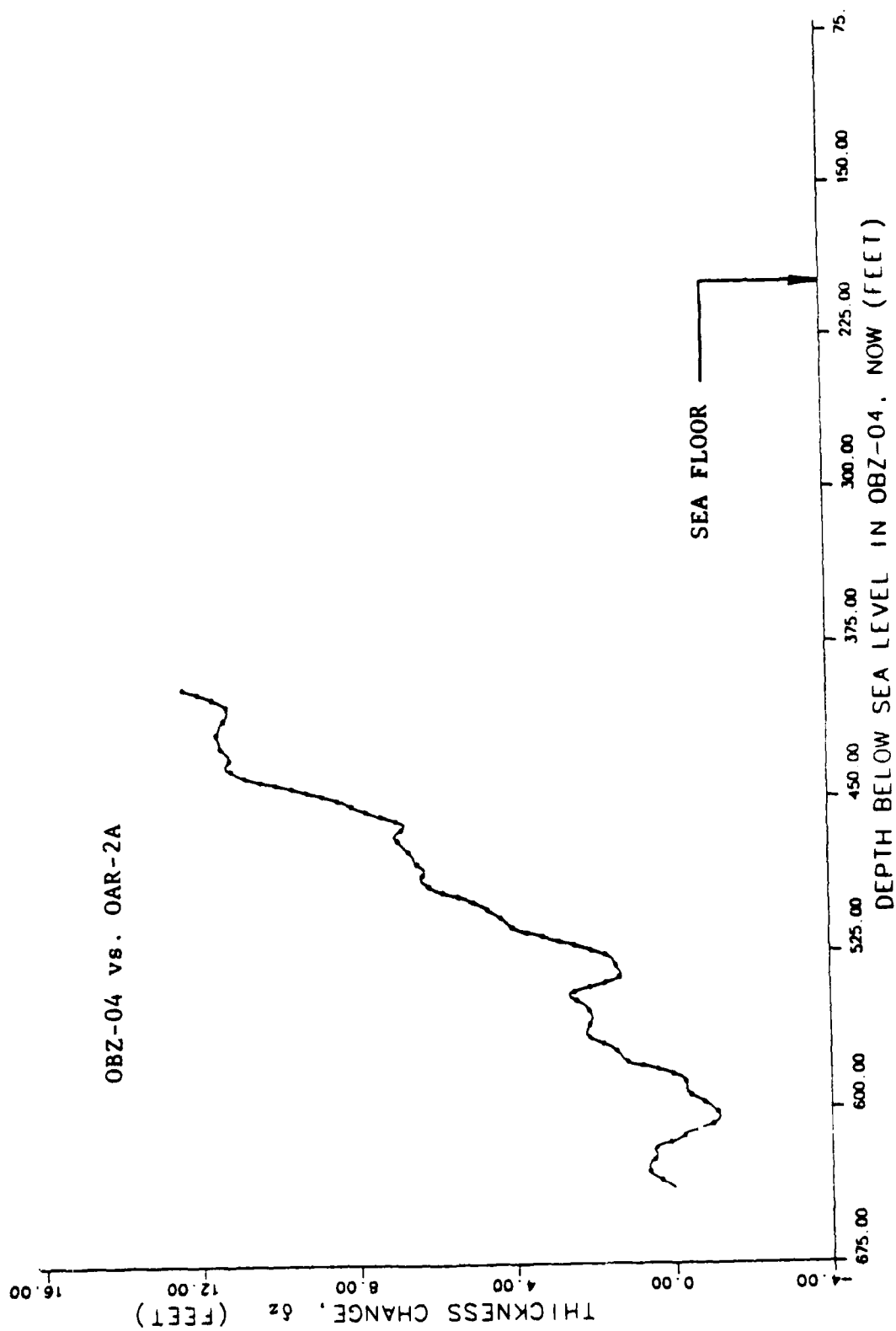


FIGURE 6-35. -- Change in rock thickness from γ - γ densities, assuming simple subsidence. Porehole OBZ-04 vs. OAR-2A.

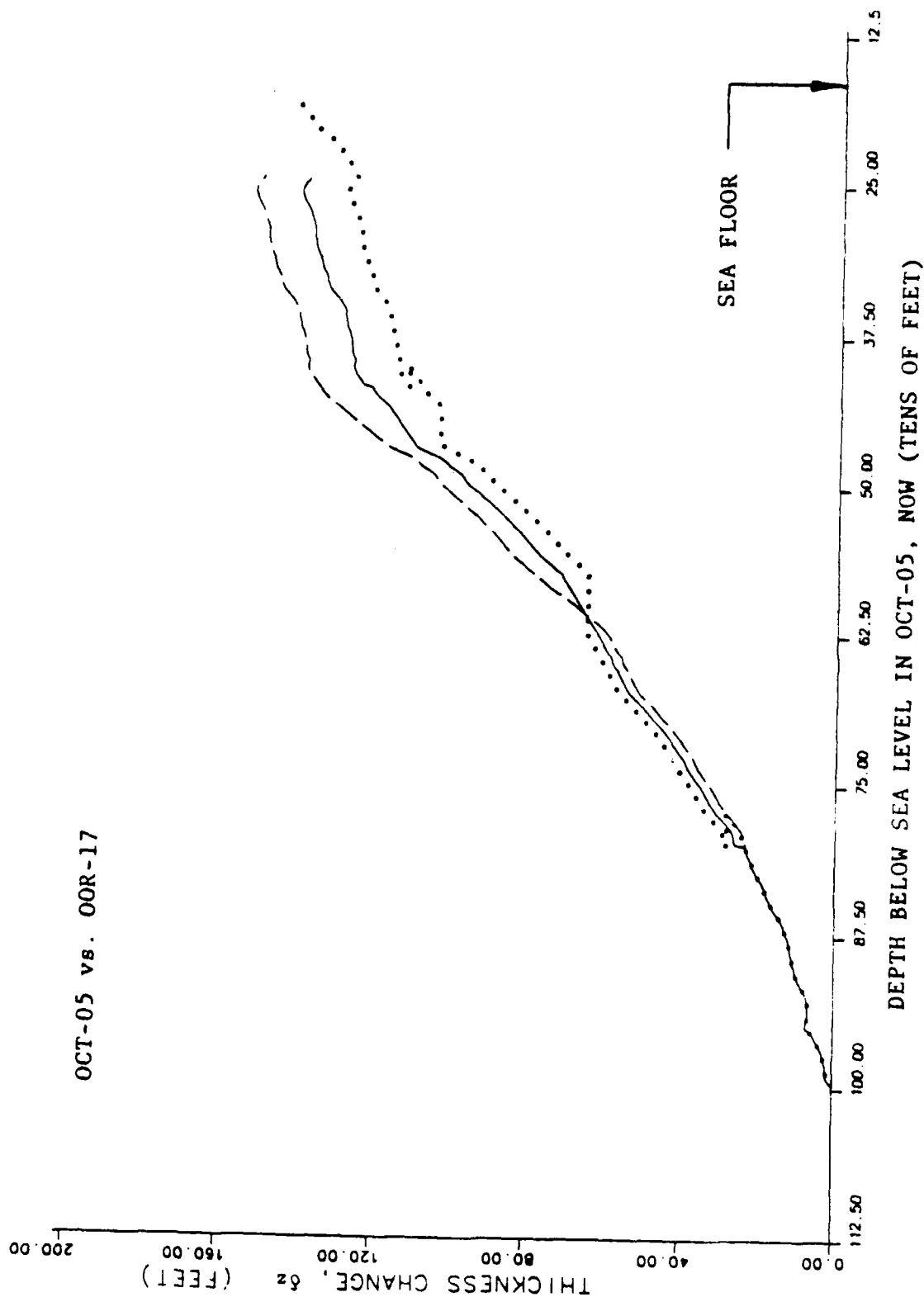


FIGURE 6-36. -- Change in rock thickness from γ - γ densities, assuming simple subsidence. Borehole OCT-05 vs. OOR-17.

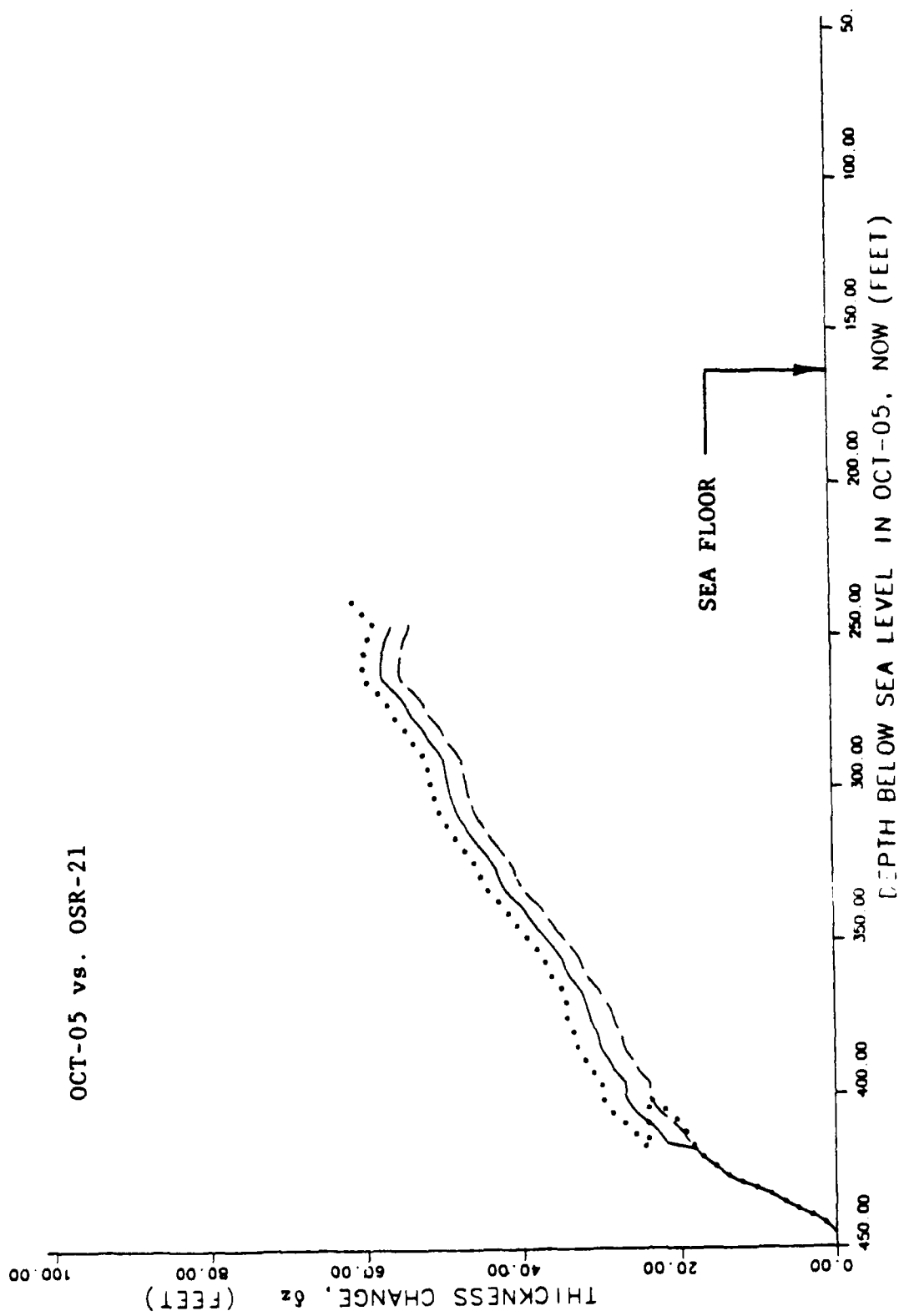


FIGURE 6-37. -- Change in rock thickness from γ - γ densities, assuming simple subsidence. Borehole OCT-05 vs. OSR-21.

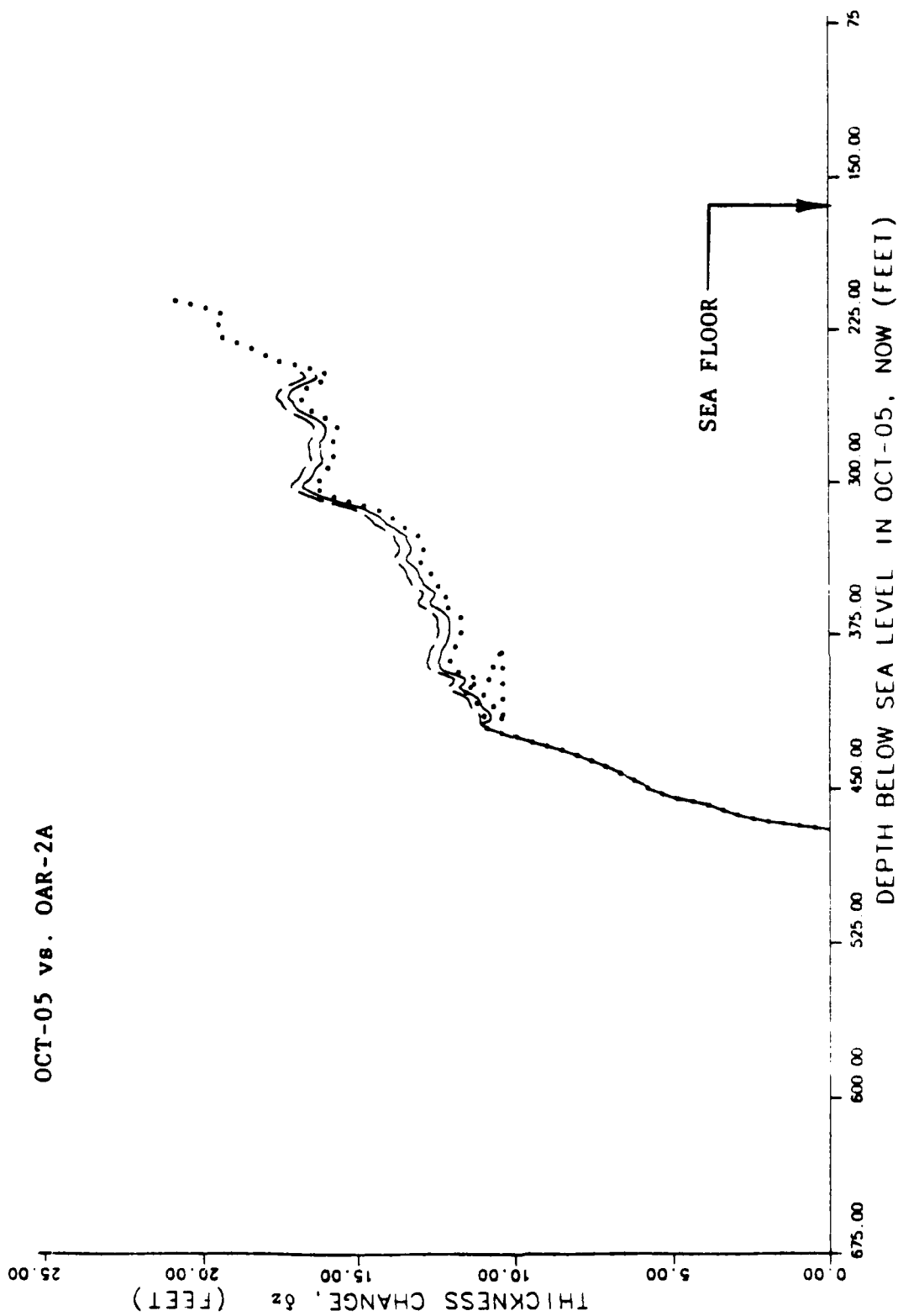


FIGURE 6-38. -- Change in rock thickness from γ - γ densities, assuming simple subsidence. Borehole OCT-05 vs. OAR-2A.

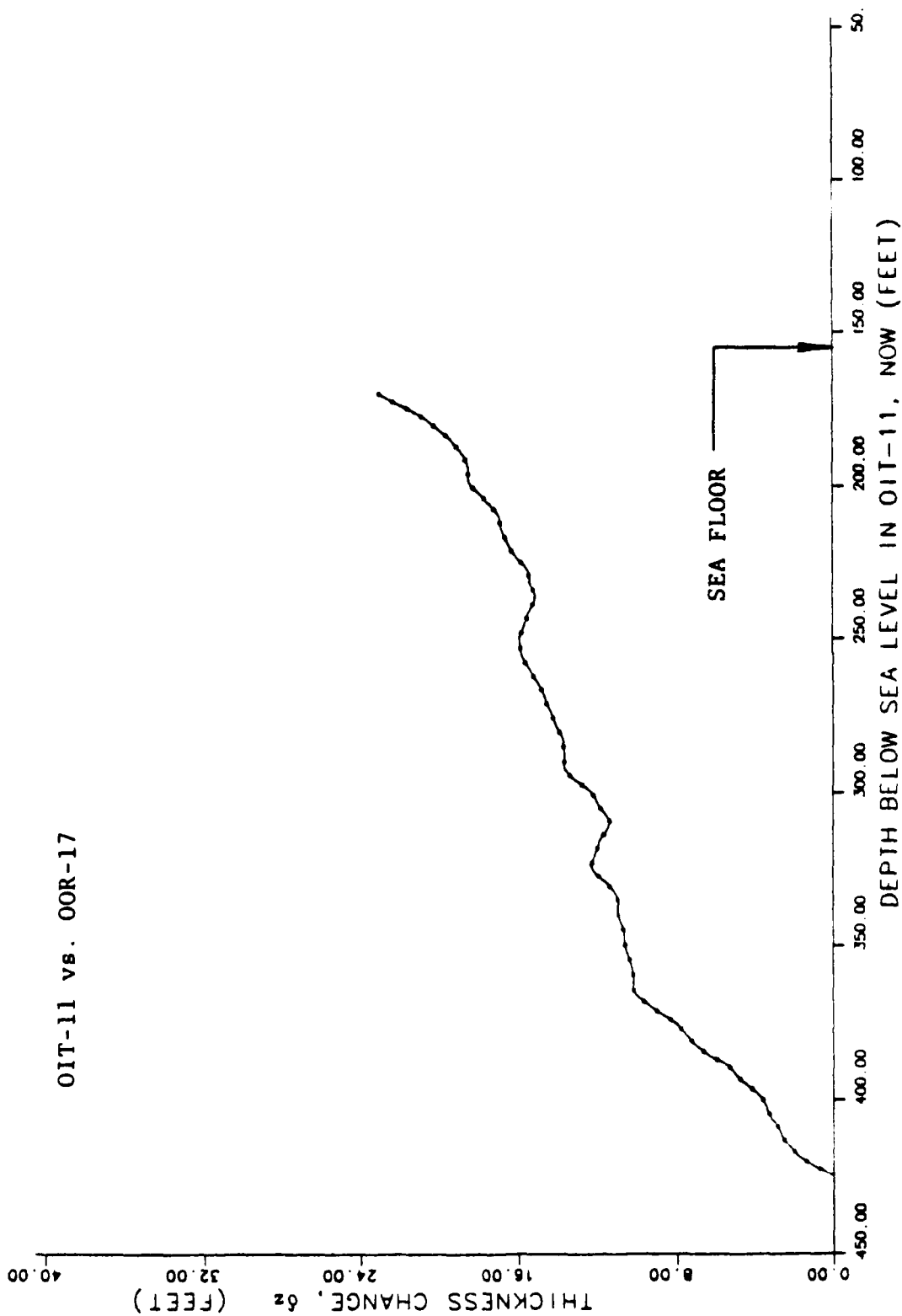


FIGURE 6-39. -- Change in rock thickness from γ - γ densities, assuming simple subsidence. Borehole OIT-11 vs. OOR-17.

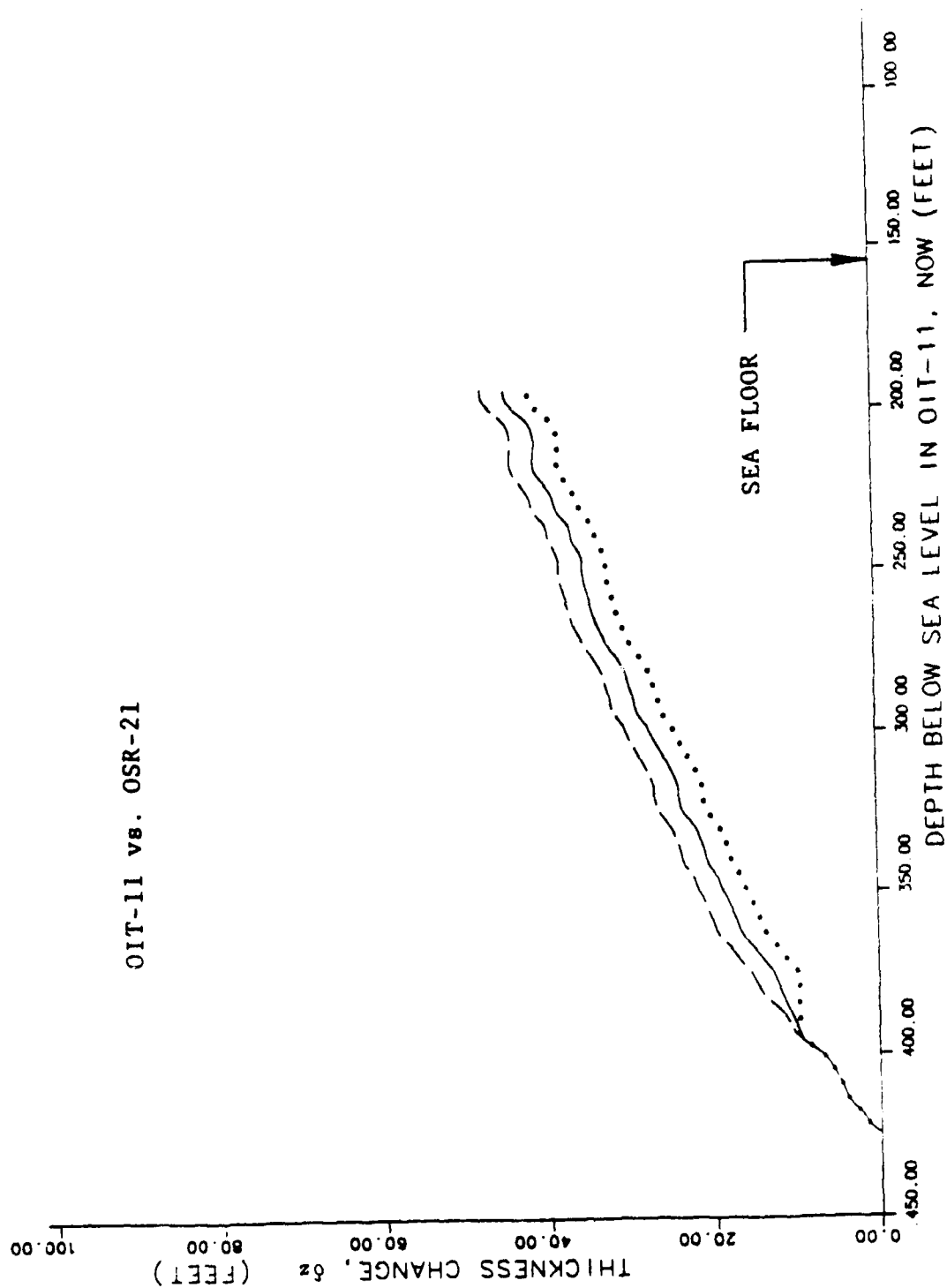


FIGURE 6-40. -- Change in rock thickness from γ - γ densities, assuming simple subsidence. Borehole OIT-11 vs. OSR-21.

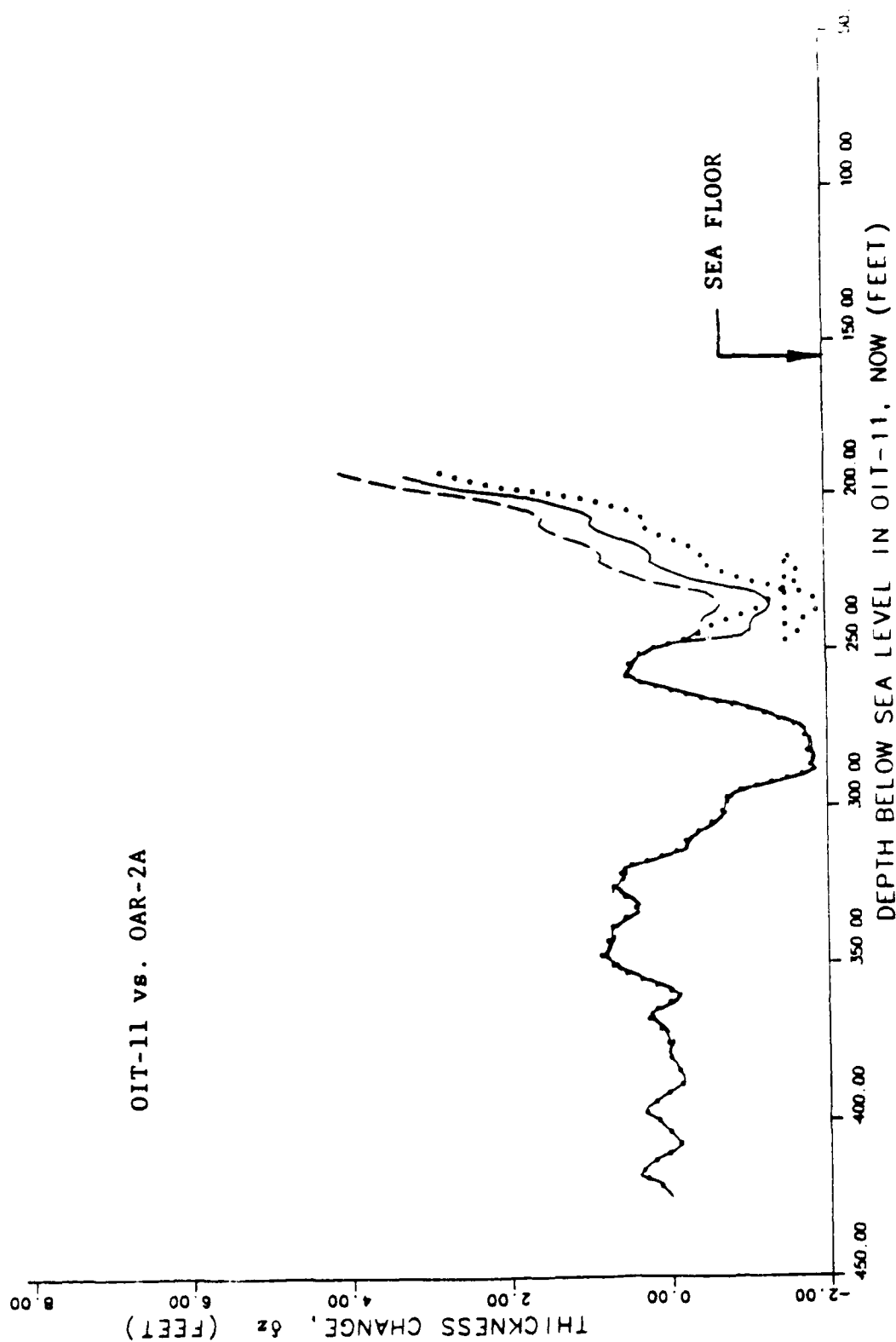


FIGURE 6-41. -- Change in rock thickness from γ - γ densities, assuming simple subsidence. Borehole OIT-11 vs. OAR-2A.

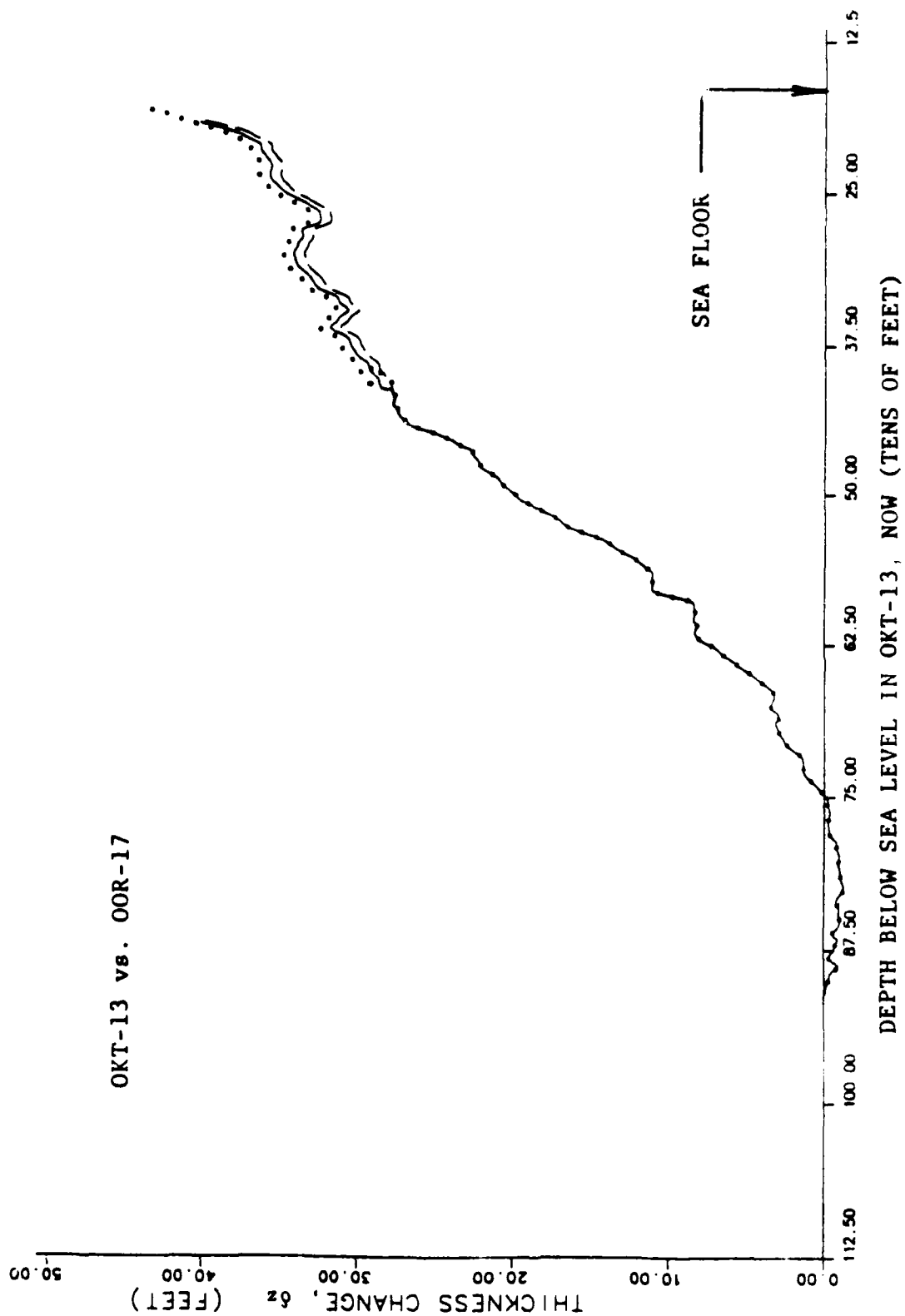


FIGURE 6-42. -- Change in rock thickness from γ - γ densities, assuming simple subsidence. Borehole OKT-13 vs. OOR-17.

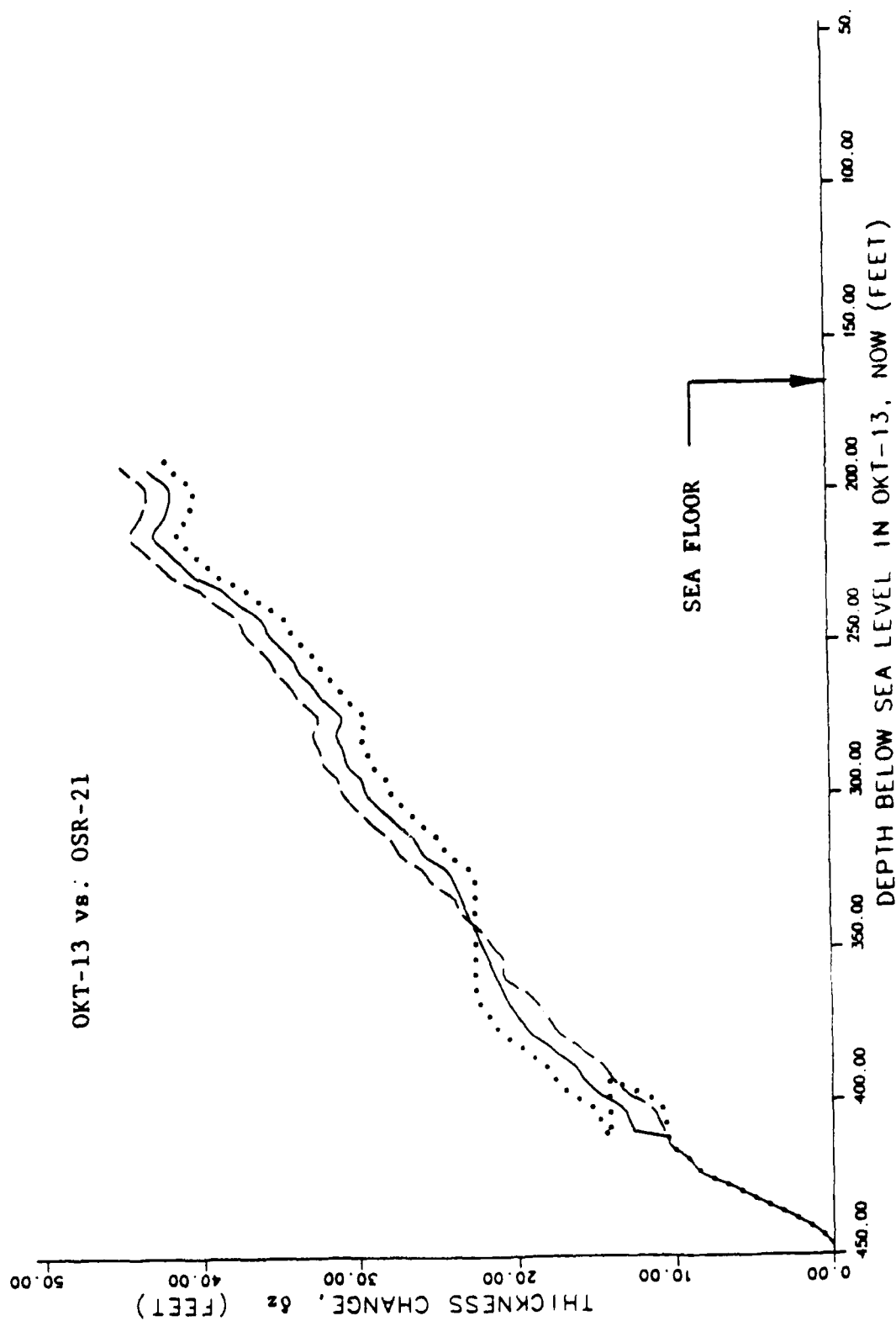


FIGURE 6-43. -- Change in rock thickness from γ - γ densities, assuming simple subsidence. Borehole OKT-13 vs. OSR-21.

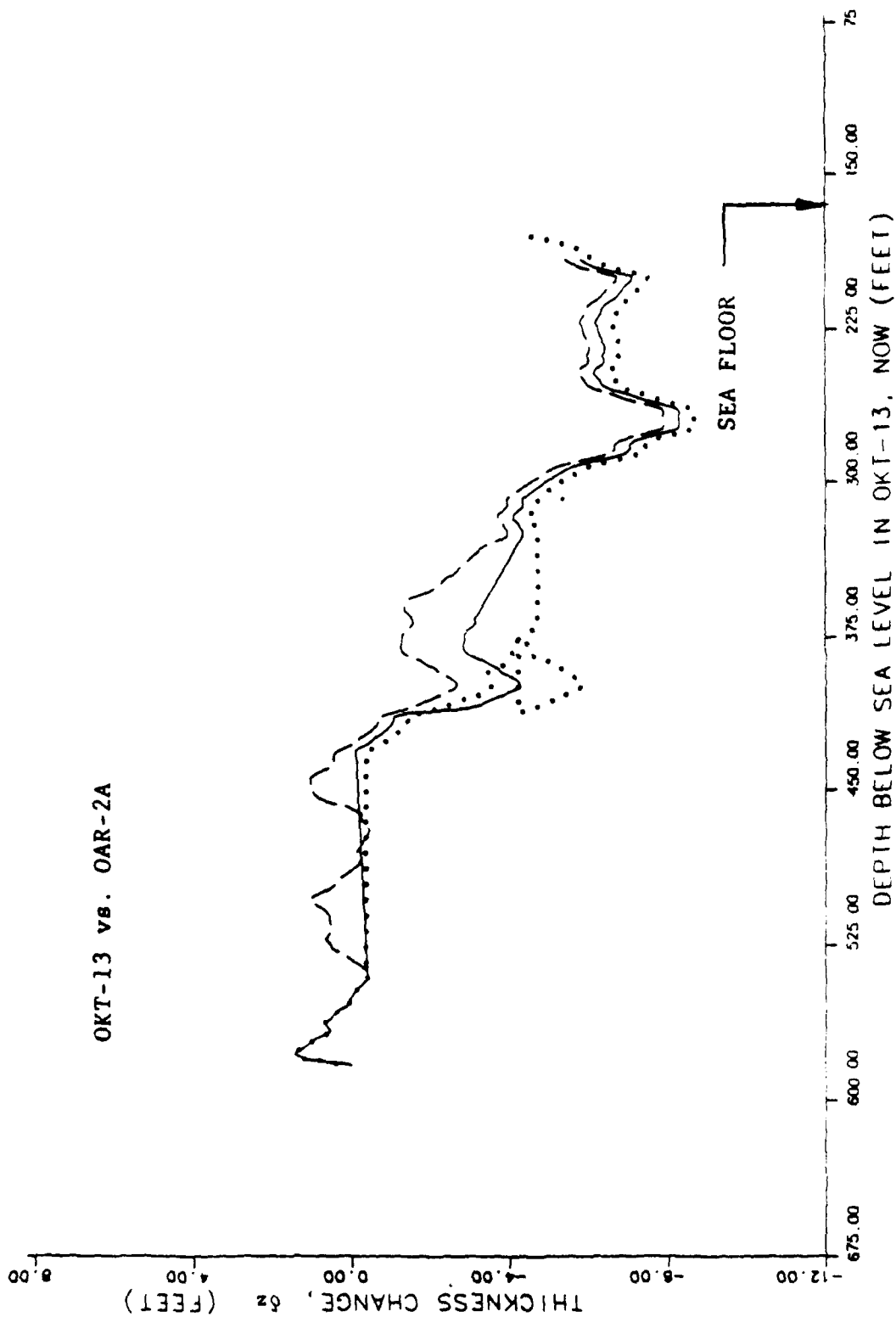


FIGURE 6-44. -- Change in rock thickness from γ - γ densities, assuming simple subsidence. Borehole OKT-13 vs. OAR-2A.

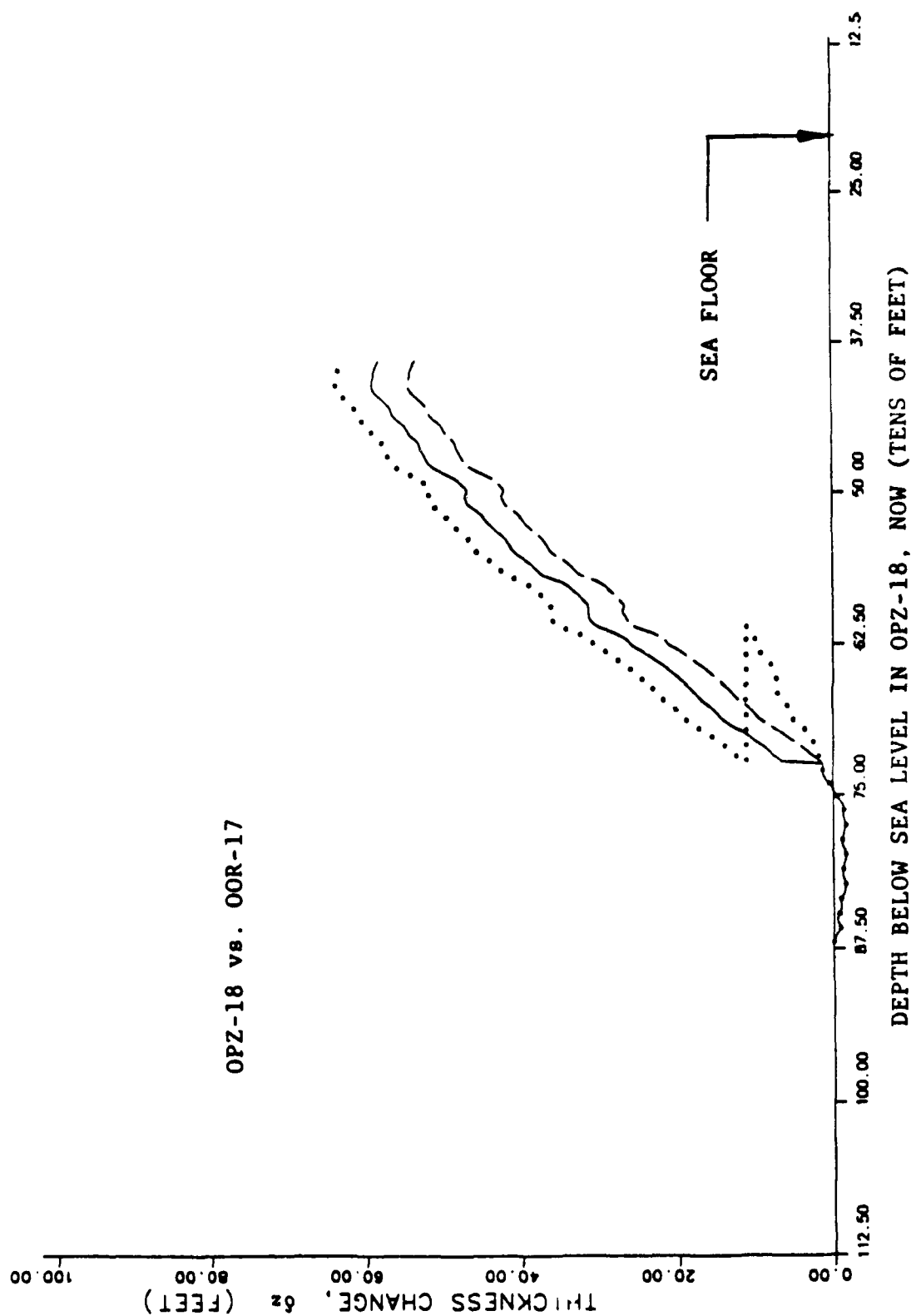


FIGURE 6-45. -- Change in rock thickness from Y-Y densities, assuming simple subsidence. Borehole OPZ-18 vs. OOR-17.

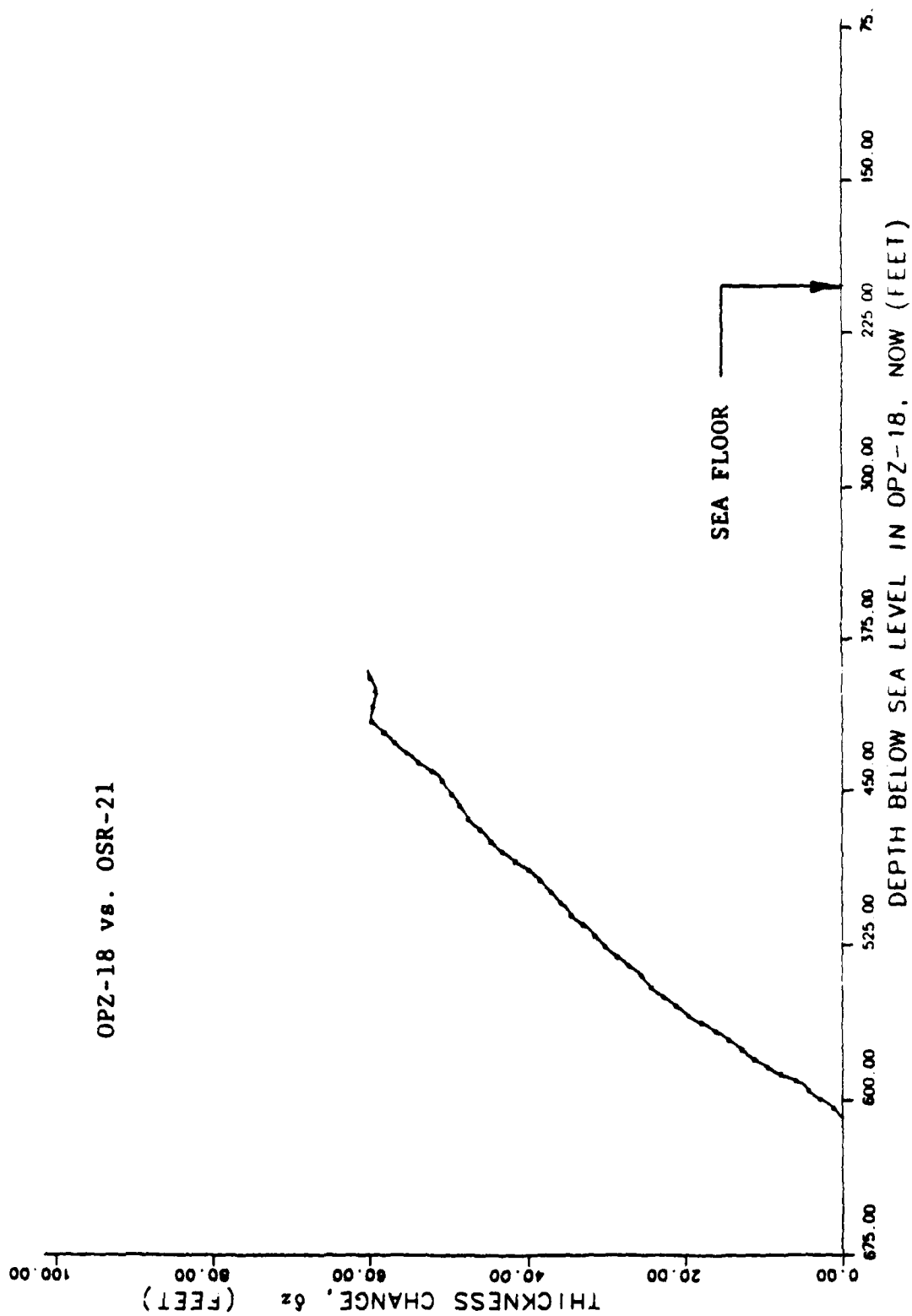


FIGURE 6-46. -- Change in rock thickness from γ - γ densities, assuming simple subsidence. Borehole OPZ-18 vs. OSR-21.

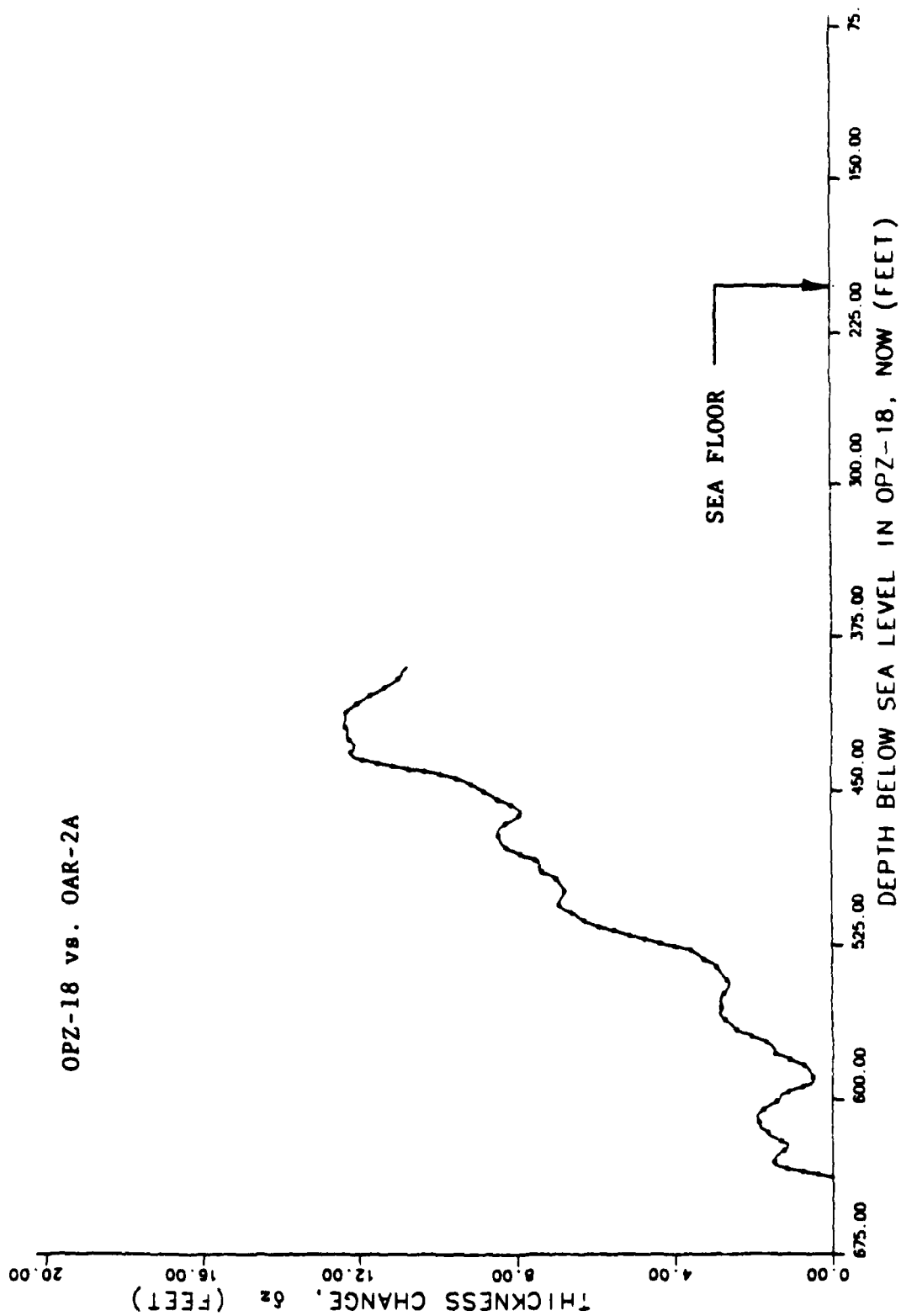


FIGURE 6-47. -- Change in rock thickness from γ - γ densities, assuming simple subsidence. Borehole OPZ-18 vs. OAR-2A.

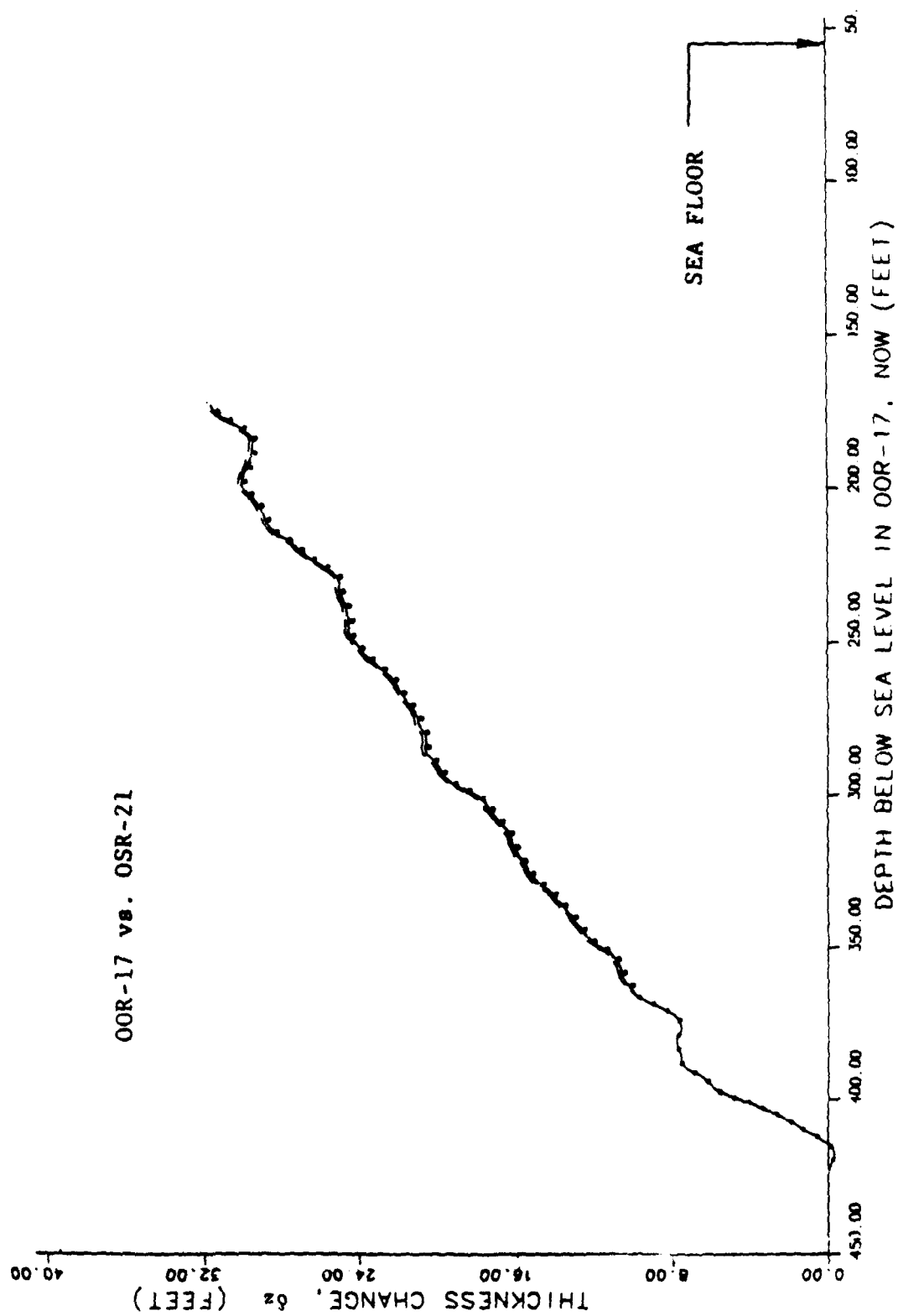


FIGURE 6-48. -- Change in rock thickness from γ - γ densities, assuming simple subsidence. Borehole 00R-17 vs. OSR-21.

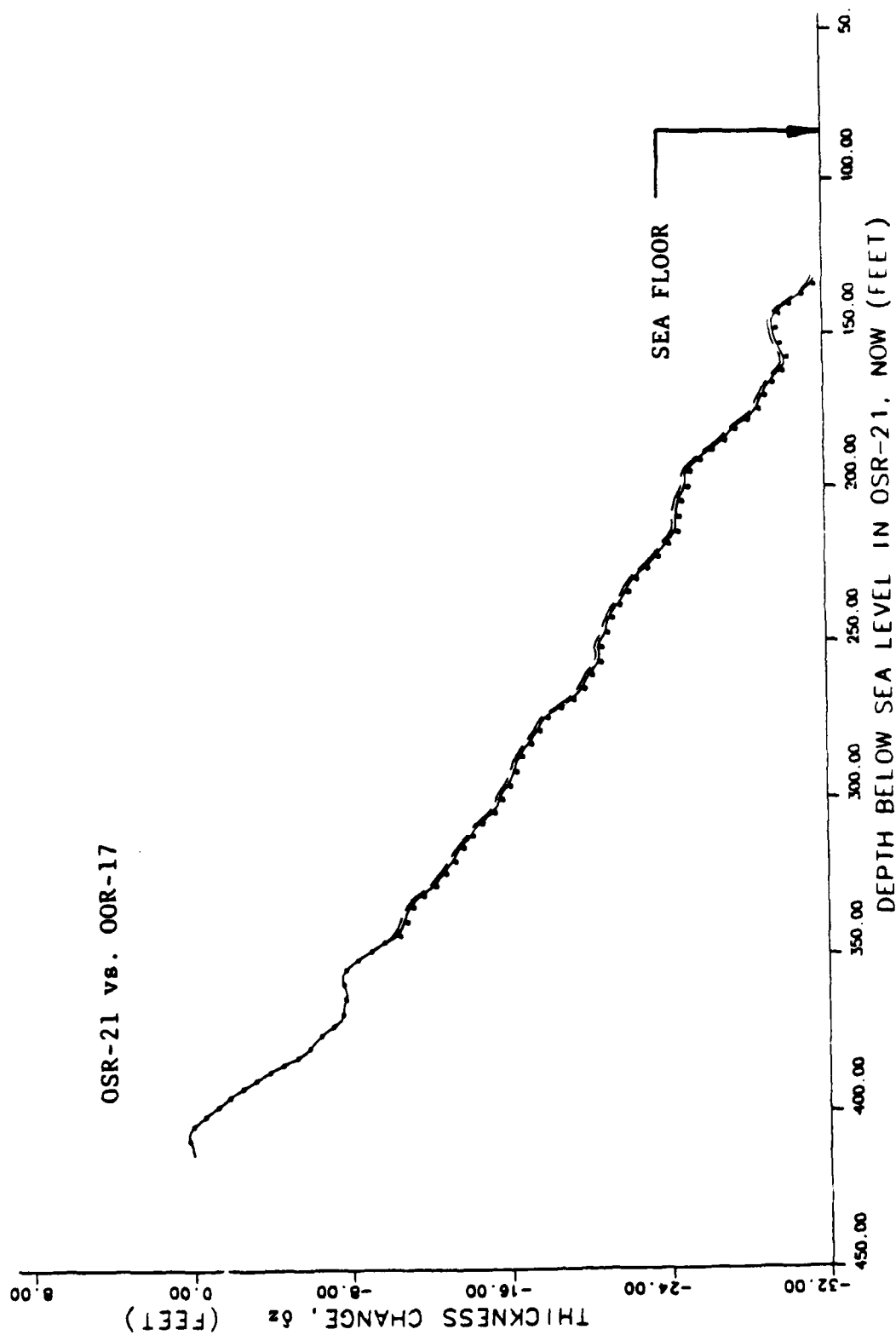


FIGURE 6-49. -- Change in rock thickness from γ - γ densities, assuming simple subsidence. Borehole OSR-21 vs. OOR-17.

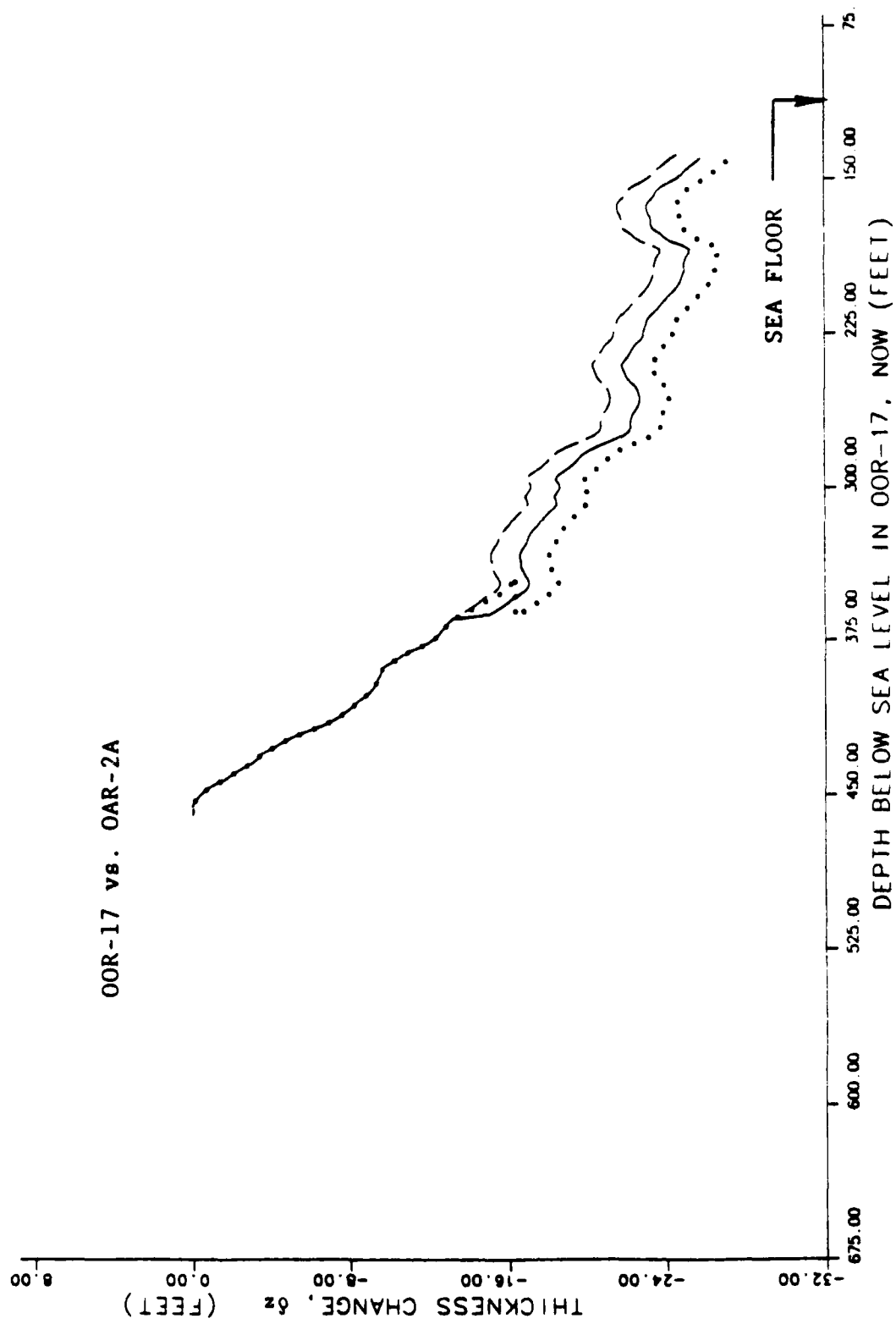


FIGURE 6-50. -- Change in rock thickness from γ - γ densities, assuming simple subsidence. Borehole OOR-17 vs. OAR-2A.

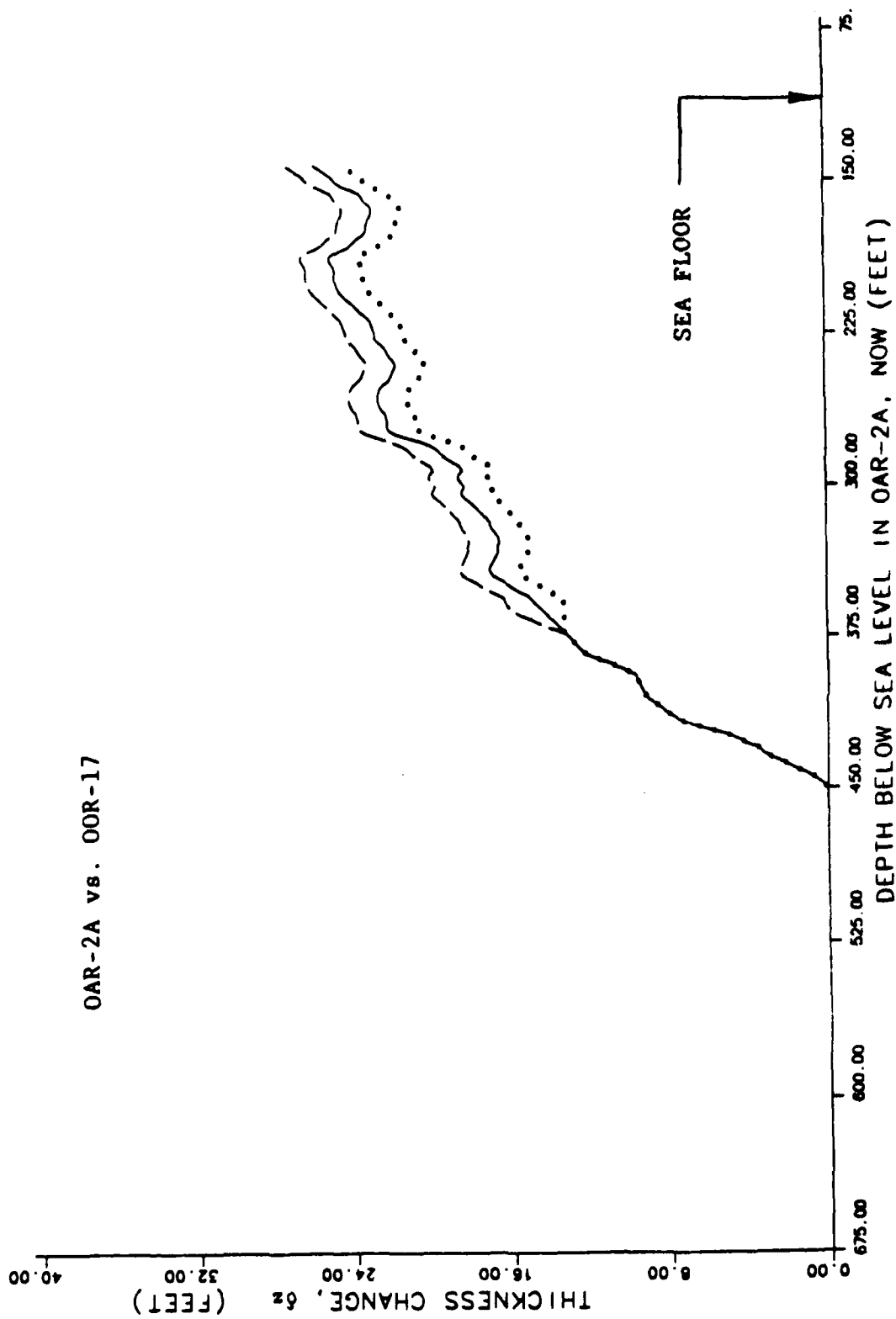


FIGURE 6-51. -- Change in rock thickness from γ - γ densities, assuming simple subsidence. Borehole OAR-2A vs. OOR-17.

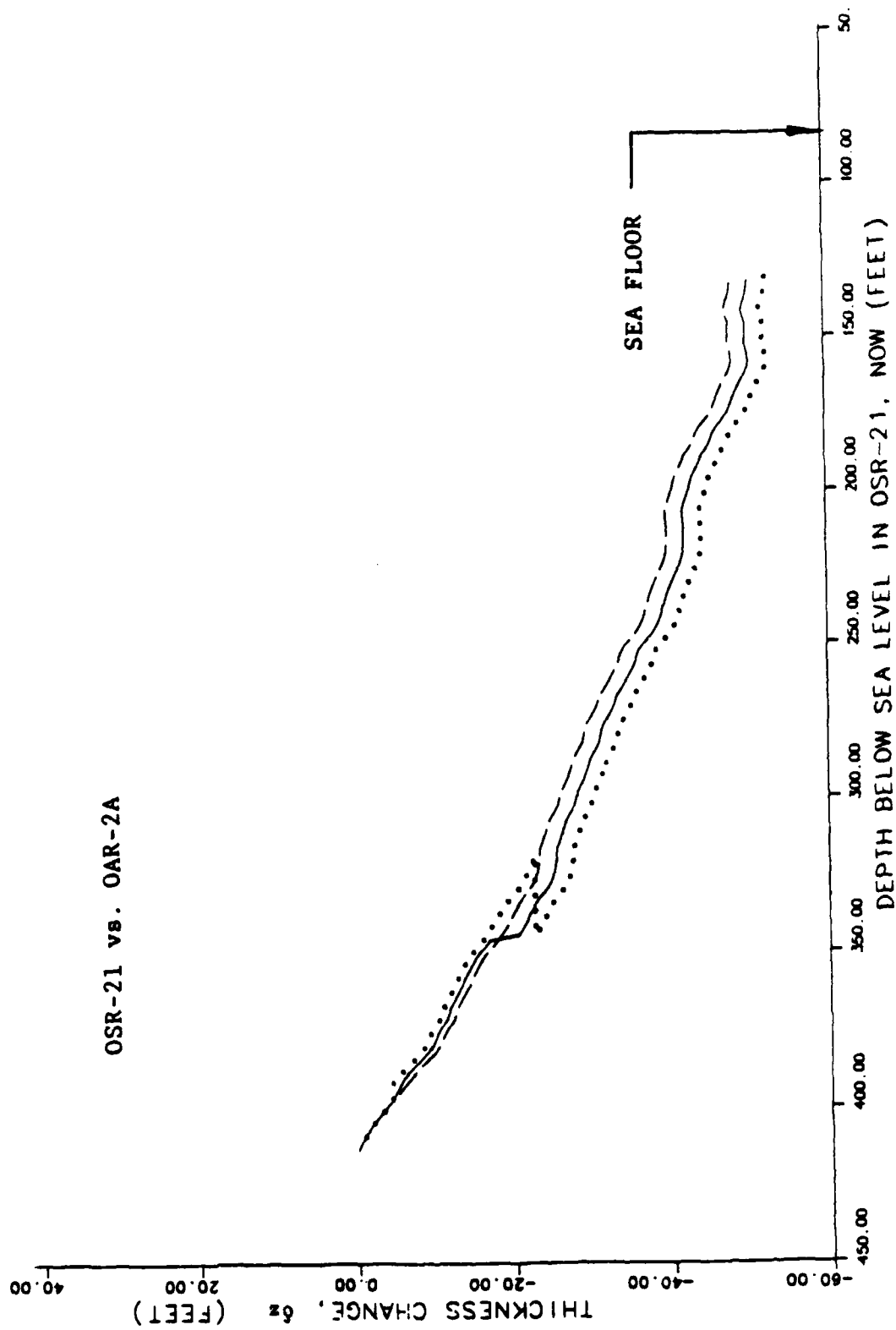


FIGURE 6-52. -- Change in rock thickness from γ - γ densities, assuming simple subsidence. Borehole OSR-21 vs. OAR-2A.

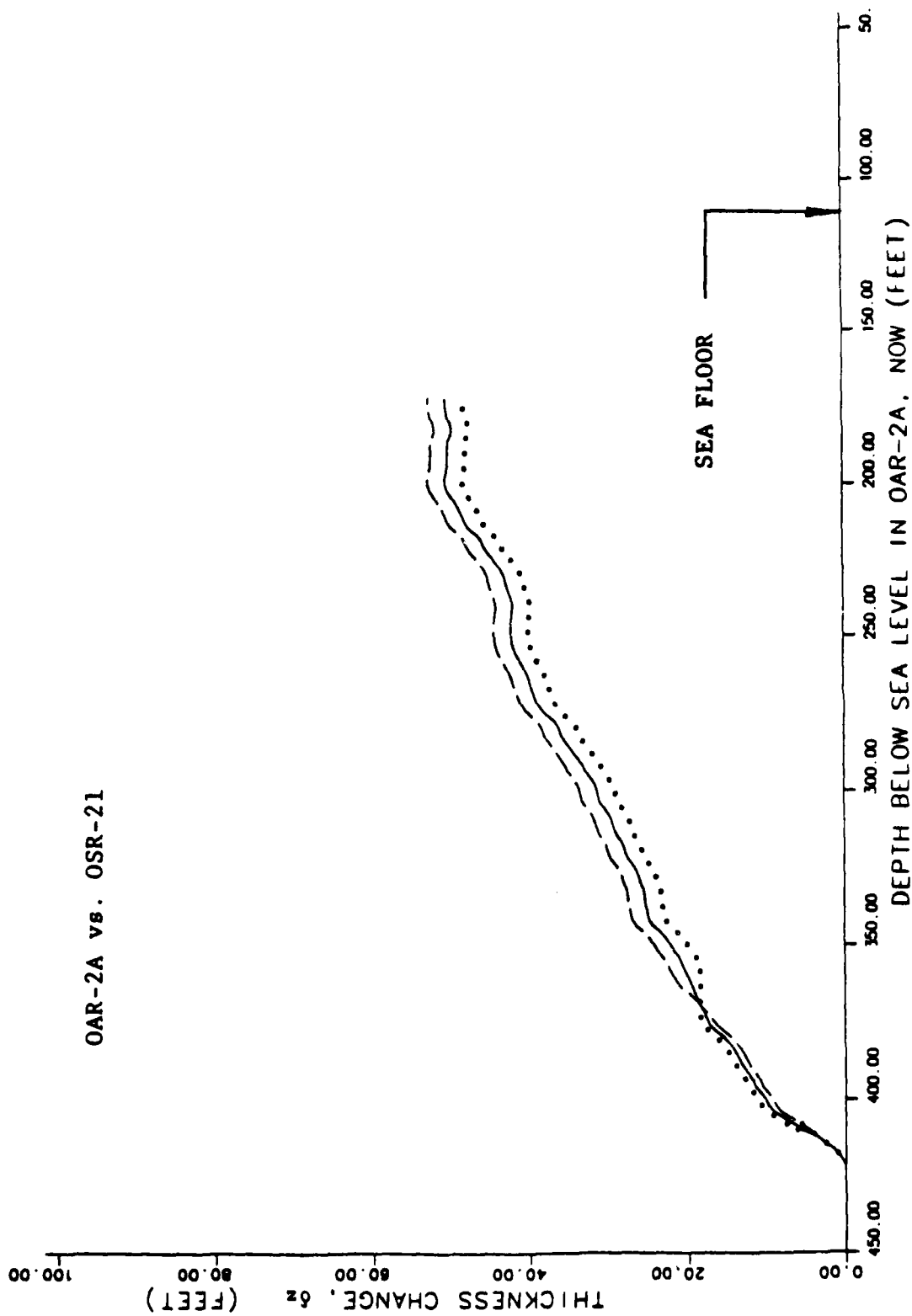


FIGURE 6-53. -- Change in rock thickness from γ - γ densities, assuming simple subsidence. Borehole OAR-2A vs. OSR-21.

CHAPTER 7:
INTEGRATION OF MATERIAL-PROPERTY UNITS, GRAVIMETRY,
AND ADDITIONAL STUDIES OF OAK AND KOA CRATERS

By

Bruce R. Wardlaw¹

INTRODUCTION

Preliminary interpretations of the geology of the OAK and KOA crater areas and of the craters themselves are presented in Wardlaw and Henry (1986a, 1986b). Since those reports, additional information was developed from analyses of borehole gravimetry, paleontologic mixing, thinning, and distribution of shocked calcite, most of which are presented in previous Chapters of the current Open-File Report. These new data require modification of the geologic interpretation of OAK and KOA craters. This Chapter incorporates these new salient data and presents a more comprehensive interpretation than that given by Wardlaw and Henry (1986b). Depths to a few horizons or zones have been reinterpreted, and all pertinent data are presented herein in corrected form as tables. These data supercede all previous information.

The most convenient way to relate the geology to crater phenomenology is to develop geologic material-property units that match the general material-property models for OAK and KOA craters. The geologic framework is reviewed briefly before presentation of the new geologic material-property units (MPs). These units will be used throughout this text in deference to previously used geologic schemes such as the sedimentary packages (SPs) of Wardlaw and Henry (1986a).

PRE-EVENT GEOLOGY OF OAK AND KOA CRATERS

The general stratigraphic sequence of Enewetak Atoll is punctuated by a series of discontinuities within the carbonate sedimentary rock column, of which nine are identified as major disconformities in the upper 1,200 ft (Wardlaw and Henry, 1986a). These major disconformities represent significant exposure and cementation surfaces over most of the atoll. Generally, pervasive cementation is confined to the reef margin (fig. 7-1a), but extends for a considerable distance beneath the lagoon beneath disconformities 5, 8, and 9 (fig. 7-2). Data from the EXPOE Project (Couch and others, 1975), which presents data from shallow boreholes drilled on islands on the reef tract, indicate that the geology is generally similar throughout the reef tract (fig. 7-1c), although the width of the cemented reef margin narrows on the leeward side of the atoll. Cementation also appears to generally decrease in areal distribution in the sequence from disconformity 5 (Pliocene) to disconformity 1

¹ Branch of Paleontology and Stratigraphy,
U.S. Geological Survey, Reston, VA 22092.

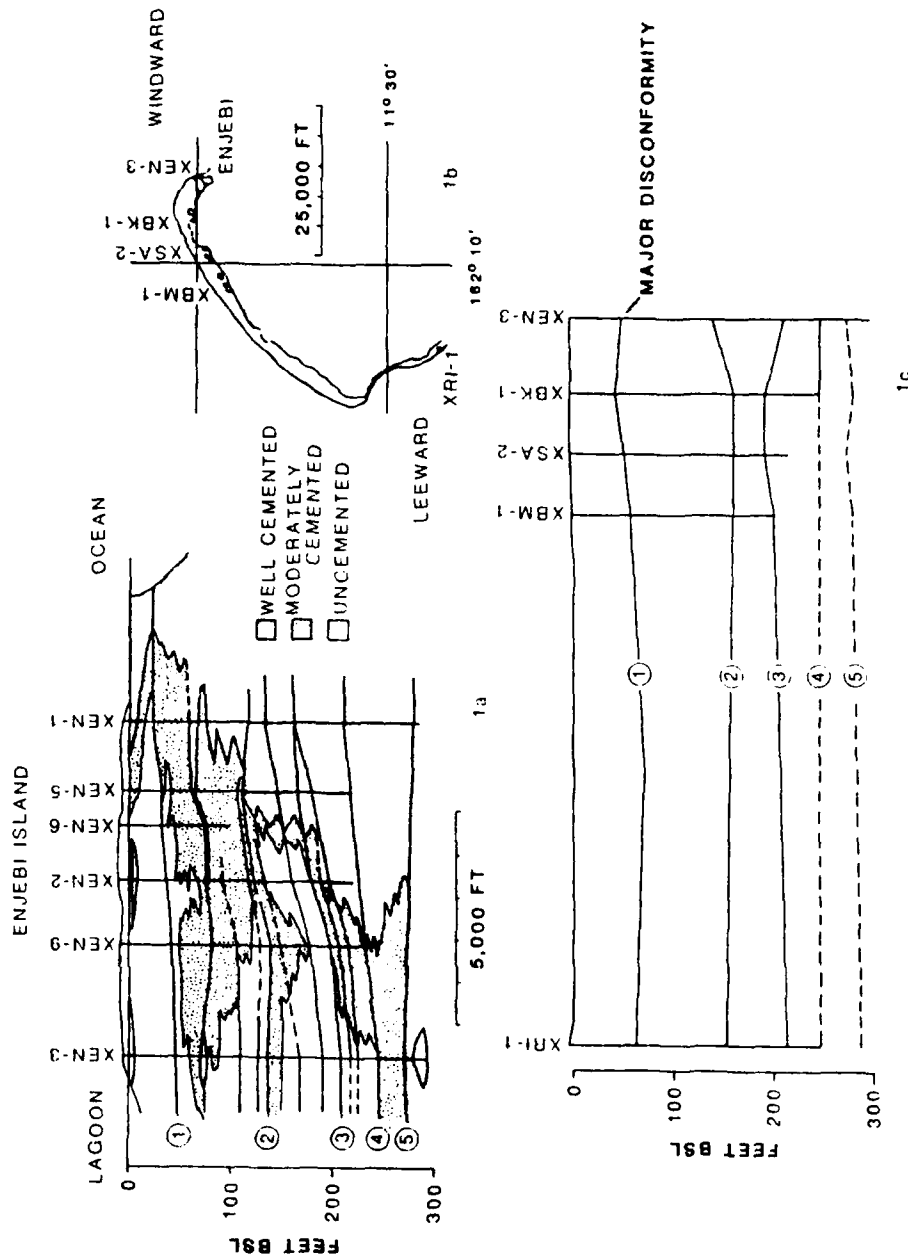


FIGURE 7-1. -- (1a) Distribution of cemented zones in shallow subsurface in transect on Enjebi Island from reef to lagoon from EXPOE cores (modified from Ristvet and others, 1978). (1b) Location of boreholes for 1c. (1c) Relationship of major discontinuities (1-5) in shallow subsurface on northern and western portion of Enewetak Atoll.

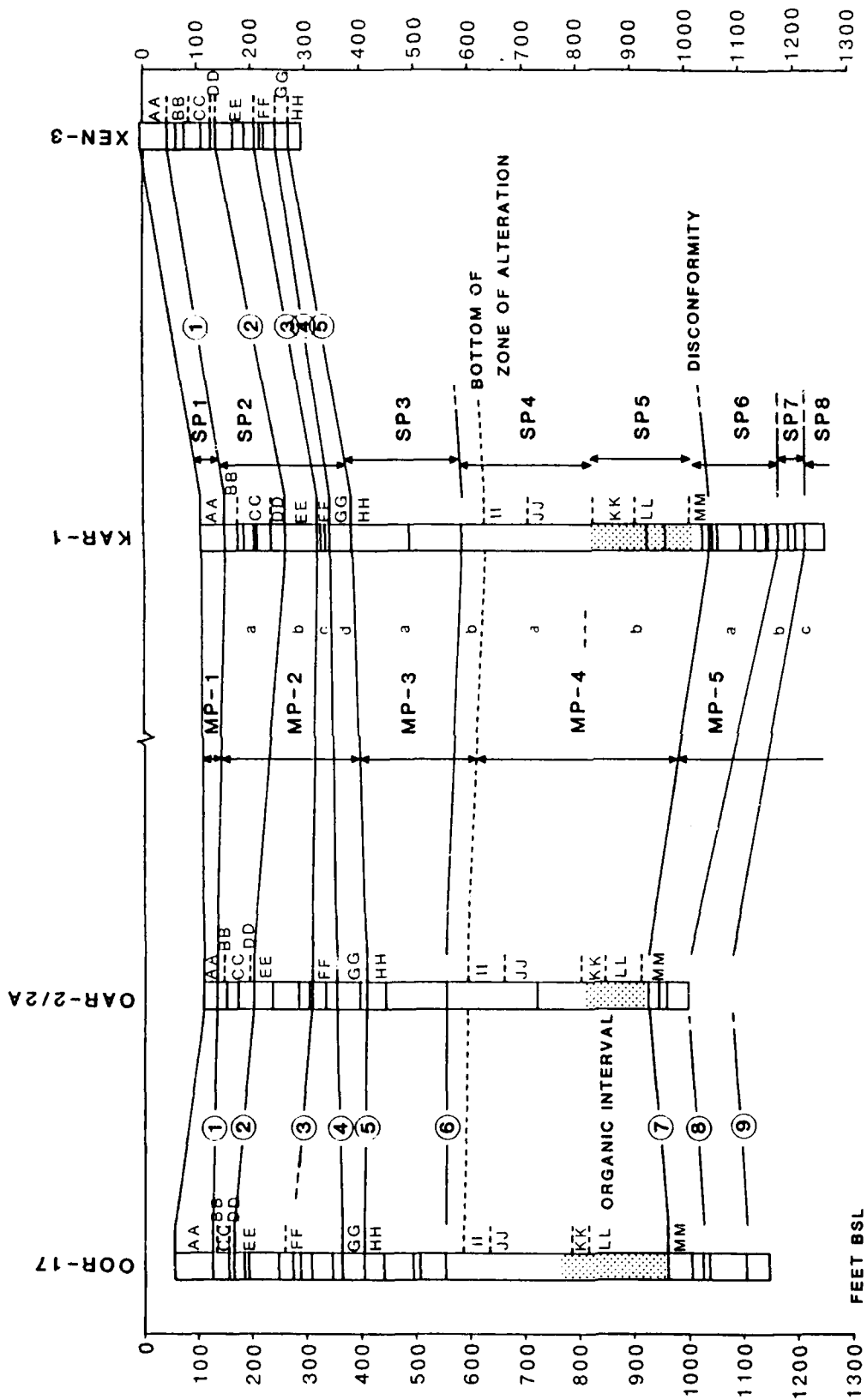


FIGURE 7-2. -- Relationship of discontinuities (shown in columns), major discontinuities (1-9), biostratigraphic zones (AA-MM), material property units (MP-1 to MP-5), and sedimentary packages (SP-1 to SP-8) in reference boreholes. Highly organic zone (SP5) is stippled in columns.

(Pleistocene) as represented in the cross section of Figure 7-1a. From disconformity 1 to the present surface, the area of cementation has increased (fig. 7-1a).

The major disconformities (Wardlaw and Henry, 1986a) and the biostratigraphic zones, based on the distribution of microfossils presented by Cronin, Brouwers, and others (1986), generally correlate readily from borehole to borehole and extend throughout the area of investigation (fig. 7-2). The sedimentary packages (SP) delimited by these disconformities (Wardlaw and Henry, 1986a) and the geologically defined material-property units (MP) proposed herein also are shown on Figure 7-2. The consistency and trends of the disconformities, the SP and MP units, and biostratigraphic zones allow reasonable prediction of pre-shot ground-zero geology for both OAK and KOA. The relationship of discontinuities, cementation zones, and general sediment type for the PEACE Program reference boreholes and the models of ground-zero geology for both OAK and KOA are shown in Figure 7-3. Excellent seismic-reflection profiles (Grow and others, 1986) allow mapping of key surfaces in the undisturbed areas away from the craters, and, combined with the pre-shot geologic models, allow mapping of the probable distribution of these surfaces in a pre-shot configuration below the crater (Wardlaw and Henry, 1986b). Figure 7-4 shows the probable pre-shot surfaces at the top of the Pleistocene (disconformity 1) and at the top of the Pliocene (disconformity 5) in the KOA and OAK areas.

The most convenient way to summarize the geology for crater considerations is in material-property (MP) units. These are units delimited by major geologic horizons that best fit the material model (viz, the geologically defined units that best conform to the mechanical properties important to cratering). Differences between the sedimentary packages (SP) and material-property units are minor (see below) but include, for example, the pervasively cemented zone that includes SP3 and the upper part of SP4 is represented as a single unit (MP-3), although it is divided by a major disconformity (6) that represents a significant exposure surface and geologic gap.

The upper 1,200 feet of sedimentary section at Enewetak is divided into five material-property units (fig. 7-3), as follows:

- MP-1** (Holocene, Sedimentary Package 1). -- Aragonitic sediments, from the surface to disconformity 1.
- MP-2** (Pleistocene, SP 2). -- Aragonitic sediments with thin calcitic limestones, from disconformity 1 to 5. This unit is subdivided by disconformities 2, 3, and 4.
- MP-3** (Upper Pliocene, SP 3 and part of SP 4). -- Cemented interval of vuggy, calcitic limestone and aragonitic or calcitic sands, from disconformity 5 to the base of the alteration zone (see Wardlaw and Henry, 1986b, p. 25 for discussion of alteration zone). This unit is subdivided by disconformity 6.
- MP-4** (Upper Miocene-Pliocene, part of SP 4, all of SP 5). -- Aragonitic sands, from base of the alteration zone to disconformity 7. High organic content and high activity on the natural gamma logs identifies a lower subunit.
- MP-5** (Miocene, SP 6, SP 7, and SP 8). -- Calcitic sands and limestones, limestone variably developed, from disconformity 7 to bottom of boreholes. This unit is subdivided by disconformities 8 and 9.

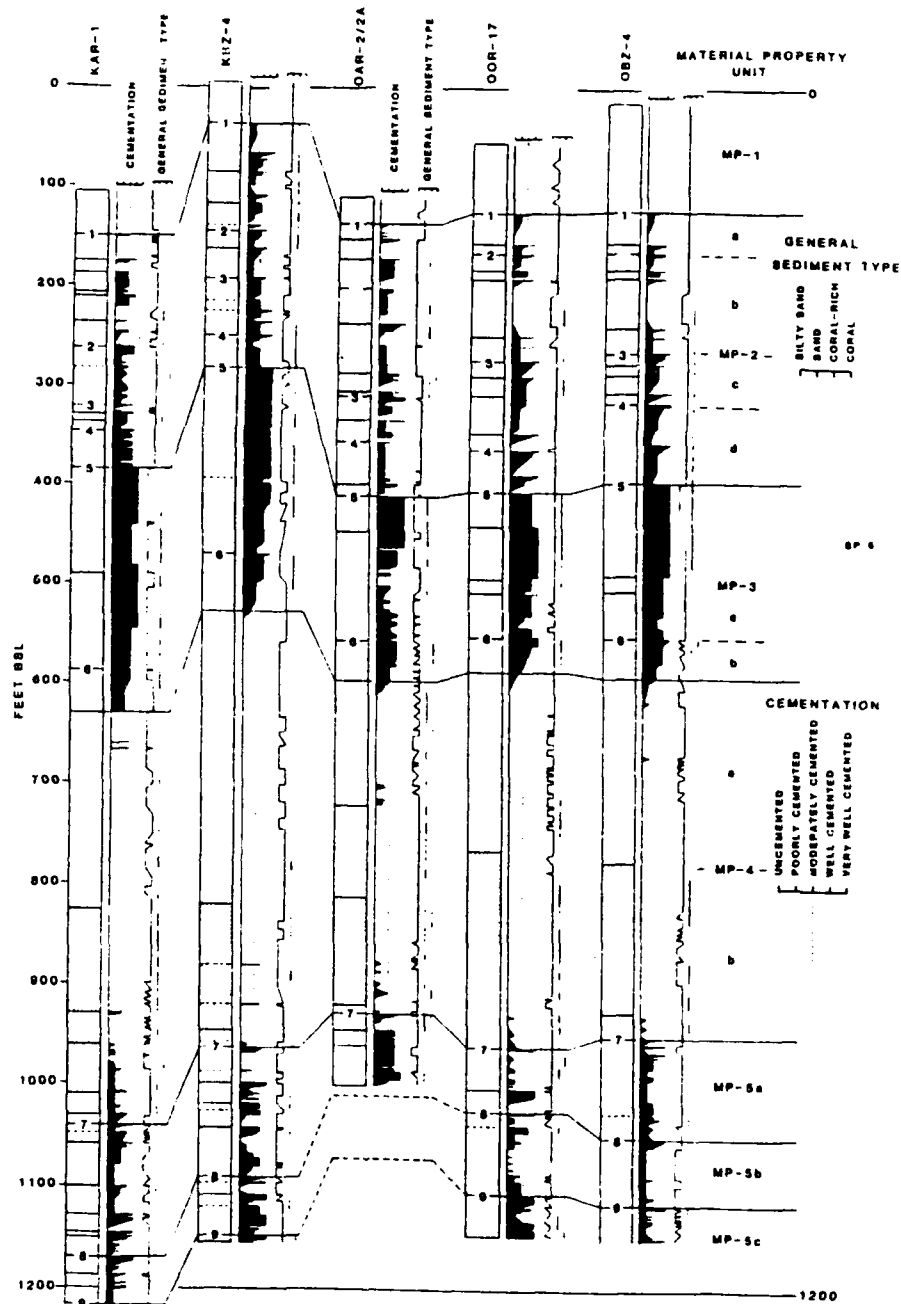


FIGURE 7-3. -- Characterization of cementation and general sediment type and relationship to material property units for reference boreholes and models for ground-zero geology. Discontinuities as lines in columns, major disconformities numbered in columns.

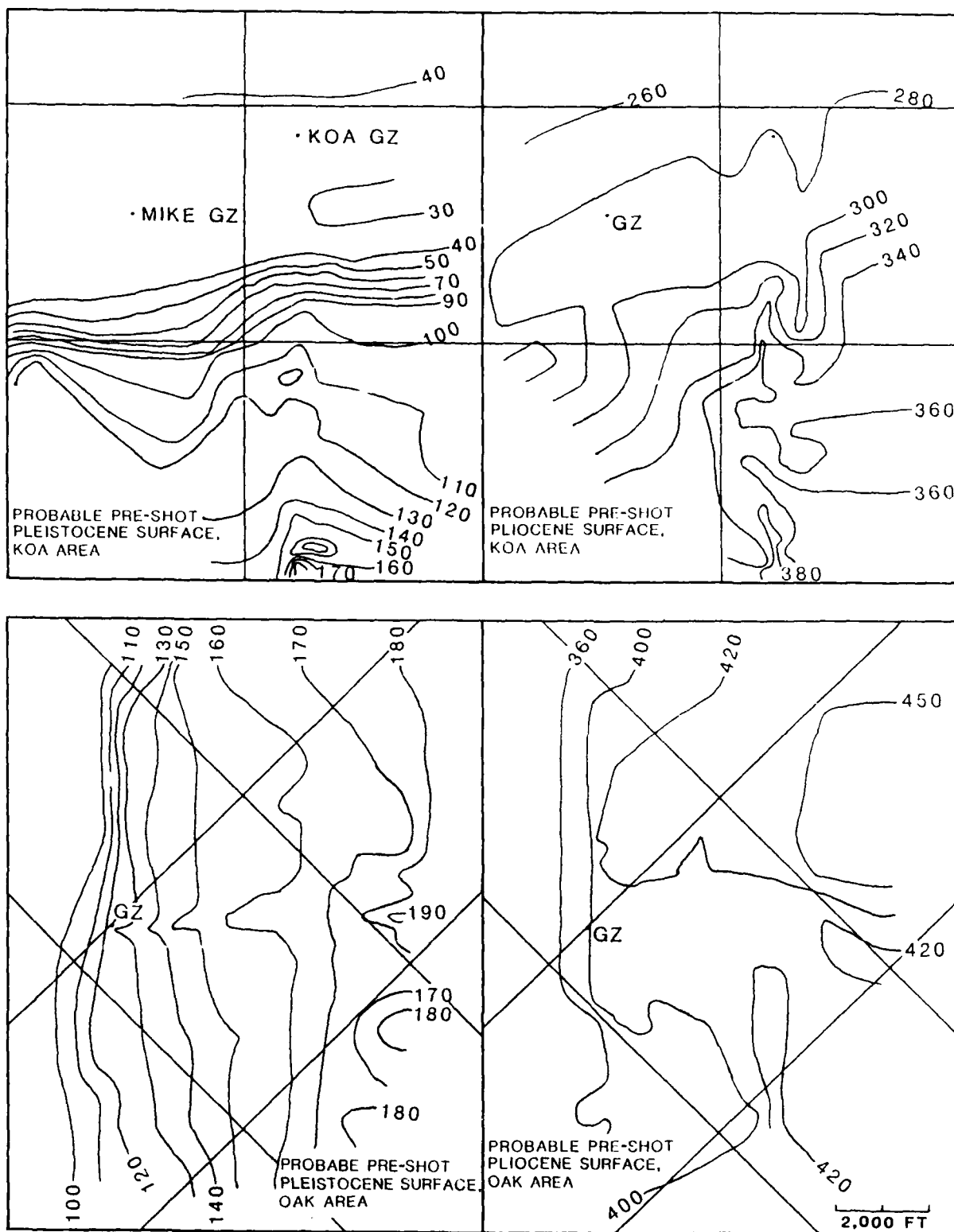


FIGURE 7-4. -- Probable pre-shot surfaces for the Pleistocene (Disconformity 1) and Pliocene (Disconformity 5) in the KOA and OAK areas. Contours in feet.

The pre-event subsurface geology in the KOA and OAK areas differs in three significant ways (fig. 7-5):

- (1). MP-2d is more consistently well-cemented in the KOA area.
- (2). MP-3 (the upper, well-cemented unit) is thicker (246 ft vs 197 ft) and shallower (top at 282 ft vs 395 ft bsl¹) in the KOA area.
- (3). MP-3 is homogeneous throughout the crater area at KOA. At OAK, this unit changes from a cemented limestone with calcitic sands beneath the reef tract to cemented limestone with aragonitic sands beneath the lagoon, and the cemented intervals appear to decrease in thickness lagoonward (contrast OAR-2/2A to OOR-17; see fig. 7-3).

In addition, the pre-event ground surfaces in OAK and KOA areas differ significantly. KOA is represented by a nearly flat shallow surface on a broad reef tract, whereas OAK is represented by a narrow, shallow reef tract, relatively steep slope, and a flat, deep lagoon bottom.

POST-EVENT GEOLOGY OF OAK AND KOA CRATERS

The excavational craters were modified profoundly by a set of processes that included shock-induced liquefaction and consolidation, subsequent flow and piping of liquefied materials from depth (both laterally and toward and/or to the surface), consequent subsidence of the region adjacent to and beneath the excavational craters, and major and repeated failures of the sidewalls of the initial and subsequent craters.

Crater Zones

OAK and KOA craters can be characterized in the subsurface by geologic, paleontologic, and seismic-reflection crater zones that, in turn, can be related to crater-event history.

Traditional crater terminology does not always adequately apply to the Enewetak craters studied; many subsurface features within the carbonate rock and sediment virtually were undescribed. Thus, limited new terminology was introduced by Wardlaw and Henry (1986b), and a few additional terms are introduced in the current Chapter (designated by an asterisk, *).

Geologic Crater Zones

1. Zone of sonic degradation (ZSD): the stratigraphic interval in which sonic velocities are depressed below expected velocities. Normal or (more correctly) pre-event sonic velocities are determined from the sonic signature of reference boreholes. On the multichannel-seismic profiles, the ZSD appears as a "fuzzy" area in which seismic reflectors are not coherent and are surrounded by an area where

¹ Below sea level is abbreviated bsl throughout this Volume.

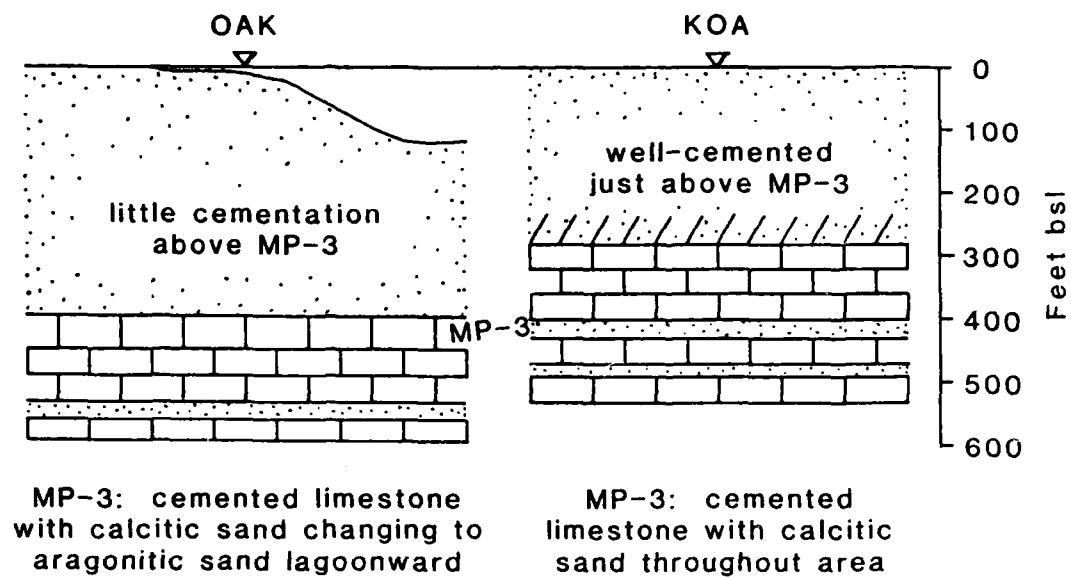


FIGURE 7-5. -- Comparison of pre-shot ground surface and subsurface geology for the OAK and KOA areas.

coherent reflectors are present but downturned. The ZSD represents units of rock and sediment that are fractured or shattered, mixed, and/or otherwise disturbed significantly enough to retard the sonic velocities relative to what they were before the nuclear events occurred. All geologic crater zones lie within the ZSD (fig. 7-6).

2. Geologic crater: the subsurface expression of the crater defined by the ZSD. The geologic crater zones encountered in the central crater are as follows:
3. Alpha 1 (α_1): Mud. Late-stage, fine-grained sediments with abundant brown, piped material in OAK.
4. Alpha 2 (α_2): Graded sand (distal) and slumps (proximal). Late-stage slope-failure and sand-turbidite flow deposits containing abundant brown, piped material. (Proximal means near material source; distal means far from the material source).
5. Beta 1a (β_{1a}): Graded Rubble. (*) This zone contains proximal rubble and distal sand (as in OPZ-18) with granules of rubblized material. The zone is transitional from the rubble below and slumps above and contains abundant brown, piped material near the top in the central crater area. Both Alpha 2 and Beta 1a show high gamma-ray activity (see fig. 7-17).
6. Beta 1s* (β_{1s}): Hiatus sand. (*) Highly shocked, uppermost unit (MP-1, Holocene) sediments.
7. Beta 1b (β_{1b}): Collapse rubble. (*) Thick rubble bed with sparse brown piped material within the zone in the central crater area. Both zones Beta 1a and Beta 1b are less distinct in the central-most part of the crater, and Beta 1s is missing in the same area because of mixing primarily due to late-stage piping.
8. Beta 2 (β_2): Transition sand. Pulverized sand within the transition paleontologic zone (see below). It has a limited lateral extent. The sand grains show fractured surfaces but no internal microfracturing.
9. Beta 3 (β_3): Rubble floatstone. Rubble in which no paleontologic mixing can be shown.
10. Gamma (γ): Fractured and displaced rock and sediment.
11. Delta (δ): Fractured but undisplaced rock and sediment.

The base of the zone of sonic degradation:

12. Epsilon (ϵ): In-place, relatively unfractured stratigraphic section; outside and beneath the geologic crater.

The geologic crater zones in the debris blanket are as follows:

13. Beta 1a* (β_{1a}^*): Graded sand and rubble *. This zone is found only in boreholes OHT-10 and OJT-12 and may be related to a large collapse and debris flow that breached the debris blanket and flowed into the

lagoon (as seen on the OAK enhanced sea-floor image, Folger and others, 1986).

14. Beta 1b* (β_{1b}^*), or Beta (β) undifferentiated: Rubble. Debris with no brown piped material.
15. Disturbed zone: This zone represents slightly altered stratigraphy with no apparent discontinuities.
16. Delta (δ) and Epsilon (ϵ): Relatively unaffected stratigraphy.

The depths to various crater zones for the transition and ground-zero boreholes for both OAK and KOA craters are given in Table 7-2, and graphically displayed in fence diagrams in Figures 7-7 to 7-10. Interpretations of geologic crater zones on seismic reflection profiles through ground-zero for both OAK and KOA crater (from Wardlaw and Henry, 1986b) are shown in Figures 7-11 and 7-12.

Paleontologic Crater Zones

The paleontologic crater zones for the **central crater** follow. The depths to various paleontologic crater zones for both OAK and KOA craters are given in Table 7-3.

1. Mixed: Fossils from various biostratigraphic zones are mixed together. This zone can be crudely divided into three subzones:
 - a. Very mixed with material from mostly upper biostratigraphic zones and piped material from deeper zones.
 - b. Mixed material from most of MP-1 and MP-2 plus piped material that decreases in degree of mixing downward.
 - c. Mixed material from mostly lower biostratigraphic zones of crater and sparse piped material.

These zones were developed for KOA crater (Wardlaw and Henry, 1986b) and are applicable to OAK with minor modification. In OAK, an additional zone, represented by the "hiatus sand" (Beta 1s), occurs between paleontologic subzones b and c in the lateral part of the crater. This unit consists predominantly of Holocene (near-surface) material and shows little mixing.

2. Transition: Transitional paleontology from mixed to unmixed.
3. Unmixed: Paleontology in normal succession showing no mixing of materials from different biostratigraphic zones.

The paleontologic crater zones for **debris blanket** are:

4. Mixed, undifferentiated: generally like unit 1b within the crater, but without piped material.
5. Transition: as above.
6. Disturbed Zone: unmixed, but sparse faunas.
7. Unmixed: as above.

GEOLOGIC CRATER ZONES

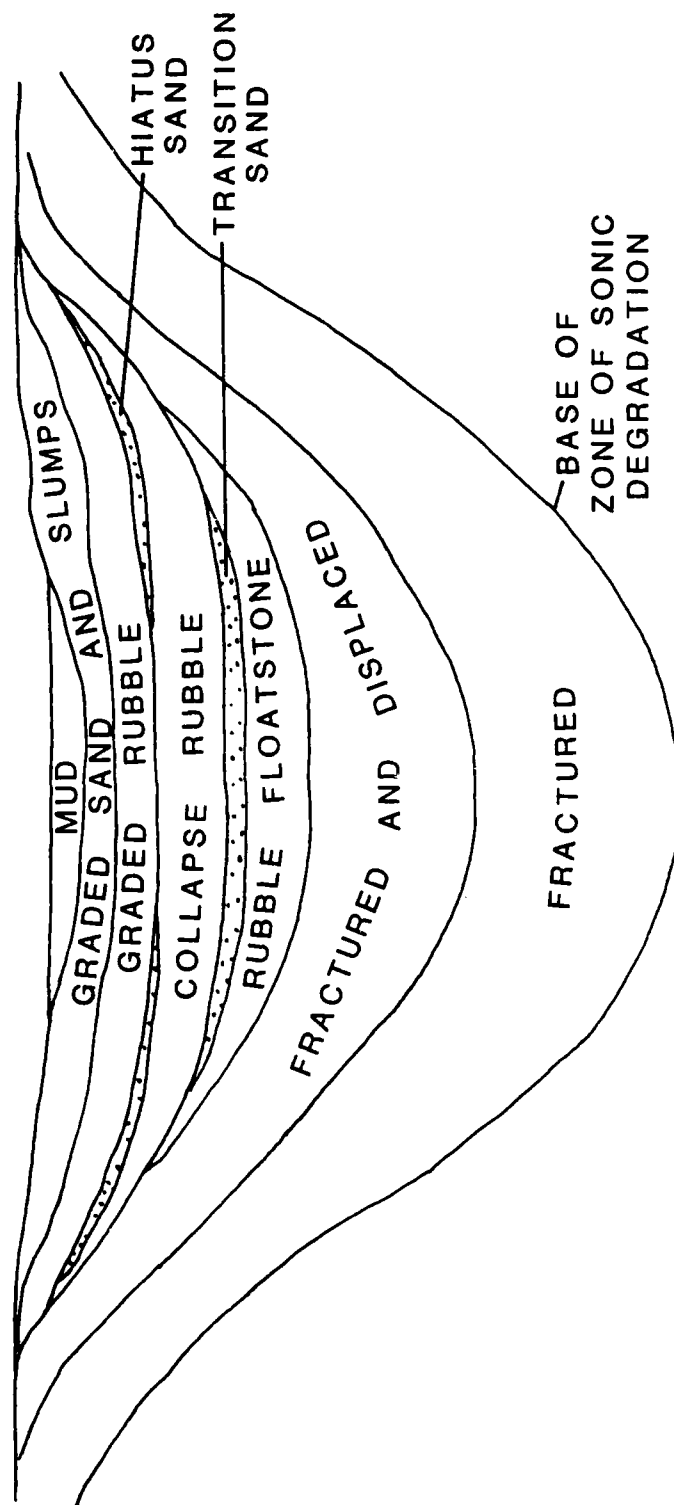


FIGURE 7-6. -- Geologic crater model.

TABLE 7-1. -- Relationship of geologic and paleontologic zones in the crater and debris blanket modified from Wardlaw and Henry (1986b). The hiatus sand { } is present only in the outer crater of OAK.

[PALEONTOLOGIC ZONES]		[GEOLOGIC ZONES]	
CENTRAL CRATER			
MIXED		ALPHA 1 (α_1) Mud	
a--Very mixed with mostly upper biostratigraphic zones and piped material		ALPHA 2 Graded sand (distal) (α_2) and slumps (proximal)	
b--Mixed material from most units 1 and 2 and piped material, generally decreasing in mixing downward		BETA 1a (β_{1a}) Graded rubble	
{Unmixed upper biostratigraphic zone}		{BETA 1s Hiatus Sand} (β_{1s})	
c--Mixed material from mostly lower biostratigraphic zones and sparse piped material		BETA 1b (β_{1b}) Collapse rubble	
TRANSITION		BETA 2 (β_2) Transition sand	
UNMIXED		BETA 3 (β_3) Rubble floatstone	
		GAMMA (γ) Fractured, displaced	
		DELTA (δ) Fractured, relatively undisplaced	
		EPSILON (ϵ) Relatively unfractured, in place	
DEBRIS BLANKET			
MIXED (undifferentiated)		BETA 1a (β_{1a}) Graded sand and rubble	
		DEBRIS (BETA)	
		BETA 1b (β_{1b}) Rubble	
TRANSITION			
DISTURBED		DISTURBED	
UNMIXED		DELTA (δ) Fractured, relatively undisplaced	
		EPSILON (ϵ) Relatively unfractured, in place	

TABLE 7-2. -- Depth (ft bsl) to tops of the crater zones in OAK and KOA boreholes. ZSD = Zone of Sonic Degradation. Boreholes listed in order of increasing distance from ground-zero.

OAK AND KOA GEOLOGIC CRATER ZONES

ZONE	ç	OBZ-4	OPZ-18	OCT-5	OTG-23	OUT-24	OKT-13	OFT-8	OIT-11
Alpha 1		198.7	201.9	163.7	-	-	164.7	130.8	155.0
Alpha 2		229.2	-	164.6	164.0	147.0	165.3	131.1	
Beta 1a		271.7	246.5	174.1	174.0	249.2	177.0	139.4	155.1
Beta 1s		-	-	244.1	219.0	278.6	190.8	152.9	-
Beta 1b		309.1	337.2	310.7	235 ?	288.0	207.0	175.4	
Beta 2		394.9	377.0	-	-	-	-	-	-
Beta 3		415.1	412.3						
Gamma		564.2	522.4	346.3	314.0	332.0	227.3	204.1	171.7
ZSD		1138.7	1082.4	863.7	842.0	830.0	831.7	639.6	697.0

ZONE	ç	OET-7	OQT-19	OHT-10	OJT-12	ODT-6	ONT-16	ORT-20	OMT-15
Alpha 1		-	-	-	-	-	-	-	-
Alpha 2		106.9	-	-	-	-	-	-	-
Beta 1a		132.3	-	137.3	143.8	87.4	-	-	-
Beta 1s		-	-	-	-	-	-	-	-
Beta 1b		-	-	145.2	155.0	-	135.1	-	110.9
Beta 2		-	-	-	-	-	-	-	-
Beta 3				[191.1]	[164.7]	-	[148.0]	-	[119.8]
Gamma		156.3	117.5	286.8	238.0	91.9	176.7	101.4	139.4
ZSD		505.1	413.3	587.1	387.0	311.6	242.7	239.0	223.0

[] denotes disturbed zone

ZONE	ç	OLT-14	ç	KBZ-4	KCT-5	KFT-8	KDT-6	KET-7
Alpha 1		-	ç	109.1	-	-	-	-
Alpha 2		-	ç	137.3	98.9	77.8	56.2	-
Beta 1a		139.7	ç	167.7	120.0	96.5	79.9	-
Beta 1s		-	ç	-	154.5	-	-	-
Beta 1b		-	ç	238.5	156.1	106.0	-	-
Beta 2		-	ç	247.2	242.5	-	-	-
Beta 3		-	ç	266.2	259.9	-	-	-
Gamma		147.2	ç	316.2	274.3	153.8	110.1	51.1
ZSD		154.2	ç	1101.1	869.2	590.4	410.0	318.2
			ç					

TABLE 7-3. -- Paleontologic crater zones and relation to the transition sand in OAK and KOA boreholes. Depths in ft below sea floor (ft bsf) are compatible with the footages presented in the paleontologic studies (Cronin, Brouwers, and others, 1986; Brouwers, Cronin, and Gibson, 1986; and Cronin and Gibson, 1987), which are consistently in feet below sea floor (bsf).

=====					
KOA CRATER					
	KBZ-4	KCT-5	KFT-8	KDT-6	
Mixed Zone	0-137.5	0-140.1	0-28.5	0-43.6	
Transition Zone	137.5-142	140.1-155.2	28.5-99.3	43.6-58.5	
Transition Sands	138.1-157.1	143.6-161.0	---	---	
=====					
OAK CRATER					
	OBZ-4	OPZ-18	OCT-5	OKT-13	
Mixed Zone	0-180	0-174	0-149	0-55	
Transition Zone	180-220	174-211	149-187	55-68	
Transition Sands	196.2-216.4	175.1-210.4	---	---	
	OFT-8	ODT-6			
Mixed Zone	0-64	1.8-4.4			
Transition Zone	64-74	---			
Transition Sands	---	---			
=====					
OAK CRATER DEBRIS BLANKET					
	OHT-10	OJT-12	ONT-16	OMT-15	OLT-14
Mixed Zone	0-54	0-20.9	0-12.9	0-8.9	0-7.5
Transition Zone	54-76	20.9-67	12.9-14.7	8.9-15.5	---
Disturbed Zone	76-149.5	67-94.2	14.7-41.6	15.5-28.5	---
=====					

Seismic Crater Zones

Grow, Lee, and others (1986) interpreted four subcrater seismic zones from the multichannel seismic-reflection records. They are, from top to bottom: (1) transparent zone, (2) zone of intense fracturing/depression, (3) zone of moderate fracturing/depression; and, 4, zone of minor fracturing/depression. The zone of minor fracturing/depression has not been defined in terms of depth. The seismic zones are compared to geologic crater zones in Table 7-4.

The transparent zone corresponds to the crater fill and the transition sand (where present). In OAK, reefward of SGZ, the base of the transparent zone is difficult to interpret because some large-scale slumps (crater fill) from the reef tract are not completely transparent seismically. The bottom of the zone of intense fracturing/depression falls within gamma, the zone of fracturing and displacement in KOA, and very near the bottom of the rubble zone in OAK. The bottom of the zone of moderate fracturing/depression appears to fall close to the gamma/delta transition or that change from fractured/displaced to fractured/in place material. The delta zone appears to be equivalent to the zone of minor fracturing/depression.

TABLE 7-4. -- Comparison of subcrater seismic zones to selected geologic crater zone boundaries for OAK and KOA craters.

SEISMIC ZONE	GEOLOGIC CRATER ZONE
KOA	
Bottom of Transparent Zone 262 ft bsl	Bottom of Transition Sand 266.2 ft bsl
Bottom of Zone of Intense Fracturing/Depression 460 ft bsl	Bottom of Rubble 316.2 ft bsl
Bottom of Zone of Moderate Fracturing/Depression 755 ft bsl	Bottom of ZSD 1101.1 ft bsl
OAK	
Bottom of Transparent Zone 361 ft bsl	Bottom of Transition Sand 377.0 ft bsl
Bottom of Zone of Intense Fracturing/Depression 590 ft bsl	Bottom of Rubble 564.2 ft bsl
Bottom of Zone of Moderate Fracturing/Depression 918 ft bsl	Bottom of ZSD 1138.7 ft bsl

CRATER FEATURES

Crater Material in the Lagoon

Muddy sediments in the northwestern portion of the lagoon (see fig. 7-13) are derived partly from crater material. Observations leading to this conclusion (Wardlaw and Henry, 1986b) include:

- (1). An anomalously high amount of low-Mg calcite in the sediments probably indicates mixing from diagenetically altered subsurface units.
- (2). The sediments have an anomalously high content of clay-size material, probably indicating crater-derived material. Normal lagoon sediments do not contain appreciable quantities of naturally produced clay-sized carbonate.
- (3). The sediments have measurable radioactivity, probably from the device-derived Cesium-137 (Ristvet and Tremba, 1986).

Thus, a substantial part of the mud in the northwestern portion of the lagoon (fig. 7-13) was derived from pulverization of sediment and rock particles by the nuclear detonations during the excavation of the craters. A considerable volume of fine-grained material was moved from the crater areas to the lagoon, although the volume of this lost material or proportion derived from each of the forty-one nuclear events other than OAK or KOA cannot be estimated.

Breach Deposit in the Lagoon

The enhanced sea-floor image of OAK crater displays a large flow deposit out into the lagoon (fig. 7-14). This feature extends out beyond the limits of the apparent crater, thus it, too, represents loss of material to the lagoon. This feature was not observed until after the field operations, so it was not sampled. The thickness or volume of the deposit is unknown. The deposit appears to represent a breach in the debris blanket through the "channel" (Peterson and Henny, Ch. 5 of this report, p. 5-15) and flow of material out onto the lagoon floor.

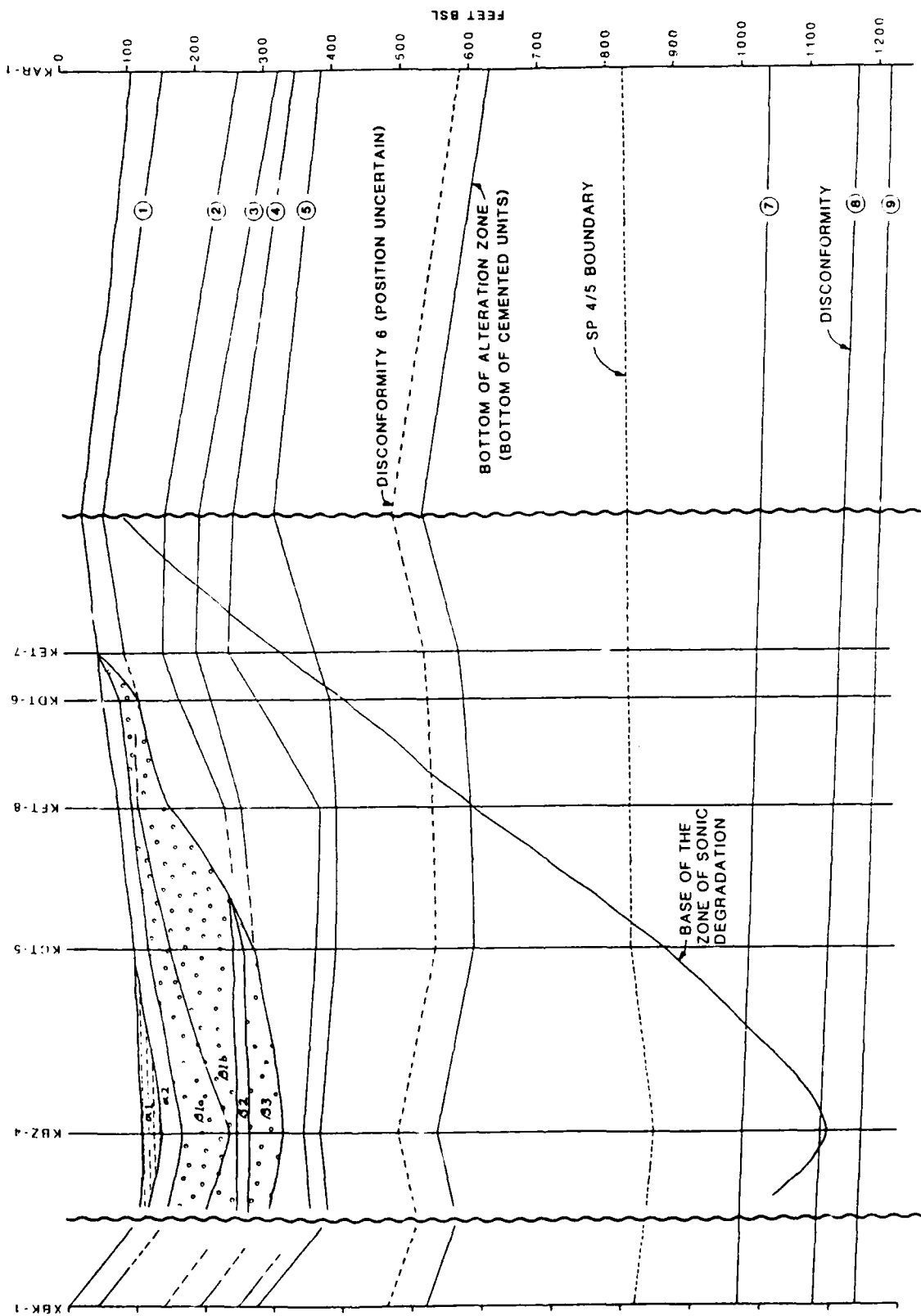


FIGURE 7-7. --- Fence diagram of KOA boreholes showing relationship of crater and geologic horizons. Scale is vertically exaggerated 2:1. Squiggly lines represent breaks to shorten the diagram.

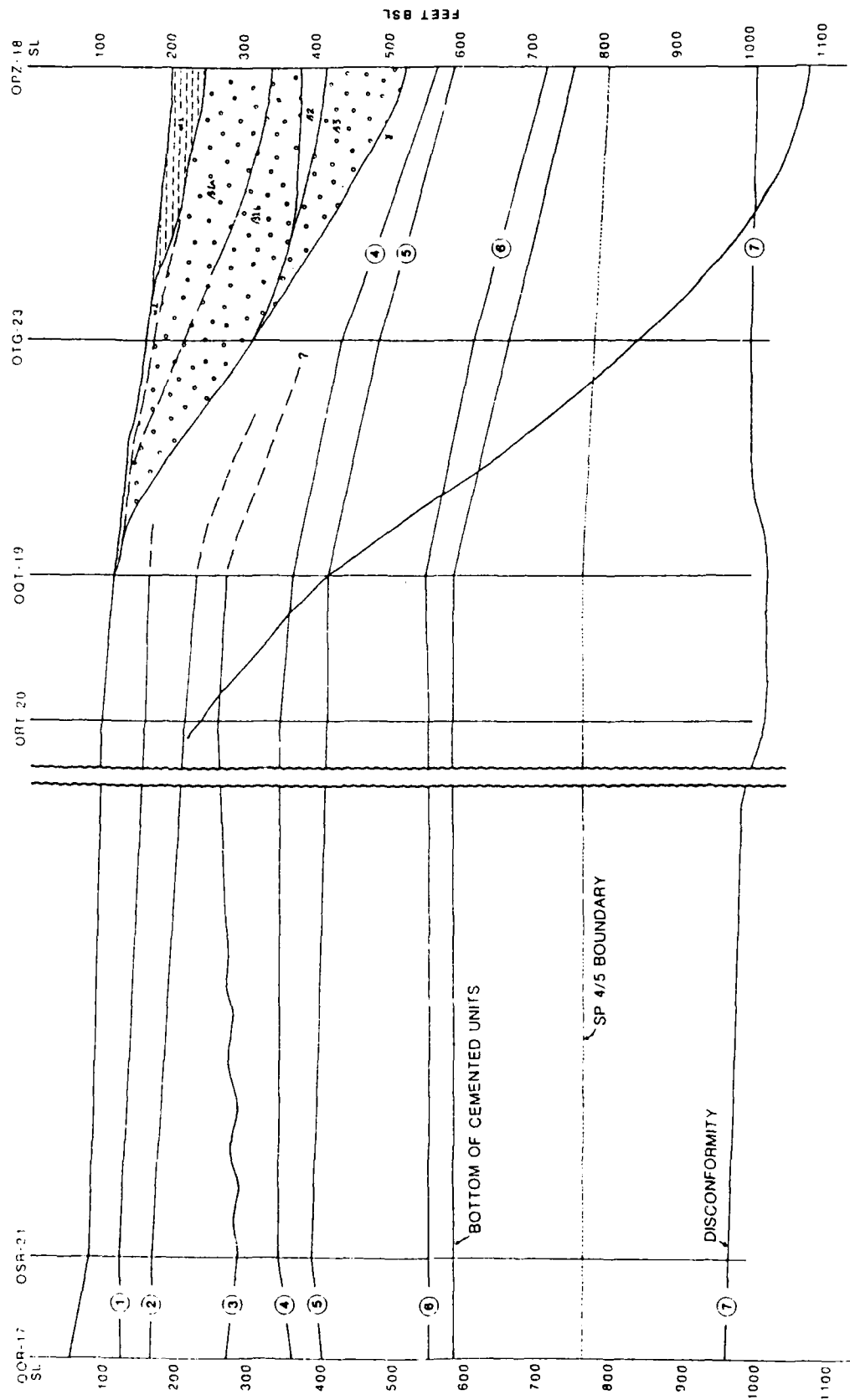


FIGURE 7-8. -- Fence diagram of OAK boreholes OOR-17 to OPZ-18 showing relationship of crater and geologic horizons. Double squiggly lines represent breaks and change in vertical exaggeration from 2:1 on right side to 4:1 on left side.

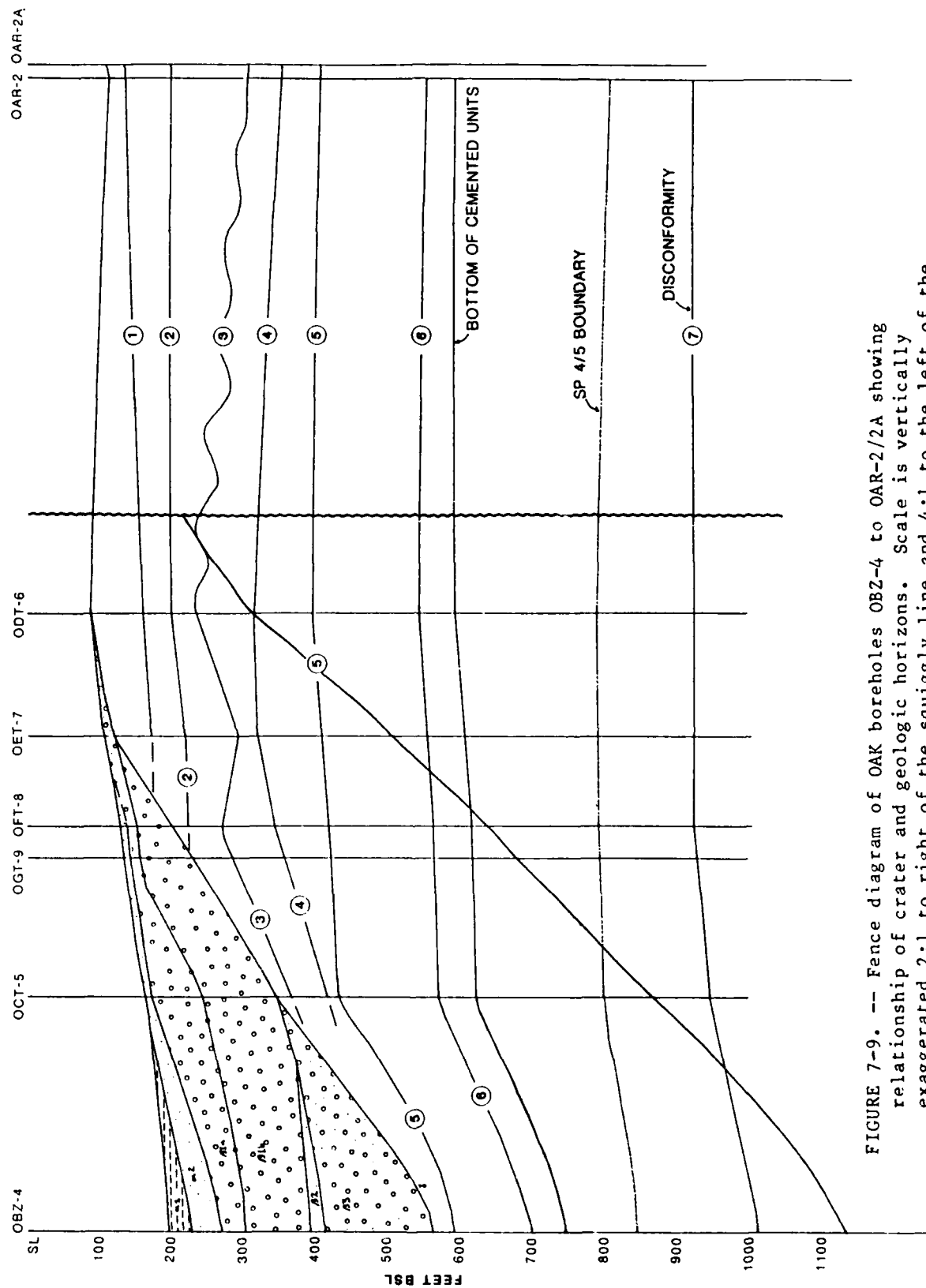


FIGURE 7-9. -- Fence diagram of OAK boreholes OBZ-4 to OAR-2/2A showing relationship of crater and geologic horizons. Scale is vertically exaggerated 2:1 to right of the squiggly line and 4:1 to the left of the line.

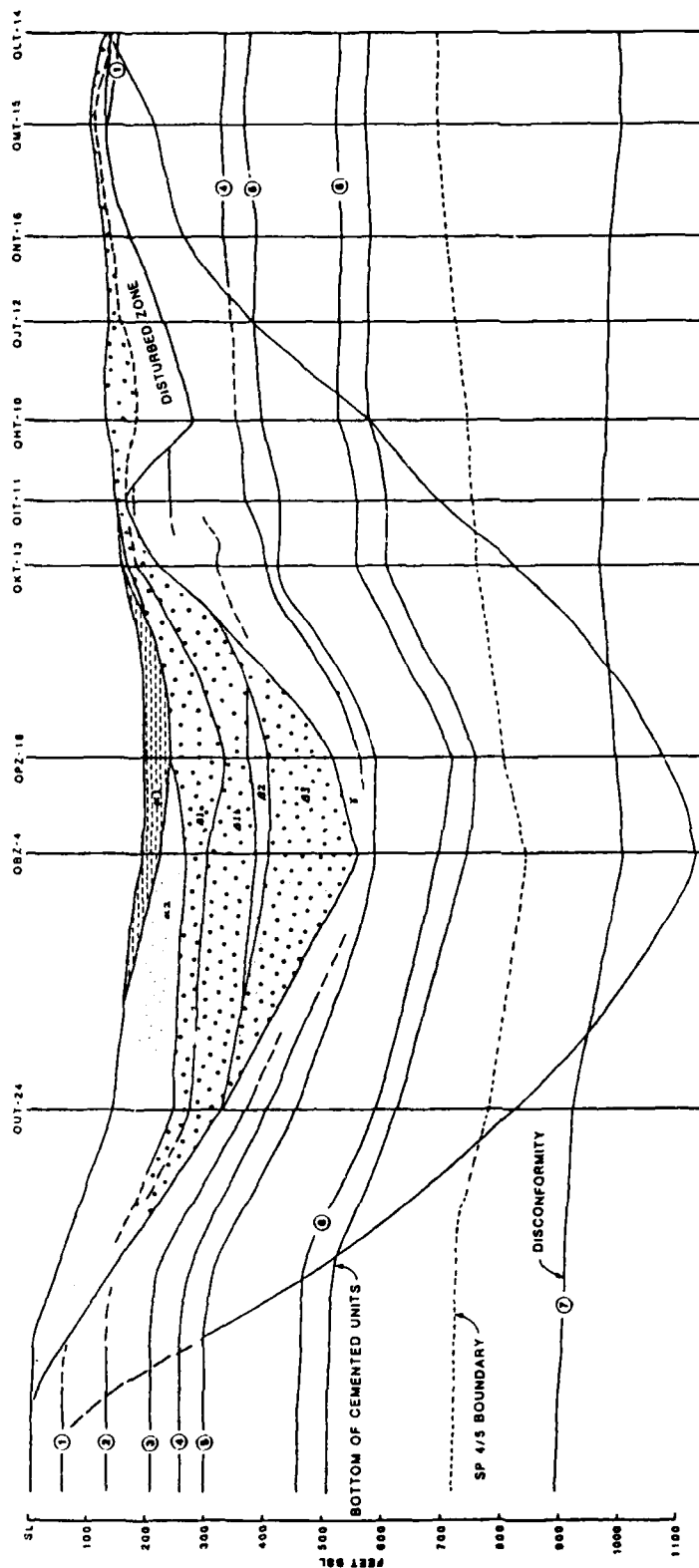


FIGURE 7-10. -- Fence diagram of OAK boreholes from reef tract to OLT-14 showing relationship of crater and geologic horizons. Scale is vertically exaggerated 2:1.

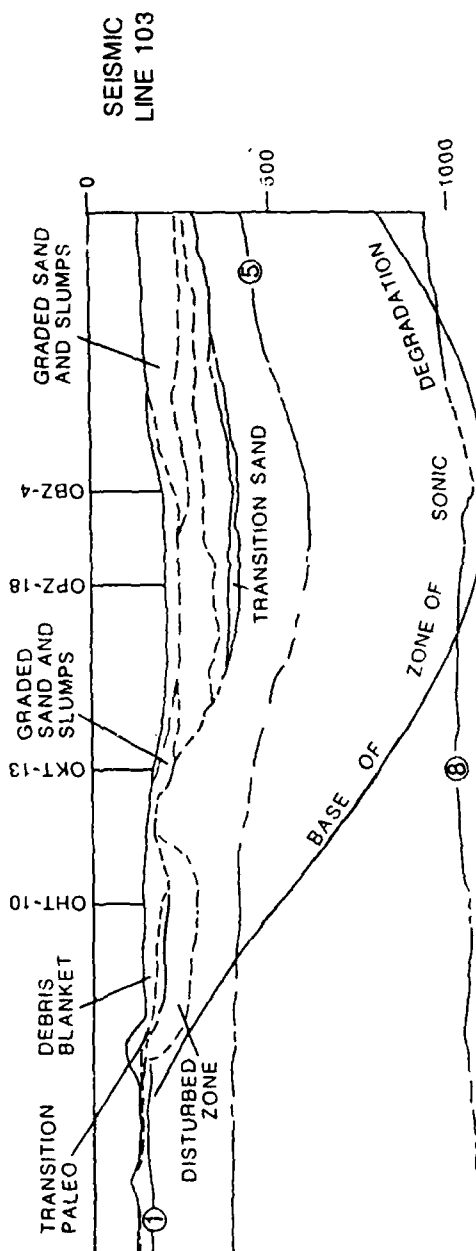


FIGURE 7-11. -- Geologic interpretation of multichannel seismic lines 101 and 103 in proximity of OAK crater (from Wardlaw and Henry, 1986b). Location of lines shown in Grow, Lee, and others (1986).

KOA CRATER

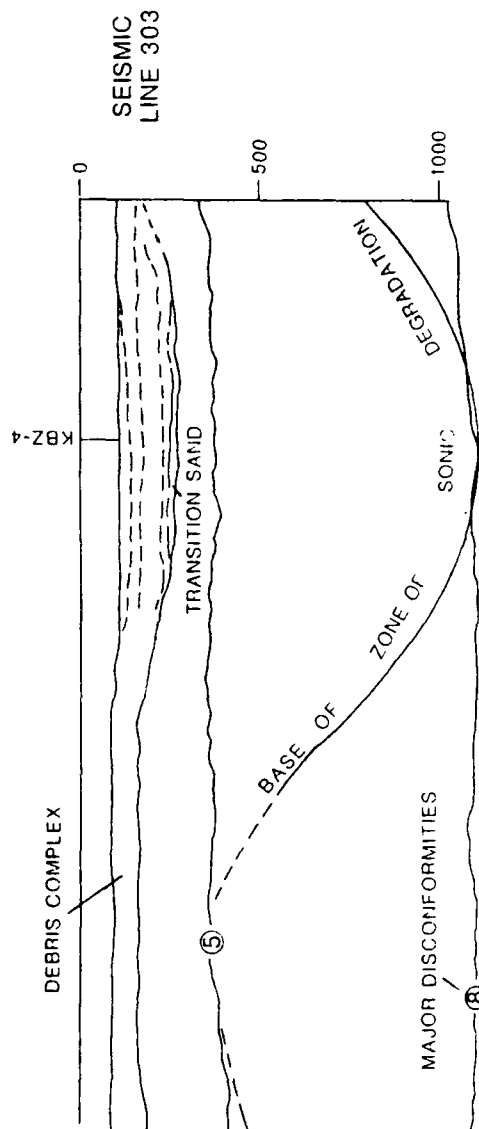
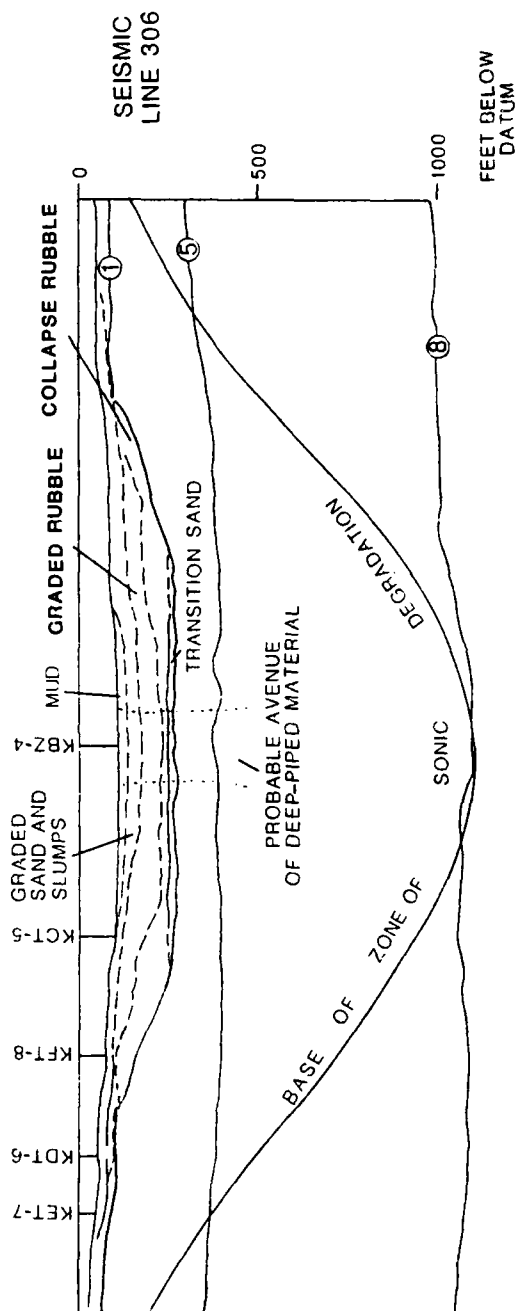


FIGURE 7-12. -- Geologic interpretation of multichannel seismic lines 303 and 306 in proximity of KOA crater (from Wardlaw and Henry, 1986b). Location of lines shown in Grow, Lee, and others (1986).

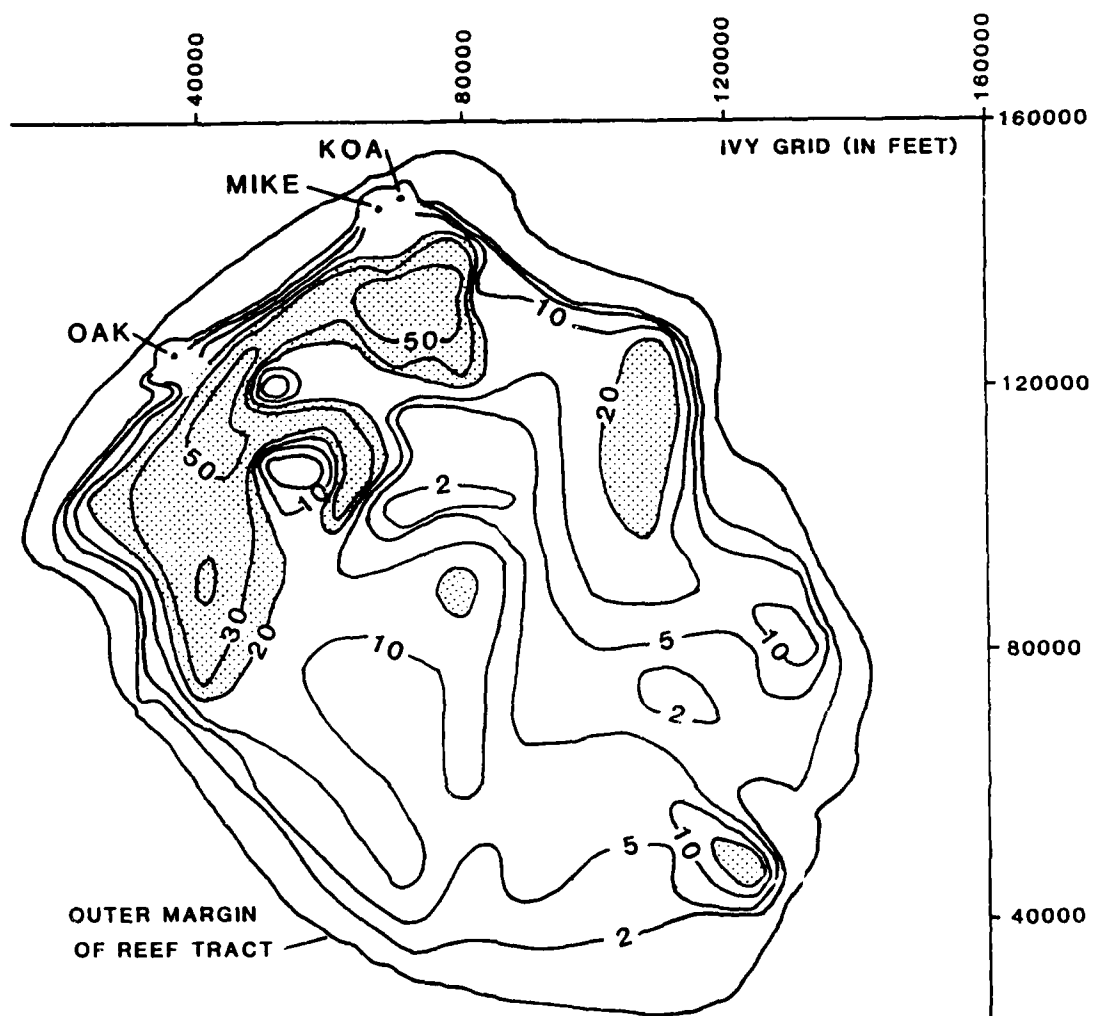


FIGURE 7-13. -- Weight percent mud in bottom sediments of lagoon. Sediments in excess of 10 percent mud are probably indicative of blast-derived mud contribution.

Piping

Brown-stained, organic-rich sediments from MP-4 were piped to the surface in substantial quantities. Several sand mounds (Halley and others, 1986) or "sand volcanoes", covered with moderate-brown, coarse-grained detritus are common on the terraces of OAK crater. This material commonly contains granule- and small-pebble-sized particles (2-64 mm) and may sparsely contain small cobble-sized materials (64-256 mm). The sand volcanoes observed are generally less than 10 ft high, are round to elongate, and are 16-33 ft across and up to 100 ft long. The eight volcanoes documented by Halley and others (1986a) are plotted on the enhanced sea-floor image (fig. 7-14). Similar features that are probably sand volcanoes are also shown. The volcanoes appear to exist in several clusters or swarms on the terraces of OAK crater. No sand volcanoes were observed in the KOA area; however, most surficial features have been obscured by extensive slumping and recent sedimentation (Folger and others, 1986).

Several thin sand dikes filled with brown-stained sediments, confirmed by paleontologic analysis to be from MP-4, were penetrated by the boreholes. These were inclined at a high angle to the borehole under the central crater region and terraces of OAK. Dikes were observed in boreholes OPZ-18 at 667.8 - 668.5 ft, OKT-13 at 615.0 to 615.2 ft, OTG-23 at 472.3 to 473.2 ft, and OFT-8 at 291.1 to 291.9 ft (all depths bsl; see Henry, Wardlaw, and others, 1986). No dikes were observed in the KOA boreholes.

Paleontologic Mixing

The distribution of mixed materials from different biostratigraphic zones within the geologic crater is complicated, but each fossil is a clue to unraveling the history of formation of crater-fill deposits. In addition to the general three to four mixed zones presented in the previous section, both KOA and OAK have an overprint of hydraulic sorting in the central region due to post-deposition upward flow of piped material from strata below the excavational crater. In KBZ-4, the piped material shows hydraulic sorting of various fossil groups (see Brouwers, Cronin, and Gibson, 1986). In OBZ-4 and OPZ-18, the faunas are depleted and represented by sparse piped material in the lower part of the crater fill (fig. 7-15; and Cronin and Gibson, 1987), thought to indicate preferential removal of contained faunas by hydraulic flow and scant deposition of MP-4 faunas.

The mixing within the crater is displayed in Figure 7-16 for OAK and Figure 7-17 for KOA. The biostratigraphic zones represented are defined in the reference boreholes in sequence of superposition and with increasing depth are: surficial (S), AA, BB, CC, DD, EE, FF, and GG. Piped material from depth designated as "piped" in the figures is represented by biostratigraphic zones II, JJ, KK, LL, and MM. Because the KOA event excavated down to the DD/EE zone boundary, most EE and all FF material in the crater-fill indicates shallow piping. Because the OAK event excavated down to a point within EE, possibly some EE and all FF and GG material in the crater-fill represents shallow piping. Each crater will be briefly discussed from bottom up (or as they filled).

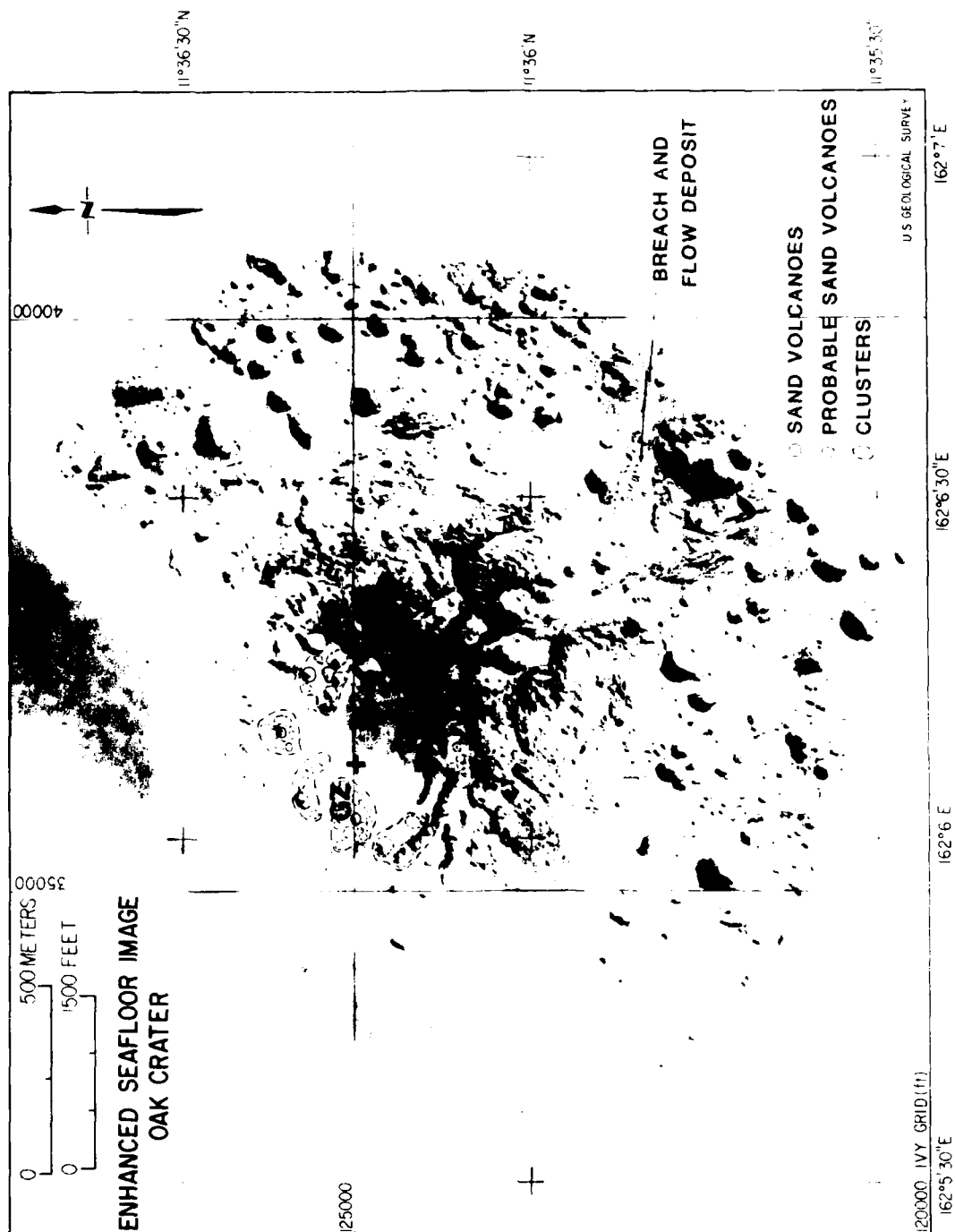


FIGURE 7-14. -- Distribution of observed (solid circles) and probable (dashed circles) sand volcanoes shown in clusters on enhanced sea-floor image of OAK crater and location of breach and flow deposit in lagoon.

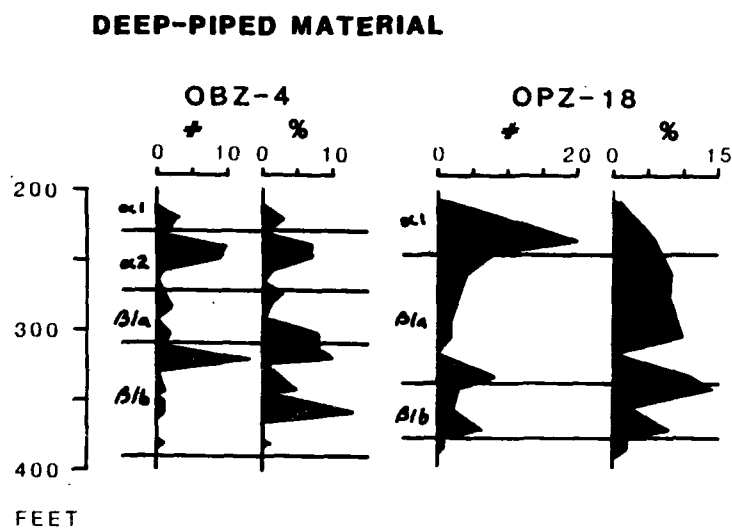


FIGURE 7-15. -- Number of specimens (#) from MP-4 and MP-5 (minor) and percent (%) of total ostracodes picked in crater zones in boreholes OBZ-4 and OPZ-18.

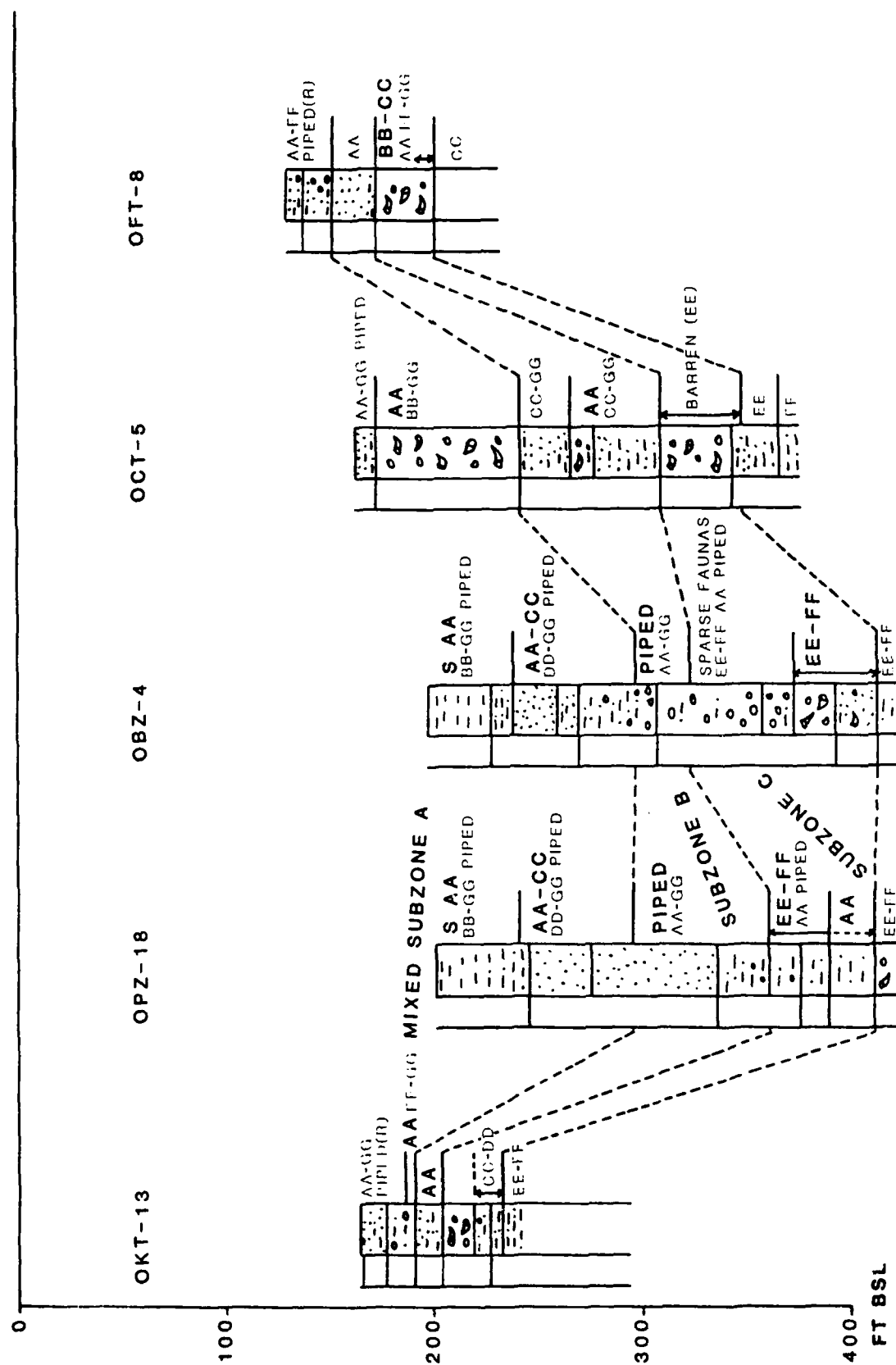


FIGURE 7-16. -- Paleontologic mixing in the mixed zone of OAK crater. Only boreholes with detailed analyses shown. Lithic symbols the same as Figure 7-19. Bold letters indicate abundant material from that particular biostratigraphic zone.

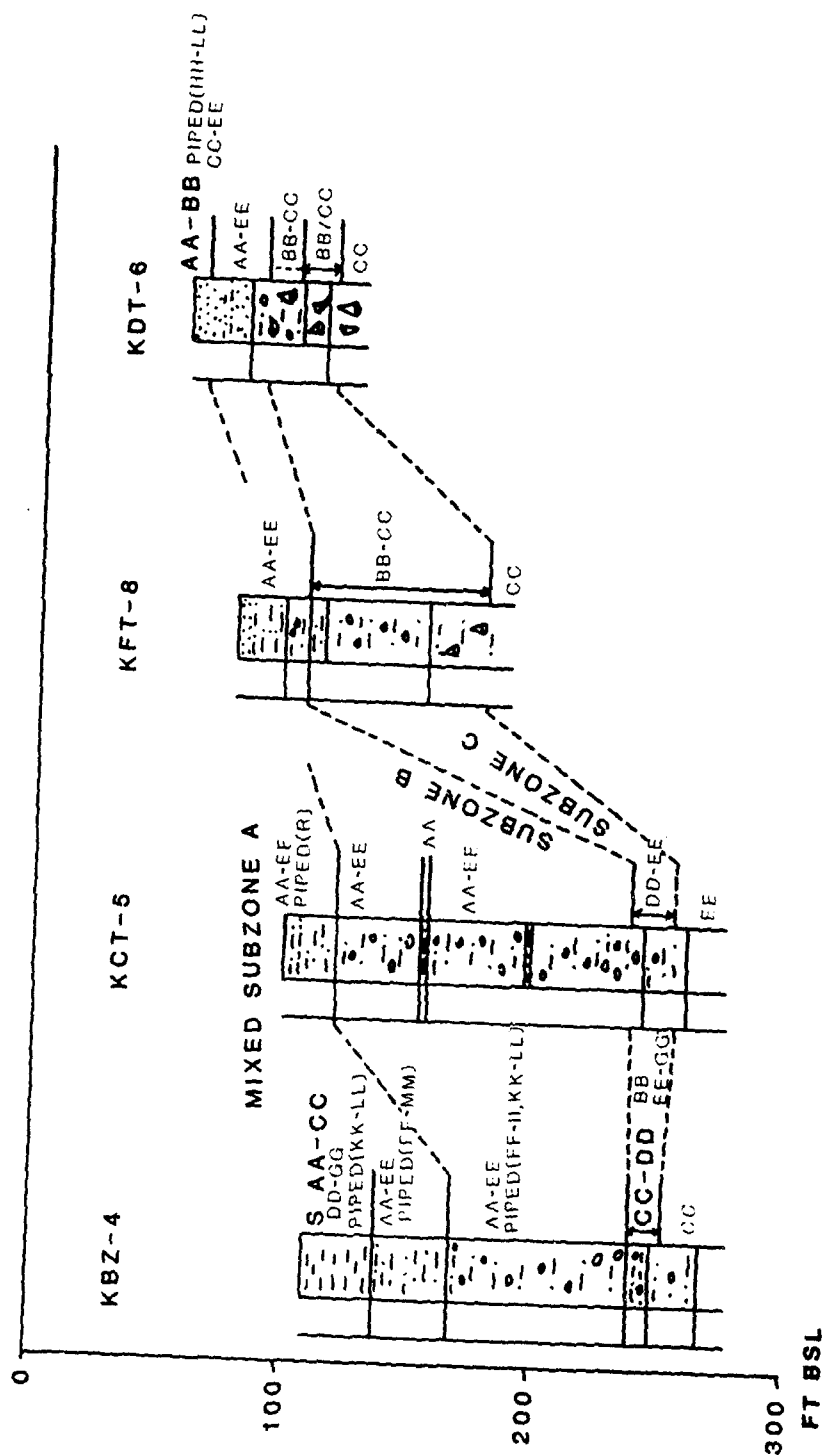


FIGURE 7-17. -- Paleontologic mixing in the mixed zone of KOA crater. Lithic symbols the same as Figure 7-19. Bold letters indicate abundant material from that particular biostratigraphic zone.

OAK Crater.

The lower mixed subzone (C, figs. 7-15 and 7-16) and the transition zone coincide for much of OAK crater (this is because of the limits of resolution, similarity of taxa in the zones, and gradational nature of these zones). This zone contains undifferentiated EE-FF material with sparse AA and deep-piped material in the central crater and of slightly mixed material from progressively stratigraphically higher zones outward to OFT-8 where it contains mostly BB-CC material.

The middle mixed subzone (B) represents a maximum of mixing of material in the central-crater area with components from zones AA-GG mixed with abundant deep-piped material in the upper part of Beta 1b and the lower part of Beta 1a. Laterally, this interval is represented by the "hiatus" sand (Beta 1s) which consists largely of AA material on top of Beta 1b. This situation is complicated at OCT-5 by an apparent local slump that covers and possibly involves the "hiatus" sand (fig. 7-16).

The upper mixed subzone (A) can be divided into two parts in the central-crater area and the inner terraces (OCT-5). In the central-crater area, the lower part consists of common AA-CC material and deep-piped and sparse DD-GG material, and the upper part consists of abundant surficial and AA components with common BB-GG and deep-piped material. Under the inner terraces (OCT-5), the upper mixed subzone consists of a lower part with abundant AA and common BB-GG material (no deep-piped material) and an upper part that is highly mixed with AA-GG and deep-piped material. Laterally, the upper mixed subzone commonly consists of very mixed AA-GG material decreasing outward to AA-FF material with sparse deep-piped material at its top. At OKT-13, the base of the upper mixed subzone (which coincides with the base of Beta 1a) is mixed with material from the underlying unit, the "hiatus" sand (Beta 1s).

Deep-piped material from MP-4 is mixed throughout the crater-fill in both OBZ-4 and OPZ-18, suggesting that the central crater bowl served as the common avenue for venting of MP-4 material. Although sand volcanoes are common on the terraces, mixing of deep-piped material from MP-4 is restricted to surface or near-surface deposits, suggesting that the volcanoes are a late-stage feature and did not represent the more common avenue of venting. Venting under the terraces probably did not take place until significant concentric fracture zones opened sufficiently in the subsiding crater to serve as conduits.

Shallow-piped material is that material in the crater-fill from shallow biostratigraphic zones that remained completely below the excavational crater. In OAK, this material is represented by components of biostratigraphic zones FF-GG. Shallow-piped material is common in the upper mixed subzone throughout the crater-fill, common in the middle mixed subzone, and sparse in the lower mixed subzone in the central crater.

KOA Crater.

The lower mixed subzone (C, fig. 7-17) and the transition zone coincide in most of KOA crater (for the same reasons as in OAK) and consist of CC-DD material with sparse BB and EE-GG material at KBZ-4, of DD-EE material at KCT-5, and of BB-CC material at KFT-8 and KDT-6.

The middle mixed subzone (B) consists of AA-EE material throughout the crater-fill. In addition, at KBZ-4, this zone contains deep-piped material that indicates hydraulic sorting in Beta 1a with FF-II ostracodes and KK-LL foraminifers, and a normal distribution of deep-piped FF-MM ostracodes and foraminifers in Alpha 2. A very thin, muddy "hiatus" sand may be preserved in KCT-5 within the middle of this unit.

The upper mixed subzone (A) is confined to Alpha zones. At KBZ-4, it is dominated by surficial (S) and AA-CC material with sparse DD-GG and deep-piped (KK-LL) material. At KCT-5, it consists of microfossils from AA-EE with very sparse deep-piped material. At KFT-8, the upper mixed subzone cannot be differentiated from the middle mixed subzone, and the whole interval consists of AA-EE material. At KDT-6, it is dominated by AA-BB with CC-EE and deep-piped (HH-LL) material.

Deep-piped material from MP-4 is mixed with other material throughout most of the crater-fill in KBZ-4. It is only found in surficial deposits in the transition boreholes. This suggests that the central bowl in KOA, which is now obscured by pervasive slumping, served as the common avenue for venting deep material from MP-4 just like in OAK.

In KOA, shallow-piped material is represented by components of biostratigraphic zones EE-GG, predominantly EE. The KOA crater-fill material shows much more pervasive shallow piping than in OAK. This shallow piping obscures some of the mixing subzones and yields fairly common mixed faunas of AA-EE. The pervasiveness of the mixing also implies that shallow piping occurred over a broad area. In addition, the paucity of samples and boreholes and a less rigorous study of the KOA material gives less definition of the mixing in KOA.

Estimates of Volume of Piped Material.

The volume of deep-piped material can be estimated with the techniques developed for the detailed paleontologic analysis of the OAK crater by Cronin and Gibson (Ch. 3 of this Report). Deep-piped material occurs only near the surface outside the central bowl and is essentially negligible in quantity. If all grain sizes behaved as those between 63 through 850 μ (the size range from which ostracodes are extracted) and if sedimentary particles of different shapes and densities (minor, all CaCO_3) behave the same as ostracode valves and carapaces, then the detailed percentages of piped ostracodes reflect the entire sedimentary assemblage (Cronin and Gibson, Ch. 3 of this report). A conservative volume estimate based on these data is 4.83 million cubic feet (5.1 % of the total volume of central bowl to a depth of 149 ft with a radius of 450 ft from GZ).

A semiquantitative approach also can be attempted for estimating the shallow-piped material in OAK. Shallow-piped material is identified as those ostracodes that characterize the FF/GG zones, those zones that remained completely below the excavational crater. Shallow-piped material is similar in distribution to deep-piped material within the central bowl, it occurs throughout the crater fill. Because of the general low abundance of FF/GG zone indicators, any patterns in the distribution within the crater-fill is difficult to discern. The crater bowl probably was an avenue for shallow

piping, and the piping probably obscures any patterns of distribution in a manner similar to that for deep-piped material. Ostracodes that characterize the FF/GG zones are typically sparse, averaging 0.4 percent in the faunas above the FF/GG zones in the reference boreholes. They average a sparing 7.5 percent in the faunas of the zones that they characterize in the reference boreholes. These ostracodes average 3.3 percent in the central crater-fill faunas. This implies a whopping 41 percent of the central crater-fill material may have been derived from the FF/GG zones. A volume estimate based on these data is 45.62 million cubic feet of shallow-piped material within the central bowl. However, unlike deep-piped material, shallow-piped material is distributed in significant quantities in Beta 1a and Alpha zones outside the central bowl, suggesting a much larger volume than that estimated for the central bowl was piped.

Paleontologic Model of Crater-Fill.

The paleontologic zonation of the crater-fill can be summarized into a simple model that is applicable to both craters studied. It is extremely relevant for constraints on timing of processes of crater-filling. It is presented in Figure 7-18. The zone of shallow-piped material coincides with that of the deep-piped material through mixed subzones B and C in the central crater but encompasses all of mixed subzone A throughout the crater. The zones of piped material indicate the relative timing of arrival of material to the surface. Shallow-piped material first arrived to the surface after the deposition of the hiatus sand (Beta 1s), which probably resulted from wash-back. Deep-piped material first arrived to the surface after the deposition of the graded rubble (Beta 1a), during deposition of Alpha.

The zone of piped material from depth has a strong overprint of mixing and hydraulic sorting in the central bowl, especially in mixed subzone B, where abundant deep-piped material was deposited. The central bowl served as the probable avenue for venting of the deep-piped material. Shallow-piped material also appears to have vented, in part, through the central region. However, shallow piping appears to have occurred throughout the crater wings which implies venting throughout the crater region.

Injection

Holocene sediment (from MP-1) appears at an anomalous depth in borehole OPZ-18 within the transition sand (390.6 to 410.0 ft bsl) and in thin dikes below the transition sand (434.5 to 435.2 ft bsl, and questionably at 415 ft). This appears to be injection of near-surface material at the base of the excavational crater.

Gamma Activity

In Enewetak boreholes, elevated gamma activity appears to reflect the following: (1) the presence of device-produced radionuclides; (2) the presence of brown-stained, organic-rich sediments from MP-4; and (3) various other factors. For example, a gamma peak of the third type occurs within muddy sediments overlying a discontinuity in OIT-11 (fig. 7-19). It appears that other peaks of the third type also can be related to thick zones of "tea-brown" (organically stained) micrite cement.

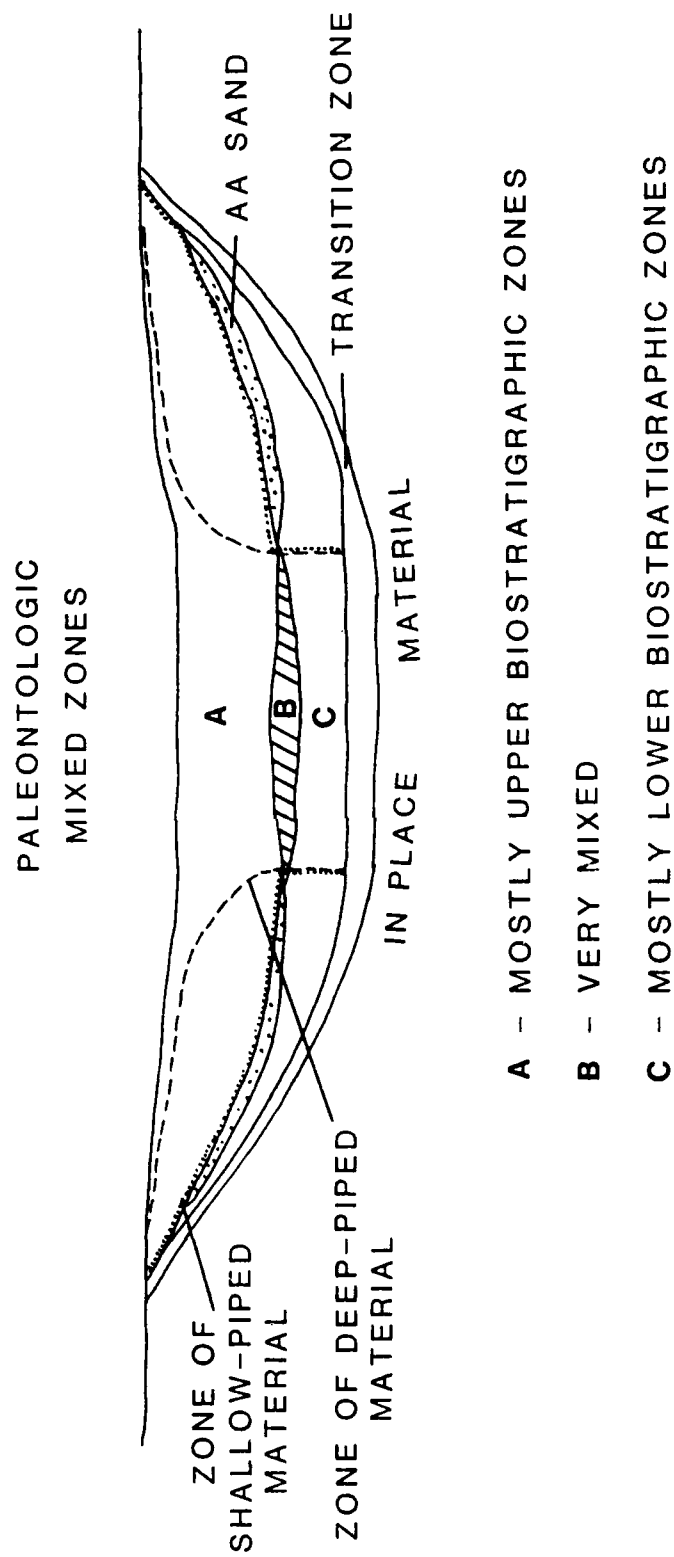


FIGURE 7-18. -- Paleontologic model of the crater-fill and the paleontologic mixed zones.

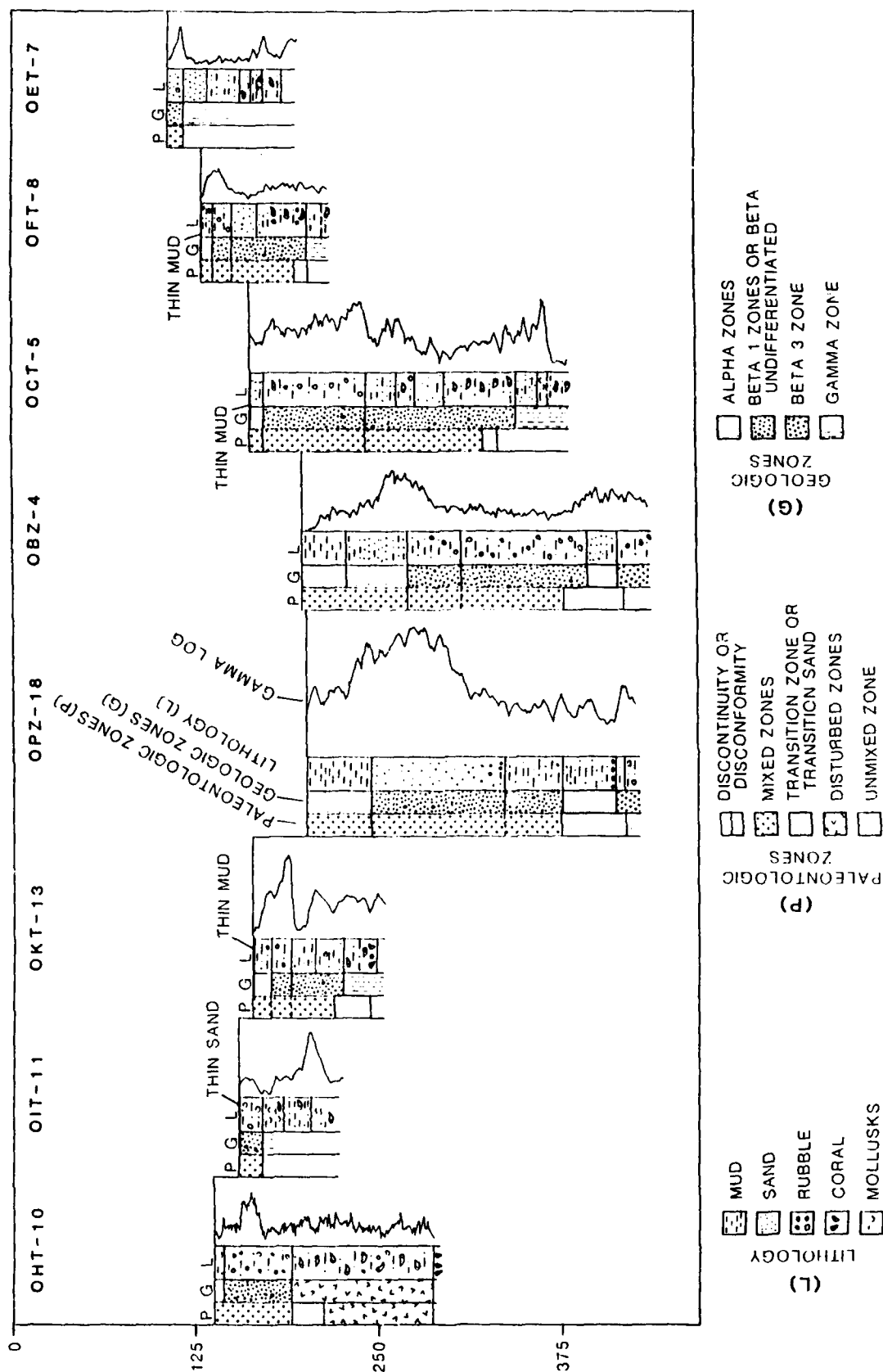


FIGURE 7-19.--Borehole lithology (L), geologic (G) and paleontologic (P) crater zones, and gamma-ray logs for selected boreholes, OAK crater. Location of boreholes shown on Figure 7-20.

Cesium-137 levels coincide directly to the gamma activity in the Alpha, Beta-1, and Beta-2 crater zones (Ristvet and Tremba, 1986). Furthermore, the gamma activity of the brown-stained, organic-rich sediments is caused largely by naturally occurring isotopes of thorium and uranium. These radionuclides were not observed within the Alpha, Beta-1, and Beta-2 crater zones.

Naturally occurring thorium and uranium isotopes were detected in borehole OIT-11 and probably account for the "other" peak (third type) in gamma activity noted above. Similarly, in borehole OHT-10, a small peak in the gamma activity probably reflects naturally occurring thorium and uranium (fig. 7-19).

Figures 7-19 and 7-20 compare the gamma log, paleontologic and geologic crater zones, and general lithologies for KOA and OAK crater areas. Only boreholes on transects with full geologic sampling and open-hole gamma logs were utilized for this comparison. Essentially, the gamma logs confirm the general trends in radionuclide abundance (Ristvet and Tremba, 1986; and fig. 7-21). The Beta-2 / Beta-3 boundary (where present) and the Beta-1 / Gamma boundary (where present) appear to represent the demarcation between occurrence and absence of device-produced radionuclides. Naturally occurring radionuclides appear to reflect the presence of deep-piped material in the Beta-3 crater zone. Device-produced radionuclides are most abundant within the bottom of Alpha-2 (graded sands) and top of Beta-1a (graded rubble) in OBZ-4 and OPZ-18, respectively. In KBZ-4, they are most abundant at the base of Alpha-1 and at the top of Alpha-2. In KCT-5, there is only a trace of radionuclides (device-produced and natural). In borehole OCT-5, device-produced radionuclides are most abundant within the lower part of the Beta-1a crater zone. In OKT-13, device-produced radionuclides show two peaks, one within Beta-1a and the other (larger) near the base of Beta 1b.

Distribution of Radionuclides

The distribution of radionuclides within OAK crater is shown in Figure 7-21 (Ristvet and Tremba, 1986). In OBZ-4, the device-produced radionuclide (Cesium-137) is common in Alpha 1, Alpha 2, and Beta 1a, with peak abundance in Alpha 2. Most of the crater-fill in OPZ-18 consists of muddier sediments than OBZ-4 and consequently contains higher concentrations of Cesium-137. In OPZ-18, radionuclides are common to Alpha 1, Beta 1a, Beta 1b, and Beta 2; the Beta 2 occurrences represent the injected material. Peak abundance is in the upper part of Beta 1a. A moderate amount of cesium is found in OKT-13 below and above the "hiatus" sand (Beta 1s), in Beta 1b, and in Beta 1a and Alpha, respectively.

Radionuclides are sparse in KOA crater and only common within KBZ-4. Here, they mimic the gamma-ray profile (fig. 7-20), with peak abundance in Alpha 1 and a trace at the base of Beta 1b and top of Beta 2.

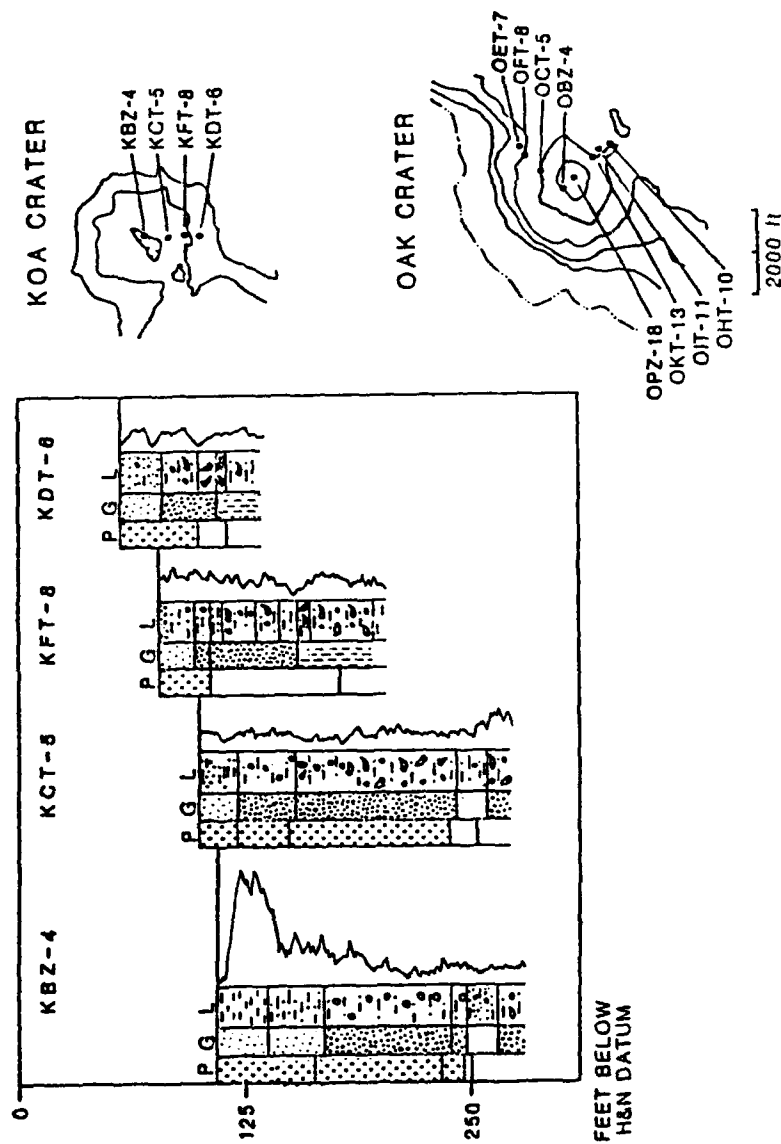


FIGURE 7-20. --- Borehole lithology (L), geologic (G) and paleontologic (P) crater zones, and gamma-ray logs for selected boreholes, KOA crater, and index maps for the KOA and OAK craters. Symbols the same as Figure 7-19.

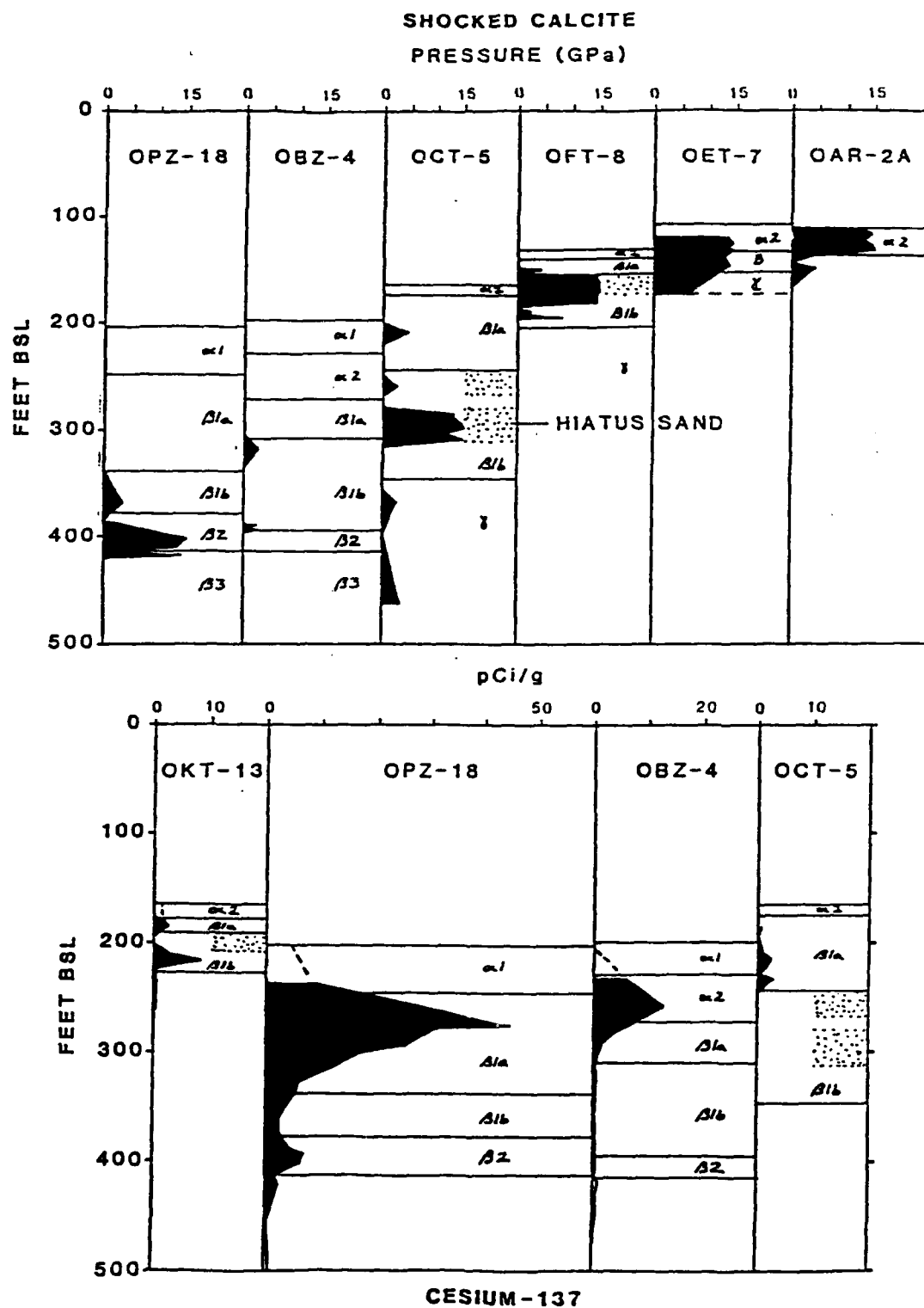


FIGURE 7-21. — Distribution of shocked calcite and Cesium-137 and relationship to crater zones in boreholes analyzed in OAK crater.

Distribution of Shocked Calcite

The distribution of shocked calcite is shown in Figure 7-21 (Polansky and Ahrens, Ch. 4 of this report). Only sparse, possibly moderately shocked calcite is present in the central crater area within Beta 1b. Highly shocked calcite is found within the injected material in OPZ-18. Under the terraces, possibly moderately shocked calcite is found in Beta 1a, Beta 1b, and Gamma with highly shocked calcite in the "hiatus" sand, Beta 1s. Outside the limits of crater-derived rubble (Beta zone), highly shocked calcite occurs in Alpha 2 and Beta in OET-7 and in Alpha 2 in OAR-2A. The material in OAR-2A represents post-event deposition of shocked calcite away from the crater, probably by the sweeping away of fine-grained ejecta from the reef tract by currents and redeposition of it in the area of OAR-2A. The material in OET-7 in graded sands (Alpha 2) seems to represent post-event deposition like that in OAR-2A. The material in OET-7 in the undifferentiated rubble apparently represents buried ejecta.

Depression and Uplift of Structural Surfaces

The surface at the top of the Pleistocene in both the OAK and KOA areas shows a pattern of central removal and lateral depression on the net-change (delta) figures (figs. 7-22A and 7-23A, respectively) derived from the pre- and post-shot surface contour maps (figs. 7-4 and 7-24). In addition, in the OAK area, two lateral depression troughs are developed along the pre-shot slope from reef to lagoon. Also, the Pleistocene surface appears to be irregularly disrupted or preserved beneath the debris blanket (dashed lines, fig. 7-22A) and irregularly uplifted near the margins of the debris blanket. The maximum current depression observed in OAK is 63 ft and in KOA is 53 ft. The maximum uplift in OAK is 14 ft. No strata in KOA are currently uplifted.

The surface at the top of the Pliocene in the OAK area (fig. 7-22B) shows central concentric depression slightly skewed toward the reef and a broad region of shallow uplift beneath both the debris blanket and the lagoon. The maximum depression is 193 ft beneath GZ. The maximum uplift appears to be about 21 ft. The Pliocene surface in the KOA area certainly was influenced by detonation of the MIKE device (fig. 7-23B). KOA shows a complicated pattern of depression with maximum depression on the lateral wings away from GZ. The pattern of depression from MIKE crater area would suggest that the area in the proximity of KOA GZ experienced 0 to 10 ft depression and the entire region from KOA GZ to MIKE experienced progressively greater depression toward MIKE. This possibly influenced the apparent lateral extension in depression roughly perpendicular to the line from KOA ground-zero to MIKE ground-zero.

COMPARISON OF OAK AND KOA CRATERS

The following comparisons and contrasts can be made between KOA and OAK craters:

- (1). The base of the zone of sonic degradation (ZSD) is similar in both craters -- 1,139 ft bsl for OAK ground-zero (GZ) and 1,101 ft bsl for KOA GZ. The ZSD appears to form a narrower cone at KOA

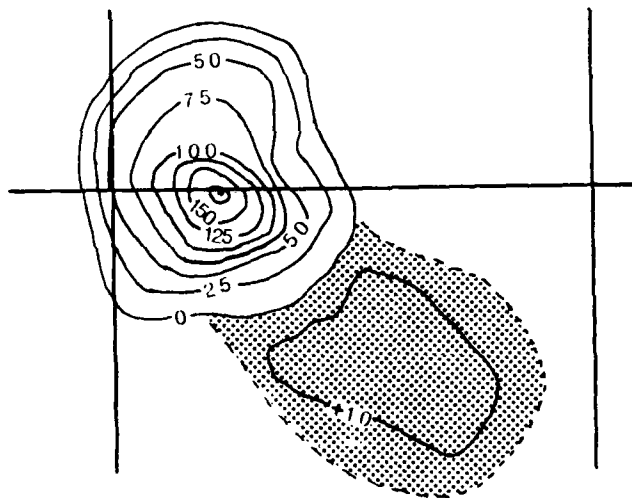
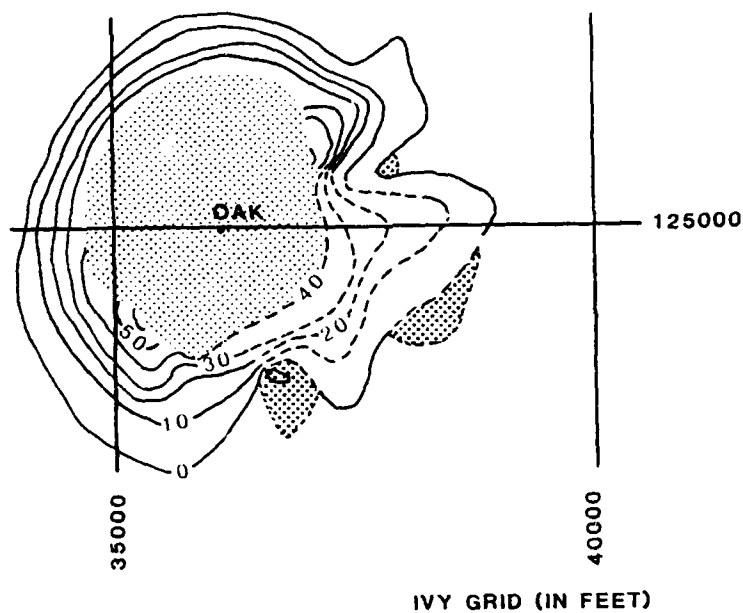


FIGURE 7-22. -- Maximum depression/uplift of Pleistocene and Pliocene surfaces, OAK crater. Pleistocene surface is projected beneath debris blanket, where it is disrupted but probably remains as several isolated outliers such as encountered in OIT-11. Surface is lightly stippled where removed, heavily stippled where uplifted.

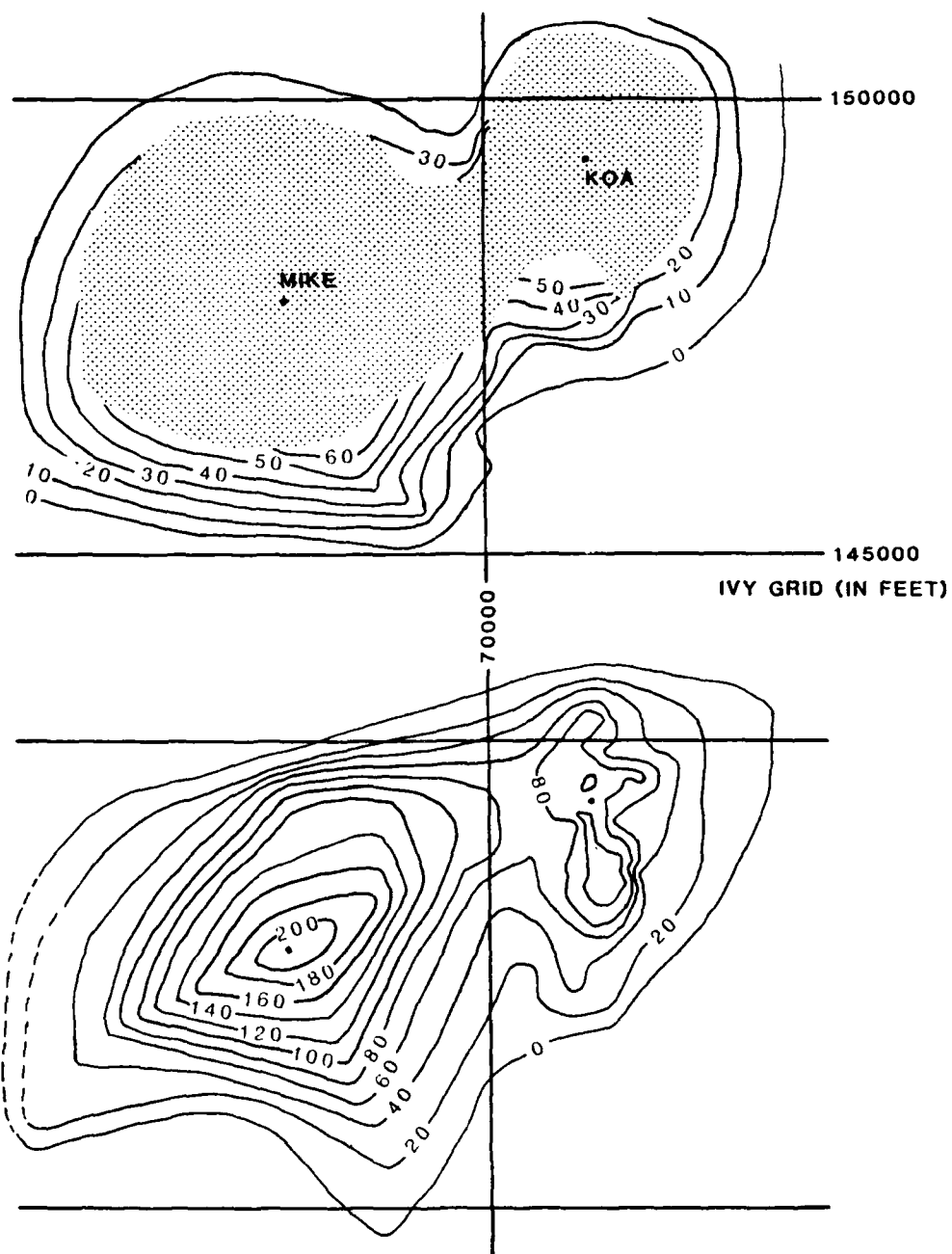


FIGURE 7-23. -- Maximum depression of Pleistocene and Pliocene surfaces, KOA crater. Surface is lightly stippled where removed.

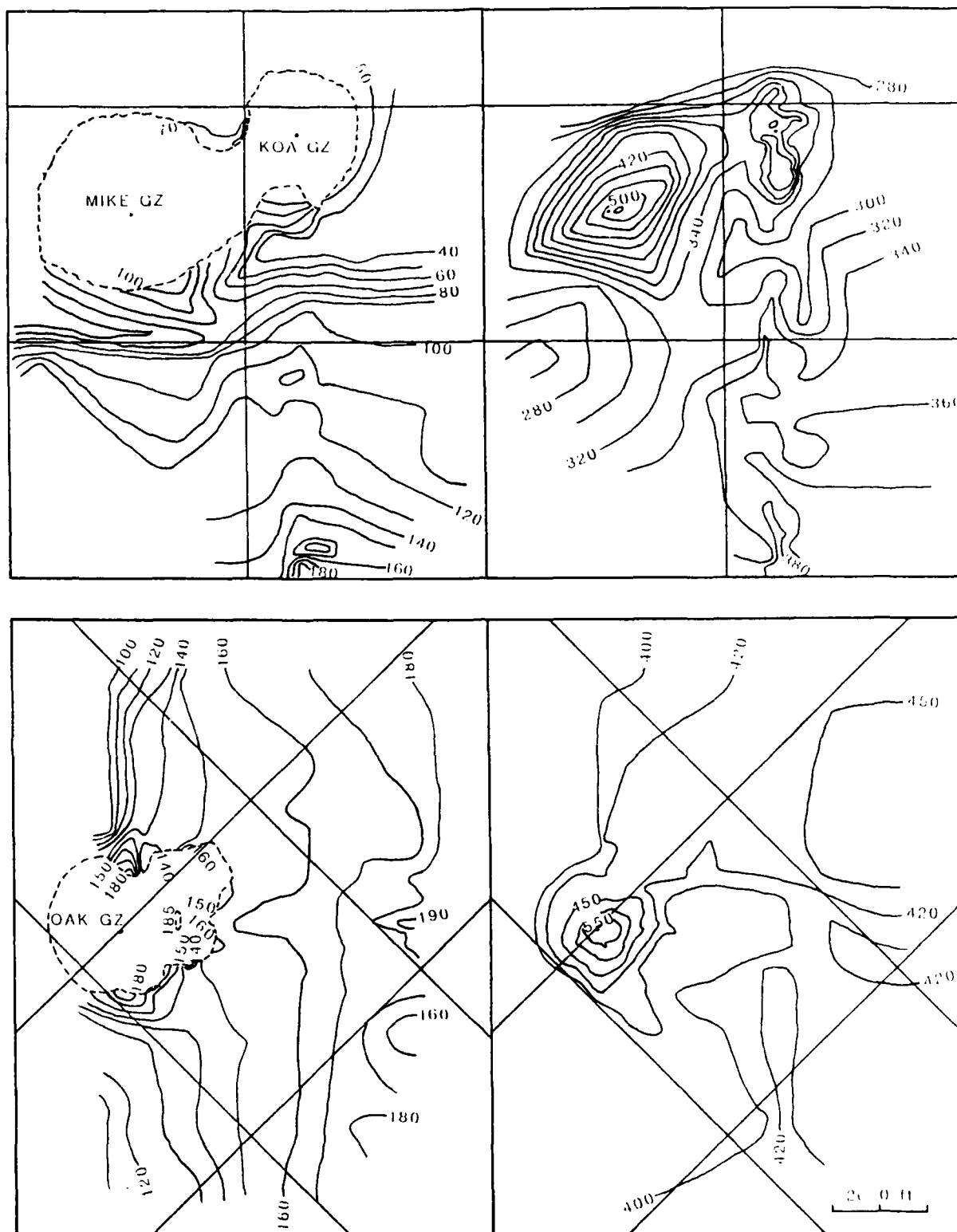


FIGURE 7-24. -- Present-day (post-shot) location of Pleistocene and Pliocene surfaces, KOA and OAK craters. Contours in ft below H&N datum (bsl).

- (2). MP-3, the significantly cemented and altered zone, was probably 246 ft thick with the top at 280 ft bsl at KOA GZ and 183 ft thick with the top at 400 ft bsl at OAK GZ.
- (3). MP-3 is depressed approximately 193 ft at OAK GZ and approximately 89 ft at KOA GZ. MP-3 shows depression and fracture at OAK and, in addition, at KOA, shows apparent rebound in the central part of the crater.
- (4). At ground-zero, the Alpha zone (mud and graded sand) is comparable between KOA and OAK; however, the Beta zone (rubble) is twice as thick at OAK. In particular, Beta 3 (rubble floatstone) is much thinner at KOA. The total lateral extent of the Beta zone is nearly the same at both craters.
- (5). The transition sand (Beta 2) is more extensive in KOA than OAK, with an average diameter of approximately 918 ft at KOA and 816 ft at OAK. The transition sand is more elongate oval at KOA than at OAK.
- (6). The collapse rubble (Beta 1b) is similar in both craters, although thicker in OAK. The Beta 1b zone thins toward the lagoon at OAK and thins toward MIKE crater at KOA.
- (7). The hiatus sand (Beta 1s) is much less extensive at KOA, presumably due to thinner and shorter-term deposition and to more extensive destruction by late-stage collapse.
- (8). The graded rubble (Beta 1a) is similar in both craters. The rubble becomes thicker and muddier in the direction of the lagoon at OAK (i.e., toward its distal margin) and in the direction of MIKE crater in KOA. For all intent and purpose, for the KOA event, MIKE served as a "lagoon" similar to the natural lagoon off OAK, but much smaller in extent.
- (9). The graded sands (Alpha 2) are similar in both craters. This zone is common throughout the KOA crater but absent near the bathymetric center (OPZ-18) of OAK crater.
- (10). Mud (Alpha 1) occupies the central region of both craters.
- (11). A debris blanket is extensive on the lagoon side of OAK; only two possible debris mounds of limited distribution exist on the MIKE-side of KOA.
- (12). Deep-piped material is common only in Alpha 2 in KOA and probably vented in a limited area at the central crater. Deep-piped material is common to Alpha 1, Alpha 2, and Beta 1a in OAK and probably vented in an extensive area of the central crater and terraces.
- (13). Shallow-piped material is common to Alpha and Beta 1a zones throughout the crater wings and found in all zones in the central crater in both craters. In KOA, it is represented by EE-GG material in the central

crater and EE material in the crater wings. In OAK, it is represented by FF/GG material throughout the crater.

- (14). KOA crater is characterized by late-time sedimentation exceeding subsidence. OAK crater, in contrast, is characterized by late-time subsidence exceeding sedimentation.
- (15). Device-produced radionuclides appear to be mostly limited to the Beta 2 and overlying zones in the craters. Radionuclides were detectable only in KBZ-4 for the KOA crater. In OAK crater, peak abundance of device-produced radionuclides progressively moves down in the crater zones away from GZ. For example, the peak abundance is in Alpha 2 in OBZ-4, at the top of Beta 1a in OPZ-18, at the bottom of Beta 1a at OCT-5, and at the bottom of Beta 1b at OKT-13.

GEOLOGIC CRATER MODEL FOR OAK AND KOA

The transition sand (Beta 2) represents the remnants of the base of the excavational crater. It is characterized by sand-sized material that is formed by fracture and pulverization, by its transitional nature from mixed paleontology to unmixed paleontology within it, and by its containing injection dikes and debris. That shocked calcite is not common within the transition sand is due to two factors: (1) the sampling technique used in which granule- and larger-sized clasts were predominantly sampled (Polansky and Ahrens, 1987, Ch. 4 of this report), and (2) the relatively low shock pressures that probably existed in this region at formation (< 15 kilobars).

The rubble floatstone (Beta 3), beneath the base of the excavational crater (Beta 2), may represent fracture and disruption of sediment and rock caused by the maximum growth of the transient crater.

The collapse rubble (Beta 1b) represents crater-sidewall and partial flap collapse. This zone reflects paleontologic mixing of zones near the base of the excavational crater. The asymmetric crater at OAK demonstrates partial sidewall and flap collapse and movement down the resulting slope away from the transient crater to form the majority of the debris blanket. The part of the flap involved in craterward collapse is that closest to the sidewall which would represent paleontologic zones contained in the sidewall itself. That the paleontologic mixing seems to reflect mixing of material from zones near the base of the crater suggests that most of this unit was deposited rapidly as a single, major, crater-wide collapse feature. This major collapse appears to have destroyed the lateral part of the excavational crater base and its sidewalls. The highly mixed material in the central crater bowl represents a variety of depositional modes that may include wash-back and piping of sufficient magnitude to keep the central bowl "boiling" (continuously mixing). This part of the unit was deposited contemporaneously with the "hiatus" sand (Beta 1s) which represents wash-back and a brief period of quasi-stabilization of the crater and deposition of post-event sediments. The "hiatus" sand is well sorted and contains the highest concentration of shocked calcite indicating deposition from wash-back and fall-back, but, curiously, contains no radionuclides. At OAK and KOA craters, the occurrences of radionuclides are spotty. The decades that have transpired since the event have allowed many radionuclides to dissipate (Ristvet and Tremba, 1986). The

remaining commonly detectable radionuclide is Cesium-137. It is associated with muddy sediments (McMurtry and others, 1985; Wardlaw and Henry, 1986b) and may have been preferentially deposited with muds, and, therefore, would not be common in well-sorted sands. Cesium-137 is involved in progressively younger and muddier deposits in the crater-fill toward ground-zero. Its absence in the "hiatus" sand probably indicates the winnowing out of silt and finer grains during the wash-back / fall-back process.

The graded rubble (Beta 1a) represents deposition probably caused by several major slumps. This indicates that subsidence significantly destabilized the existing crater margins and resulted in collapse. One such collapse in OAK appears to have originated on the reef side. Material from this collapse flowed through the crater and breached the debris blanket, leaving deposits on top of the debris blanket (OHT-10, OJT-12), and flowed out into the lagoon, as seen in the enhanced sea-floor image of OAK (fig. 7-14).

The graded sands and slumps (Alpha 2) represent late-stage, local collapse and deposition of the expanding and subsiding crater margins.

Late-stage mud (Alpha 1) represents post-event, low-energy deposition within the central crater. The differences in Alpha 1 and distal Alpha 2 sands are slight, as shown by the sediment analysis by Melzer and Patti (written communication, 1987).

The idealized distribution of these crater units is shown for a symmetric crater (KOA, fig. 7-25A) and for a asymmetric crater (OAK, fig. 7-25B). The gradational units beneath the transition sand that represent gradually less-stressed sediment and rock within the significantly fractured zone of sonic degradation are also shown.

Thinning Analysis

This analysis simply compares the pre-shot model of inferred horizon location to the measured post-shot position. The comparison of positions is shown in Figures 7-26 to 7-29 and Tables 7-5 and 7-7. The analysis is displayed graphically in Figures 7-30 and 7-31 and tabulated in Tables 7-6 and 7-8. The upper correlation line in Figures 7-30 and 7-31 correlates the pre-shot model to the probable original stratigraphic depth now preserved beneath crater-fill (where present).

Stratigraphic Density Profile

The analysis of the borehole gravity surveys (Beyer, Ristvet, and Oberste-Lehn, 1986; and Beyer, Ch. 2 of this report) provide valuable information about bulk density of the strata in the vicinity of OAK crater. By averaging the borehole-gravimetry results within stratigraphic units, the density change can be compared directly with inferred stratigraphic thinning or thickening for areas where borehole gravity surveys were taken. Figure 7-32 and Table 7-9 relate the gravimetry results to the stratigraphic units. MP-2a appears anomalously dense in the reference sections. The average of MP units 2a-c in the reference sections is utilized to compensate for this anomalous density, especially to compare to crater-fill material in the analysis.

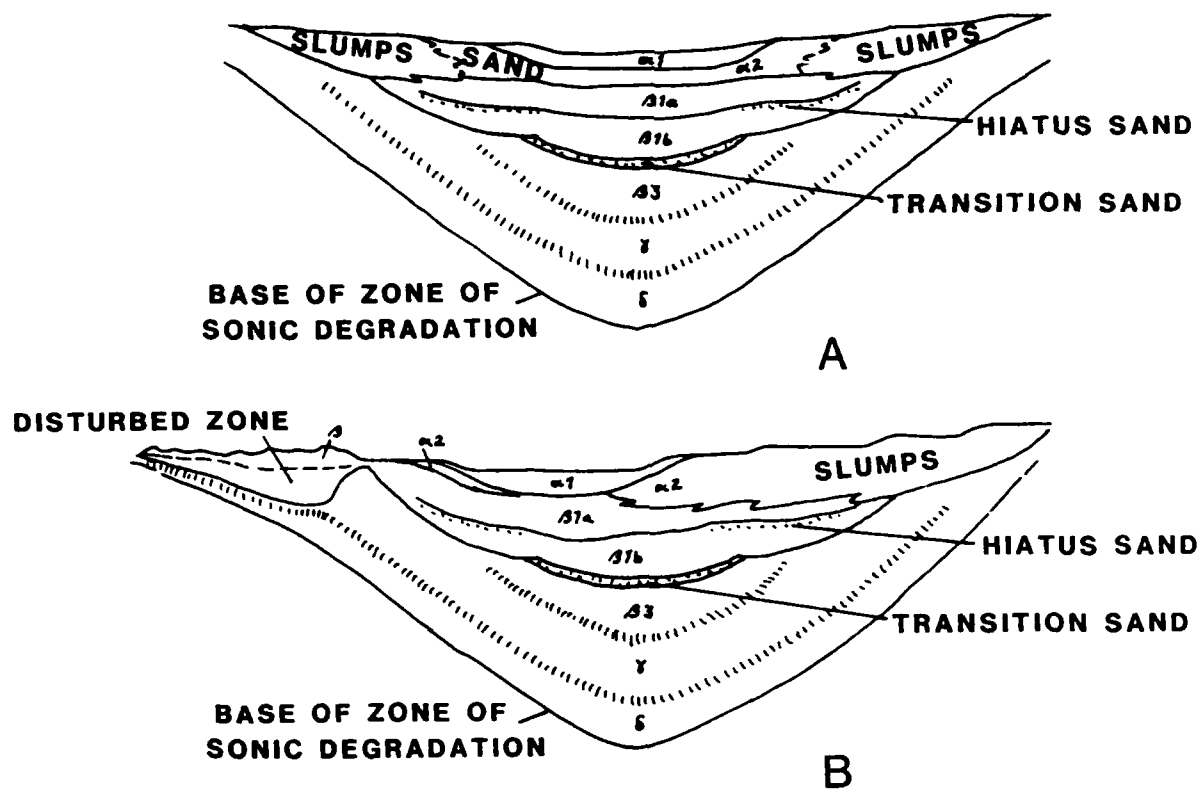


FIGURE 7-25. -- Idealized model of geologic crater for a symmetric crater (A) and an asymmetric crater developed on a significant slope (B).

TABLE 7-5. -- Depth (ft bsl) to MP unit boundaries, pre- and post-shot, OAK crater. Boreholes listed in order of increasing distance from ground zero.

UNIT	OBZ-4		OPZ-18		OCT-5		OTG-23		OUT-24	
1	14	-	47	-	16.5	-	45	-	2	-
2a	123	-	128	-	115	-	128	-	106	-
2b	165	-	166	-	155	-	168	-	145	-
2c	265	-	275	-	255	368.4	253	?	225	373.0
2d	315	-	363	568.9	305	417.9	327	434.0	276	407.0
3a	395	593.0	410	593.0	387	432.7	409	484.0	355	457.1
3b	544	701.2	555	723.5	534	572.2	544	610.0	490	592.0
4a	592	747.3	600	761.9	585	623.7	594	669.0	528	630.0
4b	775	847.7	765	809.9	785	799.7	766	787.0	784	784.0
5a	950	1013.8	956	1000.0	945	944.6	1000	1000.4	925	925.0
5b	1050	1065.1	1050	1063.0	-	-	-	-	1025	1025.0
5c	1115	1114.6	1114	1114.0	-	-	-	-	-	-

UNIT	OKT-13		OFT-8		OIT-11		OET-7		OQT-19	
1	102	-	16	-	122	-	18	-	46	-
2a	141	-	115	204.1	147	185.4	118	173.4	129	168.0
2b	170	232.9	155	223.3	209	247.4	167	220.6	195	233.9
2c	275	326.6	230	272.0	-	-	279	294.7	240	274.7
2d	362	411.6	305	344.6	345	375.0	305	320.4	330	365.3
3a	410	431.3	390	419.8	405	434.8	395	410.0	406	413.3
3b	547	564.0	535	565.0	545	562.0	540	555.0	548	548.3
4a	598	614.7	589	618.0	591	608.0	595	610.0	588	587.5
4b	766	765.8	794	794.0	758	758.0	793	793.0	767	766.5
5a	975	974.5	925	925.0	980	980.0	925	925.0	1020	1020.1
5b	1037	1036.5	-	-	-	-	-	-	-	-
5c	-	-	-	-	-	-	-	-	-	-

UNIT	OHT-10		OJT-12		ODT-6		ONT-16		ORT-20	
1	124	-	115	-	20	-	132	-	70	-
2a	152	-	149	-	116	161.5	149	-	130.5	160.6
2b	212	213.3	216	238.0	160	201.3	219	238.6	187	216.2
2c	-	-	-	-	231	231.3	-	-	243	262.7
2d	361	360.8	350	350.0	315	315.0	338	337.8	327	346.7
3a	419	403.4	405	390.3	397	397.0	407	395.2	405	411.7
3b	547	531.4	547	531.0	546	546.0	550	537.9	552	552.0
4a	600	584.0	600	584.0	594	594.0	600	588.0	586	586.4
4b	751	751.1	732	732.0	792	792.0	715	715.0	767	767.0
5a	987	987.3	991	991.0	925	925.0	994	993.8	1014	1013.5
5b	-	-	-	-	-	-	-	-	-	-
5c	-	-	-	-	-	-	-	-	-	-

(TABLE 7-5 continued on next page.)

TABLE 7-5. (continued from preceeding page.)

UNIT	OMT-15		OLT-14	
1	142	-	132	-
2a	153	140.8	158	159.4
2b	225	225.0	227	227.0
2c	-	-	-	-
2d	335	334.6	341	341.1
3a	395	373.9	399	383.8
3b	551	529.7	550	534.6
4a	600	579.0	600	585.0
4b	702	701.9	700	700.0
5a	1014	1013.5	1010	1010.2

Distance of boreholes from surface ground-zero, in feet:

OBZ-4	7
OPZ-18	335
OCT-5	658
OTG-23	804
OUT-24	858
OKT-13	989
OFT-8	1129
OIT-11	1206
OET-7	1375
OQT-19	1444
OHT-10	1462
OJT-12	1696
ODT-6	1715
ONT-16	1827
ORT-20	1846
OMT-15	2204
OLT-14	2754

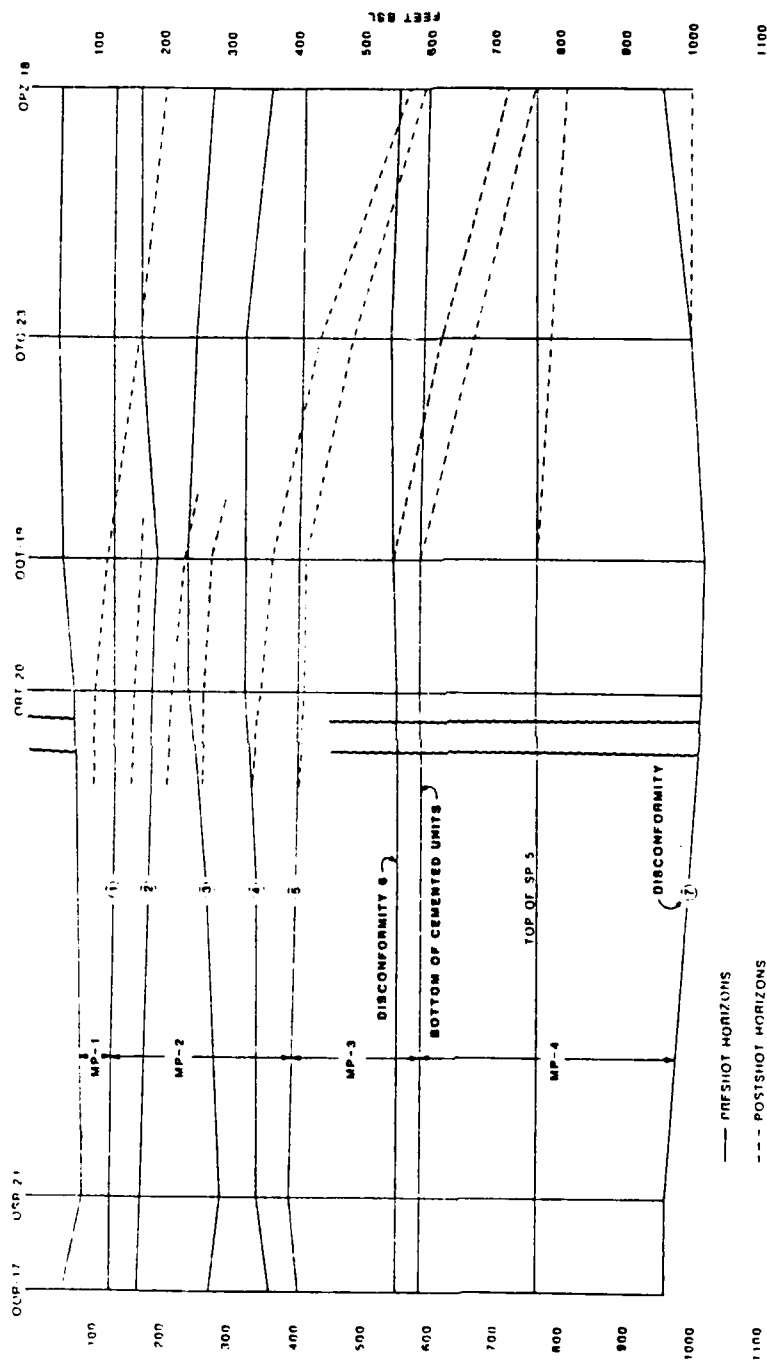


FIGURE 7-26. -- Horizon location in fence diagram from boreholes OOR-17 to OOR-18. Pre-shot location as a solid line except for unit MP-4a/4b boundary which is short dashes. Dashed line represents post-shot location where different from pre-shot location. Squiggles, breaks, and scale as in Figure 7-8.

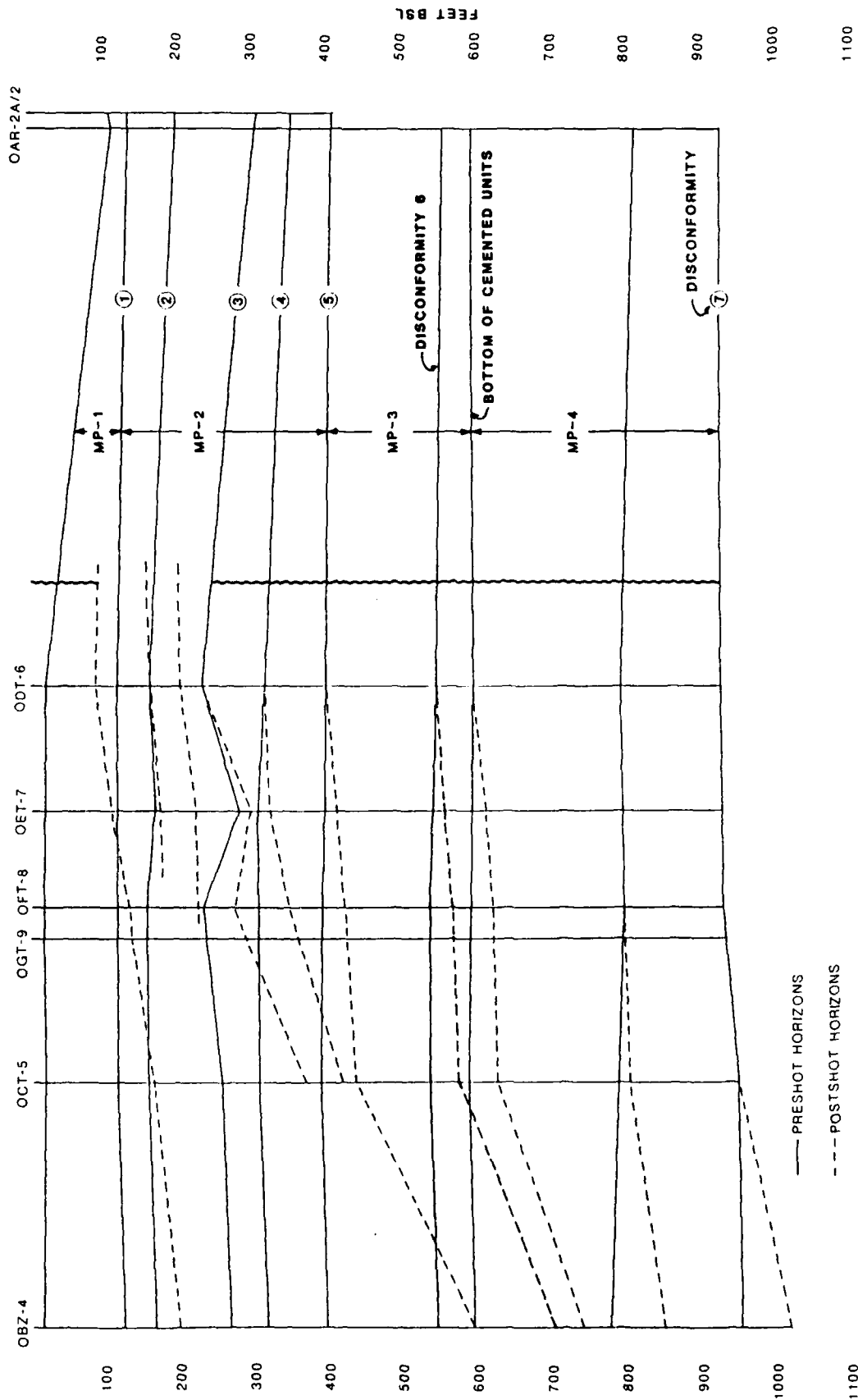


FIGURE 7-27. -- Horizon location in fence diagram from boreholes OBZ-4 to OAR-2/2A as in Figure 7-26. Squiggles, breaks, and scale as in Figure 7-9.

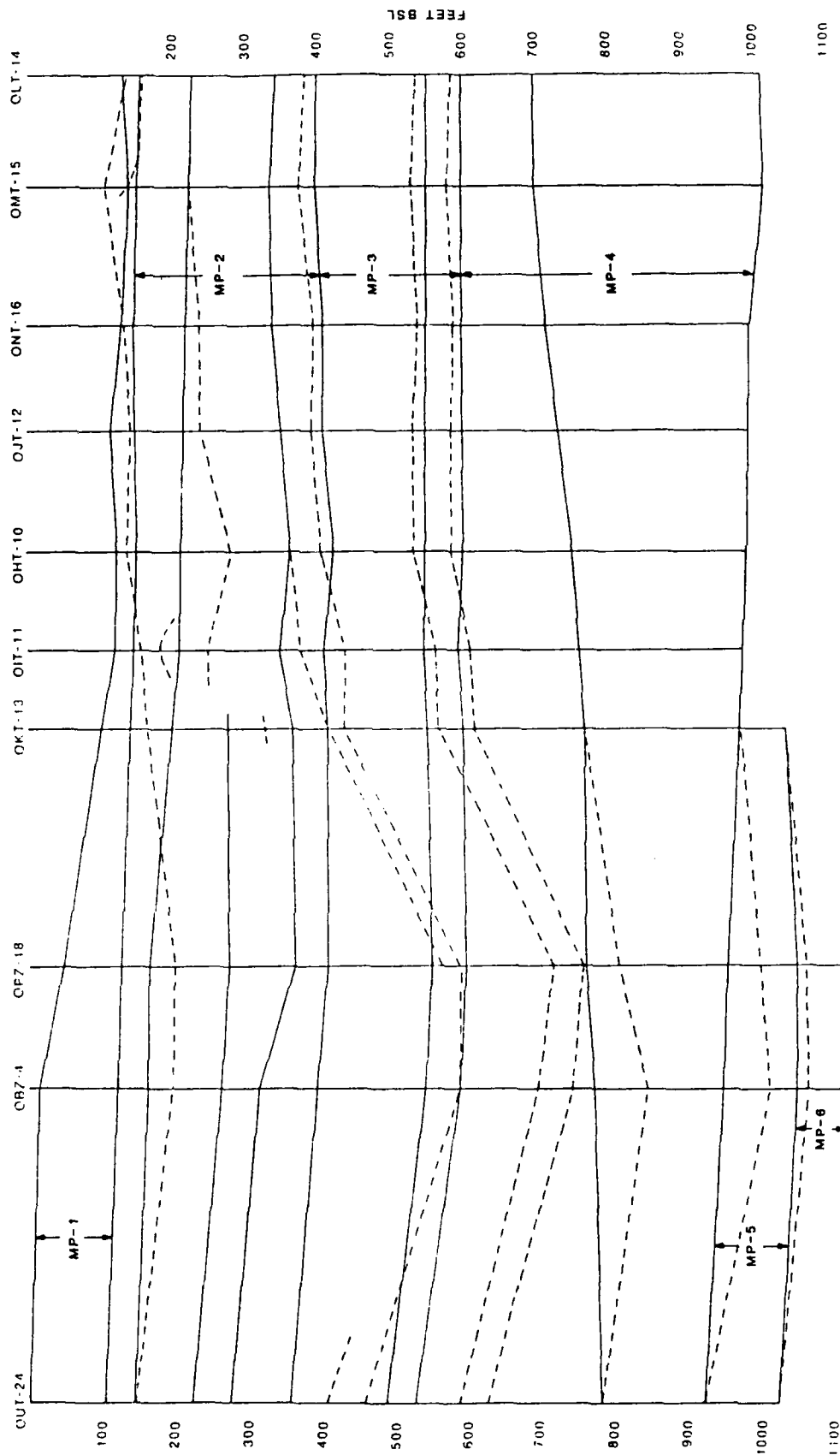


FIGURE 7-28. -- Horizon location in fence diagram from boreholes OUT-24 to OLT-14 as in Figure 7-26. Scale is vertically exaggerated 2:1.

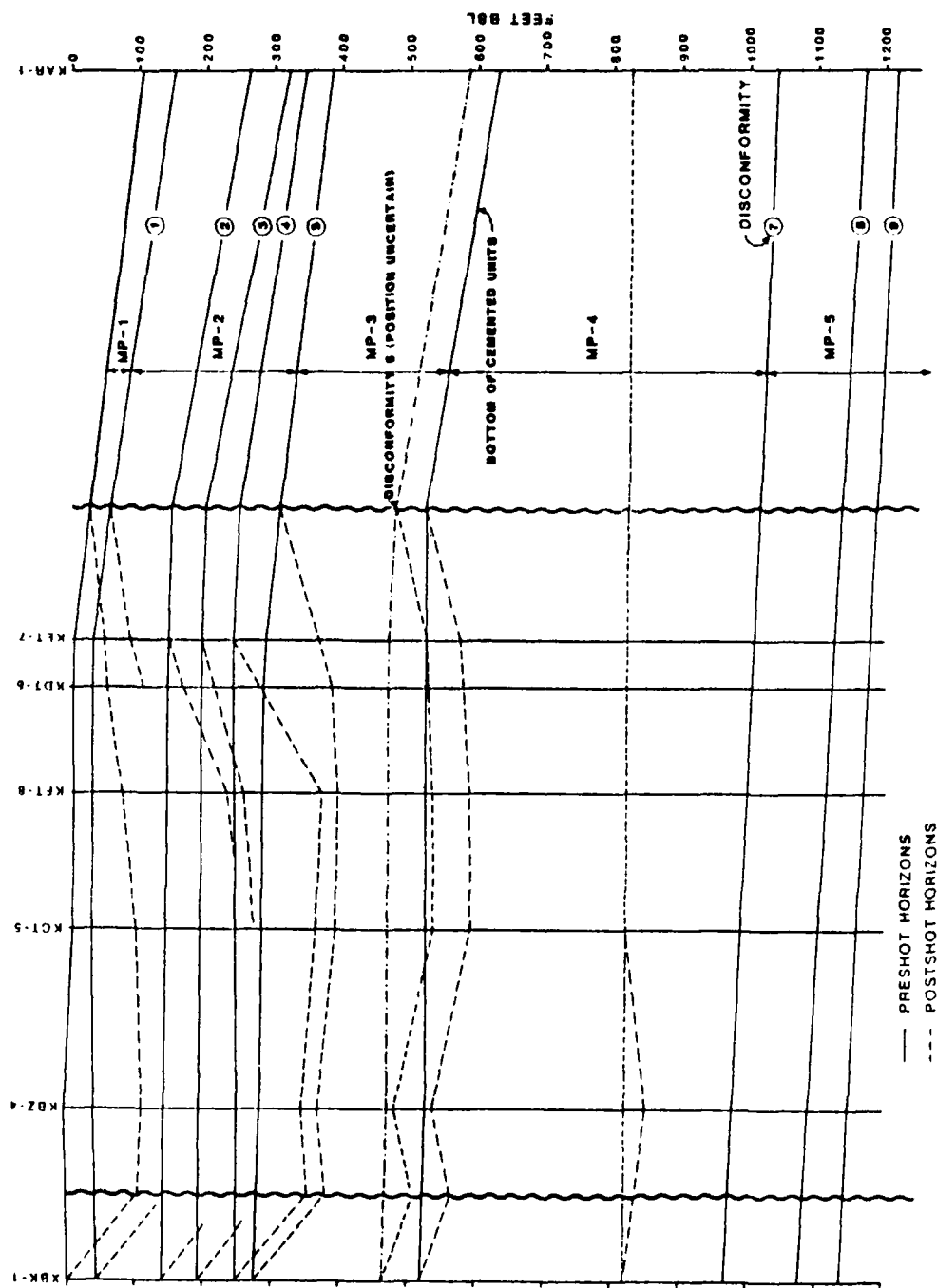


FIGURE 7-29. -- Horizon location in fence diagram from boreholes XBK-1a to KET-7 as in Figure 7-26. Squiggles, breaks, and scale as in Figure 7-7.

TABLE 7-6. -- Thinning/thickening analysis (in percent) of MP units beneath OAK crater. * = percent removed, where removal has occurred lower number indicates thinning in remaining sediments; + = percent thickened; averages indicated by brackets are weighted.

UNIT	OBZ-4	OPZ-18	OCT-5	OTG-23	OUT-24	OKT-13
1*	100	100	100	100	100	100
1	-	-	-	-	-	-
2*	28	17	40	26	28	11
2a	-	-	-	-	-	-
2b	- 02	- 08	- 47	- 19	- 30	11 15
2c	-	-	01	-	33	02
2d	-	49	69	39	37	59
3a	27 22	10 11	05 04	00 00	00 00	03 02
3b	04	15	00	00	00	01
4a	45 26	71 33	12 11	31 18	40 26	10 05
4b	05	00	09	09	00	00
5a	49 39	33 28	00	00	00	00
5b	23	20	00	00	00	00
UNIT	OFT-8	OIT-11	OET-7	OQT-19	ODT-6	ORT-20
1*	100	40	14	23	10	00
1	-	09	37	21	14	02
2*	00	00	00	00	00	00
2a	52	00	04	00	10	02
2b	35 22	06 03	34 15	09 11	68 16	17 09
2c	03	-	01	00	00	00
2d	12	00	00	37	00	17
3a	00 00	09 07	00 00	05 04	00 00	05 04
3b	00	00	00	00	00	00
4a	14 09	10 04	09 05	00	00	00
4b	00	00	00	00	00	00
5a	00	00	00	00	00	00
5b	00	00	00	00	00	00
UNIT	OHT-10	OJT-12	ONT-16	OMT-15	OLT-14	
1*	100	100	100	89	53	
1	-	-	-	-	-	
2*	09	14	02	00	00	
2a	-	-	-	+17	02	
2b	- 13	16 18	17 13	00 10	00 07	
2c	-	-	-	-	-	
2d	27	27	17	35	18	
3a	00	00	00	00	00	
3b	00	00	00	00	00	
4a	+11 +04	+12 +04	+10 +03	+21 +05	+15 +04	
4b	00	00	00	00	00	
5a	00	00	00	00	00	
5b	00	00	00	00	00	

TABLE 7-7. -- Depths (ft bsl) to MP unit boundaries, pre- and post-shot, KOA crater. Boreholes listed in order of increasing distance from ground-zero.

UNIT	KBZ-4		KCT-5		KFT-8		KDT-6		KET-7	
1	+7	-	7	-	6	-	5	-	5	-
2a	37	-	35	-	33	-	33	-	32	-
2b	145	(247.2)	146	(242.5)	146	233.1	147	166.8	148	148.0
2c	193	287.0	195	274.3	195	257.4	195	215.0	195	195.0
2d	250	344.0	246	365.4	244	372.0	243	282.0	242	242.0
3a	282	368.6	285	392.9	285	395.6	286	382.0	288	368.0
3b	470	480.7	470	-	470	-	470	-	470	-
4a	528	539.0	526	593.0	525	590.0	525	581.0	525	575.0
4b	820	848.1	820	820.0	820	820.0	820	820.0	820	820.0
5a	979	979.0	996	996.0	999	999.0	1005	1005.0	1008	1008.0
5b	1090	1089.6	-	-	-	-	-	-	-	-
5c	1147	1147.3	-	-	-	-	-	-	-	-

Distance of boreholes from ground-zero, in feet:

KBZ-4	12
KCT-5	645
KFT-8	870
KDT-6	1182
KET-7	1326

TABLE 7-8. -- Thinning/thickening analysis (in percent) of MP units beneath KOA crater, symbols as in Table 7-6.

UNIT	KBZ-4		KCT-5		KFT-8		KDT-6		KET-7	
1*	100		100		100		100		00	
1	-		-		-		-		+110	
2*	44		55		17		00		00	
2a	-		-		-		49		50	
2b	18	12	+64	+08	49	+16	00	+07	00	+08
2c	00		+78		+133		+39		00	
2d	24		30		57		+132		+173	
3a	41	31		17		19		17		13
3b	00									
4a	+05	03	23	15	23	14	19	12	17	11
4b	18		00		00		00		00	
5a	00		00		00		00		00	
5b	00		00		00		00		00	

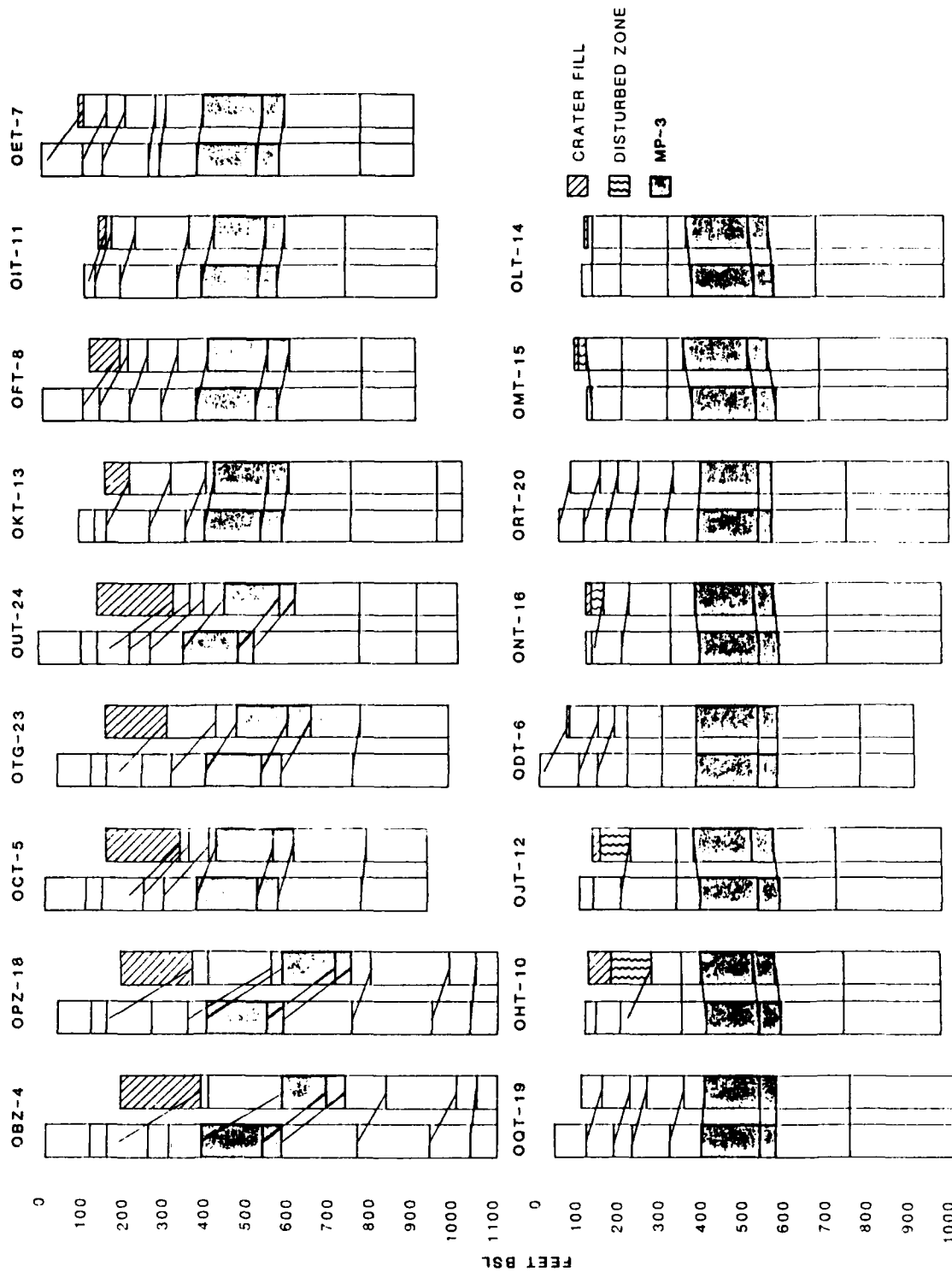


FIGURE 7-30. -- Graphic thinning analysis for OAK crater boreholes.
Correlation lines connect pre- and post-shot position of major horizons
including stratigraphic base of crater-fill.

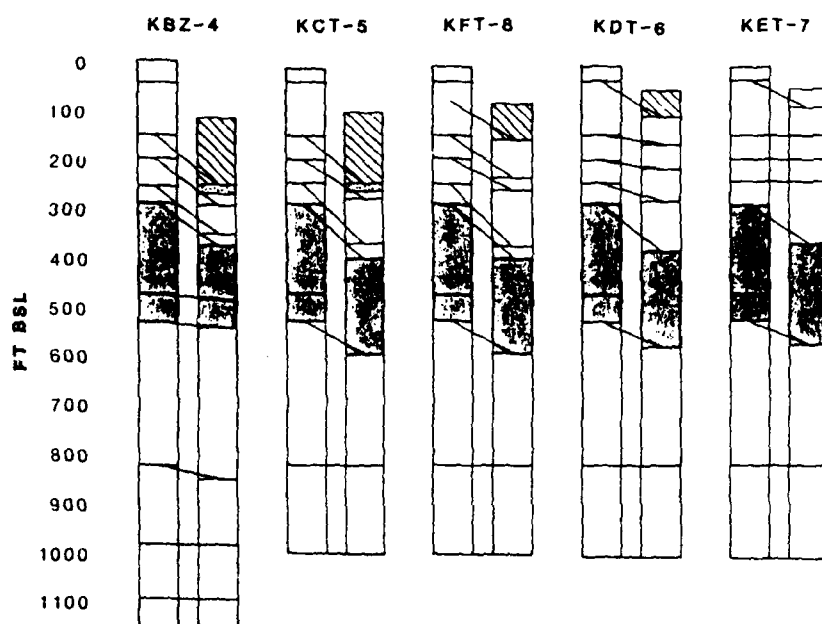


FIGURE 7-31. -- Graphic thinning analysis for KOA crater boreholes as in Figure 7-30.

TABLE 7-9. -- Stratigraphic bulk density analysis. Values in gm/cc. Change from bulk density model (the composite reference sections) is indicated in parenthesis.

AVERAGE DENSITIES FOR STRATIGRAPHIC MATERIAL PROPERTY UNITS AND CRATER ZONES						
MODEL	ORT-20	OQT-19	OTG-23	OPZ-18		
1	--	1.855	1.895	--	1.812(-.06*)	α
2a	1.965	1.923(-.02)	1.921(-.02)	--	1.876(-.02*)	β_{1a}
2b	1.908	1.918(+.01)	1.904(-)	--	1.982(+.03*)	β_{1b}
2c	1.919	1.923(-)	1.942(+.01)	2.017(+.05)	2.027(+.06*)	β_3
2d	1.920	1.985(+.03)	1.982(+.03)	2.030(+.06)	2.124(+.11)	2c
3a	1.978	1.985(-)	2.018(+.02)	2.052(+.04)	2.167(+.13)	2d
3b	1.976	--	1.950(-.01)	2.063(+.04)	2.116(+.07)	3a
4a	2.011	--	2.025(+.01)	2.150(+.07)	2.080(+.05)	3b
4b	--	--	1.959	--	2.045(+.02)	4a
					1.993(+.02)	4b

The model is the average value for units in the reference boreholes OOR-17 and OSR-21, asterisk (*) indicates the difference in bulk density from average value value of normal sediments (2a-c) which is 1.919, OQT-19 is used for model density value of unit 4b.

α = Alpha β_{1a} = Beta 1a β_{1b} = Beta 1b
 β_2 = Beta 2 β_{3a} = Beta 3a

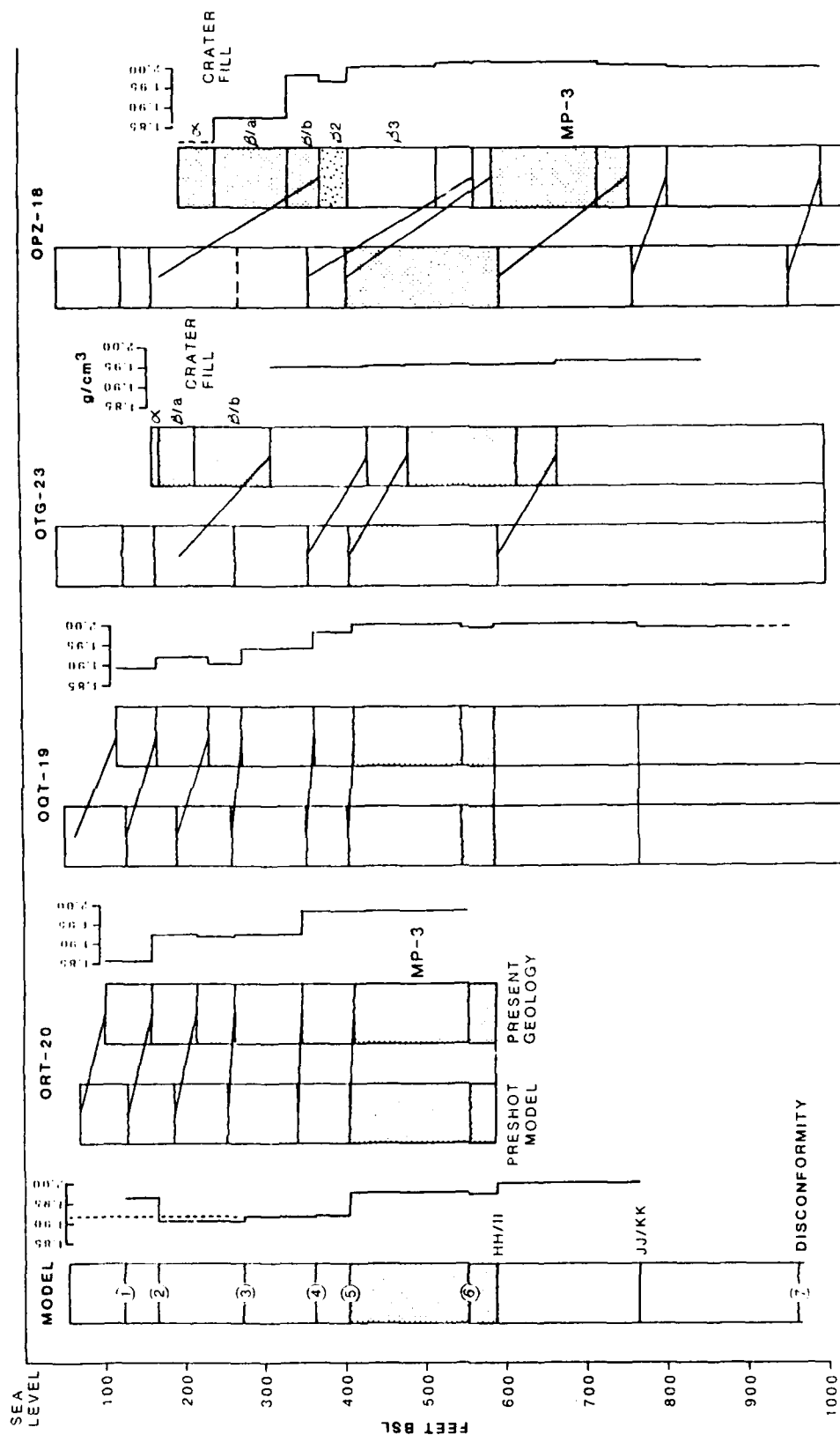


FIGURE 7-32. -- Stratigraphic density profile based on borehole gravimetry.

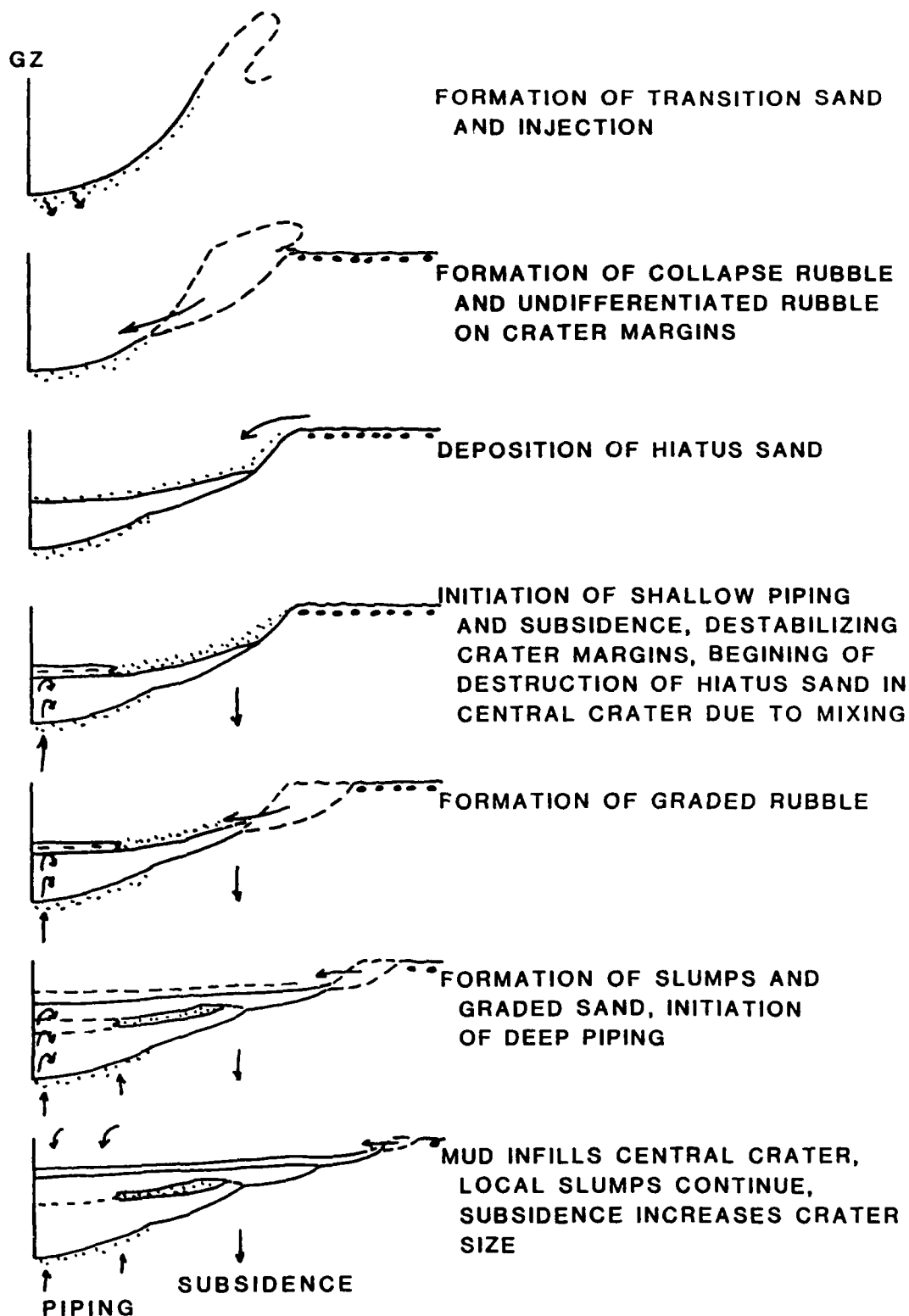


FIGURE 7-33. -- Idealized succession of major depositional events to form geologic crater. No horizontal scale is implied.

General Densification and Flow Patterns

OAK Crater.

The density values measured for the crater zones Alpha and Beta in OAK (OPZ-18) are compared to the average value of normal (undisturbed) sediments in MP-2(a-c). The author feels that the average value for MP-2a through MP-2c also adequately characterizes the upper sediments that were not measured by gamma-gamma density or borehole gravimetry (MP-1 and part of MP-2a). Material in the upper crater zones (Alpha and Beta 1a) in OAK appear to be less dense than normal sediments. Beta 1b and Beta 2 appear to be slightly more dense than normal sediments. Beta 3 has significant densification. Beneath the rubble zone (Beta), the rock and sediment occur in normal stratigraphic order, and density and thinning can be compared directly to the reference sections.

MP-2c (OPZ-18 and OTG-23) immediately subjacent to the Beta zone is moderately densified. Thinning of this unit cannot be calculated because the top of the unit is not preserved in either borehole. However, the significant densification in OPZ-18 suggests this unit behaved similar to the underlying unit, MP-2d in the area of that borehole.

MP-2d under the central crater area shows the most significant densification. However, densification cannot account entirely for the roughly 50 percent thinning of the unit over a wide area.

Densification within MP-3 accounts for most of the thinning observed within that unit except beneath the central crater. Beneath the central crater, collapse of vugs could compensate for considerable volume loss (thinning) with little observed density increase.

MP-4a shows essentially no densification under the central crater area and at least 40 percent thinning over a wide area. MP-4a and MP-4b are differentiated by organic concentration. It is probable that both units flowed and mixed obscuring their relationship in a manner so that the organics identifying MP-4b occur higher than predicted, and thinning in MP-4a is exaggerated (especially in OPZ-18). Nevertheless, the whole unit, MP-4, experienced 20 percent thinning over a wide area that is not accounted for by densification.

If the geologic pre-shot models are correct, than the stratigraphic units that show thinning is excess of that explained by densification must have been partially removed by flow. Two units under the central crater area that indicate significant flow are MP-2d and MP-4a. Material from these units previously has been shown to have been piped (vertical flow) to the surface. Material from MP-4 is involved in the majority of deep piping, but the estimated volume of that material preserved in the crater fill only accounts for a small amount of material that flowed.

It appears most of the volume lost is accounted by lateral flow. Two lines of evidence support this: (1) The density increase detected in MP-4 at the base of OTG-23 suggests lateral densification presumably from lateral

flow, and (2) The uplifted MP-3 over much of the lagoon (refer to fig. 7-21) appears to be caused by thickening of MP-4. This bulging or bulking of MP-4 clearly is visible in all the seismic-reflection survey profiles that run through the lagoon opposite the crater.

Piping (vertical flow) is clearly a post-dynamic phenomenon. The units that appear to have experienced lateral flow, also were involved with late-stage piping. These units in OAK appear to be MP-2c over a limited extent (because it was excavated in the central portion of the crater) and MP-2d, MP-4a, and MP-4b (over a wider extent). Deep piping appears to have been vented initially through the central part of the crater and subsequently through concentric fracture zones developed farther laterally (due to subsidence) represented by the piped mounds or volcanoes preserved on the terraces today. Shallow piping appears to be a more widespread phenomena over the crater area, though it too was, at least partially, vented through the central part of the crater as evidenced by the presence of shallow-piped material in all central crater zones.

KOA Crater.

By comparison with OAK crater, KOA experienced much more shallow lateral and vertical flow within its units. Thinning and bulking (thickening) is observed in MP-2b, MP-2c, and MP-2d. The thinning appears in increasing area in each lower unit and, therefore, the thickening occurs farther from ground-zero with depth. MP-3 appears more thinned than in OAK and may have experienced flow. MP-4 appears to have thinned and flowed. However, the thinning in MP-4 is complicated in its area of distribution; represented by central rebound and perhaps channeled vertical flow through the central uplift. Shallow piping appears to have been pervasive and is indicated by the common EE material in much of the mixed zone. Venting of some of the shallow-piped material in the areas of KBZ-4 and KCT-5 is suggested by the deeper mixing of this shallow-piped material in the crater fill of these boreholes.

Relative Timing of Depositional Events

The idealized succession of depositional events is shown in Figure 7-33.

For purpose of discussion, the following stages of crater development, referred to as craters, are defined:

- (1). Maximum transient crater. That crater formed when the outgoing velocity vector is zero, prior to rebound. The formation of the Beta 3 rubble beneath the excavational crater is thought to represent the maximum transient-crater growth.
- (2). Terminal transient crater. That crater formed at the end of the transient-crater phase, following rebound.
- (3). Collapse crater. That crater formed at the end of the formation of the rubble from the collapse of the sidewall/flap (early stage collapse, Beta 1b).

- (4). Initial slump crater. That crater formed at the end of the formation of late-stage collapse rubble (Beta 1a).
- (5). Apparent crater. That crater observed today, determined by extrapolation of post-shot measurements to the land or water surface at shot time (B. L. Ristvet, personal communication). This crater also has been referred to as the subsidence crater.

For OAK crater, in chronologic order from oldest to youngest, the sequence of depositional events is:

- (1). Formation of transition sand (Beta 2) at base of transient crater, dynamic lateral flow of subsurface units, air-blast deformation.
- (2). Collapse of excavational-crater wall/rim destroying lateral extent of transition sand and forming collapse rubble (Beta 1b); formation of collapse crater; initiation of liquefied (post-dynamic) flow, especially in MP-2c, MP-2d, MP-4a, and MP-4b; and initiation of subsidence.
- (3). Penecontemporaneous formation of undifferentiated rubble zone external of collapse crater by partial flap collapse in addition to prior air-blast deformation.
- (4). Penecontemporaneous formation of debris blanket by probable partial failure and movement of the excavational-crater wall/rim lagoonward.
- (5). Infilling of at least part of remaining crater bowl (collapse crater) by wash- and/or fall-back initiating deposition of "hiatus" sand (Beta 1s); and initiation of winnowing (removal in water suspension) of fine-grained sediments.
- (6). Continuation of deposition of "hiatus" sand over outer crater and contemporaneous initiation of shallow piping in the central crater; continued liquefied lateral flow and subsidence; continued winnowing.
- (7). A sequence of crater-margin collapses to form graded rubble (Beta 1a). One collapse (slump) resulted in a flow large enough to cross the crater, breach the debris blanket, and flow into the lagoon. Subsidence, piping, liquefied lateral flow, and winnowing continued. Shallow-piped material reached the surface throughout the crater before or during initiation of Beta 1a deposition.
- (8). Margin slumping and graded-sand (turbidite) deposition (Alpha 2); subsidence, piping, liquefied lateral flow, and winnowing continued. Deep-piped material reached the surface at the beginning of Alpha 2 deposition.
- (9). Late-time partial infilling of central part of the crater with mud (Alpha 1); subsidence, piping, and lateral flow continuing but progressively less. Mud deposition has continued to present. Local slumping, sand deposition, and winnowing has continued along the reef margin mainly as a consequence of natural geologic processes.

Because the OAK crater developed on a slope, the bathymetric center of the crater moved downslope at the end of early-stage collapse (generally shown as an apparent, progressively lagoonward migration of the low point of successive crater-fill units in fig. 7-25B).

For KOA crater, the events (from oldest to youngest) are:

- (1). Same as in OAK.
- (2). Same as in OAK; liquefied lateral flow especially in MP-2b, MP-2c, MP-2d, MP-4a, and MP-4b.
- (3). Penecontemporaneous formation of debris mounds by partial MIKE-ward collapse and movement of crater wall/rim.
- (4). Same as in OAK, resulting in the much-thickened section at KET-7.
- (5). Same as in OAK.
- (6). Possible deposition of a thin "hiatus" sand over outer crater (this was mostly destroyed by subsequent collapse); initiation of shallow piping; and continued liquefied lateral flow and subsidence.
- (7). A sequence of crater-margin collapse to form graded rubble; subsidence, shallow piping, and liquefied lateral flow continued.
- (8). Margin slumping and graded-sand (turbidite-flow) deposition (Alpha 2) and piping in the central part of the crater; continued but reduced subsidence and lateral flow. Deep-piped material reached the surface at the initiation of Alpha 2 deposition.
- (9). Late-time infilling of central part of the crater with mud (Alpha 1); localized slumping and sand deposition around most of crater (except near MIKE). Subsidence has lessened markedly. Deep piping has discontinued before deposition of mud (Alpha 1).

VOLUME PROBLEMS

Beyer (Ch. 2 of this report) and Trulio (Ch. 6) demonstrate that densification can only account for 8 to 15 percent of the subsidence measured in the crater wings of OAK. Yet OAK appears to be substantially a subsidence crater. Peterson and Henny (Ch. 5) show substantial late-time subsidence (post two months post-shot) by comparing the 1958 H&N post-shot map with the 1984 USGS bathymetric map. Peterson and Henny estimate an apparent (conservative) volume increase of the crater of 231 million cubic ft or 25 percent of the apparent crater volume. Piping clearly demonstrates the existence of a long-term unstable liquefied mass at depth beneath the crater.

Piping is one avenue by which this liquefied mass could achieve stability. It is the expression of liquefied flow vertically. Dikes, lagoon uplift, and densification of MP-4 laterally all demonstrate lateral flow.

Evidence for Piping and Lateral Flow

Piping is not an hypothesis but a process the results of which are observed in both OAK and KOA craters.

Surface. -- Sand volcanoes are present on the terraces of OAK crater (fig. 7-14). Their presence on the terraces indicates that deep piping persisted after the majority of Alpha deposition (slumps and sand turbidity flows) and that flow (at least vertical) is a very long-term process.

Crater-Fill. -- The volume of piped material is estimated for the crater-fill of the central bowl of OAK. Deep-piped material (biostratigraphic zones II-MM) is 4.83 million cubic ft. Shallow-piped material (biostratigraphic zones FF-GG) is 45.62 million cubic ft. Deep-piped material is only surficial outside the central bowl (i.e., on the terraces). Shallow-piped material is throughout the crater-fill above the hiatus sand (Beta 1s), so an appreciable additional volume exists but has not been calculated (further paleontologic study is needed for these estimates). Shallow piping reached the crater surface after deposition of the hiatus sand. Deep piping reached the crater surface after deposition of the graded rubble (Beta 1b). This is true for both OAK and KOA craters and suggests that shallow piping reached the surface on the order of minutes, deep piping on the order of hours, and both persisted for days. In OAK, deep- and shallow-piped material is present in the late-stage mud (Alpha 1) deposits suggesting very long-term deposition (many months). In KOA, only shallow-piped material is present in the late-stage mud (Alpha 1) deposits. Deep-piped material is present in the graded sands (Alpha 2) suggesting an ending of deep-piping at the initiation of Alpha 1 deposition in KOA (approximately 1-2 months). If the liquefied material mass exhibits vertical flow for days, why is lateral flow constrained to the dynamic phase of crater development? Material from MP-4 (deep-piped) would have an effective seal by MP-3 in most places except in the proximity of large fractures and vents. The material was depressed under the central crater and the sealed avenue of flow would be up along the lower surface of MP-3.

Subsurface. -- Unit MP-4 shows densification away from the central crater. Borehole gravimetry shows a substantial increase in density in MP-4 in OQT-23 for that part that was measured (refer to tbl. 7-9). Gamma-gamma density shows a similar substantial increase in density throughout MP-4 in OKT-13. The H&N post-shot bathymetry (Peterson and Henny, Ch. 5 of this report) shows a rise in the lagoon sea-floor depth that exceeds the thickness of the debris measured in several boreholes. This indicates uplift of the surface. As previously mentioned, MP-3 shows uplift throughout the lagoon (refer to fig. 7-22). Both these lines of evidence suggest significant lateral flow of MP-4, densifying the material laterally and uplifting the overlying sediment and rock over much of the lagoon. It appears that calculations down to the line of zero net displacement (contour D, Trulio, Ch. 6 of this report) do not adequately encompass all significant subsurface crater phenomena because much appears to happen below this line.

Loss of Material from the Crater. -- In OAK, large ejecta or debris is found entirely within the apparent crater. Halley and others (1986b) demonstrated several clasts (unspecified size, but generally cobble-sized or larger material collected by submersible) to be debris. Debris rays were observed along the reef tract, generally all within the apparent crater. The debris blanket is within the apparent crater. Where did all the material go to form the apparent crater?

Debris is indicated outside the apparent crater in three places:

- (1). In the breach and turbidite flow deposit (fig. 7-14) deposition of an unknown volume of debris is inferred from the enhanced sea-floor image.
- (2). At OAR-2A, the upper 25 ft of sediment (mostly sand) contains highly shocked material, probably ejecta swept from the reef tract and deposited at this site. This thickness could represent a substantial amount of material deposited along the toe of the slope from reef to lagoon on both the northeast and southwest sides of the crater.
- (3). In mud in the lagoon, clay-sized material is common in samples from throughout the northeastern part of the lagoon (Wardlaw and Henry, 1986b). It is probably mostly blast-derived and represents a substantial volume of fine-grained ejecta and material from the craters. Post-shot photographs show mud-laden plumes into the ocean and lagoon far beyond the apparent crater, suggesting this loss was not trivial.

The uplifted area in the lagoon near OAK (fig. 7-22) suggests that a considerable volume of material from MP-4 moved outside the apparent crater in the subsurface. If a 5-7 percent density increase accompanied this thickening it would account for an appreciable amount of the apparent crater.

SUMMARY

OAK and KOA craters are similar. They exhibit the same geologic crater zonation. The zone of sonic degradation that defines the geologic crater is very similar for both craters. OAK and KOA differ in type of device, in coupling, and in depth and radius of the various stages of crater development that are not within the scope of this paper. The KOA area was preconditioned by MIKE and possibly other devices. It contains a better, thicker cemented interval (MP-3) at shallower depths than OAK. These two factors contributed strongly to the major differences between KOA and OAK. KOA is a crater that developed early and had far less late-stage modification, as indicated by its lack of late-stage piping and diminished late-stage subsidence. OAK, on the other hand, is a crater most of which developed later and had significant late-stage subsidence and piping. It appears that as much as 66 percent of the apparent crater volume of OAK may be due to subsidence. In contrast, only about 20 percent of KOA may be due to subsidence.

Piping requires a liquefied material mass at depth. Piping lasted for months at both craters. Subsidence lasted for months at both craters. The prolonged existence of a liquefied material mass at depth is related causally to prolonged subsidence.

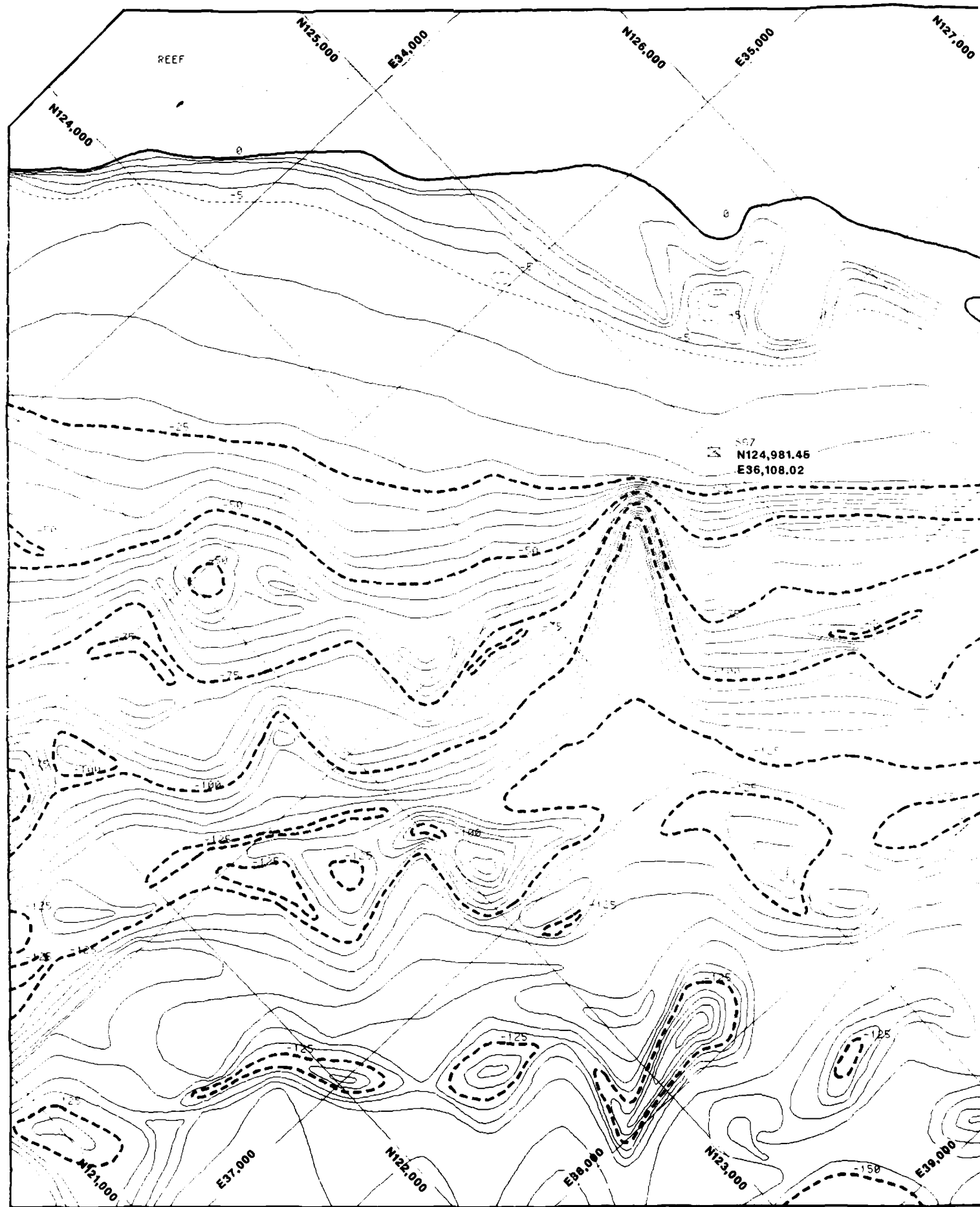
REFERENCES CITED

- Beyer, L. A., Ristvet, B. L., and Oberste-Lehn, D., 1986, Chapter 8: Preliminary density and porosity data and field techniques of borehole gravity surveys, OAK crater, in, Henry, T. W., and Wardlaw, B. R., eds., Pacific Enewetak Atoll Crater Exploration (PEACE) Program, Enewetak Atoll, Republic of the Marshall Islands; Part 3: Stratigraphic analysis and other geologic and geophysical studies in vicinity of OAK and KOA craters: U.S. Geological Survey Open-File Report 86-555, 28 p.
- Beyer, L. A., 1987, Chapter 2: Analysis of borehole gravity surveys at OAK crater, in, Henry, T. W., and Wardlaw, B. R., eds., Pacific Enewetak Crater Exploration (PEACE) Program, Enewetak Atoll, Republic of the Marshall Islands; Part 4: Additional studies of OAK and KOA craters, U.S. Geological Survey Open-File Report 87-xxx.
- Brouwers, E. M., Cronin, T. M., and Gibson, T. G., 1986, Chapter 11: Additional paleontologic studies, OAK and KOA craters, in, Henry, T. W., and Wardlaw, eds., Pacific Enewetak Atoll Crater Exploration (PEACE) Program, Enewetak Atoll, Republic of the Marshall Islands; Part 3: Stratigraphic analysis and other geologic and geophysical studies in vicinity of KOA and OAK craters: U.S. Geological Survey Open-File Report 86-555, 18 p.
- Couch, R. F., Jr., Fetzer, J. A., Goter, E. R., Ristvet, B. L., Tremba, E. L., Walter, D. R., and Wenland, V. P., 1975, Drilling operations on Eniwetok Atoll during Project EXPOE: Air Force Weapons Laboratory Technical Report AFWL-TR-75-216, Kirtland Air Force Base, New Mexico, 270 p.
- Cronin, T. M., Brouwers, E. M., Bybell, L. M., Edwards, L. E., Gibson, T. G., Margerum, R., and Poore, R. Zoro, 1986, Pacific Enewetak Crater Exploration (PEACE) Program, Enewetak Atoll, Republic of the Marshall Islands; Part 2: Paleontology and biostratigraphy application to OAK and KOA craters, U.S. Geological Survey Open-File Report 86-159, 39 p.
- Cronin, T. M., and Gibson, T. G., 1987, Chapter 3: Paleontologic evidence for sedimentary mixing at OAK crater, Enewetak Atoll, in, Henry, T. W., and Wardlaw, B. R., eds., Pacific Enewetak Crater Exploration (PEACE) Program, Enewetak Atoll, Republic of the Marshall Islands; Part 4: Additional studies of OAK and KOA craters, U.S. Geological Survey Open-File Report 87-665.
- Folger, D. W., Robb, J. M., Hampson, J. C., Davis, P. A., Bridges, P. M., and Roddy, D. J., 1986, Sidescan-sonar survey of OAK and KOA craters, in, Folger, D. W., ed., Sea-floor observations and subbottom seismic characteristics of OAK and KOA craters, Enewetak Atoll, Marshall Islands: U.S. Geological Survey Bulletin 1678, 18 p.
- Grow, J. A., Lee, M. W., Miller, J. J., Agena, W. F., Hampson, J. C., Foster, D. S., and Woellner, R. A., 1986, Multichannel seismic-reflection survey of KOA and OAK craters, in, Folger, D. W., ed., Sea-floor observations and subbottom seismic characteristics of OAK and KOA craters, Enewetak Atoll, Marshall Islands: U.S. Geological Survey Bulletin 1678, 46 p.

- Halley, R. B., Slater, R. A., Shinn, E. A., Folger, D. W., Hudson, J. H., Kindinger, J. L., and Roddy, D. J., 1986a, Observations of OAK and KOA craters from the submersible, in, Folger, D. W., ed., Sea-floor observations and subbottom seismic characteristics of OAK and KOA craters, Enewetak Atoll, Marshall Islands: U.S. Geological Survey Bulletin 1678, 32 p.
- Halley, R. B., Major, R. P., Ludwig, K. R., Peterman, Z. L., and Matthews, R. K., 1986b, Preliminary analyses of OAK debris samples, in, Folger, D. W., ed., Sea-floor observations and subbottom seismic characteristics of OAK and KOA craters, Enewetak Atoll, Marshall Islands: U.S. Geological Survey Bulletin 1678, 11 p.
- McMurtry, G. M., Schneider, R. C., Colin, P. K., Buddemeier, R. W., and Suchanek, R. H., 1985, Redistribution of fallout radionuclides in Enewetak Atoll lagoon sediments by calianassid bioturbation: *Nature*, v. 313, no. 6004, p. 674-677.
- Peterson, J. L., and Henny, R. W., 1987, Chapter 5: Bathymetric studies of OAK crater, in, Henry, T. W., and Wardlaw, B. R., eds., Pacific Enewetak Crater Exploration (PEACE) Program, Enewetak Atoll, Republic of the Marshall Islands; Part 4: Additional studies of OAK and KOA craters: U.S. Geological Survey Open-File Report 87-665.
- Polanskey, Carol, and Ahrens, T. J., 1987, Chapter 4: Shock history of PEACE samples, in, Henry, T. W., and Wardlaw, B. R., eds., Pacific Enewetak Crater Exploration (PEACE) Program, Enewetak Atoll, Republic of the Marshall Islands; Part 4: Additional studies of OAK and KOA craters: U.S. Geological Survey Open-File Report 87-665.
- Ristvet, B. L., Tremba, E. L., Couch, R. F., Jr., Fetzer, J. A., Goter, E. R., Walter, D. R., and Wendland, V. P., 1978, Geologic and geophysical investigations of the Enewetak nuclear craters: Air Force Weapons Laboratory Technical Report AFWL-TR-77-242, 300 p.
- Ristvet, B. L., and Tremba, E. L., 1986, Chapter 12: Radiation chemistry of the subsurface of OAK and KOA craters, in, Henry, T. W., and Wardlaw, B. R., eds., Pacific Enewetak Atoll Crater Exploration (PEACE) Program, Enewetak Atoll, Republic of the Marshall Islands; Part 3: Stratigraphic analysis and other geologic and geophysical studies in vicinity of OAK and KOA craters: U.S. Geological Survey Open-File Report 86-555, 15 p.
- Trulio, J. G., 1987, Chapter 6: Constraints on densification and piping in the OAK event, in, Henry, T. W., and Wardlaw, B. R., eds., Pacific Enewetak Crater Exploration (PEACE) Program, Enewetak Atoll, Republic of the Marshall Islands; Part 4: Additional studies of OAK and KOA craters: U.S. Geological Survey Open-File Report 87-665.

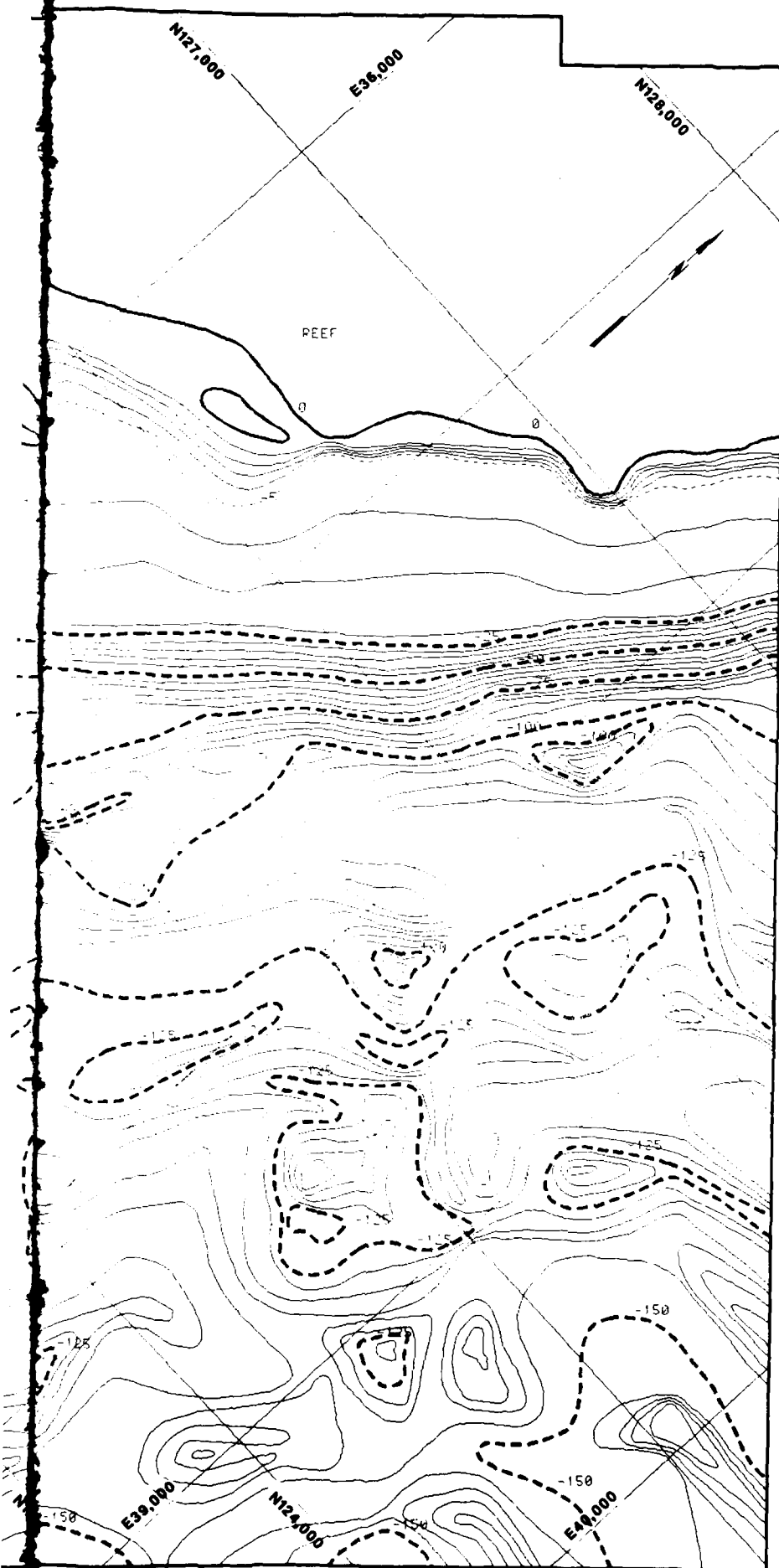
Wardlaw, B. R., and Henry, T. W., 1986a, Chapter 2: Physical stratigraphic framework, in, Henry, T. W., and Wardlaw, B. R., eds., Pacific Enewetak Atoll Crater Exploration (PEACE) Program, Enewetak Atoll, Republic of the Marshall Islands; Part 3: Stratigraphic analysis and other geologic and geophysical studies in vicinity of OAK and KOA craters: U.S. Geological Survey Open-File Report 86-555, 36 p.

Wardlaw, B. R., and Henry, T. W., 1986b, Chapter 14: Geological interpretation of OAK and KOA craters, in, Henry, T. W., and Wardlaw, B. R., eds., Pacific Enewetak Atoll Crater Exploration (PEACE) Program, Enewetak Atoll, Republic of the Marshall Islands; Part 3: Stratigraphic analysis and other geologic and geophysical studies in vicinity of OAK and KOA craters: U.S. Geological Survey Open-File Report 86-555, 39 p.



CRATER SHOT CONTOUR MAP

OPEN-FILE REPORT 87-665
PLATE 5-1



0 500 1000
HORIZONTAL SCALE (FT)

PLATE 5-1

OAK CRATER, ALICE REEF (STA. 25)
H&N (1258) PRESOT TOPOGRAPHIC AND HYDROGRAPHIC MAP

Map prepared for the PEACE Program for the Air Force Weapons Laboratory (AFWL) under the direction of the New Mexico Engineering Research Institute (NMERI) by the Technology Applications Center (TAC), December 1986.

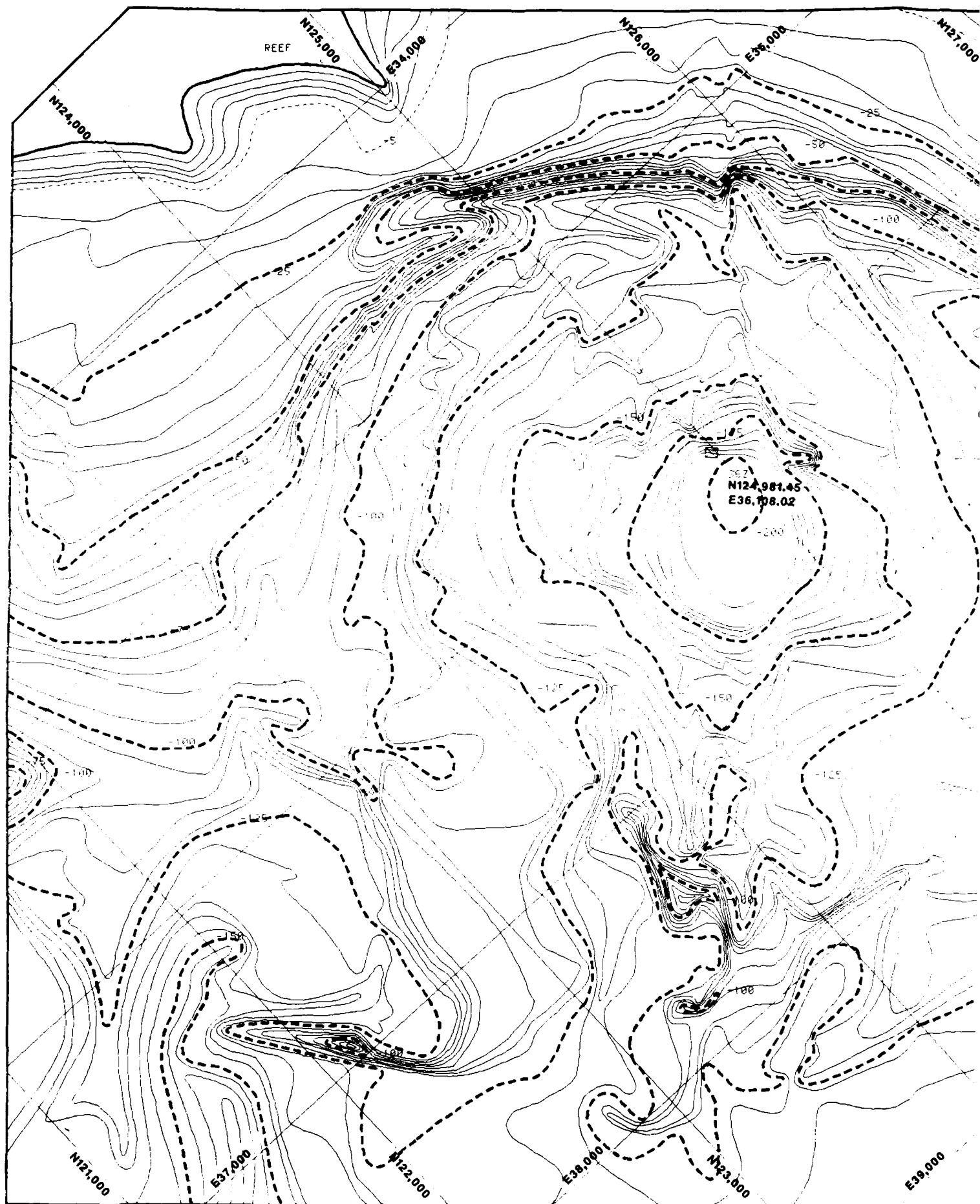
BASE MAP:

Holmes and Narver, Inc.; Blue-line copy of "Topography & Hydrography Sta. 25, Alice Reef," June 9 through 26, 1958; Sheet No. J/S 03-001-C10; dated September 13, 1958; Survey conducted for U.S. Atomic Energy Commission (AEC).

NOTES:

- Contour interval above the minus 5 ft datum is 1 ft.
- Contour interval below the minus 5 ft datum is 5 ft.
- Dotted lines represent contours above the 0 ft datum.
- Thick solid line represents 0 ft elevation.
- Dashed-dotted line represents the minus 5 ft contour.
- Dashed lines represent 75 ft contour increments below 0 ft elevation.
- Datum is 0.5 ft below Approximate Mean Low Water Springs (AMLS).
- Contour interval based on the 1958 survey.
- Surface input data: 117 coordinates, N 124.981, E 39.000, 118, 119, 120.

OAK CRATER
H&N (1958), POSTSHOT CON



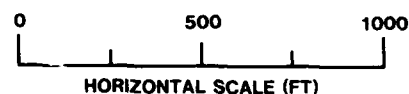
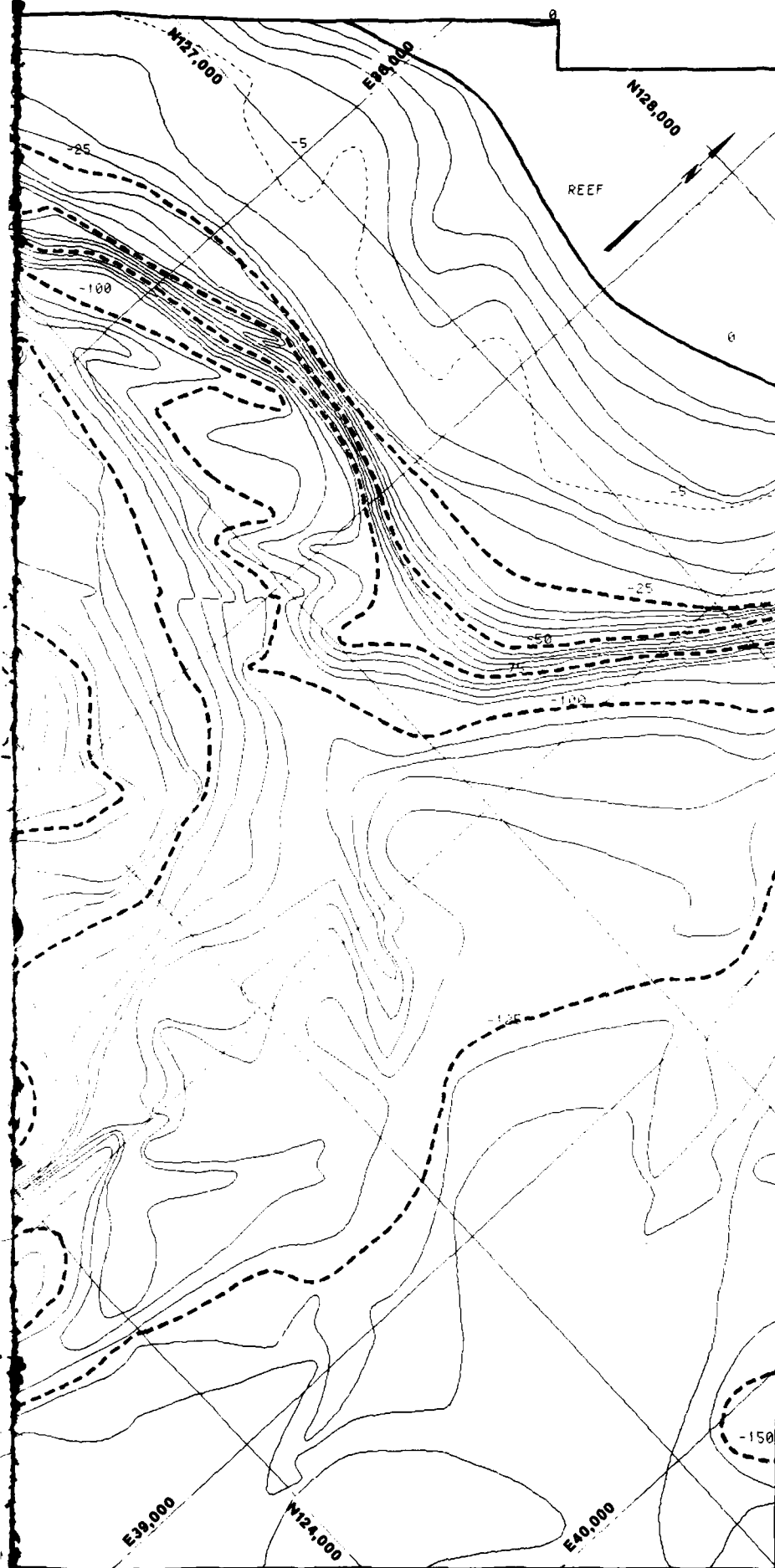


PLATE 5-2
OAK CRATER, ALICE REEF (STA. 25)
H&N (1958) PRESHOT TOPOGRAPHIC AND HYDROGRAPHIC MAP

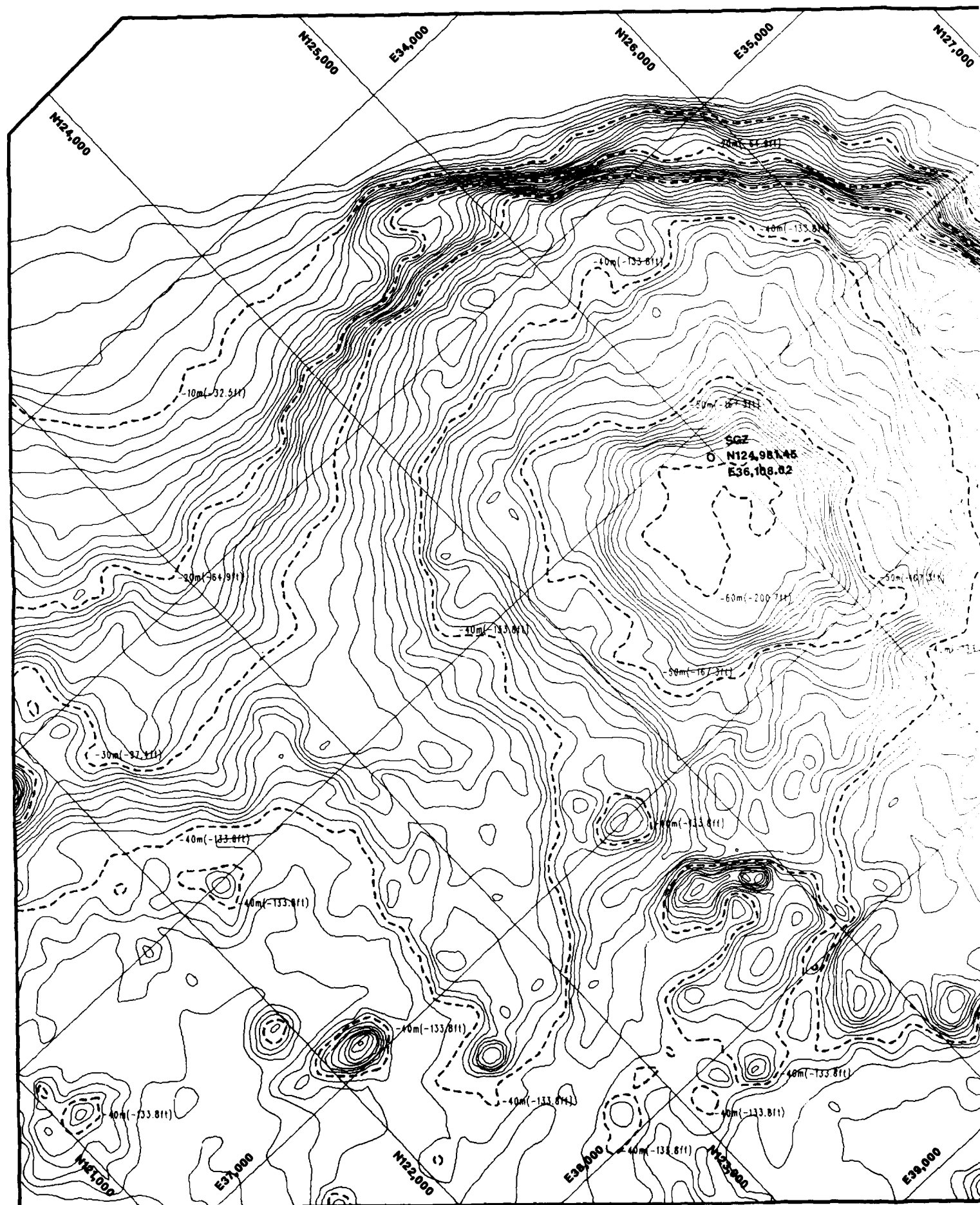
Map prepared for the PEACE Program for the Air Force Weapons Laboratory, AFML, under the direction of the New Mexico Engineering Research Institute (NEMI) by the Technology Applications Center (TAC), December 1946.

BASE MAP:

Holmes and Narver, Inc.; Blue-line copy of "Topography & Hydrography Sta. 25, Alice Reef," August 16 through September 4, 1958; Sheet No. J'S 02-001-011; dated October 1, 1958. Survey conducted for U.S. Atomic Energy Commission (AEC).

NOTES:

- Contour interval above the minus 5 ft datum is 1 ft.
- Contour interval below the minus 5 ft datum is 5 ft.
- Dotted lines represent contours above the 0 ft datum.
- Thick solid line represents 0 ft elevation.
- Dashed-dotted line represents the minus 5 ft contour.
- Dashed lines represent 25 ft contour increments below 0 ft elevation.
- Datum is 0.5 ft below Approximate Mean Low Water Spring (AMLS).
- Celestial Survey based on the IVY Grid Coordinate System (units in ft).
- Surface Ground Zero (SGZ) coordinates: N = 124,481.45 and E = 36,108.02.



POSTSHOT CONTOUR MAP

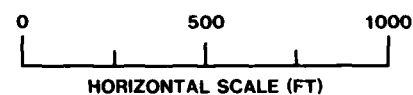
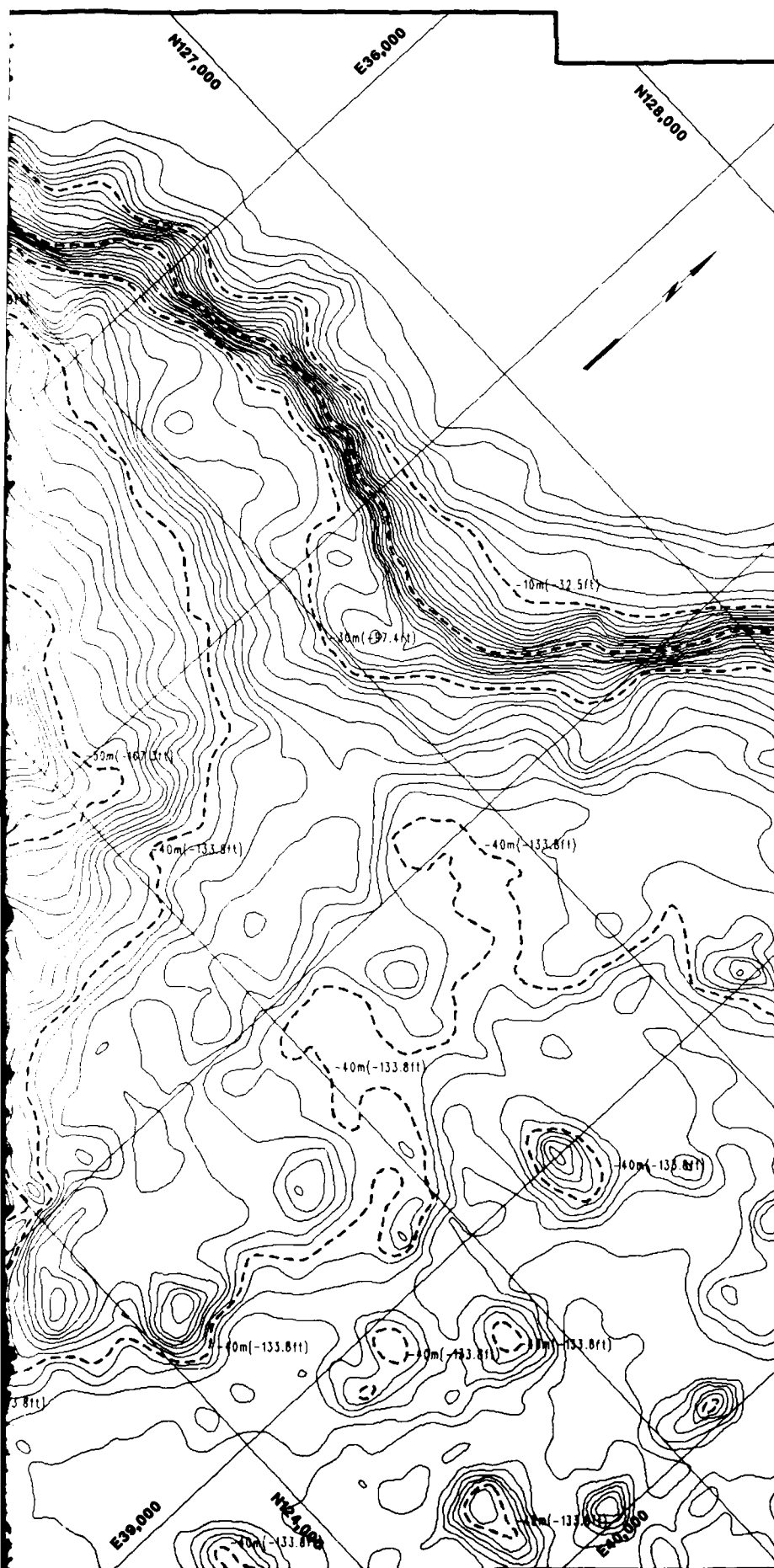


PLATE 5-3
OAK CRATER, ALICE REEF (STA. 25)
USGS (1984) POSTSHOT HYDROGRAPHIC MAP

Map prepared for the PEACE program for the Defense Nuclear Agency, Laboratory AFM, under the direction of the New Mexico Engineering Research Institute (NEMI) by the Technology Applications Center (TAC), 1984.

BASE MAP:

U.S. Geological Survey (1984), "Bathymetric Map of Oak Crater Area, Enewetak Atoll," surveyed June 1 through September 20, 1984; compiled September 1985. The base map is a mylar working-scale copy 1:6000 of the map published in 1986 in U.S. Geological Survey Bulletin 1678 as fig. 1, D. A. Survey conducted for Defense Nuclear Agency (DNA).

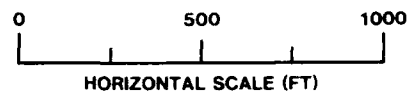
NOTES:

- Contour interval is 1 m (approximately 3.3 ft).
- Data incomplete above minus 4 m (minus 13.0 ft).
- Dashed lines represent 10 m contour intervals displayed with depth corrected values in ft.
- Data corrected for water depths as determined from Drilling Phase of PEACE Program.
- Cadastral Survey based on the IVN Grid Coordinate System (units in ft).
- Surface Ground Zero (SGZ) coordinates: N = 124,981.45 and E = 34,100.00.



OAK CRATER SHOT ISOPACH MAP, NEGATIVE Δ -RELIEF

OPEN-FILE REPORT 87-665
PLATE 5-4



LEGEND

● - BOREHOLE LOCATION WITHIN
MAPPED AREA
(BOREHOLES DRILLED 1985)

[White box]	POSITIVE Δ -RELIEF
[Horizontal lines]	NO CHANGE
[Dark gray box]	0 - 5 FT - NEGATIVE Δ -RELIEF
[Diagonal lines (top-left to bottom-right)]	5 - 10 FT
[Diagonal lines (bottom-left to top-right)]	10 - 15 FT
[Cross-hatch]	15 - 20 FT
[Stippled]	20 - 30 FT
[Vertical lines]	30 - 40 FT
[Horizontal lines]	40 - 50 FT
[Diagonal lines (top-left to bottom-right)]	50 - 60 FT
[Diagonal lines (bottom-left to top-right)]	60 - 70 FT
[Cross-hatch]	70 - 80 FT
[Stippled]	80 - 90 FT
[Vertical lines]	90 - 100 FT
[Horizontal lines]	100 - 110 FT
[Diagonal lines (top-left to bottom-right)]	110 - 120 FT
[Diagonal lines (bottom-left to top-right)]	120 - 130 FT
[Cross-hatch]	130 - 140 FT
[Stippled]	140 - 150 FT
[Vertical lines]	150 - 160 FT
[Horizontal lines]	160 - 170 FT
[Diagonal lines (top-left to bottom-right)]	170 - 180 FT
[Diagonal lines (bottom-left to top-right)]	180 - 190 FT

PLATE 5-4
OAK CRATER, ALICE REEF (STA. 25)
EARLYTIME NEGATIVE Δ -RELIEF ISOPACH MAP

Map prepared for the U.S. Navy by the U.S. Navy Hydrographic Office, Naval Hydrographic Office, 1600 Wilson Boulevard, Arlington, Virginia 22202-4302. The map is based on data collected by the U.S. Navy Hydrographic Office, 1600 Wilson Boulevard, Arlington, Virginia 22202-4302.

U.S. Navy Hydrographic Office, 1600 Wilson Boulevard, Arlington, Virginia 22202-4302. The map is based on data collected by the U.S. Navy Hydrographic Office, 1600 Wilson Boulevard, Arlington, Virginia 22202-4302.

U.S. Navy Hydrographic Office, 1600 Wilson Boulevard, Arlington, Virginia 22202-4302. The map is based on data collected by the U.S. Navy Hydrographic Office, 1600 Wilson Boulevard, Arlington, Virginia 22202-4302.

U.S. Navy Hydrographic Office, 1600 Wilson Boulevard, Arlington, Virginia 22202-4302. The map is based on data collected by the U.S. Navy Hydrographic Office, 1600 Wilson Boulevard, Arlington, Virginia 22202-4302.

U.S. Navy Hydrographic Office, 1600 Wilson Boulevard, Arlington, Virginia 22202-4302. The map is based on data collected by the U.S. Navy Hydrographic Office, 1600 Wilson Boulevard, Arlington, Virginia 22202-4302.

U.S. Navy Hydrographic Office, 1600 Wilson Boulevard, Arlington, Virginia 22202-4302. The map is based on data collected by the U.S. Navy Hydrographic Office, 1600 Wilson Boulevard, Arlington, Virginia 22202-4302.

U.S. Navy Hydrographic Office, 1600 Wilson Boulevard, Arlington, Virginia 22202-4302. The map is based on data collected by the U.S. Navy Hydrographic Office, 1600 Wilson Boulevard, Arlington, Virginia 22202-4302.

U.S. Navy Hydrographic Office, 1600 Wilson Boulevard, Arlington, Virginia 22202-4302. The map is based on data collected by the U.S. Navy Hydrographic Office, 1600 Wilson Boulevard, Arlington, Virginia 22202-4302.

U.S. Navy Hydrographic Office, 1600 Wilson Boulevard, Arlington, Virginia 22202-4302. The map is based on data collected by the U.S. Navy Hydrographic Office, 1600 Wilson Boulevard, Arlington, Virginia 22202-4302.



RATER ISOPACH MAP, POSITIVE Δ -RELIEF

OPEN-FILE REPORT 87-665
PLATE 5-5

MAP



0 500 1000
HORIZONTAL SCALE (FT)

LEGEND

● - BOREHOLE LOCATION WITHIN
MAPPED AREA
(BOREHOLES DRILLED 1985)

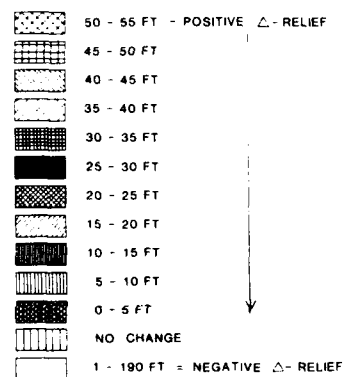


PLATE 5-5

OAK CRATER, ALICE REEF (STA.25)
EARLYTIME POSITIVE Δ -RELIEF ISOPACH MAP

Map prepared for the O&G Program for the Alaska Gas Pipeline
Laboratory, AFRL, under the direction of the New Mexico
Engineering Research Institute (NMERI), by the
Technology Applications Center (TAC), 1985.

ISOPACH MAP - Illustrating postshot distribution of
earlytime, 0.1-10 days, positive Δ -relief at the
pressure front level (atmosphere).

RAVE MAPS -

W. H. and N. V. (1985) "Wellhead of Topography &
Hydrography (14, 15, Alice Reef, June 4 through 12,
1985), Sheet No. 10-12-10-10-10, Great Southwest (1,
1985), Survey conducted for U.S. Army, County
Commission, 1985."

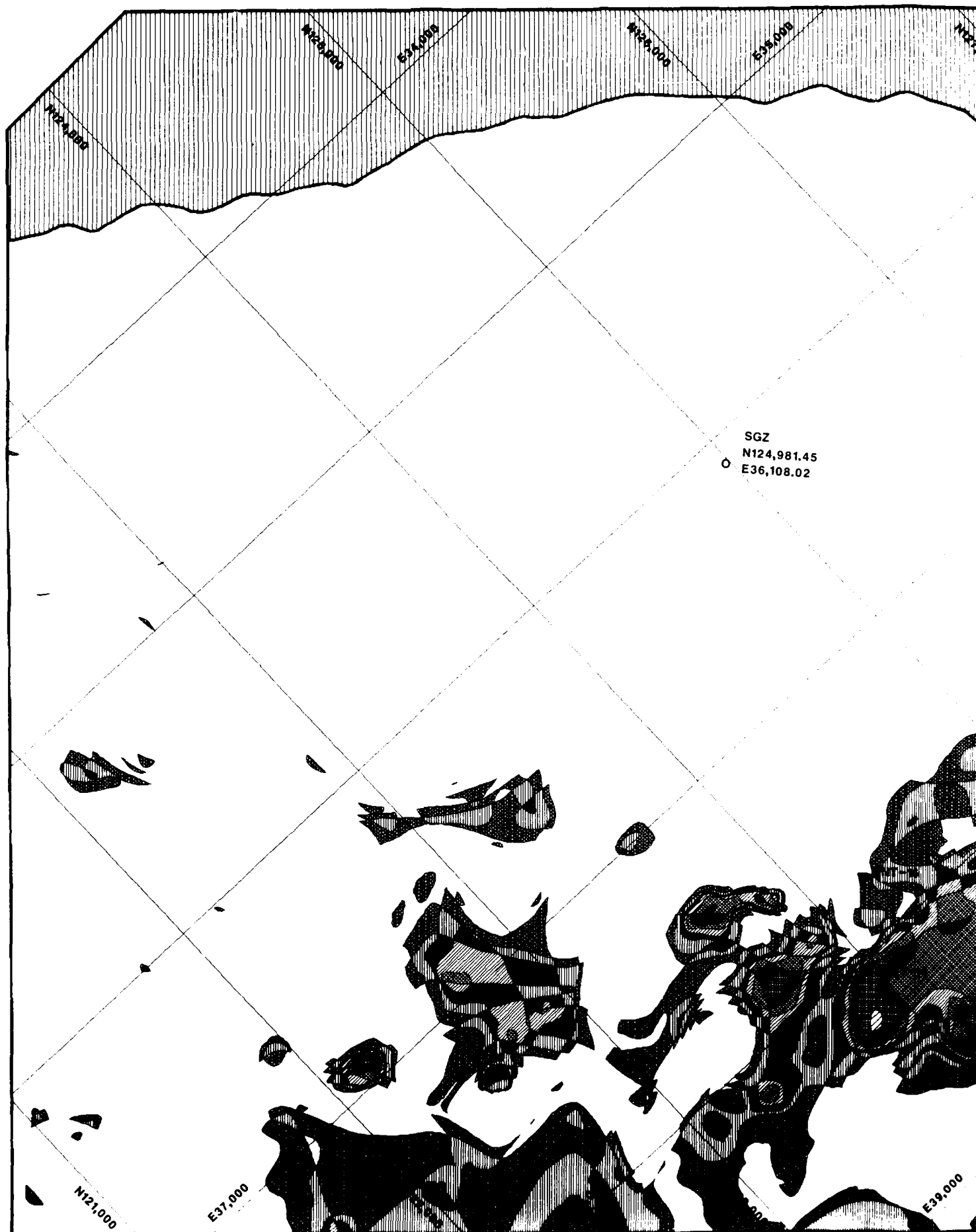
W. H. and N. V. (1985) "Wellhead of Topography &
Hydrography (14, 15, Alice Reef, August 14 through
September 1, 1985), Sheet No. 10-12-10-10-10, Great
Southwest (1, 1985), Survey conducted for U.S. Army,
County Commission, 1985."

Notes -

1. The isopach map was prepared by the
Technology Applications Center (TAC), 1985.
2. The isopach map was prepared by the Technology
Applications Center (TAC), 1985.
3. The isopach map was prepared by the Technology
Applications Center (TAC), 1985.

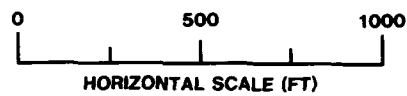






OAK CRATER AIR SHOT ISOPACH MAP, POSITIVE Δ -RELIEF

OPEN-FILE REPORT 87-665
 PLATE 5-7



LEGEND

● - BOREHOLE LOCATION WITHIN
 MAPPED AREA
 (BOREHOLES DRILLED 1985)

	50 - 55 FT - POSITIVE Δ -RELIEF
	45 - 50 FT
	40 - 45 FT
	35 - 40 FT
	30 - 35 FT
	25 - 30 FT
	20 - 25 FT
	15 - 20 FT
	10 - 15 FT
	5 - 10 FT
	0 - 5 FT
	NO CHANGE
	1 - 190 FT - NEGATIVE Δ -RELIEF

PLATE 5-7
 OAK CRATER, ALICE REEF (STA.25)
 LATETIME POSITIVE Δ -RELIEF ISOPACH MAP

Map prepared for the PLACE Program for the Air Force Weapons Laboratory (AFWL) under the direction of the New Mexico Engineering Research Institute (NMERI) by the Technology Applications Center (TAC), 1985.

ISOPACH MAP: Illustrating latetime (0 + 27 yrs) distribution of positive Δ -relief from the preshot zero (0) level datum.

RASE MAPS

Holmes and Narver, Inc.: Blue-line copy of "Topography & Hydrography Sta. 25, Alice Reef," June 3 through 24, 1958; Sheet No. J-15 37-101-010, dated September 13, 1958. Survey conducted for U.S. Atomic Energy Commission (AEC).

U.S. Geological Survey: 1964. "Bathymetric Map of Oak Crater Area, Inverness Archipelago, Surveys June 11 through September 20, 1964." Compiled September 1965. Map data map is a larger working-scale copy (1:400) of the map published in 1966 in U.S. Geological Survey Bulletin 1464 as Fig. 1, p. 84. Survey conducted for Defense Nuclear Agency (DNA).

NOTES

1. No data collected for water depths at Inverness Archipelago.

2. No data collected for water depths at Inverness Archipelago.

3. No data collected for water depths at Inverness Archipelago.

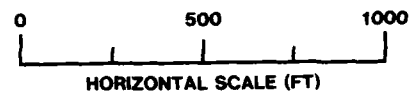
4. No data collected for water depths at Inverness Archipelago.

5. No data collected for water depths at Inverness Archipelago.



OAK CRATER POSTSHOT ISOPACH MAP, NEGATIVE Δ -RELIEF

OPEN-FILE REPORT 87-565
PLATE 5-8



LEGEND

● - BOREHOLE LOCATION WITHIN
MAPPED AREA
(BOREHOLES DRILLED 1985)

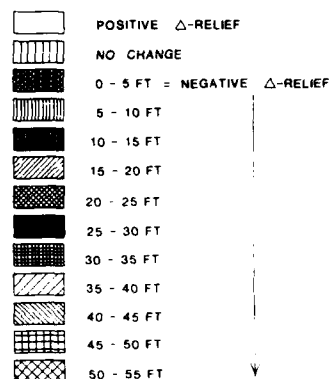


PLATE 5-8

OAK CRATER, ALICE REEF (STA. 25)

COMPARATIVE POSTSHOT ISOPACH MAP (NEGATIVE Δ -RELIEF)

Map prepared for the PEARS Program for the Air Force Weapons Laboratory, AFRL, under the direction of the New Mexico Engineering Research Institute (NEMI) by the Technology Applications Center (TAC), December 1986.

ISOPACH MAP: Illustrating postshot (0 to 47 days to failure) negative distribution of negative relief from the 465 postshot zero level datum.

RAGE MAPS:

1. Holmes and Narver, Inc., Plotting copy of Hydrographic & Hydrography Map 75, Alice Reef, August 14 through September 3, 1956. Sheet No. 115-13-731-111, dated October 11, 1956. Survey conducted for U.S. Atomic Energy Commission (AEC).

2. U.S. Geological Survey (1968), Bathymetric Map of Oak Crater Area, Eniwetok Atoll, surveyed June 11 through September 27, 1968; completed September 1968. The map is a nautical working scale (1:40,000) of the map published in 1968 by U.S. Geological Survey Bulletin 1476 as Figure 1, p. 14. Survey conducted for Atomic Nuclear Agency (ANA).

NOTES:

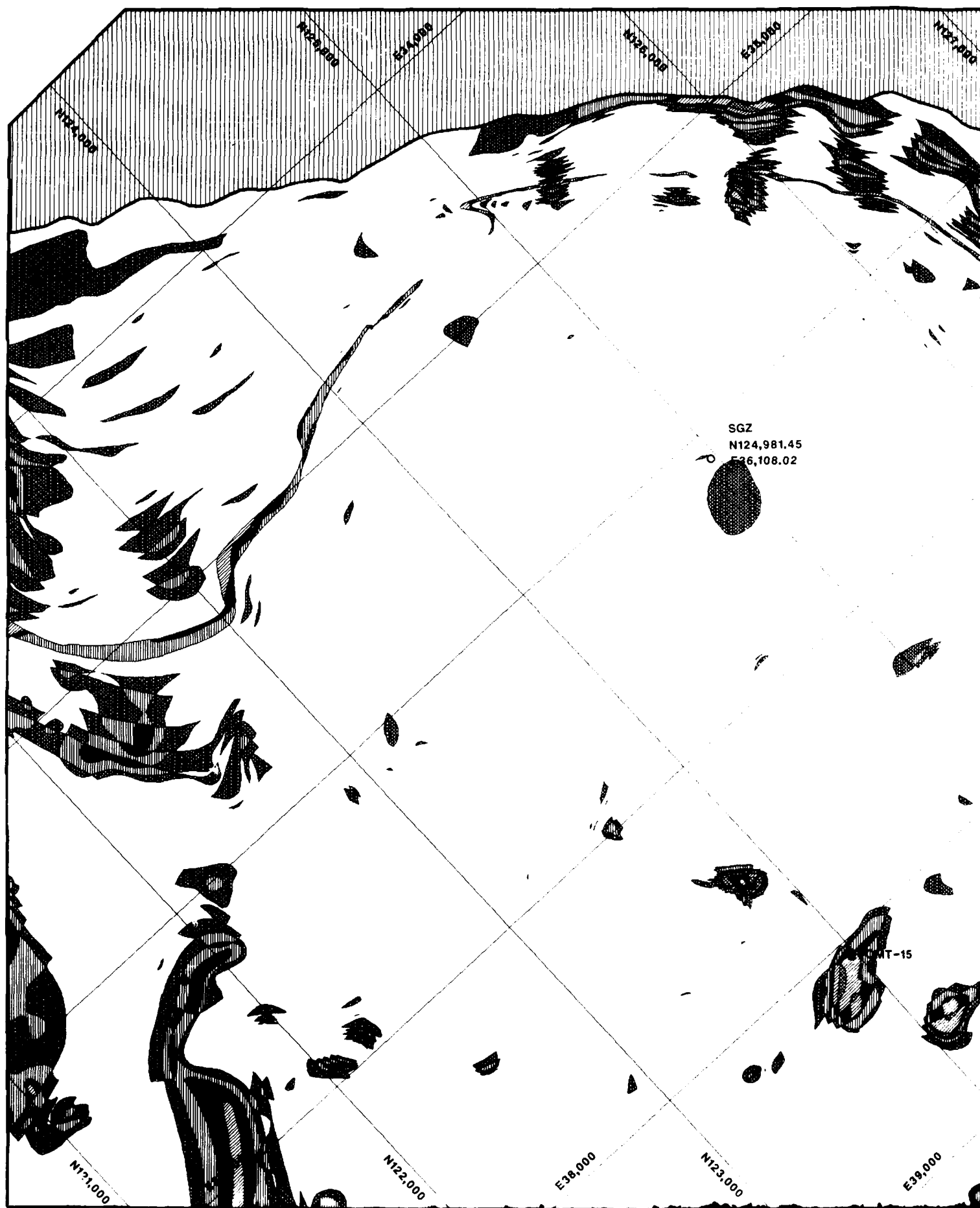
1. (54) data correction for water depth is indicated by the 100 ft depth contour line.

2. The data for the water depth is from the 1968 map.

3. The data for the water depth is from the 1968 map.

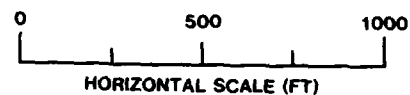
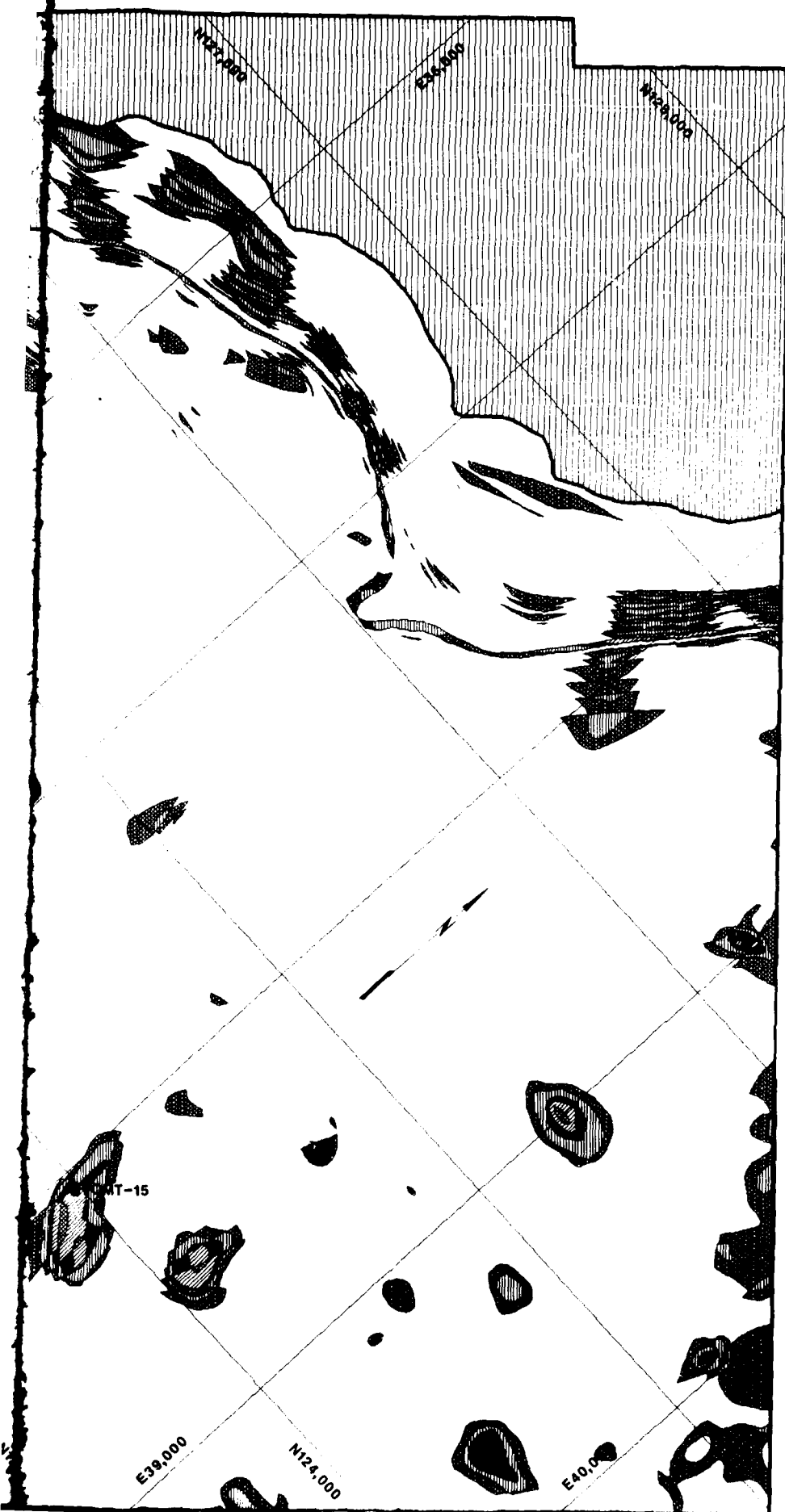
4. The data for the water depth is from the 1968 map.

OAK CRATER
USGS POSTSHOT - H&N POSTSHOT ISOPAC



SHOT ISOPACH MAP, POSITIVE Δ -RELIEF

OPEN-FILE REPORT 87- 665
PLATE 5-9



LEGEND

● - BOREHOLE LOCATION WITHIN
MAPPED AREA
(BOREHOLES DRILLED 1985)

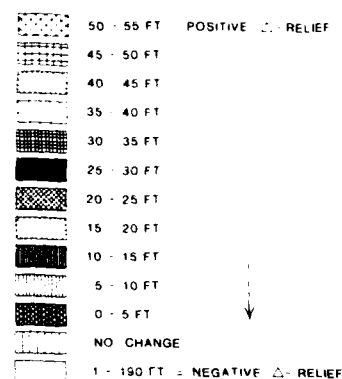


PLATE 5-9

OAK CRATER, ALICE REEF (STA.25)
COMPARATIVE POSTSHOT ISOPACH MAP (POSITIVE -RELIEF)

Mid prepared for the DEAF to give for the Director's report.
 Laboratory TIME for the production of the New Year
 Engineering Design & Construction NCES, the
 Technology Applications Center TA, etc.

FIGURE 4. Distribution of positive and negative posttest scores for the SAT.

BAGG MARI.

Holmes and Narver, Inc., Bluebeam Corp. of Minneapolis, & Hydrographer S.A. 75, 1100 Beach Avenue, August 20 through September 4, 1944. Sheet No. 10 31-27-2011, dated October 1, 1944. Survey conducted for U.S. Army Energy Commission AEC.

10. Bathymetric Survey, 1944. Bathymetric Map of the
Ordnance Survey, Sheet 11, 12, 13, 14, 15, 16, 17, 18, 19, 20, 21, 22, 23, 24, 25, 26, 27, 28, 29, 30, 31, 32, 33, 34, 35, 36, 37, 38, 39, 40, 41, 42, 43, 44, 45, 46, 47, 48, 49, 50, 51, 52, 53, 54, 55, 56, 57, 58, 59, 60, 61, 62, 63, 64, 65, 66, 67, 68, 69, 70, 71, 72, 73, 74, 75, 76, 77, 78, 79, 80, 81, 82, 83, 84, 85, 86, 87, 88, 89, 90, 91, 92, 93, 94, 95, 96, 97, 98, 99, 100, 101, 102, 103, 104, 105, 106, 107, 108, 109, 110, 111, 112, 113, 114, 115, 116, 117, 118, 119, 120, 121, 122, 123, 124, 125, 126, 127, 128, 129, 130, 131, 132, 133, 134, 135, 136, 137, 138, 139, 140, 141, 142, 143, 144, 145, 146, 147, 148, 149, 150, 151, 152, 153, 154, 155, 156, 157, 158, 159, 160, 161, 162, 163, 164, 165, 166, 167, 168, 169, 170, 171, 172, 173, 174, 175, 176, 177, 178, 179, 180, 181, 182, 183, 184, 185, 186, 187, 188, 189, 190, 191, 192, 193, 194, 195, 196, 197, 198, 199, 200, 201, 202, 203, 204, 205, 206, 207, 208, 209, 210, 211, 212, 213, 214, 215, 216, 217, 218, 219, 220, 221, 222, 223, 224, 225, 226, 227, 228, 229, 230, 231, 232, 233, 234, 235, 236, 237, 238, 239, 240, 241, 242, 243, 244, 245, 246, 247, 248, 249, 250, 251, 252, 253, 254, 255, 256, 257, 258, 259, 260, 261, 262, 263, 264, 265, 266, 267, 268, 269, 270, 271, 272, 273, 274, 275, 276, 277, 278, 279, 280, 281, 282, 283, 284, 285, 286, 287, 288, 289, 290, 291, 292, 293, 294, 295, 296, 297, 298, 299, 300, 301, 302, 303, 304, 305, 306, 307, 308, 309, 310, 311, 312, 313, 314, 315, 316, 317, 318, 319, 320, 321, 322, 323, 324, 325, 326, 327, 328, 329, 330, 331, 332, 333, 334, 335, 336, 337, 338, 339, 340, 341, 342, 343, 344, 345, 346, 347, 348, 349, 350, 351, 352, 353, 354, 355, 356, 357, 358, 359, 360, 361, 362, 363, 364, 365, 366, 367, 368, 369, 370, 371, 372, 373, 374, 375, 376, 377, 378, 379, 380, 381, 382, 383, 384, 385, 386, 387, 388, 389, 390, 391, 392, 393, 394, 395, 396, 397, 398, 399, 400, 401, 402, 403, 404, 405, 406, 407, 408, 409, 410, 411, 412, 413, 414, 415, 416, 417, 418, 419, 420, 421, 422, 423, 424, 425, 426, 427, 428, 429, 430, 431, 432, 433, 434, 435, 436, 437, 438, 439, 440, 441, 442, 443, 444, 445, 446, 447, 448, 449, 450, 451, 452, 453, 454, 455, 456, 457, 458, 459, 460, 461, 462, 463, 464, 465, 466, 467, 468, 469, 470, 471, 472, 473, 474, 475, 476, 477, 478, 479, 480, 481, 482, 483, 484, 485, 486, 487, 488, 489, 490, 491, 492, 493, 494, 495, 496, 497, 498, 499, 500, 501, 502, 503, 504, 505, 506, 507, 508, 509, 510, 511, 512, 513, 514, 515, 516, 517, 518, 519, 520, 521, 522, 523, 524, 525, 526, 527, 528, 529, 530, 531, 532, 533, 534, 535, 536, 537, 538, 539, 540, 541, 542, 543, 544, 545, 546, 547, 548, 549, 550, 551, 552, 553, 554, 555, 556, 557, 558, 559, 560, 561, 562, 563, 564, 565, 566, 567, 568, 569, 570, 571, 572, 573, 574, 575, 576, 577, 578, 579, 580, 581, 582, 583, 584, 585, 586, 587, 588, 589, 590, 591, 592, 593, 594, 595, 596, 597, 598, 599, 600, 601, 602, 603, 604, 605, 606, 607, 608, 609, 610, 611, 612, 613, 614, 615, 616, 617, 618, 619, 620, 621, 622, 623, 624, 625, 626, 627, 628, 629, 630, 631, 632, 633, 634, 635, 636, 637, 638, 639, 640, 641, 642, 643, 644, 645, 646, 647, 648, 649, 650, 651, 652, 653, 654, 655, 656, 657, 658, 659, 660, 661, 662, 663, 664, 665, 666, 667, 668, 669, 670, 671, 672, 673, 674, 675, 676, 677, 678, 679, 680, 681, 682, 683, 684, 685, 686, 687, 688, 689, 690, 691, 692, 693, 694, 695, 696, 697, 698, 699, 700, 701, 702, 703, 704, 705, 706, 707, 708, 709, 710, 711, 712, 713, 714, 715, 716, 717, 718, 719, 720, 721, 722, 723, 724, 725, 726, 727, 728, 729, 730, 731, 732, 733, 734, 735, 736, 737, 738, 739, 740, 741, 742, 743, 744, 745, 746, 747, 748, 749, 750, 751, 752, 753, 754, 755, 756, 757, 758, 759, 760, 761, 762, 763, 764, 765, 766, 767, 768, 769, 770, 771, 772, 773, 774, 775, 776, 777, 778, 779, 780, 781, 782, 783, 784, 785, 786, 787, 788, 789, 790, 791, 792, 793, 794, 795, 796, 797, 798, 799, 800, 801, 802, 803, 804, 805, 806, 807, 808, 809, 810, 811, 812, 813, 814, 815, 816, 817, 818, 819, 820, 821, 822, 823, 824, 825, 826, 827, 828, 829, 830, 831, 832, 833, 834, 835, 836, 837, 838, 839, 840, 841,

4. 10. 1991

Figure 1. The effect of the concentration of the *Agaricus bisporus* spores on the growth of *Agaricus bisporus* and *Agaricus bisporus* spores. The concentration of the spores was 10⁶ spores/ml (a), 10⁷ spores/ml (b), 10⁸ spores/ml (c), 10⁹ spores/ml (d), 10¹⁰ spores/ml (e), 10¹¹ spores/ml (f), 10¹² spores/ml (g), 10¹³ spores/ml (h), 10¹⁴ spores/ml (i), 10¹⁵ spores/ml (j), 10¹⁶ spores/ml (k), 10¹⁷ spores/ml (l), 10¹⁸ spores/ml (m), 10¹⁹ spores/ml (n), 10²⁰ spores/ml (o), 10²¹ spores/ml (p), 10²² spores/ml (q), 10²³ spores/ml (r), 10²⁴ spores/ml (s), 10²⁵ spores/ml (t), 10²⁶ spores/ml (u), 10²⁷ spores/ml (v), 10²⁸ spores/ml (w), 10²⁹ spores/ml (x), 10³⁰ spores/ml (y), 10³¹ spores/ml (z), 10³² spores/ml (aa), 10³³ spores/ml (ab), 10³⁴ spores/ml (ac), 10³⁵ spores/ml (ad), 10³⁶ spores/ml (ae), 10³⁷ spores/ml (af), 10³⁸ spores/ml (ag), 10³⁹ spores/ml (ah), 10⁴⁰ spores/ml (ai), 10⁴¹ spores/ml (aj), 10⁴² spores/ml (ak), 10⁴³ spores/ml (al), 10⁴⁴ spores/ml (am), 10⁴⁵ spores/ml (an), 10⁴⁶ spores/ml (ao), 10⁴⁷ spores/ml (ap), 10⁴⁸ spores/ml (aq), 10⁴⁹ spores/ml (ar), 10⁵⁰ spores/ml (as), 10⁵¹ spores/ml (at), 10⁵² spores/ml (au), 10⁵³ spores/ml (av), 10⁵⁴ spores/ml (aw), 10⁵⁵ spores/ml (ax), 10⁵⁶ spores/ml (ay), 10⁵⁷ spores/ml (az), 10⁵⁸ spores/ml (ba), 10⁵⁹ spores/ml (bb), 10⁶⁰ spores/ml (bc), 10⁶¹ spores/ml (bd), 10⁶² spores/ml (be), 10⁶³ spores/ml (bf), 10⁶⁴ spores/ml (bg), 10⁶⁵ spores/ml (bh), 10⁶⁶ spores/ml (bi), 10⁶⁷ spores/ml (bj), 10⁶⁸ spores/ml (bk), 10⁶⁹ spores/ml (bl), 10⁷⁰ spores/ml (bm), 10⁷¹ spores/ml (bn), 10⁷² spores/ml (bo), 10⁷³ spores/ml (bp), 10⁷⁴ spores/ml (bq), 10⁷⁵ spores/ml (br), 10⁷⁶ spores/ml (bs), 10⁷⁷ spores/ml (bt), 10⁷⁸ spores/ml (bu), 10⁷⁹ spores/ml (bv), 10⁸⁰ spores/ml (bw), 10⁸¹ spores/ml (bx), 10⁸² spores/ml (by), 10⁸³ spores/ml (bz), 10⁸⁴ spores/ml (ca), 10⁸⁵ spores/ml (cb), 10⁸⁶ spores/ml (cc), 10⁸⁷ spores/ml (cd), 10⁸⁸ spores/ml (ce), 10⁸⁹ spores/ml (cf), 10⁹⁰ spores/ml (cg), 10⁹¹ spores/ml (ch), 10⁹² spores/ml (ci), 10⁹³ spores/ml (cj), 10⁹⁴ spores/ml (ck), 10⁹⁵ spores/ml (cl), 10⁹⁶ spores/ml (cm), 10⁹⁷ spores/ml (cn), 10⁹⁸ spores/ml (co), 10⁹⁹ spores/ml (cp), 10¹⁰⁰ spores/ml (cq), 10¹⁰¹ spores/ml (cr), 10¹⁰² spores/ml (cs), 10¹⁰³ spores/ml (ct), 10¹⁰⁴ spores/ml (cu), 10¹⁰⁵ spores/ml (cv), 10¹⁰⁶ spores/ml (cw), 10¹⁰⁷ spores/ml (cx), 10¹⁰⁸ spores/ml (cy), 10¹⁰⁹ spores/ml (cz), 10¹¹⁰ spores/ml (da), 10¹¹¹ spores/ml (db), 10¹¹² spores/ml (dc), 10¹¹³ spores/ml (dd), 10¹¹⁴ spores/ml (de), 10¹¹⁵ spores/ml (df), 10¹¹⁶ spores/ml (dg), 10¹¹⁷ spores/ml (dh), 10¹¹⁸ spores/ml (di), 10¹¹⁹ spores/ml (dj), 10¹²⁰ spores/ml (dk), 10¹²¹ spores/ml (dl), 10¹²² spores/ml (dm), 10¹²³ spores/ml (dn), 10¹²⁴ spores/ml (do), 10¹²⁵ spores/ml (dp), 10¹²⁶ spores/ml (dq), 10¹²⁷ spores/ml (dr), 10¹²⁸ spores/ml (ds), 10¹²⁹ spores/ml (dt), 10¹³⁰ spores/ml (du), 10¹³¹ spores/ml (dv), 10¹³² spores/ml (dw), 10¹³³ spores/ml (dx), 10¹³⁴ spores/ml (dy), 10¹³⁵ spores/ml (dz), 10¹³⁶ spores/ml (ea), 10¹³⁷ spores/ml (eb), 10¹³⁸ spores/ml (ec), 10¹³⁹ spores/ml (ed), 10¹⁴⁰ spores/ml (ee), 10¹⁴¹ spores/ml (ef), 10¹⁴² spores/ml (eg), 10¹⁴³ spores/ml (eh), 10¹⁴⁴ spores/ml (ei), 10¹⁴⁵ spores/ml (ej), 10¹⁴⁶ spores/ml (ek), 10¹⁴⁷ spores/ml (el), 10¹⁴⁸ spores/ml (em), 10¹⁴⁹ spores/ml (en), 10¹⁵⁰ spores/ml (eo), 10¹⁵¹ spores/ml (ep), 10¹⁵² spores/ml (eq), 10¹⁵³ spores/ml (er), 10¹⁵⁴ spores/ml (es), 10¹⁵⁵ spores/ml (et), 10¹⁵⁶ spores/ml (eu), 10¹⁵⁷ spores/ml (ev), 10¹⁵⁸ spores/ml (ew), 10¹⁵⁹ spores/ml (ex), 10¹⁶⁰ spores/ml (ey), 10¹⁶¹ spores/ml (ez), 10¹⁶² spores/ml (fa), 10¹⁶³ spores/ml (fb), 10¹⁶⁴ spores/ml (fc), 10¹⁶⁵ spores/ml (fd), 10¹⁶⁶ spores/ml (fe), 10¹⁶⁷ spores/ml (ff), 10¹⁶⁸ spores/ml (fg), 10¹⁶⁹ spores/ml (fh), 10¹⁷⁰ spores/ml (fi), 10¹⁷¹ spores/ml (fj), 10¹⁷² spores/ml (fk), 10¹⁷³ spores/ml (fl), 10¹⁷⁴ spores/ml (fm), 10¹⁷⁵ spores/ml (fn), 10¹⁷⁶ spores/ml (fo), 10¹⁷⁷ spores/ml (fp), 10¹⁷⁸ spores/ml (fq), 10¹⁷⁹ spores/ml (fr), 10¹⁸⁰ spores/ml (fs), 10¹⁸¹ spores/ml (ft), 10¹⁸² spores/ml (fu), 10¹⁸³ spores/ml (fv), 10¹⁸⁴ spores/ml (fw), 10¹⁸⁵ spores/ml (fx), 10¹⁸⁶ spores/ml (fy), 10¹⁸⁷ spores/ml (fz), 10¹⁸⁸ spores/ml (ga), 10¹⁸⁹ spores/ml (gb), 10¹⁹⁰ spores/ml (gc), 10¹⁹¹ spores/ml (gd), 10¹⁹² spores/ml (ge), 10¹⁹³ spores/ml (gf), 10¹⁹⁴ spores/ml (gg), 10¹⁹⁵ spores/ml (gh), 10¹⁹⁶ spores/ml (gi), 10¹⁹⁷ spores/ml (gj), 10¹⁹⁸ spores/ml (gk), 10¹⁹⁹ spores/ml (gl), 10²⁰⁰ spores/ml (gm), 10²⁰¹ spores/ml (gn), 10²⁰² spores/ml (go), 10²⁰³ spores/ml (gp), 10²⁰⁴ spores/ml (gq), 10²⁰⁵ spores/ml (gr), 10²⁰⁶ spores/ml (gs), 10²⁰⁷ spores/ml (gt), 10²⁰⁸ spores/ml (gu), 10²⁰⁹ spores/ml (gv), 10²¹⁰ spores/ml (gw), 10²¹¹ spores/ml (gx), 10²¹² spores/ml (gy), 10²¹³ spores/ml (gz), 10²¹⁴ spores/ml (ha), 10²¹⁵ spores/ml (hb), 10²¹⁶ spores/ml (hc), 10²¹⁷ spores/ml (hd), 10²¹⁸ spores/ml (he), 10²¹⁹ spores/ml (hf), 10²²⁰ spores/ml (hg), 10²²¹ spores/ml (hh), 10²²² spores/ml (hi), 10²²³ spores/ml (hj), 10²²⁴ spores/ml (hk), 10²²⁵ spores/ml (hl), 10²²⁶ spores/ml (hm), 10²²⁷ spores/ml (hn), 10²²⁸ spores/ml (ho), 10²²⁹ spores/ml (hp), 10²³⁰ spores/ml (hq), 10²³¹ spores/ml (hr), 10²³² spores/ml (hs), 10²³³ spores/ml (ht), 10²³⁴ spores/ml (hu),